

Methods in  
Molecular Biology 2958

Springer Protocols

Yuki Hara  
Kazunori Kume *Editors*

# The Nuclear Membrane

Methods and Protocols

MOREMEDIA



Humana Press

# METHODS IN MOLECULAR BIOLOGY

*Series Editor*

**John M. Walker**

**School of Life and Medical Sciences**

**University of Hertfordshire**

**Hatfield, Hertfordshire, UK**

For further volumes:

<http://www.springer.com/series/7651>

For over 35 years, biological scientists have come to rely on the research protocols and methodologies in the critically acclaimed *Methods in Molecular Biology* series. The series was the first to introduce the step-by-step protocols approach that has become the standard in all biomedical protocol publishing. Each protocol is provided in readily-reproducible step-by-step fashion, opening with an introductory overview, a list of the materials and reagents needed to complete the experiment, and followed by a detailed procedure that is supported with a helpful notes section offering tips and tricks of the trade as well as troubleshooting advice. These hallmark features were introduced by series editor Dr. John Walker and constitute the key ingredient in each and every volume of the *Methods in Molecular Biology* series. Tested and trusted, comprehensive and reliable, all protocols from the series are indexed in PubMed.

# **The Nuclear Membrane**

## **Methods and Protocols**

Edited by

**Yuki Hara**

*Evolutionary Cell Biology Lab, Faculty of Science, Yamaguchi University, Yamaguchi, Japan*

**Kazunori Kume**

*Graduate School of Integrated Sciences for Life, Hiroshima University, Higashi-hiroshima, Japan*

*Editors*

Yuki Hara  
Evolutionary Cell Biology Lab  
Faculty of Science  
Yamaguchi University  
Yamaguchi, Japan

Kazunori Kume  
Graduate School of Integrated Sciences for Life  
Hiroshima University  
Higashi-hiroshima, Japan

ISSN 1064-3745

ISSN 1940-6029 (electronic)

Methods in Molecular Biology

ISBN 978-1-0716-4713-4

ISBN 978-1-0716-4714-1 (eBook)

<https://doi.org/10.1007/978-1-0716-4714-1>

© The Editor(s) (if applicable) and The Author(s), under exclusive license to Springer Science+Business Media, LLC, part of Springer Nature 2025

This work is subject to copyright. All rights are solely and exclusively licensed by the Publisher, whether the whole or part of the material is concerned, specifically the rights of translation, reprinting, reuse of illustrations, recitation, broadcasting, reproduction on microfilms or in any other physical way, and transmission or information storage and retrieval, electronic adaptation, computer software, or by similar or dissimilar methodology now known or hereafter developed.

The use of general descriptive names, registered names, trademarks, service marks, etc. in this publication does not imply, even in the absence of a specific statement, that such names are exempt from the relevant protective laws and regulations and therefore free for general use.

The publisher, the authors and the editors are safe to assume that the advice and information in this book are believed to be true and accurate at the date of publication. Neither the publisher nor the authors or the editors give a warranty, expressed or implied, with respect to the material contained herein or for any errors or omissions that may have been made. The publisher remains neutral with regard to jurisdictional claims in published maps and institutional affiliations.

This Humana imprint is published by the registered company Springer Science+Business Media, LLC, part of Springer Nature.

The registered company address is: 1 New York Plaza, New York, NY 10004, U.S.A.

If disposing of this product, please recycle the paper.

---

## Preface

The nucleus is a membrane-bound organelle that plays a pivotal role in numerous vital biological processes in eukaryotes, encompassing both genetic and nongenetic functions [1]. To facilitate these processes in response to intracellular and extracellular signals, specific molecules crucial for each process, such as DNA, RNA, proteins, lipids, and metabolites, must be assembled or localized in the appropriate cellular compartments at precise times. The nuclear membrane, which is composed of lipid bilayers and associated protein complexes, plays an essential role in maintaining a specific environment within the nucleus. First, the nuclear membrane serves as a physical barrier, compartmentalizing large molecules, such as genomic DNA and protein complexes involved in DNA replication and transcription, from the cytoplasm. Second, nuclear pores, which are composed of multiple proteins embedded in the nuclear membrane, actively transport specific molecules between the cytoplasm and nucleoplasm, countering free diffusion due to concentration gradient. Third, the nuclear membrane provides a platform for the organization of highly ordered chromatin structures, such as heterochromatin, through preferential localization of certain molecules, including DNA, RNA, and proteins, at the nuclear periphery.

Biological processes in the nucleus are regulated to respond to and function in the cellular environment. These processes adapt to varying conditions, such as different nutritional conditions in unicellular organisms and development and differentiation in multicellular organisms. For instance, gene expression profiles undergo remarkable changes during the transition from the differentiated state of somatic cells to the undifferentiated state of induced pluripotent stem (iPS) cells. To induce such changes in the nucleus, the properties of the nucleoplasm and nuclear membrane must be regulated. Particularly, the nuclear membrane is composed of lipids [2–4], proteins [5, 6], and interacting DNA regions [7, 8]. It exhibits local variability within the nucleus and across different cellular conditions and associated factors. These variations in the nuclear membrane influence not only the platform for protein interactions [4, 9] but also its physical properties, such as membrane stiffness [10]. Such differences contribute to the diversity in nuclear size and shape [11, 12] along with the intranuclear physical properties and functions [13] observed across cell types and species.

To comprehensively understand the mechanistic basis of how the properties of the nuclear membrane, influenced by the cellular context, drive changes in nuclear biological processes, analyzing the nuclear membrane from multiple perspectives is essential. To date, numerous experimental methodologies have been developed to investigate the configuration and functions of nuclear membranes in living cells, isolated nuclei, and individual nuclear components. Furthermore, the integration of classical cell biological analyses with recent omics approaches has rapidly advanced the accumulation of information regarding the composition of nuclear membranes. Additionally, approaches for manipulating nuclear membranes and environments *in vivo* and reconstructing them *in vitro* have enabled more precise investigations of their properties and functions using defined components. This book compiles protocols that encompass a diverse range of classical and contemporary approaches, including biochemical techniques, proteomic analyses, microscopic observations, and biophysical measurements. The objective is to offer a valuable resource for readers

investigating nuclear structure and function in the post-genomic era and inspire future studies and methodologies to ultimately create a complete *in vitro* nucleus that replicates the functional and structural complexity of its *in vivo* counterpart.

*Yamaguchi, Japan*  
*Higashi-hiroshima, Japan*

*Yuki Hara*  
*Kazunori Kume*

## References

1. Bustin M, Misteli T (2016) Nongenetic functions of the genome. *Science* 352:aad6933
2. Aviram R, Manella G, Kopelman N et al (2016) Lipidomics analyses reveal temporal and spatial lipid organization and uncover daily oscillations in intracellular organelles. *Mol Cell* 62:636–648
3. Makarova M, Peter M, Balogh G et al (2020) Delineating the rules for structural adaptation of membrane-associated proteins to evolutionary changes in membrane lipidome. *Curr Biol* 30:367–380.e8
4. Foo S, Cazenave-Gassiot A, Wenk MR, Oliferenko S (2023) Diacylglycerol at the inner nuclear membrane fuels nuclear envelope expansion in closed mitosis. *J Cell Sci* 136:jcs260568
5. Tang Y, Huang A, Gu Y (2020) Global profiling of plant nuclear membrane proteome in *Arabidopsis*. *Nat Plants* 6:838–847
6. Nastaly P, Purushothaman D, Marchesi S et al (2020) Role of the nuclear membrane protein Emerin in front-rear polarity of the nucleus. *Nat Commun* 11:2122
7. Tran JR, Zheng X, Adam SA et al (2022) High quality mapping of chromatin at or near the nuclear lamina from small numbers of cells reveals cell cycle and developmental changes of chromatin at the nuclear periphery. *Nucleic Acids Res* 50:e117
8. Robson MI, de las Heras JI, Czapiewski R et al (2016) Tissue-specific gene repositioning by muscle nuclear membrane proteins enhances repression of critical developmental genes during myogenesis. *Mol Cell* 62:834–847
9. Amm I, Weberruss M, Hellwig A et al (2023) Distinct domains in Ndc1 mediate its interaction with the Nup84 complex and the nuclear membrane. *J Cell Biol* 222:e202210059
10. Swift J, Ivanovska IL, Buxboim A et al (2013) Nuclear lamin-A scales with tissue stiffness and enhances matrix-directed differentiation. *Science* 341:1240104
11. Introini V, Kidiyoor GR, Porcella G et al (2023) Centripetal nuclear shape fluctuations associate with chromatin condensation in early prophase. *Commun Biol* 6:715
12. Katiyar A, Zhang J, Antani JD et al (2022) The nucleus bypasses obstacles by deforming like a drop with surface tension mediated by Lamin A/C. *Adv Sci (Weinh)* 9:e2201248
13. Biswas A, Muñoz O, Kim K et al (2023) Conserved nucleocytoplasmic density homeostasis drives cellular organization across eukaryotes. *bioRxiv* 2023.09.05.556409


# Contents






<i>Preface</i> .....	<i>v</i>
<i>Contributors</i> .....	<i>ix</i>
1 Lipidomic Profiling of Isolated Nuclei from Mice and Cultured Cells .....	1
<i>Nityanand Bolschette, Hanmei Bao, Xianlin Han, and Gad Asher</i>	
2 Profiling Plant Nuclear Envelope Composition Using Subtractive Proteomics .....	17
<i>Xiao Liu and Yu Tang</i>	
3 Ultrastructural Visualization of the Nuclear Envelope in HeLa Cells .....	35
<i>Sourabh Sengupta, Zhaojie Zhang, and Daniel L. Levy</i>	
4 Imaging Nuclear Envelopes Using Correlative AFM/Fluorescence Microscopy .....	45
<i>Emilie Costes, Anthony Vial, Christine Doucet, and Pierre-Emmanuel Milhiet</i>	
5 Fast Super-Resolution Live Cell Imaging of Nuclear Membrane-Endoplasmic Reticulum Dynamics .....	71
<i>Swapnil Sahoo and Abdur Rahaman</i>	
6 Immunostaining the Yeast Nuclear Membrane for Imaging by Super-Resolution Fluorescence Microscopy .....	83
<i>Emily M. Sontag</i>	
7 Visualizing Phosphatidic Acid and Diacylglycerol at the Nuclear Envelope in Fission Yeast .....	99
<i>Sherman Foo and Snezhana Oliferenko</i>	
8 Measuring Molecular Mass Densities at Subcellular Resolution Using Optical Diffraction Tomography .....	119
<i>Kyoohyun Kim, Abin Biswas, Jochen Guck, and Simone Reber</i>	
9 Quantification and Comparison of Protein Distribution on the Nuclear Membrane .....	143
<i>Paulina Nastafy and Paolo Maiuri</i>	
10 Quantifying Nuclear Shape Fluctuations During Early Mitosis .....	151
<i>Viola Introini, Giancarlo Porcella, Gururaj Rao Kidiyoor, Pietro Cicuta, and Marco Cosentino Lagomarsino</i>	
11 Micropost Arrays to Model ECM Fiber Obstacles During Cell Migration in Confinement .....	159
<i>Aditya Katiyar, Richard B. Dickinson, and Tanmay P. Lele</i>	
12 Use of Nucleoporin-Conjugated Beads to Study the Nuclear Pore Complex Assembly on the Nuclear Membrane .....	169
<i>Şükriye Bilir, Yasushi Hiraoka, and Tokuko Haraguchi</i>	

13	T4 DNA-Induced Reconstruction of Artificial Nuclei in Living Mouse Oocytes .....	183
	<i>Nao Yonezawa, Yasushi Hiraoka, Tokuko Haraguchi, and Kazuo Yamagata</i>	
14	Preparation of Nucleoplasmic Extract and Its Application in DNA End Processing .....	201
	<i>Daichi Nishiguchi, Kensuke Tatsukawa, and Tatsuro S. Takahashi</i>	
15	Liposome Flootation Assays to Study Membrane Interactions of Nucleoporins .....	225
	<i>Marianna Tatarek-Nossol and Wolfram Antonin</i>	
16	Giant Unilamellar Vesicles (GUVs) to Study Membrane Interaction of Nucleoporins .....	239
	<i>Marianna Tatarek-Nossol and Wolfram Antonin</i>	
17	One-Pot Reconstitution of GPCRs into Unilamellar Vesicles for Fluorescence-Based Phospholipid Scramblase Activity Assay .....	255
	<i>Indu Menon and Anant K. Menon</i>	
18	Identifying Genomic DNA Sequences Near the Nuclear Lamina Using Proximity Biotinylation with Ascorbate Peroxidase .....	271
	<i>Yixian Zheng, Katherine A. Bossone, Sara Debic, Ross T. A. Pedersen, and Joseph R. Tran</i>	
19	Pairing Lamin B1-DamID and Immuno-3D-FISH to Resolve and Verify Peripheral Genome Organization of Adipogenesis .....	287
	<i>Rafal Czapiewski, Jose I. de las Heras, and Eric C. Schirmer</i>	
20	Measurement of Spatial Contact Map Using Sequential FISH .....	327
	<i>Hiroaki Ohishi</i>	
	<i>Index</i> .....	343

---

## Contributors

- WOLFRAM ANTONIN • *Institute of Biochemistry and Molecular Cell Biology, Medical School, RWTH Aachen University, Aachen, Germany*
- GAD ASHER • *Department of Biomolecular Sciences, Weizmann Institute of Science, Rehovot, Israel*
- HANMEI BAO • *The Sam & Ann Barshop Institute for Longevity & Aging Studies, University of Texas Health Science Center at San Antonio, San Antonio, TX, USA*
- ŞÜKRIYE BİLİR • *Graduate School of Frontier Biosciences, Osaka University, Suita, Japan; Research Institute for Health Sciences and Technologies (SABITA), Istanbul Medipol University, Istanbul, Türkiye*
- ABIN BISWAS • *Max Planck Institute for the Science of Light, Erlangen, Germany; Max-Planck-Zentrum für Physik und Medizin, Erlangen, Germany; Max Planck Institute for Infection Biology, Berlin, Germany*
- NITYANAND BOLSHETTE • *Department of Biomolecular Sciences, Weizmann Institute of Science, Rehovot, Israel*
- KATHERINE A. BOSSONE • *Carnegie Institution for Science, Baltimore, MD, USA; Department of Biology, Johns Hopkins University, Baltimore, MD, USA*
- PIETRO CICUTA  • *Cavendish Laboratory, University of Cambridge, Cambridge, UK*
- MARCO COSENTINO LAGOMARSINO  • *IFOM ETS, The AIRC Institute of Molecular Oncology, Milan, Italy; Dipartimento di Fisica, Università degli Studi di Milano and I.N.F.N, Milan, Italy*
- EMILIE COSTES • *Centre de Biologie Structurale, INSERM, CNRS, University of Montpellier, Montpellier, France*
- RAFAL CZAPIEWSKI • *Institute of Cell Biology, University of Edinburgh, Edinburgh, UK; MRC Human Genetics Unit, Institute of Genetics and Cancer, University of Edinburgh, Edinburgh, UK*
- JOSE I. DE LAS HERAS • *Institute of Cell Biology, University of Edinburgh, Edinburgh, UK*
- SARA DEBIC • *Carnegie Institution for Science, Baltimore, MD, USA; Department of Biology, Johns Hopkins University, Baltimore, MD, USA*
- RICHARD B. DICKINSON • *Department of Chemical Engineering, University of Florida, Gainesville, FL, USA*
- CHRISTINE DOUCET • *Centre de Biologie Structurale, INSERM, CNRS, University of Montpellier, Montpellier, France*
- SHERMAN FOO • *Randall Centre for Cell and Molecular Biophysics, School of Basic and Medical Biosciences, King's College London, London, UK; The Francis Crick Institute, London, UK; Medical Research Council Laboratory of Molecular Biology, Cambridge, UK*
- JOCHEN GUCK • *Max Planck Institute for the Science of Light, Erlangen, Germany; Max-Planck-Zentrum für Physik und Medizin, Erlangen, Germany*
- XIANLIN HAN • *The Sam & Ann Barshop Institute for Longevity & Aging Studies, University of Texas Health Science Center at San Antonio, San Antonio, TX, USA; Department of Medicine, University of Texas Health Science Center at San Antonio, San Antonio, TX, USA*
- TOKUKO HARAGUCHI • *Graduate School of Frontier Biosciences, Osaka University, Suita, Japan*

- YASUSHI HIRAOKA • *Graduate School of Frontier Biosciences, Osaka University, Suita, Japan*
- VIOLA INTROINI  • *European Molecular Biology Laboratory (EMBL) Barcelona, Barcelona, Spain*
- ADITYA KATTIYAR • *Department of Biomedical Engineering, Texas A&M University, College Station, TX, USA*
- GURURAJ RAO KIDIYOOR  • *Institute for Systems Genetics, New York University School of Medicine, New York, NY, USA*
- KYOOHYUN KIM • *Max Planck Institute for the Science of Light, Erlangen, Germany; Max-Planck-Zentrum für Physik und Medizin, Erlangen, Germany*
- TANMAY P. LELE • *Department of Biomedical Engineering, Texas A&M University, College Station, TX, USA; Artie McFerrin Department of Chemical Engineering, Texas A&M University, College Station, TX, USA; Department of Translational Medical Sciences, Texas A&M University, Houston, TX, USA*
- DANIEL L. LEVY • *Department of Molecular Biology, University of Wyoming, Laramie, WY, USA*
- XIAO LIU • *State Key Laboratory of Wheat Improvement, Peking University Institute of Advanced Agricultural Sciences, Shandong Laboratory of Advanced Agricultural Sciences at Weifang, Weifang, Shandong, China*
- PAOLO MAIURI • *Department of Molecular Medicine and Medical Biotechnology, University of Naples Federico II, Naples, Italy*
- ANANT K. MENON • *Department of Biochemistry, Weill Cornell Medical College, New York, NY, USA*
- INDU MENON • *Department of Biochemistry, Weill Cornell Medical College, New York, NY, USA*
- PIERRE-EMMANUEL MILHIET • *Centre de Biologie Structurale, INSERM, CNRS, University of Montpellier, Montpellier, France*
- PAULINA NASTALY • *Division of Translational Oncology, Intercollegiate Faculty of Biotechnology, University of Gdańsk and Medical University of Gdańsk, Gdańsk, Poland*
- DAICHI NISHIGUCHI • *Graduate School of Systems Life Sciences, Kyushu University, Fukuoka, Japan*
- HIROAKI OHISHI • *Division of Gene Expression Dynamics, Medical Institute of Bioregulation, Kyushu University, Fukuoka, Japan*
- SNEZHANA OLIFERENKO • *Randall Centre for Cell and Molecular Biophysics, School of Basic and Medical Biosciences, King's College London, London, UK; The Francis Crick Institute, London, UK*
- ROSS T. A. PEDERSEN • *Carnegie Institution for Science, Baltimore, MD, USA*
- GIANCARLO PORCELLA  • *Helmholtz Zentrum München, Neuherberg, Germany*
- ABDUR RAHAMAN  • *School of Biological Sciences, National Institute of Science Education and Research, Bhubaneswar, Odisha, India; Homi Bhabha National Institute, Mumbai, India*
- SIMONE REBER • *Max Planck Institute for Infection Biology, Berlin, Germany; Berliner Hochschule für Technik, Berlin, Germany*
- SWAPNIL SAHOO  • *School of Biological Sciences, National Institute of Science Education and Research, Bhubaneswar, Odisha, India; Homi Bhabha National Institute, Mumbai, India*
- ERIC C. SCHIRMER • *Institute of Cell Biology, University of Edinburgh, Edinburgh, UK*
- SOURABH SENGUPTA • *Department of Molecular Biology, University of Wyoming, Laramie, WY, USA*

- EMILY M. SONTAG • *Department of Biological Sciences, Marquette University, Milwaukee, WI, USA*
- TATSURO S. TAKAHASHI • *Faculty of Science, Kyushu University, Fukuoka, Japan*
- YU TANG • *State Key Laboratory of Wheat Improvement, Peking University Institute of Advanced Agricultural Sciences, Shandong Laboratory of Advanced Agricultural Sciences at Weifang, Weifang, Shandong, China*
- MARIANNA TATAREK-NOSSOL • *Institute of Biochemistry and Molecular Cell Biology, Medical School, RWTH Aachen University, Aachen, Germany*
- KENSUKE TATSUKAWA • *Faculty of Science, Kyushu University, Fukuoka, Japan*
- JOSEPH R. TRAN • *Carnegie Institution for Science, Baltimore, MD, USA*
- ANTHONY VIAL • *University of Bordeaux, CNRS, Bordeaux INP, CBMN, UMR 5248, F-33360, Pessac, France*
- KAZUO YAMAGATA • *Faculty of Biology-Oriented Science and Technology, Kindai University, Kinokawa, Japan*
- NAO YONEZAWA • *Faculty of Biology-Oriented Science and Technology, Kindai University, Kinokawa, Japan*
- ZHAOJIE ZHANG • *Department of Zoology and Physiology, University of Wyoming, Laramie, WY, USA*
- YIXIAN ZHENG • *Carnegie Institution for Science, Baltimore, MD, USA*



# Chapter 1

## Lipidomic Profiling of Isolated Nuclei from Mice and Cultured Cells

Nityanand Bolshette, Hanmei Bao, Xianlin Han, and Gad Asher

### Abstract

Lipidomic methodologies, in conjunction with biochemical isolation of intracellular organelles such as the nucleus, have identified a wide variety of nuclear lipid species. The nuclear lipid composition, for example, exhibits daily changes and is controlled both by the circadian clock and feeding behavior. However, the functions of many of these lipids in the nucleus remain elusive. In this chapter we describe in detail the procedure for nuclear lipidomics; from biochemical isolation of nuclei from mouse liver and cultured cells to the unbiased lipid identification and quantification using Multi-Dimensional Mass Spectrometry Shotgun Lipidomics (MDMS-SL). The approach described herein is applicable with some modifications for different tissues and various animal models, as well as a wide variety of cultured cells. It is expected to yield new insights into various aspects of nuclear lipid composition and function in the future.

**Key words** Shotgun lipidomics, Mass spectrometry, Mouse, Liver, Cultured cells, Nuclei, Lipid metabolism

---

## 1 Introduction

Recent advancements in lipidomic methodologies have enabled the characterization and identification of an unprecedented number of lipid species. These lipids carry structural functions, which serve as energy source as well as signaling molecules [1]. The ability to harness these powerful novel technologies with traditional biochemical assays for isolation of intracellular organelles, such as the nucleus, has enabled the identification of the nuclear lipidome. The liver plays a central role in lipid metabolism [2]. We previously showed that in mouse liver, the nuclear lipid composition is highly dynamic and exhibits daily changes that are controlled by both the circadian clock and feeding behavior [3, 4]. The functions, however, of many of these lipids remain elusive. Hence, lipidomic analyses of subcellular compartments (e.g., nucleus, mitochondria) can be used to determine spatial and temporal dynamics in lipid

composition. Future studies are expected to shed more light on the mechanisms that control their accumulation in different subcellular compartments and their biological functions.

We include a detailed description of the protocol used for biochemical isolation of nuclei from mouse liver and cultured cells. Samples are then homogenized at a temperature below 4 °C to minimize enzyme activation. A pre-mixture of lipid internal standards (IS) is added prior to conducting lipid extraction for quantification of individual lipid molecular species in targeted lipid classes. Lipids are extracted using a modified Bligh and Dyer procedure [5] and analyzed using Multi-Dimensional Mass Spectrometry Shotgun Lipidomics (MDMS-SL) [6]. Identification and quantification of lipid species are performed using an automated software program [7]. Data processing (e.g., ion peak selection, baseline correction, data transfer, peak intensity comparison, and quantitation) is performed as described. At its current stage of development, this technique can provide quantitative measurement of hundreds to thousands of individual lipid species (including many regioisomers) of over 50 lipid classes, which represent >95% of the mass content of the cellular lipidome. Depending on the nature of the biological samples, the technology is expected to yield quantitative measurements of glycerophospholipids (e.g., cardiolipin, phosphatidic acid, phosphatidylcholine, phosphatidylethanolamine, phosphatidylglycerol, phosphatidylinositol, and phosphatidylserine), lyso-glycerophospholipids (e.g., lysocardiopin, lysophosphatidylcholine, and lysophosphatidylethanolamine), sphingolipids (e.g., ceramide, sphingomyelin, galactosylceramide, sulfatide, hexosylceramide, sphingosine/sphinganine, sphingoid base-1-phosphate, and psychosine), sterols (cholesterol, cholesterol ester, and some oxysterols), and glycerolipids such as diacylglycerol and triacylglycerol. These molecules are characterized according to class and biochemical structure: acyl-chain length and linkage type (if relevant) and degree of saturation (i.e., number of double bonds).

The method described herein for lipid characterization from nuclei isolated from mouse liver and cultured cells can be utilized for comprehensive characterization of the nuclear lipidome. It can be used, with slight modifications on different tissues, mouse models, and a wide variety of cultured cells, and is expected to advance our knowledge on the nuclear lipidome and its function.

---

## 2 Materials

### 2.1 Nuclei Isolation from Mouse Liver

\* Keep instruments and reagents cold during use (4 °C).

All buffers are supplemented with 0.5 mM DTT, 100 μM NaF, 100 μM Na<sub>2</sub>VO<sub>4</sub>, 0.5 μM PMSF, and 1:100 Protease Inhibitor Cocktail (CALBIOCHEM).

1. Homogenization buffer A: 0.3 M sucrose, 10 mM Hepes pH 7.6, 15 mM KCl, 2 mM EDTA, 0.15 mM spermine, 0.5 mM spermidine, 10% glycerol (prepare ~4 mL per liver sample) (*see Note 1*).
2. Homogenization buffer B: 2.2 M sucrose, 10 mM Hepes pH 7.6, 15 mM KCl, 2 mM EDTA, 0.15 mM spermine, 0.5 mM spermidine, 10% glycerol (prepare 25 mL per liver sample: 7 for homogenization, 18 for homogenate dilution) (*see Note 1*).
3. Cushion buffer: 2.05 M sucrose, 10 mM Hepes pH 7.6, 15 mM KCl, 2 mM EDTA, 0.15 mM spermine, 0.5 mM spermidine, 10% glycerol (prepare ~11 mL per liver sample) (*see Note 1*).
4. Isotonic buffer: 10 mM Hepes pH 7.6, 100 mM KCl, 0.15 mM spermine, 0.5 mM spermidine, 10% glycerol. Store in 4 °C for up to 6 months.
5. Cold phosphate-buffered saline (PBS): 137 mM NaCl, 2.7 mM KCl, 10 mM Na<sub>2</sub>HPO<sub>4</sub>, and 1.8 mM KH<sub>2</sub>PO<sub>4</sub>; adjust pH 7.4 with HCl.
6. Swinging-bucket ultracentrifuge (4 °C), we use Beckman, SW28 rotor.
7. Ultracentrifuge polycarbonate tubes, suitable for the above rotor (40 mL volume) (*see Note 2*).
8. Electric homogenizer (IKA 3720001 T-18 Ultra Turrax Digital Homogenizer, tight-fitting pestle).
9. Douncer (homogenizer): consisting of a glass tube with a tight-fitting Teflon pestle (KONTES glass 23, 15 mL capacity at least).
10. Vacuum pump.
11. Syringe (of any kind, suitable to wash a tube).
12. Spatula.
13. Microtubes (1.5 mL).
14. Delicate paper wipers (e.g., Kimwipes).
15. Three months old C57BL6 male mice.

## **2.2 Nuclei Isolation from Cultured Cells**

\*Keep instruments and reagents cold during use (4 °C). Since storing in cold may cause rust, preferably cool only prior to use.

All buffers are supplemented with 1:100 Protease Inhibitor Cocktail (Sigma).

1. Cell lysis buffer: 10 mM NaCl, 1.5 mM MgCl<sub>2</sub>, 10 mM Tris-HCl, pH 7.5, 210 mM mannitol, 70 mM sucrose, 1 mM EDTA.
2. Non salt buffer: 10 mM Tris-HCl, pH 7.5, 0.2 mM EDTA.

3. Cold phosphate-buffered saline (PBS).
4. Microtubes (1.5 mL).
5. Dounce homogenizer with glass pestle (KONTES 60 mm, pestle clearance: 0.0005–0.0025-inch, 2 mL capacity, Cat# D8938).
6. Vortex mixer.
7. Delicate paper wipers (e.g., Kimwipes).
8. Hepalcl (hepatocytes) cells.
9. DMEM high glucose medium supplemented with 10% FBS, 100 units/mL penicillin, 100 mg/mL streptomycin.
10. Humidified incubator with 5% CO<sub>2</sub>.

## 2.3 Shotgun Lipidomics

Quantity of biological samples for analysis: >0.1 mg protein of nuclei (*see* **Note 3**).

### 2.3.1 Equipment

1. Nano-ESI source device (TriVersa NanoMate, Advion Bioscience Ltd., Ithaca, NY, USA).
2. Chipsoft 8.3.1 software (TriVersa NanoMate, Advion Bioscience Ltd., Ithaca, NY, USA).
3. Mass spectrometer (Thermo TSQ Altis™ Mass Spectrometer, San Jose, CA, USA).
4. Q Exactive mass spectrometer (Thermo Fisher Scientific, San Jose, CA, USA).
5. Xcalibur™ software (Thermo Fisher Scientific, San Jose, CA, USA).
6. Microtube Pellet Pestle Rods with Motor (Daigger Scientific Inc., Vernon Hills, IL, USA).
7. Reusable culture tubes (6 mL and 10 mL) with PTFE-lined caps.
8. 5.75" disposable borosilicate glass Pasteur pipets (Thermo Fisher Scientific).
9. Vortex mixer.
10. Tabletop centrifuge.
11. Disposable soft tissue homogenizer.
12. Disposable culture borosilicate glass tube (10 mL).
13. 24-position N-EVAP nitrogen evaporator (Organomation Associates, Inc., Berlin, MA).
14. Chemical resistance 96-well microplates.
15. Calibrated micropipettes.
16. Analytical balance (0.01 mg readability).
17. Drummond pipet-aids.

18. Precellys Evolution tissue homogenizer (Bertin Technologies, France).
19. Cytation 5 imaging reader (BioTek, CA, USA).
20. Digital incubator.

### 2.3.2 Chemicals and Standards

1. Tenfold diluted PBS with water.
2. Chloroform.
3. Methanol.
4. Isopropanol.
5. Saturated lithium hydroxide in methanol.
6. Chloroform/methanol mixture (1/1, *v/v*).
7. Chloroform/methanol/isopropanol mixture (1/2/4, *v/v/v*).
8. Chloroform/methanol/isopropanol mixture (1/2/4, *v/v/v*) with 50 mM lithium hydroxide.
9. Methyl-tert-butyl ether (MTBE).
10. Deionized water.
11. Hydrochloric acid.
12. Glacial acetic acid.
13. Trimethylsilyl diazomethane solution 2.0 M in hexanes.
14. 10 mM and 50 mM lithium chloride in water.
15. BCA protein assay kit.
16. Lipid internal standards (*see Note 4*): approximately 1 mg/mL of each lipid (*see Note 5*):
  - (a) 1,2-Dimyristoleoyl-*sn*-glycero-3-phosphocholine (di14:1 PC).
  - (b) 1,2-Dipalmitoleoyl-*sn*-glycero-3-phosphoethanolamine (di16:1 PE).
  - (c) 1,2-Dipentadecanoyl-*sn*-glycero-3-phosphoglycerol (sodium salt) (di15:0 PG).
  - (d) 1,2-Dimyristoyl-*sn*-glycero-3-phospho-L-serine (sodium salt) (di14:0 PS).
  - (e) 1,2-Dimyristoyl-*sn*-glycero-3-phosphate (sodium salt) (di14:0 PA).
  - (f) 1,1',2,2'-Tetramyristoyl cardiolipin (T14:0 CL).
  - (g) 7,7,8,8-d<sub>4</sub>-Palmitic acid (d<sub>4</sub>-16:0 NEFA) (Cambridge Isotope Laboratories, Andover, MA, USA).
  - (h) N-Lauroryl sphingomyelin (N12:0 SM).
  - (i) N-Heptadecanoyl ceramide (N17:0 Cer).
  - (j) 1-Heptadecanoyl-2-hydroxy-*sn*-glycero-3-phosphocholine (17:0 lysoPC).

- (k) 1-Myristoyl-2-hydroxy-*sn*-glycero-3-phosphoethanolamine (17:0 lysoPE).
- (l) 1,2,3,4- $^{13}\text{C}_4$ -Palmitoyl-L-carnitine hydrochloride ( $^{13}\text{C}_4$ -16:0 CN) (Sigma-Aldrich, St. Louis, MO, USA).
- (m) Triheptadecenoin (T17:1 TAG) (Nu Chek, Inc. Elysian, MN).

### 3 Methods

#### 3.1 Nuclei Isolation from Mouse Liver

Preferably use 3-month-old C57BL6 male mice (the method is applicable for different mouse strains). Mice are sacrificed by cervical dislocation or carbon dioxide exposure. Livers should be harvested immediately upon sacrifice (*see Note 6*). Perform all stages on ice. *See Fig. 1*:

1. Rinse liver in cold PBS.
2. Place liver sample in glass homogenizer tube, complete volume to 5 mL with Homogenization buffer A (i.e., add ~4 mL).
3. Add 7 mL of homogenization buffer B.

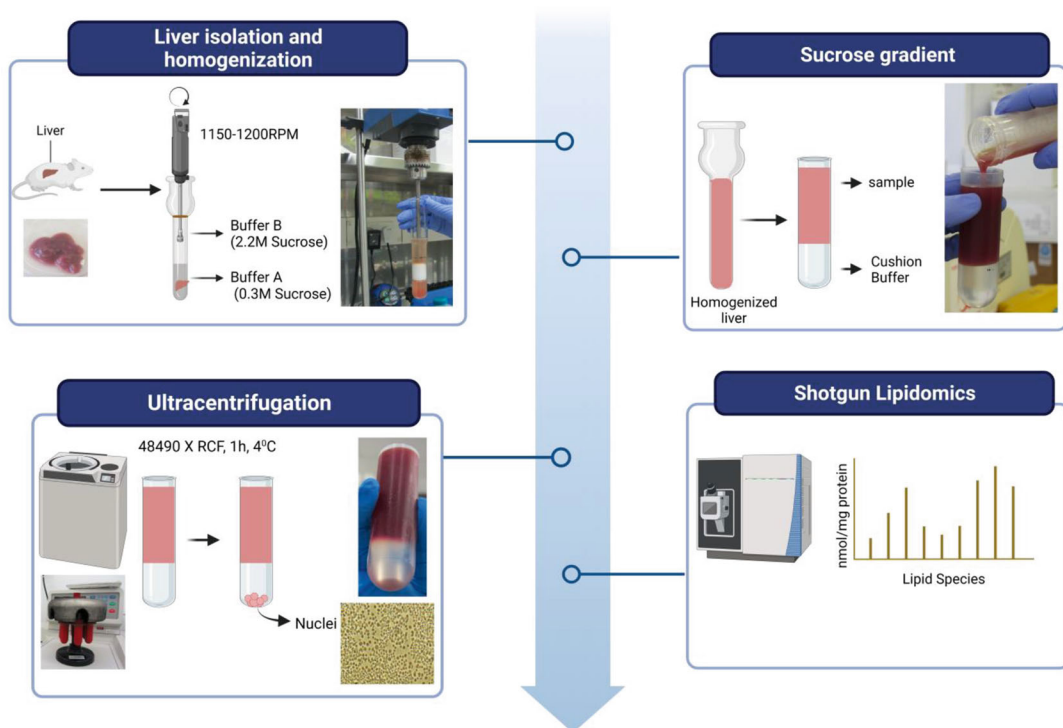


**Fig. 1** Nuclei isolation from mouse liver. Scheme representing detailed steps involved in isolation of nuclei from mouse liver for shotgun lipidomic profiling

4. Homogenize liver using tight-fitting pestle at 1150–1200 rpm (according to IKA motor setup). Run through the sample with three vertical motions. Avoid air bubbles.
5. Following homogenization add 18 mL of homogenization buffer B. Shake vigorously by hand to ensure thorough mixing.
6. Prepare the ultracentrifugation tube with 10.5 mL Cushion buffer.
7. Softly place the sample on top of the Cushion (*see Note 7*).
8. Centrifuge for 1 h, at 48,490 *g*, in 4 °C.
9. Remove the upper fat layer (using spatula or other instrument of choice such as Pasteur pipette, micro-spoon, or tweezers).
10. Remove the red fraction by the aspirator with vacuum pump (attach a pipette tip to the vacuum line for precise suction. Tilt the tube gently, insert the aspirator tip along one side, and carefully aspirate the red fraction without disturbing the lower nuclear pellet) (*see Note 8*).
11. Keep tube inverted to drain the remaining liquids. While inverted, wash the walls of the tubes with double distilled water (it is easily done using a syringe (*see Note 9*)), and dry the water with delicate paper.
12. Resuspend pellet in ~0.2 mL of isotonic buffer and transfer to microtubes (1.5 mL) (*see Note 10*).
13. Freeze samples in –80 °C, and store for lipidomic analyses.

### 3.2 Nuclei Isolation from Cell Culture

Hepalcl1 (hepatocytes) cells are cultured in DMEM high glucose medium supplemented with 10% FBS, 100 units/mL penicillin, 100 mg/mL streptomycin, and cultured at 37 °C in a humidified incubator with 5% CO<sub>2</sub> (the method is applicable for different cultured cells with some modifications).

Perform all stages on ice. *See Fig. 2*:

1. Grow the cells in 9 cm culture dish in DMEM medium until confluence.
2. Aspirate the media from the dish and wash cells with 10 mL of cold PBS.
3. Cells are dislodged (*see Note 11*) in 1 mL of cold PBS and collect in microtube (1.5 mL) on ice.
4. Centrifuge the above cell suspension at 1000 *g* for 10 min to obtain cell pellet (*see Note 12*).
5. Discard the supernatant and suspend the pelleted cells in five volumes of cell lysis buffer (buffer amount can be vary depending on cell type) and allow to swell (*see Note 13*) on ice for 10 min with intermittent mixing (no vortex).

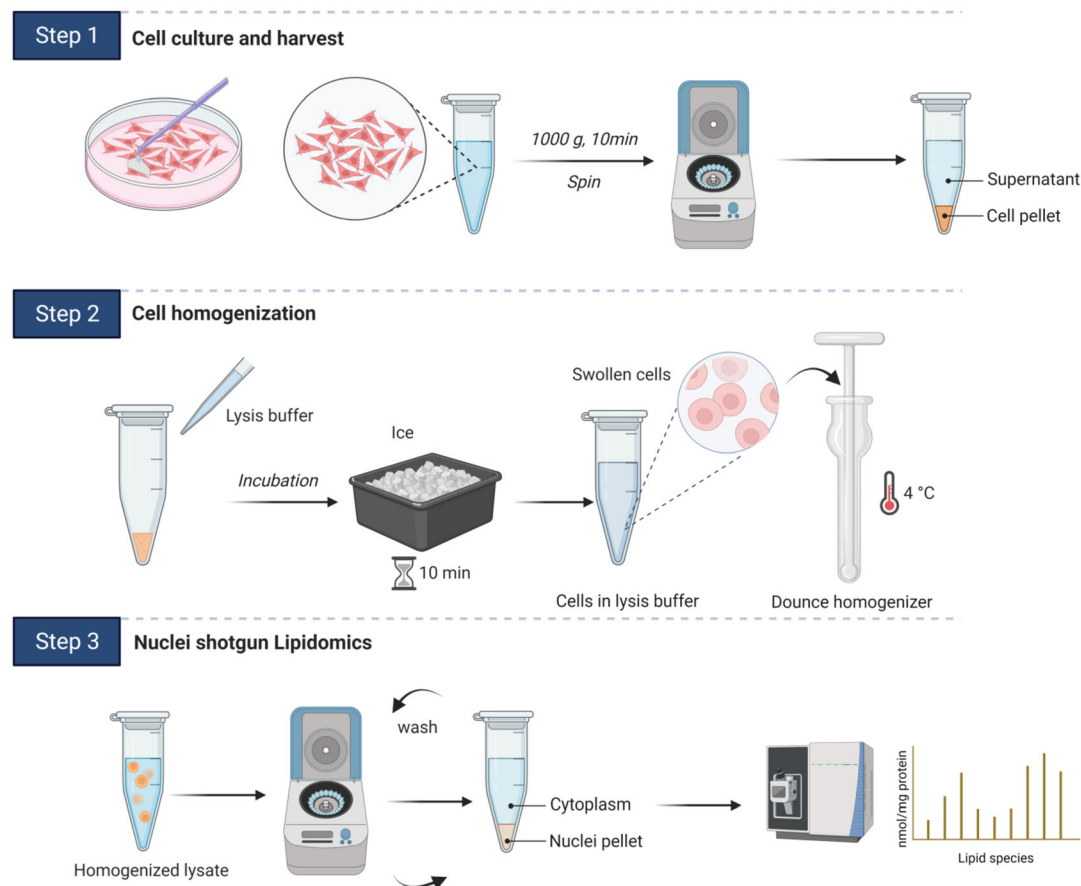


**Fig. 2** Nuclei isolation from culture cells. Scheme representing detailed steps involved in isolation of nuclei from Hepa1c1 cell line for nuclear lipidomic profiling

6. Add swollen cells in ice-cold dunce homogenizer. Perform gentle Dounce homogenization with 10–15 strokes (can be vary depending on cell types) with glass pestle (*see Note 14*). Monitor cell lysis under microscope after every five strokes (*see Note 15*).
7. Collect the homogenate in new microtube (1.5 mL) and centrifuge at 1000 *g* for 10 min at 4 °C.
8. Supernatant can be stored at –80 °C until further use as cytoplasmic extract.
9. Wash the nuclear pellet thrice (no vertex, just add buffer, tap gently, and centrifuge) with the 1 mL of non-salt buffer at 1000 *g* for 5 min.
10. After wash, remove all residual buffer and snap-freeze tube containing nuclei for lipidomic analysis.

### 3.3 Shotgun Lipidomics

#### 3.3.1 Lipid Extraction

Perform the following **steps 1** and **2** on ice:

1. For isolated nuclei samples from mice and cultured cells, keep the samples in 1.5 mL microtubes. Add 300  $\mu$ L of tenfold diluted PBS in the tube. The samples are homogenized for 1 min by using a disposable soft tissue homogenizer with an up-and-down dabbing motion.
2. Perform BCA protein assay with 5–10  $\mu$ L aliquot of the homogenate for each sample, using a 96-well microplate following the manufacturer's instructions.
3. Add 50  $\mu$ L of the pre-mixture of internal standards into a disposable culture borosilicate glass tube (10 mL), based on the protein content of the transferred homogenate sample.
4. For extraction add 4 mL of chloroform/methanol to the 10 mL glass tube, and 2 mL of 50 mM lithium chloride, and then add a precise volume of the homogenate of each sample corresponding to 0.1 mg of protein. Cap the tubes and vortex for 30 s.
5. Centrifuge at 1000  $g$  for 10 min.
6. Collect the bottom layer to a new borosilicate glass tube by a glass Pasteur pipet (*see* **Note 16**), and add 2 mL of chloroform to the residual top layer. Cap the tubes and vortex them for 30 seconds.
7. Centrifuge at 1000  $g$  for 10 min.
8. Collect the bottom layer and combine it with that collected in **step 7** in Subheading **3.3.1**.
9. Evaporate the combined chloroform layers under a nitrogen stream in the 24-position N-EVAP nitrogen evaporator.
10. Resuspend individual residue in **step 9**, Subheading **3.3.1** with 4 mL of Chloroform/Methanol mixture, and add 2 mL of 10 mM lithium chloride. Cap the tubes and vortex them for 30 s.
11. Repeat **steps 7** to **10** in Subheading **3.3.1** to re-extract the lipid layer obtained in **step 10**.
12. Resuspend individual lipid extract residue from **step 12** with chloroform/methanol mixture in a volume of 400  $\mu$ L/mg protein in original sample.
13. The liquid extracts are flushed with nitrogen using the 24-position N-EVAP nitrogen evaporator, capped, and stored at  $-20^{\circ}\text{C}$  until the following mass spectrometric analysis (Subheading **3.3.2**).

#### 3.3.2 Mass Spectrometric Analysis of Lipids

1. For shotgun lipidomics, individual lipid extract was further diluted to a final concentration of  $\sim 500$  fmol total lipids per  $\mu$ L with chloroform/methanol/isopropanol (1/2/4,  $v/v/v$ )

with or without LiOH (1%) in a Teflon-coated 96-well microplate (*see Note 17*) [8, 9]. The total lipid content in individual lipid extract was estimated based on the protein content as described in details [8].

2. Set the ionization voltage of the nanospray ionization source at 1.3 kV in the positive-ion mode, −1.3 kV in the negative-ion mode, and gas pressure at 0.55 psi. Nanospray ionization for each sample is performed by a customized sequence subroutine operated under the ChipsSoft software (*see Note 18*).
3. For mass spectrometric analysis, collect a 2-min signal averaging duration in the profile mode for each survey mass spectrometric scan (*see Note 19*). For tandem mass spectrometric analysis, set the collision gas pressure at 1.0 mTorr, vary the collision energy based on the lipid class, and collect a 3–5 min signal averaging period in the profile mode for each tandem mass spectrometric spectrum, including precursor ion scanning (PIS) and neutral loss scanning (NLS). These are sensitive and specific to the lipid class or category of lipid classes of interest. All mass spectra are automatically acquired by a customized sequence subroutine operated under Xcalibur software.

### 3.3.3 Mass Spectrometric Data Processing and Analysis

Processing of mass spectrometric analysis data, including ion peak selection, data transfer, baseline correction, peak intensity comparison, and quantification, are conducted using self-programmed Microsoft Excel macros. The results are normalized to the protein content (nmol lipid/mg protein). *See Fig. 3*.

The automated data processing to identify and quantify individual molecular species of a class of interest within a cellular lipidome is performed as follows:

1. Data loading: Tabular raw data from the mass spectra are transferred by self-programmed software directly from the Xcalibur-operated system.
2. Baseline correction: Mass spectrometry data typically exhibit a varying baseline due to chemical noise in the matrix. The baseline levels in the tabular raw data from mass spectra are the sum of baseline drift and noise level. Baseline drift is determined by averaging a set of the lowest ion intensities, while noise level is determined based on the observed accelerated intensity change from noise to signal. The precisely determined baseline level is deduced from the raw data for identification and quantification of lipid molecules.
3. Peak finding: A list of ion peaks corresponding to the molecular species within a lipid class of interest, present in the analyzed lipid extract, is generated. This is achieved by matching the  $m/z$  values of the detected ion peaks, after baseline correction in the specific scan mode (i.e., PIS or NLS), with those of

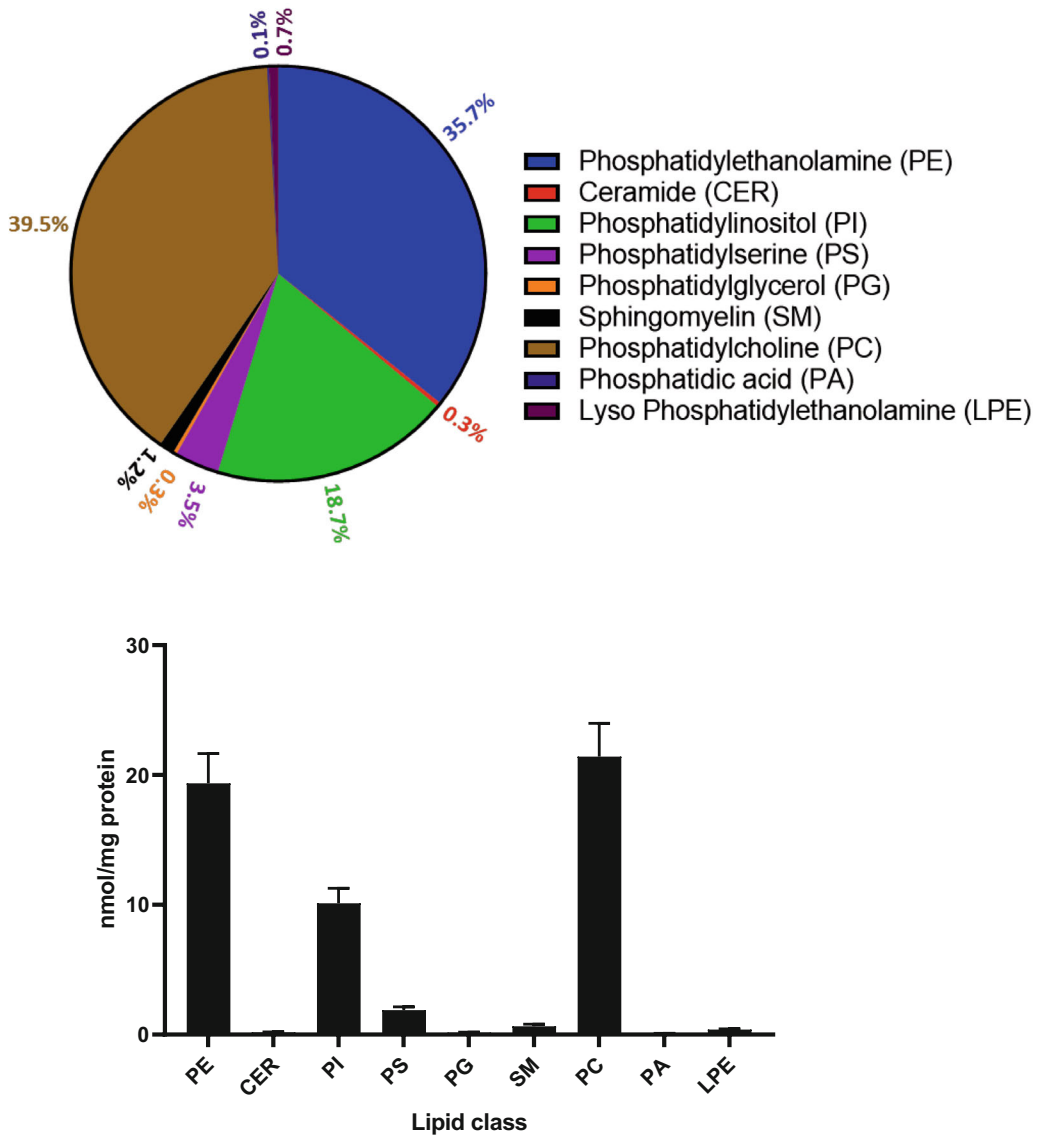


**Fig. 3** Distribution of different lipid classes in mouse liver nuclei. Distribution of different nuclear lipid species that were identified by shotgun lipidomics of mouse liver nuclei. (Lipidomic data from Aviram et al. [3] is used to plot graphs)

candidate species in the established lipid molecule database. This peak list encompasses all detectable lipid species of each specific lipid class and includes information about the total number of carbon atoms and the total number of double bonds in the aliphatic chain(s).

4. Acyl chain identification: Acyl chain moieties are identified by loading all PIS or NLS data specific to acyl chain formation. The combination of the paired aliphatic chains is determined by

restricting the total number of carbon atoms and double bonds present in the acyl chains identified for each individual species.

5. Deisotoping of electrospray mass spectra: Before quantifying lipid molecular species of interest, the effects of the presence of  $^{13}\text{C}$  isotope need to be considered [10]. There are two distinct types of effects. The first type of effect arises from the difference in carbon number between a given molecular species and the selected internal standard. The second type of effect results from the overlap of the ion peak of the species of interest ( $m/z = M$ ) with the  $^{13}\text{C}$  isotope peak of another species containing an additional double bond ( $m/z = M-2$ ) (*see Note 20*).
6. Quantification: The quantification of identified individual molecular species is conducted through either in a single-step or two-step procedure. Initially, an algorithm assesses whether there are overlapping or low-abundance peaks in the peak list of interest. If the answer is no, the quantification proceeds for the abundant and non-overlapping peaks through direct ratio-metric comparison to the ion peak intensity of the selected internal standard of the class in the survey MS scan after base-line correction and removal of  $^{13}\text{C}$  isotope effects.
7. If there are either overlapping or low-abundance peaks found in the peak list of interest, a two-step quantification is performed. The non-overlapping and abundant species, along with the exogenously added internal standards, are determined as the candidate standards for the second step of quantification. The corrected ion peak intensities of overlapping and/or low-abundance species from the class-specific PIS or NLS are used to quantify these species by ratiometric comparison with the ion-peak intensities of the candidate standards (*see Note 21*).

### 3.4 The Nuclear Lipidome

The above-described method can be used for a detailed spatial and temporal characterization of nuclear lipid composition, through biochemical isolation of nuclei from cultured cells or different mouse tissues. Moreover, this approach can be extended to other intracellular organelles that are readily biochemically isolated, such as the mitochondria. Hitherto, this approach enabled us to uncover daily oscillation in the lipid composition of the nucleus and mitochondria, regulated by feeding behavior and the circadian clock [3, 4]. Future advancements in lipidomic analyses are expected to increase the coverage of the nuclear lipidome, particularly for lipid species present in minute amounts. The biological functions of many of these nuclear lipids remain unknown, and studies using different mutant animal models and cultured cells are likely to shed light on the regulation on their nuclear accumulation as well as their biological implications.

---

## 4 Notes

1. For sucrose-containing buffers, melt sucrose on a slightly warm plate, prior to addition of other ingredients. Prepare buffers in advance, at least 1 day prior to fractionation and store in cold. This buffer can be stored in 4 °C for up to 1 month. Titer to pH with either KOH or NaOH.
2. Polycarbonate tubes exhibit more chemical resistance property than polypropylene tubes, and polycarbonate is important for reuse of tubes.
3. Else, could be performed on 10–50 mg of tissue, 10<sup>6</sup> cells, or 100 µL body fluid.
4. We purchase all of the lipid internal standards from Avanti Polar Lipids, Inc., Alabaster, AL, USA except if otherwise noted.
5. The stock solution of each single internal standard is prepared in chloroform/methanol mixture (1/1, v/v) or pure chloroform, with a concentration of approximately 1 mg/mL. The amount of each single lipid species in the pre-mixture is based on the abundance of the corresponding lipid class in the samples. The molecular species of internal standards are selected because they represent <0.1% of the endogenous cellular lipid mass levels as predetermined by ESI-MS lipid analysis.
6. Nuclei isolation can be done with a liver that has been frozen in –80 °C as long as it was not dissected into small pieces. In the case of liver analysis without fractionation, rapidly freeze the tissue in liquid nitrogen and keep frozen until lipidomics.
7. Special precaution should be taken during sample overlaying on the gradient. Materials must be cold to avoid turbulence. Transfer the sample in slope, gently on the wall of the tube. The two phases must not mix, this would destroy the separation. If mixture occurs, cease immediately and resume with the rest of the sample on top of a new Cushion. The mixed samples cannot be used.
8. Vacuum far from the pellet, tilt tube to distance the liquid from the pellet. The crude cytoplasmic fraction can be used for western blot. Collect with a pipette and store at –80 °C until further use.
9. Avoid scratching the tube for further use.
10. For maximal yield first resuspend in half the volume, transfer it, and thoroughly collect the remaining pellet with the rest.
11. Dislodge the cells with scrapper gently.
12. Cell pellet can be snap-frozen in case of whole cell lipidomic analysis.

13. Lysis buffer (hypotonic buffer) results in the swelling of the cell's cytoplasm that allow gentle rupture of cell membranes.
14. Keep the Douncer in ice while performing the strokes.
15. Mix small amount of lysate with Trypan blue dye and observe under microscope. The nuclei are stained dark, indicating uptake of the trypan blue dye (circled dark), while intact cells exclude the dye and remain bright.
16. In order to eliminate the contamination from the top layer (aqueous phase) to the bottom phase, insert the glass Pasteur pipet into the upper layer with slowly air bubbling until the pipet reaches the bottom layer. This technique helps avoid the upper layer liquid from entering the pipet. When taking the glass pipet out from the upper layer, touch the outside of the pipet on the edge of the glass tube, and promptly transfer the bottom layer to a new glass tube.
17. The total lipid concentration of a lipid extract can be estimated through the protein content or on the basis of the lipid analysis results from previous experiments, Han et al. [8]. This knowledge is useful for estimation of the concentrations of total lipids from different lipid extracts to prevent lipid aggregation during analysis through mass spectrometry. The lithium hydroxide is made of 80-time dilution of a saturated methanol solution.
18. Since sample ionization (ChipSoft) and spectral collection (Xcalibur) are operated with two separate software programs, the ionization polarity and time controlled by the ChipSoft should be matched to those of the mass spectrometer. The mass spectrometer is triggered to start collecting spectra with the start of the nanospray.
19. For the triple-quadrupole mass spectrometer, the first and third quadrupoles are used as independent mass analyzer with a mass resolution of 0.7 Th, and the second quadrupole serves as a collision cell for tandem mass spectrometry [9]. For the analysis of cardiolipin, a high-resolution mass spectrometer (at least  $\Delta m$  10,000 full width at half maximum, FWHM) is applied to detect and differentiate the doubly charged ions.
20. The isotope effects from other atoms (such as hydrogen, nitrogen, or phosphorus) are usually neglected due to extremely low abundance of its isotope or very small differences between the analyzed species and the selected internal standard.
21. The differences in the number of total carbon atoms and the number of total double bonds present in fatty acyl chains of each individual species from those of the selected standards can be considered as two important variables with multivariate least-square regression to determine the correction factors for each individual molecular species for the second-step

quantification. The linear dynamic range of quantification is extended dramatically by using this second step to quantify the overlapping and/or low-abundance species with one or more MS/MS scans through reduce background noise, increase S/N ratios of low-abundance species, and filter the overlapping molecules with class-specific PIS or NLS.

---

## Acknowledgments

We are grateful to all the members of the Asher lab for their comments on the manuscript. Graphical illustrations were generated with BioRender.com. G.A. is supported by the Abisch Frenkel Foundation for the Promotion of Life Sciences, Adelis Foundation, Susan and Michael Stern, Yotam project, and the Weizmann Institute Sustainability and Energy Research Initiative. The lipidomic study at Barshop Institute of UT Health San Antonio was partially supported by NIH grants AG 061729, P30 AG013319, and P30 AG044271.

## References

1. Horn A, Jaiswal JK (2019) Structural and signaling role of lipids in plasma membrane repair. *Curr Top Membr* 84:67–98
2. Bolshette N, Ibrahim H, Reinke H et al (2023) Asher G. Circadian regulation of liver function: from molecular mechanisms to disease pathophysiology. *Nat Rev Gastroenterol Hepatol* 20: 695–707
3. Aviram R, Manella G, Kopelman N et al (2016) Lipidomics analyses reveal temporal and spatial lipid organization and uncover daily oscillations in intracellular organelles. *Mol Cell* 62: 636–648
4. Aviram R, Wang C, Han X et al (2021) A lipidomics view of circadian biology. *Methods Mol Biol* 2130:157–168
5. Wang M, Han X (2014) Multidimensional mass spectrometry-based shotgun lipidomics. *Methods Mol Biol* 1198:203–220
6. Han X, Yang K, Gross RW (2012) Multidimensional mass spectrometry-based shotgun lipidomics and novel strategies for lipidomic analyses. *Mass Spectrom Rev* 31:134–178
7. Wang M, Wang C, Han RH et al (2016) Novel advances in shotgun lipidomics for biology and medicine. *Prog Lipid Res* 61:83–108
8. Han X (2016) *Lipidomics: comprehensive mass spectrometry of lipids*. Wiley-Blackwell
9. Han X, Yang K, Yang J et al (2006) Shotgun lipidomics of cardiolipin molecular species in lipid extracts of biological samples. *J Lipid Res* 47:864–879
10. Han X, Gross RW (2001) Quantitative analysis and molecular species fingerprinting of triacylglyceride molecular species directly from lipid extracts of biological samples by electrospray ionization tandem mass spectrometry. *Anal Biochem* 295:88–100



# Chapter 2

## Profiling Plant Nuclear Envelope Composition Using Subtractive Proteomics

Xiao Liu and Yu Tang

### Abstract

The nucleus represents a fundamental feature shared by eukaryotic cells and enclosed by a highly regulated membrane barrier, the nuclear envelope (NE). Despite numerous studies elucidating the functional significance and diversity of the NE in animals and yeast, comprehensive knowledge regarding its intricate composition and functions in plants remains limited. In this chapter, we describe subtractive proteomic approach to profile novel NE components with the model organism *Arabidopsis*, including detailed methods for isolation of nuclei using Percoll density gradients, extraction of nuclear membranes, isolation of endoplasmic reticulum enriched microsomal membranes, determination of the proteome, and validation of the enrichment at nuclear periphery. Additionally, this approach is applicable for identification of nuclear envelope protein components from diverse tissues or other plant species.

**Key words** Nuclear envelope, Endoplasmic reticulum, Plant nuclear envelope transmembrane proteins (PNETs), Subtractive proteomics, Mass spectrometry, Label-free quantification, YFP fusion

---

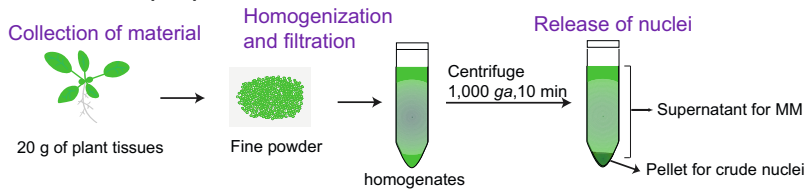
### 1 Introduction

The nuclear envelope (NE) is a conserved structure found in all eukaryotic cells, composed of two phospholipid bilayers—an outer and an inner membrane and is perforated by nuclear pore complexes (NPCs) [1]. Adjacent to the cytoplasm, the outer nuclear membrane (ONM) forms a close continuum with the endoplasmic reticulum (ER) and shares functional similarity with the peripheral ER [2, 3]. Nevertheless, some evidence suggests that ONM harbors distinctive resident proteins by physical association with cytoplasmic filaments and inner nuclear membrane (INM) spanning the NE [4]. Facing the nucleus, the INM houses prominent transmembrane proteins anchored by nuclear lamina (NL)—a peripheral and structural meshwork formed by intermediate filaments situated beneath the INM [5].

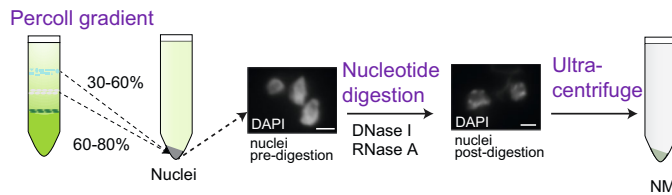
The NE plays crucial roles in a diverse range of fundamental cellular and nuclear processes [6–10]. Primarily, it acts as a physical barrier, separating transcription in the nucleus from translation in the cytoplasm. The NPC embedded within the NE is responsible for selective transport of macromolecules including proteins and RNA. This capability enables the NE to modulate gene expression and protein synthesis at the levels of mRNA processing and decay [11, 12]. Notably, the NE significantly influences genome architecture and gene expression by establishing connections with the underlying chromosome [6, 9]. Mutations of NE proteins in human cause more than 20 kinds of rare diseases, collectively termed “nuclear envelopathies,” such as Emery-Dreifuss muscular dystrophy (EDMD), Hutchinson-Gilford progeria syndrome (HGPS) [13, 14]. However, the comprehensive understanding of NE’s composition and functions in plants remains largely elusive. On one hand, many conserved NE components in animals and yeast lack homologs in plant genomes, resulting in limited sequence similarity that impedes genome-wide sequence alignment. On the other hand, the NE is physically linked to the ER and is connected with various organelles like mitochondria, chloroplasts, and the cytoskeleton facing the cytoplasm. Additionally, the INM and the nuclear lamina are intimately associated with the underlying chromatin and chromatin-regulatory proteins [6, 9]. These interconnections between the NE and its proximal organelles or protein complexes in the cell hinder the biochemical fractionation of a pure nuclear envelope. Furthermore, plant cells possess a robust cell wall crucial for maintaining structural integrity, making the aggressive disruption of the cell wall potentially damaging to organelle integrity, including the nucleus [15]. Moreover, nuclei from different tissues exhibit considerable divergence in nuclear size and shape [16, 17]. These challenges significantly complicate the extraction of intact nuclei and nuclear membrane from plant tissues. In recent years, many studies are employed multi-omic approaches utilizing isolated nuclei and nuclear proteins from various plant species such as rice, maize, tomato, and *Arabidopsis* [18–22]. However, they did not focus on the integrity and purity of the nuclei and nuclear membrane system. It is critical to explore effective biochemical methods to improve the purity of nuclei and nuclear membrane, which facilitate a deeper understanding of plant nuclear architecture and functions.

In this chapter, we present a comprehensive method employing subtractive proteomics to enrich the compositions of the nuclear envelope in plants (Fig. 1). Initially, we separate crude nuclei from whole seedlings along with the supernatant, which are used as a resource for the subsequent collection of nuclear membrane (NM) fraction and endoplasmic reticulum (ER)-enriched fraction. The resulting supernatant is utilized for the isolation of ER-enriched microsomal membranes (MMs). For nuclei isolation,

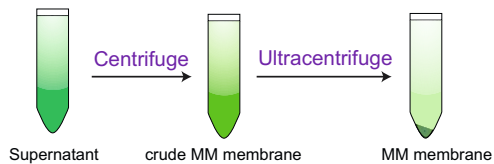
## A. Material preparation



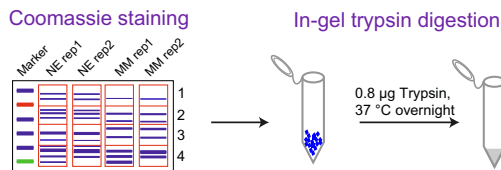
## B. Isolation of nuclei and NM



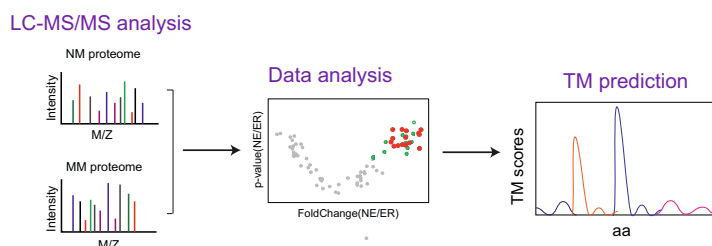
## C. Isolation of MM



## D. Protein separation and peptide preparation



## E. Identification of NE candidates



## F. Confirmation of PNET proteins

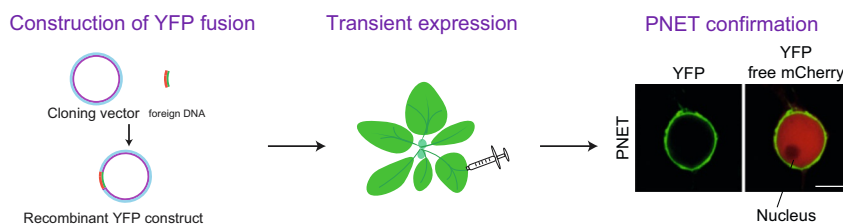


**Fig. 1** General workflow for subtractive proteomics illustrated using Arabidopsis as a plant model organism (modified from the previous publication [23]). (a) Material preparation including starting with the material collection, grinding the plant tissues into fine powder, and releasing the nuclei from the plant tissues.

we employ a rapid and efficient method involving Percoll gradient centrifugation, which aids in isolating nuclei. This process is followed by washing steps utilizing optimal detergents to eliminate any contaminated membranes surrounding the dense nuclei. Additionally, DNase and RNase are applied to digest interior nucleic acids, ensuring nucleic acid-free nuclei. These nuclei are then subjected to osmotic pressure and physical turbulence to disrupt the nuclear membrane, releasing chromatin-associated proteins. Both NM and MM fractions are separately acquired through ultracentrifugation. In addition to detailed information on the chemical fractionations of NM and MM, we provide insights into in-gel trypsin digestion and LC-MS/MS, utilizing label-free quantification to identify peptides. Furthermore, we highlight essential information about data analysis methods to enrich the identification of NE candidates. Finally, we offer a description of the validation for NE targeting using candidates with YFP fusion. Through the application of this subtractive proteomic method, we have successfully identified several uncharacterized plant nuclear envelope transmembrane proteins (PNETs) [23]. However, this method has inherent limitations. While the subtractive proteomics approach covers a significant portion of known plant nuclear envelope proteins, it may still contain contaminations from other organelles. Additionally, NE candidate proteins exhibiting low protein abundance and dual localizations at the nuclear membrane as well as other subcellular organelles might be missed using this proteomic approach. As an alternative, we have detailed another method known as proximity labeling proteomics, which has also proven effective in profiling plant NE candidates [23].

---

**Fig. 1** (continued) **(b)** Isolation of nuclei and NE. Percoll density gradient is used for isolating relatively intact and pure nuclei. The nuclear integrity is checked, and total number of nuclei is counted with DAPI staining. The nuclei are subject to nucleic acid digestion by DNase I and RNase A, and the NM is harvested by ultracentrifugation. **(c)** Isolation of MM. ER-enriched MMs are obtained by centrifugation twice from the same tissues for isolation of nuclei and NMs. **(d)** Protein separation and peptide preparation. Total NM and MM transmembrane proteins were extracted, separated by SDS-PAGE gel, and stained by Coomassie Blue. Each lane of gel is divided into four pieces for individual in-gel trypsin digestion. **(e)** Identification of NE candidates. Peptides are identified by label-free quantitative liquid chromatography tandem-mass spectrometry. Comparative data analysis and transmembrane domain prediction is applied to enrich and identify NE candidate proteins. **(f)** Confirmation of PNET proteins. The NE candidate genes are fused with YFP tag to generate recombined YFP constructs. *Agrobacterium*-mediated transformation is used to transient express the recombinant proteins. The PNET proteins are confirmed by imaging analysis with a confocal microscope

---

## 2 Materials

It is advisable to wear gloves and masks during material preparation to minimize excess keratin contamination. General equipment utilized in this chapter includes weighing scales, tissue towel, TissueLyser, water bath, vortex mixer, tube rotator, ultracentrifuge, microcentrifuge, DNase/RNase-free tubes (including 15 mL and 50 mL falcon tubes), and 1.5 mL microcentrifuge tubes. Commonly used reagents encompass liquid nitrogen, autoclaved Milli-Q (ultrapure) water, and protease inhibitor cocktail suitable for plant tissues (e.g., Sigma, P9599, 100× stock solution). All solutions in this method are prepared using ultrapure water, sterile filtered, and then stored at 4 °C unless otherwise specified. It's important to note that the fraction isolation buffer that contains spermine, spermidine, DTT, protease inhibitor cocktail, and PMSF must be fresh prepared before use.

### 2.1 Plant Material Preparation

1. *Arabidopsis thaliana* (Col-0) wild-type seeds (*see Note 1*).
2. 200 × 200 mm glass petri dishes.
3. ½ Murashige and Skoog basal medium (MS medium).
4. Phytigel (e.g., Sigma, Cat #A3301) (*see Note 2*).
5. Liquid nitrogen.
6. 50 mL falcon tubes.
7. Tweezer.
8. TissueLyser.

### 2.2 Crude Nuclei Extraction

1. 50 mL stainless metal tubes and 500 mm beads for tissue lysis (*see Note 3*).
2. Plastic Pasteur pipettes.
3. Nuclei isolation buffer (NIB1 5×): 100 mM KCl, 100 mM HEPES, pH 7.4, 69% (v/v) hexylene glycol, 0.5% (v/v) β-mercaptoethanol, 250 μM spermine, 625 μM spermidine, 5 mM phenylmethylsulfonyl fluoride (PMSF), protease inhibitor cocktail (1:20).
4. Nuclei isolation buffer 1 (NIB 1): 20 mM KCl, 20 mM HEPES, pH 7.4, 0.5% (v/v) Triton X-100, 13.8% (v/v) hexylene glycol, 0.1% (v/v) β-mercaptoethanol, 50 μM spermine, 125 μM spermidine, 1 mM phenylmethylsulfonyl fluoride (PMSF), protease inhibitor cocktail (1:100).
5. Tube rotator.
6. Miracloth (e.g., Millipore, Cat # 475855) (*see Note 4*).
7. Refrigerated centrifuge (*see Note 5*).

### **2.3 Microsomal Membrane Isolation**

1. Ultracentrifuge and the rotor (e.g., Beckman, L-80XP, Type 70 Ti).
2. The corresponding centrifuge tubes or bottles (e.g., 26.3 mL polycarbonate bottle with cap assembly, Cat#337922) (*see Note 6*).

### **2.4 Pure Nuclei Isolation**

1. Nuclei isolation buffer 2 (NIB 2): 20 mM KCl, 20 mM HEPES, pH 7.4, 13.8% (v/v) hexylene glycol, 0.1% (v/v)  $\beta$ -mercaptoethanol, 0.25% (v/v) Triton X-100, 50  $\mu$ M spermine, 125  $\mu$ M spermidine, 1 mM PMSF, protease inhibitor cocktail (1:100) (*see Note 7*).
2. Percoll gradient solutions:
  - (a) 80% (v/v) Percoll: mix eight parts of 100% Percoll with two parts of 5 $\times$  NIB 1.
  - (b) 60% (v/v) Percoll: six parts of Percoll with two parts of 5 $\times$  NIB 1 and two parts of pre-cooled water.
  - (c) 30% (v/v) Percoll: three parts of Percoll with two parts of 5 $\times$  NIB 1 and five parts of pre-cooled water.
3. Nuclei storage buffer: 50% (v/v) NIB 2 buffer: 50% (v/v) glycerol.
4. 5 mg/mL 4',6-diamidino-2-phenylindole (DAPI) solution.
5. Hemocytometer.
6. A typical fluorescence microscope.
7. 10% SHM buffer: 0.3 M sucrose, 10 mM HEPES-KOH (pH 7.4), 5 mM MgCl<sub>2</sub> solution with 2 mM DTT and protease inhibitor cocktail (1:100).
8. Refrigerated centrifuge.

### **2.5 Nuclear Membrane Isolation**

1. 10% SHM buffer.
2. DNase I dissolved at 80 U/ $\mu$ L in ultrapure H<sub>2</sub>O and stored it at  $-20^{\circ}\text{C}$  for 12 months.
3. RNase A dissolved in 20  $\mu$ g/ $\mu$ L in ultrapure H<sub>2</sub>O and stored it at  $-20^{\circ}\text{C}$  for 12 months.
4. Vortex mixer.
5. Ultracentrifuge and fixed angle rotor (e.g., Beckman, benchtop Optima Max-XP, TLA-100.3).
6. The corresponding centrifuge tubes (e.g. 13  $\times$  51 mm Thick-wall Polycarbonate Tubes for TLA-100.3, Cat# 349622).

### **2.6 Coomassie Staining**

1. 10% SDS-PAGE protein gel with 5 wells (e.g., Bio-Rad, Mini-PROTEAN<sup>®</sup> Comb, 5-well, 1.5 mm, Cat#1653363) (*see Note 8*).

2. Protein loading buffer (6×): 375 mM Tris-HCl (pH 6.8), 20% (w/v) SDS, 50% glycerol, 0.03% (w/v) Bromophenol Blue.
3. ThermoMixer.
4. Prestained Protein Ladder (e.g., Thermo Scientific, PageRuler, Cat# 26617).
5. Coomassie staining buffer: 1 g/L Coomassie Brilliant Blue G-250 in 50% methanol, 10% glacial acetic acid, 40% ultrapure H<sub>2</sub>O.
6. Destaining buffer: 50% methanol, 10% glacial acetic acid, 40% ultrapure H<sub>2</sub>O.

### **2.7 In-Gel Digestion with Trypsin and Peptide Preparation (See Note 9)**

1. Razor blades.
2. 1.5 mL low protein-binding tubes (e.g., Thermo Fisher, Cat#90410).
3. ThermoMixer.
4. 50 mM ammonium bicarbonate (NH<sub>4</sub>HCO<sub>3</sub>) in HPLC water.
5. Gel-destaining buffer: 50% (v/v) 25 mM NH<sub>4</sub>HCO<sub>3</sub> and 50% (v/v) acetonitrile (ACN).
6. 10% trifluoroacetic acid (TFA).
7. 5 mM dithiothreitol (DTT).
8. 11 mM iodoacetamide (IAA) (*see* **Note 10**).
9. Trypsin gold (e.g., Thermo Fisher Scientific, mass spectrometry grade, Cat# 90057). Prepare 1 mg/mL trypsin/Lys-C protease mix using 0.1% acetic acid. Aliquot them into PCR tubes and stored in −80 °C for future use.
10. Trypsin solution buffer: 20% (v/v) 200 mM NH<sub>4</sub>HCO<sub>3</sub>, 10% (v/v) CAN, and 70% HPLC water.
11. Peptide extraction buffer: 0.1% TFA in 50% ACN solution.
12. 0.1% formic acid (FA).
13. Integrated SpeedVac System (e.g., Eppendorf, SPD1010).

### **2.8 LC-MS Equipment and Software for Data Analysis**

1. Mobile phase A: 0.1% FA.
2. Mobile phase B: 100% ACN and 0.1% FA.
3. Thermo Orbitrap Fusion Lumos mass spectrometer (Thermo Fisher Scientific).
4. Proteome Discoverer software (Thermo Fisher Scientific) (<https://www.thermofisher.com/order/catalog/product/OPTON-30945>).

### **2.9 Data Analysis**

1. TAIR10 reference protein sequence database ([https://www.arabidopsis.org/download\\_files/Proteins/TAIR10\\_protein\\_lists/TAIR10\\_pep\\_20101214](https://www.arabidopsis.org/download_files/Proteins/TAIR10_protein_lists/TAIR10_pep_20101214)).

2. R software (<https://cran.r-project.org/mirrors.html>).
3. DESeq2 package (<https://bioconductor.org/packages/release/bioc/html/DESeq2.html>).
4. The GO enrichment analysis was performed using the AgriGO v2.0 (<http://systemsbiology.cau.edu.cn/agriGOv2/>).
5. Protein sequences were retrieved from TAIR (<https://www.arabidopsis.org/>).
6. The prediction of the transmembrane domain was performed using the SMART database (<http://smart.embl-heidelberg.de/>).

### **2.10 Confirmation of NE Localization**

1. Modified binary plant expression vector (pCAMBIA1300) with YFP tag.
2. High-fidelity DNA polymerase.
3. In-fusion cloning kit.
4. DH5 $\alpha$  competent cells.
5. LB medium.
6. LB agar supplemented with antibiotics of 25  $\mu$ g/mL Rifampicin, 50  $\mu$ g/mL kanamycin, and 50  $\mu$ g/mL gentamicin.
7. GV3101 *Agrobacterium* electrocompetent competent cells.
8. Electroporator.
9. 1 mm Cuvette.
10. Four-week-old *Nicotiana benthamiana*.
11. Spectrophotometry.
12. Needleless syringe.
13. Glass slide and cover glass.
14. Confocal microscope.

---

## **3 Methods**

For fractionation steps from Subheadings 3.2, 3.3, 3.4 and 3.5, all reagents and materials would be kept on ice throughout the process. The centrifuge, ultracentrifuge, and their rotors would be cooled to 4 °C before use. Wear gloves and masks and perform Subheadings 3.1, 3.2, 3.3, 3.4, 3.5, 3.6, 3.7 and 3.8. in a relatively clean environment.

### **3.1 Preparation of the Plant Materials**

1. Sow wild-type seeds on ½ MS medium and horizontally, grow them for 2 weeks in growth chamber.
2. Collect the whole seedlings and gently absorb the water from seedlings using paper towel.

3. Measure the weight of seedlings to 20 g and freeze immediately in 50 mL falcon tubes using liquid nitrogen. The frozen samples can be kept and stored in  $-80^{\circ}\text{C}$  for 1 month (*see Note 11*).
4. Grind the harvested seedlings into white-green powder in liquid nitrogen using TissueLyser with the setting: 40 Hz for 22 s twice (*see Note 12*).
5. Transfer the seedling powder with liquid nitrogen using a liquid nitrogen-cooled metal lab spatula into pre-cooled 50 mL falcon tubes (*see Note 13*).

### **3.2 Crude Nuclei Isolation**

1. Add 20–25 mL of ice-cold NIB 1 buffer to the powder, and stir them using a glass rod until all aggregates are disassembled and become homogenous.
2. Incubate the homogenous mixture in tube-rotator for 20 min at  $4^{\circ}\text{C}$  (*see Note 14*).
3. Filter the homogenate through double layers of Miracloth twice.
4. Centrifuge the filtrate for 15 min at  $4^{\circ}\text{C}$ , at 1000 *g* in a swing-out rotor. The supernatant and the pellet were used to prepare for MM (Subheading 3.3) and nuclei fraction (Subheading 3.4), respectively (*see Note 15*).

### **3.3 Microsomal Membrane (MM) Isolation**

1. The supernatant (**step 4** in Subheading 3.2) was centrifuged at 8000 *g* for 20 min at  $4^{\circ}\text{C}$ .
2. Carefully aspirate the supernatants to ultracentrifuge tubes using plastic Pasteur pipettes.
3. The new supernatant is subject to ultracentrifugation at 150,000 *g* for 60 min at  $4^{\circ}\text{C}$ , and the resulting pellet was collected as the endoplasmic reticulum enriched microsomal membrane (MM) fraction.

### **3.4 Pure Nuclei Isolation**

1. Resuspend the dark-green nuclei pellet (**step 4** in Subheading 3.2) in 3 mL of 80% (v/v) Percoll gradient solution, and transfer the sample to the bottom of the 15 mL centrifuge tube. On top of the sample, gently layer 3 mL of Percoll gradient solutions from bottom up: 60%, 30%, 0% (NIB 1) (*see Note 16*).
2. Carefully centrifuge the gradient samples in a swing-out rotor at 1000 *g* for 2 h at  $4^{\circ}\text{C}$  (*see Note 17*).
3. Discard the top layer of extraction buffer using pipette carefully. Use a plastic Pasteur pipette to collect nuclei from the 30–60% to 60–80% interfaces. Transfer nuclei to a clean, cold 15 mL Falcon tubes (*see Note 18*).

4. Add 10 mL NIB 2 buffer to the above nuclei fraction and mix it thoroughly using plastic Pasteur pipette.
5. Centrifuge at 1000 *g* for 10 min at 4 °C in a swing-out rotor to pellet the nuclei. Repeat the Subheading 3.4, **steps 4** and **5** (*see Note 19*).
6. The purified nuclei were resuspended with 20 mL of 10% SHM buffer (0.3 M sucrose, 10 mM HEPES-KOH (pH 7.4), 5 mM MgCl<sub>2</sub> solution) with 2 mM DTT and protease inhibitor cocktail (1:100) (*see Note 20* and **21**).
7. Transfer 50 µL into a clean 1.5 mL microcentrifuge tube (*see Note 22*).
8. Mix 10 µL of nuclei on the slide and 10 µL of 5 µg/mL DAPI solution (1000 dilutions using original solution), and transfer them to hemocytometer.
9. Count the number of total nuclei by using fluorescence microscopy (*see Note 23*).

### **3.5 Nuclear Membrane Isolation**

1. The nuclei in 10% SHM buffer (following **step 6** in Subheading 3.4) are added with 30 µL of 80 U/µL DNase I and 10 µL of 20 µg/µL RNase A (*see Note 24*).
2. Incubate the nuclei at room temperature for 60 min.
3. Transfer 5 µL of the mixture and mix with DAPI solution to check the signaling under fluorescence microscopy (*see Note 25*).
4. Vortex the nuclear buffer to disrupt the nuclei for 2 min.
5. Ultracentrifuge the digesting samples at 104,000 *g* for 60 min at 4 °C to collect the NE fraction.

### **3.6 Coomassie Staining**

1. Both NE and MM fractions were added to 150 µL of protein loading buffer with final 10% SDS to resuspend transmembrane proteins (*see Note 26*).
2. Boil them in a ThermoMixer for 10 min at 99 °C.
3. Prepare 1.5 mm 10% SDS-PAGE gel with 5 wells, and set up the protein electrophoresis apparatus.
4. Load all protein samples of NEs and MMs (*see Note 27*).
5. Separating the proteins by running at 80–100 Volts through the stacking gel and at 150 Volts through the separating gel.
6. Submerge the gel in 50 mL of Coomassie Blue staining solution.
7. Shake slowly on a laboratory shaker for 30–50 min.
8. Discard staining buffer and rinse briefly with Milli-Q water to remove most of the residual staining buffer.

9. Destain the gel using destaining solution, and replace it every 10–20 min until clear bands are observed and the background of gel becomes clean.

### **3.7 In-Gel Digestion with Trypsin**

1. Each gel lane can be excised into four small pieces, which are about 1 mm<sup>3</sup>. And transfer each piece into 1.5 mL low protein-binding tube (note: important for four pieces but not one) (*see Note 28*).
2. Destain the protein gel: add 400 µL of 25 mM NH<sub>4</sub>HCO<sub>3</sub>/50% ACN to merge the gel piece.
3. Incubate them on the ThermoMixer with a shaking speed of 800 rpm for 1–2 h at 37 °C to destain the gel (*see Note 29*).
4. The destained gel is added with 400 µL of pure ACN buffer (*see Note 30*).
5. Centrifuge shortly and remove the ACN buffer by pipetting.
6. Repeat **steps 4–5** in Subheading 3.7 once.
7. Reduce the protein gel: add 200 µL of 5 mM DTT buffer for 30 min at 45 °C (*see Note 31*).
8. Repeat **steps 4–5** in Subheading 3.7 twice.
9. Terminate the reduction reaction: add 200 µL of 11 mM IAA buffer in the dark for 20 min at room temperature.
10. Repeat **steps 4–5** in Subheading 3.7 twice.
11. Add 100 µL of 6.25 µg/mL trypsin solution to each sample (*see Note 32*).
12. Incubate the sample on the ThermoMixer with a shaking speed of 800 rpm at 37 °C overnight (at least 12 h).
13. Add 5 µL of 10% TFA buffer to each sample.
14. Transfer all digestion buffer into new low protein-binding tube.
15. Add 200 µL of 0.1% TFA in 50% acetonitrile solution into gel pieces.
16. Incubate the sample on the ThermoMixer with a shaking speed of 800 rpm for 1 h at 37 °C.
17. Transfer the solution into the tubes in **step 16** in Subheading 3.7.
18. Repeat **steps 17–18** in Subheading 3.7 once (*see Note 33*).
19. Evaporate the supernatant in a SpeedVac at room temperature for 3–4 h.
20. Add 20 µL of 0.1% TFA into each sample and centrifuge briefly (*see Note 34*).

### 3.8 Mass Spectrometry

For LC-MS/MS analysis, samples were processed using a Thermo-Dionex Ultimate 3000 HPLC system, which was directly interfaced with a Thermo Orbitrap Eclipse mass spectrometer (*see Note 35*).

1. Load the sample on a microcapillary column (e.g., 75  $\mu\text{m}$  ID, 150 mm length; Thermo Fisher Scientific).
2. Set up a constant flow rate of 0.300  $\mu\text{L}/\text{min}$  by a 120 min gradient mobile phase elution (beginning with pure mobile phase A (0% B) and ending with pure mobile phase B (0% A)) throughout the chromatography.
3. Collect full-scan MS spectra using the LTQ-Orbitrap mass spectrometer with a resolution of 120,000 at 300–1500  $m/z$  using Xcalibur 4.1 software followed by data-dependent MS/MS scans (3 s duration) in an Orbitrap (resolution: 15 k FWHM at  $m/z$  400) at 30% collision energy.
4. Search MS/MS spectra from each LC-MS/MS run using the TAIR10 database on Proteome Discoverer software (*see Note 36*).
5. Set the search criteria as follows:
  - (a) Full tryptic or no enzyme specificity is required.
  - (b) Two missed cleavages are permitted.
  - (c) Carbamidomethylation of cystine residues is set as static modification.
  - (d) Precursor ion mass tolerance is 20 ppm.
  - (e) Fragment ion mass tolerance is 0.02 Da.
  - (f) High confidence score filter ( $\text{FDR} < 1\%$ ) is used to select the “hit” peptides.

### 3.9 Data Analysis

For data analysis, we applied DEseq2 package in R software and performed data analysis to enrich candidates using MM fractions as control (*see Note 37*).

1. Download and install R and DEseq2 package.
2. Using known nuclear envelope proteins as control, we set up a cutoff which may cover most of the known NE proteins.
3. Gene IDs of all candidate proteins including these known NE proteins are input into AgriGO database for GO-Cellular Component (CC) enrichment.
4. Candidate protein sequences are downloaded from TAIR database and input into SMART protein database to predict the transmembrane domains. If TM(s) are predicted in the protein sequences, we label them as NE candidates.

### 3.10 Conformation of NE Localization by YFP Fusion Protein Expression

Use standard molecular cloning technique to construct the YFP fusions. We employed in-fusion cloning technology to construct NE candidates fused to YFP driven by the 35S constitutive promoter (*see Note 38*). The vector backbone is pCambia1300, which is modified by inserting a YFP tag after 35S promoter.

1. Design primers that contain homologous extensions.
2. PCR to amplify the cDNA or genomic DNA fragment using a high-fidelity DNA polymerase and designed primers.
3. Digest the plasmid modified pCambia1300-YFP using restriction enzymes to generate linearized vector.
4. Purify the linearized vector and PCR products from agarose gel.
5. Perform in-fusion cloning reaction by combining the linearized vector and DNA fragment.
6. Transform the in-fusion reaction mixture into DH5 $\alpha$  competent cells, and choose positive colonies by colony PCR.
7. Extract plasmid and then subject to DNA sequencing for validation.
8. Add 0.5  $\mu$ g of the plasmids that contain YFP fusions or free mCherry to *Agrobacterium tumefaciens* strain GV3101 competent cells (*see Note 39*).
9. Incubate the mixture on ice for 10 min.
10. Set up the electroporation according to the manufacturer's handbooks and perform the electroporation for mixture.
11. Add 1 mL of LB medium to the cuvette and transfer the mixture to microcentrifuge tubes.
12. Incubate the culture in a 28 °C shaker incubator for 60–90 min.
13. Plate 50–100  $\mu$ L culture on LB agar supplemented with antibiotics for positive colony selection.
14. Make overnight *Agrobacterium* culture harboring expression vectors.
15. Centrifuge the *Agrobacterium* culture at 5000 *g* for 5 min.
16. Discard the supernatant and resuspend the *Agrobacterium* using ultrapure water.
17. Measure their concentration and dilute them with water at the OD600 of 0.8–1.0.
18. Make *Agrobacterium* suspension mixtures that express NE candidate with YFP fusions and mCherry fusion in equal ratios.
19. The suspension mixtures were thoroughly mixed and gently infiltrated using a needleless syringe into 4-week-old *N. benthamiana* leaves.

20. Collect the leaves for microscopic imaging 40 h after infiltration (*see* **Note 40**).
21. YFP and mCherry fluorescence were observed using a typical confocal microscope.
22. Select and confirm the PNETs with the enrichment at nuclear envelope (*see* **Note 41**).

---

## 4 Notes

1. For mass spectrometry analysis, *Arabidopsis* seedlings, which possess a higher nucleus amount than other tissues, are utilized. Typically, about 50  $\mu\text{L}$  of *Arabidopsis* wild-type seeds are used for one replicate, and it's recommended to collect two or three biological replicate materials. The method is adaptable to other tissues of *Arabidopsis* or other higher plants, though larger amounts may be required.
2. Phytigel is recommended for preparing 1/2 MS medium. To ensure the inclusion of root tissue in whole seedlings, a concentration of 4.0 g/L of phytigel is suggested, which is slightly less than the usual concentration (5–6 g/L). Larger petri dishes (e.g., 200 mm  $\times$  200 mm  $\times$  20 mm) are typically used for healthy seedling growth.
3. Various blender-type homogenizers suitable for homogenization can be utilized. If a homogenizer isn't available, manual grinding with a fully chilled mortar and pestle in liquid nitrogen can serve as an alternative method. Caution should be taken during grinding to maintain the integrity of cells and nuclei.
4. The shapes and sizes of nuclei in different plant tissues differ significantly. For instance, in *Arabidopsis thaliana* seedlings, nuclei in epidermal cells are elongated spindle-shaped, whereas those of meristems and guard cells are nearly spherical. Using a specialized Miracloth for filtration (with a pore size of 22–25  $\mu\text{m}$  and irregular pore shape) is advised to allow most nuclei to pass through while retaining debris.
5. Prior to procedures, ensure the centrifuge and rotor are adequately pre-cooled to the desired temperature.
6. Always use the centrifuge tubes that are in good condition without any cracks or damage.
7. Triton X-100 is commonly employed to lyse cells for organelle extraction. However, high concentrations of Triton X-100 can lead to the permeabilization and breakdown of organelle membranes. Optimal concentrations for isolating intact Nuclei (NIB 1 buffer) and washing nuclei (NIB 2 buffer) are found to be 0.5% and 0.25% Triton X-100, respectively.

8. We prefer protein gel a thickness of 1.5 mm and 5 wells, allowing for the loading of approximately 200  $\mu$ L of protein sample.
9. The resulting peptides are subject to mass spectrometry following in-gel digestion. HPLC water must be used for the preparation of in-gel digestion solutions.
10. IAA, an alkylating reagent, is commonly used to halt the reduction-oxidation reaction. It's recommended to freshly prepare IAA before use and store it in the dark due to its instability.
11. Collecting 20 g of material for one replicate can be time-consuming. Collecting 4 g of material at a time helps to maintain freshness.
12. Different TissueLyers may require different parameter settings, so optimizing grinding speed and time before large-scale sample processing is essential. Effective tissue disruption and intact nuclei during grinding should be ensured, possibly by staining with DAPI.
13. It is not recommended to store the fine powder at  $-80^{\circ}\text{C}$ , and we advise to perform the subsequent steps immediately.
14. The purpose of this step is to release nuclei from the lysed cells. It is optimal to incubate the nuclei for 20 min as prolonged incubation times may disrupt the nuclei.
15. For isolation of nuclei using Percoll gradients, it is important to use a swinging-bucket rotor to maintain gradient integrity.
16. It is important to balance each tube with the corresponding cap one by one on a digital scale before ultracentrifugation. The weight of the tubes should be equilibrated by adding cold NIB1 buffer until they reach the same weight, with an error margin of 0.01 g.
17. Use one 1 mL sterile pipette tip for sample drainage, ensuring the homogenate passes through four layers of Miracloth. Gently squeeze the Miracloth with a 1 mL pipette tip when the remaining homogenate is not able to pass through. Perform filtration twice to remove most debris from the homogenate.
18. Carefully layer Percoll gradient samples using a 1 mL pipette by adding the Percoll gradient through the tube wall.
19. Set lower accelerating and decelerating speeds during centrifugation to prevent nuclei disruption and achieve migration through Percoll layers (e.g., for Eppendorf 5810R, both accelerating and decelerating speeds are 5).
20. Remove the sharp tip of the 1 mL pipette before aspirating the nuclei layer, as nuclei tend to clump together.

21. If nuclei appear green or dark yellow (indicating chloroplast contamination), wash nuclei with NIB 2 buffer two or three times to reduce contamination.
22. Reserving 50  $\mu$ L of nuclei have two purposes. One is used for counting the number of nuclei with hemocytometer, and another is as a control for the following **step 3** in Subheading 3.5.
23. The total number of nuclei for one replicate should be anticipated around  $10^9$ , which meets the quantity for proteomic analysis. If the nuclear production is lower, consider restarting the sample preparation. Nuclei can be stored in 500  $\mu$ L of nuclei storage buffer and kept in  $-80^\circ\text{C}$  for up to 1 week.
24. As the DNA and RNA of the nuclei is digested at room temperature, which might cause protein degradation at the same time. We choose higher amounts of DNase I and RNase A to minimize the protein degradation.
25. The nuclei are subject to DAPI staining to make sure most DNA disappears from the nuclei after digestion. If the digestion is not enough, incubate the nuclei with DNase I and RNase A for another 20 min at room temperature.
26. The fractions of NE and MM host many membrane lipids, and we prepare the final protein loading buffer that contains a high concentration of 10% SDS to disrupt the whole membrane system as much as possible. However, the high concentration of SDS would cause lots of bubbles when pipetting up and down to dissolve the membrane proteins. Shortly spin down the sample to devoid the bubbles when bubbles are present.
27. To prevent contamination between NE and MM fractions, it is recommended to load them on the gel intervally.
28. It is important to excise each lane into four pieces, and each piece of the gel is further cut into smaller pieces about  $1\text{ mm}^3$ , which facilitates high efficiency of in-gel trypsin digestion and high resolution of mass data.
29. You may adjust the volume of gel-destaining buffer in order to cover the total pieces of the gel.
30. Each reaction during in-gel digestion is followed by two washing steps using pure ACN buffer to eliminate the remaining reagents. Note that the protein gels are shrunk in ACN buffer, which is a normal phenomenon.
31. It is critical to do the step of reduction and alkylation of cysteine residues for high efficiency of in-gel trypsin digestion. However, the reduction is not stable and will not be maintained for a long time. Continue the following step when the reduction reaction is done.

32. The gel pieces become swollen with the addition of the trypsin buffer. If there is no buffer left after 1–2 h of digestion, it is important to add more trypsin buffer to merge the total gel pieces.
33. In order to extract as much peptide from the gel, peptide extraction twice is advisable. Totally, about 500  $\mu\text{L}$  of the supernatant containing peptide of each piece are collected.
34. The peptide powder is more stable than the peptide solution, and we recommend adding 0.1% TFA just before loading the sample to mass spectrometry.
35. Other available HPLC combined mass spectrometers work well for the identification of peptides.
36. Peptide-spectrum matches (PSM) scores for each protein identified are provided from proteome Discoverer software. We employ DESeq2 package to enrich the NE candidate proteins. Access code from the provided method website (Subheading 2.10, item 3).
37. Other convenient online services that predict the putative transmembrane domains can also be used for searching the NE candidates.
38. Prior to construction of YFP fusion, it is necessary to analyze the protein structural topology to determine which direction of YFP tag is fused to. Typically, we fuse the YFP tag to distal direction of the transmembrane domain enriched.
39. The empty vector of 35S: mCherry is transformed into *Agrobacterium* and will be co-infiltrated with NE candidates into leaves as a marker to indicate the nuclear and cytoplasm (Subheading 3.10, step 17).
40. We usually observe the YFP signal 40 h after infiltration, which is enough for expression of most candidate proteins. We have found some proteins have ER or other unanticipated abnormal localizations over time, and we advise to do imaging analysis within 48 h.
41. Due to NE and ER continuity, prefer cells with lower expression to avoid ectopic ER localization resulting from protein overexpression driven by the 35S promoter.

---

## Acknowledgments

This work is supported by the Young Taishan Scholars Program of Shandong Province and startup funds from the Peking University Institute of Advanced Agricultural Sciences (to Y.T.). We apologize to researchers whose work could not be cited due to space constraints.

## References

1. De Magistris P, Antonin W (2018) The dynamic nature of the nuclear envelope. *Curr Biol* 28:487–497
2. Agrawal A, Lele TP (2019) Mechanics of nuclear membranes. *J Cell Sci* 132:jcs.229245
3. Schirmer EC, Gerace L (2005) The nuclear membrane proteome: extending the envelope. *Trends Biochem Sci* 30:551–558
4. Bouzid T, Kim E, Riehl BD et al (2019) The LINC complex, mechanotransduction, and mesenchymal stem cell function and fate. *J Biol Eng* 13:68
5. Katta SS, Smoyer CJ, Jaspersen SL (2014) Destination: inner nuclear membrane. *Trends Cell Biol* 24:221–229
6. Pawar S, Kutay U (2021) The diverse cellular functions of inner nuclear membrane proteins. *Cold Spring Harb Perspect Biol* 13:a040477
7. D’Angelo MA, Hetzer MW (2006) The role of the nuclear envelope in cellular organization. *Cell Mol Life Sci* 63:316–332
8. Selezneva A, Gibb AJ, Willis D (2022) The nuclear envelope as a regulator of immune cell function. *Front Immunol* 13:840069
9. Tang Y (2023) Plant nuclear envelope as a hub connecting genome organization with regulation of gene expression. *Nucleus* 14:2178201
10. Fernández-Jiménez N, Pradillo M (2020) The role of the nuclear envelope in the regulation of chromatin dynamics during cell division. *J Exp Bot* 71:5148–5159
11. Wentz SR, Rout MP (2010) The nuclear pore complex and nuclear transport. *Cold Spring Harb Perspect Biol* 2:a000562
12. Dultz E, Ellenberg J (2007) Nuclear envelope. *Curr Biol* 17:154–156
13. Janin A, Bauer D, Ratti F et al (2017) Nuclear envelopopathies: a complex LINC between nuclear envelope and pathology. *Orphanet J Rare Dis* 12:147
14. Braun DA, Lovric S, Schapiro D et al (2018) Mutations in multiple components of the nuclear pore complex cause nephrotic syndrome. *J Clin Invest* 128:4313–4328
15. Anderson CT, Kieber JJ (2020) Dynamic construction, perception, and remodeling of plant cell walls. *Annu Rev Plant Biol* 71:39–69
16. Cantwell H, Dey G (2022) Nuclear size and shape control. *Semin Cell Dev Biol* 130:90–97
17. Meier I, Griffis AH, Groves NR et al (2016) Regulation of nuclear shape and size in plants. *Curr Opin Cell Biol* 40:114–123
18. Sikorskaite S, Rajamäki M-L, Baniulis D et al (2013) Protocol: optimised methodology for isolation of nuclei from leaves of species in the solanaceae and Rosaceae families. *Plant Methods* 9:31
19. Jones AME, MacLean D, Studholme DJ (2009) Phosphoproteomic analysis of nuclei-enriched fractions from *Arabidopsis thaliana*. *J Proteome* 72:439–451
20. Bae MS, Cho EJ, Choi EY et al (2003) Analysis of the *Arabidopsis* nuclear proteome and its response to cold stress. *Plant J* 36:652–663
21. Khan MM, Komatsu S (2004) Rice proteomics: recent developments and analysis of nuclear proteins. *Phytochemistry* 65:1671–1681
22. Lu Y, Wei L, Wang T (2015) Methods to isolate a large amount of generative cells, sperm cells and vegetative nuclei from tomato pollen for “omics” analysis. *Front Plant Sci* 6:391
23. Tang Y, Huang A, Gu Y (2020) Global profiling of plant nuclear membrane proteome in *Arabidopsis*. *Nat Plants* 6:838–847



# Chapter 3

## Ultrastructural Visualization of the Nuclear Envelope in HeLa Cells

Sourabh Sengupta, Zhaojie Zhang, and Daniel L. Levy

### Abstract

Transmission electron microscopy (TEM) is a powerful tool that has been used for the visualization of biological materials since the 1940s. This technique permits the detailed observation of cellular organelles and other intracellular structures as well as infectious agents, like viruses. Important insights about the structure and function of the cell nucleus have been gleaned using TEM. Here we present a method for visualization of the nuclear envelope in cultured HeLa cells using TEM. The method covers cell culturing, fixation, embedding, sectioning, staining, and visualization. This approach is particularly useful to understand how the ultrastructure of the nuclear envelope is affected by cell culture conditions, genetic manipulations, and stress treatments.

**Key words** Nucleus, Nuclear envelope, HeLa cells, Transmission electron microscopy

---

### 1 Introduction

Among the many organelles present inside the cell, the nucleus serves many important functions. First observed and then named in the early 1800's [1], the nucleus is bound by a double-membraned nuclear envelope which is continuous with the endoplasmic reticulum in many cells. This envelope contains pores, which are formed by a set of proteins called nucleoporins that constitute the nuclear pore complex (NPC) [2–4]. Selective transport of proteins and RNAs takes place through these NPCs [5, 6]. Alterations in nuclear size and shape are associated with cell differentiation, developmental progression, and certain diseases, notably cancer in which nuclear morphology is frequently altered [7, 8]. Variations in nuclear structure are also seen across species [9], aging [10], and diseases like laminopathies [11]. Studying the mechanisms that regulate nuclear structure is an area of active research.

The first published report of a biological sample imaged by transmission electron microscopy (TEM) was of a cultured fibroblast originating from a chick embryo [12], the first time that cellular organelles were revealed at such a high level of resolution. Since then, electron microscopy techniques have been developed to visualize viruses [13], Golgi bodies [14], mitochondria [15], muscle tissue [16], and many other cellular and subcellular structures [17]. In this protocol we describe the technique to visualize the ultrastructure of the nuclear envelope in cultured HeLa cells. This technique can be applied to other cell types besides HeLa cells and is useful to visualize how different culture conditions, genetic manipulations, and stress treatments affect nuclear envelope structure.

---

## 2 Materials

Prepare all solutions in ultrapure water unless indicated otherwise. Cell culture solutions, Sato's lead, and glutaraldehyde should be stored at 4 °C, while all other solutions can be stored at room temperature. Be sure to follow all waste disposal regulations as per local and/or institutional guidelines.

### 2.1 Cell Culture

1. HeLa cells (ATCC, CRM-CCL-2).
2. Eagle's Minimum Essential Medium (EMEM) (ATCC, 30-2003), Earle's Balanced Salt Solution, non-essential amino acids, 2 mM L-glutamine, 1 mM sodium pyruvate, and 1500 mg/L sodium bicarbonate.
3. Fetal bovine serum (FBS) (ATCC, 30-2020).
4. Penicillin-streptomycin (Pen/Strep) (Gibco, 15140148), 10,000 U/mL.
5. CO<sub>2</sub> incubator.
6. Inverted microscope.
7. Tissue culture-treated cell culture flasks (T-25 or T-75) (VWR, 10062-872, 10060-860).

### 2.2 Fixation and Embedding

1. Cell scrappers.
2. Phosphate buffered saline (PBS) (pH 7.4), sodium chloride 137 mM, potassium chloride 2.7 mM, sodium phosphate dibasic 10 mM, potassium phosphate monobasic 1.8 mM, pH adjusted to 7.4 with hydrochloric acid.
3. Glutaraldehyde (EM grade).
4. Osmium tetroxide (OsO<sub>4</sub>).
5. Uranyl acetate.

6. Ultrapure water.
7. Ethanol.
8. Propylene oxide.
9. SPURR, Low Viscosity Embedding Kit (Electron Microscopy Sciences 14300).
10. BEEM<sup>®</sup> capsules size 00 (Electron Microscopy Sciences, 69910-01).
11. 65 °C oven.
12. Tube rotator (VWR, 76595-828).

### **2.3 Trimming the Resin Block Containing the Cells**

1. Fine sharp razor blade.
2. Ultramicrotome for TEM sectioning.
3. Glass knife.
4. Brightfield microscope.

### **2.4 Making Ultrathin Sections for Visualization**

1. Diamond knife.
2. Formvar/Carbon 200 Mesh copper grids (Electron Microscopy Sciences, FCF200-Cu-50).
3. Filter paper.

### **2.5 Staining with Lead to Increase Contrast**

1. Grid Staining Pad (Electron Microscopy Sciences, 71187).
2. Petri dish.
3. Sato's lead solution [18], lead citrate 0.4% (w/v), lead nitrate 0.3% (w/v), lead acetate 0.3% (w/v), sodium citrate 2% (w/v), 1 N sodium hydroxide solution 18% (v/v).
4. Potassium hydroxide.

### **2.6 Mounting Samples and Visualization**

1. Transmission electron microscope (Hitachi H-7650).
2. Perfect Handle & Loop Set (Electron Microscopy Sciences, 70944).

---

## **3 Methods**

### **3.1 Cell Culture**

1. Media for cell culture is prepared with EMEM containing 10% FBS and 1X Pen/Strep (*see Note 1*). This medium can be stored for a few weeks at 4 °C.
2. Upon receiving the frozen vial of cells, thaw as per the ATCC handling instructions (*see Note 2*).
3. Grow cells in T25 or T75 tissue culture-treated cell culture flasks in a 37 °C incubator with 5% CO<sub>2</sub> maintained inside the incubator.

4. Allow cells to grow for 24–48 h, and check for confluency using an inverted microscope (*see Note 3*).
5. For ultrastructural observation, cells should be grown to a confluency of 75–80%.
6. Once the cells have reached the desired level of confluency, proceed to the next step of fixing and embedding the cells.

### **3.2 Fixation and Embedding**

1. Aspirate off the medium and wash cells twice with 1X PBS.
2. Primary fixation: Add 2 mL of freshly prepared 2.5% glutaraldehyde in 1X PBS to the T25 flask, gently spread it evenly over the surface, and incubate the flask at room temperature for 1.5 h (*see Note 4*).
3. Scrape the cells from the surface of the flask using a cell scraper. Be gentle during this step while also ensuring to scrape off as many cells as possible.
4. Collect the scrapped cells into 2 mL tubes, and centrifuge the tubes at 300 *g* for 5 min at room temperature to pellet the cells (*see Note 5*).
5. Discard the supernatant and wash cells twice by resuspending in 1X PBS and centrifuging as before.
6. Secondary fixation: After two washes with 1X PBS, pellet cells as before and resuspend them in 2% OsO<sub>4</sub> (freshly prepared in water). Incubate for 1.5 h at room temperature (*see Note 6*).
7. Pellet the cells by centrifuging at 300 *g* for 5 min and discard the supernatant.
8. Wash cells three times with deionized water by resuspending the cells in deionized water and pelleting them down each time.
9. En bloc staining: Resuspend the cell pellet in 2% uranyl acetate (water solution). Incubate the suspension for 1.5 h at room temperature. Uranyl acetate enhances the contrast of cells.
10. Wash cells two times with deionized water by resuspending the cells in deionized water and pelleting them down each time.
11. Dehydration (**Steps 11–14**): after pelleting the cells by centrifugation and removing the supernatant, resuspend the cell pellet in a 30% ethanol solution (made with ultrapure water). Incubate the suspension for 5 min at room temperature, and then pellet the cells by centrifuging at 300 *g* for 5 min.
12. Repeat the above step sequentially with 50%, 70%, and 90% ethanol (each prepared with ultrapure water).
13. After the 5-min incubation in 90% ethanol, pellet the cells by centrifuging at 300 *g* for 5 min at room temperature. Discard the supernatant, resuspend the cells in 100% ethanol, and incubate for 5 min. Pellet the cells by centrifuging at 300 *g* for 5 min.

14. Repeat the above 100% ethanol dehydration step three times to ensure complete dehydration (*see* **Note 7**).
15. Transition: Remove the supernatant and resuspend the cell pellet in 100% propylene oxide. Incubate the cell suspension for 15 min at room temperature (*see* **Note 8**).
16. Infiltration (**Steps 16–18**): Pellet the cells by centrifuging at 300 *g* for 5 min at room temperature. Resuspend the cell pellet in 1 mL of 2:1 propylene oxide/resin solution (2 parts propylene oxide to 1 part SPURR resin). Incubate the cells on a tube rotator at room temperature for 3 h (*see* **Note 9**).
17. Pellet the cells, discard the supernatant, and resuspend the cells in 1 mL of 1:2 propylene oxide/resin solution. Incubate the suspension overnight on a tube rotator at room temperature.
18. Pellet the cells, remove the supernatant, and resuspend the cells in 1 mL of 100% resin. Incubate this suspension on a tube rotator at room temperature for 2 h. Repeat this step with fresh 100% resin and incubate for 2 h.
19. Embedding: Pellet the cells. Discard 90–95% of the supernatant. Resuspend the cell pellet in the remaining resin and transfer this suspension into a BEEM<sup>®</sup> capsule, taking care that the cells remain concentrated at the bottom of the capsule. Fill the capsule completely with resin.
20. Place the capsule in a 65 °C oven overnight to polymerize the resin.

### **3.3 Trimming the Resin Block Containing the Cells**

1. Using a fine sharp razor blade, cut the sides of the BEEM<sup>®</sup> capsule. Carefully remove the resin block making sure not to scratch the surface of the resin. Visual inspection of the resin block will reveal darkly stained brownish-black regions that correspond to the stained cells. Regions of the block without cells will be yellowish-gold in color.
2. Mount the resin block onto the sample holder of the ultramicrotome. Trim the block to an irregular trapezoid shape, removing portions of the block without cells that are yellowish-gold in color.
3. Use a glass knife to slice off 2–3  $\mu\text{m}$  sections of the trimmed resin. Examine these sections using a brightfield microscope to identify sections that contain the most cells. Stained cells exhibit increased contrast and can be visualized easily under a brightfield microscope by their brownish-black color. Also carefully examine the sections to ensure good dehydration and infiltration as evidenced by an absence of holes in the resin.
4. Upon reaching a section with a sufficient number of cells, trim the block further while keeping the cell-containing region

intact. The final trimmed block should be trapezoidal in shape, with the base having a maximum length of 0.5 mm.

5. Use this trimmed block to slice ultrathin sections using a diamond knife.

### **3.4 Making Ultrathin Sections for Visualization**

1. Carefully place the diamond knife on the knife holder of the ultramicrotome. Make sure to set the knife to the correct angle (typically  $6^\circ$ ).
2. Align the diamond knife edge and the trimmed resin block so they are exactly parallel to each other. To accomplish this, use the objective lens of the ultramicrotome to focus on the knife edge. Then using the built-in lamp of the ultramicrotome, move the knife edge so that it is parallel to the base of the trimmed resin block. This step often requires multiple adjustments of the block in the x-y and/or z planes (*see Note 10*).
3. Fill the “boat” of the diamond knife with deionized water, ensuring the surface of the water is flat.
4. Manually set the cutting window of the ultramicrotome and set the parameters to slice thin sections 50 nm in thickness. To minimize mechanical vibrations and air flow while sectioning, use a divider to shield the sample and diamond knife from the external environment.
5. Discard the first few slices that float on the surface of the water of the boat. Collect slices that have a silvery appearance using the “perfect loop.”
6. Transfer the thin sections onto Formvar/Carbon-coated copper grids. Using a piece of filter paper, very carefully wick off all of the water that might be associated with the mesh and/or sections.

### **3.5 Staining with Lead to Increase Contrast**

1. Place the grids onto a grid staining pad, and place the pad in a Petri dish containing potassium hydroxide pellets, which help to eliminate carbon dioxide.
2. Keep the grids in a potassium hydroxide environment for 2–5 min so that the Petri dish environment is free from carbon dioxide.
3. Add a few drops of Sato’s lead solution onto each grid and incubate for 20–30 min to increase the contrast of cellular structures.
4. Quickly remove the lead solution by dipping the staining pad in deionized water multiple times.
5. Allow the samples to air dry.

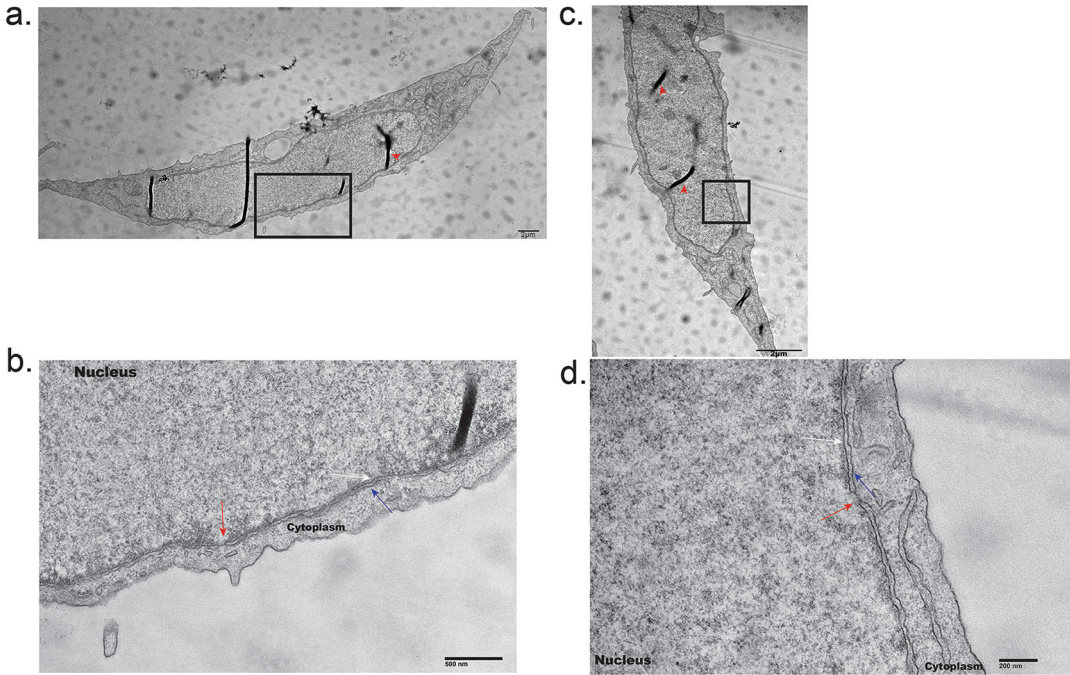


**Fig. 1** TEM images of cultured HeLa cells and nuclei. **(a)** Low magnification micrograph of an entire cell. Thick black lines (red arrow heads) are thin section folds commonly seen in cell-containing regions. The scale bar is 2  $\mu\text{m}$ . **(b)** High magnification micrograph of the inset region denoted in **(a)**. The red arrow indicates a nuclear pore complex (NPC). The blue and white arrows denote the outer and inner nuclear membranes, respectively. The scale bar is 500 nm. **(c)** Low magnification micrograph of an entire cell. Thick black lines (red arrow heads) are thin section folds commonly seen in cell-containing regions. The scale bar is 2  $\mu\text{m}$ . **(d)** High magnification micrograph of the inset region denoted in **(c)**. The red arrow indicates an NPC. The blue and white arrows denote the outer and inner nuclear membranes, respectively. The scale bar is 200 nm

### 3.6 Mounting Samples and Visualization

1. Once the grid is dry, place it on the specimen holder of the TEM.
2. Place the specimen holder in the vacuum chamber and set up the instrument.
3. A high voltage around 80 kV is normally used for observing biological samples, as this voltage provides a good balance between contrast and resolution.
4. Locate the cells using the visualization window. Scan across the entire x-y plane to obtain a comprehensive image of the nuclear envelope. See Fig. 1 for example images. The nucleus can be distinguished from the cytoplasm because of its darker contrast around which is visible the distinct double membrane structure of the nuclear envelope. For HeLa cells, the nucleus is the largest organelle inside the cell.

---

## 4 Notes

1. The percentage of FBS can be varied in cell culture media from 8% to 20% depending on cell type and growth rate [19]. Alternatives to FBS have also been identified [20].
2. Place medium in a 37 °C water bath for at least 15 min before thawing cells.
3. Different strains of HeLa cells have different doubling times, ranging between 17.5 and 32.3 h [21]. Also, cell culture conditions like media and FBS percentage influence cell growth, and hence it is advised to empirically standardize those conditions to have cells with 75–80% confluency.
4. Alternate fixation methods can be used if needed. For example, for cell types that are strongly adherent, add glutaraldehyde to the media in the flask to a final concentration of 2.5%, scrape off the cells, pellet the cells by centrifugation at 300 *g* for 5 min, remove the supernatant, and resuspend the cells in 2.5% glutaraldehyde in 1X PBS. Glutaraldehyde is toxic and should be disposed of properly. Work in a fume hood and wear gloves when handling glutaraldehyde.
5. Fixing and embedding involve multiple centrifugation and cell pelleting steps. To ensure that the cell structure is preserved, it is advised to centrifuge at speeds not more than 300 *g*. Additionally, to resuspend the cell pellets, avoid using pipettes, and instead resuspend by tapping the centrifuge tubes.
6. We have also tested a 1% OsO<sub>4</sub> solution and found that to be effective. OsO<sub>4</sub> is highly toxic and should be disposed of properly. Work in a fume hood and wear gloves at all times.
7. Shorter dehydration could result in incomplete water removal, while longer dehydration may cause membrane loss. To ensure 100% dehydration, use a freshly opened bottle of ethanol to avoid moisture contamination.
8. Propylene oxide functions as a transition step because it mixes well with both ethanol and resin.
9. SPURR resin is prepared as per the manufacturer's instructions. Briefly, the components are mixed as mentioned in the instructions with the catalyst being added last. It is advised to prepare the resin in a fume hood. Mix the components very gently to avoid formation of air bubbles. Unpolymerized resin can be used up to 3 days after mixing the components. Any unused resin should be polymerized and discarded. Volumes added to cells should be at least ten times the cell pellet volume.
10. Ensuring that the diamond knife edge and trimmed resin block are perfectly aligned to each other in a parallel manner is of critical importance to ensure sections of uniform thickness.

## Acknowledgments

Work in the Levy lab is supported by the National Institutes of Health/National Institute of General Medical Sciences (R35GM134885 and P20GM103432).

## References

1. Pederson T (2010) "Compact" nuclear domains: reconsidering the nucleolus. *Nucleus* 1(5):444–445. <https://doi.org/10.4161/nucl.1.5.13056>
2. Gall JG (1964) Electron microscopy of the nuclear envelope. In: *The nuclear membrane and nucleocytoplasmic interchange*. Springer Vienna, Vienna, pp 4–25. [https://doi.org/10.1007/978-3-7091-5476-2\\_2](https://doi.org/10.1007/978-3-7091-5476-2_2)
3. Alber F, Dokudovskaya S, Veenhoff LM et al (2007) The molecular architecture of the nuclear pore complex. *Nature* 450(7170):695–701. <https://doi.org/10.1038/nature06405>
4. Fernandez-Martinez J, Rout MP (2009) Nuclear pore complex biogenesis. *Curr Opin Cell Biol* 21(4):603–612. <https://doi.org/10.1016/j.ceb.2009.05.001>
5. D'Angelo MA, Hetzer MW (2008) Structure, dynamics and function of nuclear pore complexes. *Trends Cell Biol* 18(10):456–466. <https://doi.org/10.1016/j.tcb.2008.07.009>
6. Hoelz A, Debler EW, Blobel G (2011) The structure of the nuclear pore complex. *Annu Rev Biochem* 80:613–643. <https://doi.org/10.1146/annurev-biochem-060109-151030>
7. Jevtic P, Levy DL (2014) Mechanisms of nuclear size regulation in model systems and cancer. *Adv Exp Med Biol* 773:537–569. [https://doi.org/10.1007/978-1-4899-8032-8\\_25](https://doi.org/10.1007/978-1-4899-8032-8_25)
8. Chow KH, Factor RE, Ullman KS (2012) The nuclear envelope environment and its cancer connections. *Nat Rev Cancer* 12(3):196–209. <https://doi.org/10.1038/nrc3219>
9. Levy DL, Heald R (2010) Nuclear size is regulated by importin alpha and Ntf2 in *Xenopus*. *Cell* 143(2):288–298. <https://doi.org/10.1016/j.cell.2010.09.012>
10. Scaffidi P, Misteli T (2006) Lamin A-dependent nuclear defects in human aging. *Science* 312(5776):1059–1063. <https://doi.org/10.1126/science.1127168>
11. Goldman RD, Shumaker DK, Erdos MR et al (2004) Accumulation of mutant lamin A causes progressive changes in nuclear architecture in Hutchinson-Gilford progeria syndrome. *Proc Natl Acad Sci USA* 101(24):8963–8968. <https://doi.org/10.1073/pnas.0402943101>
12. Porter KR, Claude A, Fullam EF (1945) A study of tissue culture cells by electron microscopy: methods and preliminary observations. *J Exp Med* 81(3):233–246. <https://doi.org/10.1084/jem.81.3.233>
13. Claude A, Porter KR, Pickels EG (1947) Electron microscope study of chicken tumor cells\*. *Cancer Res* 7(7):421–430
14. Dalton AJ (1951) Observations of the Golgi substance with the electron microscope. *Nature* 168(4267):244–245. <https://doi.org/10.1038/168244b0>
15. Palade GE (1952) The fine structure of mitochondria. *Anat Rec* 114(3):427–451. <https://doi.org/10.1002/ar.1091140304>
16. Hodge AJ, Huxley HE, Spiro D (1954) Electron microscope studies on ultrathin sections of muscle. *J Exp Med* 99(2):201–206. <https://doi.org/10.1084/jem.99.2.201>
17. Masters BR (2008) History of the electron microscope in cell biology. In: *Encyclopedia of life sciences*. Wiley. <https://doi.org/10.1002/9780470015902.a0021539>
18. Sato T (1968) A modified method for lead staining of thin sections. *J Electron Microsc* 17(2):158–159
19. Khasawneh RR, Al Sharie AH, Abu-El Rub E et al (2019) Addressing the impact of different fetal bovine serum percentages on mesenchymal stem cells biological performance. *Mol Biol Rep* 46(4):4437–4441. <https://doi.org/10.1007/s11033-019-04898-1>
20. Fang CY, Wu CC, Fang CL et al (2017) Long-term growth comparison studies of FBS and FBS alternatives in six head and neck cell lines. *PLoS One* 12(6):e0178960. <https://doi.org/10.1371/journal.pone.0178960>
21. Tang L (2019) Investigating heterogeneity in HeLa cells. *Nat Methods* 16(4):281. <https://doi.org/10.1038/s41592-019-0375-1>



# Chapter 4

## Imaging Nuclear Envelopes Using Correlative AFM/Fluorescence Microscopy

Emilie Costes, Anthony Vial, Christine Doucet,  
and Pierre-Emmanuel Milhiet

### Abstract

The nuclear envelope (NE) is the hallmark of eukaryotic cells. It is a complex structure composed of two concentric lipid bilayers separated by a 50 nm lumen. While the outer nuclear membrane is continuous with the endoplasmic reticulum, the inner nuclear membrane contains a unique set of proteins. Methods have been developed several decades ago to prepare NEs from *Xenopus laevis* oocytes, exposing inner and outer nuclear membranes, which makes them ideal samples for probe scanning methods such as atomic force microscopy (AFM). In addition, biochemical preparations of human NEs have been valuable tools to investigate the structure of their nuclear pore complexes (NPCs). However, recent data have highlighted that membrane tension loss during NE preparation changes the morphology of NPCs. In this chapter, we outline a novel approach to extract nuclei from cultured mammalian cells, affix them onto glass substrates, and gently open them, thereby maintaining membrane tension and preserving NPC structure for subsequent AFM imaging of both inner and outer nuclear membranes. Furthermore, we detail a protocol for immuno-labeling and correlative imaging by AFM/dSTORM (direct Stochastic Optical Reconstruction Microscopy). Additionally, we provide comprehensive guidance on data analysis, in particular for proper correlation of the optical and AFM images. Notably, the sample preparation steps only require basic materials. The procedures described here could be easily extended to other cellular models such as plant cells or cells isolated from animal tissues.

**Key words** Nuclear envelope, Nuclear pore complex (NPC), Mammalian cells, Atomic force microscopy (AFM), Fluorescence microscopy, Single-molecule localization microscopy (SMLM), Direct stochastic optical reconstruction microscopy (dSTORM)

---

## 1 Introduction

The nuclear envelope (NE) is a defining feature of eukaryotic cells. It plays a crucial role, serving to protect the genetic material within the nucleus. Moreover, the physical separation it provides between transcription and translation components allows an important level

---

Authors “Emilie Costes” and “Anthony Vial” have equally contributed to this chapter.

Yuki Hara and Kazunori Kume (eds.), *The Nuclear Membrane: Methods and Protocols*, Methods in Molecular Biology, vol. 2958, [https://doi.org/10.1007/978-1-0716-4714-1\\_4](https://doi.org/10.1007/978-1-0716-4714-1_4),  
© The Author(s), under exclusive license to Springer Science+Business Media, LLC, part of Springer Nature 2025

of gene expression regulation. The NE is composed of two lipid bilayers separated by a lumen (the perinuclear space) that ranges from 20 nm in yeast to 50 nm in higher eukaryotes. The outer nuclear membrane (ONM) is continuous with the endoplasmic reticulum (ER), while the inner nuclear membrane (INM) contains a unique set of proteins and is underlined by the nuclear lamina, providing structural support to the nucleus. Nuclear pore complexes (NPCs) are located at sites where the ONM and INM fuse, tightly controlling the exchange of molecules between the nucleus and the cytoplasm.

NPCs are composed of a cylindrical scaffold, embedded in the NE, capped by two asymmetrical domains, the cytoplasmic filaments and the nuclear basket. The scaffold also forms a central channel filled with disordered proteins. While the structure and molecular organization of the scaffold are known with sub-nanometer resolution, the details of the peripheral domains remain poorly defined [1–6]. Notably, these domains are systematically missing from high-resolution cryo-electron microscopy (cryo-EM) structures, likely due to their high variability, which causes them to disappear during particle averaging and reconstruction. Beyond resolving the structure of these heterogeneous domains, there is increasing interest in describing and understanding NPC variability [7–9]. A powerful tool for studying the topography and mechanical properties of such variable and dynamic objects at the single-molecule level is atomic force microscopy (AFM). Unlike cryo-EM, AFM does not require data averaging to provide detailed topographies with nanometric resolution. It also delivers mechanical information. It is thus a technique of choice to probe the heterogeneous structure of NPCs' peripheral domains. Since AFM does not provide (nor requires) chemical and specific signature, it can be advantageously correlated with single-molecule localization microscopy (SMLM): indeed, the two approaches have similar lateral resolutions on biological samples (5–15 nm), and this combination enables the unique triple correlation between topography, mechanical properties, and molecular composition [9, 10].

Since AFM is a contact technique, NEs need to be extracted from cells before imaging. Traditionally, nuclear envelopes have been isolated from *Xenopus laevis* oocytes [11–14], which have large nuclei that can be manually torn open with tweezers. The isolated nuclear envelope is then spread on an electron microscopy grid, a mica disc, or a glass coverslip, with portions of the outer and inner nuclear membranes facing up [15]. Chromatin is gently washed out, leaving the nuclear envelope ready for imaging after fixation [15]. While the *Xenopus* system has been valuable for imaging NEs by AFM, it has limitations. These include its specificity to embryonic stages and the availability of fewer tools for techniques like immunofluorescence compared to those available for mammalian systems. Transferring this technology to human

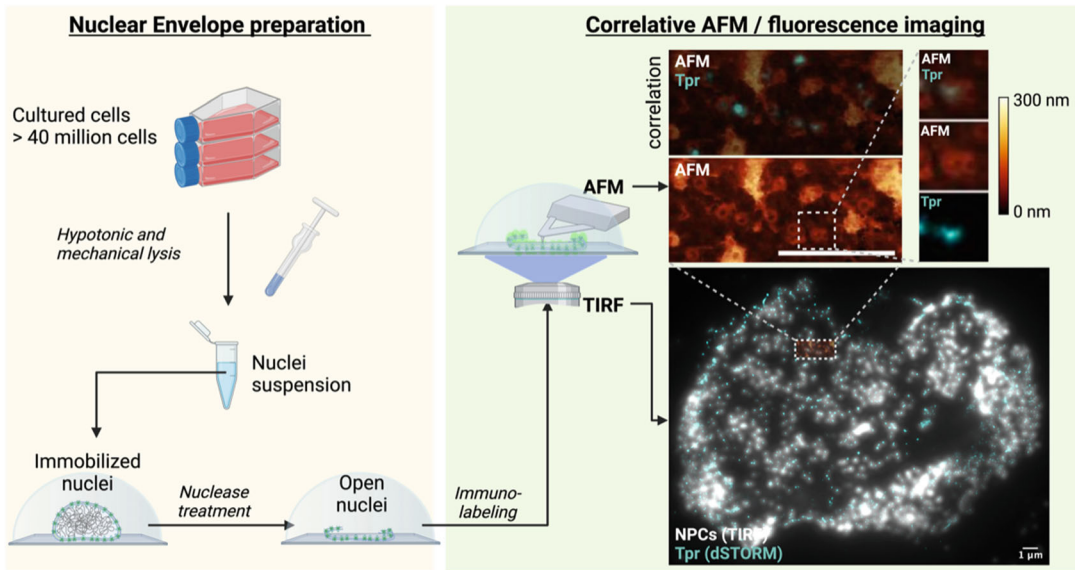


**Fig. 1** Schematic summary of nuclear envelope preparation for correlative AFM/dSTORM imaging. The right panel shows an open nucleus extracted from U2OS cells. NPCs have been immuno-labeled with mAb414, a monoclonal antibody that recognizes FG repeats, and anti-Tpr, a nucleoporin of the basket. mAb414 was imaged by diffraction-limited TIRF (total internal reflection fluorescence) microscopy (white) while Tpr was imaged by dSTORM (cyan). An area of the inner nuclear membrane was imaged by AFM and overlaid with the dSTORM image. Scale bars = 1  $\mu$ m. (The data in this figure were already published in *Nanoscale* [9]. Figure-created with BioRender.com)

cells opens up new possibilities for research, including genetic engineering using techniques like CRISPR-Cas, small interfering RNA (siRNA), and fusion of various tags for visualization or manipulation.

In this chapter, we detail an approach to isolate NEs from cultured human cells and image them by correlative AFM/SMLM [9], while preserving membrane tension. Indeed, it was shown recently that the classical approach of preparing NEs from nuclei suspensions alters the diameter of its NPCs [1, 16]. This is most likely because the membrane tension is lost. In the method we present in this chapter, the nuclei are immobilized on glass prior to opening and chromatin removal. This immobilization step presumably preserves the tension in the NE, since we did not observe any change in the diameter of NPCs [9]. The protocol presented here describes all steps related to cell culture, coverslips preparation, nuclear extraction and opening, fluorescent labeling, dSTORM imaging, AFM imaging, and image reconstruction and correlation (Fig. 1). Note that the methods presented here were optimized for U2OS cells and NPC labeling. This workflow should in principle work for any cell line or cells isolated from animal tissues, or plants, but several steps might require specific optimization.

## 2 Materials

### 2.1 Cell Preparation

The reagents listed here are those we routinely use for U2OS culture. In case other cell lines are used, they should be cultured as usual, with appropriate reagents.

1. U2OS cells (ATCC).
2. DMEM, high glucose, supplemented with GlutaMAX and pyruvate.
3. Fetal bovine serum to supplement culture medium at 10%.
4. Phosphate buffer solution (PBS): 137 mM NaCl, 2.7 mM KCl, 10 mM Na<sub>2</sub>HPO<sub>4</sub>, and 1.8 mM KH<sub>2</sub>PO<sub>4</sub>, pH 7.4.
5. Trypsin: Enzyme Express (1X) TrypLE™.
6. 75 cm<sup>2</sup> tissue culture flasks, sterile.

### 2.2 Coverslip Cleaning

1. Wheaton labeling containers.
2. 25 mm H1.5 coverslips (*see Note 1*).
3. Acetone.
4. 95% ethanol.
5. 1 M KOH (*see Note 2*).

### 2.3 Nuclei Extraction

1. 100X cOmplete™ protease inhibitor cocktail (PIC): 1 pellet of EDTA-free cOmplete™ protease inhibitor (Roche) resuspended in 500 µL of Milli-Q water. Stored at −20 °C.
2. Hypotonic Buffer: 50 mM Tris pH 7.5, 1 mM DTT, 1X PIC (*see Note 3*).
3. S500 sucrose buffer: 10 mM HEPES pH 7.5, 2.5 mM MgCl<sub>2</sub>, 50 mM KCl, 500 mM Sucrose, 1 mM DTT, 1× PIC (*see Note 3*).
4. 1 mL Dounce tissue grinder with a tight-fitting pestle (tube length 88 mm, borosilicate glass 3.3, DWK Life Sciences) (*see Note 4*).
5. Glass slides (76 × 26 mm, 1.1 mm thickness) and coverslips (25 mm high-precision type 1.5 glass coverslips of 0.17 mm thickness).
6. Numeration cells (Bio-Rad).

### 2.4 Nuclei Immobilization and Opening

1. Poly-L-Lysine solution (PLL): 0.1% (w/v) in water.
2. NE-A: 0.1 mM MgCl<sub>2</sub>, 1 mM DTT + 30 U DNase I + 250 U RNase A.
3. NE-B: 20 mM Tris pH 8.5, 10% sucrose, 0.1 mM MgCl<sub>2</sub>, 1 mM DTT.

4. S500 sucrose buffer (*see* Subheading 2.3).
5. Optional: 32% PFA (*see* Note 5).

## 2.5 Fluorescent Labeling

1. PBS (*see* Note 6).
2. Goat serum (*see* Note 7).
3. Blocking buffer: PBS + 3% goat serum.
4. Primary antibodies: mAb414 (BioLegend #902901), anti-Lamin B1 (Thermo Scientific #PA5-19468), anti-Tpr (Abcam #ab84516).
5. Secondary antibodies conjugated to an organic fluorescent dye (*see* Note 8).
6. Optional: HALO or SNAP ligands conjugated to an organic fluorescent dye (e.g., SNAP-Surface Alexa Fluor 647, NEB) (*see* Note 9).
7. Optional: Hoechst 33342 (1 mg/mL stock solution) nucleic acids stain.

## 2.6 Direct Stochastic Optical Reconstruction Microscopy (dSTORM)

1. Attofluor cell chamber (Invitrogen) (*see* Note 10).
2. Gloxy buffer: PBS supplemented with 10% glucose, 0.5 mg/mL glucose oxidase, 0.04 mg/mL catalase, 35 mM mercaptoethylamine (MEA) (*see* Note 11). This buffer has to be freshly prepared just before the experiment.
3. Optional: Fluorescent TetraSpeck microbeads (*see* Note 12).
4. Epi-fluorescence/total internal reflection fluorescence (TIRF) microscopy was performed with an inverted microscope equipped with an oil immersion Zeiss  $\alpha$ -Plan-Apochromat 100 $\times$ , 1.46 NA DIC objective, three visible lasers (488 nm, Thorlabs 50 mW; 561 nm, Coherent Sapphire 100 mW; 642 nm, MPB 1 W), an AOTF controlled by a LabVIEW program, to modulate the excitation laser power and select the wavelength [10] and an emCCD camera (iXON Ultra897, Andor technologies).

## 2.7 Atomic Force Microscopy

1. Nuclei buffer: 10 mM HEPES pH 7.5, 2.5 mM MgCl<sub>2</sub>, 83 mM KCl, 17 mM NaCl.
2. AFM probes (Bruker MSNL or Olympus OTR4 cantilevers with 0.1 and 0.08 mN/m spring constant, respectively).
3. AFM microscope (JPK Nanowizard 4, Bruker Nano GmbH) is a tip scanning setup mounted on an inverted optical microscope. Imaging is performed in quantitative imaging (QI) mode (*see* Note 13).

## 2.8 General Materials and Equipment

1. Class II biosafety cell culture hood.
2. Cell counter.
3. Incubator.
4. Centrifuge for 15 mL and 50 mL tubes.
5. Bath sonicator.
6. Fume hood.

## 2.9 Softwares

Below is a list of open source softwares used for data analysis. This list does not include the proprietary softwares to run the microscopes and to acquire data from the camera and the atomic force microscope. Additional analysis can be performed by custom scripts written in MATLAB, Python, or any other programming language:

1. Fiji (<https://imagej.net/software/fiji/downloads>) [17] with the plugin ThunderSTORM (<https://zitmen.github.io/thunderstorm/>) [18].
2. Icy (<https://icy.bioimageanalysis.org/>) [19] with the plug-in ec-CLEM [20].
3. Gwyddion (<http://gwyddion.net/>) [21].

---

## 3 Methods

### 3.1 Cell Preparation: Four Days Before Nuclei Preparation

The following cell preparation protocol refers to U2OS cells, whose doubling time is roughly 24 h. In case other cell lines are used, passages should be adapted to have cells at confluence in the flasks the day of the nuclei preparation. Note that cells have to be amplified before nuclei preparation in order to seed five to six 75 cm<sup>2</sup> flasks 4 days before nuclei extraction:

Warm up DMEM, PBS, and trypsin before cell preparation (*see Note 14*).

1. Wash the cells twice with 10 mL of PBS per 75 cm<sup>2</sup> flask.
2. Remove the PBS and add 2 mL of trypsin per flask. Remove the excess of trypsin and put the flasks in the incubator (37 °C) for 5 min.
3. Resuspend the cells with 10 mL of fresh DMEM. Collect 10 µL of the suspension, load a cell counting chamber, and count using the cell counter (it is also possible to use Neubauer counting chambers).
4. Prepare five to six 75 cm<sup>2</sup> flasks by filling them with 20 mL of fresh media. Add 1.3 million of cells per flask (*see Note 15*) which corresponds to a volume of  $\frac{1.3 \cdot 10^6}{\text{cell density (cells/mL)}}$  mL of resuspended cells. Gently shake the flasks to disperse the cells and put them in the incubator (37 °C, 5% CO<sub>2</sub>) for 4 days until nuclei extraction.

### 3.2 Coverslip Cleaning

For SMLM, glass coverslips need to be extensively cleaned, as described below:

1. Place 25 mm high-precision (H1.5) glass coverslips in a Wheaton labeling jar.
2. Sequentially wash them with acetone, ethanol, and water. For each washing step, cover the coverslips with liquid, and then gently pour the liquid out of the Wheaton jar along one corner of the jar to prevent coverslips from falling (*see Note 16*).
3. Remove water and replace with 1 M KOH.
4. Sonicate the coverslips for 20 min in 1 M KOH.
5. Rinse them ten times with Milli-Q water (*see Note 17*).
6. Sonicate the coverslips in Milli-Q water for 20 min.
7. Let the coverslips dry completely before use. Cover them to prevent them from getting dusty (*see Notes 18 and 19*).

### 3.3 Nuclei Extraction

1. Warm up PBS, trypsin, and cell growth media.
2. Thaw Hypotonic Buffer and sucrose S500 buffer, supplement them with DTT (final concentration = 1 mM) and PIC (1X), and keep on ice until use. Also place the Dounce and a 2 mL Eppendorf tube on ice until use.
3. Flasks of cells (75 cm<sup>2</sup>) previously prepared should be confluent. Wash the cells twice with 10 mL of PBS for each flask, and then add 2 mL of trypsin in each flask, make sure that it is dispersed over the entire surface and remove the excess of trypsin. Put the flasks back into the incubator (37 °C, 5% CO<sub>2</sub>) for 5 min. Check under the microscope that the cells are well detached.
4. Collect the cells from all flasks in a total volume of 30 mL of fresh DMEM, and place them in a Falcon tube. Take a 10 µL sample to count the cells as described above (*see Note 20*). Pellet the cell suspension by centrifuging at 300 *g* for 5 min at 4 °C.
5. Remove the DMEM and resuspend the pellet in 30 mL of PBS, pellet at 300 *g* for 5 min at 4 °C.
6. Remove the PBS and resuspend the pellet in 20 mL of Hypotonic Buffer, pellet at 200 *g* for 5 min at 4 °C (*see Note 21*).
7. Remove the Hypotonic Buffer and resuspend the pellet in 0.7–1 mL of Hypotonic Buffer (*see Note 22*).
8. Let stand on ice for 1 h; the cells will swell due to osmotic equilibration with the Hypotonic Buffer. They will also sediment toward the bottom of the tube. The excess of Hypotonic Buffer can be gently removed with a pipet tip.

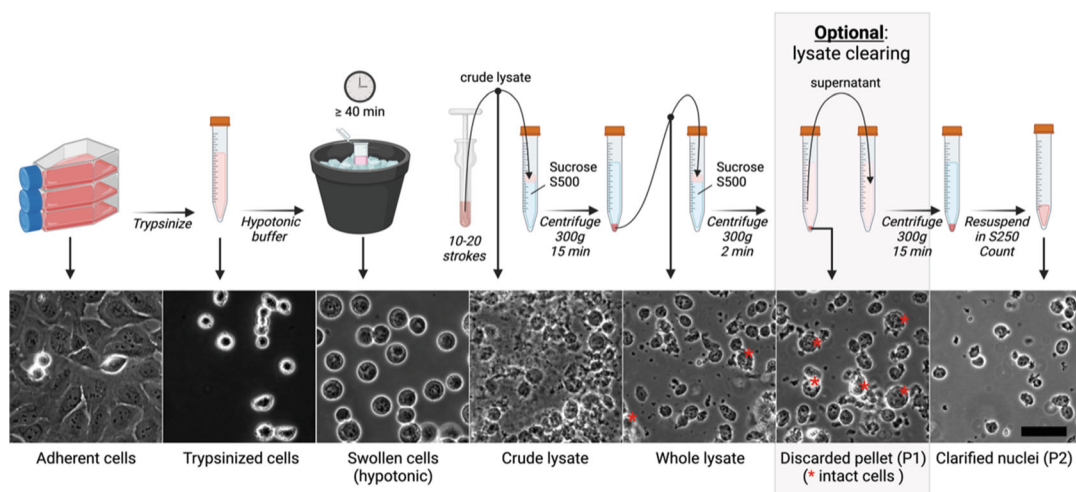


**Fig. 2** Schematic view of the nuclei extraction process from cultured cells. Representative images of the distinct stages of preparation are shown to illustrate the morphological evolution of the system. The red stars indicate contaminating intact cells in the nuclei preparation. These can be efficiently eliminated during an optional centrifugal clearing. Scale bar = 50  $\mu\text{m}$ . (Figure created with BioRender.com)

9. Transfer the suspension of swollen cells into the Dounce, avoiding the formation of air bubbles.
10. Mechanically break the cells by performing successive strokes with the tight pestle (make sure to avoid bubbles by always keeping the extremity of the pestle under the liquid surface). Start checking the nuclei preparation under the microscope after 8 strokes (*see Note 23*). To do this, extract 10  $\mu\text{L}$  of suspension from the Dounce without removing the pestle by gently inserting the extremity of a 10  $\mu\text{L}$  pipet tip between the pestle and the wall of the reservoir while the pestle is all the way down. Extracted nuclei appear dark under a transmitted light microscope, whereas the remaining intact cells appear as larger refringent bright spheres (Fig. 2).
11. Stop actioning the pestle when cell lysis reaches around 95% or nuclei start to break (*see Note 23*).
12. Extract the pestle from the Dounce, minimizing air bubbles as much as possible (*see Note 24*). To do so, slowly raise the pestle until its extremity reaches just below the cell suspension surface. Then rapidly extract the pestle. Carefully load the cell lysate on top of 5 mL of sucrose S500 in a 15 mL tube and spin for 15 min at 300  $g$  at 4  $^{\circ}\text{C}$ .
13. Remove the supernatant and resuspend the pellet in 500  $\mu\text{L}$  of Hypotonic Buffer. Load the resuspended pellet on top of 5 mL of S500 in a 15 mL tube, and spin again for 15 min at 300  $g$  at 4  $^{\circ}\text{C}$ .

14. Remove the supernatant and resuspend the pellet (P0) into 500  $\mu\text{L}$  of S500.

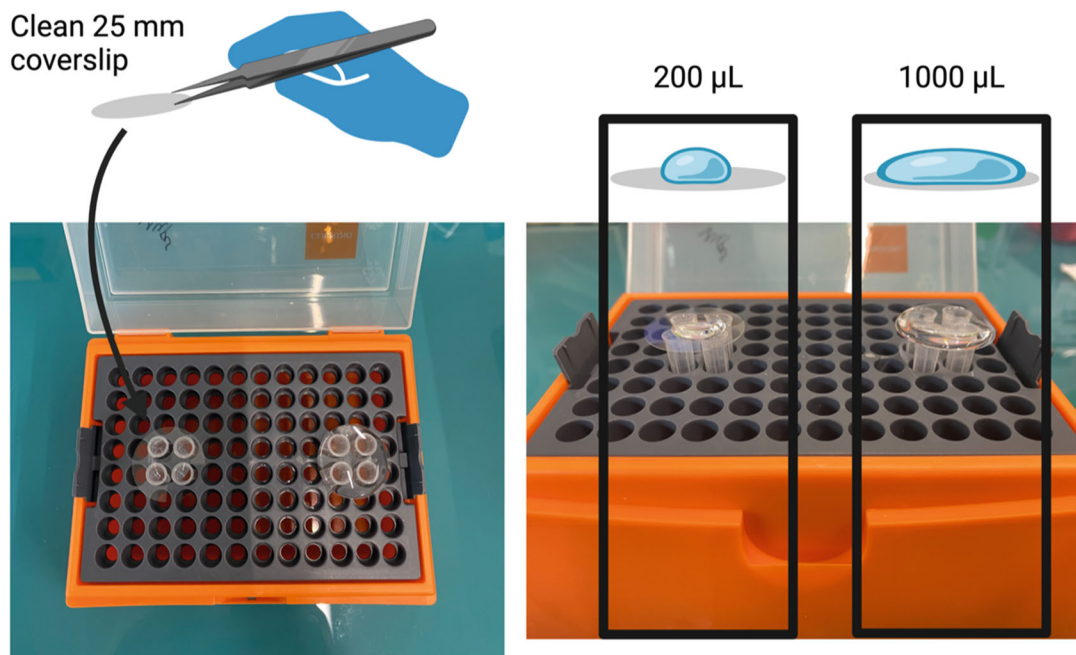
*Optional: clearing step (see Note 25).* If cell lysis is below 90%, a clearing step can be added at **step 13** in Subheading 3.3 to remove unbroken cells: Spin the cells resuspended in S500 for 2 min at 300  $g$  at 4  $^{\circ}\text{C}$ ; keep the pellet (P1), which contains most unbroken cells and a fraction of bona fide nuclei. Collect the supernatant, transfer it to a clean 15 mL tube, and spin it for 15 min at 300  $g$ . Remove the supernatant and resuspend the pellet P2, which should contain over 90% nuclei, in 500  $\mu\text{L}$  of S500.

15. Dilute P0 or P1 and P2 with Hypotonic Buffer to reach 2 million nuclei per mL.
16. To dissociate nuclei, gently pipet them up and down 100 times with a P200, making sure to avoid air bubbles.
17. If nuclei are not mounted on glass the same day, they can be stored in a tube at 4  $^{\circ}\text{C}$  for 1–2 days into a 50/50 mixture of Hypotonic Buffer/S500.

### 3.4 Nuclei Immobilization and Opening

For all these steps, the clean, 25 mm glass coverslips are placed in equilibrium on the base of tips placed in an empty rack (Fig. 3). Edges of the coverslip should not touch the plastic to avoid drop wetting. This is important to form droplets of 200  $\mu\text{L}$  to 1 mL at the surface of the coverslips. Ideally, water is added to the bottom of the chamber to maintain environmental humidity and limit evaporation. Note that if the nuclei express fluorescent proteins, they should be protected from light until imaging:

1. Place each coverslip in equilibrium in the incubation chamber.
2. Load a 500  $\mu\text{L}$  drop of Poly-L-lysine (PLL), diluted at 1:10 in water and filtered (0.01% final concentration), on each 25 mm high-precision H1.5 clean glass coverslip for 2 min at room temperature.
3. Aspirate the drop of PLL with a pipet until complete removal of the liquid.
4. Load 250  $\mu\text{L}$  of purified nuclei on the coverslips, and let them incubate for 15 min at room temperature. To make sure that nuclei are not aggregated, pipet them up and down 10–20 times with the P200 before deposit. The drop only covers the center of the coverslip, but this is fine since the edges cannot be imaged when the coverslip is placed in the Attofluor.
5. Remove the excess of nuclei suspension and gently rinse the coverslips four times with 500  $\mu\text{L}$  of sucrose S500 buffer.
6. Per coverslip, prepare 200  $\mu\text{L}$  of NE-A and 800  $\mu\text{L}$  of NE-B (see Note 26). Prewarm NE-A and NE-B at 37  $^{\circ}\text{C}$ .



Base of tips placed in an empty rack

**Fig. 3** Coverslip stand for nuclei immobilization and labeling. Left panel displays a 25 mm coverslip stand. Water can be added at the bottom to limit evaporation of the sample. Right panel illustrates the appearance of a 200  $\mu\text{L}$  drop and a 1000  $\mu\text{L}$  drop placed on a 25 mm coverslip

7. Remove the S500 from the coverslip. Cover the nuclei with 200  $\mu\text{L}$  of NE-A. After 30 s, add 800  $\mu\text{L}$  of NE-B, and gently pipet up and down three to four times to homogenize the solution. Incubate for 35 min at room temperature.
8. Rinse twice with 500–1000  $\mu\text{L}$  of S500 buffer.
9. Place each coverslip in a well of a 6-well plate, with 1 mL of S500.
10. *Optional: chemical fixation (see Note 27)*. Per coverslip, prepare 500  $\mu\text{L}$  of 4% PFA, diluted in S500 (*see Note 5*). Cover the nuclei with the solution, and incubate for 5 min at room temperature. Rinse four times with S500, and store the coverslips at 4 °C in S500 until fluorescent labeling.

### 3.5 Fluorescent Labeling

A combination of up to four fluorescent labels can be simultaneously imaged on most microscopes. Primary antibodies can be combined without restriction if they are directly coupled to organic dyes. Otherwise, only antibodies raised in orthogonal hosts can be combined for indirect immuno-labeling. Note that Hoechst labeling is convenient to analyze the quality of the nuclei preparation (Fig. 4) but is not recommended for SMLM. In the following

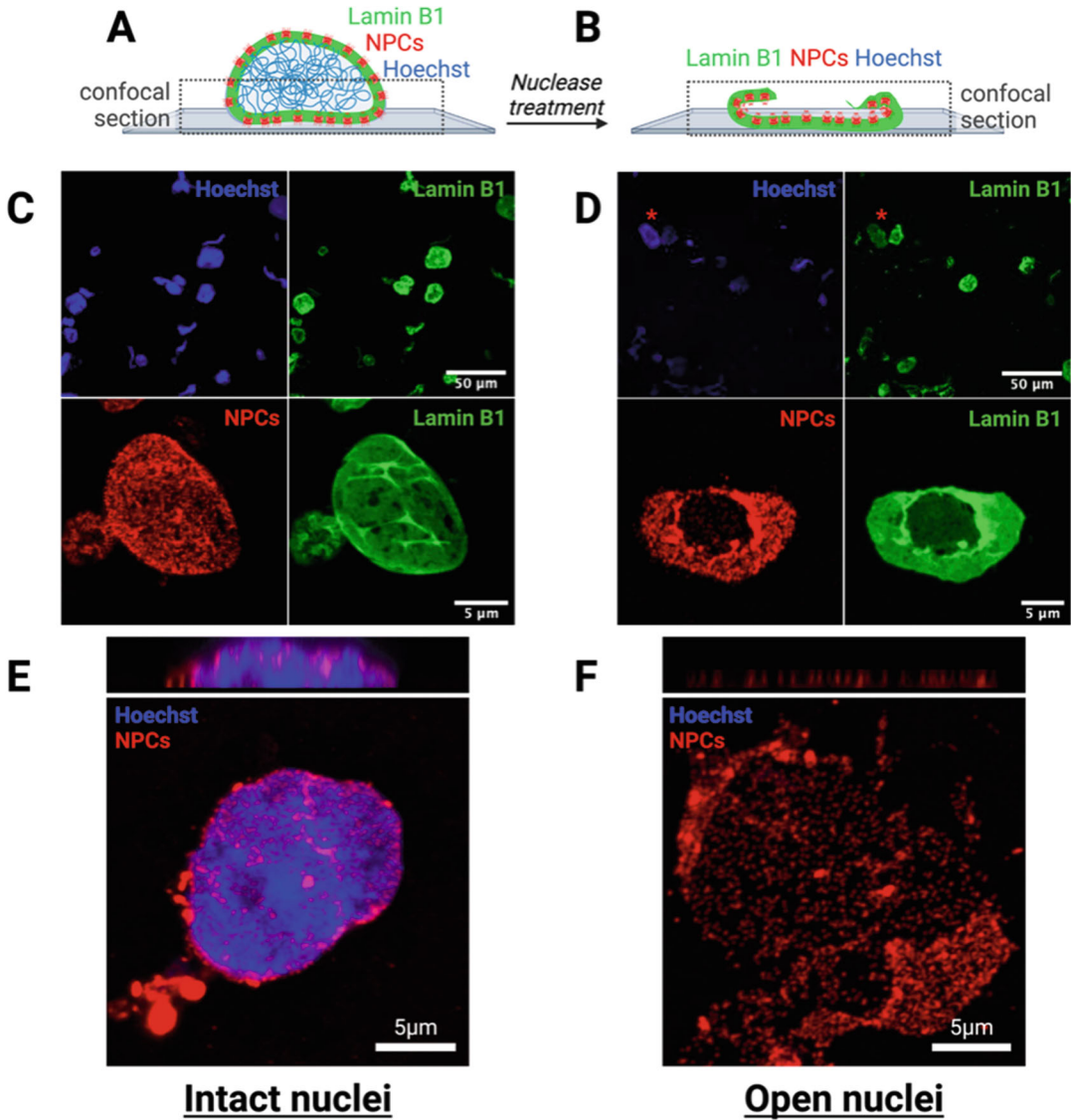


**Fig. 4** Confocal images of nuclei extracted from U2OS cells, labeled with Hoechst (blue), anti-Lamin B1 (green), and mAb414 (red). Note that in this case, intact nuclei were permeabilized before immuno-labeling. (a, c, e) untreated, intact nuclei. (b, d, f) nuclei treated by hypotonic shock and nuclease treatments. (c, d) confocal single stacks. In (d), most nuclei are devoid of chromatin and open. The nucleus identified by a red star still contains chromatin; this is most likely a contaminating intact cell. The open area in nuclei is inferred from the differences in intensity for NPCs and LaminB1 signals. (e, f) xz and xy confocal imaging of an intact (e) vs open (f) nucleus. (Data in e and f were already published in Nanoscale [9]. Figure created with BioRender.com)

section, we will describe the procedure for fluorescent labeling with Hoechst (chromatin), anti-Lamin B1 (Lamin B1 forms a meshwork at the INM) [22, 23], and mAb414 (NPCs) [24, 25]. But any other combination could be used.

Coverslips with open nuclei are placed in a 6-well plate, one coverslip per well. All incubations are performed at room temperature:

1. Incubate immobilized nuclei with 500  $\mu$ L of blocking buffer (PBS + 3% goat serum) for 10 min.
2. Prepare the primary antibodies solution: per coverslip, 500  $\mu$ L of blocking buffer + anti-Lamin B1 (raised in Rabbit) + mAb414 (raised in Mouse) at appropriate dilutions. For TIRF or confocal imaging, anti-Lamin B1 and mAb414 are used at 1:1000 dilutions from commercial stocks; for dSTORM, they are used at 1:200 dilutions.
3. Remove the blocking buffer and add the primary antibodies solution. Incubate for 1 h.
4. Rinse three times with 500  $\mu$ L of blocking buffer. The first two washes are rapid (just exchange buffers). Let the third wash incubate for 5 min.
5. Prepare the secondary antibodies solution: per coverslip, 500  $\mu$ L of blocking buffer + anti-Rabbit coupled to Alexa Fluor 594 + anti-Mouse coupled to Alexa Fluor 647 at appropriate dilutions. For TIRF or confocal imaging, secondary antibodies are used at 1:2000 dilutions from commercial stocks (1  $\mu$ g/mL); for dSTORM, they are used at 1:200 dilutions (10  $\mu$ g/mL). For conventional microscopy, Hoechst can be added to this solution at 1  $\mu$ g/mL.
6. Remove the blocking buffer and add the secondary antibodies solution. Incubate for 30 min.
7. Rinse three times as in **step 4** in Subheading 3.5.
8. Finally rinse with S500 or with nuclei buffer if AFM is performed directly after labeling.

When initially practicing nuclear envelope extraction, it is advisable to evaluate the quality of the nuclei preparation using confocal microscopy. This technique enables the imaging of large fields of view and the acquisition of z-stacks (Fig. 4). For confocal microscopy, coverslips are mounted on glass slides with an appropriate mounting medium (*see Note 28*). Keep in mind that in intact nuclei, immuno-labeling of nuclear proteins will require a permeabilization step—0.1% of Triton-X100 can be added to the blocking solution.

Once the preparation conditions are optimized, samples can be prepared for correlative AFM/TIRF (dSTORM) microscopy as described above.

### 3.6 Fluorescent Imaging

For correlative microscopy, it is recommended to acquire the fluorescence image first. We have noticed significant photobleaching of the sample induced by the AFM laser when AFM is performed first. In addition, importing the fluorescence image in the AFM acquisition software allows to choose regions of interest according to the fluorescent signal. However, the AFM tip calibration on glass should be performed before placing the sample on the stage (*see next section*).

dSTORM imaging is performed on an AFM/SMLM correlative setup [10] in total internal reflection fluorescence (TIRF) mode. The setup is equipped with a 100× oil immersion objective (Zeiss Plan apoCHROMAT, NA 1.46), an additional ×1.6 magnification in the emission path and an Andor iXon Ultra 897 EMCCD 512 × 512 pixels camera:

1. Place the sample with immuno-labeled open nuclei in the Attofluor, and fill it with 1 mL of imaging buffer (here: Gloxy buffer) extemporaneously prepared. Cover the Attofluor with a 25 mm clean coverslip to limit oxygen contact. This “lid” should be in contact with the imaging buffer. Try to minimize air bubbles.
2. Either use Brightfield or epifluorescence microscopy to localize an open nucleus (*see Note 29*).
3. When a nucleus of interest is visualized with epifluorescence microscopy, switch the fluorescence mode to TIRF. When the critical angle is reached, the fluorescence intensity should increase and background due to out-of-focus molecules should disappear.
4. For dSTORM imaging, increase the laser power. The fluorescence first increases, as all fluorophores are efficiently excited. After a few seconds, the fluorescence signal decreases, as excited fluorophores are progressively transitioning to their dark state.
5. Wait until you see blinking, meaning that most fluorophores are stochastically switching between their on and off state [26, 27]. Start the movie acquisition when you see individual molecules blinking. Photoactivation with a 405 nm laser can increase the blinking frequency of some fluorophores, like Alexa Fluor 647 [28]. In this case, the 405 nm and 640 nm lasers are shone alternatively, and the power of the 405 nm laser is progressively increased during the movie acquisition to keep a constant rate of 10–20 emitting molecules per frame.
6. We usually acquire 30,000 frames, with an exposure time of 30 ms and a laser power of 500 mW. But these settings should be adjusted according to the microscope, laser power, and fluorescent labeling.

Keep in mind that Gloxy buffer acidifies over time [29]; thus it needs to be changed every 2 h.

### 3.7 Atomic Force Microscopy

Before fluorescence imaging, the AFM cantilever spring constant should be calibrated on glass [30]. This is particularly important to extract mechanical data.

The workflow described below is the one we use with our JPK Nanowizard 4. Some steps—like the AFM/optical alignment—might differ with other AFM microscopes:

1. Mount an AFM probe with typical spring constant around 0.1 N/m and tip radius below 15 nm (*see* Subheading 2.7 for recommended tips and **Note 30**) on the cantilever holder. Align the AFM laser at the end of the cantilever and center the reflected beam on the photodiode.
2. Mount a clean coverslip in the Attofluor or use a glass bottom petri dish (WPI) filled with few mL of Nuclei buffer used for AFM imaging.
3. Once in liquid, re-center the reflected beam on the photodiode. Calibrate the deflection sensitivity and the spring constant of the cantilever by performing a force-distance curve and recording the cantilever thermal noise.
4. Place the sample with immobilized nuclei on the microscope/AFM stage. Remove the imaging buffer and replace it with nuclei buffer.
5. Use widefield/brightfield or fluorescence microscopy images to visually localize a nucleus (*see* **Note 30**). To perform correlative AFM/fluorescence microscopy, first acquire the fluorescence images. Then leave the sample in place, and position the AFM scanning head onto the stage, without moving anything.
6. Visually align the AFM tip position on the center of the nucleus. To do so, first approach the AFM probe toward the surface with the step motors until the cantilevers can be visualized slightly out of focus in the field of view of the camera.
7. Translate the position of the AFM head and thus of the cantilever, with head displacement micrometric screws so that the end of the cantilever, where the tip is located, is centered on the nucleus.
8. Import the optical image of the nucleus in the AFM acquisition software (*see* **Note 31**).
9. Set the AFM imaging parameters. Imaging modes based on off-resonance force curves, like quantitative imaging or Peak-Force Tapping, are recommended. Maximum force setpoint below 300 pN allows imaging with minimal force applied to the nuclear envelopes. A ramp length of at least a few hundreds of nanometers is necessary (typically 200–300 nm) with a tip approach speed below 30  $\mu\text{m/s}$ .

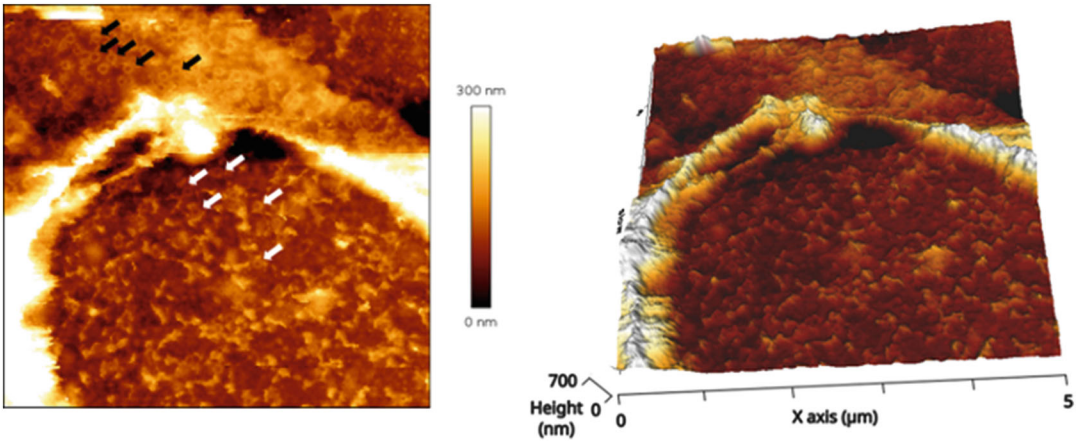


**Fig. 5** 2D and 3D representation of the AFM image of an open nucleus. (*Left*) 2D AFM image of an open nucleus with height color scale truncated to 300 nm to highlight NPCs which are visible as rings both on the ONM and INM (respectively black and white arrows). (*Right*) 3D representation of the same image with the full height scale which allows us to observe the hole in the nuclear envelope. (Data were already published in Nanoscale [9]. Scan width is 5  $\mu\text{m}$  on both images)

10. Approach the AFM tip to the surface and start scanning an area of approximately 5  $\mu\text{m}$  in width. Try to avoid areas with very high or steep topographical features which could result in tip contamination. These areas can generally be spotted on the fluorescence image by moving the focus up and down. Importantly the acquisition time per image has to stay relatively low (typically below 20 min) to avoid AFM image distortion due to the drift between the tip and the sample. This is especially important for correlation with dSTORM images.
11. Readjust the optical image in the AFM acquisition software to align it with the structure imaged by AFM. This is easier when a border of the nucleus opening is visible in the AFM image, although such imaging induces a higher risk of tip contamination. A typical AFM image of a well-open nucleus is presented in Fig. 5 where NPCs can be seen on the INM and ONM. Once the AFM and fluorescence images are properly aligned, select narrower areas of interest for high-resolution AFM imaging.

### 3.8 Analysis

#### 3.8.1 dSTORM

The stack of dSTORM images is then analyzed to reconstruct a super-resolved image. The main steps of this process are the detection of single molecule localizations in each frame, drift correction, localization filtering, and image rendering (Fig. 6). We use Fiji and its plugin ThunderSTORM for all these steps, but other SMLM reconstruction softwares or custom-built algorithms can be used as well [31]:

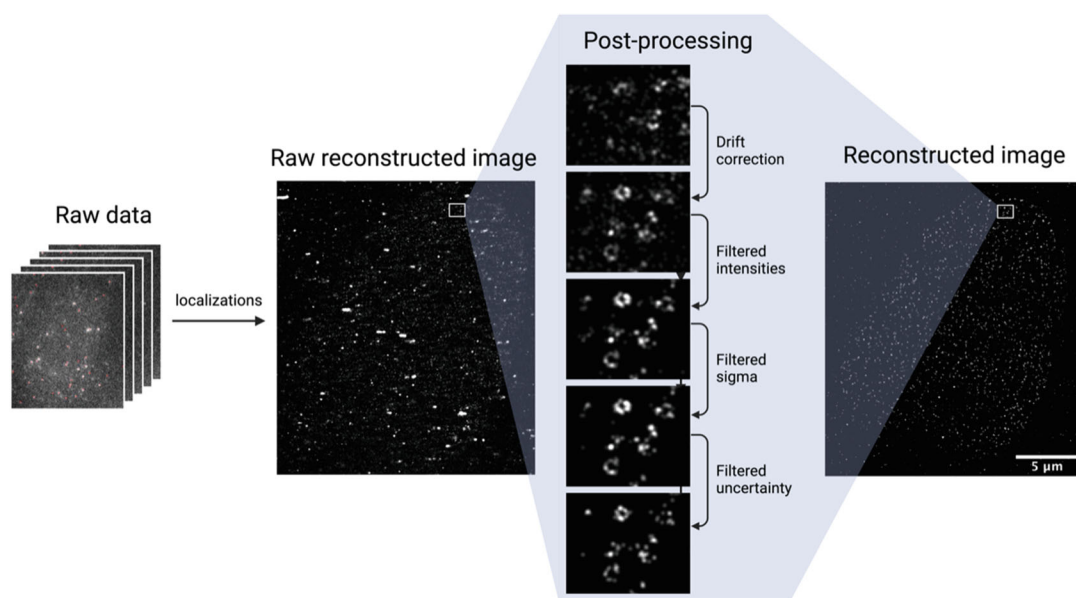


**Fig. 6** Illustration of dSTORM post-processing using ThunderSTORM. Localizations are fitted from each acquired frame and compiled into a raw reconstructed map. A zoomed area is shown to illustrate the effect of the successive corrections and filters applied. Drift correction was performed by cross-correlation. The following filters were applied: 500 counts < Intensities < 5000 counts; 90 nm < Sigma < 180 nm; 10 nm < Uncertainty < 20 nm. The entire final reconstructed image is shown in the right panel. (Figure created with BioRender.com)

1. Open the movie in TIFF virtual stack mode for the process to be faster (*see Note 32*).
2. Set the camera parameters in ThunderSTORM (Plugins > ThunderSTORM > Camera setup): Fill the pixel size (in nm), the photoelectrons per A/D count, the base level (in A/D counts), and the EM gain (camera gain). The pixel size has to be experimentally measured, for example, using a  $10\ \mu\text{m} \times 10\ \mu\text{m}$  calibration grid (Thorlabs) imaged with white transmitted light. The other camera parameters can be retrieved from the camera specification sheet. The EM gain is the one used during acquisition.
3. Run ThunderSTORM analysis by selecting Plugins > ThunderSTORM > Run analysis. While running, the detected localizations are indicated on the frames of the acquisition stack as red dots and the localization map is progressively constructed.
4. Save the raw localizations (unfiltered, uncorrected) as a .csv file. This file can be open later (Plugins > ThunderSTORM > Import/export > Import results).
5. Correct drift: Drift correction is performed according to fiducial markers if they were added to the sample. In this case, at least four beads should be present in the image, well spread

around the nucleus of interest. Drift correction by cross-correlation also works well (*see* **Note 33**). At this stage, recognizable structures appear in the reconstructed image. In particular, if NPC components of the scaffold are labeled, rings with a typical eightfold symmetry and a diameter around 100 nm should be visible.

6. Save the drift-corrected localizations as a .csv file.
7. Filter localizations: for each parameter the distribution of values can be visualized by clicking on “Plot histogram.” Select the range of values directly on the histogram. Click “Apply ROI to filter”; this will automatically define the boundaries of the filter. Click “Apply” on the main ThunderSTORM window; the rendered image is then updated to reflect the changes.
8. Frame: in dSTORM it can happen that an important fraction of fluorophores has not reached the dark state in the first frames of the movie. This results in a high localization density, and potentially a lower precision of localizations. It is common to filter out the first 1000 frames of the movie.
9. Intensity: the range of intensities corresponding to “real” localizations can be estimated by tracing intensity profiles along bona fide localizations in the raw data. The baseline (= background) and intensity of the peak can be estimated from this and used to apply a proper intensity filter.
10. Sigma: this is the standard deviation of the fitted PSF. The range of values will depend on the fluorophore wavelength. For Alexa Fluor 647, this value should be between 90 and 160 nm but will be ultimately chosen according to the histogram. Wider sigma typically appears for out-of-focus localizations.
11. Uncertainty: this is the localization precision. These values will depend on the image quality, in particular the signal-to-noise ratio.
12. Remove duplicates: Detected localizations that converge to the same position can be removed by setting the distance threshold (in nm). This distance should be less than the localization precision.
13. Merging: Localizations appearing in subsequent frames can be merged. Again, the maximum distance should be lower than the uncertainty.
14. Save the processed list of localizations as a .csv file.
15. The corresponding reconstructed image can be rendered by clicking on “Visualization.” Several rendering methods are available. The pixel size can be defined by choosing the “Magnification” parameter. Save the reconstructed images for further analysis.

## 3.8.2 AFM

AFM image analysis can be performed using manufacturer AFM analysis software (such as JPK Data Processing) as well as the free and open-source software Gwyddion. The following steps for data treatment are described for Gwyddion, but similar functions and processes can be found in other softwares:

1. Open the AFM image file.
2. Correct the mean image plane: Data Process > Level > Plane Level.
3. Correct line alignment: Data Process > Correct Data > Align Rows. “Median difference” method usually works fine but other methods like “Median” or “Polynomial (degree = 2)” can be used.
4. If scars—segments or lines where the AFM feedback loop failed—are present, remove them: Data Process > Correct Data > Remove scars. Check that this treatment does not introduce artifacts in the image.
5. Set the zero level of the height value so that the lowest topography in the AFM image is fixed to zero: Data Process > Level > Fix Zero.
6. Range of height visible can be adjusted with the “Color Range Tool.” The color gradient can be changed (e.g., to “Gwyddiont.net” palette) by right-clicking on the height color scale to the right of the image.
7. When the AFM image treatment is complete, a TIFF file can be created through “File > Save as...” and then adding the .tiff extension in the name of the saved file. At this step, the user can modify the characteristics of the TIFF file to include a lateral color scale for example. For correlation with the optical image using Icy, save the AFM image as TIFF with the following parameters: Zoom = 1, no “Value scale”; untick “Draw frame.”

Imaging modes based on off-resonance force curves, like quantitative imaging, allow to save the force curves at each pixel of the AFM images for further mechanical analysis to determine, for example, the Young’s modulus of the sample. In case this type of analysis is of interest, we recommend applying the Hertz/Sneddon model with the appropriate tip geometry parameters (*see Note 34 [32]*). We also suggest paying attention to the tip-surface geometry of contact which can affect Young’s modulus analysis. Finally, the sample’s indentation has to remain negligible relative to the sample’s thickness to avoid substrate contribution to the Young’s modulus calculated value.

### 3.8.3 Correlation

Correlation can be directly performed in the AFM acquisition software if it permits image import. However since dSTORM requires long data analysis, it can also be performed post-acquisition using AFM data processing softwares or the ec-CLEM plugin [20] in the Icy software (*see Note 35*). In all cases, camera pixel size and dSTORM reconstructed image pixel size have to be calibrated prior to acquisition.

For correlation in the JPK Nanowizard 4 software:

1. Import the optical image as an 8-bit or RGB TIFF image in the software by setting the optical image pixel size.
2. Translate the optical image in the AFM software visualization framework relative to the AFM images to align the external shape of the nuclear envelope (*see Note 36*).
3. Refine the correlation using labeled nuclear envelope components visible on both AFM and optical/fluorescence images. For example, if NPCs are labeled, their distribution in the nuclear envelope generally shows a very specific pattern easily recognizable on both optical and AFM images that could be matched (Fig. 7).

For correlation in the Icy ec-CLEM plugin:

1. Open the Icy software and ec-CLEM plugin.
2. Import the optical image and the 2D grayscale AFM image, previously saved as TIFF files.
3. Select “2D (X,Y,[T])” transformation, or “non rigid (2D or 3D)” if sample drift has introduced some distortion in the AFM image.
4. Select the optical image as the image to be transformed and resized, and the AFM image as the image which will not be modified—in the place of the EM image asked by ec-CLEM.
5. Follow the ec-CLEM protocol for correlation: place a landmark point first on the AFM image (for instance, for NPCs, select the center of a recognizable NPC ring in the AFM image). Then adjust the position of the corresponding point that appeared in the optical image, to reach the desired corresponding location (i.e., center of a fluorescent spot), and right-click. Repeat this operation until you have at least three landmark points.
6. At this moment a transformation matrix (translation or translation + distortion, depending on the chosen mode) will be calculated by the software for the correlation. You can place as many points as you want to refine the correlation.
7. Overlaid images can then be visualized in the Icy software or exported in the desired format.

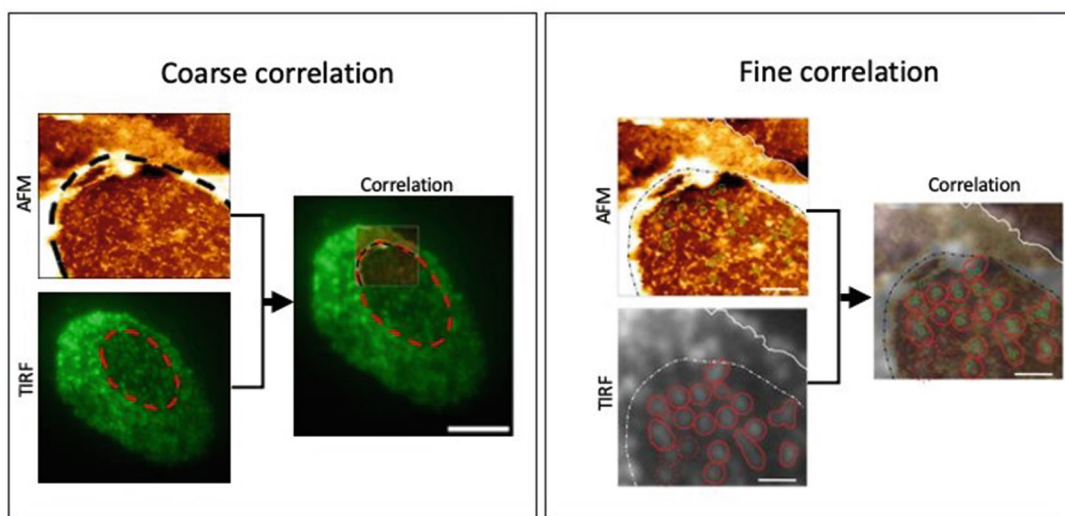


**Fig. 7** AFM/TIRF correlation. (*Left*) The border of the hole in the nucleus is delineated in black on the AFM scan and in red in the TIRF image. Alignment of this border helps aligning coarsely the AFM scanned area on the TIRF image. The color range for the AFM image is 0–300 nm, and the scale bar is 5  $\mu\text{m}$ . (*Right*) NPCs are contoured in red on the TIRF image. Due to the diffraction limit, individual NPCs may not always be resolvable; in such cases, clusters of NPC islands are delineated. In the AFM image, NPC rings are contoured in green. The distribution pattern of the NPCs helps verify or refine the correlation between the two images. However, this correlation is not perfect: some fluorescent NPCs are not detected in the AFM image, indicated by dashed contours. This discrepancy can result from poor AFM image quality in specific areas or contaminating membrane debris covering the NPCs. Significant drift during AFM scanning can cause deformation along the slow scanning axis, leading to misalignment over the entire field of view. In such cases, a transformation matrix, such as the one provided by the ec-CLEM plugin in Icy, may be necessary. The color range for the AFM image is 0–300 nm, and the scale bar is 2  $\mu\text{m}$ . (Data used for this figure were already published in Nanoscale [9])

## 4 Notes

1. High-quality glass is extremely important for SMLM.
2. As KOH reacts with glass, this solution should be stored in plastic bottles for long-term storage.
3. Buffers without DTT and Complete can be prepared in large quantities and stored as 30 mL aliquots at  $-20\text{ }^{\circ}\text{C}$ . DTT and Complete are added extemporaneously.
4. 1 mL Dounce tissue grinders can be found with different tube diameters. The nuclei extraction procedure described in this protocol is adapted to a tube diameter of 11 mm. Smaller diameters may require lower cell suspension volumes.
5. PFA should be handled under a fume hood and discarded in an appropriate container to be treated as chemical waste.

6. If you use PBS, make sure it does not contain  $Mg^{2+}$  ions as these will inhibit the trypsin activity.
7. Goat serum will serve as a blocking agent to reduce non-specific labeling. It can be replaced by other blocking agents such as bovine serum albumin (BSA) for instance. But note that detergents should be absolutely prohibited to preserve membrane integrity.
8. The organic dye should be compatible with dSTORM experiments. We usually use Alexa Fluor 647. Note that if another dye is used, the imaging buffers may be different or optimized.
9. Can be used if cells express proteins fused to SNAP- or HALO-tags.
10. The Attofluor cell chamber is modified, with the upper metallic part truncated to accommodate the JPK AFM head. Depending on the AFM microscope used, if the commercial Attofluor chamber is used, its large height might prevent engagement of the AFM tip on the surface since the Attofluor upper ring will touch first the AFM head.
11. This Gloxy buffer is optimized to promote stochastic blinking of Alexa Fluor 647 dyes, while preventing their photobleaching. However, different dyes might require other specific imaging buffers.
12. Fluorescent beads will help correct lateral drift happening during long acquisitions. This step is performed in the post-processing steps. However, drift can also be corrected in the absence of beads by cross-correlation.
13. A force curve length of a few hundreds of nanometers (typically 200–300 nm) is necessary to achieve proper imaging in off-resonance force curve-based imaging modes like JPK QI or Bruker PeakForce. Other similar modes based on photothermal-induced tip movement might not be able to reach this length and thus not be suited for such imaging.
14. Water bath at 37 °C can be used; however, it is sometimes a source of contamination. We usually have the media warm up at room temperature for 1 h before cell preparation.
15. The number of cells to add per flask needs to be adjusted depending on the cell line used.
16. Acetone should be manipulated under a fume hood and collected in an appropriate container to be treated as chemical waste.
17. KOH should be collected in an appropriate container to be treated as chemical waste.
18. Another option is to dry the coverslips under air flow or any inert gas flow.

19. If coverslips are not used right after cleaning, they can be stored in ethanol or Milli-Q water for a few days.
20. At least 40 million cells are needed to have a good quality of nuclei preparation.
21. This rinsing step with Hypotonic Buffer is crucial to remove all traces of salt present in the PBS.
22. The volume you use to resuspend the pellet needs to be adjusted both depending on the volume, geometry of the Dounce, and the number of cells you started with since the more concentrated the cell suspension, the more efficient the cell lysis will be. Moreover, the total volume (cells + buffer) should be large enough to ensure that the course of the pestle within the suspension will be long enough to provide correct mechanical pressure.
23. The optimal number of strokes will depend on the cell density, force applied, and tight fitting of the pestle with the Dounce reservoir. This should be empirically determined. Note that excessive mechanical strokes will lead to nuclei breakage. The released chromatin will then tend to aggregate with intact nuclei, dramatically decreasing the quality of the nuclei preparation. With experience, the number of strokes to apply will be reproducibly identified.
24. Contact between air bubbles and nuclei promotes nuclei breakage.
25. Note that this optional clearing step will eliminate most remaining intact cells, but a number of nuclei will also be discarded. Importantly, nuclei in P2 are smaller than nuclei discarded in P1. The necessity of performing the clearing step should thus be carefully evaluated, depending on the performance of cell lysis and the benefit/risk of having a percentage of intact cells in the nuclei preparation. Extracted nuclei can usually be identified under the microscope and selected accordingly. However, proximity of intact cells can interfere with AFM imaging: indeed, if the cantilever contacts a neighboring intact cell—which is higher than nuclei—this will deteriorate the image quality of the target nucleus.
26. NE-A and NE-B can be prepared in large quantities without DTT and stored at  $-20^{\circ}\text{C}$  as 200, 800  $\mu\text{L}$  aliquots, respectively. DTT has to be added extemporaneously to reach 1 mM final concentration.
27. Chemical fixation is not mandatory: as nuclei are open, immuno-labeling is performed without permeabilization, which is compatible with unfixed samples. However, chemical fixation stabilizes the samples for up to 4–5 days. Otherwise, imaging should be performed within 24 h or significant deterioration will be observed.

28. In order to preserve the 3D architecture of the nuclei, it is advised to avoid hardening mounting media. We usually use Vectashield (VectorLabs).
29. Intact nuclei can be easily located thanks to their distinctive phase contrast. For open nuclei their lower phase contrast makes it difficult to find them in brightfield. Visualization with fluorescence is thus recommended. If the cell line you are using has a nuclear protein genetically fused to a fluorescent protein, it is recommended to use it to find the nuclei instead of the dSTORM fluorophore. Otherwise, decrease the laser power to avoid photobleaching of the dSTORM fluorophore.
30. In our experience, Bruker MSNL-E with nominal spring constant of 0.1 N/m, nominal tip radius of 2 nm, and Olympus OTR4 cantilever with nominal spring constant of 0.08 N/m and nominal tip radius of 7 nm are the best suited for high-resolution AFM images of nuclear envelopes but other probes like, for example, Nanosensors qp-BioT and qp-BioAC, can also be used.
31. The optical image can be either a brightfield image, a fluorescence TIRF image or the reconstructed dSTORM image. The image pixel size on the camera must have been calibrated prior to the experiment for accurate correlation for every objective used. Other image alignment processes can be used like AFM tip registration where the tip position is pinpointed directly, but this method is less accurate in our opinion.
32. Most acquisitions are split in separate files due to size limitation. First concatenate the files into a single stack using the FiJI > Image > Stacks > Tools > Concatenate menu.
33. In some rare cases, drift correction by cross-correlation does not work properly on unfiltered localizations. In this case, it is worth trying again after filtering.
34. Refer to the application note by JPK/Bruker Nano GmbH ([https://www.bruker.com/en/products-and-solutions/microscopes/bioafm/resource-library/determining-the-elastic-modulus-of-biological-samples-using-the-atomic-force-microscope/\\_jcr\\_content/root/sections/section/sectionpar/twocolumns/contentpar-2/calltoaction.download-asset.pdf/primaryButton/jpk-app-elastic-modulus.14-1.pdf](https://www.bruker.com/en/products-and-solutions/microscopes/bioafm/resource-library/determining-the-elastic-modulus-of-biological-samples-using-the-atomic-force-microscope/_jcr_content/root/sections/section/sectionpar/twocolumns/contentpar-2/calltoaction.download-asset.pdf/primaryButton/jpk-app-elastic-modulus.14-1.pdf)).
35. Ec-CLEM is a plugin developed for Correlative Light and Electron Microscopy (CLEM) to correlate EM and fluorescence microscopy images. Since the problem is the same as in AFM/Fluorescence correlative microscopy, this plugin can be used by replacing the EM image by an AFM image. It is important that the image with the largest pixel size will have its size modified in the Icy software.

36. To properly correlate the optical and AFM images, it is important to visualize at least partially the border of the nucleus, or its opening. However, these areas are often the steepest and the most difficult to image in AFM and often result in AFM tip contamination. We recommend limiting the time spent imaging these areas to the minimum necessary for rough correlation.

---

## Acknowledgments

We thank L. Costa for inspiring discussions about AFM imaging and analysis, and E. Margeat, J.B. Fiche, and A. Le Gall for their contribution to building and maintaining the TIRF microscope. We thank A. Gehin and E. Margeat for critically reading this manuscript. The CBS is a member of the France-BioImaging (FBI) and the French Infrastructure for Integrated Structural Biology (FRISBI), two national infrastructures supported by the French National Research Agency (ANR-10-INBS-04-01 and ANR-10-INBS-05, respectively). This work was supported by a grant from the French Research Agency (ANR-16-CE11-0004-01) and a Plan Cancer 2016 Equipment grant. E. Costes is supported by a fellowship from the French Research Ministry.

## References

1. Mosalaganti S, Obarska-Kosinska A, Siggel M et al (2022) AI-based structure prediction empowers integrative structural analysis of human nuclear pores. *Science* 376:eabm9506
2. Zhu X, Huang G, Zeng C et al (2022) Structure of the cytoplasmic ring of the *Xenopus laevis* nuclear pore complex. *Science* 376:eabl8280
3. Schwartz TU (2022) Solving the nuclear pore puzzle. *Science* 376(6598):1158–1159
4. Bley CJ, Nie S, Mobbs GW et al (2022) Architecture of the cytoplasmic face of the nuclear pore. *Science* 376:eabm9129
5. Petrovic S, Samanta D, Perriches T et al (2022) Architecture of the linker-scaffold in the nuclear pore. *Science* 376:eabm9798
6. Fontana P, Dong Y, Pi X et al (2022) Structure of cytoplasmic ring of nuclear pore complex by integrative cryo-EM and AlphaFold. *Science* 376:eabm9326
7. Stanley GJ, Fassati A, Hoogenboom BW (2018) Atomic force microscopy reveals structural variability amongst nuclear pore complexes. *Life Sci Alliance* 1:e201800142
8. Sabinina VJ, Hossain MJ, Hériché J-K et al (2021) Three-dimensional superresolution fluorescence microscopy maps the variable molecular architecture of the nuclear pore complex. *Mol Biol Cell* 32:1523–1533
9. Vial A, Costa L, Dosset P et al (2023) Structure and mechanics of the human nuclear pore complex basket using correlative AFM-fluorescence superresolution microscopy. *Nanoscale* 15: 5756–5770
10. Dahmane S, Doucet C, Le Gall A et al (2019) Nanoscale organization of tetraspanins during HIV-1 budding by correlative dSTORM/AFM. *Nanoscale* 11:6036–6044
11. Jarnik M, Aeby U (1991) Toward a more complete 3-D structure of the nuclear pore complex. *J Struct Biol* 107:291–308
12. Rangl M, Nevo R, Lashkovich I et al (2011) Stable, non-destructive immobilization of native nuclear membranes to micro-structured PDMS for single-molecule force spectroscopy. *ChemPhysChem* 10:1553–1558
13. Enss K, Danker T, Schlune A et al (2003) Passive transport of macromolecules through *Xenopus laevis* nuclear envelope. *J Membr Biol* 196:147–155

14. Shahin V, Albermann L, Schillers H et al (2005) Steroids dilate nuclear pores imaged with atomic force microscopy. *J Cell Physiol* 202:591–601
15. Allen TD, Rutherford S, Murray S et al (2007) A protocol for isolating *Xenopus oocyte* nuclear envelope for visualization and characterization by scanning electron microscopy (SEM) or transmission electron microscopy (TEM). *Nat Protoc* 2:1166–1172
16. Schuller AP, Wojtynek M, Mankus D et al (2021) The cellular environment shapes the nuclear pore complex architecture. *Nature* 598:667–671
17. Schindelin J, Arganda-Carreras I, Frise E et al (2012) Fiji: an open-source platform for biological-image analysis. *Nat Methods* 9: 676–682
18. Ovesný M, Křížek P, Borkovec J et al (2014) ThunderSTORM: a comprehensive ImageJ plug-in for PALM and STORM data analysis and super-resolution imaging. *Bioinformatics* 30:2389–2390
19. de Chaumont F, Dallongeville S, Chenouard N et al (2012) Icy: an open bioimage informatics platform for extended reproducible research. *Nat Methods* 9:690–696
20. Heiligenstein X, Paul-Gilloteaux P, Raposo G et al (2017) eC-CLEM: a multidimension, multimodel software to correlate intermodal images with a focus on light and electron microscopy. *Methods Cell Biol* 140:335–352
21. Nečas D, Klapetek P (2012) Gwyddion: an open-source software for SPM data analysis. *Open Phys* 10:181–188
22. Shimi T, Kittisopikul M, Tran J et al (2015) Structural organization of nuclear lamins A, C, B1, and B2 revealed by superresolution microscopy. *Mol Biol Cell* 26:4075–4086
23. Kittisopikul M, Virtanen L, Taimen P et al (2019) Quantitative analysis of nuclear lamins imaged by super-resolution light microscopy. *Cells* 8(4):361
24. Davis LI, Blobel G (1986) Identification and characterization of a nuclear pore complex protein. *Cell* 45:699–709
25. Aris JP, Blobel G (1989) Yeast nuclear envelope proteins cross react with an antibody against mammalian pore complex proteins. *J Cell Biol* 108:2059–2067
26. Vogelsang J, Steinhauer C, Forthmann C et al (2010) Make them blink: probes for super-resolution microscopy. *ChemPhysChem* 11: 2475–2490
27. Finan K, Flottmann B, Heilemann M (2013) Photoswitchable fluorophores for single-molecule localization microscopy. *Methods Mol Biol* 950:131–151
28. Vaughan JC, Jia S, Zhuang X (2012) Ultra-bright photoactivatable fluorophores created by reductive caging. *Nat Methods* 9:1181–1184
29. Nahidiazar L, Agronskaia AV, Broertjes J et al (2016) Optimizing imaging conditions for demanding multi-color super resolution localization microscopy. *PLoS One* 11:e0158884
30. Proksch R, Schäffer TE, Cleveland JP et al (2004) Finite optical spot size and position corrections in thermal spring constant calibration. *Nanotechnology* 15:1344
31. Sage D, Pham T-A, Babcock H et al (2019) Super-resolution fight club: assessment of 2D and 3D single-molecule localization microscopy software. *Nat Methods* 16:387–395
32. Sneddon IN (1965) The relation between load and penetration in the axisymmetric boussinesq problem for a punch of arbitrary profile. *Int J Eng Sci* 3:47–57



# Chapter 5

## Fast Super-Resolution Live Cell Imaging of Nuclear Membrane-Endoplasmic Reticulum Dynamics

Swapnil Sahoo  and Abdur Rahaman 

### Abstract

The nuclear membrane undergoes continuous remodelling during the life cycle of all eukaryotic cells. The endoplasmic reticulum remains continuous with the nuclear membrane and regulates this nuclear remodeling process. Here in this chapter, we describe in detail a protocol for high-speed imaging of nuclear membrane/endoplasmic reticulum dynamic structure in live cell using fluorescent endoplasmic reticulum resident marker (GFP-KDEL). We used super-resolution microscope to capture this dynamic event. This protocol will help visualize the dynamic changes in nuclear membrane/endoplasmic reticulum structure at different cell cycle stages and understand the role of various cellular factors in this process.

**Key words** Nuclear membrane, Endoplasmic reticulum, Super-resolution, High-speed imaging, Live cell imaging

---

### 1 Introduction

Nuclear envelope (NE) is a double membrane structure and acts as a physical barrier between the nucleoplasm and cytoplasm that protects the genetic material from cytosolic exposure [1]. It is a highly dynamic structure and undergoes continuous remodelling [1, 2]. In higher eukaryotes, though nuclear envelope breaks down and reforms during cell division, it expands during interphase to accommodate increased nuclear volume [1, 3]. Lower eukaryotes such as yeast and ciliates undergo closed mitosis and involve nuclear expansion during cell division [4, 5].

NE is continuous with endoplasmic reticulum (ER) and depends on it for membrane components necessary for maintaining

---

**Supplementary Information** The online version contains supplementary material available at [https://doi.org/10.1007/978-1-0716-4714-1\\_5](https://doi.org/10.1007/978-1-0716-4714-1_5).

Yuki Hara and Kazunori Kume (eds.), *The Nuclear Membrane: Methods and Protocols*, Methods in Molecular Biology, vol. 2958, [https://doi.org/10.1007/978-1-0716-4714-1\\_5](https://doi.org/10.1007/978-1-0716-4714-1_5),  
© The Author(s), under exclusive license to Springer Science+Business Media, LLC, part of Springer Nature 2025

dynamic nuclear membrane structure [5–7]. The physical continuity and functional integration of ER with nuclear membrane are critical for maintaining cellular homeostasis and defect of which results in various pathophysiological disorders [8, 9].

*Tetrahymena* is a single-cell ciliate that harbors a transcriptionally silent germline micronucleus (MIC) and a phenotypically active macronucleus (MAC). In a particular stage of sexual reproduction (conjugation), the nuclear remodelling is profound where the small MIC expands many folds to generate new MAC [10]. This large change in nuclear membrane structure makes this organism a suitable model to study nuclear remodelling [11, 12].

In order to visualize the dynamic NE/ER structure in real time, we have employed super-resolution microscopy combined with high-speed image acquisition. This method is able to image dynamic NE/ER structure at high spatiotemporal resolution (100 nm spatial resolution and ~3.7 millisecond per frame time resolution) and thereby enable demonstration of fast nuclear remodelling events in real time (Fig. 1 and Movie 1).

Fluorescently labelled ER probes are often used to visualize NE/ER structure, many of which potentially interfere with the normal functioning of ER. For example, ER-Tracker dye available with many leading manufacturers (Invitrogen, Cell Signal Technologies, MedChemExpress, Lumiprobe, etc.) employs glibenclamide, which binds to sulfonylurea receptors of ATP-sensitive K<sup>+</sup> channels and alter ER function. Moreover, expression of this receptor in the cellular compartments other than ER in some specialized cells may lead to erroneous result. In *Tetrahymena*, exogenous dyes including ER tracker are accumulated in food vacuoles and give high-intensity fluorescence, thereby interfering with capturing the specific NE/ER signal in live cells. In order to circumvent this problem, a tetra-peptide (KDEL) fused at the C-terminus of a secretory fluorescent protein targeted to the lumen of ER is routinely used to observe NE/ER structure [13–15]. Though this method has been developed using *Tetrahymena* cell, it can be easily adopted for any eukaryotic cell that is tractable for transgene expression.

---

## 2 Materials

Prepare all the solutions in autoclaved Milli-Q water and molecular-grade reagents. We store the reagents at –20 °C unless mentioned otherwise.

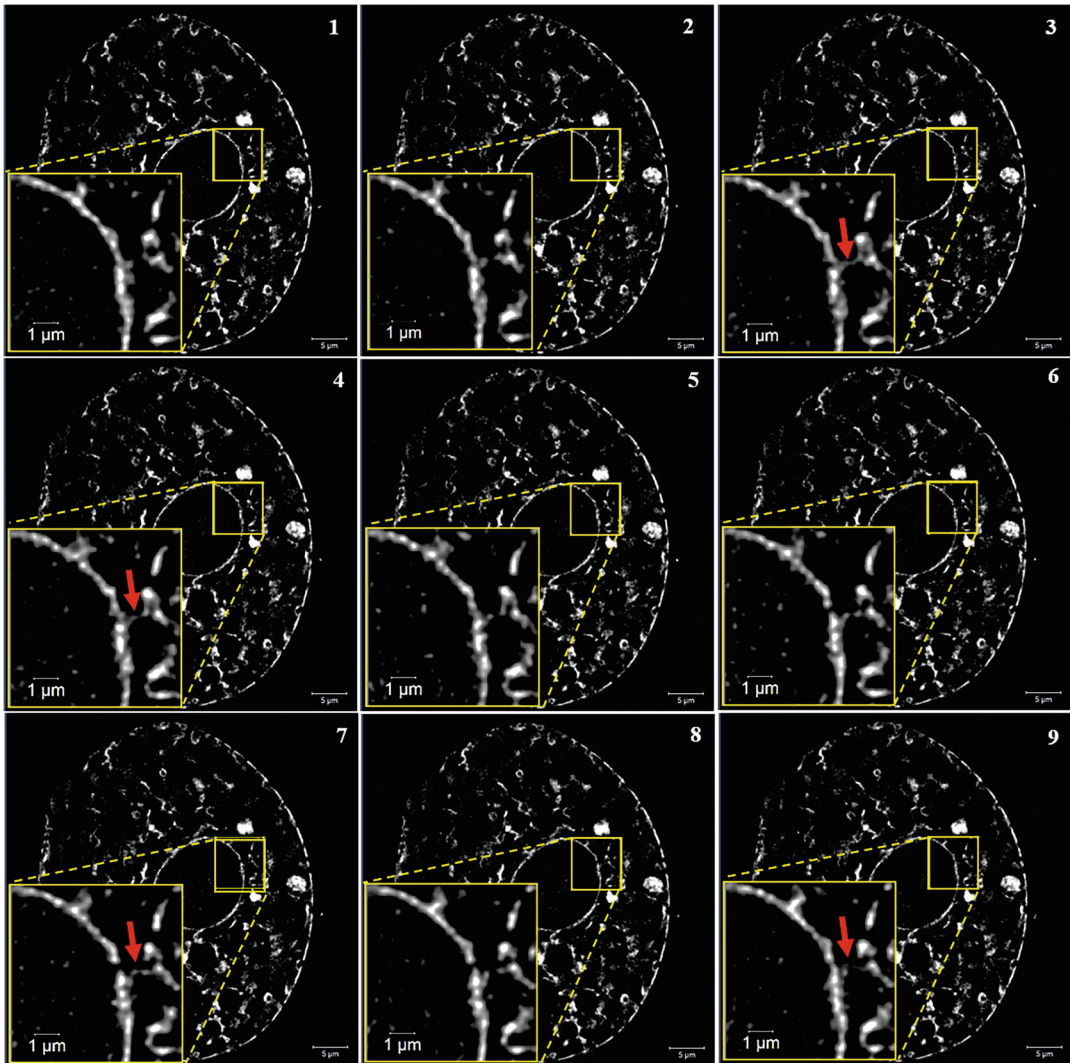


**Fig. 1** Fast live cell imaging of nuclear membrane/endoplasmic reticulum dynamics by super-resolution microscopy. High-speed super-resolution imaging of a live *Tetrahymena* cell expressing an ER marker (GFP-KDEL) was performed at 270 frames per second, and a movie at 15 frames per second is generated (Movie 1a). A part of the movie is cropped and the zoomed in version is shown in Movie 1b. Nine consecutive frames (collected at an interval of ~3.7 milliseconds) from the movie are presented here to visualize the ER/NE dynamics. The ER connection with nuclear envelope is indicated by a red arrow inside the enlarged yellow-boxed region. Appearance of a distinct connection of ER with NE can be seen in frame number 3, which starts disappearing in frame number 4, again reappearing in frame number 7. This imaging at high spatial and temporal resolution allows capturing the dynamic appearance and reappearance of ER-NE connections

## 2.1 *Tetrahymena* Culture

Prepare the media in Milli-Q water, autoclave for 40 min, and store at room temperature. Following are the composition of various media used:

1. *Tetrahymena* cells (B2086 or CU428).
2. *Tetrahymena* growth media (SPP): 2% proteose peptone (Gibco), 0.2% glucose (Sigma), 0.1% yeast extract (Gibco), and 0.003% ferric EDTA (Sigma) (*see Note 1*).
3. *Tetrahymena* starvation media (DMC medium): 0.17 mM sodium citrate, 0.1 mM  $\text{NaH}_2\text{PO}_4$ , 0.1 mM  $\text{Na}_2\text{HPO}_4$ , 0.65 mM  $\text{CaCl}_2$ , 0.1 mM  $\text{MgCl}_2$  (*see Note 2*).
4. PSA: Antimicrobial and antifungal cocktail containing penicillin, streptomycin, and amphotericin B (Hi-Media). The SPP media is always supplemented with PSA.
5. Selection media: SPP media supplemented with 60  $\mu\text{g}/\text{mL}$  blasticidin and 1  $\mu\text{g}/\text{mL}$   $\text{CdCl}_2$ .
6. Incubator: New Brunswick Innova 42 incubator shaker.
7. Centrifuge device: Thermo Scientific Sorvall Legend XTR centrifuge equipped with TX-750 swinging bucket rotor and 50 mL tube adaptors.
8. Centrifuge tubes: Nalgene PC Conical-Bottom Centrifuge Tubes. It is advisable to these tubes to pellet *Tetrahymena* cells to avoid cell loss.
9. Culture flask: Borosil Erlenmeyer (Conical) Flask with screw cap.

## 2.2 *Biolistic* Transformation

1. GFP-KDEL *ncvB* expression construct (*see Note 3*).
2. Particle delivery system: Bio-Rad PDS-1000 | He System.
3. Accessories: Bio-Rad Gold Microcarriers 1  $\mu\text{m}$  in 50% glycerol, macrocarriers, macrocarrier holders, 900 psi rupture discs, stopping screen.
4. Spermidine: A stock of 0.1 M spermidine in water, and store aliquots of 100  $\mu\text{L}$  at  $-20^\circ\text{C}$ .
5. Calcium chloride: A stock of 2.5 M calcium chloride solution in Milli-Q water and store at  $-20^\circ\text{C}$ .
6. Glass petri plates: Glass petri plates compatible with the Bio-Rad system with Whatman paper #1 inside it. Wrap it with aluminum foil and sterilize by autoclaving.
7. Blasticidin S hydrochloride: A stock of 30  $\text{mg}/\text{mL}$  Blasticidin S (Sigma) in autoclaved Milli-Q water. Sterilize this solution by passing it through 0.2  $\mu\text{m}$  filter, and store aliquots of 50  $\mu\text{L}$  at  $-20^\circ\text{C}$ .

8. Cadmium chloride ( $\text{CdCl}_2$ ): A stock of 1 mg/mL cadmium chloride (Sigma) in autoclaved Milli-Q water and sterilize the solution using 0.2  $\mu\text{m}$  filter.
9. 96-well plate.
10. 24-well plate.

### 2.3 Super-Resolution Observation

1. Microscope (Zeiss SIM<sup>2</sup> Elyra 7 microscope; FSet77 HE triple band filter for visualization, laser line: 488 nm for acquisition of images).
2. Micro-centrifuge tube.
3. Glass slides (25.4 mm  $\times$  76.2 mm, thickness, 1–1.2 mm).
4. Cover glass (18 mm  $\times$  18 mm, No. 1.5).
5. Petroleum jelly (we used Vaseline).

---

## 3 Methods

### 3.1 *Tetrahymena* Culturing and Starvation

1. Culture *Tetrahymena* cells (B2086 or CU428) in SPP media at 30 °C under shaking at 90 rpm till the required density ( $3 \times 10^5$  cells/mL) is reached.
2. Centrifuge the culture at 1200  $g$  for 1 min.
3. Wash the cells twice with DMC media.
4. Resuspend the cell pellet with DMC media (same volume as the initial culture).
5. Starve the cells in 1000 mL flask for 16–18 h at 30 °C under shaking (90 RPM) (*see* **Notes 4** and **5**).

### 3.2 Biolistic Transformation

This procedure of biolistic transformation of *Tetrahymena thermophila* is adapted from the methods by *Chalker et al.* [16].

#### 3.2.1 Particle Preparation

1. Weigh about 60 mg gold microparticles in a low-retention tube.
2. Add 1 mL of freshly prepared 70% molecular-grade ethanol.
3. Vortex it for 3–5 min and incubate for 15 min in room temperature.
4. Centrifuge at 1000  $g$  for 5 s to pellet the microparticles and discard the supernatant.
5. Repeat **steps 2–4** thrice.
6. Add 1 mL of sterile water to the pellet and then allow it to settle for 1 min.
7. Spin the tube at 1000  $g$  for 3 s to pellet the microparticles and discard the supernatant.
8. Resuspend the microparticles in 1 mL of 50% glycerol, and make aliquots of 50  $\mu\text{L}$  to be stored at  $-20$  °C.

### 3.2.2 Particle Coating

Perform all the steps of particle coating at 4 °C, unless mentioned otherwise.

1. Recover one tube containing 50 µL gold particle suspension from -20 °C and vortex for 15–20 min in the cold room (at 4 °C).
2. Keep three pipettes set at 12 µL (for DNA), 62.5 µL (for CaCl<sub>2</sub>), and 32.5 µL (for spermidine).
3. Add 12 µL of digested DNA, 62.5 µL of CaCl<sub>2</sub> and 32.5 µL of spermidine with 5 s interval in the sequence mentioned.
4. Continue vortexing for another 10 min.
5. Spin the coated particles at 1000 *g* for 5 s in room temperature. Discard the supernatant.
6. Add 150 µL of 70% ethanol through the wall of the tube, and follow the preceding step (**step 5**).
7. Repeat **step 6** with 100% ethanol.
8. Resuspend the coated particles in 40 µL of 100% ethanol to be used for transformation.

### 3.2.3 Biolistic Bombardment

1. Keep all the accessories required for gene gun, as mentioned in Subheading 2.2, inside the laminar hood.
2. Mix the coated particles vigorously by tapping. Dispense 10 µL of this suspension on the macro-carrier, and let it dry completely, preferably by placing it inside desiccator.
3. Add ~1 mL of DMC to the Whatman paper placed in the glass petri plate. Remove any air bubble from the Whatman paper using sterile forceps.
4. Take 50 mL of SPP media supplemented with PSA in 250 mL flask.
5. Collect the starved cells ( $\sim 2 \times 10^5$  cells/mL) from the incubator and spin at 1100 *g* for 1 min in a 50 mL Nalgene conical bottom centrifuge tube.
6. Discard the supernatant, and resuspend the cell pellet with 500 µL of DMC media.
7. Spread the resuspended cells at the center of Whatman paper.
8. Assemble all the components such as rupture disc, stopping screen, and macro-carrier, and place the petri plates with the cells inside the chamber before the bombardment.

### 3.2.4 Recovery of Transformants

1. Collect the bombarded cells with 1 mL of SPP media, transfer it to 50 mL of SPP media, and incubate overnight at 25 °C without shaking.

2. To obtain the transformant, add blasticidin (60  $\mu\text{g}/\text{mL}$ ) and  $\text{CdCl}_2$  (1  $\mu\text{g}/\text{mL}$ ) to transformed cells before transferring to a sterile 96-well plate (125  $\mu\text{L}/\text{well}$ ) (*see* **Note 6**).
3. Incubate the plate at 30 °C (*see* **Note 7**).
4. Monitor the plate to select the transformant (generally we obtain the transformant within a week. But sometime it may take up to 2 weeks).
5. Once the well is confluent with healthy dividing cells, transfer about 50  $\mu\text{L}$  of culture to 1 mL selection media in a sterile 24-well plate.
6. Passage the culture for two to three times in the selection media (*see* **step 5** in Subheading 2.1) before checking the expression.
7. To check the expression, inoculate the transformant in SPP media.
8. Induce the expression by adding 2  $\mu\text{g}/\text{mL}$   $\text{CdCl}_2$  to the culture ( $0.25 \times 10^5$  cells/mL), and incubate for 3 h before checking the expression.
9. Check the expression using a fluorescence microscope (Ex/Em of 488/512).
10. Select transformant that expresses GFP-KDEL and maintain in the selection media at room temperature (*see* **Note 8**).

### 3.3 Super-Resolution Microscopy

1. Express GFP-KDEL as mentioned in the above section except use 0.5  $\mu\text{g}/\text{mL}$   $\text{CdCl}_2$  (*see* **Note 9**).
2. Centrifuge 1.5 mL culture at 1200 *g* for 2 min in a micro-centrifuge tube.
3. Remove the media leaving around 30  $\mu\text{L}$  to resuspend the cell pellet.
4. Remove the dust particle from the slide and cover glass with 70% ethanol by using nonabrasive lint-free paper.
5. Apply petroleum jelly on the four corners of a cover glass (18 mm  $\times$  18 mm) (*see* **Note 10**).
6. Take 4  $\mu\text{L}$  of cell suspension on a slide, and place the cover glass on the drop without introducing any air bubble.
7. Gently press the four corners of the cover glass such that the drop spreads uniformly.
8. Place the slide onto the microscope slide holder for imaging in a Zeiss SIM<sup>2</sup> Elyra 7 microscope.
9. Start the Zeiss ZEN-Black application.
10. Use FSet77 HE triple band filter within “*Locate*” tab to visualize the fluorescence and adjust the focus.

11. Switch to “*Acquisition*” tab and set the parameters: (*see Note 11*).
12. *Laser*: Switch on 488 nm laser line.
13. *Imaging setup*: Switch to Apotome mode. Select the 1× lens and BP-495-550 + BP 570–620 filter.
14. *Acquisition mode*: Select Plan Apochromat 63×/1.4NA objective. Set frame size to 512 × 512 (X\*Y) (*see Note 12*). Make sure that averaging number is 1, bit-depth is 8 bit, and grating is set to three phases.
15. *Channels*: Add one track and switch on 488 nm laser line. Set the exposure time to 1 ms. Adjust the laser power such that the intensity value is ~1000.
16. *Time series*: Set cycles as per the requirement (*see Note 13*) and interval to 0.0 ms.
17. Click on *Start Experiment* to begin acquisition.
18. After acquisition is over, switch to the “*Processing*” Tab and set parameters.
19. *Method*: Select SIM.
20. *Method Parameters*: Select the acquired image. Tick mark the *SIM*<sup>2</sup> and *Burst Mode* (*see Note 14*).
21. Click on “*Apply*” to process the acquired data.

---

## 4 Notes

1. *Tetrahymena* is highly sensitive to detergent in the culture media. To ensure complete removal of detergent, the flasks must be properly washed with bleach, detergent, and 70% ethanol and left with water overnight. We then autoclave the culture flasks for 20 min before the final autoclave of SPP media which is for 40 min.
2. To prepare DMC, add all the components except CaCl<sub>2</sub> and MgCl<sub>2</sub> to autoclaved Milli-Q water. Prepare separate stock solutions for CaCl<sub>2</sub> and MgCl<sub>2</sub>. Autoclave each of these solutions for 40 min, and cool it before adding CaCl<sub>2</sub> and MgCl<sub>2</sub>. One can also use 10 mM Tris, pH 7.5 for starvation in place of DMC.
3. The *ncvB* vector used here was originally developed by Bowman et al. [17]. Take about 20 µg of GFP KDEL *ncvB* plasmid, and linearize it with Sfi I restriction enzyme. Use this linearized fragment containing GFP KDEL for biolistic transformation. GFP KDEL is integrated at the chromosomal *MTT1* locus of *T. thermophila* by homologous recombination [11, 18].

4. While starving the cells, we keep the culture volume as one tenth of the volume of the flask for better aeration. For example, we use 1000 mL flask to starve 100 mL culture. However, one fifth culture volume is used for growing *Tetrahymena* cells in SPP media.
5. For pelleting large volume of *Tetrahymena* culture, centrifuge in a swinging bucket rotor for maximum recovery.
6. We plate two different densities: aliquoting of transformed culture without dilution in one plate and a fivefold diluted culture in another. Add blasticidin (60  $\mu\text{g/mL}$ ) and  $\text{CdCl}_2$  (1  $\mu\text{g/mL}$ ) to culture before plating.
7. Place the 96-well plate in a moist chamber. The moisture can be maintained in a box by placing a petri plate containing autoclaved Milli-Q water without a lid. This ensures that the media does not dry up during prolonged incubation.
8. For short-term storage of transformant, incubate at room temperature and passage once in a week.
9. The density of the culture is important for optimal expression of GFP-KDEL. When expressed at high density ( $>1.5 \times 10^5$  cells/mL), a large number of food vacuoles appear which may interfere with the acquisition of the NE/ER dynamic structures. We found that a density of  $0.25 \times 10^5$  cells/mL is good for optimal imaging.
10. Using minimal amount of petroleum jelly ensures that the cells are immobilized between the glass slide and the cover glass. Using this method it can be imaged up to 30 min before the cells begin to burst. Pressing of the cover glass is important for effectively immobilizing the cells.
11. Snapshots of settings for acquisition and processing are provided in Fig. 2.
12. By reducing the frame size to  $256 \times 256$ , the temporal resolution can be further improved.
13. It should be noted that higher number of cycles may lead to excessive bleaching of the sample. Therefore, we take about 100 cycles per acquisition. However, this may vary from sample to sample.
14. *Burst mode* will only be highlighted if correct settings are used during the image acquisition.

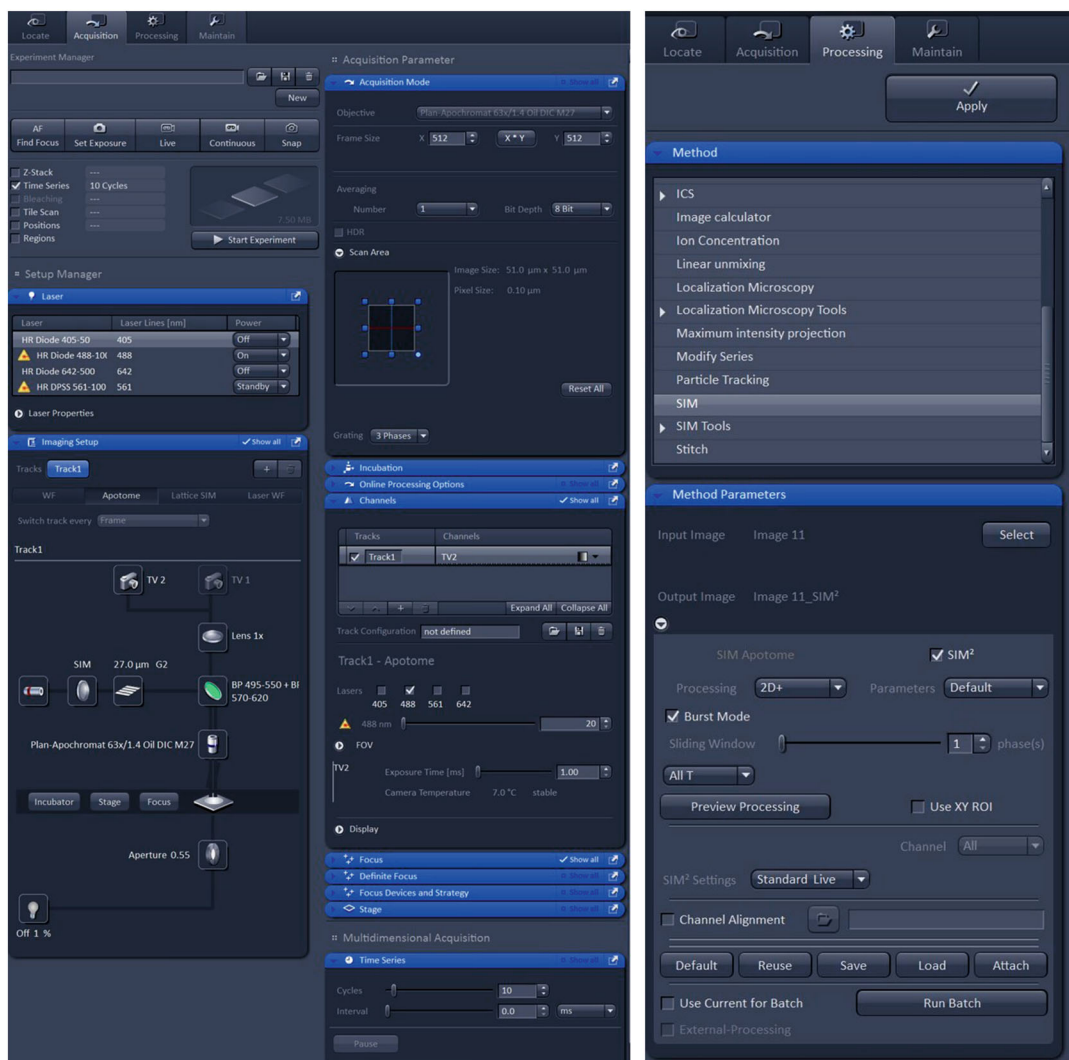


**Fig. 2** Snapshots showing parameters for image acquisition (left panel) and processing (right panel) in Zeiss ZEN-Black application

## Acknowledgments

We thank the imaging facility at School of Biological Sciences, NISER-Bhubaneswar.

## References

1. De Magistris P, Antonin W (2018) The dynamic nature of the nuclear envelope. *Curr Biol* 28(8):R487–R497
2. Dey G, Baum B (2021) Nuclear envelope remodelling during mitosis. *Curr Opin Cell Biol* 70:67–74
3. Zhironkina OA, Kurchashova SY, Pozhrsksaia VA et al (2016) Mechanisms of nuclear lamina growth in interphase. *Histochem Cell Biol* 145(4):419–432
4. Takemoto A, Kawashima SA, Li JJ et al (2016) Nuclear envelope expansion is crucial for proper chromosomal segregation during a closed mitosis. *J Cell Sci* 129(6):1250–1259
5. Barger SR, Penfield L, Bahmanyar S (2022) Coupling lipid synthesis with nuclear envelope remodeling. *Trends Biochem Sci* 47(1):52–65
6. Cooper G, Adams K (2022) *The cell: a molecular approach*. Oxford University Press
7. Pawar S, Ungricht R, Tiefenboeck P et al (2017) Efficient protein targeting to the inner nuclear membrane requires Atlastin-dependent maintenance of ER topology. *elife* 6:e28202
8. Rayavarapu S, Coley W, Nagaraju K (2012) Endoplasmic reticulum stress in skeletal muscle homeostasis and disease. *Curr Rheumatol Rep* 14(3):238–243
9. Ungricht R, Kutay U (2017) Mechanisms and functions of nuclear envelope remodelling. *Nat Rev Mol Cell Biol* 18(4):229–245
10. Ruchle MD, Orias E, Pearson CG (2016) Tetrahymena as a unicellular model eukaryote: genetic and genomic tools. *Genetics* 203(2):649–665
11. Rahaman A, Elde NC, Turkewitz AP (2008) A dynamin-related protein required for nuclear remodeling in Tetrahymena. *Curr Biol* 18(16):1227–1233
12. Kar UP, Dey H, Rahaman A (2021) Cardiolipin targets a dynamin-related protein to the nuclear membrane. *elife* 10:e64416
13. Carter SD, Hampton CM, Langlois R et al (2020) Ribosome-associated vesicles: a dynamic subcompartment of the endoplasmic reticulum in secretory cells. *Sci Adv* 6(14):eaay9572
14. Denecke JR, Rycke D, Botterman J (1992) Plant and mammalian sorting signals for protein retention in the endoplasmic reticulum contain a conserved epitope. *EMBO J* 11(6):2345–2355
15. Bannai H, Inoue T, Nakayama T et al (2004) Kinesin dependent, rapid, bi-directional transport of ER sub-compartment in dendrites of hippocampal neurons. *J Cell Sci* 117(Pt 2):163–175
16. Chalker DL (2012) Transformation and strain engineering of Tetrahymena. *Methods Cell Biol* 109:327–345
17. Bowman GR, Elde NC, Morgan G et al (2005) Core formation and the acquisition of fusion competence are linked during secretory granule maturation in Tetrahymena. *Traffic* 6(4):303–323
18. Cowan AT, Bowman GR, Edwards KF (2005) Genetic, genomic, and functional analysis of the granule lattice proteins in Tetrahymena secretory granules. *Mol Biol Cell* 16(9):4046–4060



# Chapter 6

## Immunostaining the Yeast Nuclear Membrane for Imaging by Super-Resolution Fluorescence Microscopy

Emily M. Sontag

### Abstract

The ability to image biological samples beyond the diffraction limit (super-resolution) has opened a world of new discoveries in molecular biology. Super-resolution fluorescence microscopy requires specific fluorophores that often require immunostaining with labeled antibodies to achieve the necessary parameters for imaging. Budding yeast *Saccharomyces cerevisiae* is a common model organism used in cell biology, genetics, and molecular biology. However, yeast are difficult to immunostain due to the cell wall that hinders antibody penetration. In this chapter, I describe the methods we use for immunostaining yeast to visualize the nuclear membrane with the necessary efficiency for imaging by super-resolution fluorescence microscopy. I discuss approaches and optimizations to prepare samples for different imaging techniques including Structured Illumination Microscopy (SIM) and Stochastic Optical Reconstruction Microscopy (STORM). Super-resolution imaging can then be used to determine the precise location of proteins within the nuclear membrane, or if perinuclear proteins reside inside or outside the nucleus. The methods can be extended to other techniques requiring antibody penetration into yeast cells.

**Key words** Super-resolution microscopy, SIM, STORM, Yeast, Nuclear membrane, Immunostaining, Antibody

---

### 1 Introduction

The nuclear membrane is a hotbed of cellular activities ranging from chromatin organization, regulation of gene expression, and DNA repair to regulation of nuclear-cytoplasmic trafficking and even quality control of mRNA and proteins. The outer nuclear membrane is continuous with the ER, is studded with ribosomes, and shares proteins with the ER [1–3]. The intermembrane space between the inner and outer nuclear membranes is connected to the lumen of the ER [1]. The inner and outer nuclear membranes are connected via nuclear pore complexes (NPC) and the linker of nucleoskeleton and cytoskeleton (LINC) complex [2, 3]. The inner nuclear membrane has a distinct proteome and lipid composition, including the presence of a specialized protein quality control

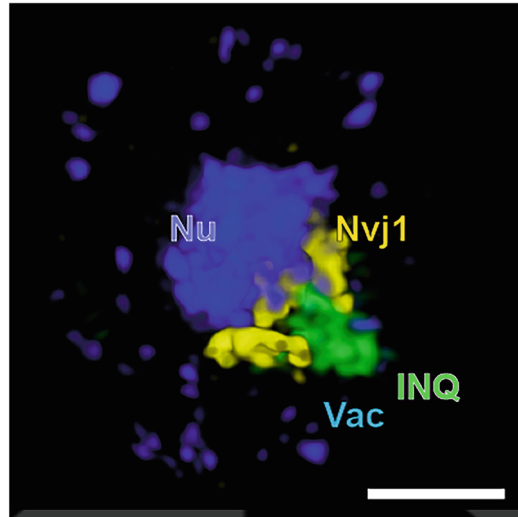


**Fig. 1** Representative SIM image of WT yeast cell co-expressing NLS-DsRed-Luciferase (green) with Nvj1-sfGFP (yellow) after 2 h incubation at 37 °C with 100  $\mu$ M MG132. The NLS-Luciferase inclusion can be seen extruding through the NVJ toward the vacuole. (Reproduced from [8] with permission)

system termed inner nuclear membrane-associated degradation (INMAD) that is analogous to ER-associated degradation (ERAD) [4, 5]. The storage for improperly assembled nuclear pore complexes (SINC) compartment is specialized for quality control of nuclear pore complexes in the nuclear envelope that may be degraded in the vacuole [6, 7]. Our recent work has highlighted another mechanism of protein quality control at the nuclear envelope that results in the removal of misfolded proteins from the nucleus by budding into the vacuole (Fig. 1) [8].

Budding yeast is frequently used as a model organism to study protein quality control mechanisms, including those at the nuclear envelope, due to the easy genetic manipulations, fast growth, and conservation of protein quality control systems between yeast and mammalian cells. Yeast lack lamin proteins, the intermediate filaments that form a meshwork of fibers on the inside of the inner nuclear membrane [9, 10]. Therefore, researchers must rely on visualizing components of the nuclear envelope to determine the boundary of the nucleus and resolve the location of a molecule of interest as inside or outside of the nucleus. One solution has been to rely on fluorescent protein tags on nuclear membrane proteins such as Heh1 or Pom33 to visualize the inner and outer nuclear membranes, respectively. Proteins localizing to the nuclear envelope can be found via the Yeast GFP Fusion Localization Database (YeastGFP) [11] hosted by the Saccharomyces Genome Database (SGD), and these GFP-tagged proteins are readily available through the Yeast GFP Clone Collection from Invitrogen.

Fluorescent protein tags do have limitations including rapid photobleaching, particularly the GFP-S65T variant used in the Yeast GFP Clone Collection, limited color palette, and the small number of blinking fluorophores for super-resolution techniques like Stochastic Optical Reconstruction Microscopy (STORM). In order to utilize Structured Illumination Microscopy (SIM) to pinpoint the precise location of protein quality control compartments within yeast, we needed fluorophores that could withstand thousands of images taken from multiple angles at each slice through the sample without photobleaching and introducing artifacts into the three-dimensional reconstruction of the cell. We chose to supplement the signal from the fluorescent protein tags with antibodies to the tags and to the Nsp1 nuclear pore complex protein to visualize the nuclear envelope as the boundary of the nucleus [8, 12]. Immunostaining yeast is very difficult due to the cell wall that inhibits antibody penetration into the center of the cell where the nuclear membrane often resides. We have therefore developed a protocol for high-quality immunostaining of yeast to enable the use of super-resolution microscopy techniques like SIM and STORM. This protocol can easily be adapted to other organisms with a cell wall, as well as other techniques that require antibody labeling of subcellular structures.

---

## 2 Materials

Prepare all solutions in ultrapure water using analytical grade reagents. Store all solutions at 4 °C unless otherwise specified. Follow all safety protocols for working with and disposing of hazardous materials, particularly the  $\text{NaN}_3$  and paraformaldehyde.

### 2.1 Preparing Cover Glass for Super-Resolution Imaging

1. High Precision #1.5H cover glass, any size (*see Note 1*).
2. 1 M HCl.
3. Forceps or tweezers for handling cover glass.
4. Glass petri dish (*see Note 2*).
5. Ultrapure water.
6. 70% ethanol.
7. Lint-free delicate task wipers (such as Kimwipes).
8. 0.1% (w/v) poly-L-lysine solution in  $\text{H}_2\text{O}$ .
9. Aluminum foil.

### 2.2 Harvesting and Fixing Cells

1. 16% paraformaldehyde.
2. Chilled methanol ( $-20\text{ }^\circ\text{C}$ ).
3. SHA buffer: 1 M sorbitol, 50 mM HEPES pH 6.8, 1 mM  $\text{NaN}_3$ .

**2.3 Spheroplasting**

1. SHA + 0.2%  $\beta$ -mercaptoethanol.
2. Zymolyase (Zymo prod # E1005).
3. SHA + 0.1% Triton X-100.

**2.4 Immunostaining Cells**

1. Blocking buffer: 1% nonfat dry milk, 0.5 mg/mL Bovine Serum Albumin, 200 mM NaCl, 50 mM HEPES-KOH pH 7.5, 1 mM  $\text{NaN}_3$ , 0.1% Tween-20.
2. Antibodies to antigens of interest (*see* **Notes 3–4**).
3. Fluorescently labeled secondary antibodies.
4. 0.1% Bovine Serum Albumin (BSA).
5. Phosphate buffered saline (PBS; 1X): 137 mM NaCl, 2.7 mM KCl, 10 mM  $\text{Na}_2\text{HPO}_4$ , 1.8 mM  $\text{KH}_2\text{PO}_4$ .
6. DNA stain (optional).
7. Aluminum foil (optional).
8. Multi-well plate (optional).

**2.5 Mount Cover Glass to Slides**

1. Microscope slides.
2. Mounting media (*see* **Note 5**).

**2.6 Structured Illumination Microscopy**

1. Optically matched objective oil (*see* **Note 6**).
2. 100 $\times$  objective (*see* **Note 7**).
3. Diode lasers and filter sets for the fluorophores used to label samples (*see* **Note 8**).
4. Three emCCD cameras (*see* **Note 9**).
5. Channel-specific optical transfer functions (OTF) and registration files (*see* **Note 10**).

---

**3 Methods**

All procedures are performed at room temperature unless otherwise indicated.

**3.1 Preparing Cover Glass for Super-Resolution Imaging**

1. Add 10 mL of 1 M HCl to a glass petri dish (*see* **Note 11**).
2. Place high-performance cover glass #1.5H into petri dish using forceps to ensure that the cover glass is in a single layer and not overlapping.
3. Incubate at room temperature for 4 h.
4. Carefully remove cover glass from the dish and wash 10 times with ultrapure  $\text{H}_2\text{O}$ . Rinses can be performed by holding cover glass with forceps over a sink and applying  $\text{H}_2\text{O}$  with a squeeze

bottle, or by dipping cover glass into a beaker of ultrapure H<sub>2</sub>O.

5. Wash cover glass five times with 70% ethanol by squeeze bottle or dipping.
6. Dry cover glass by touching a corner to a lint-free delicate task wiper to remove excess liquid.
7. Place cover glass between fresh task wipers until completely dry.
8. Add 50  $\mu$ L of poly-L-lysine solution to make a spot on the aluminum foil, one for each cover glass.
9. Place the clean, dry cover glass on top of the spot of poly-L-lysine solution so that the poly-lysine is spread evenly across the cover glass between the glass and the foil.
10. Incubate for 30 min at room temperature.
11. Wash cover glass with ultrapure H<sub>2</sub>O.
12. Dry as above in **steps 6–7** in Subheading **3.1**.
13. Store dry, coated cover glass in a protective box at 4 °C (*see Note 12*). Cover glass can be stored for several weeks.

### **3.2 Harvesting and Fixing Cells**

Obtain yeast to be visualized in an actively growing mid-log phase culture. Yeast from stationary phase cultures typically have altered cell walls that make spheroplasting and staining more difficult:

1. Add 16% paraformaldehyde directly to the yeast culture at a final concentration of 4% (*see Notes 13–14*).
2. Incubate for 15 min at room temperature. Do not exceed 20 min or the nucleus will become deformed and fluorescent protein tags can become denatured and decrease the fluorescent signal (*see Note 15*).
3. Pellet cells at 8000 $\times g$  for 30 s.
4. Remove and discard the supernatant according to safety procedures for using paraformaldehyde.
5. Resuspend cells in 1 mL of chilled methanol (–20 °C) for every 1 mL of initial culture.
6. Incubate samples for 20 min at –20 °C.
7. Pellet cells at 8000 $\times g$  for 30 s and discard the supernatant.
8. Resuspend in 1 mL of SHA buffer (*see Note 16*).

### **3.3 Spheroplasting**

1. Pellet cells at 8000 $\times g$  for 30 s and discard the supernatant.
2. Resuspend in 1 mL of SHA + 0.2%  $\beta$ -mercaptoethanol for every 1 mL of initial culture.
3. Add 25 units per mL Zymolyase (*see Note 17*).
4. Incubate at room temperature for 30 min with occasional mixing (*see Note 18*).

5. Pellet cells at  $1000\times g$  for 2 min at 4 °C and discard the supernatant (*see* **Notes 19–20**).
6. Resuspend in 500  $\mu\text{L}$  of SHA + 0.1% Triton X-100 for every 1 mL of initial culture (*see* **Note 21**).
7. Incubate for 10 min at room temperature.
8. Pellet cells at  $1000\times g$  for 2 min at 4 °C and discard the supernatant.
9. Resuspend in 250  $\mu\text{L}$  of SHA (*see* **Note 22**).

### **3.4 Immunostaining Cells**

Cells can be immunostained in suspension or after mounting to cover glass. Each method has advantages and disadvantages. Staining cells in suspension results in less background staining and typically has a greater number of cells with antibody labeling. However, staining in suspension uses more reagents including the expensive antibodies, has greater cell loss from frequent removal of supernatant, and has a risk of crushing the cells due to repeated centrifugation. Conversely, staining mounted samples uses less reagents with little cell loss or crushing from the centrifugation but often has higher background and fewer stained cells than when staining in suspension. A careful consideration of the nature of the yeast sample, for instance, having few or fragile cells, and the drawbacks of each method is necessary. Additionally, certain antibodies and dyes work better in suspension or on mounted samples, so optimization of individual reagents is often necessary to ensure the highest quality results. The Notes section highlights ways to improve staining and includes the tradeoffs of those modifications to consider.

#### **3.4.1 Staining Cells in Suspension**

1. Pellet cells at  $1000\times g$  for 2 min at 4 °C and discard the supernatant.
2. Resuspend in 500  $\mu\text{L}$  of blocking buffer (*see* **Note 23**).
3. Incubate at room temperature for 1 h with occasional gentle inversion to mix.
4. Pellet cells at  $1000\times g$  for 2 min at 4 °C and discard the supernatant.
5. Resuspend in 250  $\mu\text{L}$  of primary antibody in blocking buffer (*see* **Notes 24–26**).
6. Incubate cells at 4 °C overnight (*see* **Notes 27–28**).
7. Pellet cells at  $1000\times g$  for 2 min at 4 °C and discard the supernatant (*see* **Note 29**).
8. Wash cells five times in 500  $\mu\text{L}$  of cold blocking buffer. A wash is a gentle resuspension in blocking buffer followed by pelleting at  $1000\times g$  for 2 min at 4 °C (*see* **Notes 30–31**).

9. Resuspend cells in 250  $\mu\text{L}$  of secondary antibody in blocking buffer (*see* **Notes 32–33**).
10. Incubate cells at room temperature for 1 h with occasional gentle inversion to mix.
11. Pellet cells at  $1000\times g$  for 2 min at 4  $^{\circ}\text{C}$  and discard the supernatant.
12. Resuspend in DNA stain in blocking buffer if desired (*see* **Note 34**).
13. Incubate for 5 min at room temperature.
14. Pellet cells at  $1000\times g$  for 2 min at 4  $^{\circ}\text{C}$  and discard the supernatant.
15. Wash cells five times in 500  $\mu\text{L}$  of cold blocking buffer.
16. Resuspend in 250  $\mu\text{L}$  of 0.1% BSA (*see* **Note 35**).
17. Add an appropriate volume of sample to get good density of cells on the poly-lysine-coated coverslip (*see* **Notes 36–37**).
18. Incubate for 15 min at room temperature to allow the cells to settle and bind to the poly-lysine.
19. Aspirate the remaining liquid (*see* **Note 38**).
20. Wash cells with 1 mL of cold 1X PBS by flowing it across the adhered cells (*see* **Note 39**) (Fig. 2).

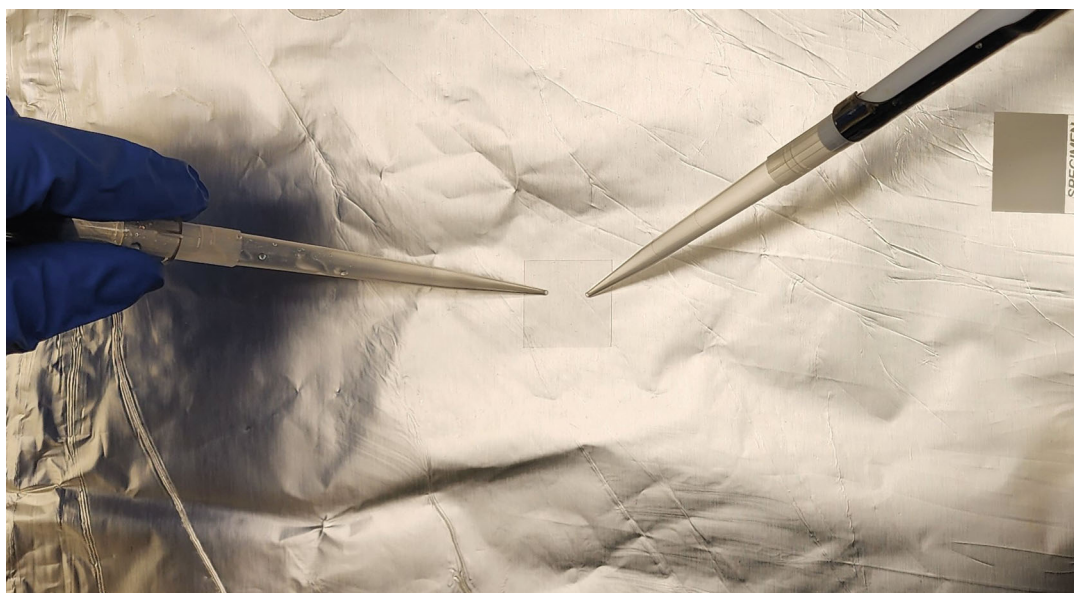


**Fig. 2** Image of washing cells on the cover glass. (a) Hold the micropipettor in one hand and vacuum in the other. (b) Flow the buffer out of the micropipettor, across the cells, and into the vacuum. Try to keep the flow rate constant so the cells do not dry or flood

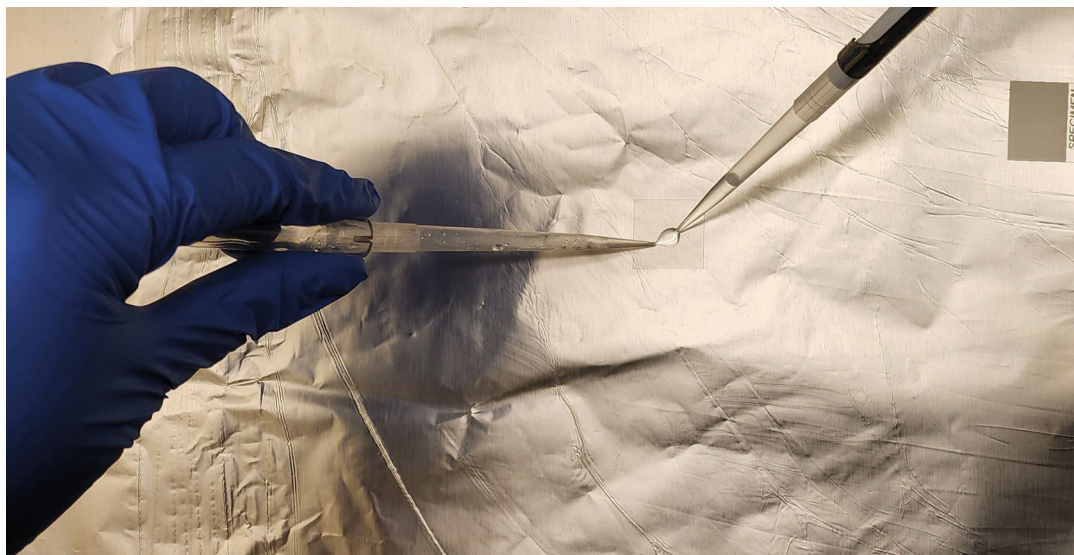


**Fig. 2** (continued)

### 3.4.2 Staining Cells on Coverslips/Slides

1. Adhere cells from **step 9** in Subheading [3.3](#) to poly-lysine-coated cover glass by adding an appropriate volume of sample to get good density of cells on the poly-lysine-coated coverslip (*see* **Notes 40–41**).
2. Incubate for 15 min at room temperature to allow the cells to settle and bind to the poly-lysine.
3. Aspirate the remaining liquid (*see* **Note 42**).
4. Block for 1–2 h in 0.1% BSA to prevent background binding to coverslip (*see* **Note 35**).
5. Follow the same protocol as above in **steps 5–15** in Subheading [3.4.1](#) except add 50  $\mu\text{L}$  of each solution to coverslips instead of resuspending cells in solutions. Solutions should be made with 0.1% BSA instead of blocking buffer (*see* **Notes 35 and 40**).

### 3.5 Mount Cover Glass to Slides

This section may be omitted if the microscopy technique requires access to the sample, i.e., STORM where the buffers must be changed to maximize blinking and minimize photobleaching:

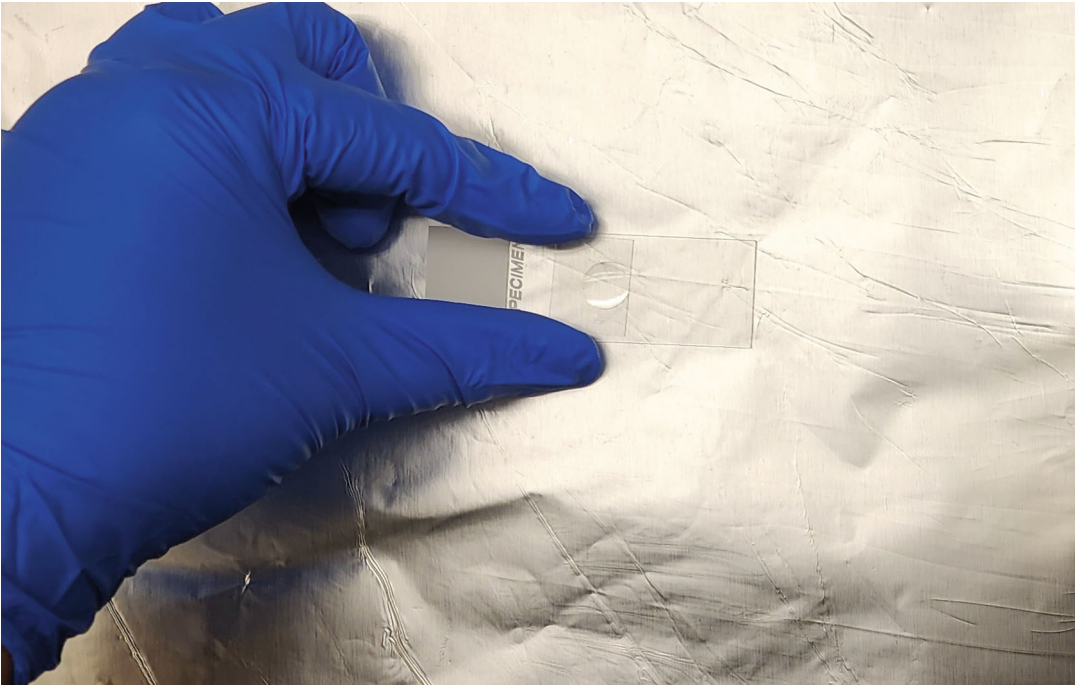
1. Apply sufficient amount of appropriate mounting media to the microscope slide to cover the sample, but not enough that excess media is outside of the cover glass. Minimize bubbles in mounting media when pipetting (*see* **Note 41**).
2. Invert the cover glass and place it on the mounting media with cells facing down into the media (*see* **Note 42**) (*Fig. 3a*).

3. Ensure that there are no bubbles in the mounting media. Bubbles can be removed by applying gentle pressure to the cover glass and moving the bubble out from under the cover glass (*see Note 43*) (Fig. 3b).
4. Allow slides to cure overnight at room temperature in the dark (*see Note 44*).
5. Seal coverslips to slides with nail polish or other sealant (*see Note 45*).

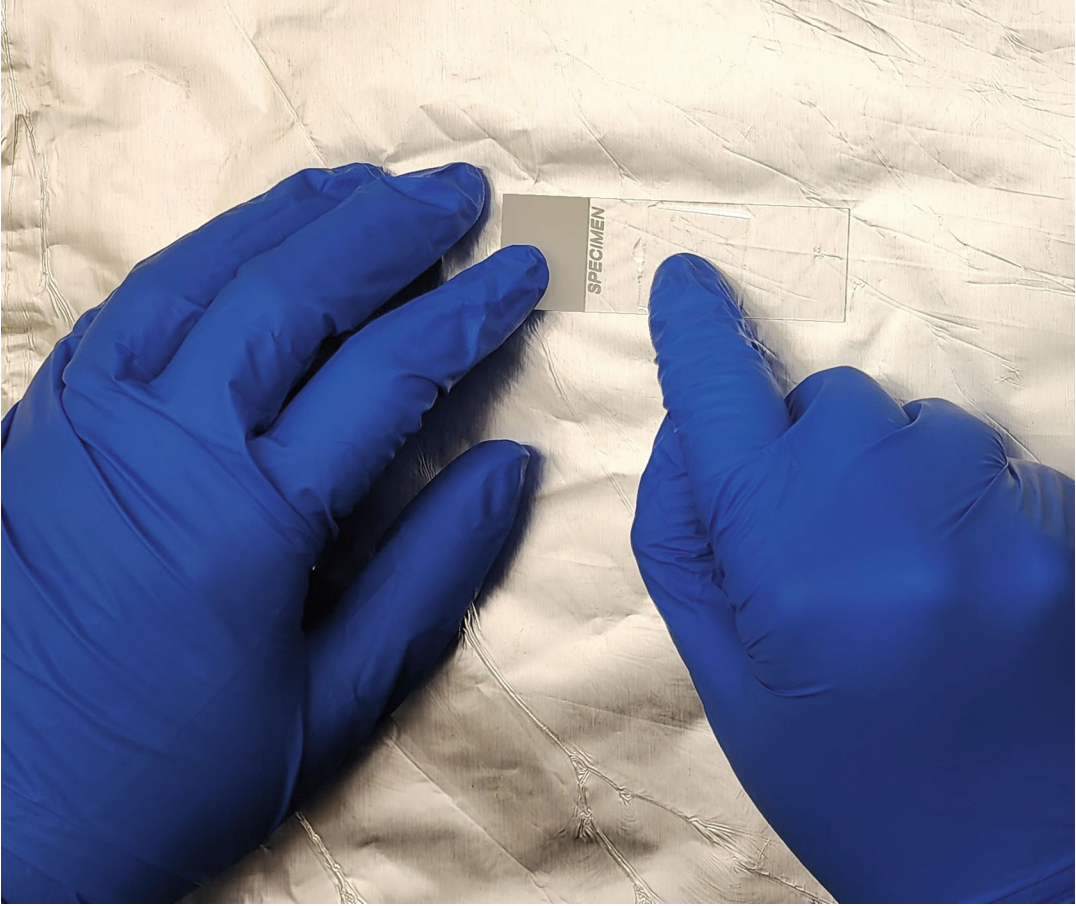
### 3.6 Minimizing Artifacts in SIM Imaging

Image acquisition varies significantly based on the optical setup and commercial platform used. Each user should receive extensive training on the microscope prior to use to ensure images are acquired correctly:

1. Utilize high-precision cover glass to minimize refractive index changes due to aberrations in the glass.
2. Minimize exposure times to reduce photobleaching and drift during acquisition. There should be no more than 30% bleaching across the entire z-stack of images (*see Note 46*). SIM



**Fig. 3** Image of mounting cover glass to slide. **(a)** Hold the cover glass at a 45° angle over the mounting media on the slide. Gently place cover glass onto mounting media on slide by allowing one side to touch first and then the other to push bubbles out as the cover glass is applied. **(b)** Remove any remaining bubbles from under cover glass by applying gentle pressure to move the bubbles to the edge of the cover glass and out the side



**Fig. 3** (continued)

requires many images as multiple phases and rotations must be acquired at each individual z plane.

3. Include two to three z slices below and above the cell to ensure that none of the structures are missing from the reconstructions.
4. Ensure that the number and spacing of the z-stack slices are acquired using the Nyquist sampling rate for the sample. The Nyquist rate is  $2\times$  the highest frequency of the signal and is dependent on the optical setup of the microscope. If the distance between the z slices is too large, then information will be missing from the resulting reconstruction. If the distance between the z slices is too small, then photobleaching will become an issue and introduce artifacts in the reconstruction. Many commercial software platforms will include information on the correct Nyquist sampling rate for the experiment. Nyquist rate calculators are also available online (*see Note 47*).

5. Haloing or doubling of the signal during acquisition indicates that the objective oil is not properly matched. Clean the lens and slide and then try an oil with a different refractive index to ensure a proper match. If the flaring of the signal is in the direction of the cover glass, then the refractive index of the oil is too high and a lower number should be used. If the flaring is away from the cover glass, then use a higher refractive index oil (*see* **Note 48**).
6. If there is a honeycomb pattern to the signal, that indicates that there is diffuse labeling or low signal-to-noise ratio. SIM works best with discrete structures as diffuse signals are difficult to reconstruct from the Fourier transforms. This is frequently seen with DAPI staining. There are a number of different approaches to remedy the honeycomb artifact. Three of the most common are outlined below:
  - Acquire the channel with the diffuse signal using widefield instead of SIM and incorporate the widefield images into the reconstruction.
  - Increase the signal-to-noise ratio by adjusting the exposure time, laser power, and neutral density (%T).
  - Utilize a higher Wiener filter constant (*see* **Note 49**). These filters remove high-frequency data but sacrifice resolution.

---

## 4 Notes

1. Cover glass already coated with poly-lysine and ready to use can be purchased from many different vendors. Pre-coated cover glass can sometimes have debris that is difficult to remove, and the poly-lysine coating can be uneven. If purchasing pre-coated cover glass, then reagents in Subheading 2.1 and methods in Subheading 3.1 may be omitted.
2. A small, short-walled beaker or a staining jar with cover glass holders may be used instead of the glass petri dish.
3. Animals used to generate polyclonal antibodies often have natural antibodies to yeast. Polyclonal antibodies therefore often recognize the yeast cell wall, including remnants remaining after spheroplasting. Antibodies that recognize the cell wall and create problematic nonspecific staining can be precleared as described in **Note 21**.
4. Single-domain antibodies, called nanobodies, are highly specific and high affinity camelid antibodies that can be produced recombinantly and labeled with a fluorophore of choice. These are excellent for staining yeast as they are small, and therefore

easily penetrate the spheroplasted yeast, and they will not have the issue of recognizing yeast cell walls discussed in **Note 3**.

5. Hardening mounting media offers superior anti-fade for super-resolution microscopy but can flatten the cells and deform the subcellular structures (such as nuclei), particularly in the Z-dimension. Wet mounting media better preserves the shape of the cells but does photobleach more rapidly than hardening mounting media. These are also called “setting” and “non-setting” mounting media.
6. In order to prevent artifacts from differences in refractive index, the objective oil needs to have the same refractive index as the mounting media. Commercial mounting media will list a refractive index in the product information. Based on the curing and conditions, this can vary slightly. The listed refractive index for the mounting media is a good place to start and then adjust as discussed in Subheading 3.6, step 5.
7. Note the numerical aperture (NA) of the objective used. Increasing the NA results in higher-resolution images. The data shown in Fig. 1 was taken using a 100×/1.4 NA PlanApo oil immersion objective from Olympus.
8. Typical wavelengths are 405 nm (blue/DAPI), 488 nm (green/GFP), 568 nm (orange-red/RFP), and 647 nm (far red/mKate2) diode lasers with standard filter sets.
9. Cameras will be equipped as part of the SIM microscope at the appropriate angles for generating the pattern shifts that provide the Moiré fringes which undergo Fourier transformation to create the high-resolution reconstructions of the sample.
10. These are specific for each microscope and optical set up. Instructions for obtaining these files will vary with each commercial platform and should be provided during training on the microscope. Registration files will also periodically be updated to ensure that the different laser lines overlay correctly during reconstruction. The registration files from when the images were *acquired* should be used for reconstruction, not the most recent files available.
11. If there is still debris present during the super-resolution imaging that interferes with the results, an acetone wash step can be added prior to the 1 M HCl. If this is still insufficient, the cover glass can be washed with piranha solution of hydrogen peroxide and sulfuric acid. This solution is extremely corrosive and is only recommended if absolutely necessary.
12. We use the box that the cover glass was stored in prior to cleaning and coating. If there is foam in the box that seems to be adding debris to the cover glass at the storage step, it can

be removed and replaced with lint-free delicate task wipers to protect the cover glass while in storage.

13. Wear proper protective equipment when working with paraformaldehyde including gloves, lab coat, eye protection, and work in a fume hood when possible.
14. Cells can be aliquoted into smaller volumes to minimize the amount of paraformaldehyde used unless the manipulation is very transient, such as a heat shock where removal from heat will start the recovery before fixation is complete.
15. Fixation can be done at 37 °C if the cells are heat stressed to keep cells from recovering before fixation is complete.
16. Fixed cells can be stored in SHA buffer at 4 °C for 1–2 days before continuing to Subheading 3.3.
17. Lyticase can be used instead at 134 U/mL for 75–90 min at 37 °C.
18. Concentration and duration of zymolyase (or lyticase) can be optimized by removing a few  $\mu$ L of cells periodically and imaging under white light on the microscope to visualize the remaining cell wall.
19. Be gentle from this point on as cells are easily lysed once the cell wall has been removed.
20. The cell pellet can be difficult to see, particularly as the protocol progresses. Ensuring sufficient starting material and following the Notes to minimize cell loss will make the pellet easier to visualize throughout the protocol. The pellet will appear smaller and more transparent than the initial cell pellet.
21. The cell pellet often appears “fluffier” and whiter at this stage.
22. Cells can be stored at 4 °C for 1–2 days before continuing to Subheading 3.4.
23. The volume of blocking buffer can be adjusted to the number of cells in the sample to minimize reagent use and reduce cell rupture. Ensure sufficient volume for adequate mixing, as samples that are too dense do not stain efficiently. Generally, 0.5 mL of solution per 1 mL of initial culture is a good balance.
24. Ensure that this volume is sufficient to allow good mixing. Samples that are too dense do not stain well, and samples that are too diluted cause cells to rupture. If incubating overnight, a slightly denser sample will minimize cell loss without a huge loss of staining efficiency.
25. Concentrations generally range from 1:100 to 1:1000 with a typical concentration of 1:500. Primary antibodies for different antigens can be mixed provided they can be recognized by different secondary antibodies. Fluorescently labeled nanobodies can be added here or during the incubation with secondary antibodies.

26. Polyclonal antibodies that recognize cell walls will need to be precleared before use. This can be done by adding 100  $\mu\text{L}$  of yeast culture to a tube and pellet cells at  $8000\times g$  for 30 s. Wash cells three times with 1 mL of 1X PBS. Resuspend cells in the 250  $\mu\text{L}$  of primary antibody in blocking buffer. Incubate for 2 h at room temperature with occasional mixing. Pellet cells by centrifugation at  $8000\times g$  for 30 s. Remove the antibody-containing supernatant into a new tube to be incubated with the spheroplasts in **step 9** in Subheading 3.4.1. Precleared antibodies can be made in large quantities and then small aliquots stored at  $-20\text{ }^{\circ}\text{C}$  for later use.
27. Incubation can be done for 2 h at room temperature, but typically overnight incubation results in better staining. Overnight incubation can result in more cell loss than the 2-h incubation.
28. Gentle mixing on a rotator can improve staining but can increase cell loss.
29. Generally, reusing the primary antibody causes diminished staining and increased background, but this can be tested for each primary antibody to determine if it can be reused or should be discarded.
30. Cold 1X PBS can be used in place of blocking buffer but results in more cell loss from rupture.
31. The number of washes can be reduced to three times if working with few or fragile cells, or if the antibody has low background staining. Reducing washes will increase the number of cells but can also increase background staining.
32. The typical concentration for fluorescently labeled secondaries is 1:1000. As with the primary antibodies, these can be mixed as long as they recognize different antigens and should be discarded after use.
33. From this point on, keep samples in the dark as much as possible to minimize quenching of the fluorescent dyes on the secondary antibody. Samples in a rack may be wrapped in foil or placed in a drawer.
34. Any nucleic acid dye counterstain can be used here if desired. This step can be omitted if the mounting media contains the dye. Typical concentration of DAPI and Hoechst 33342 is 1:1000.
35. Blocking buffer can be used, but milk adheres to the polylysine-coated coverslips and makes large debris with green autofluorescence that can interfere with imaging.
36. Determining the appropriate volume is trial and error, but generally 50  $\mu\text{L}$  is a good starting point. If there is sufficient

sample, multiple coverslips with different amounts of cells can be generated to ensure one is a good density for imaging.

37. Minimize clumping of the cells by mixing the sample well before adding to the cover glass.
38. You can allow the sample to dry completely to maximize cell adherence to the cover glass, but this often leads to deformed cells.
39. This is easiest by using a micropipettor of 1X PBS with one hand and a vacuum line with the other (Fig. 2). For best results, keep a constant flow rate of the buffer.
40. Place cover glass cell side up into the wells of a multi-well plate to keep them contained and keep from mixing up the samples.
41. Typically 25–30  $\mu\text{L}$  for a  $22 \times 22$  mm cover glass.
42. Gently hold the cover glass between the thumb and index finger at a 45-degree angle relative to the slide (Fig. 3a). Slowly lower the cover glass onto the mounting media so that one side touches first and then the other. This minimizes the number of air bubbles under the cover glass that can interfere with imaging.
43. Be very careful as the glass can crack easily (Fig. 3b).
44. Staining can be observed by carefully imaging on a regular fluorescence microscope. The mounting media should be completely cured to ensure it is at the correct optical density before continuing with super-resolution microscopy. Even wet mount media can need time to cure even though it does not harden. Check the user manual to determine if the mounting media needs to be cured to reach the final optical density.
45. Be very careful if using wet mounting media as the coverslips will move and can disrupt the samples.
46. If using a low value of neutral density filter (%T), and then increase the exposure time. If using a high %T, then reduce the exposure time.
47. The calculator from Scientific Volume Imaging works well to calculate Nyquist rate and point spread functions based on experimental setups. <https://svi.nl/Nyquist-Calculator>
48. It is best to match the refractive index for one color if doing multicolor imaging. For best results, optimize for the most red-shifted color or the most important color of the sample.
49. Typical values for our images range from 0.001 to 0.003. Honeycombs in the DAPI signal were resolved using 0.005 or higher. Report these values in the methods section.

## Acknowledgments

I would like to thank Sarah Rolli for critical reading of the manuscript. Funding for this work was provided by the Way Klingler Early Career Faculty Award to EMS.

## References

1. Walters AD, Bommakanti A, Cohen-Fix O (2012) Shaping the nucleus: factors and forces. *J Cell Biochem* 113(9):2813–2821. <https://doi.org/10.1002/jcb.24178>
2. Taddei A, Gasser SM (2012) Structure and function in the budding yeast nucleus. *Genetics* 192(1):107–129. <https://doi.org/10.1534/genetics.112.140608>
3. Meseroll RA, Cohen-Fix O (2016) The malleable nature of the budding yeast nuclear envelope: flares, fusion, and fenestrations. *J Cell Physiol* 231(11):2353–2360. <https://doi.org/10.1002/jcp.25355>
4. Bahmanyar S, Schlieker C (2020) Lipid and protein dynamics that shape nuclear envelope identity. *Mol Biol Cell* 31(13):1315–1323. <https://doi.org/10.1091/mbc.E18-10-0636>
5. Smoyer CJ, Jaspersen SL (2019) Patrolling the nucleus: inner nuclear membrane-associated degradation. *Curr Genet* 65(5):1099–1106. <https://doi.org/10.1007/s00294-019-00971-1>
6. Webster BM, Colombi P, Jäger J et al (2014) Surveillance of nuclear pore complex assembly by ESCRT-III/Vps4. *Cell* 159(2):388–401. <https://doi.org/10.1016/j.cell.2014.09.012>
7. Webster BM, Thaller DJ, Jager J et al (2016) Chm7 and Heh1 collaborate to link nuclear pore complex quality control with nuclear envelope sealing. *EMBO J* 35(22):2447–2467. <https://doi.org/10.15252/embj.201694574>
8. Sontag EM, Morales-Polanco F, Chen J-H et al (2023) Nuclear and cytoplasmic spatial protein quality control is coordinated by nuclear–vacuolar junctions and perinuclear ESCRT. *Nat Cell Biol* 25(5). <https://doi.org/10.1038/s41556-023-01128-6>
9. Dittmer TA, Misteli T (2011) The lamin protein family. *Genome Biol* 12(5):222. <https://doi.org/10.1186/gb-2011-12-5-222>
10. Peter A, Stick R (2015) Evolutionary aspects in intermediate filament proteins. *Curr Opin Cell Biol* 32:48–55. <https://doi.org/10.1016/j.ceb.2014.12.009>
11. Engel SR, Aleksander S, Nash RS, Wong ED, Weng S, Miyasato SR, Sherlock G, Cherry JM (2025) *Saccharomyces Genome Database: Advances in Genome Annotation, Expanded Biochemical Pathways, and Other Key Enhancements*. *Genetics*. 2024 Nov 12: iyae185. <https://doi.org/10.1093/genetics/iyae185>. PMID:39530598
12. Rolli S, Langridge CA, Sontag EM (2024) Clearing the JUNQ: the molecular machinery for sequestration, localization, and degradation of the JUNQ compartment. *Front Mol Biosci* 11:1427542. <https://doi.org/10.3389/fmolb.2024.1427542>



## Visualizing Phosphatidic Acid and Diacylglycerol at the Nuclear Envelope in Fission Yeast

Sherman Foo and Snezhana Oliferenko

### Abstract

Although the outer membrane of the nuclear envelope is continuous with the endoplasmic reticulum, temporally regulated and functionally significant differences in membrane lipid composition may exist between the two nuclear membranes and between the outer nuclear membrane and the endoplasmic reticulum. Biochemical approaches to probing lipid composition are challenged when lipid dynamics must be analyzed with fine spatiotemporal resolution, for instance, within the cell cycle of a single cell. Here we describe a method to probe the distribution of phosphatidic acid and diacylglycerol, two interconvertible biosynthetic precursors for other membrane glycerophospholipids, in living cells of the model fission yeast *Schizosaccharomyces pombe*. We show how genetically encoded fluorescent biosensors can be constructed and optimized and present a protocol to probe and quantify phosphatidic acid and diacylglycerol levels specifically at the inner nuclear membrane.

**Key words** Phosphatidic acid, Diacylglycerol, Nuclear envelope, Fission yeast, Microscopy

---

### 1 Introduction

Lipids are a major class of biomolecules present in all organisms. They form the bulk of biological membranes delimiting cells and eukaryotic organelles, determine the function of membrane-associated proteins, and may act as signaling and storage molecules. Lipid repertoire differs between, and even within, different cellular membranes, which is likely achieved through a combination of transport and compartmentalized metabolism [1]. Although the nuclear envelope (NE) can be considered a subdomain of the endoplasmic reticulum, its two constituent membranes may differ in metabolic capabilities and the abundance of specific lipids. For instance, the inner nuclear membrane (INM), traditionally thought to be metabolically silent, has been recently shown to house lipid

biosynthetic reactions, such as the synthesis of storage lipid triacylglycerol [2], and the formation of CDP-choline, the rate-limiting step in the production of phosphatidylcholine [3].

Dynamic changes in lipid distribution across different membranes may have profound implications for cellular physiology [4–10], but they are notoriously difficult to study [1, 11]. Recent exciting mass spectrometry-based methodologies and the advent of fluorescent and photoactivatable lipid derivatives have begun to tackle the complexity of lipid transport and metabolism in living cells [12–16]. Yet, these strategies are technically demanding and/or struggle with reporting changes in the subcellular distribution of endogenous lipids in single cells on functionally relevant timescales. A simple alternative is utilizing genetically encoded fluorescent lipid biosensors, typically built on protein domains recognizing specific lipid classes. Such biosensors, e.g., for phosphatidic acid (PA), diacylglycerol (DG), phosphatidylcholine, and sterols, have been used in a range of experimental systems [4, 17–26].

We have developed a suite of nuclear and cytoplasmic PA and DG biosensors for the use in the fission yeasts *Schizosaccharomyces pombe* and *Schizosaccharomyces japonicus* [4]. This advance has allowed us to discover the critical roles of the DG kinase Dgk1 and the DG cholinephosphotransferase Ept1 in boosting glycerophospholipid synthesis, which enables NE expansion required for “closed” mitosis of *S. pombe*. Importantly, we have optimized biosensor designs used previously in other experimental systems and provided suggestions on their expression levels [4].

The PA sensor was constructed by removing an endogenous nuclear localization sequence (NLS) within the codon-optimized Q2 helix of the *Saccharomyces cerevisiae* transcriptional factor Opi1 [24], introducing a G120W point mutation predicted to increase PA-binding selectivity [23], and duplicating the helix to stabilize it at the membrane. The DG sensor was based in duplicated codon-optimized rat protein kinase C DG-binding domain [22]. In our published designs, both biosensors were expressed under the control of the medium-strength *S. pombe cdc15* promoter and tagged at the C-terminus with a glutathione S-transferase (GST) tag and green fluorescent protein (GFP) (Fig. 1). GST serves as a means of increasing protein bulk, preventing passive protein diffusion through the nuclear pores. Appending or omitting the SV40 NLS at both ends of the lipid-binding module allowed us to probe lipid enrichment at the INM or in the cytoplasm, respectively (Fig. 2). Both sensor designs have been validated by modulating the cellular abundance of PA and DG and by mutating amino acids known to mediate binding to the target lipids [4].

Here, we describe how basic manipulation of the biosensors can be performed, followed by the protocol to probe PA and DG enrichment at the INM in *S. pombe*. We will replace the GFP

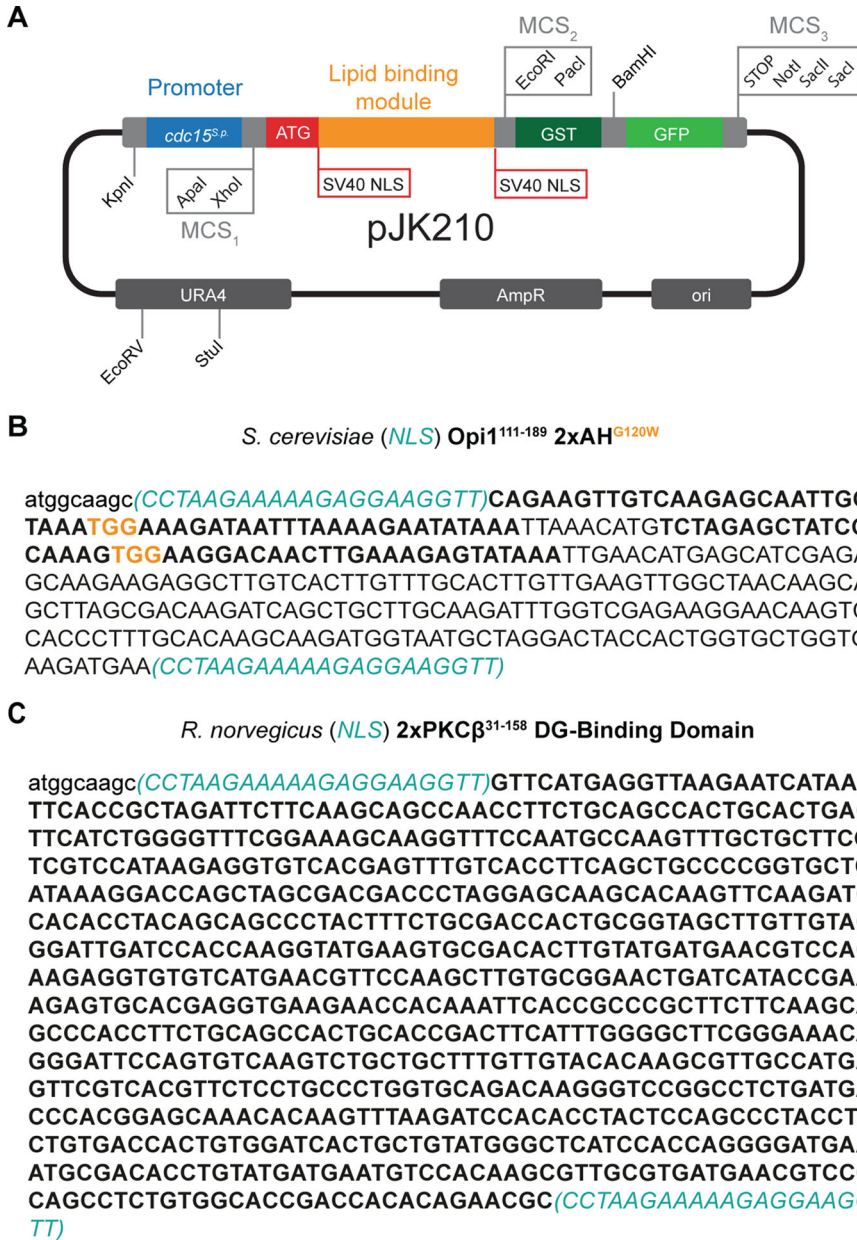


**Fig. 1** (a) Diagram depicting the plasmid design for expressing lipid sensors in the study [4]. The lipid sensors consist of a lipid-binding module (reengineered duplicated *S. cerevisiae* Opi1 PA-binding amphipathic helix or duplicated *Rattus norvegicus* PKC $\beta$  DG-binding domain) under the control of the *S. pombe* *cdc15* promoter, with a C-terminal GST tag and GFP. Restriction enzyme sites and the multiple cloning sites (MCS) are depicted in grey. In the NLS versions of the sensors, the lipid-binding module is flanked by two SV40 NLS motifs on both ends. (b) DNA sequence of the PA lipid sensor module. It consists of two consecutive *S. cerevisiae* Opi1 amphipathic helices each containing a G120W point mutation. The amphipathic helices are indicated in bold, mutations indicated in orange, and SV40 NLS motifs in cyan. (c) DNA sequence of the DG lipid sensor module. The DG lipid sensor consists of two consecutive *R. norvegicus* PKC $\beta$  DG-binding domains indicated in bold and the SV40 NLS motifs in cyan

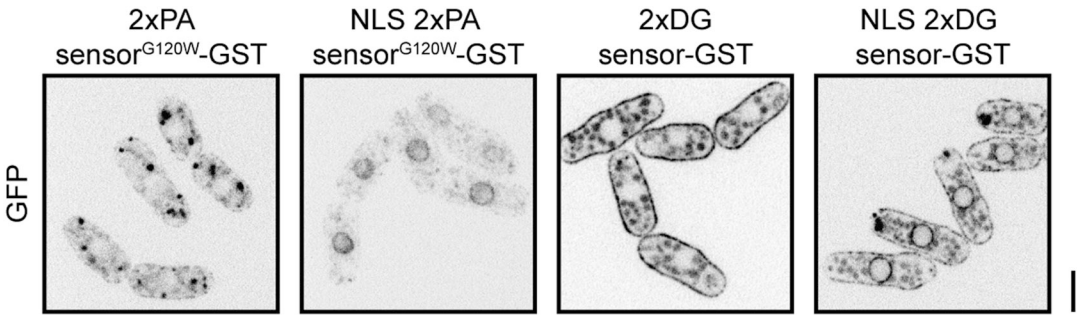


**Fig. 2** Single-plane spinning-disk confocal images of *S. pombe* expressing the cytoplasmic and NLS PA and DG GFP-based sensors. Scale bars: 5  $\mu$ m

fluorophore with mCherry as an example workflow. Similarly, the promoter, GST tag, or selection marker can be swapped out using appropriate DNA fragments and restriction enzymes as necessary. In terms of choosing endogenous promoters of different strengths, PomBase, an excellent curated database, contains the regulatory context of all *S. pombe* genes [27], and there is increasing amount of information on *S. japonicus*, in a sister database JaponicusDB [28].

## 2 Materials

### 2.1 Polymerase Chain Reaction

1. Template DNA (any mCherry-containing plasmid).
2. Forward and reverse primers (100  $\mu$ M).
3. KAPA HiFi PCR Kit (Roche).
4. dNTP mix (10 mM).
5. PCR-grade water.
6. 8-strip PCR tubes and caps.
7. PCR machine.
8. UltraPure Agarose (Thermo Scientific).
9. Tris Acetate EDTA (TAE) buffer (Thermo Scientific).
10. GelRed Nucleic Acid Stain (Sigma-Aldrich).
11. Sub-Cell GT DNA electrophoresis cell and combs (Bio-Rad).
12. PowerPac Basic Power Supply (Bio-Rad).
13. DNA ladder.
14. GelDoc system.
15. Macherey-Nagel NucleoSpin Gel and PCR Clean-up Kit (Fisher Scientific).
16. Ethanol.
17. Benchtop centrifuge for 1.5 mL microcentrifuge tubes.
18. Nanodrop (Thermo Scientific).

19. Microcentrifuge tubes.
20.  $-20^{\circ}\text{C}$  freezer.

## **2.2 Molecular Cloning**

1. mCherry PCR insert (1  $\mu\text{g}$ ).
2. Vector (1  $\mu\text{g}$ ) (*see* **Note 1**).
3. Restriction enzymes and buffer (NEB).
4. PCR-grade water.
5. Microcentrifuge tubes.
6. Heat block.
7. UltraPure Agarose (Thermo Scientific).
8. Tris Acetate EDTA (TAE) buffer (Thermo Scientific).
9. GelRed Nucleic Acid Stain (Sigma-Aldrich).
10. Sub-Cell GT DNA electrophoresis cell and combs (Bio-Rad).
11. PowerPac Basic Power Supply (Bio-Rad).
12. DNA ladder.
13. GelDoc system.
14. Scalpel.
15. Macherey-Nagel NucleoSpin Gel and PCR Clean-up Kit (Fisher Scientific).
16. Ethanol.
17. Benchtop centrifuge for 1.5 mL microcentrifuge tubes.
18. Nanodrop (Thermo Scientific).
19.  $-20^{\circ}\text{C}$  freezer.
20. T4 DNA ligase and buffer (NEB).
21. 5-alpha competent *E. coli* cells (NEB).
22. SOC media: 2% tryptone, 0.5% yeast extract, 10 mM NaCl, 2.5 mM KCl, 10 mM  $\text{MgCl}_2$ , 10 mM  $\text{MgSO}_4$ , and 20 mM glucose.
23. LB plates: 1% peptone, 0.5% yeast extract, 0.5% NaCl (w/v), 1.5% (w/v) agar supplemented with 100  $\mu\text{g}/\text{mL}$  ampicillin.
24.  $37^{\circ}\text{C}$  incubator.

## **2.3 Miniprep and Analytical Digestion**

1. 13 mL snap-cap tubes.
2. LB media: 1% peptone, 0.5% yeast extract, 0.5% NaCl (w/v), supplemented with 100  $\mu\text{g}/\text{mL}$  ampicillin.
3.  $37^{\circ}\text{C}$  shaking incubator.
4. Benchtop centrifuge for 15 mL tubes.
5. Thermo Scientific GeneJet Miniprep Kit.
6. Ethanol.

7. Restriction enzymes and buffer (NEB).
8. Microcentrifuge tubes.
9. Heat block.
10. 6× gel loading dye (NEB).
11. UltraPure Agarose (Thermo Scientific).
12. Tris Acetate EDTA (TAE) buffer (Thermo Scientific).
13. GelRed Nucleic Acid Stain (Sigma-Aldrich).
14. Sub-Cell GT DNA electrophoresis cell and combs (Bio-Rad).
15. PowerPac Basic Power Supply (Bio-Rad).
16. DNA ladder.
17. GelDoc system.
18. −20 °C freezer.

#### **2.4 Yeast Molecular Genetics and Husbandry**

1. *S. pombe* strains (*see* **Note 1**).
2. Glass flasks for yeast cultures.
3. Benchtop centrifuge for 50 mL tubes.
4. Benchtop centrifuge for 1.5 mL tubes.
5. Benchtop spectrometer.
6. Reagent grade water.
7. Microcentrifuge tubes.
8. LiAc-TE buffer: 0.1 M lithium acetate, 10 mM Tris-HCl pH 7.5, 1 mM EDTA.
9. LiAc-TE-PEG buffer: LiAc-TE, 40% PEG4000.
10. Carrier DNA (10 mg/mL Sonicated Salmon Sperm DNA).
11. Heat block.
12. DMSO.
13. Edinburgh Minimal Medium (EMM) plates: 14.7 mM potassium hydrogen phthalate, 15.5 mM Na<sub>2</sub>HPO<sub>4</sub>, 93.5 mM NH<sub>4</sub>Cl, 2% (w/v) glucose and 2% (w/v) agar supplemented with 5.2 mM MgCl<sub>2</sub>, 0.1 mM CaCl<sub>2</sub>, 13.4 mM KCl, 0.282 mM Na<sub>2</sub>SO<sub>4</sub>, 4.2 μM pantothenic acid, 81.2 μM nicotinic acid, 55.5 μM inositol, 40.8 nM biotin, 8.09 μM boric acid, 2.37 μM MnSO<sub>4</sub>, 1.39 μM ZnSO<sub>4</sub>, 0.74 μM FeCl<sub>2</sub>, 0.25 μM molybdic acid, 0.60 μM KI, 0.16 μM CuSO<sub>4</sub>, and 4.76 μM citric acid. Uracil selection plates are further supplemented with leucine, histidine, and adenine (225 mg/L each).
14. 30 °C incubator.
15. Sterile inoculation loop.
16. MasterPure Yeast DNA Purification Kit (LGC group).
17. Ethanol.
18. Isopropanol.

19. Forward and reverse genotyping primers (100  $\mu$ M).
20. PCR materials (*see* Subheading 2.1).
21. Cryotubes.
22. Glycerol.
23.  $-80^{\circ}\text{C}$  freezer.

## 2.5 Imaging

1. Glass microscopy slides.
2. Coverslips.
3. Fluorescence microscope system, e.g., spinning disk confocal.
4. UltraPure agarose.
5. Edinburgh Minimal Medium (EMM) medium 14.7 mM potassium hydrogen phthalate, 15.5 mM  $\text{Na}_2\text{HPO}_4$ , 93.5 mM  $\text{NH}_4\text{Cl}$  and 2% (w/v) glucose supplemented with 5.2 mM  $\text{MgCl}_2$ , 0.1 mM  $\text{CaCl}_2$ , 13.4 mM KCl, 0.282 mM  $\text{Na}_2\text{SO}_4$ , 4.2  $\mu$ M pantothenic acid, 81.2  $\mu$ M nicotinic acid, 55.5  $\mu$ M inositol, 40.8 nM biotin, 8.09  $\mu$ M boric acid, 2.37  $\mu$ M  $\text{MnSO}_4$ , 1.39  $\mu$ M  $\text{ZnSO}_4$ , 0.74  $\mu$ M  $\text{FeCl}_2$ , 0.25  $\mu$ M molybdic acid, 0.60  $\mu$ M KI, 0.16  $\mu$ M  $\text{CuSO}_4$ , and 4.76  $\mu$ M citric acid. Uracil selection plates are further supplemented with leucine, histidine, and adenine (225 mg/L each).
6. Yeast extract with supplements (YES) medium: 0.5% (w/v) yeast extract, 3% (w/v) glucose, supplemented with uracil, leucine, histidine, and adenine (225 mg/L each).
7. Heat block.
8. Microcentrifuge tubes.
9. Benchtop centrifuge.
10. Wax or nail polish.

---

## 3 Methods

### 3.1 PCR of Region of Interest

1. Figure 1a shows an overview of the design and restriction sites used in the construct of the sensors. The DNA sequences of the PA and DG lipid sensors can be found in Fig. 1b, c, respectively. All sensors are cloned into pJK210-based plasmid backbone for integration into the *ura4* locus of *S. pombe* (Fig. 2) [29] (*see* Note 1).
2. Design primers for PCR of a fluorophore of interest. For further details on good primer design, refer to this in-depth guide by Álvarez-Fernández [30] or Dieffenbach and colleagues [31].
3. In this section, we use mCherry as an example molecular cloning workflow, to enable co-localization of a protein of

interest tagged with GFP together with an mCherry-tagged lipid sensor (*see* **Notes 2–4**). Alternatively, Gibson assembly or similar approaches can be used to swap out these components as necessary [32].

4. Primers targeting the 5' and 3' ends of the mCherry gene are designed and procured commercially. The forward primer should include a BamHI restriction site at its 5' end, while the reverse primer contains a Stop codon, followed by a NotI (or SacII or SacI) restriction site at its 3' end. Check that the sequence of the fluorophore of interest does not contain these restriction sites.
5. Using an mCherry-containing plasmid template, perform PCR reaction (*see* Table 1) according to the manufacturer's instructions. In this case, we use KAPA HiFi (Roche).
6. Divide 100  $\mu$ L reaction into four PCR tubes containing 25  $\mu$ L reaction each.
7. Run gradient PCR (e.g., 60–70  $^{\circ}$ C; *see* Table 2) to amplify the mCherry DNA sequence 711 bp plus additional cloning adaptors).
8. Meanwhile, prepare 1.5% agarose gel for DNA electrophoresis. Prepare gel tray and combs for casting of gel. Add 0.75 g of UltraPure agarose in 50 mL of TAE buffer in a glass flask, microwave for 1–2 min till fully dissolved. Next, add 5  $\mu$ L of GelRed Nucleic Acid Stain (*see* **Note 5**).
9. Mix 2  $\mu$ L of each PCR reaction from **step 6** with 1  $\mu$ L of NEB 6 $\times$  gel loading dye. Load the samples into four wells of the agarose gel. Load 5  $\mu$ L of DNA ladder in an empty well, and run DNA electrophoresis at constant 120 V for 30 min or until the DNA ladder is resolved.

**Table 1**  
**KAPA HiFi PCR reaction**

Reagent	Volume
5 $\times$ KAPA HiFi buffer	20 $\mu$ L
10 mM dNTP mix	3 $\mu$ L
10 $\mu$ M forward primer	3 $\mu$ L
10 $\mu$ M reverse primer	3 $\mu$ L
Template DNA (e.g., plasmid with mCherry sequence)	1–5 <i>ng</i>
1 U/ $\mu$ L KAPA HiFi DNA polymerase	2 $\mu$ L
PCR-grade water	Up to 100 $\mu$ L
<b>Total volume</b>	<b>100 <math>\mu</math>L</b>

**Table 2**  
**KAPA HiFi PCR cycling protocol**

Step	Temperature	Duration	Cycles
Initial denaturation	95 °C	3 min	1
Denaturation	98 °C	20 s	34
Annealing	60–70 °C	15 s	
Extension	72 °C	15 s/kb	
Final extension	72 °C	5 min	1
Completion	12 °C	∞	1

10. Image agarose gel on a GelDoc system, repeat PCR if necessary with the appropriate annealing temperature.
11. Clean up the PCR reaction using a PCR cleanup kit (e.g., Macherey-Nagel NucleoSpin Gel and PCR Clean-up Kit) following the manufacturer's instructions. Elute final product with 30–50 µL of water.
12. Measure concentration of eluted DNA and store at –20 °C for future use.

### 3.2 Molecular Cloning

1. Prepare two restriction digest reaction mix for the PCR product (mCherry DNA fragment) and vector (e.g., pSO1070) (see Table 3).
2. Perform restriction digest for 1 h at the optimal temperature. This is 37 °C for BamHI-HF and NotI-HF (see Note 6).
3. Add 6 µL of NEB 6× gel loading dye and run the restriction digest reaction on a 1.5% agarose gel (see step 8 in Subheading 3.1). Excise the products from the gel using a clean scalpel. There should be one band at approximately 700 bp for the PCR digest and two bands for the vector digest corresponding to GFP and the rest of the vector.
4. Extract and clean up the products using a PCR/Gel cleanup kit (e.g., Macherey-Nagel NucleoSpin Gel and PCR Clean-up Kit) following the manufacturer's instructions. Elute final product with 20–25 µL of water.
5. Measure concentration of eluted DNA. Store at –20 °C for future use.
6. Ligation of insert into vector (see Note 7, Table 4).
7. Mix by gentle pipetting, incubate at room temperature for 1 h.
8. Add ligation mix directly to a tube of thawed competent *Escherichia coli* cells (e.g., NEB 5-alpha Competent *E. coli*).
9. Incubate on ice for 30 min, heat shock at 42 °C for 30 s before returning tube to ice for 2 min.

**Table 3**  
**Restriction digest reaction**

Reagent	Volume
CutSmart buffer	3 $\mu\text{L}$
DNA	1–2 $\mu\text{g}$
Restriction enzyme #1 (BamHI-HF)	1 $\mu\text{L}$
Restriction enzyme #2 (NotI-HF)	1 $\mu\text{L}$
PCR-grade water	Up to 25 $\mu\text{L}$
<b>Total volume</b>	<b>30 <math>\mu\text{L}</math></b>

**Table 4**  
**Ligation reaction**

Reagent	Volume
T4 DNA ligase buffer (10 $\times$ )	2 $\mu\text{L}$
Insert DNA	13 $\mu\text{L}$ ( <i>see Note 7</i> )
Vector DNA	4 $\mu\text{L}$ ( <i>see Note 7</i> )
T4 DNA ligase	1 $\mu\text{L}$
<b>Total volume</b>	<b>20 <math>\mu\text{L}</math></b>

10. Recover in SOC media for 30 min at 37 °C.
11. Plate cells on LB plates containing 100  $\mu\text{g}/\text{mL}$  ampicillin, and incubate overnight at 37 °C.

### **3.3 Miniprep and Analytical Digestion**

1. In 13 mL snap-cap tubes, inoculate four colonies of transformed *E. coli* separately into 3 mL LB media containing 100  $\mu\text{g}/\text{mL}$  ampicillin.
2. Grow bacteria cultures overnight at 37 °C with constant shaking.
3. Pellet cells by centrifugation at >4000 g for 5 min at room temperature. Decant medium.
4. Use a miniprep kit of choice to purify plasmid DNA (e.g., Thermo Scientific GeneJet Plasmid Miniprep Kit) following the manufacturer's instructions.
5. Measure concentration of eluted DNA. Store at –20 °C for future use.
6. Prepare a restriction digestion reaction master mix (*see Table 5*).

**Table 5**  
**Analytical digest master mix**

Reagent	Volume
CutSmart buffer	6 $\mu$ L
H <sub>2</sub> O	42 $\mu$ L
Restriction enzyme #1 (BamHI-HF)	2 $\mu$ L
Restriction enzyme #2 (NotI-HF)	2 $\mu$ L
<b>Total volume</b>	<b>52 <math>\mu</math>L</b>

- Aliquot 13  $\mu$ L of the master mix into four PCR or microcentrifuge tubes.
- Add 2  $\mu$ L of plasmid DNA from the four minipreps from **step 5** to each 13  $\mu$ L analytical digest reactions.
- Incubate digestion reactions at optimal temperature for the restriction enzymes of choice for 30 min (e.g., 37 °C) (*see Note 6*).
- Add 3  $\mu$ L of NEB 6 $\times$  gel loading dye to each restriction digest, mix well.
- Prepare 1.5% agarose gel for DNA electrophoresis (*see step 8* in Subheading 3.1).
- Load all 18  $\mu$ L of the restriction digest from **step 9** into four wells of the agarose gel. Load 5  $\mu$ L of DNA ladder, and run DNA electrophoresis at constant 100 V for 30 min.
- Image the agarose gel. Positive clones should have a band corresponding to the mCherry insert of approximately 700 bp and a larger band corresponding to the rest of the vector.
- Sanger sequence the positive clones to confirm the absence of unwanted mutations. Store the plasmids at -20 °C for future use.

### 3.4 *S. pombe* Chemical Transformation

- Linearize vector at the *ura4* marker with StuI restriction enzyme (*see* Subheading 3.2, Table 3). Purify the linearized plasmid using a PCR clean up kit, e.g., Macherey-Nagel NucleoSpin Gel and PCR Clean-up Kit) following the manufacturer's instructions, and measure the DNA concentration.
- Grow 20 mL of *S. pombe* strains of required genotypes (e.g., NemI-mNeonGreen expressing cells) to OD<sub>595</sub> = 0.5 or  $1 \times 10^7$  cells/mL, typically in Yeast Extract with Supplements (YES) medium.
- Prepare reagents for chemical transformation. LiAc-TE and LiAc-TE-PEG.

4. Pellet cells via centrifugation at 1000 *g* for 2 min and remove supernatant.
5. Wash cells by resuspending pellet in 20 mL of water followed by centrifugation at 1000 *g* for 2 min. Decant supernatant.
6. Resuspend cell pellet in 1 mL water and transfer to a clean microcentrifuge tube.
7. Pellet cells via centrifugation at 1000 *g* for 2 min and remove supernatant.
8. Wash cells once in 1 mL of LiAc-TE followed by centrifugation at 1000 *g* for 2 min. Remove supernatant by aspirating with a pipette.
9. Resuspend cell pellet in 100  $\mu$ L of LiAc-TE. Add 2  $\mu$ L of carrier DNA (10 mg/mL Sonicated Salmon Sperm DNA) and 1–2  $\mu$ g linearized plasmid DNA to the cell mixture.
10. Add 260  $\mu$ L of LiAc-TE-PEG and mix gently.
11. Incubate for 30–60 min at 30 °C.
12. Add 43  $\mu$ L of DMSO and incubate cells at 42 °C for 5 min.
13. Pellet cells via centrifugation at 1000 *g* for 2 min and wash once with 1 mL of water. Resuspend washed cells in 500  $\mu$ L of water and plate on two Edinburgh Minimum Media (EMM) lacking uracil (EMM ura<sup>−</sup>) selective plates. Incubate at 30 °C for 3–4 days.
14. For a more detailed *S. pombe* transformation protocol, refer to this protocol by Moreno and colleagues [33]. Other transformation protocols, such as electroporation, can be used [34].

### 3.5 Selection and Genotyping

1. *S. pombe* colonies will have formed following 3–4 days of growth on selective medium. We typically select eight colonies and restreak them on a fresh EMM ura<sup>−</sup> plate using a sterile inoculation loop or pipette tip. Incubate plate in a 30 °C incubator for 1–2 days.
2. When restreaked colonies have grown sufficiently, perform genomic DNA extraction as described below:
3. Scrape a single yeast colony of approximately 2 mm in diameter from the agar plate.
4. Lyse cells and extract genomic DNA using a genomic DNA extraction kit (e.g., MasterPure Yeast DNA Purification Kit, Biosearch Technologies) following the manufacturer's instructions.
5. Measure DNA concentration.
6. Perform PCR genotyping on the genomic DNA using primers flanking the integration site to confirm the integration of vector in the *ura4* locus (see steps 5–10 in Subheading 3.1).

7. Alternatively, strains containing the integrated lipid sensors can be crossed with strains containing mutants or markers of interest (*see* Moreno et al. [33]).
8. Freeze positive clones for future use: scrape remaining restreaked yeast containing the integrated vector from the selective plate using a 10  $\mu$ L inoculation loop and transfer it into a cryotube containing 1 mL of 50% glycerol and 50% YES medium. Resuspend yeast by pipetting up and down and store at  $-80^{\circ}\text{C}$  for future use.

### **3.6 Quick Imaging to Check for the Presence of the Lipid Sensor**

1. When performing a quick screen for the presence of the lipid sensor of interest, restreaked yeast colonies can be checked under a fluorescence microscope using the appropriate imaging settings for the genetically encoded fluorophore of choice, as follows:
2. Pipette 2  $\mu$ L of YES or EMM medium onto a glass microscope slide.
3. Using a pipette tip, scrape a small amount of restreaked yeast from the selective plates, and dab it onto the medium droplet three to four times to resuspend it. Place a glass cover slip on the droplet and check for fluorescence.
4. An example of *S. pombe* expressing a protein of interest, the lipin phosphatase Nem1, tagged with mNeonGreen together with the mCherry-tagged PA or DG lipid sensor is shown in Fig. 3.

### **3.7 Live Cell Imaging**

1. Frozen yeast stocks can be restreaked directly on YES plates or EMM ura<sup>-</sup> plates by scraping a small amount of frozen material with a clean pipette tip. Incubate at  $30^{\circ}\text{C}$  for 1–3 days until colonies are formed. We typically restreak these once again allowing them to grow overnight. This step ensures that cells are outside of stationary phase when inoculated in liquid media for imaging.
2. Inoculate freshly restreaked cells in 10–20 mL appropriate liquid medium. Culture in a shaking incubator overnight at  $30^{\circ}\text{C}$ . Use cells for imaging at  $\text{OD}_{595} = 0.3\text{--}0.6$  or  $\sim 1 \times 10^7$  cells/mL. If cell culture overgrew the target  $\text{OD}_{595}$ , dilute it to  $\text{OD}_{595} = 0.1\text{--}0.2$ , and continue growing until the required density is reached.
3. Centrifuge 1 mL of cell culture in a microcentrifuge tube at  $1000 g$  for 2 min and remove supernatant by decanting (*see* Note 8).

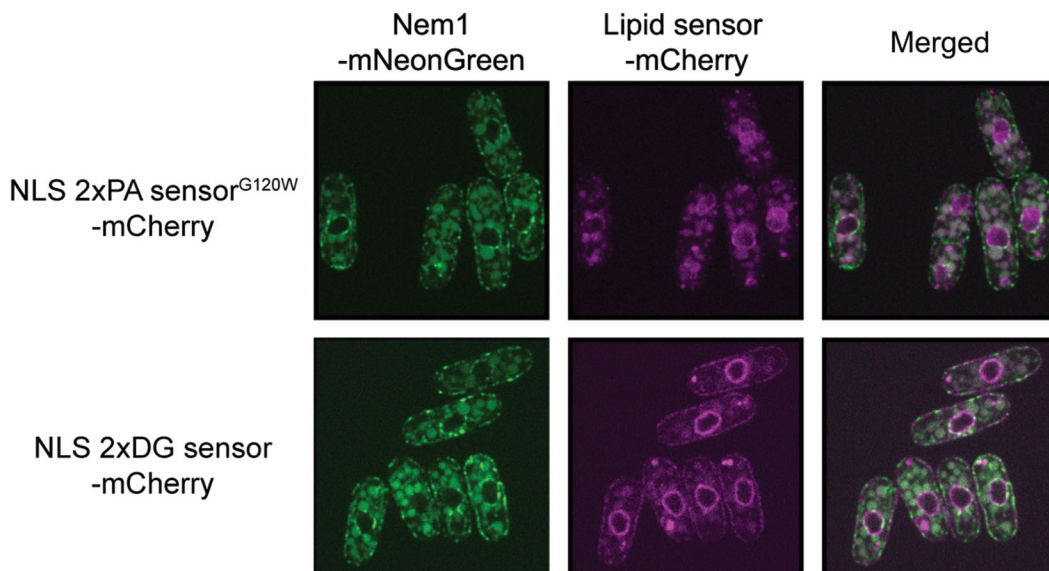


**Fig. 3** Single-plane spinning-disk confocal images of *S. pombe* cells co-expressing the ER-localized Lipin phosphatase Nem1-mNeonGreen together with the mCherry tagged NLS PA and DG sensors. Scale bars: 5  $\mu$ m

4. For snapshots, resuspend the pellet in 20–50  $\mu$ L of media, and place 2  $\mu$ L of cells on a glass microscope slide, cover with a cover slip and image cells, as appropriate.
5. For imaging *S. pombe* cells over a longer periods of time to produce time-lapse movies or montages (*see* Fig. 3 in [4]), or for quantification of changes in lipid sensor distribution over time, live cell imaging on agarose pads should be performed. This is described in detail by Pemberton [35] but we provide a brief protocol below.
6. Prepare 20 mL YES media with 1% agarose. Dissolve the agarose by briefly microwaving the solution. Aliquot 1 mL of the solution into microcentrifuge tubes for future use.
7. To prepare agarose pads for imaging, melt an aliquot from **step 6** using a 95 °C heat block for 5–10 min. If further use of molten agarose medium is required, transfer the aliquot to a 65 °C heat block to prevent it from burning (*see* **Note 9**).
8. Meanwhile, prepare a glass slide and two pieces of cardboard or tape to act as spacers. Place the spacers on the two ends of the glass slide.
9. Mix the melted aliquot of 1% agarose by inverting the tube, and pipette 50–80  $\mu$ L onto the middle of the glass slide.
10. Gently place another glass slide on the top, flattening the agarose drop. The second slide should rest on the two spacers on either side (*see* **Note 10**).

11. After about 30–60 s, the agarose pad will have solidified. Gently slide the second glass slide off, keeping the agarose pad in the middle of the first slide.
12. Allow the agarose pad to dry for 1 min. Prepare *S. pombe* cells for imaging as outlined above (*see* **steps 1–3** in Subheading **3.7**). Gently resuspend the cell pellet in 20–50  $\mu\text{L}$  of media and place 0.8–1  $\mu\text{L}$  of cells on the agarose pad.
13. Gently cover the pad with a glass coverslip, avoiding air bubbles, and seal it with wax or nail polish.
14. Incubate the prepared slide in the temperature-controlled microscope set-up (e.g., using an Okolab Cage Incubator) to allow it to acclimatize to the imaging temperature (*see* **Note 11**).
15. Image cells as required.

### **3.8 Optional Spectral Autofluorescence Image Correction by Regression (SAIBR) Protocol**

1. To reduce autofluorescence in the green channel, we recommend exploring the SAIBR method [36]. The SAIBR plugin for FIJI, together with detailed instructions and sample data-sets, is available online at [https://github.com/goehringlab/saibr\\_fiji\\_plugin](https://github.com/goehringlab/saibr_fiji_plugin).
2. Briefly, image the strains containing GFP-tagged lipid sensors using the green channel using appropriate microscopy settings. At the same time, image the strains in the red channel with the same settings for autofluorescence correction in SAIBR. Additionally, image 3–5 fluorophore-negative samples (e.g., wild-type cells) using the green and red channels with the same settings for calibration of the plug-in.
3. Download and install the plug-in from the link above.
4. Open the plug-in in *Plugins*  $\rightarrow$  *SAIBR*.
5. Calibrate using 3–5 fluorophore-negative control samples (e.g., wild-type cells). Set the green channel as the Primary Channel and red channel as the Predictor Channel.
6. Specify regions of interest (ROI) around the cells.
7. Run calibration.
8. Check the scatterplot for a good 1:1 relationship across the range of values for all images and a high  $R^2$  value of  $>0.9$ .
9. Adjust the Gaussian Blur value and rerun the calibration if necessary.
10. Once satisfied with the calibration, save calibration and return to the main menu.
11. Open the image files to be corrected.

12. Check that the parameters for correction are set according to the calibration performed. Set the green channel as the Primary Channel and the red channel as the Predictor Channel.
13. Click on *Run correction* to perform autofluorescence correction on the image.
14. Repeat the process for the other image files to be processed.

### **3.9 Quantification of PA and DG Sensor Intensity at the INM**

1. We typically quantify PA and DG sensor intensities at the INM (or other cellular locations, such as the cortex) using the segmented line function in Fiji/ImageJ [37]:
2. Right click on the Straight Line function button to switch to the segmented line function. Double-click the segmented line function button to adjust the line width to 5 pixels or an appropriate size to encompass the region of interest.
3. Use the Set Measurements function under the Analyze menu and set it to display the mean grey value, perimeter and area, and any other measurements of interest.
4. Select a cell of interest (e.g., a dividing cell).
5. Outline the region of interest (i.e., the fluorescence from the lipid sensor at the INM), and use the Measure function (under the Analyze menu). The Measure function will display the values as selected in **step 3**.
6. Repeat this measurement for every time point in the montage taken for the cell of interest.
7. Transfer the data to a data analysis software of choice (e.g., Microsoft Excel, GraphPad Prism).
8. The sensor intensity at the INM can be divided by the intensity at the cortex to normalize the readings, to account for photobleaching.
9. Next, plot the rate of sensor signal decay at the INM against time for the cell of interest.
10. Repeat **steps 4–9** in Subheading 3.9 for other dividing cells.
11. Linear regression of the sensor signal decay of each individual cell can be calculated. The gradient calculated is the rate of sensor intensity decay at the INM.

---

## **4 Notes**

1. The lipid biosensor constructs (*see* Table 6) and *S. pombe* strains expressing them (*see* Table 7) have been validated extensively [4]. Plasmids and *S. pombe* strains can be obtained via request from the authors. Representative spinning disk confocal

microscopy images of the strains in Table 7 can be found in Fig. 2.

2. The presence of restriction sites flanking the promoter, lipid binding module, GST biochemical tag, and GFP fluorophore allows for the replacement of any of the components with suitable alternatives (e.g., different promoter, alternative biochemical tags such as MBP, HA; alternative fluorophores such as mCherry or mNeonGreen) (*see also* Notes 3 and 4).
3. Care should be taken when choosing an appropriate promoter for overexpression of PA and DG sensors, as strong overexpression, e.g., using the strong *tdh1* promoter [38] may lead to NE morphology defects (*see* Fig. S2D in [4]).
4. It should be noted that further optimization of the lipid sensors might be necessary for different species. For example, we have observed that the abundance of both nuclear and cytoplasmic PA sensors is significantly weaker in *S. japonicus*, as compared

**Table 6**  
**Plasmid information**

Plasmid	Insert	Description
pSO1074	PA sensor	pJK210-promoter <sup><i>cdc15</i></sup> -PA sensor (Opi1 <sup>111-189, G120W</sup> 2xAH)-GST-GFP
pSO1070	NLS PA sensor	pJK210-promoter <sup><i>cdc15</i></sup> -NLS PA sensor (NLS <sup>SV40</sup> -Opi1 <sup>111-189, G120W</sup> 2xAH-NLS <sup>SV40</sup> )-GST-GFP
pSO1079	DG sensor	pJK210-promoter <sup><i>cdc15</i></sup> -DG sensor (PKCβ <sup>31-158</sup> 2xbinding domain)-GST-GFP
pSO1080	NLS DG sensor	pJK210-promoter <sup><i>cdc15</i></sup> -NLS DG sensor (NLS <sup>SV40</sup> -PKCβ <sup>31-158</sup> 2xbinding domain-NLS <sup>SV40</sup> )-GST-GFP

**Table 7**  
**Yeast strain information**

Strain	Lipid sensor	Genotype
SO8772	PA sensor	<i>ura4<sup>+</sup>::promoter<sup><i>cdc15</i></sup>-PA sensor-GST-GFP</i> <i>ade6-704 ura4-294 leu1-32 h<sup>-</sup></i>
SO8760	NLS PA sensor	<i>ura4<sup>+</sup>::promoter<sup><i>cdc15</i></sup>-NLS PA sensor-GST-GFP</i> <i>ade6-704 ura4-294 leu1-32 h<sup>-</sup></i>
SO8766	DG sensor	<i>ura4<sup>+</sup>::promoter<sup><i>cdc15</i></sup>-DG sensor-GST-GFP</i> <i>ade6-704 ura4-294 leu1-32 h<sup>-</sup></i>
SO8767	NLS DG sensor	<i>ura4<sup>+</sup>::promoter<sup><i>cdc15</i></sup>-NLS DG sensor-GST-GFP</i> <i>ade6-704 ura4-294 leu1-32 h<sup>-</sup></i>

to *S. pombe* [4]. This is not due to the promoter usage, as the DG sensors driven by the same regulatory elements are expressed well. It is possible that the sensor stability could be affected by differences in acyl chain composition in the two species [4, 39].

5. Volume of agarose gel depends on the DNA gel electrophoresis system used.
6. If the restriction enzymes have two different optimal temperatures, perform the digest for 30 min at the lower temperature followed by 30 min at the higher temperature.
7. Ligation ratio 1:3 up to 1:8 of vector/insert. Use an online ligation calculator (e.g., the NEBioCalculator at <https://nebiocalculator.neb.com/#!/ligation>) to determine the amount and volume required, as this depends on both the concentration and size of the respective fragments.
8. Avoid centrifuging cells for imaging at high speeds to reduce stress.
9. Once molten, the agarose-containing medium kept at 65 °C can be used to make more agarose pads on the same day.
10. Optimal agarose pad thickness is approximately 1–2 mm. It can be adjusted by using spacers of appropriate thickness.
11. Live cell imaging is typically performed at 30 °C for *S. pombe* cells, unless working with temperature-sensitive mutants or temperature shift-based experiments.

---

## Acknowledgments

This research was funded in whole, or in part, by the Wellcome Trust (103741/Z/14/Z; 220790/Z/20/Z) grants awarded to S.O. and supported by the Francis Crick Institute, which receives its core funding from Cancer Research UK (CC0102), the UK Medical Research Council (CC0102), and the Wellcome Trust (CC0102). For the purpose of Open Access, the author has applied a CC-BY public copyright license to any Author Accepted Manuscript version arising from this submission.

## References

1. Harayama T, Riezman H (2018) Understanding the diversity of membrane lipid composition. *Nat Rev Mol Cell Biol* 19:281–296. <https://doi.org/10.1038/nrm.2017.138>
2. Vance JE (2015) Phospholipid synthesis and transport in mammalian cells. *Traffic* 16:1–18. <https://doi.org/10.1111/tra.12230>
3. Haider A, Wei Y-C, Lim K et al (2018) PCYT1A regulates phosphatidylcholine homeostasis from the inner nuclear membrane in response to membrane stored curvature elastic stress. *Dev Cell* 45:481–495. <https://doi.org/10.1016/j.devcel.2018.04.012>
4. Foo S, Cazenave-Gassiot A, Wenk MR, Oliferenko S (2023) Diacylglycerol at the inner

- nuclear membrane fuels nuclear envelope expansion in closed mitosis. *J Cell Sci* 136: 260568. <https://doi.org/10.1242/jcs.260568>
5. Makarova M, Gu Y, Chen J-S et al (2016) Temporal regulation of lipin activity diverged to account for differences in mitotic programs. *Curr Biol* 26:237–243
  6. Barbosa AD, Sembongi H, Su W-M et al (2015) Lipid partitioning at the nuclear envelope controls membrane biogenesis. *MBoC* 26:3641–3657. <https://doi.org/10.1091/mbc.E15-03-0173>
  7. Villani M, Subathra M, Im Y-B et al (2008) Sphingomyelin synthases regulate production of diacylglycerol at the Golgi. *Biochem J* 414: 31–41. <https://doi.org/10.1042/BJ20071240>
  8. Carlton JG, Jones H, Eggert US (2020) Membrane and organelle dynamics during cell division. *Nat Rev Mol Cell Biol* 21:151–166. <https://doi.org/10.1038/s41580-019-0208-1>
  9. Cullen PJ, Carlton JG (2012) Phosphoinositides in the mammalian endo-lysosomal network. *Subcell Biochem* 59:65–110. [https://doi.org/10.1007/978-94-007-3015-1\\_3](https://doi.org/10.1007/978-94-007-3015-1_3)
  10. Barbosa AD, Lim K, Mari M et al (2019) Compartmentalized synthesis of triacylglycerol at the inner nuclear membrane regulates nuclear organization. *Dev Cell* 50:755–766. <https://doi.org/10.1016/j.devcel.2019.07.009>
  11. Laguerre A, Schultz C (2018) Novel lipid tools and probes for biological investigations. *Curr Opin Cell Biol* 53:97–104. <https://doi.org/10.1016/jceb.2018.06.013>
  12. Iglesias-Artola JM, Nadler A (2023) The road to quantitative lipid biochemistry in living cells. *Acc Chem Res* 56:810–820. <https://doi.org/10.1021/acs.accounts.2c00804>
  13. Schultz C, Brügger B (2023) Chemical tools for lipid cell biology. *Acc Chem Res* 56:983. <https://doi.org/10.1021/acs.accounts.3c00225>
  14. Kuerschner L, Thiele C (2022) Tracing lipid metabolism by alkyne lipids and mass spectrometry: the state of the art. *Front Mol Biosci* 9:880559. <https://doi.org/10.3389/fmolb.2022.880559>
  15. John Peter AT, Kornmann B (2024) Uncovering mechanisms of interorganelle lipid transport by enzymatic mass tagging. *FEBS Lett*. <https://doi.org/10.1002/1873-3468.14810>
  16. John Peter AT, Petrungaro C, Peter M, Kornmann B (2022) METALIC reveals interorganelle lipid flux in live cells by enzymatic mass tagging. *Nat Cell Biol* 24:996–1004. <https://doi.org/10.1038/s41556-022-00917-9>
  17. Ganesan S, Sosa Ponce ML, Tavassoli M et al (2019) Metabolic control of cytosolic-facing pools of diacylglycerol in budding yeast. *Traffic* 20:226–245. <https://doi.org/10.1111/tra.12632>
  18. Romanauska A, Köhler A (2018) The inner nuclear membrane is a metabolically active territory that generates nuclear lipid droplets. *Cell* 174:700–715. <https://doi.org/10.1016/j.cell.2018.05.047>
  19. Kay JG, Koivusalo M, Ma X et al (2012) Phosphatidylserine dynamics in cellular membranes. *Mol Biol Cell* 23:2198–2212. <https://doi.org/10.1091/mbc.e11-11-0936>
  20. Tanimura A, Nezu A, Morita T et al (2002) Interplay between calcium, diacylglycerol, and phosphorylation in the spatial and temporal regulation of PKC $\alpha$ -GFP. *J Biol Chem* 277: 29054–29062. <https://doi.org/10.1074/jbc.M201130200>
  21. Vermeer JEM, van Wijk R, Goedhart J et al (2017) In vivo imaging of diacylglycerol at the cytoplasmic leaflet of plant membranes. *Plant Cell Physiol* 58:1196–1207. <https://doi.org/10.1093/pcp/pcx012>
  22. Lučić I, Truebestein L, Leonard TA (2016) Novel features of DAG-activated PKC isozymes reveal a conserved 3-D architecture. *J Mol Biol* 428:121–141. <https://doi.org/10.1016/j.jmb.2015.11.001>
  23. Hofbauer HF, Gecht M, Fischer SC et al (2018) The molecular recognition of phosphatidic acid by an amphipathic helix in Opi1. *J Cell Biol* 217:3109–3126. <https://doi.org/10.1083/jcb.201802027>
  24. Loewen CJR, Gaspar ML, Jesch SA et al (2004) Phospholipid metabolism regulated by a transcription factor sensing phosphatidic acid. *Science* 304:1644–1647. <https://doi.org/10.1126/science.1096083>
  25. Marek M, Vincenzetti V, Martin SG (2020) Sterol biosensor reveals LAM-family Ltc1-dependent sterol flow to endosomes upon Arp2/3 inhibition. *J Cell Biol* 219: e202001147. <https://doi.org/10.1083/jcb.202001147>
  26. Maekawa M, Yang Y, Fairn GD (2016) Perfringolysin O theta toxin as a tool to monitor the distribution and inhomogeneity of cholesterol in cellular membranes. *Toxins (Basel)* 8:67. <https://doi.org/10.3390/toxins8030067>
  27. Harris MA, Rutherford KM, Hayles J et al (2022) Fission stories: using PomBase to understand *Schizosaccharomyces pombe* biology.

- Genetics 220:iyab222. <https://doi.org/10.1093/genetics/iyab222>
28. Rutherford KM, Harris MA, Oliferenko S, Wood V (2022) JaponicusDB: rapid deployment of a model organism database for an emerging model species. Genetics 220:iyab223. <https://doi.org/10.1093/genetics/iyab223>
  29. Keeney JB, Boeke JD (1994) Efficient targeted integration at leu1-32 and ura4-294 in *Schizosaccharomyces pombe*. Genetics 136:849–856. <https://doi.org/10.1093/genetics/136.3.849>
  30. Álvarez-Fernández R (2013) Explanatory chapter: PCR primer design. Methods Enzymol 529:1–21. <https://doi.org/10.1016/B978-0-12-418687-3.00001-X>
  31. Dieffenbach CW, Lowe TM, Dveksler GS (1993) General concepts for PCR primer design. PCR Methods Appl 3:S30–S37. <https://doi.org/10.1101/gr.3.3.s30>
  32. Gibson DG, Young L, Chuang R-Y et al (2009) Enzymatic assembly of DNA molecules up to several hundred kilobases. Nat Methods 6:343–345. <https://doi.org/10.1038/nmeth.1318>
  33. Moreno S, Klar A, Nurse P (1991) Molecular genetic analysis of fission yeast *Schizosaccharomyces pombe*. Methods Enzymol 194:795–823. [https://doi.org/10.1016/0076-6879\(91\)94059-1](https://doi.org/10.1016/0076-6879(91)94059-1)
  34. Murray JM, Watson AT, Carr AM (2016) Transformation of *Schizosaccharomyces pombe*: electroporation procedure. Cold Spring Harb Protoc 2016:pdb.prot090951. <https://doi.org/10.1101/pdb.prot090951>
  35. Pemberton LF (2014) Preparation of yeast cells for live-cell imaging and indirect immunofluorescence. In: Smith JS, Burke DJ (eds) Yeast genetics: methods and protocols. Springer, New York, pp 79–90
  36. Rodrigues NTL, Bland T, Borrego-Pinto J et al (2022) SAIBR: a simple, platform-independent method for spectral autofluorescence correction. Development 149:dev200545. <https://doi.org/10.1242/dev.200545>
  37. Schindelin J, Arganda-Carreras I, Frise E et al (2012) Fiji: an open-source platform for biological-image analysis. Nat Methods 9:676–682. <https://doi.org/10.1038/nmeth.2019>
  38. Vještica A, Marek M, Nkosi PJ et al (2020) A toolbox of stable integration vectors in the fission yeast *Schizosaccharomyces pombe*. J Cell Sci 133:jcs240754. <https://doi.org/10.1242/jcs.240754>
  39. Makarova M, Peter M, Balogh G et al (2020) Delineating the rules for structural adaptation of membrane-associated proteins to evolutionary changes in membrane lipidome. Curr Biol 30:367–380. <https://doi.org/10.1016/j.cub.2019.11.043>



# Chapter 8

## Measuring Molecular Mass Densities at Subcellular Resolution Using Optical Diffraction Tomography

Kyoohyun Kim, Abin Biswas, Jochen Guck, and Simone Reber

### Abstract

Biological systems intricately regulate their density and volume throughout their life cycles and in response to physiological changes. Mass density, as a fundamental physical quantity, plays significant roles in biological processes such as differentiation, cell growth, protein synthesis, and condensate formation. Loss of density homeostasis on the other hand can have severe consequences including cellular senescence and disease states. Recent developments in biophotonics now enable high-resolution density quantification, providing new insights into the biophysical properties of cells and subcellular structures. One such technique is optical diffraction tomography (ODT), which offers label-free, high-resolution measurements of mass density distribution based on refractive index (RI) measurements. In this chapter, we present a comprehensive guide to implementing ODT for quantitative characterization of mass density distribution in biological systems, including in vivo (adherent cell culture) and in vitro (*Xenopus* egg extract) samples. We begin by detailing the optical setups, emphasizing key considerations for optimizing tomography acquisition. Subsequently, we introduce preparation protocols tailored to biological samples in various types of sample carriers and offer guidance on standard image acquisition and data analysis procedures. Finally, we address the challenges posed by the linear relationship between RI and mass density in complex substances, offering strategies for overcoming these limitations.

**Key words** Mass density, Nucleoplasm, Cytoplasm, Optical diffraction tomography, Label-free imaging

---

### 1 Introduction

The nuclear membrane provides a selective barrier that physically separates two compartments: the nucleoplasm and the cytoplasm, each possessing unique macromolecular identities and functions. Components essential for DNA replication and RNA transcription are enriched in the nucleoplasm, whereas the cytoplasm is packed with components necessary to enable protein translation. While the absolute solute concentration (density) and composition can vary

---

Authors “Kyoohyun Kim” and “Abin Biswas” have equally contributed to this chapter.

Yuki Hara and Kazunori Kume (eds.), *The Nuclear Membrane: Methods and Protocols*, Methods in Molecular Biology, vol. 2958, [https://doi.org/10.1007/978-1-0716-4714-1\\_8](https://doi.org/10.1007/978-1-0716-4714-1_8),  
© The Author(s), under exclusive license to Springer Science+Business Media, LLC, part of Springer Nature 2025

significantly between compartments, cell types and different species [1–4], there appear to be some common features. For example, cellular density shows very little variability for a given cell type and is consistently maintained through the cell cycle [5] and during early development [4]. Perturbing cytoplasmic density can influence biological function by altering the global rates of protein translation and degradation [6], can affect cytoskeletal dynamics [7] and has been linked to altered physiological states such as senescence [8]. But how does one reliably measure this basic biophysical property?

Traditionally, density gradient centrifugation has been used to identify and separate cells of different densities [9]. Modern methods to measure density include suspended channel microresonators [10] or optical techniques such as quantitative phase imaging (QPI) [11, 12]. QPI has emerged as a precise and robust method to quantify subcellular densities with high spatial resolution. One promising variant of this technique is optical diffraction tomography (ODT), which can be conceptualized as a three-dimensional (3D) extension of QPI. ODT quantitatively measures the 3D refractive index (RI), from which the mass density of biological samples can be calculated. Hence, ODT enables comprehensive characterization of biological biochemistry and morphology. Since the RI is an intrinsic optical property of materials, ODT offers a direct, label-free imaging approach, circumventing the need for complex sample preparation and reducing the risk of photobleaching, phototoxicity, and quenching commonly associated with fluorescence techniques. What can we learn by measuring the mass density with subcellular resolution?

ODT has been used to investigate the material properties of protein-rich ensembles like the metaphase spindle [13], to precisely measure the concentration of macromolecules within condensates both *in vitro* and *in vivo* [14–19] and to assay biophysical transitions during stressed cellular states in diverse organisms [20, 21]. Surprisingly, recent work using ODT has revealed that the cell's nucleus exhibits a lower mass density as the cytoplasm, with a nucleocytoplasmic (NC) density ratio consistently below 1 [4, 5]. This was observed across multiple eukaryotic species [4, 5] and remained robust even under significant perturbations to cell cycle progression, cytoskeleton polymerization, and chromatin compaction [5]. In addition to mass density measurements, the 3D tomograms obtained from ODT can be used to detect morphological changes by directly measuring volume without using exogenous dyes. Combining the mass density and volume information can provide the dry mass. Additionally, with sufficient knowledge of the sample, one can also estimate the volume fraction of a specific component, as has been demonstrated for protein condensates [18, 19]. In addition to quantitative characterization, the parameters measured and derived from RI measurements can

enrich or constrain physical models that quantitatively describe biological processes such as nuclear-to-cytoplasmic volume and density ratios [4, 22, 23].

In this chapter, we offer an overview of the setup and experimental methodologies employed for conducting mass density characterization of biological samples using ODT. We outline a range of optical setups, preparation protocols tailored to biological in vivo (adherent cell culture) and in vitro (*Xenopus* egg extract) samples, address potential challenges encountered during measurements, and offer guidance on standard data analysis procedures. Furthermore, we present examples of nuclear and cytoplasmic mass density measurements in HeLa cells and *Xenopus* egg extracts. We conclude with a discussion on the technical challenges of ODT measurements and offer possible solutions.

---

## 2 Preparing for ODT Measurements

In this section, we provide a detailed description of a general optical setup suitable for imaging both in vivo and in vitro systems. Our goal is to accommodate a wide range of experimental conditions and sample types, enabling researchers to apply the same setup across various biological contexts and quantitatively characterize subcellular mass densities. We here focus on nuclei and the cytoplasm, but such measurements can easily be extended to mitochondria [24, 25], lipid droplets [26–28], or other subcellular regions of interest. Specifically, we focus on two representative systems: adherent mammalian cells cultured on 2D surfaces for in vivo imaging, and cytoplasmic extracts prepared from *Xenopus laevis* frog eggs for in vitro reconstituted systems.

### 2.1 ODT Setup

QPI measures the optical phase delay experienced by light passing through samples. This phase delay occurs because the RI values of samples are typically higher than those of the surrounding medium, causing the speed of light passing through the samples to slow down and resulting in phase retardation. Traditional imaging detectors, however, can only detect the intensity of light, as the frequency of light in the visible range is hundreds of terahertz while the fastest electronics can only measure wave frequencies up to gigahertz, leading to the loss of phase delay information. QPI employing interferometry enables the phase delay measurements by recording interference patterns (hologram), which encode phase delay information. It can be retrieved with Fourier transform-based calculations (*see* Subheading 4.1.2). The phase delay measured,  $\phi(x, y)$ , is the integral of RI contrast between samples,  $n$ , and the medium,  $n_m$ , along the axial direction, as  $\phi(x, y) = \frac{2\pi}{\lambda} \int [n(x, y, z) - n_m] dz$ , where  $\lambda$  is the wavelength of

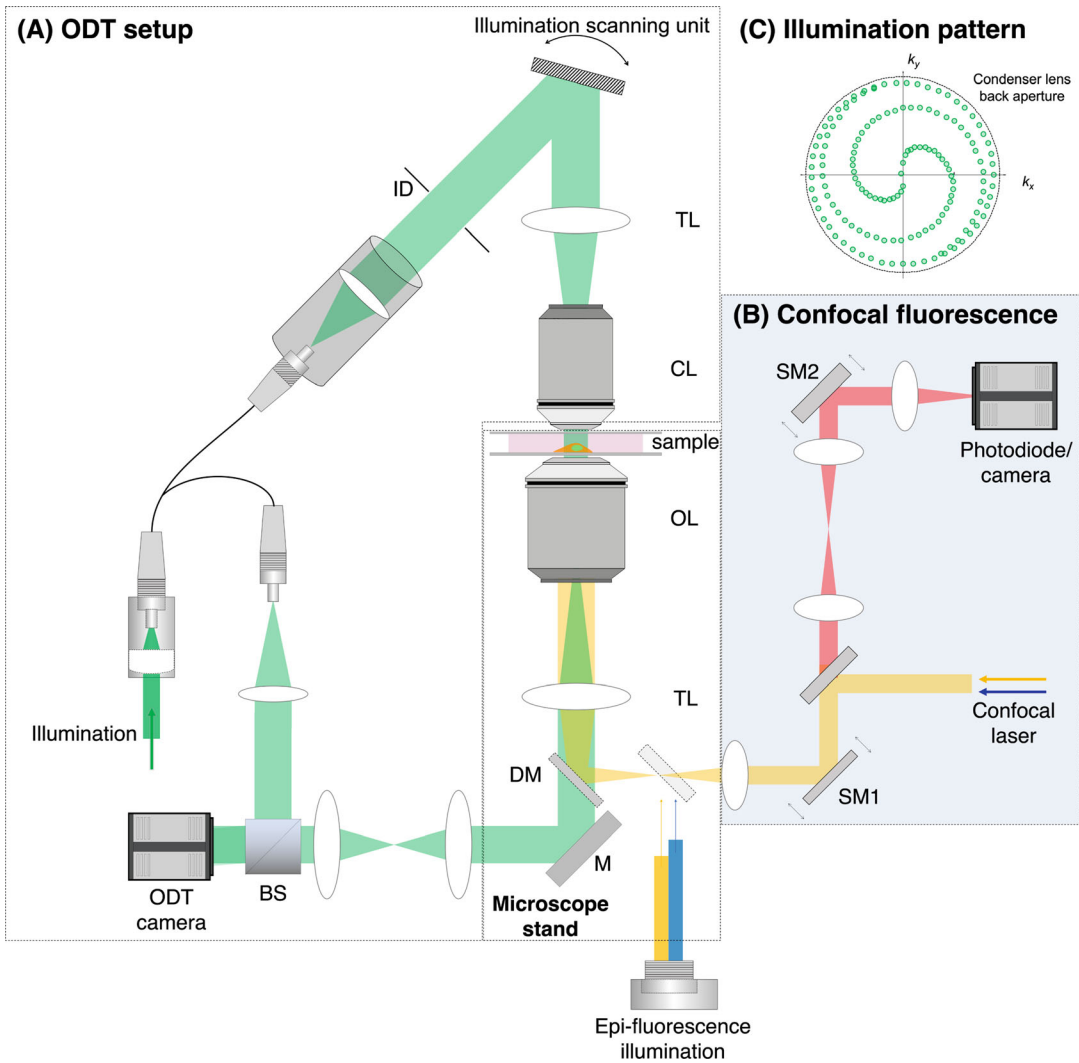


**Fig. 1** Schematic of the optical setup for ODT. **(a)** Typical schematic of the optical setup for ODT. *ID* iris diaphragm, *TL* tube lens, *CL* condenser lens, *OL* objective lens, *DM* dichroic mirror, *M* mirror, *BS* beam splitter. Epi-fluorescence illumination can be combined in the optical setup and the same ODT camera can detect the fluorescence emission signals. **(b)** Alternatively, a confocal fluorescence microscope can be attached to the ODT setup. *SM* scanning mirror. **(c)** Spatial frequency of the spiral illumination pattern for the current ODT setup

light; to fully characterize the 3D RI distribution from measured phase delay maps, tomographic measurements are necessary, forming the basis of ODT.

The experimental ODT setup employs Mach-Zehnder interferometry to capture multiple optical fields from diverse incident angles (Fig. 1). The optical setup can be built around a commercially available microscope stand (such as Axio Observer 7, Zeiss, Germany or Olympus IX81 series, Olympus, Japan) or a custom-

made microscope stand. A collimated illumination beam is split into two paths via a beamsplitter. One path serves as a reference beam, while the other path serves as a sample beam to illuminate the sample positioned on the stage of an inverted microscope through a tube lens and an objective lens. The scattered light from the sample is collected by a high numerical aperture (NA) objective lens in the inverted microscope. The sample beam and the reference beam interfere at the camera plane to generate the interference patterns. For tomographic acquisition, the illumination scanning unit is positioned at the conjugate plane of the sample in the upper part of the sample beam. Multiple interference patterns are sequentially generated by scanning different illumination angles impinging on the sample. These interference patterns are then measured to reconstruct a 3D RI tomogram using the calculation steps outlined in Subheading 4.1.2.

Several considerations should be taken into account when choosing the illumination source and its wavelength, objective lenses, and the illumination scanning unit. These factors can significantly impact the quality and resolution of the tomographic images. For detailed insights into these considerations, please refer to Subheading 6 (*see Notes 1–4*).

#### 2.1.1 Combination with Fluorescence

Integrating the optical setup for ODT with epi-fluorescence or confocal fluorescence microscopy offers the advantage of acquiring additional molecular specificity, facilitating the determination of local RI and mass density of biological materials and subcellular compartments of interest (Fig. 1b). Moreover, fluorescence images can serve as masks for segmenting subcellular organelles, enabling quantitative analysis of their dry mass, mass density, and volume.

For epi-fluorescence microscopy, the excitation beam path can be coupled using a dichroic beamsplitter, and the epi-fluorescence image can be detected using the same ODT camera, simplifying the colocalization of RI tomograms and epi-fluorescence images. On the other hand, confocal fluorescence microscopy offers higher imaging contrast and enhanced spatial resolution of fluorescence images but requires careful registration of the field of view (FOV) between the ODT camera and a detector (camera or photodiode) in confocal fluorescence microscopy.

In addition to determining the local RI and dry mass of subcellular organelles through colocalization of RI tomograms and fluorescence images, 3D confocal fluorescence images can aid in estimating the 3D morphology of samples. This information can be utilized for regularization with high accuracy, effectively mitigating the missing cone artifact [29] (*see Subheading 4.1.3*).

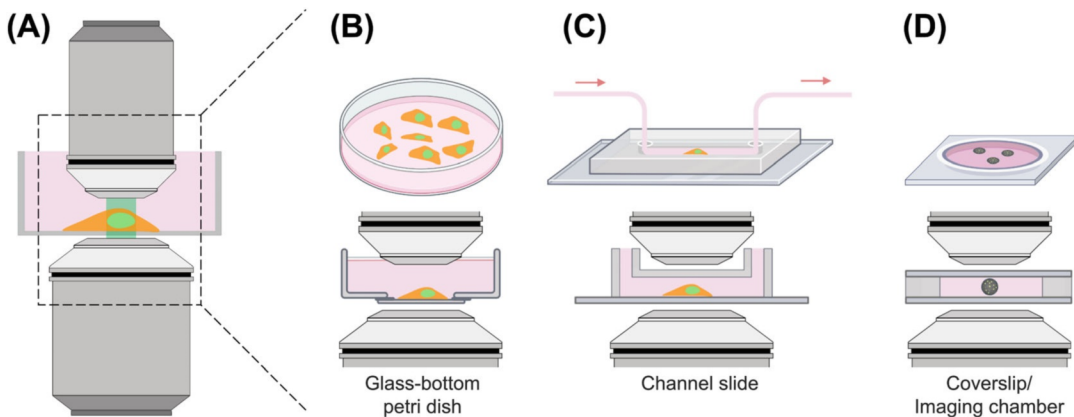


**Fig. 2** Schematic of various sample mounting methods for ODT measurements. **(a)** The dashed lines indicate the placement of samples mounted between a condenser and objective lens. **(b–d)** Top (upper row) and side (lower row) views of each sample mounting method. **(b)** In vivo samples cultured on a glass-bottom petri dish. If a water-dipping objective lens is used as the condenser lens, it is immersed in the culture medium. **(c)** In vivo samples cultured inside a channel slide. Fluidic pressure pumps and flow switches can be attached for sophisticated flow control. **(d)** In vitro samples in an imaging chamber made of two coverslips. (Figure 2b–d were created with BioRender)

## 2.2 Sample Preparation

Depending on the biological question and context, density can be determined in vivo as well as in in vitro systems. Here, we showcase one representative system each: adherent mammalian cells cultured on 2D surfaces for in vivo imaging, and cytoplasmic extracts prepared from *Xenopus laevis* frog eggs for in vitro imaging. In this chapter, we present preparation protocols suitable for live samples, taking advantage of the minimal phototoxicity inherent to ODT. The optical intensity of the collimated laser beam at the sample plane in the current ODT setup is less than  $0.005 \mu\text{W}/\mu\text{m}^2$ , whereas the typical optical intensity of a laser focus on the sample for confocal fluorescence microscopy is around  $400 \mu\text{W}/\mu\text{m}^2$ . It is worth noting that the laser beam for ODT illumination is *collimated*, resulting in exposure to an extremely low dose of laser illumination for each sample. Additionally, the preparation protocols are applicable to fixed samples, although it is important to note that chemical fixation may alter the morphology [30] and RI values in biological samples [31].

Since the samples are mounted in the limited space between the objective and condenser lenses (Fig. 2a), a variety of mounting methods utilizing different types of carriers are employed to accommodate both in vivo and in vitro samples, each tailored to their specific cell types and research objectives.

### 2.2.1 Preparation for In Vivo Samples

Adherent mammalian cells typically exhibit well-defined morphology and attachment to the substrate, making them ideal for high-resolution imaging. The flattened and spread-out shape of adherent

cells allows for clear visualization of nuclear and cytoplasmic compartments and even finer structures such as the nuclear envelope (Fig. 4e). For ODT measurements, cells can be mounted using various carriers, such as glass-bottom petri dishes, channel slides, or coverslips with spacers.

1. Glass-bottom petri dish (Fig. 2b)

Glass-bottom petri dishes from various manufacturers (e.g., FluoroDish from World Precision Instruments GmbH or ibi-treated  $\mu$ -Dish from ibidi GmbH) offer an optimal environment for both cell culture and high-resolution imaging within the same dish. This is due to their glass bottom surface, which has the thickness of a coverslip, and a lid that secures a sterile environment. The cells are subcultured in a glass-bottom petri dish at least 1 day prior to the measurement. For a petri dish with a 35 mm diameter, a suspension of  $4\text{--}9 \times 10^4$  cells/ml should result in a 50% confluent HeLa cell layer within a day. If the ODT setup does not have a stage-top incubator to maintain the  $\text{CO}_2$  concentration, the culture medium is exchanged to  $\text{CO}_2$ -independent medium (18045088, Thermo Fisher Scientific, Inc.) or Leibovitz L-15 medium (21083027, Thermo Fisher Scientific, Inc.) prior to imaging. If the ODT setup utilizes a condenser lens with a long working distance, the lid of the petri dish can remain closed, preserving the sterile environment for an extended period. However, if a water-dipping objective lens is employed as a condenser, the lid of the petri dish must be opened. In this configuration, the condenser lens is immersed in the culture medium of the petri dish when it is positioned correctly along the optical axis.

2. Channel slide (Fig. 2c)

Channel slides, like  $\mu$ -Slide I Luer from ibidi GmbH, offer a convenient and efficient method for quickly replacing medium or applying drugs during experiments. Integration of flow control components including pressure pumps and fluidic valves enables rapid exchange of culture medium, facilitating high-speed time-lapse measurements of the instantaneous RI changes of cells requiring imaging of the same FOV over time, such as cell detachment or hyper/hypo-osmotic stress within a short time frame.

3. Coverslip (Fig. 2d)

The simplest method to mount samples involves sandwiching them between two coverslips. This approach is efficient and straightforward, particularly suitable for cells in suspension like blood or yeast cells, which may easily become defocused if using glass-bottom petri dishes or channel slides. By sandwiching the cells in suspension between coverslips, the samples remain in a focal plane, ensuring optimal imaging conditions.

To prevent sample compression by the upper coverslip, a proper spacer can be placed between the coverslips. This spacer can be made from punched double-sided sticky tape or obtained commercially as Secure-Seal™ Spacer.

Despite being sandwiched between coverslips, cells in suspension may still exhibit movement within the FOV due to thermal fluctuations or active motion. This motion can lead to motion blurring artifacts that degrade the quality of reconstructed tomograms. To immobilize the samples and mitigate motion artifacts, the sample surface can be treated with substances like poly-L-lysine (P4707, Sigma-Aldrich), lectin (L1395, Sigma-Aldrich), or Cell-Tak (Corning). Alternatively, an agar gel pad can be used between the coverslips to provide a stable environment for the samples [32].

#### 4. Correlative fluorescence imaging.

Combined with fluorescence microscopy (*see* Subheading 2.1.1), the local mass density in a subcellular region of interest can be easily determined from fluorescence staining with live dyes (i.e., Hoechst 33342 or SYTO™ for nuclei). For example, we were interested whether the nucleus changes its density through the cell cycle. To this aim, we used HeLa human cervical cancer cells transfected with the fluorescence ubiquitination cell cycle indicator (FUCCI) cell cycle sensor [33] are used. The FUCCI marker emits monomeric Kusabira-Orange 2 (mKO2) at the G1 stage and monomeric Azami-Green 1 (mAG1) at the G2 stage.

#### 2.2.2 Preparation for In Vitro Samples

The cell-free *Xenopus* egg extract system is prepared by crushing *Xenopus* eggs with a high-speed centrifuge. Extracts present a unique opportunity to directly probe and perturb material properties in a cytoplasm enriched with macromolecules at physiological concentrations. The open nature of the system allows users to add in fluorescent dyes, drugs, and other molecules of interest easily. Importantly, the system supports the in vitro reconstitution of intracellular organelles like the metaphase spindle or nuclei. These organelles are relatively large (tens of microns in length), are functional and can be easily measured using fluorescent and label-free imaging techniques. Recently, we have utilized the extract system to examine the biochemical and biophysical mechanisms regulating nuclear mass density [4]. For details regarding the preparation of cytoplasmic extracts, isolation of a chromatin source such as sperm nuclei and in vitro nuclear assembly, we urge readers to look at detailed protocols that have been published previously [34–38]. We suggest using coverslips to image reconstituted organelles (*see* below):

### 1. Coverslip (Fig. 2d)

As mentioned in Subheading 2.2.1, coverslips provide an affordable and efficient mounting alternative that provides a thin sample layer and optimal imaging conditions. When using coverslips for imaging *Xenopus* egg extracts, ensure that the coverslip is clean and free from debris by gently wiping the glass surface with lens-paper and ethanol. Depending on the coverslip size ( $18 \times 18 - 24 \times 40$  mm), 5–10  $\mu\text{L}$  of extract can be sandwiched between two coverslips. Despite being sandwiched, assembled nuclei remain functional and are both import and replication competent [4, 36]. To prevent squashing, coverslips with spacers can also be used. In our experience, chambers with a height of up to 100  $\mu\text{m}$  can be used without loss in tomogram quality. Additionally, ODT allows users to measure subtle RI (and mass density) changes between the reconstituted organelles and the cytoplasm (*see* Fig. 5), due to its enhanced sensitivity [5].

### 2.2.3 In Vivo and In Vitro Perturbations

Nuclear morphology and density can be perturbed in both cultured cells or *Xenopus* egg extracts using multiple strategies. Here we provide a brief overview of some relevant biophysical and biochemical perturbations.

#### 1. In Vivo Biochemical Perturbations

The cellular nucleus represents a complex system in biophysics and biomechanics, subject to tension from the cytoskeleton and anchored to the cell membrane. Consequently, disruptions in cytoskeleton polymerization may perturb the pressure equilibrium across the nuclear envelope, leading to alterations in nuclear mass density. Chemical treatments such as cytochalasin D and nocodazole induce the depolymerization of actin and microtubules, respectively, leading to changes in mass density in the nucleoplasm and cytoplasm, which can be captured by ODT. Additionally, chromatin compaction within the nucleus can be directly modulated by chemicals like trichostatin A (which induces decondensation) and anacardic acid (which induces condensation), allowing for monitoring of cellular responses in ODT measurements [5].

#### 2. In Vitro Biochemical Perturbations

In addition to biochemical perturbations using drugs and small molecule inhibitors, the extract system allows for perturbations that would usually not be tolerated well by cultured cells. These include perturbations directed towards modifying chromatin state by cross-linkers or extreme alterations in osmotic conditions. Further, it is possible to generate unique phenotypes in vitro such as poreless nuclei using the calcium chelator BAPTA [39] or to directly target a protein/complex of interest during the establishment of nucleoplasmic and cytoplasmic compartments.

### 3 Tomogram Acquisition

Image acquisition is facilitated by a custom-written MATLAB GUI software available in Github (Table 1), which enables the control of various components including the camera, the microscope stage, and the digital acquisition box (e.g., National Instruments (NI)-DAQ) for applying voltage to the Galvanomirror and triggering signals to the camera and laser shutter.

#### 3.1 Initialization

1. Mount the samples using an appropriate carrier such as a petri dish, coverslips, or microfluidic channels (*see* Subheading 2.2).
2. In the acquisition software, establish connections with the digital acquisition box and camera.
3. Place the objective lens and condenser lens at the correct axial position. If using an immersion objective lens, apply a drop of immersion medium.
4. Adjust the axial position of the objective lens to achieve sample focus (Fig. 3, lower row). The best sample focus is achieved at the plane with the minimized diffraction from samples.
5. Close the iris diaphragm (ID in Fig. 1a) to locate the beam center. If the condenser lens is mounted on an x-y kinematic optic mount, adjust its x and y positions to place the beam center in the center of the camera FOV.
6. Place the condenser lens at the correct axial position to ensure that the beam center remains stationary while the Galvanomirror changes the angle of illumination (Fig. 3, upper row). Open the iris diaphragm fully to secure the maximum beam size.

#### 3.2 Data Acquisition

1. Locate the sample of interest within the FOV of the camera. The FOV available to the user will depend on the NA of the objective lens, total magnification, camera pixel number, and

**Table 1**  
**List of custom-made scripts and software**

1 Tomogram acquisition	<a href="https://github.com/OpticalDiffractionTomography/ODT_Image_Acquisition">https://github.com/OpticalDiffractionTomography/ODT_Image_Acquisition</a>
2 Tomogram reconstruction	<a href="https://github.com/OpticalDiffractionTomography/ODT_Reconstruction">https://github.com/OpticalDiffractionTomography/ODT_Reconstruction</a>
3 Open source tomogram visualization	tomviz, <a href="https://tomviz.org/">https://tomviz.org/</a> ImageJ/FIJI (clear volume) <a href="https://imagej.net/plugins/clearvolume">https://imagej.net/plugins/clearvolume</a>
4 Segmentation/analysis of in vivo samples	<a href="https://github.com/OpticalDiffractionTomography/NucleiAnalysis">https://github.com/OpticalDiffractionTomography/NucleiAnalysis</a>
5 Segmentation of in vitro samples	<a href="https://sites.imagej.net/SCF-MPI-CBG/">https://sites.imagej.net/SCF-MPI-CBG/</a>

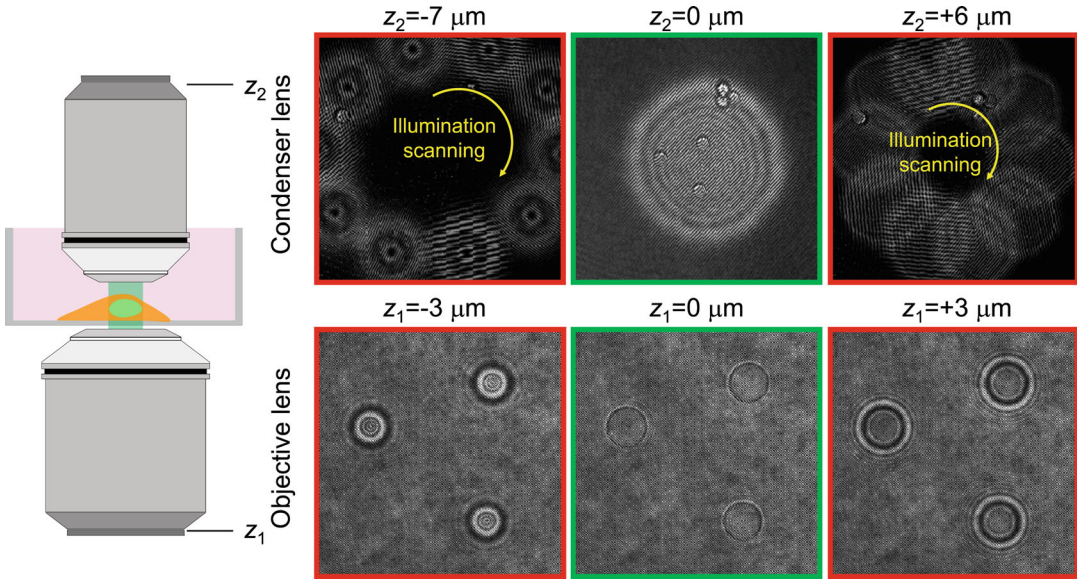


**Fig. 3** The process of finding the correct axial position of both the objective lens (lower row) and the condenser lens (upper row). The samples shown here are silica beads in water. The optimal sample focus is identified at the plane with minimal diffraction from the samples (indicated by the green box). The proper axial position of the condenser lens is obtained when the beam center remains stationary while the Galvanomirror changes the angle of illumination (indicated by the green box). Conversely, if the condenser lens position is incorrect, the beam position changes with variations in the angle of illumination

camera pixel size, and it should fulfill the Nyquist-Shannon theorem for hologram formation [40]. The FOV of the current setup is  $100 \times 100 \mu\text{m}$ , with the  $63\times$  objective lens with an NA of 1.3 and the camera pixel size of  $5.5 \mu\text{m}$  (XIMEA GmbH, MQ042MG-CM-TG). For fluorescently labeled samples use either confocal fluorescence or epi-fluorescence imaging mode to find the sample.

2. Capture a series of holograms with various incident angles. Note that acquiring holograms with a larger number of different illumination angles can fill more of the 3D Fourier space during tomogram reconstruction (*see* Subheading 4.1.2), leading to more accurate tomograms, albeit at the cost of longer acquisition times. To strike a balance between tomogram quality and acquisition speed, we opt to scan 150 different illumination angles at a camera frame rate of 150 Hz, which enables us to achieve a tomogram acquisition time of 1 s. For optimal imaging conditions and to mitigate potential photodamage or phototoxicity, it is advantageous to conduct ODT imaging before fluorescence imaging. Given the longer acquisition time required for fluorescence imaging compared to ODT, this sequential approach ensures consistent imaging conditions for both modalities.

3. For samples with simple geometry and homogeneous RI distribution, such as red blood cells and microspheres, our current setup requires a minimum of 10 azimuthal angles. With this configuration, we can achieve a tomogram acquisition rate of up to 15 Hz, maintaining more than 95% of correlation with the tomogram reconstructed with full angles [41].
4. The maximum scanning angle in ODT is determined by the NA of the condenser and objective lens and illuminating samples with larger azimuthal angles improve axial resolution in reconstructed tomograms. Hence, the illumination pattern should cover the entire area within the back aperture of the condenser lens. To minimize mechanical errors associated with the Galvanomirror, our current ODT setup utilizes a spiral illumination pattern that encompasses the maximum boundary of the back aperture of the condenser lens, alongside the normal illumination angle (Fig. 1c).
5. Capture a series of holograms within a FOV devoid of any sample. These holograms serve the purpose of compensating for the background phase gradients induced along the optical paths (*see* Subheading 4.1.1).
6. If the sample size exceeds the FOV of the camera, acquire multiple FOVs and stitch the tomograms together [42]. Ensure an overlap of approximately 20% between adjacent FOVs. When utilizing a motorized stage on the microscope, record the positions of the stage and stitch the reconstructed tomograms accordingly. In cases where a manual stage is used, determine the relative positions of FOVs by identifying the position of the maximum peak of the 2D cross-correlation between adjacent FOVs.
7. The data generated by the current MATLAB GUI software is stored in .mat file format, which is compatible with MATLAB. The recorded interference patterns within a FOV typically has a size of approximately 150 MB (uint8,  $1024 \times 1024 \times 150$  for  $x$ ,  $y$ , and angles).
8. The phase retardation in the 2D quantitative phase image is generated by the difference in the RI between the object and the surrounding. Thus, the absolute RI of the medium or the extract needs to be independently measured by an Abbe refractometer (e.g., 2WAJ, Arcarda GmbH, Germany) as a reference.

---

## 4 Data Analysis

### 4.1 Post-processing

#### 4.1.1 Field Retrieval

Complex optical fields comprising both amplitude and phase delay information are extracted from the recorded holograms using a field retrieval algorithm based on Fourier transform (Fig. 4a, b)

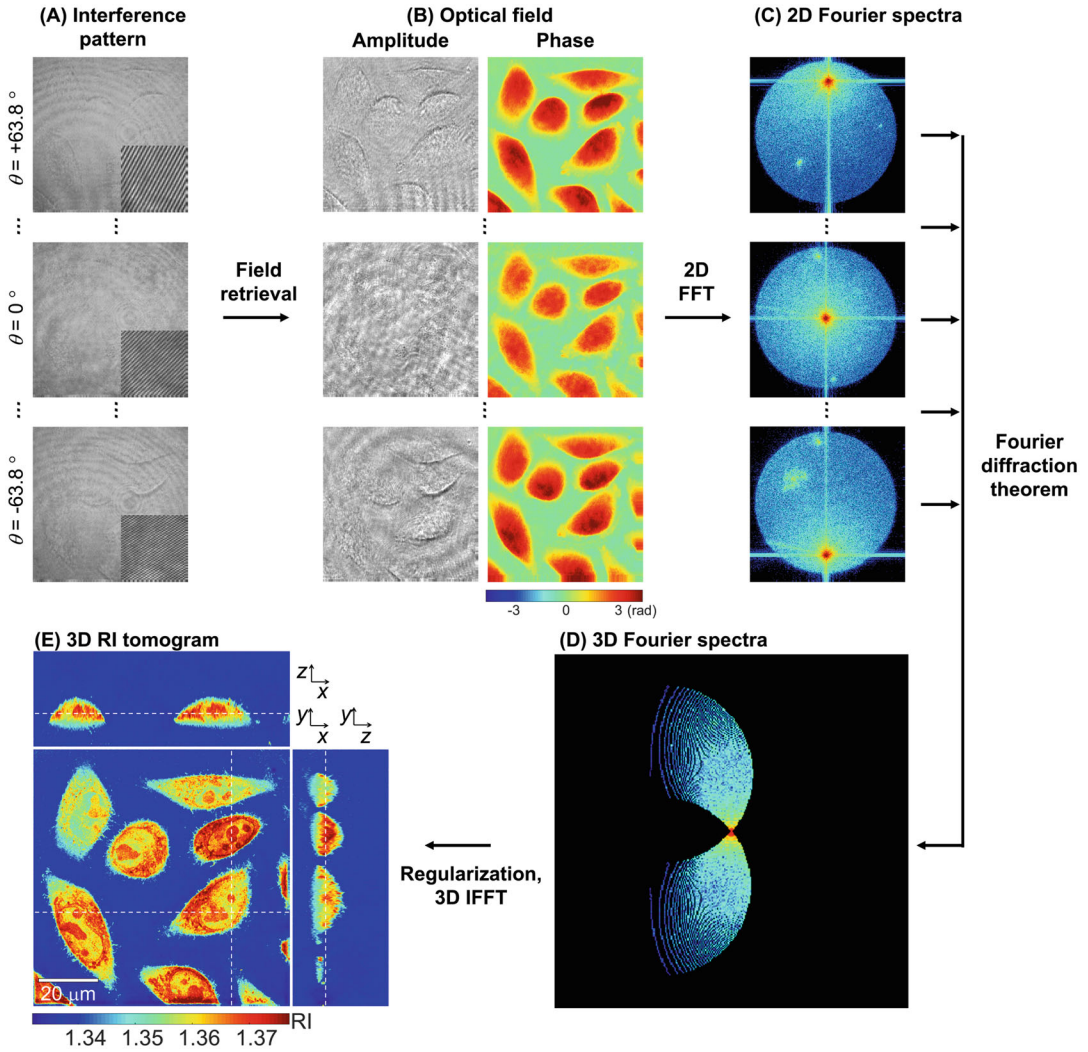


**Fig. 4** Flow chart of data evaluation for ODT. (a) Interference patterns measured with various incident angles of illumination. (b) Optical fields consisting of amplitude and phase retrieved from the measured interference patterns in (a). (c) The 2D Fourier spectra of the optical fields in (b) accordingly. (d) The 3D Fourier space where the 2D Fourier spectra in (c) are mapped according to the Fourier diffraction theorem. (e) The cross-sectional slices of the reconstructed RI tomograms along the  $x$ - $y$ ,  $y$ - $z$ , and  $x$ - $z$  axes. The color ranges in (b) and (e) represent phase values and RI, respectively

[43]. The retrieved phase delay at each angle is subtracted by the phase delay of the background FOV, in order to compensate for any phase gradients induced along the optical paths. As a result, a series of complex optical fields consisting of amplitude and phase delay maps with various incident angles are retrieved (Fig. 4b).

#### 4.1.2 Tomogram Reconstruction

The reconstruction of the 3D RI distribution of the samples is accomplished by applying the Fourier diffraction theorem to the retrieved complex optical fields, utilizing the first-order Rytov approximation [44, 45]. Briefly, the 2D Fourier spectra of each complex optical field (Fig. 4c) are mapped into the 3D Fourier space, whose coordinates are shifted according to the Fourier diffraction theorem (Fig. 4d), and the inverse 3D Fourier transform of the mapped 3D Fourier spectra results in the 3D RI tomogram (Fig. 4e). Further details regarding tomogram reconstruction can be found elsewhere [46]. The MATLAB script for ODT reconstruction is available in Github (Table 1).

The first-order Rytov approximation we have used for tomogram reconstruction assumes single light scattering within the biological samples. This approximation remains valid for reconstructing RI tomograms of a layer of adherent cells and nuclei in *Xenopus* egg extract, given the typical scattering mean free path of biological samples (approximately 100  $\mu\text{m}$ ). However, to extend the analysis to larger and optically denser specimens, recent advancements have led to the development of computational algorithms that account for multiple photon scattering in the sample [47–49]. By employing such algorithms, the application of the ODT setup can be extended to biological samples with a thickness larger than 100  $\mu\text{m}$  and multiple light scattering such as tissues or organoids.

#### 4.1.3 Regularization

The condenser and objective lens of ODT techniques have a finite NA, which limits their angle range of illumination and detection. Consequently, the Fourier space exhibits an inaccessible region corresponding to spatial frequencies beyond the maximum capabilities of the imaging system. This issue, known as the missing cone problem, results in shape elongation and underestimated RI values in reconstructed tomograms.

To address the missing cone problem and improve tomogram quality, several iterative algorithms have been proposed. These algorithms leverage a priori information about the object, such as non-negativity constraint, edge-preserving regularization, and total-variation regularization. Detailed information about these algorithms and comparative studies for reconstructing the 3D RI distribution of biological samples via ODT can be found elsewhere [50]. Additionally, machine-learning algorithms based on the beam propagation method offer another avenue for alleviating the missing cone problem [51].

#### 4.1.4 Visualization

Visual representation of the 3D RI tomogram can be achieved by displaying cross-sectional slices along each axis:  $x$ - $y$ ,  $x$ - $z$ , and  $y$ - $z$  (Fig. 4e). Additionally, the maximum projection of an RI tomogram along the axial direction can be utilized to easily identify the RI distribution of samples located at different axial planes. 3D

rendering can be accomplished using MATLAB Volume Viewer or open-source software such as tomviz or ImageJ/FIJI Clear volume (Table 1).

## 4.2 Quantitative Characterization

### 4.2.1 Segmentation

For the quantitative analysis of the reconstructed 3D RI tomograms, accurate segmentation of the sample is crucial. A common approach is to employ the Otsu's thresholding method, which effectively separates regions occupied by samples from the background. Subsequently, the watershed algorithm can be applied to identify individual objects, such as cells or nuclei from the segmented RI tomograms. Several thresholding strategies are available both in MATLAB and FIJI, either as standalone plugins or already incorporated into the base software. Further refinement of segmentation can be achieved by integrating fluorescence images (Fig. 5b, d). This additional information enables enhanced quantitative analysis of individual subcellular compartments, including nuclei and cytoplasm.

For example, the 3D segmentation of HeLa cells and their nuclei is performed using custom-written MATLAB scripts, which are available in GitHub (Table 1). For 3D segmentation in *Xenopus* egg extracts, nuclei can either be segmented manually or using the 3D volume manager plugin (part of the Bio Image Analysis Toolbox from the Scientific Computing Facility, MPI-CBG (Table 1).

Recent advancements in machine learning have introduced sophisticated segmentation algorithms based on neural networks, enabling accurate delineation of cellular boundaries between attached neighboring cells [52], determination of cell cycles [53], and identification of subcellular organelles without fluorescence labeling [54, 55]. The use of these advanced segmentation algorithms promises to extend the capabilities of ODT in quantitative analysis.

### 4.2.2 Extracting Quantitative Parameters

Physical properties that can be derived from segmented masks include mass density, volume, and dry mass (Fig. 5d, h). Each voxel in the reconstructed tomogram represents the mean RI of all substances within the voxel. The mass density of each compartment is directly calculated from the mean RI value within the segmented masks, since in most biological samples, the RI value,  $n(x,y,z)$ , is linearly proportional to the mass density of the material,  $\rho(x,y,z)$ , as  $n(x,y,z) = n_m + \alpha\rho(x,y,z)$ , where  $n_m$  is the RI value of the surrounding medium and  $\alpha$  is an RI increment [56, 57]. The RI increment ( $dn/dc$ ) is a molecular-specific quantity that determines the change of RI values in a solution with varying solute concentration. The RI increment is particularly important in polymer physics and biochemistry where different substances have characteristic RI increments (e.g.,  $\alpha = 0.143$  mL/g for sucrose in water [58] and  $\alpha = 0.177$  mL/g for sodium chloride in water [59], respectively). In complex biological solutions, however, different

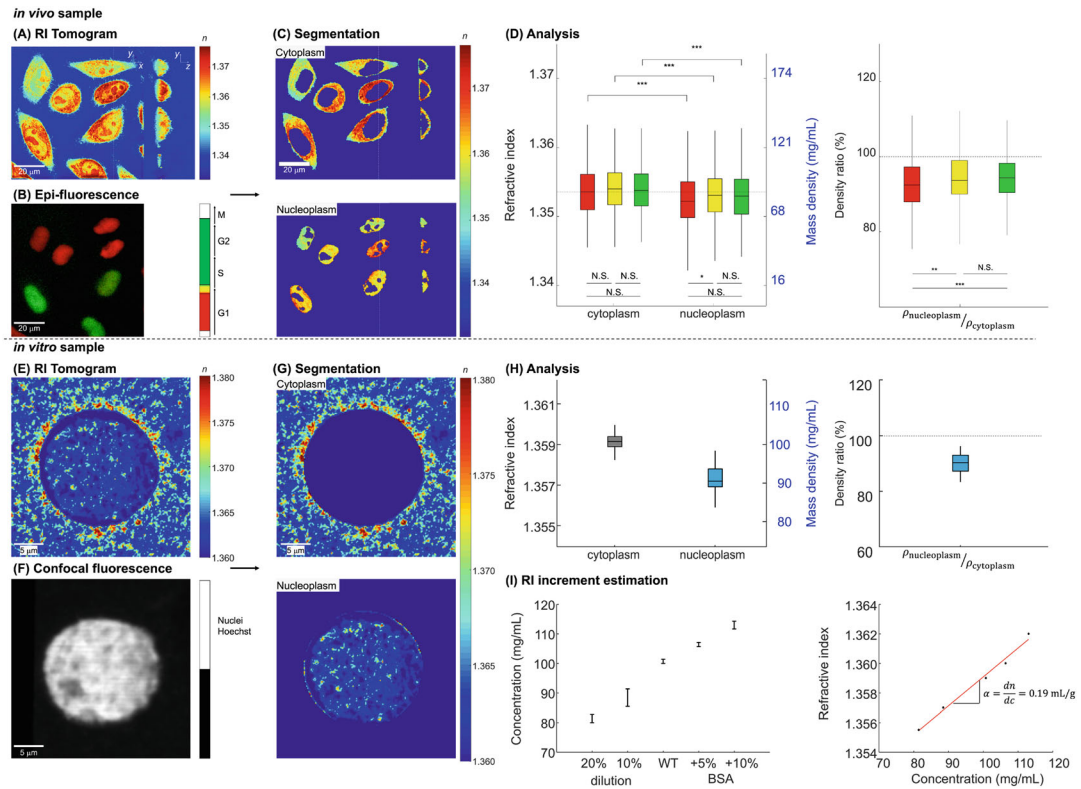


**Fig. 5** Flow chart of in vivo (a–d) and in vitro (e–i) ODT data analysis. (a, e) The reconstructed RI tomograms. (b, f) The epi-fluorescence image of FUCCI-stained cell nuclei (b) and the confocal fluorescence image of Hoechst 33342-stained nuclei from *Xenopus* egg extract in the same FOV of a and e, respectively. (c, g) The segmented masks for cytoplasm (top) and nucleoplasm (bottom). (d, h) The mean RI and mass density of cytoplasm and nuclei of HeLa cells at different cell cycle progression (d) and in the *Xenopus* egg extract (h). The right panels describe the relative mass density ratio between nucleoplasm and cytoplasm (N/C density ratio). Note that the dashed lines represent the N/C density ratio of 1. (i) For *Xenopus* extract, the RI increment,  $\alpha$ , can be directly measured by independent measurements of protein concentration modulated with BSA (addition) or CSF-XB buffer (dilution) and RI values. (Figure 5d is modified from [5])

macromolecules with unknown composition ratios will contribute to the RI. Thus, final mass density will be sensitive to the choice of the RI increment value (*see* discussion below). In addition to mass density, the volume of the compartments is extracted by adding up the number of voxels in the corresponding binary mask, and the dry mass of the compartments is calculated by integrating the mass density inside the corresponding binary mask.

In a simple two-substance mixture of protein and nucleic acids in water, the linear proportionality between RI and mass density is maintained. Based on this, in our studies we use an RI increment of 0.19 mL/g valid for protein and nucleic acids, which in cells make up ~70% of the dry mass [1, 60–62]. However, this assumption may exhibit variation across different cell compartments depending

on their composition, particularly in membrane-rich regions such as the perinuclear region. To address this challenge and accurately account for the mixture of proteins, nucleic acids, or phospholipids, more sophisticated labeling and multi-channel fluorescence imaging can accurately identify areas enriched with various substances. For example, chromatin and lipid-rich membranes can be labeled with Hoechst-33342, and DiOC6, respectively, allowing the use of appropriate RI increments for each region, such as  $\alpha = 0.190$  mL/g for chromatin and  $\alpha = 0.135$  mL/g for membranes [61]. Additionally, the absolute concentration of different molecules could be directly measured using the intensity of Raman scattering signals [63]. A recent study also proposed the theoretical framework for estimating the correct mass density from the RI measurement using Monte-Carlo simulations as well as Gaussian propagation of uncertainty [64].

For in vitro samples, concerns regarding RI increment can be addressed by directly measuring the RI increment of *Xenopus* extract through independent measurements of protein concentration and RI values. Protein concentration can be measured using the Bradford assay, followed by perturbations with BSA (addition) or CSF-XB buffer (dilution) to modulate protein concentration. The RI of each solution can be measured using an Abbe refractometer. Plotting RI values against average protein concentrations indeed reveals a linear relationship with a slope of 0.19 mL/g, consistent with previously measured RI increments for proteins and nucleic acids (Fig. 5i) [60]. Even more precise RI increment calculations for polydisperse solutions like the cytoplasm necessitates knowledge of chemical composition, achievable through techniques like Raman spectroscopy combined with predictive biophysical models as mentioned in the last paragraph. Extracts provide an additional advantage when dealing with complex mixtures: the molecular complexity of *Xenopus* extracts can be simplified by fractionation to remove individual components like mitochondria, ribosomes, or sugars such as glycogen, which have different RI increments.

---

## 5 Conclusion

ODT emerges as a powerful technique for the quantitative characterization of mass density distribution within biological samples, offering invaluable insights into the biophysical properties of sub-cellular compartments. In particular, our studies on the mass density difference between nucleoplasm and cytoplasm in vivo and in vitro samples highlight the significance of ODT in unraveling fundamental biological characteristics. Through the comprehensive overview in this chapter, we hope to outline the optical setup,

sample preparation protocols for *in vivo* and *in vitro* samples, and data analysis pipelines in detail, which are all crucial for the application of ODT. We envision that the application of ODT will further provide the uncharted discoveries in biophysical studies.

---

## 6 Notes

1. Selection of illumination source: The simple illumination source for ODT would be a laser beam with a long coherence length ( $l_c$ ) (e.g.  $l_c > 50$  meter for single longitudinal mode laser series, CNI Laser, China, or  $l_c > 100$  meter for Torus 532, Laser Quantum, United Kingdom). This ensures that interference patterns can be generated in Mach-Zehnder interferometry setups, where the optical path difference between the sample and reference beam should be shorter than the coherence length of the laser beam. Consequently, the longer coherence length of the laser beam provides greater flexibility for the optical path of both the sample beam and the reference beam. The use of laser or light emitting diode with the short coherence length can provide improved tomogram quality by reducing laser speckle noise and unwanted interference patterns from multiple reflections at any reflective surface. It requires fine adjustment of optical path length by placing a (active) delay line along the reference beam [65, 66].

The wavelength of the illumination beam can be chosen with considerations including spatial resolution (shorter wavelength), phototoxicity (longer wavelength), and easy access for the optical alignment (visible range). The use of specific wavelengths for illumination can be considered to image certain biological materials with specific RI dispersion peaks such as DNA [67] or hemoglobin ( $\lambda = 420$  nm) [68]. Hyperspectral ODT can provide the RI values of biological samples throughout the various range of wavelengths [69].

2. Selection of illumination scanning unit: For tomographic acquisition, samples were illuminated from various different incident angles, and the scanning angles can be systematically controlled by various types of devices shaping the wavefront of the illumination, including Galvanomirror, spatial light modulator (SLM), or digital micromirror device (DMD). The choice of device depends on their optical characteristics and suitability for the specific experimental setup. In a nutshell, the Galvanomirror offers a straightforward method for controlling the illumination beam angle through voltage-induced tilting of its mirrors, albeit with potential limitations in scanning speed due to mirror inertia. Wavefront shaping devices like SLM or DMD, utilizing liquid crystal or micromirror arrays, ensure

high stability in ODT measurements without mechanical parts and can correct wavefront distortions for improved accuracy [70, 71]. However, the SLM and DMD's limited diffraction efficiency results in reduced illumination beam power, necessitating complex pattern generation to section address undesired diffraction effects and minimize speckle noise [72, 73]. For a detailed comparison of illumination scanning units, further information is available elsewhere [74].

3. Selection of objective lenses and their effects in lateral/axial resolution: The ODT setup requires two objective lenses; one acts as a condenser lens illuminating the samples, and the other collecting the scattering signals from the samples. The spatial resolution of ODT is theoretically defined by the maximum spatial frequency in the reconstructed Fourier spectra. This parameter is primarily determined by the wavelength of light,  $\lambda$ , the NA of a condenser and an objective lens,  $\text{NA}_{\text{illu}}$  and  $\text{NA}_{\text{obj}}$ , respectively, and the RI value of the immersion media  $n_i$ . As a result, the lateral and axial resolution of ODT can be expressed as  $\lambda/[2(\text{NA}_{\text{illu}} + \text{NA}_{\text{obj}})]$  and  $\lambda/\left[2n_i - \sqrt{n_i^2 - \text{NA}_{\text{illu}}^2} - \sqrt{n_i^2 - \text{NA}_{\text{obj}}^2}\right]$ , respectively [75]. Hence, the use of both objective lenses having higher NA can provide the improved spatial resolution. The equation above also indicates that the NA of the condenser lens,  $\text{NA}_{\text{illu}}$ , significantly influences the spatial resolution, implying the importance of using a high NA condenser lens. However, using a high NA lens with a shorter working distance (typically  $\sim 100 \mu\text{m}$ ) necessitates the use of immersion medium and imposes constraints on sample thickness and carrier geometry. Immersion oil must be applied between the objective lens and sample carriers (such as glass slides or coverslips in Fig. 2c, d) to ensure optical contact. Alternatively, a water-dipping objective lens can be immersed directly into a glass-bottom petri dish (Fig. 2b), allowing the use of a high NA condenser lens to access the samples even with a shorter working distance. However, opening the container lid may affect the sterile conditions of the samples during long-term measurements. On the other hand, the use of a long working distance objective lens as a condenser lens (e.g., Zeiss Epiplan-Neofluar 50x, WD = 9.1 mm; Olympus LMPLFLN 50x, WD = 10.6 mm) offers the flexibility of sample preparation. The cultured cells on the glass bottom petri dish or even in a thicker culture flask can be mounted without opening the container lid, which can maintain the healthy physiology of the cells for a longer time. However, it is noteworthy that the lower NA of the objective lens may result in poorer axial resolution.

## Acknowledgments

The authors thank all present and former members of the labs for ongoing discussions and support. The authors acknowledge funding through the Max Planck Society to JG and SR. SR thanks the Rosalind-Franklin Scientist-in-Residence (RFSR) Program of the Max-Planck-Zentrum für Physik und Medizin (MPZPM) for additional funding.

## References

1. Milo R, Phillips R (2015) Cell biology by the numbers. Garland Science. <https://doi.org/10.1201/9780429258770>
2. Neurohr GE, Amon A (2020) Relevance and regulation of cell density. Trends Cell Biol 30: 213–225. <https://doi.org/10.1016/j.tcb.2019.12.006>
3. Liu X, Oh S, Kirschner MW (2022) The uniformity and stability of cellular mass density in mammalian cell culture. Front Cell Dev Biol 10:1017499. <https://doi.org/10.3389/fcell.2022.1017499>
4. Biswas A, Muñoz O, Kim K et al (2023) Conserved nucleocytoplasmic density homeostasis drives cellular organization across eukaryotes. bioRxiv 20230905556409. <https://doi.org/10.1101/2023.09.05.556409>
5. Kim K, Guck J (2020) The relative densities of cytoplasm and nuclear compartments are robust against strong perturbation. Biophys J 119:1946–1957. <https://doi.org/10.1016/j.bpj.2020.08.044>
6. Chen Y, Huang J-H, Phong C et al (2024) Viscosity-dependent control of protein synthesis and degradation. Nat Commun 15:2149. <https://doi.org/10.1038/s41467-024-46447-w>
7. Molines AT, Lemièrre J, Gazzola M et al (2022) Physical properties of the cytoplasm modulate the rates of microtubule polymerization and depolymerization. Dev Cell 57:466–479.e6. <https://doi.org/10.1016/j.devcel.2022.02.001>
8. Neurohr GE, Terry RL, Lengfeld J et al (2019) Excessive cell growth causes cytoplasm dilution and contributes to senescence. Cell 176:1083–1097.e18. <https://doi.org/10.1016/j.cell.2019.01.018>
9. Work TS, Work E (1981) Laboratory techniques in biochemistry and molecular biology: pt.3. Immunochemical techniques for the identification and estimation of macromolecules. Elsevier/North-Holland Biomedical Press
10. Burg TP, Godin M, Knudsen SM et al (2007) Weighing of biomolecules, single cells and single nanoparticles in fluid. Nature 446:1066–1069. <https://doi.org/10.1038/nature05741>
11. Lee K, Kim K, Jung J et al (2013) Quantitative phase imaging techniques for the study of cell pathophysiology: from principles to applications. Sensors 13:4170–4191. <https://doi.org/10.3390/s130404170>
12. Park Y, Depeursinge C, Popescu G (2018) Quantitative phase imaging in biomedicine. Nat Photonics 12:578–589. <https://doi.org/10.1038/s41566-018-0253-x>
13. Biswas A, Kim K, Cojoc G et al (2021) The *Xenopus spindle* is as dense as the surrounding cytoplasm. Dev Cell 56:967–975.e5. <https://doi.org/10.1016/j.devcel.2021.03.013>
14. Guillén-Boixet J, Kopach A, Holehouse ASAS et al (2020) RNA-induced conformational switching and clustering of G3BP drive stress granule assembly by condensation. Cell 181: 346–361.e17. <https://doi.org/10.1016/j.cell.2020.03.049>
15. Hugonnet H, Kim YW, Lee M et al (2021) Multiscale label-free volumetric holographic histopathology of thick-tissue slides with sub-cellular resolution. Adv Photonics 3:026004. <https://doi.org/10.1117/1.AP.3.2.026004>
16. Schlüßler R, Kim K, Nötzel M et al (2022) Correlative all-optical quantification of mass density and mechanics of subcellular compartments with fluorescence specificity. eLife 11: e68490. <https://doi.org/10.7554/eLife.68490>
17. Kim T, Yoo J, Do S et al (2023) RNA-mediated demixing transition of low-density condensates. Nat Commun 14:2425. <https://doi.org/10.1038/s41467-023-38118-z>
18. Ng SC, Biswas A, Huyton T et al (2023) Barrier properties of Nup98 FG phases ruled by FG motif identity and inter-FG spacer length. Nat Commun 14:747. <https://doi.org/10.1038/s41467-023-36331-4>

19. Beck T, van der Linden L-M, Borchers WM et al (2024) Optical characterization of molecular interaction strength in protein condensates. *Mol Biol Cell* 35:ar154. <https://doi.org/10.1091/mbc.E24-03-0128>
20. Abuhattum S, Kim K, Franzmann TM et al (2018) Intracellular mass density increase is accompanying but not sufficient for stiffening and growth arrest of yeast cells. *Front Phys* 6: 131. <https://doi.org/10.3389/fphy.2018.00131>
21. Kim K, Gade VR, Kurzchalia TV et al (2022) Quantitative imaging of *Caenorhabditis elegans* dauer larvae during cryptobiotic transition. *Biophys J* 121:1219–1229. <https://doi.org/10.1016/j.bpj.2022.02.031>
22. Lemi re J, Real-Calderon P, Holt LJ et al (2022) Control of nuclear size by osmotic forces in *Schizosaccharomyces pombe*. *elife* 11: e76075. <https://doi.org/10.7554/eLife.76075>
23. Rollin R, Joanny J-F, Sens P (2023) Physical basis of the cell size scaling laws. *elife* 12: e82490. <https://doi.org/10.7554/eLife.82490>
24. Dong D, Huang X, Li L et al (2020) Super-resolution fluorescence-assisted diffraction computational tomography reveals the three-dimensional landscape of the cellular organelle interactome. *Light Sci Appl* 9:11. <https://doi.org/10.1038/s41377-020-0249-4>
25. Soto JM, Rodrigo JA, Alieva T (2021) Partially coherent optical diffraction tomography toward practical cell study. *Front Phys* 9: 666256. <https://doi.org/10.3389/fphy.2021.666256>
26. Kim K, Lee S, Yoon J et al (2016) Three-dimensional label-free imaging and quantification of lipid droplets in live hepatocytes. *Sci Rep* 6:36815. <https://doi.org/10.1038/srep36815>
27. Park S, Ahn JW, Jo Y et al (2020) Label-free tomographic imaging of lipid droplets in foam cells for machine-learning-assisted therapeutic evaluation of targeted nanodrugs. *ACS Nano* 14:1856–1865. <https://doi.org/10.1021/acsnano.9b07993>
28. Abuhattum S, Kotzbeck P, Schl  bler R et al (2022) Adipose cells and tissues soften with lipid accumulation while in diabetes adipose tissue stiffens. *Sci Rep* 12:10325. <https://doi.org/10.1038/s41598-022-13324-9>
29. Guo R, Barnea I, Shaked NT (2021) Limited-angle tomographic phase microscopy utilizing confocal scanning fluorescence microscopy. *Biomed Opt Express* 12:1869. <https://doi.org/10.1364/BOE.419598>
30. Kletter T, Reusch S, Cavazza T et al (2022) Volumetric morphometry reveals spindle width as the best predictor of mammalian spindle scaling. *J Cell Biol* 221:e202106170. <https://doi.org/10.1083/jcb.202106170>
31. Baczewska M, Eder K, Ketelhut S et al (2021) Refractive index changes of cells and cellular compartments upon paraformaldehyde fixation acquired by tomographic phase microscopy. *Cytom Part A* 99:388–398. <https://doi.org/10.1002/cyto.a.24229>
32. Skinner SO, Sep  lveda LA, Xu H et al (2013) Measuring mRNA copy number in individual *Escherichia coli* cells using single-molecule fluorescent in situ hybridization. *Nat Protoc* 8:1100–1113. <https://doi.org/10.1038/nprot.2013.066>
33. Sakaue-Sawano A, Kurokawa H, Morimura T et al (2008) Visualizing spatiotemporal dynamics of multicellular cell-cycle progression. *Cell* 132:487–498. <https://doi.org/10.1016/j.cell.2007.12.033>
34. Murray AW (1991) Cell cycle extracts. *Methods Cell Biol* 36:581–605. [https://doi.org/10.1016/S0091-679X\(08\)60298-8](https://doi.org/10.1016/S0091-679X(08)60298-8)
35. Hannak E, Heald R (2006) Investigating mitotic spindle assembly and function in vitro using *Xenopus laevis* egg extracts. *Nat Protoc* 1: 2305–2314. <https://doi.org/10.1038/nprot.2006.396>
36. Chen P, Levy DL (2018) Nucleus assembly and import in *Xenopus laevis* egg extract. *Cold Spring Harb Protoc* 2018:pdb.prot097196. <https://doi.org/10.1101/pdb.prot097196>
37. Good MC, Heald R (2018) Preparation of cellular extracts from xenopus eggs and embryos. *Cold Spring Harb Protoc* 2018: pdb.prot097055. <https://doi.org/10.1101/pdb.prot097055>
38. Reusch S, Biswas A, Hirst WG et al (2020) Affinity purification of label-free tubulins from xenopus egg extracts. *STAR Protoc* 1:100151. <https://doi.org/10.1016/j.xpro.2020.100151>
39. Macaulay C, Forbes DJ (1996) Assembly of the nuclear pore: biochemically distinct steps revealed with NEM, GTP gamma S, and BAPTA. *J Cell Biol* 132:5–20. <https://doi.org/10.1083/jcb.132.1.5>
40. Popescu G (2011) Quantitative phase imaging of cells and tissues. McGraw Hill Professional
41. Kim K, Kim KS, Park H et al (2013) Real-time visualization of 3-D dynamic microscopic objects using optical diffraction tomography. *Opt Express* 21:32269–32278. <https://doi.org/10.1364/OE.21.032269>

42. Stępień P, Krauze W, Kujawińska M (2022) Preprocessing methods for quantitative phase image stitching. *Biomed Opt Express* 13: 439045. <https://doi.org/10.1364/BOE.439045>
43. Cuche E, Marquet P, Depeursinge C (2000) Spatial filtering for zero-order and twin-image elimination in digital off-axis holography. *Appl Opt* 39:4070–4075. <https://doi.org/10.1364/AO.39.004070>
44. Wolf E (1969) Three-dimensional structure determination of semi-transparent objects from holographic data. *Opt Commun* 1:153–156. [https://doi.org/10.1016/0030-4018\(69\)90052-2](https://doi.org/10.1016/0030-4018(69)90052-2)
45. Sung Y, Choi W, Fang-Yen C et al (2009) Optical diffraction tomography for high resolution live cell imaging. *Opt Express* 17:266–277. <https://doi.org/10.1364/oe.17.000266>
46. Kim K, Yoon H, Diez-Silva M et al (2014) High-resolution three-dimensional imaging of red blood cells parasitized by *Plasmodium falciparum* and *in situ* hemozoin crystals using optical diffraction tomography. *J Biomed Opt* 19:011005. <https://doi.org/10.1117/1.JBO.19.1.011005>
47. Lim J, Ayoub AB, Antoine EE et al (2019) High-fidelity optical diffraction tomography of multiple scattering samples. *Light Sci Appl* 8:82. <https://doi.org/10.1038/s41377-019-0195-1>
48. Chowdhury S, Chen M, Eckert R et al (2019) High-resolution 3D refractive index microscopy of multiple-scattering samples from intensity images. *Optica* 6:1211–1219. <https://doi.org/10.1364/OPTICA.6.001211>
49. Lee M, Hugonnet H, Park Y (2022) Inverse problem solver for multiple light scattering using modified born series. *Optica* 9:177. <https://doi.org/10.1364/OPTICA.446511>
50. Lim J, Lee K, Jin KH et al (2015) Comparative study of iterative reconstruction algorithms for missing cone problems in optical diffraction tomography. *Opt Express* 23:16933–16948. <https://doi.org/10.1364/OE.23.016933>
51. Chung H, Huh J, Kim G et al (2021) Missing cone artifact removal in ODT using unsupervised deep learning in the projection domain. *IEEE Trans Comput Imaging* 7:747–758. <https://doi.org/10.1109/TCI.2021.3098937>
52. Lee M, Lee Y-H, Song J et al (2020) Deep-learning-based three-dimensional label-free tracking and analysis of immunological synapses of CAR-T cells. *elife* 9:e49023. <https://doi.org/10.7554/eLife.49023>
53. He YR, He S, Kandel ME et al (2022) Cell cycle stage classification using phase imaging with computational specificity. *ACS Photonics* 9:1264–1273. <https://doi.org/10.1021/acsp Photonics.1c01779>
54. Kandel ME, He YR, Lee YJ et al (2020) Phase imaging with computational specificity (PICS) for measuring dry mass changes in sub-cellular compartments. *Nat Commun* 11:6256. <https://doi.org/10.1038/s41467-020-20062-x>
55. Jo Y, Cho H, Park WS et al (2021) Label-free multiplexed microtomography of endogenous subcellular dynamics using generalizable deep learning. *Nat Cell Biol* 23:1329–1337. <https://doi.org/10.1038/s41556-021-00802-x>
56. Barer R (1952) Interference microscopy and mass determination. *Nature* 169:366–367. <https://doi.org/10.1038/169366b0>
57. Popescu G, Park Y, Lue N et al (2008) Optical imaging of cell mass and growth dynamics. *Am J Physiol Physiol* 295:C538–C544. <https://doi.org/10.1152/ajpcell.00121.2008>
58. Greenwood CT, Hourston DJ (1975) Specific refractive index increments of certain polysaccharide systems. *Polymer (Guildf)* 16:474–476. [https://doi.org/10.1016/0032-3861\(75\)90001-4](https://doi.org/10.1016/0032-3861(75)90001-4)
59. Becker A, Köhler W, Müller B (1995) A scanning Michelson interferometer for the measurement of the concentration and temperature derivative of the refractive index of liquids. *Ber Bunsenges Phys Chem* 99:600–608. <https://doi.org/10.1002/bbpc.19950990403>
60. Zhao H, Brown PH, Schuck P (2011) On the distribution of protein refractive index increments. *Biophys J* 100:2309–2317. <https://doi.org/10.1016/j.bpj.2011.03.004>
61. Zangle TA, Teitell MA (2014) Live-cell mass profiling: an emerging approach in quantitative biophysics. *Nat Methods* 11:1221–1228. <https://doi.org/10.1038/nmeth.3175>
62. Alberts B (2017) *Molecular biology of the cell*. Garland Science
63. Bailey M, Gardner B, Alunni-Cardinali M et al (2021) Predicting the refractive index of tissue models using light scattering spectroscopy. *Appl Spectrosc* 75:574–580. <https://doi.org/10.1177/0003702820984482>
64. Möckel C, Beck T, Kaliman S et al (2024) Estimation of the mass density of biological matter from refractive index measurements. *Biophys Rep* 4:100156. <https://doi.org/10.1016/j.bpr.2024.100156>

65. Sung Y (2018) Spectroscopic microtomography in the visible wavelength range. *Phys Rev Appl* 10:054041. <https://doi.org/10.1103/PhysRevApplied.10.054041>
66. Park C, Lee K, Baek Y et al (2020) Low-coherence optical diffraction tomography using a ferroelectric liquid crystal spatial light modulator. *Opt Express* 28:39649. <https://doi.org/10.1364/OE.405418>
67. Sung Y, Choi W, Lue N et al (2012) Stain-free quantification of chromosomes in live cells using regularized tomographic phase microscopy. *PLoS One* 7:e49502. <https://doi.org/10.1371/journal.pone.0049502>
68. Wang J, Deng Z, Wang X et al (2015) Measurement of the refractive index of hemoglobin solutions for a continuous spectral region. *Biomed Opt Express* 6:2536. <https://doi.org/10.1364/BOE.6.002536>
69. Jung J, Kim K, Yoon J et al (2016) Hyperspectral optical diffraction tomography. *Opt Express* 24:2006–2012. <https://doi.org/10.1364/OE.24.002006>
70. Kuś A, Krauze W, Kujawińska M (2015) Active limited-angle tomographic phase microscope. *J Biomed Opt* 20:111216. <https://doi.org/10.1117/1.JBO.20.11.111216>
71. Shin S, Kim K, Yoon J et al (2015) Active illumination using a digital micromirror device for quantitative phase imaging. *Opt Lett* 40:5407–5410. <https://doi.org/10.1364/OL.40.005407>
72. Goorden SA, Bertolotti J, Mosk AP (2014) Superpixel-based spatial amplitude and phase modulation using a digital micromirror device. *Opt Express* 22:17999. <https://doi.org/10.1364/oe.22.017999>
73. Lee K, Kim K, Kim G et al (2017) Time-multiplexed structured illumination using a DMD for optical diffraction tomography. *Opt Lett* 42:999–1002. <https://doi.org/10.1364/OL.42.000999>
74. Kim K, Yoon J, Shin S et al (2016) Optical diffraction tomography techniques for the study of cell pathophysiology. *J Biomed Photonics Eng* 2:020201. <https://doi.org/10.18287/JBPE16.02.020201>
75. Lauer V (2002) New approach to optical diffraction tomography yielding a vector equation of diffraction tomography and a novel tomographic microscope. *J Microsc* 205:165–176. <https://doi.org/10.1046/j.0022-2720.2001.00980.x>



## Quantification and Comparison of Protein Distribution on the Nuclear Membrane

Paulina Nastały and Paolo Maiuri

### Abstract

The nuclear membrane also referred as nuclear envelope (NE) encloses the nucleoplasm of the cell and acts as a barrier between the nuclear DNA and the cytoplasm. Recent studies suggest that the composition of proteins at the NE is not even throughout the whole membrane and can show zones with accumulation of some proteins inner and outer nuclear membrane protein, emerin, lamin A/C, or nesprin-2 in relation to cells' polarization. Here we propose a methodology that combines immunofluorescent staining with quantitative imaging to prepare maps of protein distribution frequency that can serve to compare protein distribution on nuclear membrane.

**Key words** Nuclear membrane, Nuclear envelope, Frequency distribution map, Confocal microscopy, Quantitative imaging

---

### 1 Introduction

The nuclear membrane also referred as nuclear envelope (NE) encloses the nucleoplasm of the cell and acts as a barrier between the nuclear DNA and the cytoplasm. Recent studies suggest that the composition of proteins at the NE is not even throughout the whole membrane and can show zones with accumulation of some components. Some studies reported a tension-induced basal-to-apical polarization of lamin A/C in mouse embryonic fibroblasts [1, 2]. When several proteins of the NE were mapped in front-to-rear oriented cells (including lamin A/C, EMD, nesprin-1, LAP2a, and many more), their distribution along the nuclear membrane in a polarized cell was not uniform [3, 4]. They were instead organized in a biased fashion that follows the cellular polarization with emerin being one of the key proteins involved in the transmission of the polarity [3, 4]. These findings were further confirmed in the cytomegalovirus infection, where intranuclear polarity in emerin can control nuclear actin filaments

that spatially segregate viral DNA from inactive histones and host DNA, which leads to maximization of virus replication [5]. Additionally, some NE proteins, as nesprin-2, can accumulate at the front of the nucleus during migration through narrow constrictions [6]. Therefore, quantification and comparison of protein distribution on nuclear membrane is a useful method to study nuances in NE organization in a quantitative manner. Here, we describe a method to quantify and compare proteins at the nuclear membrane that can be easily adapted to address multiple scientific questions regarding the architecture and composition of nuclear membrane in various cell types.

---

## 2 Materials

### 2.1 Cell Culture

1. Human hTERT-immortalized retinal pigment epithelium cell line, hTERT RPE-1 (American Type Culture Collection, ATCC). As ensured by ATCC, this is a human cell line with a modal chromosome number of 46 that occurs in 90% of the cells. Any kind of adherent cell line can be used. To couple your results with the 3D organization of the DNA in the nucleus, you can find the list of recommended cell lines from the 4D Nucleome Consortium (*see Note 1*).
2. Media for cell culture (for hTERT RPE-1 DMEM:F12 supplemented with 10% fetal bovine serum (FBS)).
3. Hemocytometer or cell counter.
4. Trypan Blue.
5. Cell culture vessels.
6. Coverslips coated with extracellular matrix (ECM) proteins (e.g., fibronectin, collagen I, or laminin) and/or coverslips coated with micro-patterns of your interest (*see Note 2*).

### 2.2 Immuno-fluorescent Staining and Imaging

1. 1X phosphate-buffered saline (PBS): 137 mM NaCl, 2.7 mM KCl, 10 mM Na<sub>2</sub>HPO<sub>4</sub>, pH adjusted to 7.4.
2. 4% paraformaldehyde in 1X PBS.
3. 0.1% Triton-X in 1X PBS.
4. 1% bovine serum albumin/1X PBS.
5. Primary antibodies (e.g., anti-lamin A/C, anti-lamin B1, anti-emerin).
6. Secondary antibodies (dedicated fluorophore-conjugated antibody against the primary antibody).
7. 300 nM DAPI solution in 1X PBS (*see Note 3*).

8. Mounting medium (e.g., VECTASHIELD Antifade Mounting Medium VectorLabs, ProLong Glass Thermo Fisher Scientific).
9. Confocal microscope equipped with motorized stage, appropriate lasers, objectives of 40× or 63×, and software.

### **2.3 Frequency Distribution Map Preparation**

1. ImageJ software.
2. TurboReg ImageJ plugin (<https://bigwww.epfl.ch/thevenaz/turboreg/>).
3. R studio (<http://www.r-project.org/>).

---

## **3 Methods**

### **3.1 Cell Culture**

1. Determine the total number of cells and % viability (e.g., using a hemocytometer, cell counter, and Trypan Blue exclusion). If necessary, add growth media to the cells to achieve the desired cell concentration, and recount the cells.
2. Dilute cell suspension to the seeding density recommended for the cell line, pipet the appropriate volume into cell culture vessels containing coverslips (coated with dedicated extracellular matrix protein and micro-pattern), and return the cells to the incubator.
3. Grow the plated cells in the dedicated medium for 8–72 h to enable spreading on the surface. Observe the cells under the microscope to reach optimal cell density to be able to visualize single cells.

### **3.2 Immuno- fluorescent Staining and Imaging**

Perform immunofluorescent staining according to you optimized protocol. For each combination use one to two antibodies against nuclear membrane proteins (e.g., to detect lamin A/C, lamin B1, emerin, nesprin-1, SUN2, MAN1) and a marker to orient the cells (e.g., centrosome marker as pericentrin, Golgi marker as Giantin, ER marker as KDEL, cytoskeleton marker as phalloidin or alpha-tubulin). Below you can find a simplified protocol that you can modify accordingly:

1. Replace the growth media to 4% paraformaldehyde/1X PBS, and incubate the microscopic slide with the desired cells (prepared in **step 3** in Subheading **3.1**) for 10 min at room temperature.
2. Wash the cells in 1X PBS three times.
3. Replace the buffer to 0.1% Triton-X/1X PBS, and incubate the slide with cells for 5 min at room temperature.
4. Wash the cells in 1X PBS three times.

5. Replace the buffer to 1% bovine serum albumin/1xPBS, and incubate the slide with cells for 15 min at room temperature.
6. Replace the buffer to 1% bovine serum albumin/1X PBS with primary antibody (e.g., anti-lamin A/C, anti-lamin B1, anti-emerin), and incubate the slide with cells for 45–60 min at room temperature.
7. Wash the cells in 1x PBS three times.
8. Replace the buffer to 1% bovine serum albumin/1X PBS with secondary antibody and incubate the slide with cells for 45–60 min at room temperature.
9. Wash the cells in 1x PBS three times.
10. Repeat the **steps 5–9** in Subheading 3.2 for the second and/or third round of immunostaining using different primary/secondary antibodies.
11. Replace the buffer to 300 nM DAPI solution in 1X PBS, and incubate the slide for 5 min at room temperature.
12. Wash the cells in 1X PBS three times.
13. Mount the coverslips of microscopic slides using the mounting medium and proceed to microscopic imaging. You can secure the coverslip on the microscopic slide with transparent nail polish.
14. Image single cells using a confocal microscope (Fig. 1a, b). Ensure that the nucleus is well spread and the nuclear envelope is intact, not wrinkled (*see Note 4*).
15. For each experiment, select randomly at least ten single cells, preferably >30 cells/experiment that can be then pooled to obtain a final map.

### 3.3 Frequency Distribution Map Preparation

To produce the distribution map, process images using ImageJ software [7, 8] with TurboReg ImageJ plugin.

1. Project all the Z-stacks of the obtained images. Use the “Z Project” command in ImageJ to sum all the slices of the acquired Z-stacks. At this step, prepare one image of each channel per cell.
2. Image orientation (Fig. 1c): Rotate all the images in the same direction so that the cells are positioned in the same direction. You can use the channel of interest, e.g., channel with Golgi or ER marker that serves to mark the front part of a cell, and all the cells can be oriented in the same direction regarding front-to-rear polarity [3].
3. Choose a reference cell (*see Note 5*). All the other cells will be registered according to the reference cell.

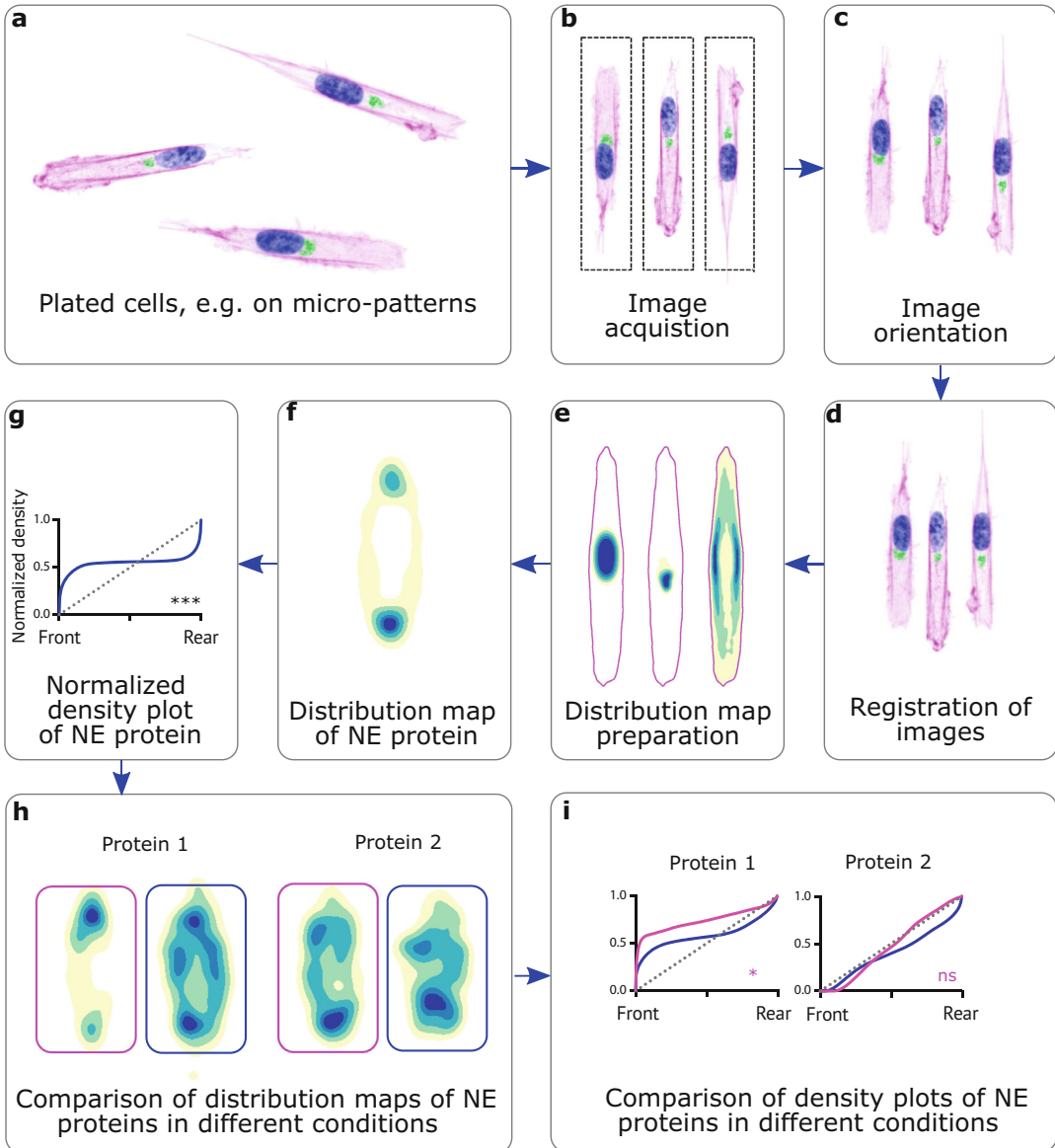


**Fig. 1** A scheme of protein map distribution frequency preparation and comparison. (Adapted from [3]). Panels **a–d** contain F-actin (magenta), nucleus (DAPI staining in blue), Golgi (green). Panels **e, f, h** contain distribution map with pseudo-coloring

- Registration of channels in the reference cell: First determine the registration channel to be used (e.g., in our case, we decided the DAPI staining as the registration channel to register the nuclei of the cell population). All the remaining channels (e.g., Golgi and ER staining in our case) will be aligned in function of this one. It could be the pattern itself; cytoskeleton components, like actin; or the nucleus, using DAPI.

5. Registration of images: (Fig. 1d): Run for each cell the TurboReg ImageJ plugin [9]. First set the registration channel image of the cell as source and the registration channel image of the reference cell as target. Set “rigid body” algorithm to find the combination of rotation and translation of the source to fit the target. Apply the same roto-translation to the other channels of the source cell. Repeat the above operation for each cell. Because TurboReg is scriptable, all these operations can be automatized in a macro.
6. Distribution map preparation (Fig. 1e, f). For each channel, combine all the registered images in a single stack. Now you should have a stack of the dimension of your sample for each channel separately including the referenced channels (Fig. 1e) and your channels of interest (in our case, staining images against favorite NE proteins; magnified image example in Fig. 1f).
7. Normalized density plot of NE proteins (Fig. 1g): Segment the stack corresponding to the channel/color of interest. Use the same algorithm to compute an appropriate threshold value for each image in the stack, e.g., in our case the stack was segmented using threshold value for each image in the stack using TopHat (value 20) filter [3, 10]. Then divide the stack for 255; all pixels over the threshold would then be equal to one to produce a binary image (*see* **Note 6**).
8. Produce the map (Fig. 1h, i). Project the stack of interest making a sum of all the images in the stack. Rescale the image to the desired size. As the human eye can perceive relatively few shades in one image, it is better to use a pseudo-coloring to make images can make data more visible. You can use the desired lookup table for the color-coded representation as presented in Fig. 1e, f, h (*see* **Note 7**). While for some proteins a biased distribution was evident already at the single cell level, for others it becomes evident only after averaging several single cell images [3].
9. Obtain at least 30 single cells for each experiment to reach at least ~100 cells. For each map cells from at least three independent experiments should be analyzed. Using ImageJ draw a straight line across your map to plot a distribution profile, and test it against signal that shows a uniform distribution (Fig. 1g).
10. Statistics and reproducibility. The two-sided Kolmogorov–Smirnov test can be used to compare protein distribution with uniform distribution (Fig. 1g). The statistical difference of distribution maps between two samples can be tested using R studio.

### 3.4 Comparison of Distribution Maps

1. Produce the map of the protein of your interest in different conditions. We used cells micro-patterned on 10  $\mu\text{m}$  lines that were oriented by the front-to-rear polarity (Golgi marker was used to orient the cells). Project the stack of interest making a sum of all the images in the stack. Rescale the image. Use the desired lookup table for the pseudo-color-coded representation (Fig. 1h).
2. Using ImageJ draw a straight line across your map to plot a distribution profile in different conditions and compare them using the two-sided Cramér–von Mises test using R studio (Fig. 1i).

---

## 4 Notes

1. Cell lines recommended by the 4D Nucleome Consortium <https://www.4dnucleome.org/cell-lines/>.
2. Coverslips with micro-patterns can be purchased from commercial sources (e.g., CYTOO).
3. We usually prepare 300  $\mu\text{M}$  DAPI intermediate dilution and dilute it 1:1000 in 1X PBS before the staining.
4. It is very convenient to use the confocal microscope with motorized stage in order to select multiple cells, set the Z-stack distance (we recommend using 0.3–0.6  $\mu\text{m}$ ) and range, and then let the system acquire multiple positions. We routinely use 60 $\times$  oil immersion objective and acquire images with Z-stacks of 0.3  $\mu\text{m}$  of focal plane.
5. It is important to choose the reference cell carefully: it must be as much as possible representative of the population with possibly centered nuclei (od shape representative to the population) and accurate and reliable high-quality immunofluorescent staining with low background of your markers of interest.
6. If the goal is to only produce a qualitative distribution and not a quantitative frequency map, skip this step. It is important to notice that at this point, the information associated with the intensity (density) of the signal is lost. Only the frequency of the signal over the threshold on that particular position will be considered.
7. For the pseudo-color-coded map you can choose different variants of LUTs, e.g., that pass the color-blinded requirements, you can easily download them and install them in ImageJ, e.g., from this website: [https://imagej.net/ij/download/luts/NucMed\\_Image\\_LUTs/](https://imagej.net/ij/download/luts/NucMed_Image_LUTs/).

## Acknowledgments

This work was supported by the Polish National Science Centre grant 2020/39/D/NZ3/00882 for PN. PM is supported by the Italian Association for Cancer Research (AIRC), Investigator Grant #24976 and by the Ministero dell'Università e della Ricerca (MUR), PRIN/PNRR2022 #P2022F3YRF.

## References

1. Ihalaainen TO, Aires L, Herzog FA et al (2015) Differential basal-to-apical accessibility of lamin A/C epitopes in the nuclear lamina regulated by changes in cytoskeletal tension. *Nat Mater* 14:1252–1261. <https://doi.org/10.1038/nmat4389>
2. Kim D-H, Wirtz D (2015) Cytoskeletal tension induces the polarized architecture of the nucleus. *Biomaterials* 48:161–172. <https://doi.org/10.1016/j.biomaterials.2015.01.023>
3. Nastaly P, Purushothaman D, Marchesi S et al (2020) Role of the nuclear membrane protein Emerin in front-rear polarity of the nucleus. *Nat Commun* 11:2122. <https://doi.org/10.1038/s41467-020-15910-9>
4. Nastaly P, Maiuri P (2022) Cellular polarity transmission to the nucleus. In: Kloc M, Kubiak JZ (eds) *Nuclear, chromosomal, and genomic architecture in biology and medicine. Results and problems in cell differentiation*, vol 70. Springer, Cham. [https://doi.org/10.1007/978-3-031-06573-6\\_21](https://doi.org/10.1007/978-3-031-06573-6_21)
5. Procter DJ, Furey C, Garza-Gongora AG et al (2020) Cytoplasmic control of intranuclear polarity by human cytomegalovirus. *Nature* 587:109–114. <https://doi.org/10.1038/s41586-020-2714-x>
6. Davidson PM, Battistella A, Déjardin T et al (2020) Nesprin-2 accumulates at the front of the nucleus during confined cell migration. *EMBO Rep* 21:e49910. <https://doi.org/10.15252/embr.201949910>
7. Rueden CT, Schindelin J, Hiner MC et al (2017) ImageJ2: ImageJ for the next generation of scientific image data. *BMC Bioinform* 18:529. <https://doi.org/10.1186/s12859-017-1934-z>
8. Schneider CA, Rasband WS, Eliceiri KW (2012) NIH image to ImageJ: 25 years of image analysis. *Nat Methods* 9:671–675. <https://doi.org/10.1038/nmeth.2089>
9. Thévenaz P, Ruttimann UE, Unser M (1998) A pyramid approach to subpixel registration based on intensity. *IEEE Trans Image Process* 7:27–41. <https://doi.org/10.1109/83.650848>
10. Poli A, Pennacchio FA, Ghisleni A et al (2023) PIP4K2B is mechanoresponsive and controls heterochromatin-driven nuclear softening through UHRF1. *Nat Commun* 14:1432. <https://doi.org/10.1038/s41467-023-37064-0>



## Quantifying Nuclear Shape Fluctuations During Early Mitosis

Viola Introini , Giancarlo Porcella , Gururaj Rao Kidiyoor ,  
Pietro Cicuta , and Marco Cosentino Lagomarsino

### Abstract

This chapter presents a detailed methodology for monitoring nuclear shape fluctuations and their correlation with chromatin condensation, developed for our analyses of early prophase, but applicable to other contexts. Nuclear shape dynamics play a key role in mitotic progression, and understanding the mechanical and biophysical properties associated with the fast-paced fluctuations may offer insights into key cellular processes like chromatin condensation and nuclear envelope breakdown. By employing live-cell imaging and computational analysis such as segmentation and flickering spectroscopy techniques, this approach leverages high-resolution temporal tracking of nuclear shape changes during cell cycle progression to derive insights into the mechanical forces driving chromatin condensation and nuclear envelope instabilities leading to the nuclear envelope breakdown. The experimental protocol provides a step-by-step guide for synchronizing HeLa cells at a specific cell-cycle transition and manipulating chromatin condensation and cytoskeletal structures through pharmacological perturbations. The data analysis section includes methods for extracting relevant biophysical parameters, such as nuclear effective tension and nuclear invaginations, as well as image-processing analysis, to correlate nuclear deformations with chromatin dynamics. We hope this robust and accessible workflow will serve as a powerful tool for exploring the mechanical coupling between chromatin condensation and nuclear structure across different conditions, which is crucial for our fundamental understanding of the nuclear function, as well as relevant for diseases resulting in nuclear abnormalities and disrupted cellular functions.

**Key words** Nuclear shape fluctuations, Chromatin condensation, Mitotic progression, Prophase, Nuclear envelope breakdown, Live-cell imaging, Nuclear mechanics

---

### 1 Introduction

The eukaryotic nucleus plays a fundamental role in several cellular processes, including genome organization, transcription regulation, and mitotic progression. Additionally, it serves as a central mechanosensory hub of the cell, responding to both internal and

---

Authors “Viola Introini” and “Giancarlo Porcella” have equally contributed to this chapter.

Yuki Hara and Kazunori Kume (eds.), *The Nuclear Membrane: Methods and Protocols*, Methods in Molecular Biology, vol. 2958, [https://doi.org/10.1007/978-1-0716-4714-1\\_10](https://doi.org/10.1007/978-1-0716-4714-1_10),  
© The Author(s), under exclusive license to Springer Science+Business Media, LLC, part of Springer Nature 2025

external mechanical forces [1, 2]. Throughout the cell cycle, the nuclear envelope (NE) undergoes significant dynamic changes, particularly at the G2/M transition, as chromatin condenses and the NE disassembles during nuclear envelope breakdown (NEBD) [3]. Chromatin condensation, a hallmark of early prophase, is critical for the faithful segregation of chromosomes during mitosis.

These events are tightly linked to mechanical forces generated both within the nucleus and by the surrounding cytoskeleton. Studies have shown that the seconds-to-minutes time scale fluctuations of the nuclear envelope are cell-cycle dependent, acting as indicators of cell cycle stages [4]. These fluctuations are not merely passive but result from a combination of active nonequilibrium drives and passive relaxation processes. As such, they can provide insights into the mechanical coupling between chromatin behavior and nuclear architecture, as well as on the multiple equilibrium and nonequilibrium mechanical perturbations that affect the nuclear surface. In particular, the relationship between chromatin condensation and nuclear shape dynamics during early prophase remains relatively underexplored.

Our research in this direction has revealed that nuclear shape fluctuations in early prophase are driven by mechanical processes that involve both chromatin dynamics and cytoskeletal forces [5]. These fluctuations can be divided into two distinct phases: (1) initial inward transient centripetal fluctuations, driven primarily by chromatin condensation and (2) later stage more pronounced deformations mainly orchestrated by microtubule networks from centrioles, which destabilize the NE and lead to NEBD.

This chapter presents a detailed protocol for real-time tracking and quantification of nuclear shape fluctuations throughout the HeLa cell cycle. By analyzing nuclear displacements in early prophase by inducing chromatin condensation or perturbing cytoskeletal dynamics, this approach helps in dissecting the complex mechanical interactions between chromatin and the nuclear envelope.

The key steps in this method are the following:

1. Synchronization of HeLa cells at the G1/S or G2/M transition.
2. Live-cell imaging of nuclear shape fluctuations using confocal microscopy.
3. Perturbation of nuclear and cytoskeletal properties using pharmacological agents.
4. Quantitative analysis of nuclear shape fluctuations and inward invaginations during prophase, determining nuclear effective tension and bending modulus.
5. Correlation analysis of nuclear shape changes with chromatin condensation events.

---

## 2 Materials

### 2.1 *HeLa Cell Culture*

1. HeLa cells.
2. DMEM with GlutaMAX: Dulbecco's Modified Eagle Medium supplemented with 10% FBS and 1% penicillin-streptomycin.
3. Phosphate-buffered saline (PBS): 137 mM NaCl, 2.7 mM KCl, 10 mM Na<sub>2</sub>HPO<sub>4</sub>, and pH adjusted to 7.4.
4. Fibronectin (Bovine Plasma Fibronectin), 1 mg/mL stock prepared in PBS, and added to cells at a final concentration of 1 µg/mL.
5. Penicillin-streptomycin.
6. Lipofectamine2000 (Invitrogen).
7. Sterilized 35 mm glass-bottom imaging dishes.
8. Incubator (37 °C, 5% CO<sub>2</sub>, CellXpert C170o CO<sub>2</sub> Incubator).
9. H2B-mCherry and emerin-GFP plasmids.

### 2.2 *Cell Synchronization and Treatment with Pharmacological Agents*

1. CDK1 Inhibitor (RO-3306): 1 mM stock prepared in DMSO and added to cells at a final concentration of 10 µM, for the arresting of cells in G2/M phase.
2. Thymidine Block Solution: 10 mM stock prepared in PBS and added to cells at a final concentration of 2 mM, for cell cycle synchronization in the G1-S phase.
3. Calyculin 100 µM stock prepared in DMSO and added to cells at a final concentration of 5 nM, used to induce rapid chromatin condensation.
4. Latrunculin A 1 mM stock prepared in DMSO and added to cells at a final concentration of 1 µM, used to depolymerize actin filaments and perturb cytoskeletal dynamics.

### 2.3 *Live-Cell Imaging of Nuclear Shape Fluctuations*

1. Confocal spinning disk microscope (Olympus) equipped with IX83 inverted microscope provided with an IXON 897 ultra camera (Andor), attached with ×100 silicone immersion objective (Refractive Index = 1.406; Numerical Aperture = 1.35). A temperature- and CO<sub>2</sub>-controlled incubator maintains cells during live imaging experiments.
2. CellSens Dimension 1.18 image acquisition software for capturing high-speed live-cell images.
3. Temperature-controlled live-cell imaging chamber.
4. Fiji ImageJ.

### 2.4 *Image Processing and Analysis*

MATLAB R2022a MathWorks<sup>®</sup>.

### 3 Methods

#### 3.1 HeLa Cell Culture

1. Prepare fibronectin-coated glass-bottom dishes with a solution of 10  $\mu\text{g}/\text{mL}$  fibronectin in PBS, incubate for 30 min at 37 °C, remove the solution, and rinse with PBS.
2. Plate HeLa cells expressing desired fluorescent markers (e.g., H2B-mCherry) in DMEM with 10% FBS and 1% penicillin-streptomycin to reach around 60–70% confluency on the day of transfection with the additional fluorescent markers (*see Note 1*).
3. For visualization of chromatin and nuclear envelope dynamics, transfect HeLa cells with H2B-mCherry and emerin-GFP plasmids 36–48 h before imaging (*see Fig. 1a*). Lipofectamine2000 (Invitrogen) is used for transfecting fluorescent markers of the nuclear envelope (e.g., emerin pEGFP-C1) or the cytoskeleton (e.g., pmScarlet-i\_alphaTubulin\_C1).
4. Maintain cells in a 5%  $\text{CO}_2$  humidified incubator at 37 °C.

### Biophysical quantification of nuclear shape fluctuations

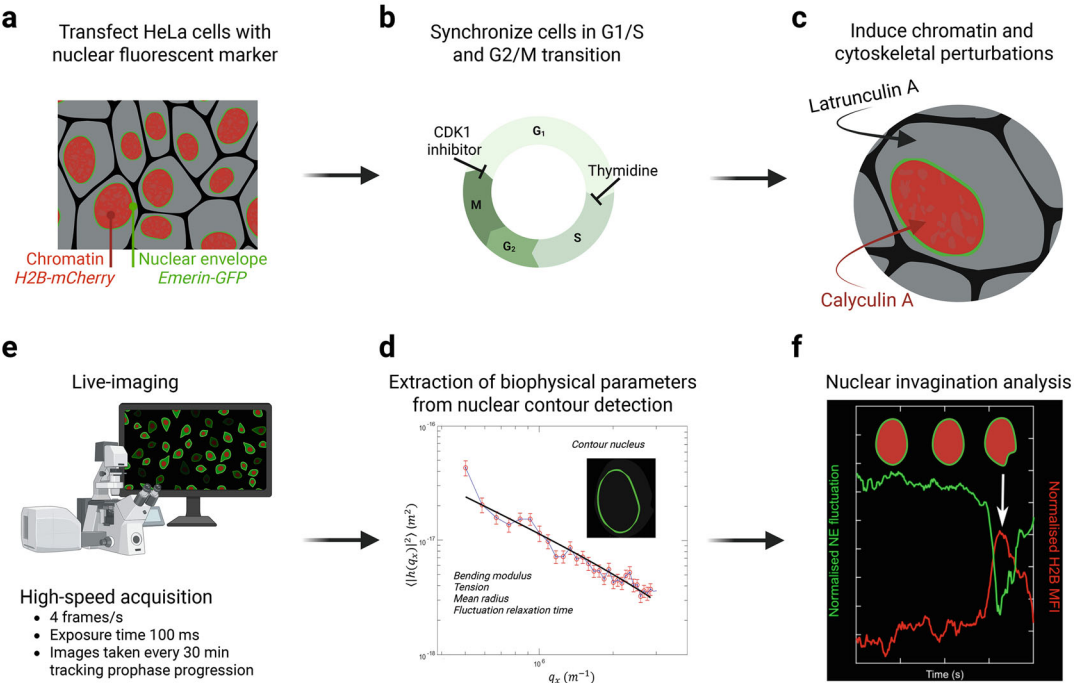


**Fig. 1** Step-by-step illustrated protocol for real-time detection and image analysis of nuclear envelope fluctuations correlated with chromatin changes during the cell cycle. (Schematics created in BioRender)

### 3.2 Cell Synchronization and Treatment with Pharmacological Agents

1. Treat cells with thymidine block solution for 14 h to block them in G1/S transition, as in Fig. 1b.
2. Wash with PBS and release the block by adding fresh medium for 7 h.
3. Re-block by treating cells again with thymidine block solution for 18 h (*see* Fig. 1b).
4. After the second thymidine block, treat cells with 10  $\mu$ M CDK1 inhibitor for 16 h.
5. Calyculin A treatment (Fig. 1c): treat synchronized cells with 5 nM calyculin A for 20 min to induce premature chromatin condensation. Capture time-lapse images during and after treatment using the same acquisition setting.
6. Latrunculin A treatment (Fig. 1c): apply 1  $\mu$ M latrunculin A for 20 min to disrupt actin filaments. Monitor the nuclear shape fluctuations before and after treatment.

### 3.3 Live-Cell Imaging of Nuclear Shape Fluctuations

Place the glass-bottom dish with transfected HeLa cells in a temperature-controlled live-cell imaging chamber.

1. Ensure that the chamber is pre-warmed to 37 °C and equilibrated with 5% CO<sub>2</sub>.
2. Using the 100 $\times$  silicone immersion objective and low laser power (*see* **Note 2**), select the desired number of cells expressing both fluorescent markers (H2B-mCherry for chromatin, emerin-GFP for the NE), making sure to select a sufficiently high number of cells (*see* **Note 3**).
3. Set the microscope software to acquire images at four frames per second (100 ms exposure time per frame). High-speed acquisition is crucial to capture fast nuclear membrane fluctuations (“flickering”).
4. Before launching the acquisition, gently wash the cells three times with PBS, add fresh medium. This will release the cells from the G2/M block and will prompt them to enter prophase. Be gentle during the wash to avoid flushing cells from the dish and losing them from the selected field of view (*see* **Note 4**).
5. Adjust the focus until a crisp emerin-GFP nuclear envelope signal is visible (*see* **Note 5**). Capture 500 frames per session for each experimental condition, with images taken at regular intervals (every 30 min) to track progression through prophase. Nuclear flickering is observed in the early prophase before nuclear envelope deformation and breakdown (refer to Fig. 1d).
6. Save the time-lapse images as .avi videos or formats that could be open by the Analysis software.

### 3.4 Image Processing and Analysis

#### 3.4.1 Nuclear Flickering Spectroscopy

1. Run the flickering algorithm developed in house and implemented in MATLAB available at the GitHub repository <https://github.com/vi211/Flickering-Nuclei>.
2. Run the “Nuclei” script and follow the GUI interactive instructions, selecting the .avi video for analysis (*see Note 6*).
3. The first frame of the video will appear and manually select the nuclear contour by clicking the center of the nucleus and one point on the contour. The algorithm will detect the nuclear outline for each frame with subpixel resolution (*see Note 7*).
4. As shown in Fig. 1e, obtain the mean equatorial radius, effective tension  $\sigma$ , and bending modulus  $\kappa$  for each nuclear envelope, by fitting the resulting static spectrum of fluctuation amplitudes with the formula.
5.  $\left\langle |h(q_x, y=0)|^2 \right\rangle = \frac{K_B T}{L} \frac{1}{2\sigma} \left[ \frac{1}{q_x} - \frac{1}{\sqrt{\frac{\sigma}{\kappa} + q_x^2}} \right]$  for modes 5–34.  
Avoid lower modes, because they are influenced by the nucleus shape, well as higher modes, which are affected by the noise of the acquisition exposure time (*see Notes 8 and 9*).
6. From the dynamics of the nuclear fluctuations, relaxation time is obtained by fitting the autocorrelation function of the fluctuation amplitudes for each mode with a single exponential, as in [6, 7] (*see Note 10*).

#### 3.4.2 Nuclear Invagination Analysis

1. Plot heat maps or polar plots of nuclear invaginations as deviation from the mean contour for each frame, by subtracting the mean of the contour shape for the first ten frames as a reference from the contour of each frame.
2. To correlate invagination dynamics with chromatin condensation as in Fig. 1f, analyze the mean fluorescence signal of the histones labelled H2B-mCherry adjacent to segments of the nuclear envelope in the presence or absent of invaginations, and calculate the Pearson correlation coefficient.
3. The same procedure is used to investigate effect of microtubules in creating invaginations by labelling tubulin.
4. Plot 3D kymographs of nuclear envelope surface using z as time-lapse images.
5. Plot the skewness of the distribution of NE contours using the *skewness* MATLAB function to quantify inward vs outward nuclear deformations.

---

## 4 Notes

1. The expression of two fluorescent markers is not always well tolerated by cells in culture. Make sure to monitor the cell state before imaging, and to seed enough cells to have enough healthy cells expressing both markers.

2. Given the cell continuous exposure to laser light during the fast-paced acquisition bursts, it is important to keep laser power as low as possible, i.e., 3–5% power to avoid photobleaching.
3. Cell synchronization at G2/M is not achieved with 100% efficiency. Is thus important to select an excess of cell expressing both markers for the acquisition before washing the RO3306 out, as not all of them will proceed into mitosis.
4. Use a Pasteur pipette to gently but thoroughly wash away RO3306-containing media before release, as persisting CDK1-inhibitor will decrease the number of cells going through cell division.
5. To facilitate image analysis for contour detection, a good contrast between the nuclear envelope and chromatin signal is necessary. Select for imaging cells that express a bright enough emerin-GFP signal to aid image analysis boundary recognition.
6. If the original emerin fluorescent signal is dim for the automatic detection of the cell contour by the flickering algorithm, use ImageJ to adjust the contrast.
7. The theoretical basis of membrane flickering spectroscopy and the details of the algorithm detecting the nuclear contours and fluctuation amplitudes are published and can be consulted for further details [6, 7].
8. Although the system is out of equilibrium, if we assume that active forces play the role of an increased “effective temperature,” then it is possible to use the standard model for fluctuations to extract effective biophysical parameters. While this is a reasonable assumption, there are also situations where picturing active forces as an effective temperature may be too simplistic. Importantly, these measured effective parameters are not the same as the underlying biophysical ones but a by-product of constitutive parameters and the action of active forces.
9. Two significant technical differences are introduced from previous work by Chu et al. [4]. (1) Accounting for projection of fluctuations on the equator in the measured shape fluctuations leading to correct  $q$  dependencies in limiting behaviors:  $\langle h(q_x, y=0)^2 \rangle \sim q^{-1}$  for low modes, if dominated by tension ( $\sigma \gg \kappa q_x^2$ ); instead, at large  $q$ , there is a bending-dominated regime  $\langle h(q_x, y=0)^2 \rangle \sim q^{-3}$  for ( $\sigma \ll \kappa q_x^2$ ). In the range we consider, which is the whole experimentally accessible range, both terms are contributing to the deformation energy, and the slope is an intermediate power law. This is fortunate, because it means that this approach is able to address both tension and bending. (2) Mean-square displacement of nuclear fluctuations is plotted as function

of wave vector rather than wave number to avoid averaging together fluctuations of different wavelengths from nuclei of different sizes.

10. The range of modes that can be studied dynamically is limited by the camera acquisition rate, as well as by the other factors that limit also the static analysis. Higher modes decay too fast to be captured by images at frame rates of a fraction of a second, hence are not accessible by the standard methods described here.

---

## Acknowledgments

V.I. was supported by Marie Skłodowska-Curie Actions post-doctoral fellowship FEBRIS [101026717], M.C.L. was supported by the Italian Association for Cancer Research (AIRC), grant AIRC-IG (REF: 23258). P.C. was supported by the Engineering and Physical Sciences Research Council (EPSRC) (EP/R011443/1). Work of G.R.K. and G.P. was supported by Italian Association for Cancer Research (AIRC) AIRC-IG REF: 21416. G.R.K. was supported by Marie Curie Initial Training Networks (ITN, FP7 aDDress) and by an Italian Association for Cancer Research (AIRC) fellowship.

## References

1. Miroshnikova YA, Wickström SA (2022) Mechanical forces in nuclear organization. *Cold Spring Harb Perspect Biol* 14(1): a039685. <https://doi.org/10.1101/cshperspect.a039685>
2. Kirby TJ, Lammerding J (2018) Emerging views of the nucleus as a cellular mechanosensor. *Nat Cell Biol* 20(4):373–381. <https://doi.org/10.1038/s41556-018-0038-y>
3. Lima JT, Ferreira JG (2024) Mechanobiology of the nucleus during the G2-M transition. *Nucleus* 15(1):2330947. <https://doi.org/10.1080/19491034.2024.2330947>
4. Chu F-Y, Haley SC, Zidovska A (2017) On the origin of shape fluctuations of the cell nucleus. *Proc Natl Acad Sci USA* 114:10338–10343. <https://doi.org/10.1073/pnas.1702226114>
5. Introini V, Kidiyoor GR, Porcella G et al (2023) Centripetal nuclear shape fluctuations associate with chromatin condensation in early prophase. *Commun Biol* 6(1):715. <https://doi.org/10.1038/s42003-023-05074-9>
6. Yoon YZ, Hong H, Brown A et al (2009) Flickering analysis of erythrocyte mechanical properties: dependence on oxygenation level, cell shape, and hydration level. *Biophys J* 97(6): 1606–1615. <https://doi.org/10.1016/j.bpj.2009.06.028>
7. Kariuki SN, Marin-Menendez A, Introini V et al (2020) Red blood cell tension protects against severe malaria in the Dantu blood group. *Nature* 585(7826):579–583. <https://doi.org/10.1038/s41586-020-2726-6>



# Chapter 11

## Micropost Arrays to Model ECM Fiber Obstacles During Cell Migration in Confinement

Aditya Katiyar, Richard B. Dickinson, and Tanmay P. Lele

### Abstract

Micropost arrays are a valuable platform for studying cell migration in controlled microenvironments. These arrays enable researchers to mimic how migrating cells deform their nuclei in reaction to physical constraints presented by extracellular matrix (ECM) fibers during processes such as wound healing and cancer metastasis. By tuning micropost patterns and sizes, researchers can not only explore the impact of confining spaces created by such patterns on cell migration, signaling, and nuclear deformation but also simultaneously quantify cell-generated forces and forces of nuclear deformation. This paper outlines methods to design and fabricate ECM fiber mimicking micropost arrays for use in fundamental studies of confining cell migration.

**Key words** Nuclear mechanics, Microfabrication, Confining cell migration

---

### 1 Introduction

Biological processes such as wound healing and cancer invasion involve the migration of cells through confining spaces in the interstitium. Extracellular matrix (ECM) fibers present obstacles that cells must overcome in order to migrate [1]. In particular, cells must squeeze the nucleus, which is the largest organelle in the cell, into these spaces. Being composed of structures such as the nuclear lamina and chromatin [2], the nucleus mechanically resists deformation and imposes a limit on the smallest cross-section that cells can move through [3, 4]. It has been shown that cells cannot migrate through confinement if the confining space is less than 10% of the cross-sectional area of the nucleus [5]. Thus, understanding how cells deform their nuclei to navigate through these tight spaces, and how the nucleus might limit migration, is essential for a complete understanding of cell migration in the tissue interstitium.

In vitro model systems have proved to be powerful in visualizing nuclear deformation during confining cell migration. One type of model system involves polydimethylsiloxane (PDMS) devices that provide smooth, contiguous surfaces of narrow cross-section, through which the nucleus must be squeezed for cells to migrate [3, 6]. While such model systems mimic contiguous surfaces that may be present in tissue, they do not effectively mimic any fibrous obstacles that may impede cellular motion in tissue. An alternative approach is to present cells migrating on a 2D surface with a “forest” of upright, slender, soft microposts [7]. Choosing the micropost dimensions and patterns in such a way that the interpost distance is smaller than nuclear sizes enables the study of nuclear deformation as it is squeezed through slender obstacles like ECM fibers. Adjusting the height, diameter, and the Young’s modulus of the material that the microposts are made of allows the tuning of the stiffness of the microposts to be of the same order of magnitude as individual ECM fibers. This paper outlines the methods for the fabrication of micropost arrays and for the use of these arrays for cell migration and nuclear deformation studies.

---

## 2 Materials

### 2.1 *Micropost Design and Fabrication*

1. Designing software (Autodesk, AutoCAD 2018).
2. Maskless aligner (Heidelberg Instruments, MLA-150 DWL 66 laser writer).
3. Contact aligner (Karl Suss, MA-6 contact aligner).
4. P-type silicon wafer (100 mm diameter) (MTI Corporation, SIBa101D0525C1R1US).
5. AZ1512 photoresist (MicroChemicals, 1A001512).
6. Chrome-coated glass mask (University Wafer, 272336).
7. (Tridecafluoro-1, 1, 2, 2-tetrahydrooctyl)-1-trichlorosilane (T2492, UCT Inc., Bristol, PA, USA) for Chemical Vapor Deposition.
8. Vacuum Desiccator (SP Bel-Art, B002VBW9SM).
9. Deep Reactive Ion Etching equipment (Oxford DRIE).
10. Oxygen plasma etcher (PlasmaEtch, PE-25).
11. 4:1 AZ-300MIF solution (developer) (MicroChemicals, 1004145).
12. SYLGRAD 184 Silicone Elastomer Kit (Dow Corning, Midland, MI, USA) for PDMS (dimethylpolysiloxane).
13. Scanning electron microscope.
14. Glass-bottom dishes (No. 1.5, 35 mm, FD35-100, WPI Inc., Sarasota County, FL, USA).

15. 22 mm × 22 mm glass coverslips (No. 1.5) or glass bottom dish.
16. 100% ethanol.
17. Silane solution (T-2492, UCT Inc.)

## 2.2 Preparing Microposts for Cell Culture

1. 200-proof ethanol.
2. 70% ethanol.
3. 40% ethanol.
4. DI water.
5. Rhodamine-fibronectin (r-FN).
6. 1X PBS (Phosphate-buffered saline).
7. 4% paraformaldehyde (PFA).
8. Suitable cell culture media.
9. Pipettes (20–200  $\mu$ L and 1–10  $\mu$ L).
10. Vacuum Aspirator.
11. Cell culture incubator.
12. Live-cell or fixed-cell fluorescent probes (optional).

## 2.3 Deflection Measurements

Image Analysis software (Mathworks, Matlab 2019a).

---

# 3 Methods

## 3.1 Micropost Design and Fabrication

We designed the micropost patterns in AutoCAD 2018.

### 3.1.1 Designing Micropost Patterns

1. Choose the side length of the hexadecagon so that it encloses an area equivalent to the average cell spreading area (*see Note 1*).
2. Ensure the center-to-center distance between microposts results in a minimum edge-to-edge distance that is less than the average nuclear diameter (*see Note 2*).
3. Array the hexadecagon pattern onto an area of 1 cm by 1 cm.

### 3.1.2 Patterning and Etching

1. Coat a P-type silicon wafer (diameter 100 mm) with a 1-micron layer of AZ1512 photoresist.
2. Pattern the AutoCAD design onto a chrome-coated glass mask using a Maskless aligner.
3. Mount the glass mask on the silicon wafer using a contact aligner and expose the photoresist-coated wafer to ultraviolet (UV) light through the glass mask.

4. Use a UV source with a wavelength of 365 nm (i-line), an intensity of 10 mW/cm<sup>2</sup>, and an exposure duration of 5–10 s, ensuring optimal transfer of the mask pattern onto the photoresist layer.
5. Develop the wafer by immersing it in a 4:1 AZ-300MIF solution for 60–90 s at room temperature.
6. Monitor the process visually or use a microscope to ensure that the unexposed areas of the photoresist layer are fully removed, leaving behind the desired micropost pattern.
7. Adjust the development time slightly if necessary based on the photoresist thickness and exposure conditions.
8. Place the wafer in the Deep Reactive Ion Etching equipment and perform etching using the Bosch process. Use SF<sub>6</sub> (50 sccm) for etching, C<sub>4</sub>F<sub>8</sub> (90 sccm) for passivation, at a chamber pressure of 20 mTorr, platen temperature of –20 °C, and RF power of 200 W.
9. Etch for 10–15 min depending on the desired depth, monitoring intermittently for uniformity using a scanning electron microscope, and repeat the development and etching steps iteratively until the desired micropost height is achieved.
10. After etching, transfer the wafer to an oxygen plasma cleaner. Perform oxygen plasma treatment with an oxygen flow rate of 80 sccm, pressure of 100 mTorr, and RF power of 150 W, for 10 min or until the photoresist is fully removed. Inspect the wafer to ensure no residue remains.
11. Apply a ~50 nm thick coating of (tridecafluoro-1,1,2,2-tetrahydrooctyl)-1-trichlorosilane on the wafer using Chemical Vapor Deposition (CVD). Place the clean wafer in a vacuum desiccator with 1 mL of the undiluted silane solution, and maintain a static vacuum for 1–2 h to ensure uniform coating (*see Note 3*).

### 3.1.3 Preparing Negative Molds

1. To prepare a negative mold from the patterned master silicon wafer using PDMS (dimethylpolysiloxane), mix the silicon elastomer kit at a base-to-cross-linking agent ratio of 10:1 (w/w).
2. Cure the PDMS mixture at 60 °C for 2 h.
3. Peel the negative mold from the wafer and cut it into blocks containing the patterned area.

### 3.1.4 Fabricating PDMS Microposts

1. Evenly spread a thin layer of uncured PDMS, mixed at a base-to-cross-linking agent ratio of 10:1 (w/w), over a block of the negative mold (*see Note 4*).
2. Carefully press the block onto a glass-bottom dish or a glass coverslip.

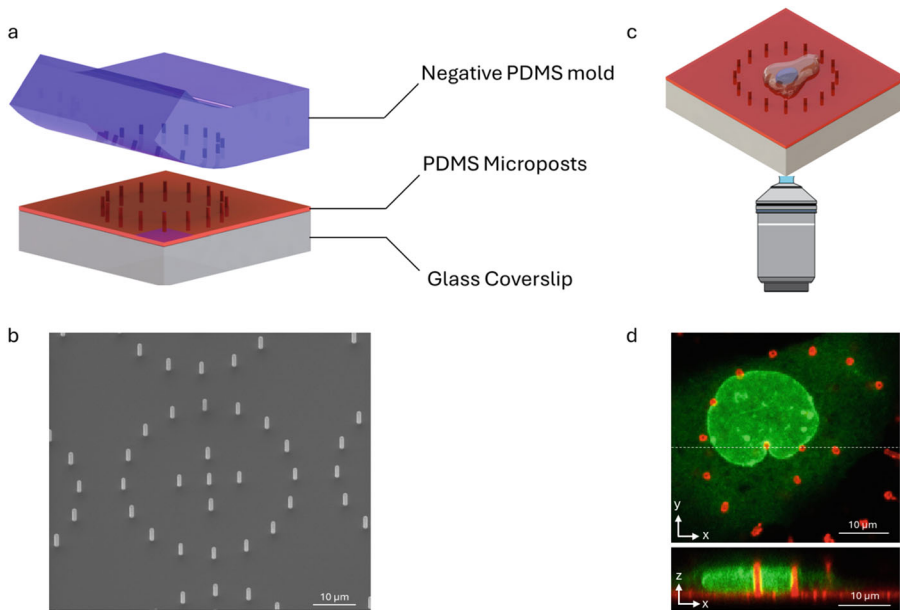


**Fig. 1** (a) Schematic illustrating the setup of PDMS microposts (red), formed after peeling away the negative PDMS mold (blue) from the glass coverslip (gray). (b) SEM image of PDMS microposts. (c) Schematic showing cells seeded on the microposts. (d) High-resolution confocal image of a cell expressing GFP-BAF and microposts labeled with r-FN (top panel), with the bottom panel showing the  $x$ - $z$  reconstruction of the same nucleus

3. Cure the dish with the negative mold at 60 °C for 2 h to form the micropost topology on the glass surface.
4. Carefully peel off the negative mold after curing (*see* Fig. 1a, b).
5. Submerge the newly cast molds in 100% ethanol for further processing.

### 3.2 Imaging for Cell Culture with Microposts

#### 3.2.1 Washing Micropost

1. Begin by replacing the 200-proof ethanol with 70% ethanol through serial dilutions, followed by a subsequent dilution to 40% ethanol (*see* Notes 5–8).
2. Pipette and aspirate with DI water 3 times to remove 40% ethanol (*see* Note 9).

#### 3.2.2 Coating with Rhodamine-Fibronectin (r-FN)

1. Add ~20 μL of 1 μM r-FN solution to the remaining DI water without physically disturbing the dish.
2. Mix gently using a 1–10 μL pipette.
3. Incubate the microposts with r-FN for 2 h.
4. Wash the r-FN solution three times with 1X PBS.
5. Aspirate all the PBS from the corner of the dish or well (*see* Note 10).
6. Add cell media to the dish, aspirate, and repeat this process three times to ensure thorough removal of any residual PBS.

**3.2.3 Seeding Cell**

1. Before seeding cells, add at least 2 mL of cell media to the 35 mm dish.
2. Seed cells drop-by-drop over the glass area.
3. Maintain cell confluence below 50% to facilitate optimal cell migration.
4. Mix the cell suspension by pipetting gently using a 20–200  $\mu$ L pipette.
5. Incubate the cells (*see* **Note 11**).

**3.2.4 Live-Cell Imaging**

1. Wash the sample with 1X PBS and replace the media.
2. Add appropriate live-cell stains and incubate.
3. Make sure the microposts are within the working distance of the objective of choice else flip the coverslip upside down for imaging.
4. The sample is now ready for imaging (*see* Fig. 1c, d and **Note 12**).

**3.2.5 Fixed-Cell Imaging**

1. Aspirate all media.
2. Wash the sample three times with 1X PBS.
3. Fix the cells with 4% paraformaldehyde (PFA) for 15–18 min at room temperature.
4. After fixation, wash the sample three times with 1X PBS.
5. The sample is now ready for staining.

**3.3 Deflection Measurements**

1. As migrating cells deform their nuclei against the labeled microposts, capture confocal Z-stacks in a time-lapse format using the desired microscopy.
2. Utilize MATLAB 2019a or a similar image processing software for automated analysis.
3. Implement centroid-detection-based particle-tracking routines to track micropost centroids.
4. Process raw images with bandpass filters and brightness thresholds to isolate the cross-sections of the top and bottom of the microposts from background noise.
5. Fit 2-D Gaussians to pixel intensities around the top and the bottom micropost section to determine the centroid positions, respectively.
6. Identify the peak of the Gaussian fit as the micropost centroid.
7. Calculate the deflection vector as the difference between the centroids of the bottom and top of each micropost.
8. Subtract the deflection vector just before nuclear contact from subsequent time points.

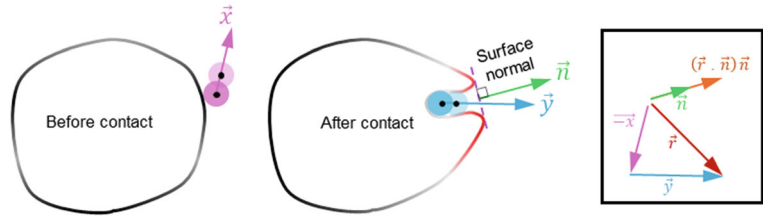


**Fig. 2** The schematic illustrates the calculation of a differential deflection vector ( $\rightarrow_r$ ) as the change in the micropost's deflection after contacting the nucleus, followed by its projection onto the normal to the deformed nuclear surface (*see Note 15*)

9. Draw a line connecting the two protruding nuclear surfaces adjacent to the micropost.
10. Rotate this line  $90^\circ$  to determine the normal direction.
11. Determine the differential deflection vector component along the normal direction in successive frames by calculating cosines of the angle between the normal vector and the differential deflection vector (*see Fig. 2*).
12. Use  $\omega = \frac{8EI}{r^3} \delta$  to quantify the uniformly distributed force exerted by microposts on the nucleus (*see Notes 13 and 14*).
13. Multiply the uniformly distributed load force per unit length by the micropost length ( $5 \mu\text{m}$ ) to determine the total force exerted during nuclear contact.

## 4 Notes

1. For example, we placed the circles of diameter  $1 \mu\text{m}$  on the corners of an equilateral hexadecagon with a side length of  $7.71 \mu\text{m}$  to customize the micropost patterns for NIH 3T3 fibroblasts which have an average spreading area of  $\sim 1200 \mu\text{m}^2$ .
2. For example, in the design we tested, the edge-to-edge distance between adjacent micropost was  $6.6 \mu\text{m}$  which is less than the average nuclear diameter of  $\sim 10 \mu\text{m}$  for NIH 3T3 fibroblasts.
3. This treatment facilitates minimal adhesion of PDMS to the wafer, ensuring ease of peeling the negative mold.
4. Spreading 20 microliters of PDMS over an area of approximately 1 cm by 1 cm on the negative PDMS mold will result in a thin film with a thickness of 50–70 microns. This thickness is within the working distance of high numerical aperture, high magnification objectives such as  $40\times$  or  $60\times$ , facilitating high-resolution imaging.

5. PDMS is hydrophobic. Place the dish or well plate on a perfectly flat surface before aspirating to avoid drying out the microposts. If dried out, the microposts may bend and stick to the bottom surface.
6. Add solutions drop by drop along the sides of the dish to minimize strong convective currents.
7. Do not add solutions directly onto the glass area; rather, add it towards the edge of the well or dish.
8. Leave at least 1 mL of solution or always maintain a minimum liquid depth of around 1 cm in the dish during aspiration.
9. During the last DI water wash, leave the microposts submerged in 2–3 mL of DI water for at least 15 min to allow adsorbed ethanol to diffuse out followed by pipetting more water and aspirating.
10. If the r-FN coating is effective, PDMS will retain a thin layer of water despite the aspiration of all liquid.
11. To facilitate the clear visualization of nuclear shape, it is recommended that cells express a nuclear envelope GFP-tagged protein-like GFP-laminA or GFP-BAF. Additionally, F-actin can be visualized using Lifeact or similar approaches, allowing for the study of cytoskeletal dynamics together with nuclear dynamics.
12. For optimal imaging quality and effective optical sectioning of microposts, it is essential to use a high numerical aperture (NA) objective. We utilized a 60 $\times$ /1.4 NA oil immersion objective to capture high-resolution images. The pinhole size was set to 1 Airy Unit (AU) with a 488 nm laser, corresponding to an optical section thickness of approximately 600 nm. To satisfy the Nyquist criterion, a z-step size of 250 nm was used, with a time resolution set to either 5 or 10 min.
13. In  $\omega = \frac{8EI}{r^4}$ ,  $\omega$  represents the uniformly distributed force exerted by the nucleus across the length of the micropost.  $E$  is the Young's modulus of PDMS, measured to be  $2.21 \pm 0.04$  MPa for PDMS mixed at a 10:1 base-to-cross-linking agent ratio and cured at 60 °C for 2 h,  $I = \frac{\pi r^4}{4}$  is the area moment of inertia of the circular cross-section of the micropost of radius  $r$ , and  $l$  is the length of the micropost.  $\delta$  is the measured deflection of the top of the micropost relative to micropost bottom.
14. Flexural rigidity ( $EI$ ) is calculated using the formula  $EI = E \times I$ , where  $E$  represents Young's modulus and  $I$  denotes the second moment of inertia for cylindrical geometry. Collagen fibers have a characterized Young's modulus ranging from 100 to 360 MPa and an average diameter of  $0.41 \pm 0.09$   $\mu$ m [8], yielding calculated flexural rigidity ( $EI$ ) between

$1.37 \times 10^{-16} \text{ Nm}^2$  and  $4.94 \times 10^{-16} \text{ Nm}^2$ . The PDMS microposts fabricated using the methods described here, with a diameter of 1 micron and a Young's modulus of  $2.21 \pm 0.04 \text{ MPa}$ , have an equivalent  $EI$  of  $\sim 1.11 \times 10^{-16} \text{ Nm}^2$ , similar to that of the collagen fibers.

15. All deflection vectors are calculated by subtracting the centroid of the top of the micropost from that of the bottom. The vector  $\vec{x}$  represents the deflection of the microposts before nuclear contact, while  $\vec{y}$  denotes the deflection vector after nuclear contact. The unit vector  $\vec{n}$  is directed normal to the nuclear surface after contact with the micropost. The vector  $\vec{r}$  is the difference between  $\vec{x}$  and  $\vec{y}$ .

---

## Acknowledgments

Tanmay P. Lele, CPRIT Scholar in Cancer Research, acknowledges support from NIH U01 CA225566, CPRIT Established Investigator Award RR200043, and NSF awards 2412520 and 2226157.

## References

1. Jana A, Tran A, Gill A et al (2022) Sculpting rupture-free nuclear shapes in fibrous environments. *Adv Sci (Weinh)* 9(25):e2203011
2. Lele TP, Dickinson RB, Gundersen GG (2018) Mechanical principles of nuclear shaping and positioning. *J Cell Biol* 217(10):3330–3342
3. Mistriotis P, Wisniewski EO, Bera K et al (2019) Lammerding, K. Konstantopoulos, Confinement hinders motility by inducing RhoA-mediated nuclear influx, volume expansion, and blebbing. *J Cell Biol* 218(12):4093–4111
4. Denais CM, Gilbert RM, Isermann P et al (2016) Lammerding, Nuclear envelope rupture and repair during cancer cell migration. *Science* 352(6283):353–358
5. Wolf K, Te Lindert M, Krause M et al (2013) Physical limits of cell migration: control by ECM space and nuclear deformation and tuning by proteolysis and traction force. *J Cell Biol* 201(7):1069–1084
6. Davidson PM, Sliz J, Isermann P et al (2015) Design of a microfluidic device to quantify dynamic intra-nuclear deformation during cell migration through confining environments. *Integr Biol (Camb)* 7(12):1534–1546
7. Katiyar A, Zhang J, Antani JD et al (2022) The nucleus bypasses obstacles by deforming like a drop with surface tension mediated by lamin A/C. *Adv Sci (Weinh)* 9(23):e2201248
8. Dutov P, Antipova O, Varma S et al (2016) Measurement of elastic modulus of collagen type I single fiber. *PLoS One* 11(1):e0145711



# Chapter 12

## Use of Nucleoporin-Conjugated Beads to Study the Nuclear Pore Complex Assembly on the Nuclear Membrane

Şükriye Bilir, Yasushi Hiraoka, and Tokuko Haraguchi

### Abstract

Reassembly of the nuclear pore complex (NPC) at the end of mitosis is a key event for establishing a functional nuclear envelope. However, the role of each NPC component (Nup) in NPC reassembly remained unclear. Here, we describe a method using artificial beads conjugated with an anti-GFP antibody. In this method, such beads are introduced into living cells expressing the Nup of interest fused with GFP to tether the specific Nup around the beads. By examining the Nup-conjugated beads in mitotic telophase cells, it is possible to investigate the role of the specific Nup of interest in NPC formation on the nuclear membrane.

**Key words** Anti-GFP antibody-conjugated bead, Nup-bead, Nucleoporin, Nuclear pore complex, Live-cell imaging, Live CLEM imaging

---

### 1 Introduction

The NE is a dynamic structure that disassembles at the beginning of mitosis and reassembles at the end of mitosis. NPCs also disassemble and reassemble during mitosis. NPC reassembly occurs in conjunction with NE reformation. Kinetic analysis using live-cell imaging of dividing cells showed that NPC subcomplexes sequentially assemble on chromatin to form functional NPCs [1]. Furthermore, it has been shown that NPCs insert into sheet-like membranes generated from the endoplasmic reticulum cisternae during telophase [2–4]. However, it remains unclear how nucleoporins and membrane components function in assembling NPCs at the end of mitosis.

To understand the complex process of NPC assembly that occurs simultaneously with NE reformation at the end of mitosis, we have developed an experimental system using artificial beads [5, 6]. In this method, when anti-GFP antibody-conjugated beads are introduced into living cells expressing a GFP-tagged protein of

interest, the GFP-tagged protein can be assembled onto the beads (Fig. 1). Therefore, by observing the events that occur around the beads, one can reveal the functions of target proteins in NE and NPC assemblies. This bead-dependent method is effective in revealing the function of target molecules in a specific time and space, even when the target molecules change their localization dynamically, such as during mitosis [6]. By observing beads using various microscopy tools such as fluorescence live-cell imaging and “Live CLEM” [7, 8], which is a combination of fluorescence live-cell imaging and correlated light-electron microscopy, it is possible to link the dynamic properties of molecules of interest to the ultrastructure of cells.

## 2 Materials

### 2.1 Beads Incorporation into Living Cells Using Transfection Reagents

1. HeLa cells expressing GFP-Nup133.
2. Culture medium: Dulbecco’s modified Eagle medium (DMEM) supplemented with 10% fetal bovine serum (FBS).
3. 35 mm glass-bottom culture dishes with an addressing grid on the coverslip (designated as “a gridded coverslip”) (*see Note 1*).
4. 1.6  $\mu\text{m}$ -diameter magnetic beads conjugated with anti-GFP monoclonal antibody (D153-11, MBL) (*see Note 2*).
5. Bead stock solution: Add 500  $\mu\text{L}$  PBS (cell culture grade) to a 1.5 mL microcentrifuge tube. Add 5  $\mu\text{L}$  of bead mixture purchased from MBL (D153-11). Vortex the bead + PBS mixture and place it on a magnetic rack (Fig. 2a). Leave it for 1 min until the beads are collected in the magnet area. Then, remove the PBS solution. Add fresh 500  $\mu\text{L}$  of PBS and repeat the same washing step three times. After the final washing, remove PBS and add 20  $\mu\text{L}$  of fresh PBS. Stored at 4 °C.
6. Transfection reagent kit (*see Note 3*).
7. 1.5 mL microcentrifuge tubes.
8. Magnetic racks for 1.5 mL microcentrifuge tubes.
9. Microliter pipettes and tips.
10. Clean bench.
11. Vortex mixer.

### 2.2 Live-Cell Imaging Using Fluorescence Microscopy

1. Fluorescence microscope (*see Note 4*).
2. Temperature controlling equipment (*see Note 5*).
3. 100 ng/ $\mu\text{L}$  Hoechst 33342 (a fluorescent dye for staining chromosomes) dissolved in DW. Store in the dark at 4 °C.

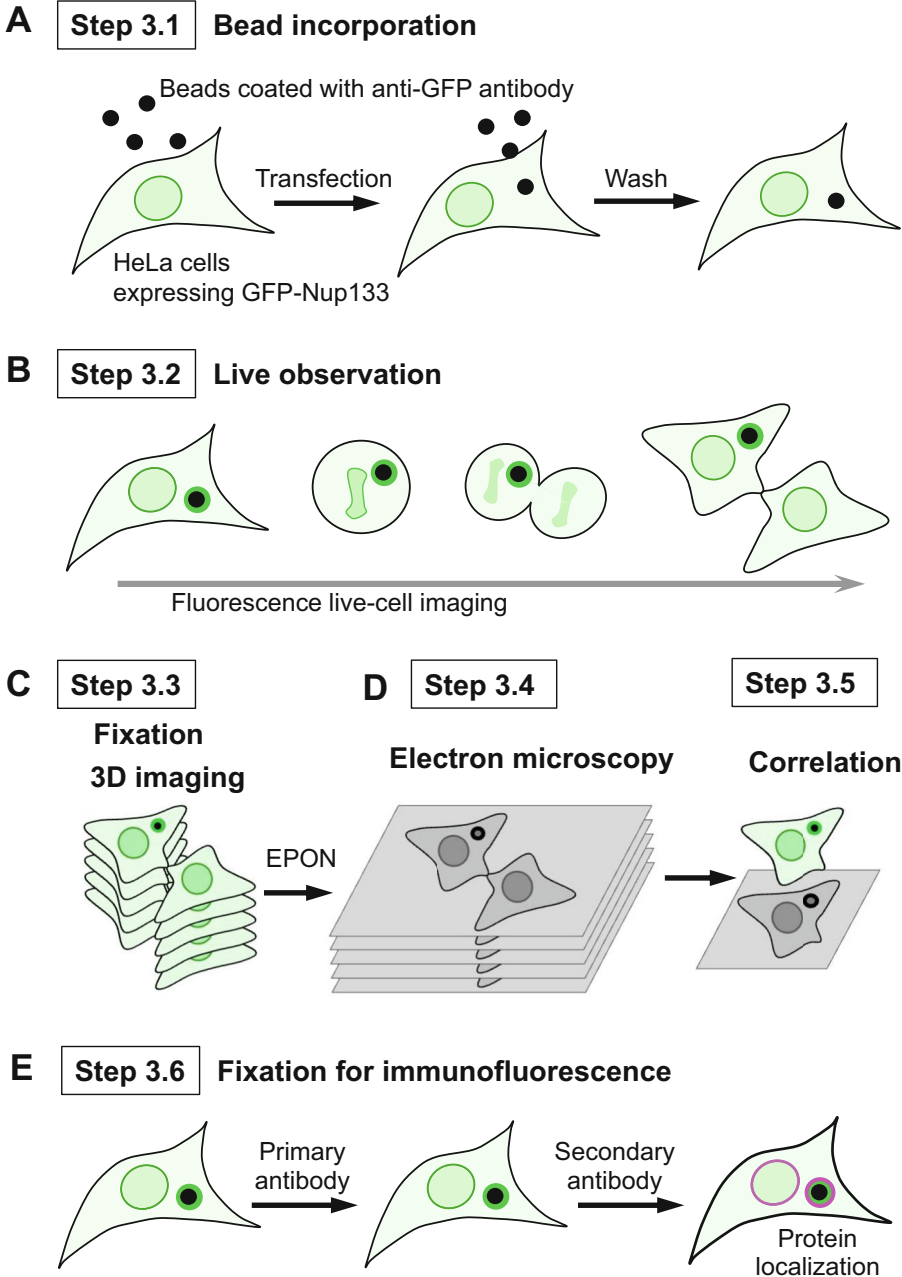


**Fig. 1** General steps to follow from bead incorporation to microscopic observation. **(a)** Steps of bead incorporation into cells as described in Subheading 3.1. **(b)** Steps of live-cell imaging as described in Subheading 3.2. **(c)** Steps of chemical fixation of cells for Live CLEM analysis as described in Subheading 3.3. Cells are fixed at the timing of your interest during live-cell imaging. **(d)** Steps of electron microscopy for CLEM analysis as described in Subheadings 3.4 and 3.5. **(e)** Steps of indirect immunofluorescence staining as described in Subheading 3.6. Subheading 3.2 of live-cell imaging can be skipped

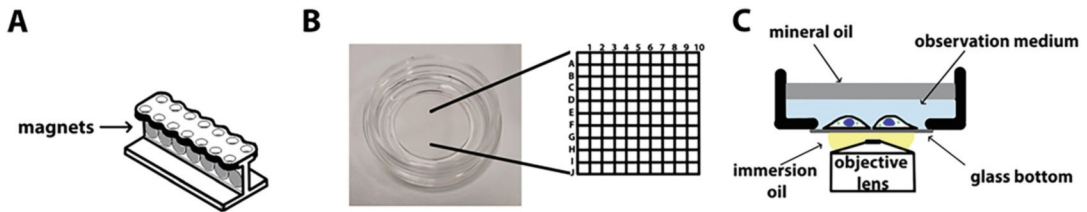


**Fig. 2** (a) A typical magnetic rack to prepare magnetic beads for the experiments. (b) A typical glass-bottom culture dish with a gridded coverslip. (c) A typical live-cell imaging setup with mineral oil on top

4. Observation medium: DMEM without phenol red, including 25 mM HEPES (pH, 7.4), 10% FBS, and 80 µg/mL Kanamycin.
5. Mineral oil.

### 2.3 Fixation for CLEM

Use reagents of the highest grade. Use ultrapure deionized water (DW) for all stock solutions.

1. Refrigerator.
2. 10× PBS stock solution for immunofluorescence: Measure 80.1 g of NaCl, 14.4 g of Na<sub>2</sub>HPO<sub>4</sub>, 2 g of KCl, and 2.7 g of KH<sub>2</sub>PO. Dissolve them in an 800 mL of DW. Bring pH to 7.4 by adding HCl. Make up the volume to 1 L with DW. This stock solution can be stored at room temperature (approximately 26 °C).
3. PBS for immunofluorescence: Took 100 mL of 10× PBS and bring to 1 L with water.
4. 10% glutaraldehyde solution: Dilute 1 mL of 25% glutaraldehyde (electron microscopy grade, nacalai tesque, Kyoto, Japan, No. 17003-92) with PBS to 2.5 mL. This amount is suitable for specimens in five 35 mm dishes.

### 2.4 Sample Preparation for CLEM

1. Fume hood.
2. Horizontal rotary shaker.
3. Desiccator.
4. Heating oven (60 °C).
5. Ultramicrotome (Leica UC6): equipped with a light microscope with a 1× ~ 4× objective lens (for observing the address on epoxy blocks).
6. Diamond knife (DiATOME Ultra 45°).
7. 2× phosphate buffer (PB): Prepare 0.2 M Na<sub>2</sub>HPO<sub>4</sub> solution, adjust pH to 7.4 with 0.2 M NaH<sub>2</sub>PO<sub>4</sub> and autoclave.
8. 0.1 M PB for electron microscopy: Dilute 3 mL 2× PB (pH 7.4) with DW to 6 mL. Use 6 mL 1× PB per one culture dish.

9.  $2\times$  osmium tetroxide ( $\text{OsO}_4$ ) solution: Wear gloves. Use a fume hood during the following processes. Ampules containing 0.5 g  $\text{OsO}_4$  crystals from EMS (#19120) are used. Scratch the neck of the ampule with an ampule cutter (do not break). Place the scratched ampule into a glass bottle specialized for  $\text{OsO}_4$ . Wrap the  $\text{OsO}_4$  bottle with Parafilm. Shake the bottle until the  $\text{OsO}_4$  ampule breaks. Add 25 mL of DW to the bottle. Incubate the  $\text{OsO}_4$  solution at  $4^\circ\text{C}$  until the solution becomes clear. Store at  $4^\circ\text{C}$ .
10. 1%  $\text{OsO}_4$ : Wear gloves and use a fume hood. Mix 150 mL of  $2\times$   $\text{OsO}_4$  and 150 mL of  $2\times$  PB. Use 300 mL per one culture dish.
11. 30%, 50%, 70%, 90%, and 100% EtOH: Use the highest grade of EtOH (99.5% purity) as 100% EtOH; dilute 30, 50, 70, 90, and 100 mL of 100% EtOH with DW to 100 mL.
12. 100% EPON: Utilize the EPON812 resin embedding kit (TAAB No. T024) comprising 30.5 g of EPON 812, 15.2 g of DDSA (dodecenyl succinic anhydride), and 17.1 g of MNA (methyl nadic anhydride). Homogenize the reagents until a homogeneous solution is achieved. Add 0.75 mL of DMP-30 (2,4,6-tridimethylamino methyl phenol; epoxy accelerator) to the mixture and thoroughly blend until uniform. Use promptly or preserve in a 12 mL syringe at  $-20^\circ\text{C}$  (use within approximately 1 month). Prior to use, equilibrate the stored solution to room temperature to prevent reagent moisture absorption.
13. 10%, 30%, 50%, 70%, and 90% EPON: Mix 100% EPON with 100% EtOH at a ratio of 1:9, 3:7, 1:1, 7:3, and 9:1. Use 1 mL of each solution per one culture dish.
14. 2% uranyl acetate: Wear gloves. Place 0.2 g uranyl acetate into a polypropylene (conical) tube. Adjust the volume to 10 mL with DW and rotate until the solution becomes clear. Filter using a syringe filter (pore size,  $0.22\ \mu\text{m}$ ) and store in a polystyrene (Spitz) tube in the dark at  $4^\circ\text{C}$ . The reagent should be stored overnight before use.
15. 4% uranyl acetate: Wear gloves. Place 0.4 g uranyl acetate into a polypropylene (conical) tube. Adjust the volume to 10 mL with DW and rotate until the solution becomes clear. Filter using a syringe filter (pore size,  $0.22\ \mu\text{m}$ ) and store in a polystyrene (Spitz) tube in the dark at  $4^\circ\text{C}$ . The reagent should be stored overnight before use.
16. Lead staining solution (SIGMA, 18-0875-2; containing 0.3% lead nitrate and 0.3% lead acetate): Filter with a syringe filter ( $0.22\ \mu\text{m}$  pore size) and store in a Spitz tube at  $4^\circ\text{C}$ .
17. Fine-tip Pasteur pipette.
18. Electron microscope (JOEL JEM-1400 in this case).
19. 3-slit grids; hole size, 340 nm (Nisshin EM, No. 2486).

20. Grid stick kit (Nisshin EM, No. 4361).
21. Grid cases (Nisshin EM, No. 2731).

### **2.5 Correlation Between Fluorescence Microscopy**

1. Photoshop software.

### **2.6 Immuno- fluorescence Sample Preparation**

1. 16% formaldehyde solution (EM grade, Polyscience inc. 18814).
2. 3.7% formaldehyde solution: Add 600 µL of 16% formaldehyde solution (EM grade, Polyscience inc. 18814) directly to 2 mL DMEM culture medium or PBS.
3. 0.1% Triton X-100 in PBS: Dissolve 0.1 mL of Surfact Amps X-100 (Pierce 28314) in 9.9 mL of PBS.
4. 1% BSA in PBS: Dissolve 1 g of bovine serum albumin (BSA) in 100 mL PBS. Aliquot it and store at  $-20^{\circ}\text{C}$ .
5. Primary antibody (e.g., anti-Nup107 antibody (Novus Biologicals, NBP1 76926, Littleton, CO, USA) in this case).
6. Secondary antibody (e.g., Alexa Fluor 594 conjugated secondary antibodies (goat anti-rabbit IgG, Carlsbad, CA, USA in this case).
7. Wet chamber.
8. Bench top shaker.

---

## **3 Methods**

We use HeLa cells expressing GFP-Nup133 to analyze the Nup bead-dependent NPC formation by Live CLEM imaging [6].

### **3.1 Beads Incorporation into Living Cells Using Transfection Reagents (Fig. 1a)**

1. Use a glass-bottom dish with a gridded coverslip to culture cells (Fig. 2b) (*see Note 1*).
2. Place 2 mL of cell suspension into the dish and culture the cells for about 1 day in a  $\text{CO}_2$  incubator at  $37^{\circ}\text{C}$ . Cultured cell amount of  $1.5 \times 10^5$  cells per dish is optimal (*see Note 6*) (As an example, we use HeLa cells expressing GFP-Nup133 suspended in the DMEM culture medium supplemented with 10% FBS).
3. After 1 day incubation, prepare a mixture of beads and transfection reagent. For this, the Effectene transfection reagent kit from Qiagen is used (*see Note 3*). Mix 10 µL buffer EC (supplied with the kit) with 1.5 µL of anti-GFP bead solution in a 1.5 mL microcentrifuge tube. Add 1 µL of Effectene reagent (supplied with the kit) to this mixture. Stir the mixture vigorously by using a vortex mixer. After 15 min at room temperature, add 80 µL of culture medium to the tube.

4. Remove the culture medium from cells in the glass bottom dishes. Then add the prepared mixture of beads and Effectene transfection reagent to the cells on the glass area. For dishes with 10 mm glass area, this amount of the bead mixture is generally sufficient to cover the entire glass area.
5. Incubate cells with the bead mixture at 37 °C for 1 h (*see Note 7*). After 1 h, wash the cells with prewarmed culture medium twice (*see Note 8*) and add 2 mL of culture medium to the dish (*see Note 9*). Place the dish back in the incubator. After 1 day of incubation, cells are ready to be observed on a fluorescence microscope (*see Note 10*).

### **3.2 Live-Cell Imaging Using Fluorescence Microscopy (Fig. 1b)**

1. Before starting live-cell imaging, stain the cells with Hoechst 33342 for chromosome visualization. For this, add 2  $\mu$ L of Hoechst 33342 stock solution (100 ng/ $\mu$ L) to 2 mL of culture medium and place this medium on a 35 mm glass-bottom dish. Incubate the cells with Hoechst 33342-containing culture medium for 15 min at 37 °C in a CO<sub>2</sub> incubator.
2. After 15 min, replace the culture medium with 1.5 mL of observation medium. Incubate the cells in the observation medium for 2 more hours at 37 °C.
3. Transfer the gridded dish onto a fluorescence microscope stage (*see Note 11*). Remove the lid of the dish and layer the culture medium with ~500  $\mu$ L of mineral oil to prevent evaporation during observation (Fig. 2c, *see Note 12*).
4. Observe the living cells using a fluorescence microscope for the desired period at appropriate intervals (*see Note 13*). An example of cells observed by live-cell imaging is shown in Fig. 3a.
5. Make notes (hand drawings) of the position and shape of the cells of interest in relation to the address on a gridded coverslip (*see Note 14*).

After this step, depending on the purpose of the experiment, proceed either to Subheadings 3.3, 3.4 and 3.5 for Live CLEM or to Subheading 3.6 for immunofluorescence.

### **3.3 Fixation for Live CLEM (Fig. 1c)**

For Live CLEM, the following fixation must be used:

1. At an appropriate time point during live-cell observation, fix the cells by adding 500  $\mu$ L of 10% glutaraldehyde directly to the dish (*see Note 15*). This results in a final concentration of 2.5% glutaraldehyde in the dish.
2. After incubating the cells for 1 h at room temperature, wash them with PBS three times (*see Note 16*).
3. Keep the fixed cell in 4 °C overnight. The next day they will be ready for 3D observation (*see Note 17*).

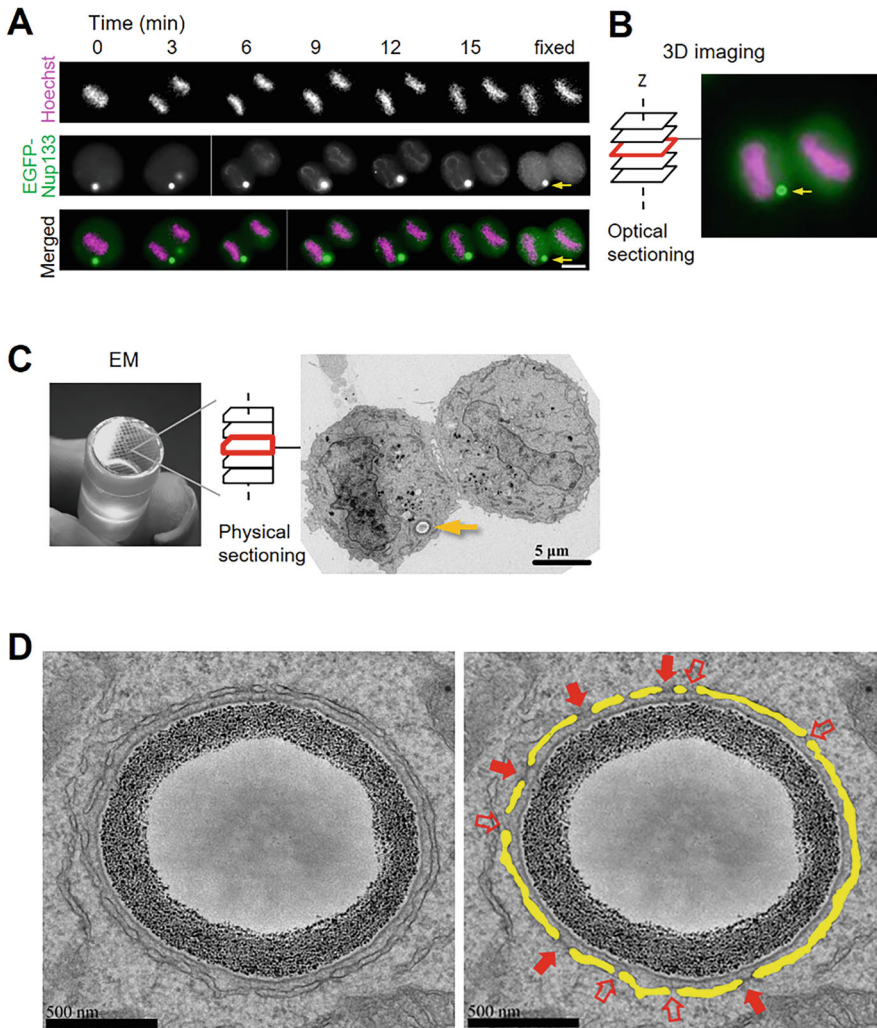


**Fig. 3** A typical bead-dependent NPC assembly on the membrane obtained by this protocol. **(a)** Live-cell imaging of a GFP-Nup133 stably expressing HeLa cell with an incorporated bead inside. The bead is marked with yellow arrows. Hoechst 33342 (DNA, magenta) and EGFP-Nup133 (green) in a merged image. Numbers on the top indicate timing from the anaphase transition. Cells were fixed at the indicated times. Scale bar, 10 µm. **(b)** An optical section image of the same cell in **(a)**. A single optical section image is shown. **(c)** Sample preparation for EM. The bead is found in serial sections marked with a yellow arrow. Scale bar, 5 µm. **(d)** A typical membranal structure that can form around beads of GFP-Nup133. Scale bar, 500 nm. (Right) Modeled image. The double-layered membrane is colored in yellow. NPC-like structures are shown with filled red arrows. Membranal openings are marked with open red arrows. Scale bar, 500 nm

4. Take three-dimensional (3D) images of target cells at the 200 nm focus intervals using a fluorescence microscope (Fig. 3b, see Note 18).

After fixing the cells during live-cell imaging, the same cells are imaged in 3D. This imaging makes it easier to find target areas within a cell during electron microscopy (EM) observation by matching the shapes of the cell and nucleus.

### 3.4 Sample Preparation for Electron Microscopy (Fig. 1d)

Wear gloves for the following **steps 1–12**. Details of this step are described previously [8].

1. Wash the cells three times with 2 mL of PB for 1 min each. Remove PB, and add 1% OsO<sub>4</sub> in PB. Leave the cells at room temperature for 1 h to post-fix the cells.
2. Remove the 1% OsO<sub>4</sub> solution and wash with DW three times. After washing, add 2% uranyl acetate. Incubate at room temperature for 1 h in a fume hood.
3. Remove the uranyl acetate solution and wash with DW three times. After washing, subject the cells to the dehydration step. For dehydration, incubate the cells in 30%, 50%, 70%, 90%, and 100% EtOH sequentially for 1 min for 30%, 3 min for 50%, and 5 min for the rest.
4. Remove the 100% EtOH solution, add 10% EPON, and shake for 3 min. Repeat this step with the 30%, 50%, and 70% EPON solutions. Replace the 70% EPON solution with the 90% EPON solution and incubate for 10 min with shaking.
5. Remove the 90% EPON solution completely and add 100% EPON. Shake for 1 h. After shaking, replace the EPON solution with fresh 100% EPON, put a lid on the dish, and leave the dish in the desiccator overnight without shaking.
6. The next day, replace the EPON with fresh 100% EPON, and leave the dish in the desiccator for 3 h without shaking.
7. Remove 100% EPON using a fine-tip Pasteur pipette. Place a tube filled 80% with EPON upside down onto the coverslip of the glass-bottom dish.
8. Incubate for 48 h at 60 °C to allow the EPON to polymerize.
9. Remove the epoxy block from the dish. After removal, the surface of the epoxy block should have an imprint of the cover glass grid.
10. After removing the block, place it to the ultramicrotome and section it using a diamond knife. Collect the serial sections in order, to a three slid grid.
11. After collecting all sections, stain them with 4% uranyl acetate for 15 min using a grid stick. Wash the sections with DW three times. Then, soak the grid stick in lead stain solution for 1 min and wash again with DW three times.
12. Leave the grids at room temperature until they are dry. After drying, store the grids in a grid case in a desiccator.
13. Observe the specimens using an electron microscope (JEOL JEM-1400 in this case) with 80 kV.

### 3.5 Correlation Between Fluorescence Microscopy (FM) and EM Images (Fig. 1d)

1. Find the EM sections, in which the regions of interest appear by comparing the EM images with the FM 3D images.
2. Compare the FM image with the EM image by eye and find the corresponding structure (*see Note 19*). Examples of EM images of cells observed by FM are shown in Fig. 3c, d.
3. Merge FM images with EM images using Photoshop or other software if necessary (this last step may not be required).

### 3.6 Immuno- fluorescence Sample Preparation (Fig. 1e)

After Subheading 3.2, if the beads are to be marked for specific NE or NPC proteins, the following steps of immunofluorescence are used:

1. Fix cells with 3.7% formaldehyde solution for 15 min. Add 600  $\mu$ L of 16% formaldehyde solution (EM grade, Polyscience inc. 18814) to 2 mL culture medium directly (*see Note 20*).
2. After fixation, wash the cells with PBS three times each for 10 min on a bench top shaker.
3. Permeabilize the cells with 0.1% Triton X-100 in PBS for 5 min (*see Note 21*).
4. Block the cells with 1% BSA in PBS for 1 h at room temperature (approximately 26 °C).
5. Treat them with a primary antibody of interest diluted in 1% BSA in PBS overnight in a wet chamber at 4 °C (*see Note 22*).
6. Next day, wash the cells three times with PBS.
7. Treat the same cells with the secondary antibody diluted in 1% BSA in PBS for 3 h at room temperature (*see Note 23*).
8. Take fluorescence images for GFP-positive beads. An example of GFP-positive beads stained with anti-Nup107 antibody is shown in Fig. 4.

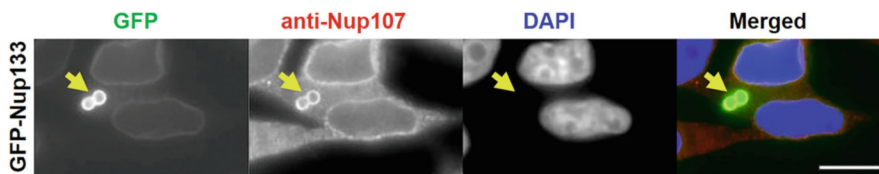


**Fig. 4** A typical immunofluorescence image obtained by this protocol. A GFP-positive bead with GFP-Nup133 around it is marked with yellow arrows. GFP-Nup133 (green), anti-Nup107 (red), DAPI (blue) in a merged image. Scale bar, 15  $\mu$ m

---

## 4 Notes

1. The gridded coverslips are for subsequent EM observation. Otherwise, regular glass-bottom dishes can be used.
2. Anti-GFP-conjugated beads with a diameter of 3  $\mu\text{m}$  (MBL D153-9) are more suitable; however, they are no longer available from the company.
3. For the introduction of beads into cells, any commercially available transfection reagents can be used, but the most efficient in our trials was Effectene reagent. This is because Effectene breaks through endosomal membranes more efficiently [9].
4. We use a DeltaVision microscope system, based on a wide-field fluorescence microscope (IX70, Olympus), equipped with high-sensitivity cameras, such as CCD or sCMOS, and an objective lens with low levels of chromatic aberration.
5. This is the equipment necessary for live-cell imaging. This equipment should control the temperature of the dish together with the objective to avoid focus drift. The main advantage is that the cell temperature can be maintained constant (at an optimal temperature), but an additional advantage is that it can reduce focus drift due to temperature fluctuations during observation.
6. The number of cells per 35 mm dish may vary from  $1 \times 10^5$  to  $2 \times 10^5$ . Too many cells will affect their health during live-cell observation. Thus, we recommend passing no more than  $2 \times 10^5$  cells per dish.
7. As the incubation time increases during bead incorporation, the number of beads taken up by a single cell increases, often leading to unhealthy cells and eventually cell death. Furthermore, the presence of multiple beads within a single cell makes observations difficult, for example, by producing overlapping bead images.
8. For less expensive means, it is also possible to use prewarmed DMEM without FBS to wash the cells. However, it is best to use culture medium with FBS for better cell conditions.
9. It is important to remove unattached beads from the cells. Too many unattached beads left around the cells will make it difficult to observe GFP-positive beads.
10. GFP-positive beads can be observed after 4–5 h of incubation. Thus, the live-cell observation can be started at this time. However, live-cell imaging at this stage may result in fewer cells containing GFP-positive beads and compromised cell

health. Therefore, we recommend observing live cells the day after bead incorporation.

11. If using a non-gridded dish, mark the dish for orientation when placing it on a fluorescence microscope stage. We put a mark on the outer side of the dish at the 6 o'clock position with a solvent resistant marker. This way allows us to easily find the targeted cell for subsequent EM sample preparation and IF observation.
12. In our experience, the container in which mineral oil is stored (a glass dropper bottle) may affect cell health. We recommend storing mineral oil in a glass bottle with no rubber attachment. The dropper bottle with rubber suction may cause health problems during live-cell observation.
13. For live-cell imaging using a DeltaVision fluorescence microscope system, we use an oil-immersion objective lens UApo/340 ( $\times 40$ , NA = 1.35, Olympus, Tokyo, Japan).
14. It is recommended to draw the shape of neighboring cells together with the target cell. This step makes it easier to find the target cell during EM sample preparation.
15. Glutaraldehyde is added directly to the dish after taking the last image during live observation. Take another image after fixation. As the microscope focus may change during this step, it should be adjusted to the target cell again. It is also important to add glutaraldehyde slowly, drop by drop, to avoid disturbing the attachment of the cells. Otherwise, the target cell may detach from the glass surface.
16. Washing with PBS can be extended until the mineral oil is removed from the dish. Be careful to leave any mineral oil in the dish because it may cause improper images during the 3D imaging steps. It is again also important to wash gently to avoid detaching the cells from the surface.
17. After glutaraldehyde fixation, cells will have a high background for fluorescence. Thus, in our experience, it is strongly recommended to keep cells at 4 °C overnight. This reduces the background while taking 3D images.
18. For 3D imaging using a DeltaVision microscope system, we use an oil-immersion objective lens PLAPON60xOSC ( $\times 60$ , NA = 1.40, Olympus, Japan).
19. When comparing FM and EM images, the best way is to follow the shape of the nucleus. Hoechst dye on FM 3D images generally merges with the EM images. By comparing the shape of the nucleus, the target area can be easily found during EM imaging.
20. Methanol can also be used for fixation instead of formaldehyde. In our experience, some antibodies give better results

with methanol fixation. For this fixation method, cells are incubated with ice-cold 100% methanol for 30 min instead of formaldehyde. The same IF method is followed, skipping the permeabilization with Triton X-100 step.

21. For permeabilization of cells, other detergents may also be used, but Triton X-100 was the most effective for our purpose. Additionally, for different cell types, the incubation time may need to be adjusted accordingly.
22. Primary and secondary antibodies in this step must be chosen so that they do not cross-react with the anti-GFP antibody of the beads. Since the GFP antibody uses a mouse monoclonal antibody, antibodies for immunofluorescence staining must be from sources other than mouse.
23. To increase or decrease the signal, the incubation time can be adjusted.

---

## Acknowledgments

This work was supported by KAKENHI grants JP23K05636 to YH, and JP25116006 and JP18H05528 to TH.

## References

1. Dultz E, Zanin E, Wurzenberger C et al (2008) Systematic kinetic analysis of mitotic dis- and reassembly of the nuclear pore in living cells. *J Cell Biol* 180(5):857–865
2. Lu L, Ladinsky MS, Kirchhausen T (2011) Formation of the postmitotic nuclear envelope from extended ER cisternae precedes nuclear pore assembly. *J Cell Biol* 194(3):425–440
3. Doucet CM, Esmery N, de Saint-Jean M et al (2015) Membrane curvature sensing by amphipathic helices is modulated by the surrounding protein backbone. *PLoS One* 10(9):e0137965. <https://doi.org/10.1371/journal.pone.0137965>
4. Otsuka S, Steyer AM, Schorb M et al (2018) Postmitotic nuclear pore assembly proceeds by radial dilation of small membrane openings. *Nat Struct Mol Biol* 25(1):21–28. <https://doi.org/10.1038/s41594-017-0001-9>
5. Kobayashi S, Koujin T, Kojidani T et al (2015) BAF is a cytosolic DNA sensor that leads to exogenous DNA avoiding autophagy. *Proc Natl Acad Sci USA* 112(22):7027–7032. <https://doi.org/10.1073/pnas.1501235112>
6. Bilir Ş, Kojidani T, Mori C et al (2019) Roles of Nup133, Nup153 and membrane fenestrations in assembly of the nuclear pore complex at the end of mitosis. *Genes Cells* 24(5):338–353. <https://doi.org/10.1111/gtc.12677>
7. Haraguchi T, Kojidani T, Koujin T et al (2008) Live cell imaging and electron microscopy reveal dynamic processes of BAF-directed nuclear envelope assembly. *J Cell Sci* 121:2540–2554
8. Haraguchi T, Osakada H, Koujin T (2015) Live CLEM imaging to analyze nuclear structures at high resolution. *Methods Mol Biol* 1262:89–103. [https://doi.org/10.1007/978-1-4939-2253-6\\_6](https://doi.org/10.1007/978-1-4939-2253-6_6)
9. Kobayashi S, Kojidani T, Osakada H et al (2010) Artificial induction of autophagy around polystyrene beads in non-phagocytic cells. *Autophagy* 6:36–45



## T4 DNA-Induced Reconstruction of Artificial Nuclei in Living Mouse Oocytes

Nao Yonezawa, Yasushi Hiraoka, Tokuko Haraguchi,  
and Kazuo Yamagata

### Abstract

Fertilization involves a specialized nuclear formation process distinct from that of somatic cells, and reconstitution methods are useful for understanding its underlying mechanisms. Recently, we successfully reconstructed a nuclear-like structure, termed an “artificial nucleus,” in living mouse oocytes by microinjecting solutions of T4 DNA (~166 kbp). This achievement allowed us to identify the physicochemical properties necessary for nuclear formation. In this paper, we describe a method for constructing artificial nuclei using T4 DNA solutions, which will contribute to future studies on the mechanisms of nuclear formation.

**Key words** Artificial nucleus, Mouse oocyte, T4 DNA, Microinjection, Live-cell imaging, Indirect immunofluorescence staining

---

### 1 Introduction

During fertilization, a special type of nucleus called the “pronucleus” is formed. The genomes of the sperm and egg each give rise to male and female pronuclei, which are enclosed by the nuclear envelope. This unique stage features two nuclei of different origin within a single cell. Research on the molecular mechanisms of fertilization often employs a “reductionism” approach, where specific molecules are identified, and their functions are inferred using techniques such as gene knockout. This approach has highlighted the significance of certain molecules in fertilization and development. However, questions remain about where, when, and to what extent these molecules contribute to nuclear formation.

To address these gaps, a “reconstructive approach” can be employed. This approach seeks to replicate biological phenomena by combining defined factors to reconstruct systems that closely resemble natural ones. Unlike reductionism, it also allows the

consideration of physicochemical factors alongside molecular factors. By integrating both reductionism and reconstructive approaches, we can achieve deeper understanding of life mechanisms.

While many studies on nuclear construction have utilized cultured cells in a reductionism approach [1–3], a reconstructive approach may be particularly beneficial for studying pronuclear formation after fertilization [4]. Therefore, we aimed to identify factors required for pronuclear formation using a reconstructive approach with mouse oocytes. When DNA-coated magnetic beads (3  $\mu\text{m}$  in diameter, coated with ~8 kilobase pairs of linear plasmid DNA) were introduced into mouse oocytes immediately after fertilization, nucleus-like structures similar to cell nuclei formed around the beads [4]. However, these “artificial nuclei” lacked nuclear transport function, suggesting that DNA-coated beads were insufficient to fully replicate sperm function. We hypothesized that additional factors are required for functional nuclear construction.

Recently, we addressed this limitation by developing a new method. Instead of the plasmid DNA-coated beads, we microinjected long-stranded DNA (T4 DNA, ~166 kbp) directly into activated mouse oocytes. By carefully controlling the DNA concentration and its microinjection timing, we successfully constructed artificial nuclei with nuclear transport activity that closely resembled natural pronuclei at the electron-microscopic level [5].

In this paper, we describe methods for preparing oocytes and microinjecting T4 DNA solution, as well as live-cell imaging and immunostaining methods used to reconstruct artificial nuclei within mouse oocytes. Each step is detailed to ensure better reproducibility of results (Fig. 1).

---

## 2 Materials

### 2.1 Oocyte Collection

1. 10–18 weeks old ICR female mice: Purchase from Japan SLC, Inc.
2. KSOM<sup>AA</sup> medium: KSOM<sup>AA</sup> medium containing 0.1% w/v BSA [6, 7].
3. Pregnant mare serum gonadotropin (PMSG): Purchase from Asuka Animal Health Co. Ltd. as “Serotropin.”
4. Human chorionic gonadotropin (hCG): Purchase from Asuka Animal Health Co. Ltd. as “Gonotropin 3000.”
5. Hyaluronidase (Sigma-Aldrich, Type-IS, H3506).
6. Liquid paraffin (Nacalai Tesque Inc., 26117-45).
7. 35-mm non-treated dish (Iwaki, 1000-35).
8. Micropipette.

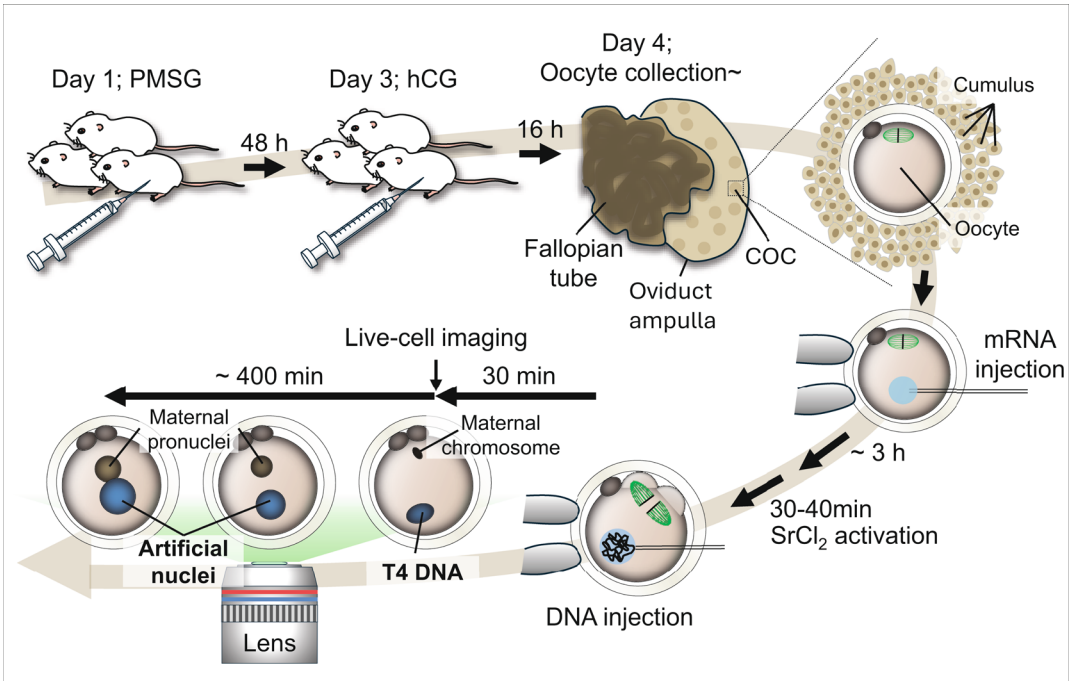


**Fig. 1** Experimental scheme for creating artificial cell nuclei in a mouse oocyte. Scheme of the experiment from days 1 to 4. Mice are administrated with pregnant mare serum gonadotropin (PMSG) on day 1 and with human chorionic gonadotropin (hCG) on day 3 (48 h later). The mice are then dissected, and the cumulus-oocyte complexes (COCs) are collected from the oviductal ampulla. After removing the cumulus cells, the oocytes are injected with mRNA and cultured in a medium containing  $\text{SrCl}_2$  for 30–40 min to activate oocyte maturation, allowing the resumption of meiosis. Following activation, the oocytes are injected with DNA solution. Live-cell imaging should begin within 30 min after DNA microinjection to capture the process of artificial cell nucleus formation

9. Mouth pipette: A handmade tool made by combining a glass capillary with multiple plastic tubing (*see Note 1*).
10. Tweezers.
11. Stereo microscope (*see Note 2*).
12. Stage-top warm plate (Tokai Hit Co., Ltd., Thermo Plate, MATS-55SZX2B).

## 2.2 Preparation of *In Vitro* Transcribed RNA

1. pcDNA3.1-histone H2B-mCherry-poly (A) [8] (*see Note 3*).
2. Restriction enzymes (*Xho* I; New England Biolabs).
3. Phenol–chloroform.
4. Chloroform.
5. Ethanol.
6. Ultrapure water, DNase- and RNase-free (*see Note 4*).
7. RiboMAX™ Large-Scale RNA Production System T7 (Promega, P1320).

8. Ribo m<sup>7</sup>G Cap Analog (Promega, P1711).
9. MicroSpin™ S-200 HR Columns (Cytiva, 27-5120-01).
10. Spectrophotometer.
11. −80 °C freezer.
12. Gel electrophoresis apparatus.

### 2.3 Preparation of DNA

1. T4 DNA (T4GT7, 166,644 bp): Purchase from Nippon Gene (catalog number, 318-03971) (*see Note 5*).
2. 3 M sodium acetate: We use premade reagent 3 M sodium acetate buffer solution (pH 5.2) purchased from Nacalai Tesque (catlog number: 06893-24).
3. Tris-EDTA solution (TE): TE buffer solution (pH 8.0) Nacalai Tesque (catalog number: 06990-25).

### 2.4 Microinjection of RNA Probes

1. HEPES-CZB medium [9].
2. HEPES-CZB containing 12% polyvinylpyrrolidone (PVP-HEPES-CZB).
3. 60-mm non-treated dish (Iwaki, 1010-60).
4. Micromanipulator (Narishige, MN-4).
5. Inverted microscope (Olympus, IX-73). Two objective lenses, 4× UPLFLN (numerical aperture (NA), 0.13) and 20× LUCPLFLN (NA, 0.45), are used.
6. Microinjector (Narishige, IM-21) (*see Note 6*).
7. Pneumatic manual microinjector (Eppendorf, CellTram Air 5176).
8. Piezo-drive manipulator (Eppendorf, PiezoXpert®).
9. Holding pipette: A handmade tool crafted from glass capillaries (Sutter, B100-75-10) (*see Note 7*).
10. Microinjection needle: A handmade tool crafted from glass capillaries (Sutter, B100-75-10) (*see Note 8*).

### 2.5 Strontium Activation of Oocyte

1. KSOM<sup>AA</sup> medium containing 5 mM SrCl<sub>2</sub> and 2.25 μM EGTA.
2. 6% CO<sub>2</sub> incubator.

### 2.6 Microinjection of DNA

1. The same as Subheading 2.4 microinjection of RNA probes.

### 2.7 Live-Cell Imaging

1. KSOM<sup>AA</sup>PVA medium: Protein-free KSOM<sup>AA</sup> medium containing 0.00025% polyvinyl alcohol (average molecular weight 30,000–70,000; Merck) and 100 μM EDTA (Merck).
2. 35-mm glass-bottom dish (No. 1.5 coverslip, glass diameter 14 mm; MATTEK).

3. Inverted fluorescence microscope system: A spinning disk confocal super-resolution fluorescence microscopy system (Yokogawa Electric Corp., CSU-W1 SoRa) is used [10, 11] (*see Note 9*).
4. Objective lens (Olympus, UPLANSAPO 40×/1.25, silicone-immersion).
5. Stage top incubator (Tokai Hit, STXG-IX3WX-SET).
6. Optical power meter (Yokogawa Electric Corp., TB200).
7. Wire-type thermocouple thermometer (Tokai Hit, TSU-200F).

## 2.8 Immunostaining

1. 96-well plate.
2. 4% formaldehyde solution in phosphate buffer (PB), pH 7.0 (Sigma-Aldrich, HT5011).
3. 0.02% PVA dissolved in PBS (PVA/PBS): Prepare a 10% (w/v) PVA stock solution by dissolving 1 g of PVA in 10 mL of PBS. Once the PVA has completely dissolved, filter the solution. Dilute 1  $\mu$ L of the stock solution with 500  $\mu$ L of PBS.
4. 0.2% Triton X-100 dissolved in PBS (Triton X-100/PBS): Prepare a 10% stock solution by adding 300  $\mu$ L of Triton X-100 to 2.7 mL of PBS. To prepare the working solution, mix 4  $\mu$ L of the stock solution with 196  $\mu$ L of PBS.
5. 3% (w/v) bovine serum albumin (BSA) dissolved in PBS (BSA/PBS): Prepare the solution by dissolving 15 g of BSA (Nacalai Tesque, 01863-48) in 500 mL of PBS and filtering.
6. Primary antibody (e.g., anti-NPC and anti-lamin B1 antibody).
7. Secondary antibody (e.g., CF 555-conjugated goat anti-mouse IgG (H + L) antibody (Biotium, 20231-1), Cyanine 5-conjugated goat anti-rabbit IgG (H + L) antibody (Invitrogen, A10523)).
8. 4', 6-diamidino-2-phenylindole (DAPI).

---

## 3 Methods

### 3.1 Oocyte Collection

Mouse is maintained in a temperature-controlled room at approximately 23 °C, with relative humidity at around 50%, and a 12/12 h light/dark cycle. Animals have free access to water and commercial food pellets.

1. Induce superovulation for female ICR mice (10–18 weeks-old) by intraperitoneal injections of 10 IU pregnant mare serum gonadotropin (PMSG) on day 1 and 10 IU human chorionic gonadotropin (hCG) on day 3 (Fig. 1).

2. Create 100- $\mu$ L and 20- $\mu$ L droplets of KSOM<sup>AA</sup> medium on a 35-mm dish, and then cover them with liquid paraffin (Fig. 2a).
3. 15–17 h after the hCG injection (on day 4, Fig. 1), collect cumulus-oocyte complexes (COCs) from the oviductal ampullae on the 35-mm dish filled with liquid paraffin using a tweezer under a stereo microscope (Fig. 2b, c).
4. Transfer the COCs using a tweezer to a 100- $\mu$ L droplet of KSOM<sup>AA</sup> medium covered with liquid paraffin, which is pre-warmed at 37.5 °C on a stage top warm plate equipped on the stereo microscope stage (*see* **Note 10**) (Fig. 2d).
5. Add hyaluronidase (150 U/mL) to the 100- $\mu$ L droplet using a micropipette and incubate for 5 min to disperse the cumulus cells (*see* **Note 11**) (Fig. 2e).
6. After dispersing the cumulus cells, select oocytes and transfer them to the adjacent droplet using a mouth pipette (Fig. 2f, g, j).
7. Select only metaphase II oocytes and transfer them to the 20- $\mu$ L droplet of KSOM<sup>AA</sup> medium (*see* **Note 12**) (Fig. 2h, i).

### 3.2 Preparation of In Vitro Transcribed RNA

The method for in vitro transcription of fluorescent probes (RNA probes) has been described elsewhere [10–12]. The method is briefly described below.

1. Linearize plasmid DNA (at least 5  $\mu$ g) using a restriction enzyme that has a single digestion site immediately downstream of the poly (A) sequence. Use *Xho* I for pcDNA3.1-histone H2B-mCherry-poly (A).
2. Purify the linearized plasmid by phenol-chloroform treatment, followed by chloroform treatment and ethanol precipitation using RNase-free reagents.
3. Dissolve the purified linear plasmid in fresh ultrapure water at a concentration of 0.5  $\mu$ g/ $\mu$ L.
4. Use 3–4  $\mu$ L of the plasmid solution (1.5–2  $\mu$ g DNA) as the template in a 20  $\mu$ L reaction for RNA transcription.
5. Transcribe the RNA using the RiboMAX<sup>TM</sup> Large-Scale RNA Production System T7, following the manufacturer's protocol. Add the Ribo m7G cap analog to stabilize the RNA in the ooplasm.
6. Treat the transcribed RNA with RQ-1 RNase-free DNase from the RNA production kit.
7. Purify the RNA by phenol-chloroform treatment, chloroform treatment, and ethanol precipitation.
8. Dissolve the RNA in 20  $\mu$ L of fresh ultrapure water.

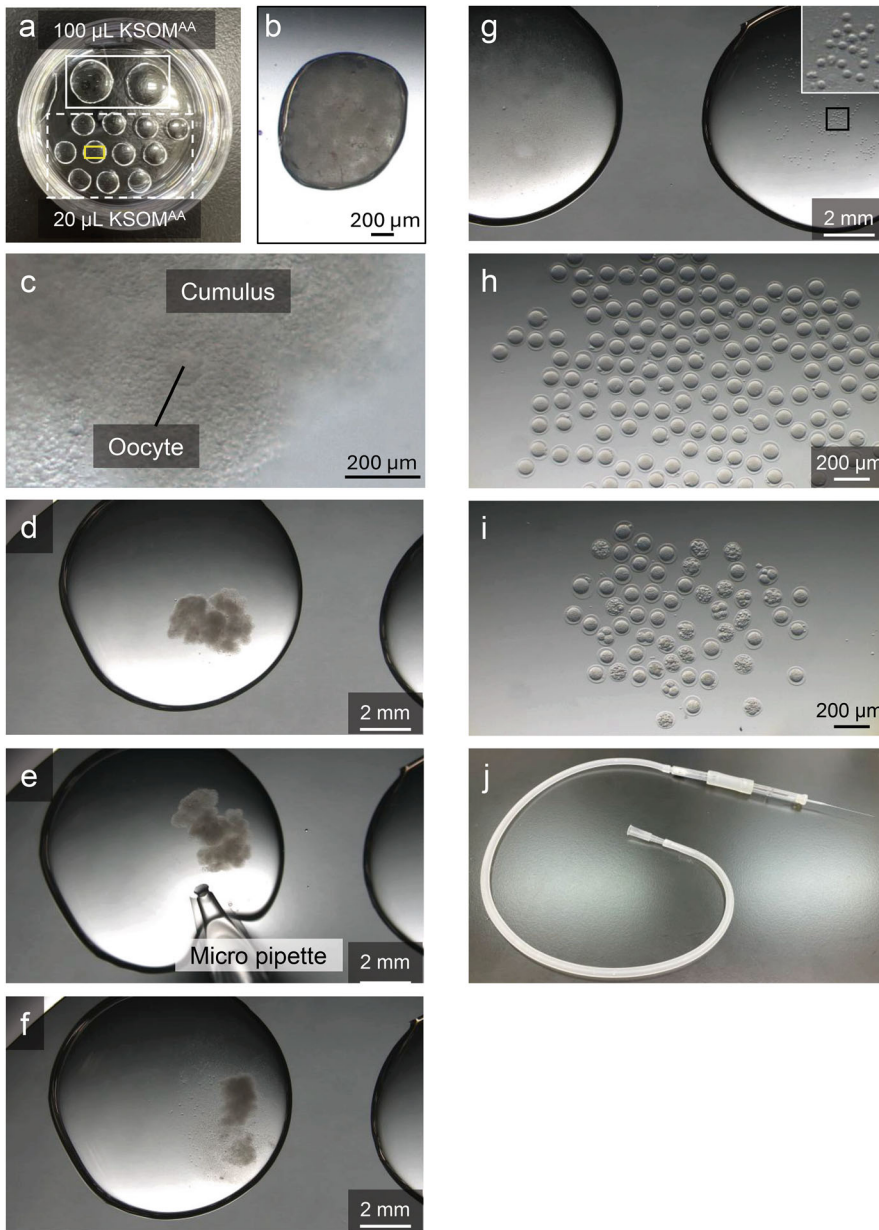


**Fig. 2** Oocyte collection. (a) Droplets of KSOM<sup>AA</sup> medium on a 35-mm plastic dish covered with liquid paraffin. Solid and dashed boxes indicate areas containing 100-μL and 20-μL droplets, respectively. The white box is enlarged in (d–g). Enlarged views of 20-μL droplets are shown in (h) and (i); (h) shows the yellow-boxed region. (b) Cumulus-oocyte complexes (COCs) in a dish filled with liquid paraffin. (c) Enlarged view of a single COC in the KSOM<sup>AA</sup> medium. (d) COCs in a 100-μL droplet of KSOM<sup>AA</sup> medium. (e) Hyaluronidase addition to the droplet using a micropipette. (f) Five min after hyaluronidase addition, oocytes are released from cumulus cells. (g) Cumulus cell-free oocytes are transferred into the right droplet. The inset in the upper right shows a magnification of the boxed area. (h) Typical view of oocytes in a 20-μL droplet. Only metaphase II oocytes are selected. Note that some oocytes may rarely undergo parthenogenesis. (i) Degenerated and fragmented oocytes, which are removed from normal oocytes by transferring them into separate droplets. (j) A handmade mouth pipette used to transfer oocytes between droplets

9. Remove free rNTPs using a MicroSpin™ S-200 HR column as follows: First, equilibrate the column with fresh ultrapure water, spin to remove the water, and repeat five times. Second, add the RNA solution to the column and spin down. Third, elute RNA using 20  $\mu\text{L}$  of water multiple times.
10. Measure the RNA concentration in each fraction using a spectrophotometer.
11. Verify the size, degradation, and quantity of the transcribed RNA via denaturing electrophoresis.
12. Combine two to three fractions and adjust the RNA concentration to approximately 100 ng/ $\mu\text{L}$  (*see Note 13*).
13. Store RNA in microliter aliquots at  $-80^\circ\text{C}$  to avoid repeated freeze-thaw cycles.

### 3.3 Preparation of DNA

1. Dilute 10–20  $\mu\text{g}$  of DNA (T4 DNA) with TE or ultrapure water to a total volume of 350  $\mu\text{L}$  (*see Note 14*).
2. Add 35  $\mu\text{L}$  (1/10th volume of DNA solution) of 3 M sodium acetate to the DNA solution.
3. Purify the DNA by performing 400  $\mu\text{L}$  phenol-chloroform treatment, 400  $\mu\text{L}$  chloroform treatment, and 800  $\mu\text{L}$  ethanol precipitation (*see Note 15*).
4. Dissolve the precipitate (DNA) in approximately 20  $\mu\text{L}$  of water (*see Note 16*).
5. Measure the DNA concentration using a spectrophotometer and electrophoresis, and adjust to the required concentration by adding water. Store until use (*see Note 17*).

### 3.4 Microinjection of RNA Probes

The RNA probe, such as mRNA encoding histone H2B-mCherry, must be injected several hours before the start of imaging, during which time the fluorescent molecules are translated from the probe.

1. Set the holding pipette to the pneumatic manual microinjector on one side (typically the left side) of the inverted microscope (*see Note 7*).
2. Set the microinjection needle to the water-filled microinjector equipped with a piezo-drive manipulator on the other side (typically the right side) of the inverted microscope (*see Note 8*).
3. Dilute the RNA probe (e.g., histone H2B-mCherry RNA; *see Subheading 3.2*) to 10 ng/ $\mu\text{L}$  in ultrapure water.
4. Place an aliquot (0.3  $\mu\text{L}$ ) into a micromanipulation chamber (e.g., the lid of 60 mm dish) (Fig. 3a, b).
5. Create 8- $\mu\text{L}$  droplets of PVP-HEPES-CZB medium and 8- $\mu\text{L}$  droplets of HEPES-CZB medium in the same chamber, and then cover them with liquid paraffin (Fig. 3b).

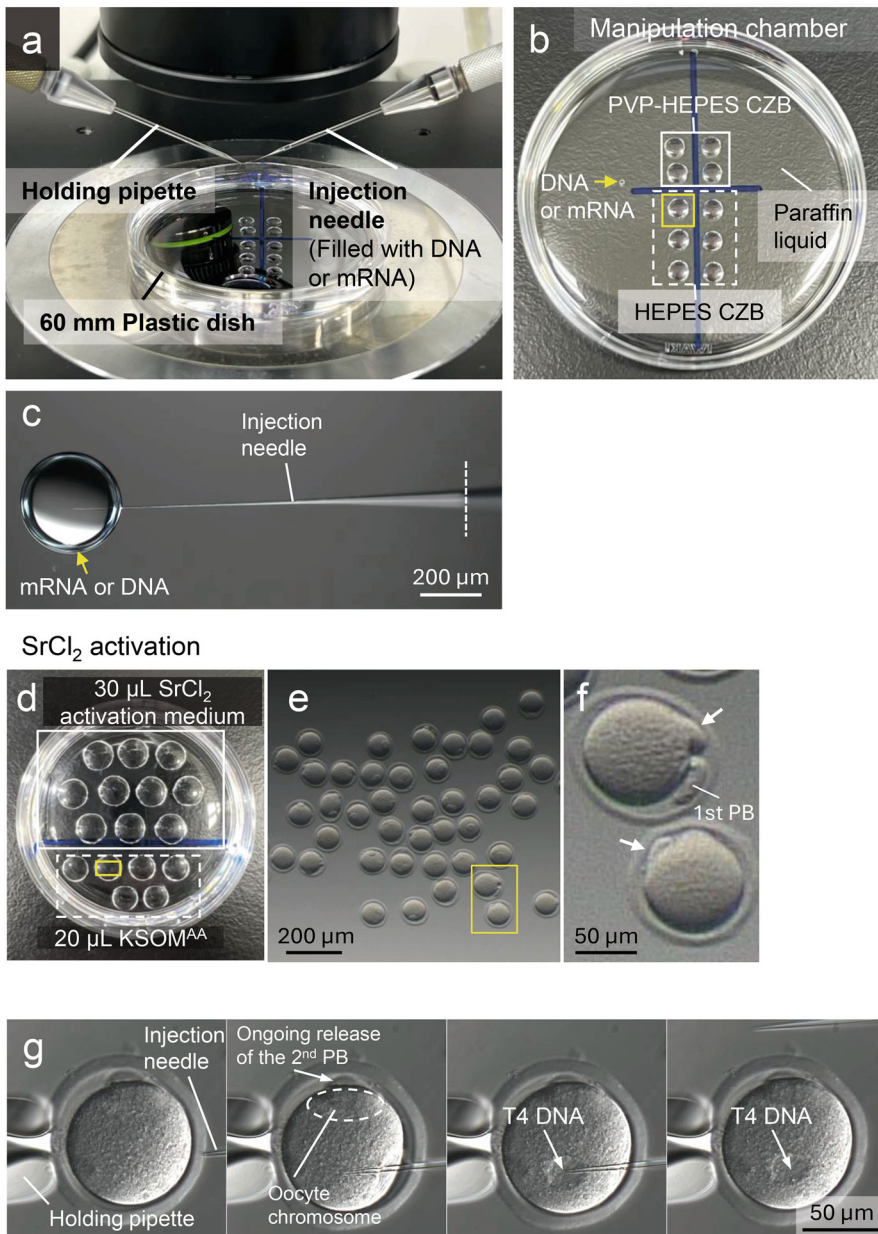


**Fig. 3** Microinjection of mRNA and DNA and strontium activation. **(a)** Microinjection setup on an inverted microscope. The needle on the left is the holding pipette used to retain the oocyte, and the needle on the right is used to inject mRNA or DNA. The bottom shows a 60 mm dish, serving as the micromanipulation chamber for microinjection. **(b)** A micromanipulation chamber with 8- $\mu\text{L}$  droplets containing PVP-HEPES-CZB (white solid box) and HEPES-CZB (white dotted box) in liquid paraffin. Yellow arrows indicate the position of 0.3- $\mu\text{L}$  droplets containing mRNA or DNA. An enlarged view of the yellow boxed region is shown in **(g)**. **(c)** Microinjection needle filled with mRNA or DNA. **(d)**  $\text{SrCl}_2$  activation medium on a 35 mm plastic dish. **(e)** Oocytes after 30–40 min of incubation in  $\text{SrCl}_2$  medium. An enlarged view of the yellow boxed region is shown in **(f)**. **(f)** Image of anaphase II oocytes. Successful parthenogenesis is confirmed by the release of the second polar body. White arrows indicate positions of the second polar body. **(g)** DNA microinjection to a mouse oocyte. In this example, 250 ng/ $\mu\text{L}$  T4 DNA solution was injected into cytoplasm, avoiding the polar body (dashed circle) to prevent extrusion of chromosomes during the second meiotic division

6. Transfer the micromanipulation chamber to the stage of inverted microscope.
7. Transfer metaphase II oocytes to the HEPES-CZB medium (Fig. 3b).
8. Hold the oocyte by the holding pipette (Fig. 3a).
9. Wash the inner wall of the glass microinjection needle by aspirating and spitting out PVP-HEPES-CZB medium once, to prevent the RNA from sticking to the needle.
10. Aspirate the RNA solution into the glass microinjection needle (*see Note 18*) (Fig. 3c).
11. Break the zona pellucida and oolemma of the oocytes with the microinjection needle applying piezo pulses generated by a piezo-drive manipulator.
12. Inject a few picoliters of the RNA solution into the ooplasm and remove the needle after microinjection (*see Note 19*).
13. Transfer the oocytes to a 20- $\mu$ L droplet of the KSOM<sup>AA</sup> medium (Fig. 2a).
14. Incubate the oocytes in a 6% CO<sub>2</sub> incubator at 37 °C for 3 h or more (*see Note 20*).

### 3.5 Strontium Activation of Oocyte

1. Create 30- $\mu$ L droplets of KSOM<sup>AA</sup> medium containing 5 mM SrCl<sub>2</sub> and 2.25  $\mu$ M EGTA and 20- $\mu$ L droplets of KSOM<sup>AA</sup> medium without these compounds, in a 35-mm dish, and then cover them with liquid paraffin (Fig. 3d).
2. Transfer metaphase II oocytes fluorescently labeled with RNA probes (*see Subheading 3.4*) to the 30- $\mu$ L droplet containing SrCl<sub>2</sub> on the stage top warm plate (set at 37.5 °C) on the stereo microscope stage.
3. Incubate for approximately 30 min at 37 °C in a 6% CO<sub>2</sub> incubator for strontium activation (Fig. 3e, f).
4. Check whether oocytes have reached anaphase II using the stereo microscope. If not, incubate for an additional 10 min. Identify anaphase II oocytes by the presence of a second polar body (*see Note 21*) (Fig. 3f).
5. Wash the oocytes by transferring them to a 20- $\mu$ L droplet containing KSOM<sup>AA</sup> medium (*see Note 22*) (Fig. 3e).
6. Transfer anaphase II oocytes to another 20- $\mu$ L droplet of KSOM<sup>AA</sup> medium (Fig. 3e, f), repeating one or two times.
7. Keep the oocytes at 37 °C in the 6% CO<sub>2</sub> incubator until DNA microinjection (*see Note 23*).

### 3.6 Microinjection of DNA

1. Dilute the DNA (obtained in Subheading 3.3) to 250 ng/ $\mu$ L in ultrapure water (*see* **Note 24**).
2. Place an aliquot (0.3  $\mu$ L) onto a micromanipulation chamber (e.g., the lid of 60 mm dish) (Fig. 3a, b).
3. Place 8- $\mu$ L droplets of HEPES-CZB medium and 8- $\mu$ L droplets of PVP-HEPES-CZB in the same chamber, and then cover them with liquid paraffin (Fig. 3b).
4. Prepare a holding pipette and set the pipette on the inverted microscope. (*see* **Note 25**).
5. Prepare a microinjection needle on and set the microinjection needle on the inverted microscope (*see* **Note 26**).
6. Place the micromanipulation chamber on the inverted microscope stage, pre-cooled to approximately 18 °C using a cooling gel pack (*see* **Note 27**).
7. Wash the inner wall of the microinjection needle by aspirating and spitting out the HEPES-CZB medium once, to prevent DNA from sticking to the needle.
8. Aspirate the DNA solution into the microinjection needle (*see* **Notes 18, 28**) (Fig. 3c).
9. Transfer anaphase II oocytes to the HEPES-CZB medium in the chamber (*see* **Note 29**).
10. Break the zona pellucida and oolemma of the oocytes with the microinjection needle applying piezo pulses generated by a piezo-drive manipulator.
11. Inject a few picoliters of DNA solution into the oocytes using a microinjector and remove the needle (*see* **Note 30**) (Fig. 3g).
12. Leave the DNA-injected oocytes in the HEPES-CZB medium on the inverted microscope stage (kept at approximately 18 °C) for 10–30 min (*see* **Note 27**).
13. Transfer the oocytes into a 20- $\mu$ L droplet of KSOM<sup>AA</sup> medium and incubate them at 37 °C in a 6% CO<sub>2</sub> incubator until live-cell observation.

### 3.7 Live-Cell Imaging

A spinning disk confocal super-resolution fluorescence microscopy system (Yokogawa Electric Corp., CSU-W1 SoRa), based on an Olympus inverted fluorescence microscope (IX-73) [10, 11], is used.

1. Use an optical power meter to measure the laser power emitted from the objective lens. The required output power may vary depending on the specimens and probe, but for this chapter, 0.1 mW at 561 nm is recommended (*see* **Note 31**) (Fig. 4a, b).

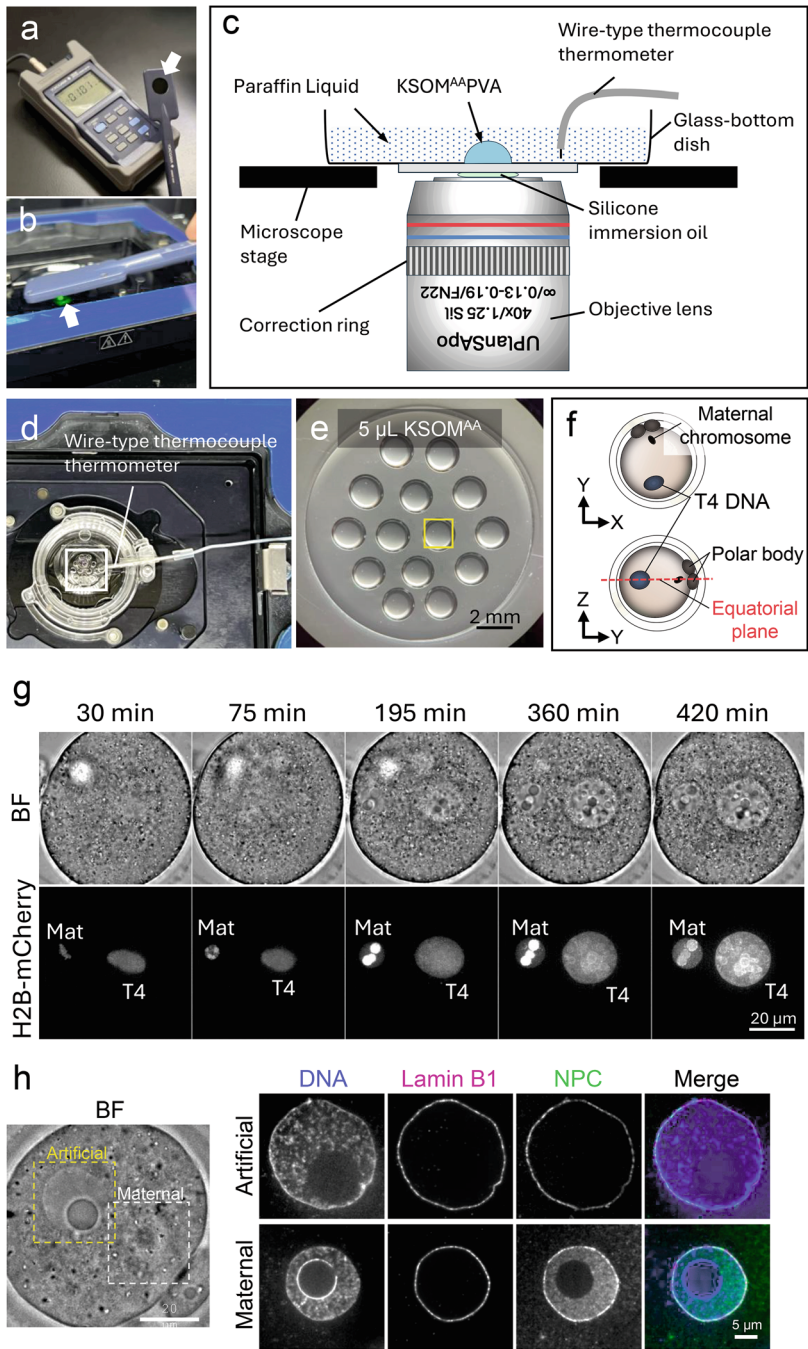


**Fig. 4** Live-cell imaging of mouse oocytes. **(a)** Optical power meter used to measure laser power. The arrow indicates the hole where the laser light enters. **(b)** Measuring the laser power emitted from the objective lens. **(c)** Fluorescence microscope setup for live-cell imaging. A silicone immersion lens is used, as the oocyte is approximately 90- $\mu$ m thick in diameter. Before starting live-cell imaging, the correction ring should be adjusted to minimize blur. During imaging, the temperature is monitored with a wire-type thermocouple thermometer. **(d)** Microscope stage for live-cell imaging. The white box is enlarged in **(e)**. **(e)** Droplets of KSOM<sup>AA</sup>PVA medium (5  $\mu$ L) used for live-cell imaging, each containing one oocyte. The yellow box is enlarged in **(f)**. **(f)** Schematic showing an oocyte positioned at the bottom of a glass-bottom dish, with the polar body visible. It is preferable that oocytes are set so that T4 DNA, polar bodies, and maternal chromosomes are

2. Transfer the oocytes into 5- $\mu$ L droplets of KSOM<sup>AA</sup>PVA medium spotted on a glass-bottom dish (*see* **Note 32**), aligning the polar bodies at the equator (Fig. 4c, f).
3. Transfer the glass-bottom dish to the stage top incubator on the microscope stage maintained at 37 °C. Confirm the temperature in the dish using a wire-type thermocouple thermometer (*see* **Note 33**) (Fig. 4c–f).
4. Observe the oocyte using the fluorescence microscope system through an objective lens (UPLANSAPO 40 $\times$ /1.25, Olympus, silicone immersion). A typical example of time-lapse images of histone H2B-mCherry is shown (*see* **Note 34**) (Fig. 4g).

### 3.8 Immunostaining

Immunostaining of oocytes is performed using 96-well plates. The reaction and washing process is carried out by transferring samples (oocytes) using a mouth pipette into wells containing 40  $\mu$ L of various solutions one after the other.

1. Aspirate oocytes into the tip of a mouth pipette filled with 4% formaldehyde in PB.
2. Transfer the oocytes into a well of a 96-well plate containing 4% formaldehyde/PB for fixation, and incubate for 20 min at room temperature (RT, approximately 26 °C).
3. Wash twice with 0.02% PVA/PBS for 15 min at RT.
4. Incubate twice with 0.2% Triton X-100/PBS for 15 min at RT for permeabilization.
5. Incubate twice in 3% BSA/PBS for 15 min at RT to remove residual Triton X-100.
6. Incubate once in 3% BSA/PBS for 60 min at RT for blocking nonspecific binding of antibodies.
7. Incubate with the primary antibody diluted in 3% BSA/PBS overnight at 4 °C.
8. Wash twice with 3% BSA/PBS for 60 min at RT.

**Fig. 4** (continued) aligned in the equatorial plane. **(g)** Example of fluorescence live-cell imaging of a mouse oocyte. The upper and lower panels show bright-field and histone H2B-mCherry fluorescence images. 3D images (0.5  $\mu$ m  $\times$  61 z-sections) were taken every 15 min. Maximum projection images of selected time frames are shown. “MAT” indicates maternal pronuclei, and “T4” refers to T4 DNA-induced artificial nuclei. **(h)** Example of immunostained image of a mouse oocyte fixed 300 min after microinjection with 250 ng/ $\mu$ L T4 DNA at anaphase II. The leftmost image shows a bright field (BF) image. The upper-right panels show fluorescence (FL) images of the T4 DNA-induced artificial nuclei (yellow-boxed region), while the lower-right panels show the maternal pronuclei (white-boxed region). The merged image shows DNA stained with DAPI (blue), lamin B1 (magenta), and nuclear pore complex (NPC, green). The images are single-plane views of the nuclei. Scale bar, 20  $\mu$ m (BF image), 5  $\mu$ m (FL images)

9. Incubate with the secondary antibody diluted in 3% BSA/PBS for 60 min at RT.
10. Wash twice with PBS containing 0.5 µg/mL DAPI for 60 min at RT.
11. Observe under the fluorescence microscope. A typical example of an oocyte stained with anti-NPC and anti-lamin B1 antibodies is shown (Fig. 4h).

---

## 4 Notes

1. A mouth pipette consists of a glass capillary (inner diameter 1.1–1.2 mm, outer diameter 1.5–1.6 mm, Paul Marienfeld, 2900000) and plastic tubing (Kokugo, Styrenic Elastomer 20-200-02-02, and 02-200-07-02) (*see* Fig. 2j).
2. We use a stereo zoom microscope (Olympus SZX12) equipped with a transmitted light LED stand (SZX2-ILLTQ) and an LED light guide light source (SZX2-CDB).
3. This plasmid contains an extended polyadenine sequence at the 3' end of the coding region to enhance mRNA stability and transcription efficiency [12].
4. DNA and RNA for microinjection are dissolved in fresh ultra-pure water to avoid introducing DNase, RNase, or contaminants into oocytes. We use water from the PURELAB flex 3 system, certified to contain <5 pg/mL DNase and <1 ng/mL RNase.
5. Artificial nuclei can also be made using lambda DNA (48,502 bp, Nippon Gene, 318-00414; Tokyo, Japan). As a control, we typically use plasmid DNA, pGADT7 AD (7987 bp, Clontech, 630442, Clontech Laboratories, Inc., Mountain View, CA, USA) [5].
6. While injectors were originally filled with oil, we now use water-filled tubes for easier handling and cleaning.
7. Making the holding pipette: A glass capillary (Sutter, B100-75-10) is pulled using a puller (Sutter, P-1000IVF). The tip is broken with a microforge (Narishige, MF-900) to achieve an outer diameter of 50–80 µm. The tip is then rounded smoothly using the microforge.
8. Making the microinjection needle: A glass capillary (Sutter, B100-75-10) is pulled using a puller (Sutter, P-1000IVF). The tip is broken off with a microforge (Narishige, MF-900) to achieve an outer diameter of less than 1 µm. The tip of the needle should not be round.

9. We use a spinning disk confocal super-resolution fluorescence microscopy system (Yokogawa Electric Corp., CSU-W1 SoRa), based on an Olympus inverted fluorescence microscope (IX-73), equipped with an sCMOS camera (Photometrics, Prime 95B), a silicone-immersion objective lens with low chromatic aberration (UPLANSAPO 40 $\times$ /1.25, Olympus), and a 4 $\times$  tube lens.
10. Preincubate droplets for at least 6 h in a CO<sub>2</sub> incubator to ensure gas equilibrium.
11. Minimize oocyte exposure to hyaluronidase.
12. Complete removal of cumulus cells at this stage facilitates subsequent microinjection and observation.
13. High absorbance at 260 nm in later fractions indicates free NTPs. After confirming RNA transcription via electrophoresis, combine the two or three most abundant fractions for further use.
14. Commercially available DNA is unsuitable for microinjection and must be purified before microinjection.
15. Prepare 70% ethanol for DNA washing immediately before use, as delays reduce DNA solubility in water.
16. Long-stranded DNA is highly insoluble in water and requires storage at 4 °C for up to 2 weeks for complete dissolution, which can be confirmed with a stereomicroscope. TE buffer dissolves DNA faster (about 1 day), but introducing large amounts of TE should be avoided in oocytes, as it may affect oocyte development.
17. Store purified DNA at –30 °C in single-use aliquots to avoid freeze-thaw cycles, which inhibit the formation of artificial nuclei resembling natural ones.
18. After aspirating the RNA or DNA solution into the needle, maintain positive needle pressure to prevent the surrounding media (e.g., culture medium or liquid paraffin) from entering the needle during approach.
19. Avoid injecting mRNA or DNA into the oocyte's metaphase II spindle in order to prevent spindle disruption, visible under a relief contrast microscope (IX-71, Olympus) as a smooth area at the oocyte periphery.
20. Fluorescent proteins expressed from the RNA probe become detectable 3 h after RNA microinjection.
21. Prolonged incubation from the collection of oocytes to strontium activation can delay activation. After transferring to SrCl<sub>2</sub> medium, ensure oocytes are in anaphase II. If not, incubate for at least 10 min until they reach anaphase II.

22. To remove  $\text{SrCl}_2$ , transfer oocytes to a 20- $\mu\text{L}$  droplet of KSO- $\text{M}^{\text{AA}}$  medium at least twice.
23. Limit the number of oocytes in a droplet to no more than 1 oocyte per 1  $\mu\text{L}$  of medium.
24. DNA concentrations between 100 and 500  $\text{ng}/\mu\text{L}$  are suitable for artificial nucleus formation, but lower concentrations (e.g., 20  $\text{ng}/\mu\text{L}$ ) may lead to failure [5]. Higher concentrations, however, increase DNA viscosity, making manipulation difficult.
25. The holding pipette used for RNA microinjection can be reused for DNA microinjection; there is no need to prepare a new one.
26. Use freshly made needles of approximately 1  $\mu\text{m}$  in diameter for DNA microinjection. If the needle is too large or aged, the DNA may stick to it, making release difficult, and the cytoplasm may adhere to the needle.
27. Reducing the temperature of the microscope stage to approximately 18  $^{\circ}\text{C}$  is known to promote the repair of oocyte membrane damage caused by DNA microinjection [13]. Therefore, leave the oocytes in HEPES-CZB medium on the microscope stage at 18  $^{\circ}\text{C}$  for 10–30 min after DNA microinjection.
28. If DNA is drawn up to the white line in the glass lumen (Fig. 3c), rinse the lumen with HEPES-CZB to this line to avoid contamination.
29. The oocyte cell cycle stage at the time of DNA microinjection is critical for successful artificial nuclear formation. Anaphase II is optimal, but metaphase II or telophase II is also acceptable. Microinjection during interphase results in incomplete artificial nuclei, lacking nuclear pore complexes and nuclear transport activity [5].
30. When removing the needle, do so slowly. With highly concentrated or long-stranded DNA, the cytoplasm may be withdrawn with the needle.
31. We use a laser power meter (Yokogawa Electric Corp., TB200).
32. We place one oocyte per droplet to ensure that a single oocyte is present within the observation field.
33. Ensure temperature stability at 37  $^{\circ}\text{C}$  before starting imaging.
34. Glass in a glass-bottom dish may expand or contract with temperature fluctuations. To properly adjust the correction ring, wait for 30–120 min after transferring the sample to the microscope for the glass to stabilize.

## References

1. Haraguchi T, Kojidani T, Koujin T et al (2008) Live cell imaging and electron microscopy reveal dynamic processes of BAF-directed nuclear envelope assembly. *J Cell Sci* 121: 2540–2554
2. Lu L, Ladinsky MS, Kirchhausen T (2011) Formation of the postmitotic nuclear envelope from extended ER cisternae precedes nuclear pore assembly. *J Cell Biol* 194:425–440
3. Olmos Y, Hodgson L, Mantell J et al (2015) ESCRT-III controls nuclear envelope reformation. *Nature* 522:236–239
4. Suzuki Y, Bilir Ş, Hatano Y et al (2019) Nuclear formation induced by DNA-conjugated beads in living fertilised mouse egg. *Sci Rep* 9:8461
5. Yonezawa N, Shindo T, Oda H et al (2024) Reconstruction of artificial nuclei with nuclear import activity in living mouse oocytes. *Genes Cells* 29:820–837
6. Ho Y, Wigglesworth K, Eppig JJ et al (1995) Preimplantation development of mouse embryos in KSOM: augmentation by amino acids and analysis of gene expression. *Mol Reprod* 41:232–238
7. Biggers JD (2022) Thoughts on embryo culture conditions. *Reprod Biomed* 4(Suppl 1): 30–38
8. Yamagata K, Suetsugu R, Wakayama T (2009) Long-term, six-dimensional live-cell imaging for the mouse preimplantation embryo that does not affect full-term development. *J Reprod Dev* 55:324–350
9. Chatot CL, Ziomek CA, Bavister BD (1989) An improved culture medium supports development of random-bred 1-cell mouse embryos in vitro. *J Reprod Fertil* 86:679–688
10. Hatano Y, Mashiko D, Tokoro M et al (2022) Chromosome counting in the mouse zygote using low-invasive super-resolution live-cell imaging. *Genes Cells* 27:214–228
11. Hatano Y, Yonezawa N, Tokoro M et al (2025) Chromosome counting at meiosis and mitosis of mouse oocytes and embryos using super-resolution live-cell imaging and CRISPR/dCas9 mediated live-FISH. *Methods Mol Biol* 2872:21–35
12. Yamagata K (2010) DNA methylation profiling using live-cell imaging. *Methods* 52:259–266
13. Kimura Y, Yanagimachi R (1995) Intracytoplasmic sperm injection in the mouse. *Biol Reprod* 54:709–720



## Preparation of Nucleoplasmic Extract and Its Application in DNA End Processing

Daichi Nishiguchi, Kensuke Tatsukawa, and Tatsuro S. Takahashi

### Abstract

The nucleoplasmic extract (NPE) of *Xenopus laevis* eggs contains a physiological concentration of nuclear proteins that recapitulate a functional nuclear environment. This system has been widely used to study key nuclear processes, including DNA replication, repair, transcription, and chromatin assembly. Its soluble nature, free from membrane fractions and insoluble structures, enables direct analysis of nuclear responses to specific DNA structures and lesions. Here, we describe an NPE preparation protocol with our modifications and its application in the processing of DNA double-strand breaks, a critical step in homology-directed repair.

**Key words** Nucleoplasmic extract, *Xenopus laevis*, DNA double-strand break, End resection

---

### 1 Introduction

Cell-free extracts of unfertilized eggs from the African clawed frog, *Xenopus laevis*, serve as a powerful model system for studying various cellular processes, including cell cycle regulation, DNA replication, and mitosis. Crude extracts of *Xenopus* eggs, called low-speed supernatant (LSS), contain both cytoplasmic and nuclear proteins as well as nuclear membrane vesicles and retain the ability of cell-cycle regulated nuclear formation, DNA replication, and mitotic entry [1–3]. When demembranated sperm chromatin, a natural chromatin substrate for frog eggs, is added to interphase LSS, the nuclear envelope assembles around chromatin to form functional nuclei, which concentrate nuclear proteins in the nucleus and exclude cytoplasmic proteins via active nuclear transport. This process facilitates a complete round of DNA replication: Exposure of sperm chromatin to LSS allows the loading of the Mcm2–7 complex onto DNA, a process that is mediated by ORC, Cdc6, and Cdt1 [4]. Subsequently, nuclear transport stimulates the initiation of DNA replication by concentrating multiple initiation

factors that convert Mcm2–7 into the replicative DNA helicase complex. At the same time, nuclear transport prevents additional Mcm2–7 loading by negatively regulating Cdt1 through multiple mechanisms, including the concentration and activation of a natural Cdt1 inhibitor, Geminin [5–7]. DNA replication in this system is associated with chromatin assembly and sister-chromatid cohesion. Upon entry into mitosis, nuclear envelope breakdown and chromosome condensation shape mitotic chromatid pairs attached through cohesion.

The major limitation of this powerful system is that most nuclear reactions require the assembly of functional nuclei. Since nuclear assembly depends on a critical mass of DNA, relatively small DNA molecules, such as bacterial plasmids, do not efficiently support nuclear assembly and, therefore, are not suitable substrates for most nuclear processes in LSS [8]. In addition, nuclear envelope assembly limits the handling of DNA substrates. For example, a conventional method for recovering chromatin-bound proteins from LSS requires the permeabilization of the nuclear membrane with detergents before the centrifugal isolation of chromatin. To overcome these limitations, Walter and Newport developed a nucleus-free *Xenopus* egg extract system [9]. Since the primary role of nuclear assembly is to concentrate nuclear proteins, a simple way to bypass this step is to prepare a highly concentrated extract of nuclear proteins. They successfully prepared such an extract, which they called the nucleoplasmic extract or NPE, by collecting a large number of nuclei assembled in LSS. NPE concentrates typical nuclear proteins by ~30-fold compared to LSS while efficiently excluding cytoplasmic proteins [9]. Moreover, they showed that NPE recreates a functional nuclear environment that supports cell cycle-regulated DNA replication of any DNA substrates including plasmid DNA [9, 10]; the incubation of DNA templates in a cytoplasmic extract of *Xenopus* eggs called high-speed supernatant (HSS) stimulates Mcm2–7 loading, and the subsequent addition of NPE mimics nuclear transport to promote the initiation of DNA replication. NPE also recapitulates many other nuclear processes, such as various DNA repair reactions occurring on specific DNA structures and lesions [11–14, 25, 19]. The use of NPE has been thoroughly reviewed previously [15].

Since NPE is an extract from nuclei assembled in LSS, it has unique characteristics distinct from crude egg extracts such as LSS and HSS. During the early development of amphibian eggs, transcription is suppressed until a certain stage of embryonic development known as the midblastula transition (MBT), which occurs at the twelfth cleavage of fertilized eggs in *Xenopus laevis*. Seminal studies by Newport and Kirschner demonstrated that transcriptional activation is primarily regulated by a critical nucleus-to-cytoplasm ratio corresponding to the MBT [16, 17]. Presumably due to the high nucleus-to-cytoplasm ratio in LSS during NPE

preparation, NPE is permissive to transcription, unlike LSS and HSS [18, 19]. A caveat of using NPE arises also from its unique preparation process: The enrichment of nuclear proteins in NPE can be somewhat uneven across different factors. Since NPE is a soluble fraction of nuclei that have undergone one round of DNA replication in LSS, factors tightly associated with post-replicative chromatin, such as cohesin, are preferentially removed during NPE preparation. Nevertheless, the large stockpile of nuclear proteins in *Xenopus* eggs ensures that this does not significantly compromise the functionality of NPE. For instance, cohesins remain enriched by approximately tenfold in NPE compared to LSS [20, 21].

NPE preparation has been comprehensively documented in previous protocol articles [22–24], allowing us to focus here on specific aspects. In this section, we describe our latest modifications to the NPE preparation protocol, applied primarily to prevent apoptosis during the nuclear assembly step. We also outline a method to prevent the initiation of DNA replication during NPE preparation, a modification that improves the recovery of materials consumed during DNA replication. Finally, we present an application of NPE for studying DNA double-strand break (DSB) processing [14]. Since DSB end resection occurs only in the nuclear environment, the use of NPE is essential to recapitulate this event on a defined DNA substrate *in vitro*.

---

## 2 Materials

All buffers and solutions should be prepared using ultrapure water. Store stock solutions at room temperature unless otherwise specified.

### 2.1 Sperm Chromatin Preparation

1. Frog water: Chlorine is generally harmful to amphibians and should be removed.
2. Male adult *Xenopus laevis*: ~80 g body weight.
3. 10× buffer X: 100 mM Hepes-NaOH (pH 7.5), 800 mM KCl, 150 mM NaCl, 50 mM MgCl<sub>2</sub>, and 10 mM EDTA in H<sub>2</sub>O.
4. Buffer X + 0.2 M sucrose: 0.2 M sucrose in 1× buffer X. Prepare 100 mL from 10× buffer X (*see Note 1*).
5. Buffer X + 2.0 M sucrose: 2.0 M sucrose in 1× buffer X. Prepare 10 mL.
6. Buffer X + 2.3 M sucrose: 2.3 M sucrose in 1× buffer X. Prepare 10 mL.
7. Buffer X + 2.5 M sucrose: 2.5 M sucrose in 1× buffer X. Prepare 10 mL.
8. Benzocaine solution: 100 mg/mL benzocaine in ethanol. Prepare 5 mL.

9. 18 G needles.
10. Surgical scissors.
11. Single-edged razor blades.
12. 15 mL screw-cap conical centrifuge tubes.
13. 5 mL ultracentrifuge tubes: Beckman Coulter, CA, USA, # 344057.
14. 14 mL round-bottom tubes: Corning, NY, USA, # 352059.
15. Centrifuges with swinging-bucket rotors (we use the NS-1 rotor [TOMY Seiko, Tokyo, Japan] and the TMS-21 rotor [TOMY Seiko] for low-speed centrifugation and the SW55Ti rotor [Beckman Coulter] for ultracentrifugation).
16. Dithiothreitol (DTT) solution: 1 M DTT in H<sub>2</sub>O. Store at –20 °C as small aliquots.
17. Aprotinin/leupeptin solution: 10 mg/mL aprotinin and 10 mg/mL leupeptin in H<sub>2</sub>O. Store at –80 °C as small aliquots.
18. Buffer X + 0.2 M sucrose, protease inhibitors (PIs), DTT: 0.2 M sucrose in 1× buffer X. Add 10 µg/mL aprotinin, 10 µg/mL leupeptin, and 1 mM DTT from 10 mg/mL and 1 M stock solutions, respectively, just before use. Prepare 2 mL.
19. Triton X-100 solution: 10% (w/v) Triton X-100 in H<sub>2</sub>O.
20. Buffer X + 0.5 M sucrose, BSA, PIs, DTT: 0.5 M sucrose and 30 mg/mL Bovine serum albumin (BSA) in 1× buffer X. Add 10 µg/mL aprotinin, 10 µg/mL leupeptin, and 1 mM DTT from 10 mg/mL and 1 M stock solutions, respectively, just before use. Prepare 10 mL.
21. Buffer X + 0.2 M sucrose, BSA, PIs, DTT: 0.2 M sucrose and 30 mg/mL BSA in 1× buffer X. Add 10 µg/mL aprotinin, 10 µg/mL leupeptin, and 1 mM DTT from 10 mg/mL and 1 M stock solutions, respectively, just before use. Prepare 10 mL.
22. Flame-sealed Pasteur pipette: Heat-seal the narrow tip of a 5¼-inch glass Pasteur pipette to make a small stirring rod.
23. Hoechst solution: 200 mM sucrose, 10 mM Hepes-NaOH (pH 7.5), 7.4% formaldehyde, and 8 µg/mL Hoechst 33258 in H<sub>2</sub>O.
24. Hemocytometer.
25. Liquid nitrogen.

## **2.2 Nucleoplasmic Extract Preparation**

1. 26 G needles.
2. 2.5 mL syringes.
3. 5 L buckets.

4. Female adult *Xenopus laevis*: >120 g body weight.
5. Pregnant mare serum gonadotropin (PMSG): Dissolve in 0.6% NaCl to prepare a 250 IU/mL solution. Store at 4 °C for up to 2 weeks.
6. Human chorionic gonadotropin (HCG): Dissolve in 0.6% NaCl to prepare a 2000 IU/mL solution. Store at 4 °C for up to 2 weeks.
7. 10× MMR: 1 M NaCl, 20 mM KCl, 5 mM MgSO<sub>4</sub>, 25 mM CaCl<sub>2</sub>, 50 mM Hepes, 1 mM EDTA in H<sub>2</sub>O. Adjust the pH to 7.8 with NaOH. Store at 4 °C.
8. 10× ELB salts: 25 mM MgCl<sub>2</sub>, 0.5 M KCl, 100 mM Hepes. Adjust the pH to 7.7 with KOH. Filter sterilization. Store at 4 °C.
9. 2.2% cysteine solution: Dissolve 88 g of L-cysteine-HCl in 1–2 L H<sub>2</sub>O. Adjust the pH to 7.8 using NaOH, and bring the volume to 4 L.
10. 0.5× MMR: Dilute 10× MMR with H<sub>2</sub>O.
11. 1× ELB: 250 mM sucrose, 1 mM DTT, and 50 µg/mL cycloheximide in 1× ELB salts.
12. Plastic beakers.
13. Glass rods.
14. 9-inch glass Pasteur pipettes.
15. 14 mL round-bottom tubes.
16. 50 mL polycarbonate centrifuge tubes.
17. Aprotinin/leupeptin solution.
18. Cycloheximide solution: 10 mg/mL cycloheximide in H<sub>2</sub>O. Store at –80 °C as small aliquots.
19. Cytochalasin B solution: 5 mg/mL cytochalasin B in dimethyl sulfoxide (DMSO). Store at –20 °C as small aliquots.
20. DTT solution.
21. Nocodazole solution: 5 mg/ml nocodazole in DMSO. Store at –20 °C as small aliquots.
22. Centrifuges with swinging-bucket rotors (we use the NS-1 rotor for low-speed centrifugation and the SW41 [Beckman Coulter] and SW55Ti rotors for ultracentrifugation).
23. Spatula.
24. Disposable plastic Pasteur pipettes.
25. 50 mL screw-cap conical centrifuge tubes.
26. Parafilm.
27. ATP solution: Dissolve adenosine triphosphate (ATP) in H<sub>2</sub>O to a final concentration of 0.2 M. Adjust the pH to 7.0–8.0

with NaOH (pH test paper can be used) since ATP is a highly acidic compound. Store at  $-20^{\circ}\text{C}$  as small aliquots.

28. PC solution: 1 M phosphocreatine (PC) in  $\text{H}_2\text{O}$ . Store at  $-20^{\circ}\text{C}$  as small aliquots.
29. CPK solution: Dissolve creatine phosphokinase (CPK) to a final concentration of 5 mg/mL in 10 mM Hepes-NaOH (pH 7.5), 50 mM NaCl, and 50% (v/v) glycerol. Store at  $-20^{\circ}\text{C}$ .
30. 220,000/ $\mu\text{L}$  sperm chromatin: Store at  $-80^{\circ}\text{C}$  as 90  $\mu\text{L}$  aliquots.
31. Glass test tubes:  $13 \times 100$  mm,  $12 \times 105$  mm, and  $10 \times 90$  mm.
32. Hoechst solution.
33. Liquid nitrogen.

### **2.3 DSB End Resection Assay in NPE**

1. Plasmid DNA.
2. Restriction enzymes that generate 3'-protruding ends, such as *ApaI* and *PstI*.
3. Phenol/chloroform: A 1:1 mixture of TE-saturated phenol and chloroform. Store at  $4^{\circ}\text{C}$ .
4. EtOH-NaAc: Add 3 M sodium acetate solution (pH 7.0) to 99.5% ethanol to a final concentration of 0.1 M.
5. 80% (v/v) ethanol.
6. 10:1 TE: 10 mM Tris-HCl (pH 7.4) and 1 mM EDTA in  $\text{H}_2\text{O}$ .
7. Terminal deoxynucleotidyl transferase (TdT): New England Biolabs, MA, USA, #M0315S.
8. 10 $\times$  TdT buffer: 500 mM potassium acetate, 200 mM Tris-acetate (pH 7.9), 100 mM magnesium acetate. Store at  $-20^{\circ}\text{C}$ .
9. 10 $\times$   $\text{CoCl}_2$  solution: 2.5 mM  $\text{CoCl}_2$  in  $\text{H}_2\text{O}$ . Store at  $-20^{\circ}\text{C}$ .
10. dATP solution. Dilute 100 mM dATP (Cytiva, MA, USA, #28-4065-51) in  $\text{H}_2\text{O}$  to a final concentration of 10 mM. Store at  $-20^{\circ}\text{C}$ .
11. 10:20 TE: 10 mM Tris-HCl (pH 7.4) and 20 mM EDTA in  $\text{H}_2\text{O}$ .
12. ATP regeneration system (ATP-RS): Mix 1 volume of ATP solution (final concentration: 67 mM), 2 volumes of PC solution (667 mM), and 0.1 volume of CPK solution (166  $\mu\text{g}/\text{mL}$ ).
13. NPE.
14. Stop buffer: 1% (w/v) sodium dodecyl sulfate (SDS) and 20 mM EDTA in  $\text{H}_2\text{O}$  (*see Note 2*).

15. 2× SDS sample buffer: 100 mM Tris-HCl (pH 6.8), 0.2 M DTT, 4% (w/v) SDS, 0.1% (w/v) bromophenol blue, and 20% (v/v) glycerol in H<sub>2</sub>O. Store at −20 °C.
16. Proteinase K solution: 20 mg/mL proteinase K in H<sub>2</sub>O. Store at −20 °C as small aliquots.
17. RNaseA solution: 10 mg/mL RNaseA in H<sub>2</sub>O. Store at −20 °C.
18. S1 nuclease: Takara Bio, #2410.
19. 10× rCutSmart buffer: New England Biolabs, #B6004S.
20. Glycogen solution: 20 mg/mL glycogen (Nacalai tesque, Kyoto, Japan, #07592-21) in H<sub>2</sub>O.
21. 0.8% agarose gel: 0.8% (w/v) agarose in 0.5× TBE buffer.
22. 10× TBE buffer: 0.89 M Tris base, 0.89 M Boric Acid, and 20 mM EDTA in H<sub>2</sub>O.
23. SYBR Gold nucleic acid gel stain: Thermo Fisher Scientific, #S11494. Store at −20 °C as small aliquots.
24. Amersham Typhoon Scanner 5 system (Cytiva).
25. SDS-PAGE gels.
26. Polyvinylidene fluoride (PVDF) membrane: Cytiva, #10600023.
27. Skim milk.
28. Phosphate-buffered saline with Tween 20 (PBST): 137 mM NaCl, 8.1 mM Na<sub>2</sub>HPO<sub>4</sub>, 2.68 mM KCl, 1.47 mM KH<sub>2</sub>PO<sub>4</sub>, and 0.05% (w/v) Tween 20 in H<sub>2</sub>O.
29. Chk1 antibody: Santa Cruz Biotechnology, #sc8408. Use at 1:500 dilution in PBST.
30. phospho-Chk1 antibody: Cell Signaling Technology, #2341. Use at 1:1000 dilution in PBST.
31. BSA.
32. Fluorescent-dye conjugated secondary antibodies.

#### **2.4 DNA Pull-Down Assay in NPE**

1. EZ-Link Amine-PEG3-Biotin: Thermo Fisher Scientific, MA, USA, #21347. Dissolve in coupling buffer to a final concentration of 50 mM. Store at −80 °C as small aliquots.
2. HiTrap NHS-activated sepharose HP 1 mL column: Cytiva, #17071601.
3. 1 mL syringes.
4. 5 mL syringes.
5. 1 mM HCl.
6. Coupling buffer: 0.2 M NaHCO<sub>3</sub> and 0.5 M NaCl in H<sub>2</sub>O. Adjust the pH to 8.3 with NaOH.

7. Blocking buffer: 0.5 M Ethanolamine and 0.5 M NaCl in H<sub>2</sub>O. Adjust the pH to 8.3 with NaOH.
8. Washing buffer: 0.1 M Acetic acid and 0.5 M NaCl in H<sub>2</sub>O. Adjust the pH to 4.0 with HCl.
9. Single-edged razor blades.
10. Phosphate-buffered saline (PBS): 137 mM NaCl, 8.1 mM Na<sub>2</sub>HPO<sub>4</sub>, 2.68 mM KCl, and 1.47 mM KH<sub>2</sub>PO<sub>4</sub> in H<sub>2</sub>O.
11. NaN<sub>3</sub> solution: 20% (w/v) NaN<sub>3</sub> in H<sub>2</sub>O. Store at 4 °C.
12. Restriction enzymes that recognize non-palindromic sequences.
13. Phenol/chloroform.
14. 80% (v/v) ethanol.
15. EtOH-NaAc.
16. S-400 HR column: Cytiva, #27514001.
17. Biotinylated hairpin oligonucleotide adaptor.
18. T4 DNA ligase: NIPPON GENE, Tokyo, Japan #311-00406.
19. 10× ligation buffer: 500 mM Tris-HCl (pH 7.9), 100 mM MgCl<sub>2</sub>, 200 mM DTT, and 10 mM ATP.
20. Restriction enzyme that generates 3'-protruding termini.
21. Sepharose CL-4B: Cytiva, #17015001.
22. Open-top column: Econo-Column Chromatography Column, 0.5 × 10 cm (Biorad, MA, USA, #7370512).
23. TdT.
24. 10× TdT buffer.
25. 10× CoCl<sub>2</sub> solution.
26. 10:20 TE.
27. 1 mg/mL streptavidin: New England Biolabs, #N7021S.
28. Binding buffer: 5 mM Tris-HCl (pH 7.4), 1 M NaCl, 0.5 mM EDTA, and 0.1% (w/v) Triton X-100 in H<sub>2</sub>O.
29. Centrifuge with swinging-bucket rotor (we use the TMS21 rotor).
30. 1× ELB salts: Dilute 10× ELB salts to 1× with H<sub>2</sub>O.
31. NPE.
32. ATP-RS.
33. ELB salts containing 0.2% Triton X-100: 0.2% (w/v) Triton X-100 in 1× ELB salts. Store at 4 °C.
34. ELB salts containing 0.5 M sucrose: 0.5 M sucrose in 1× ELB salts. Store at 4 °C.
35. Stop buffer containing 3 mM biotin: 1% (w/v) SDS, 20 mM EDTA, and 3 mM biotin in H<sub>2</sub>O.

36. Proteinase K solution.
37. RNaseA solution.
38. Glycogen solution.
39. 0.8% agarose gel.
40. 0.8% alkaline agarose gel: 0.8% (w/v) agarose in 50 mM NaOH and 1 mM EDTA.
41. SYBR Gold nucleic acid gel stain.
42. 2× SDS sample buffer.
43. SDS-PAGE gels.
44. PVDF membrane.

### 3 Methods

#### 3.1 Sperm Chromatin Preparation

All procedures are carried out at room temperature unless otherwise stated. This protocol is intended for 6–10 male frogs.

1. Dissolve 5 mL of 100 mg/mL benzocaine solution in 1 L of frog water to obtain a 0.05% benzocaine solution.
2. Anesthetize a male frog in 0.05% benzocaine until it no longer exhibits a sucking reflex. This process takes approximately 4–6 min (*see Note 3*).
3. Euthanize the frog by pithing it with an 18 G needle (Fig. 1a).
4. Isolate the testes. Cut open the abdominal skin and abdominal muscles of the frog with surgical scissors and pull out the intestine. The testes are attached to the intestine and visceral fat by the mesentery, and sometimes it is not easy to identify. The testes are elliptical-shaped organs, whiter and firmer than

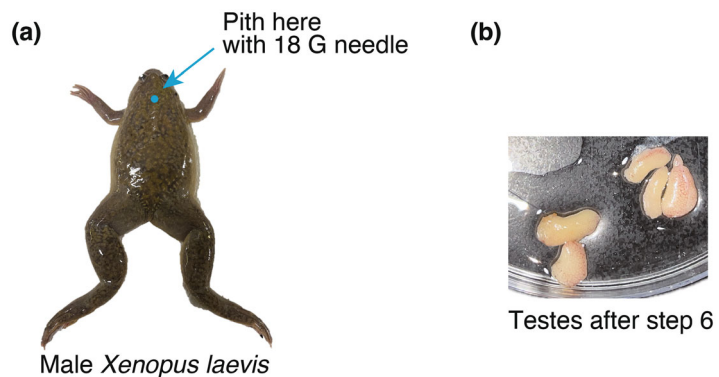


**Fig. 1** Isolation of testes from male *Xenopus laevis*. (a) Male *Xenopus laevis*. Pith the top of the spinal cord at the junction with the skull (blue arrow) using an 18 G needle. (b) Isolated testes, as described in **step 5** in Subheading 3.1

the visceral fat and intestine (*see* Fig. 1b). Snip the testes away from the connecting organs.

5. Remove any blood from the testes by gently rolling them on a piece of paper towel; then place the testes in a small petri dish containing approximately 2–3 mL of buffer X + 0.2 M sucrose (Fig. 1b).
6. Repeat **steps 2–5** for 6–10 male frogs.
7. Remove as much buffer as possible from the isolated testes. Finely mince the testes into small pieces by chopping them extensively using two new razor blades (*see* **Note 4**).
8. Add 2–3 mL of buffer X + 0.2 M sucrose to the testes and transfer the minced pieces into a 15 mL screw-cap conical centrifuge tube (Tube A) using a cut-off P1000 tip.
9. Rinse the petri dish with a small amount of buffer X + 0.2 M sucrose and transfer the buffer containing minced pieces to Tube A.
10. Vortex Tube A for 1 min vigorously and centrifuge it for 10 s in a swinging-bucket rotor at 200 *g* to pellet large debris.
11. Transfer the supernatant to a new 15 mL screw-cap conical centrifuge tube (Tube B).
12. Repeat **steps 9–11** until Tube B is filled with the supernatant (*see* **Note 5**). At this point, the supernatant in Tube A from **step 10** should not appear very cloudy.
13. Centrifuge Tube B in a swinging-bucket rotor at 230 *g* for 50 s to pellet tissue pieces; then transfer the supernatant to a 14 mL round-bottom tube.
14. Add 12 mL of buffer X + 0.2 M sucrose to Tube B, vortex the tube vigorously for 1 min, and centrifuge at 230 *g* for 50 s. Transfer the supernatant to a new 14 mL round-bottom tube.
15. Centrifuge both 14 mL round-bottom tubes at 2600 *g* for 10 min in a swinging-bucket rotor (NS-1) to pellet the sperm.
16. During the centrifugation, prepare sucrose step gradients in two 5 mL ultracentrifuge tubes by overlaying 4.3 mL of buffer X + 2.3 M sucrose onto 0.3 mL of buffer X + 2.5 M sucrose.
17. Resuspend the sperm pellet from **step 15** thoroughly in 0.8 mL of buffer X + 2 M sucrose. Split the mixture in half and overlay each half onto the sucrose step gradient.
18. Thoroughly stir the interface between the sperm and 2.3 M sucrose using a flame-sealed Pasteur pipette (*see* **Note 6**).
19. Centrifuge the sucrose step gradients at 74,600 *g* for 100 min. Red blood cells should float on top of the 2.3 M sucrose layer, while sperm should settle at the bottom. Remove the debris, which forms a membranous layer on top of the gradients, using

a flamed Pasteur pipette. If a cloudy layer remains in the middle of the tubes, remix with a flamed Pasteur pipette and centrifuge for another 20 min.

20. Carefully aspirate off the top half of the gradient containing the red blood cells and transfer the remaining sucrose cushion into 4 new 14 mL round-bottom tubes (*see* **Note 7**).
21. Add 500  $\mu$ L of buffer X + 0.2 M sucrose to each pellet, pipette up and down with a P1000 tip, then transfer the sperm to the 4 14 mL round-bottom tubes. Any gray spots at the bottom of the 5 mL tubes indicate incomplete sperm recovery.
22. Dilute the sperm suspension in each 14 mL round-bottom tube to a final volume of 12 mL (48 mL total) with buffer X + 0.2 M sucrose, mix well, and centrifuge in a swinging-bucket rotor (NS-1) at 10,000 *g* for 30 min.
23. Carefully aspirate off the supernatant and thoroughly resuspend the sperm pellet in 0.5 mL each of buffer X + 0.2 M sucrose, PIs, DTT (2 mL total). Transfer the sperm suspension into two 1.5 mL round-bottom snap-cap tubes (1.5 mL microtubes).
24. Add Triton X-100 to a final concentration of 0.4% (w/v) and incubate for 30 min with gentle rotation at 4 °C. This step removes the sperm membrane.
25. Prepare 4 new 1.5 mL microtubes containing 0.5 mL of buffer X + 0.5 M sucrose, BSA, PIs, DTT. Overlay one-fourth of the sperm suspension (approximately 500  $\mu$ L per tube) onto the 0.5 M sucrose buffer in each tube. Centrifuge at 2200 *g* for 3 min at 4 °C in a swinging-bucket rotor (TMS-21).
26. Carefully remove the supernatant and resuspend each pellet in 0.2 mL of buffer X + 0.2 M sucrose, BSA, PIs, and DTT (0.8 mL total). Transfer the sperm suspension to 4 new 1.5 mL microtubes, and dilute each to 0.7 mL with buffer X + 0.2 M sucrose, BSA, PIs, and DTT (2.8 mL total). Centrifuge at 2200 *g* for 3 min at 4 °C in a swinging-bucket rotor (TMS-21) (*see* **Note 8**).
27. Repeat **step 26** once, combining four tubes into two (1.4 mL total).
28. Resuspend the sperm pellet in 1 mL each of buffer X + 0.2 M sucrose, BSA, PIs, and DTT (2 mL total); then combine the suspensions. Mix well.
29. Take 3  $\mu$ L of the sperm suspension, add 30  $\mu$ L of Hoechst solution, and dilute with sterile water to a final volume of 300  $\mu$ L. Count the sperm using a hemocytometer under a fluorescence microscope with the UV/DAPI channel. Note that sperms settle rapidly. Always withdraw a sample immediately after mixing.

30. Dilute the sperm suspension to 220,000/ $\mu$ L with buffer X + 0.2 M sucrose, BSA, PIs, and DTT, aliquot into 90  $\mu$ L portions, and freeze in liquid nitrogen.

### 3.2 Nucleoplasmic Extract Preparation

We prepare NPE essentially based on previously published protocols [22–24]. Our major modification is the use of ultracentrifugation for LSS preparation, which helps remove mitochondria from LSS and prevents apoptosis during NPE preparation. This protocol is intended for 12–20 frogs.

1. Inject 0.3 mL of 250 IU/mL PMSG solution subcutaneously into a female frog along the leg using a 2.5 mL syringe and 26 G needle (*see Note 9*). Frogs should be primed with PMSG at least 2 days, but no more than 7–8 days, before the secondary HCG injection to induce ovulation.
2. Inject 0.3 mL of 2000 IU/mL HCG solution subcutaneously into a female frog along the leg using a 2.5 mL syringe and 26 G needle. Place the frog in a 5 L bucket containing 2.5 L frog water with 100 mM NaCl (dissolve 14.7 g of NaCl in 2.5 L) (*see Note 10*). The secondary injection should be performed 22 h before the desired egg collection time.
3. Pre-warm an adequate volume of ultrapure water at 22 °C overnight for buffer preparation.
4. On the morning of NPE preparation, prepare 4 L of 2.2% cysteine-HCl, 2 L of 0.5 $\times$  MMR, and 2 L of 1 $\times$  ELB. Pre-warm the buffers at 22 °C.
5. Set the centrifuge and swinging-bucket rotor to 22 °C (*see Note 11*). Thaw the aprotinin/leupeptin solution and cytochalasin B solution before egg collection.
6. Remove the frogs from buckets and visually assess the quality of the eggs. Discard batches of very poor quality eggs, such as those that are mostly white, swollen, or stringy. Collect the eggs into plastic beakers, ensuring not to combine different batches at this stage. Inspect the quality of the eggs under a stereo microscope. Good quality eggs exhibit a clear separation between the pigmented animal hemisphere and the white vegetal hemisphere, with a visible spot at the top corresponding to the position of the germinal vesicle.
7. Combine batches of eggs judged to be of good or acceptable quality into a 2 L plastic beaker.
8. Remove as much water as possible; then add 2.2% cysteine solution to nearly fill the beaker. Stir gently with a glass rod to draw all the eggs into the vortex, stop stirring, and allow the eggs to settle. Repeat these procedures for ~2 min; then discard the cysteine solution (*see Note 12*).

9. Add 2.2% cysteine solution to nearly fill the beaker and repeat **step 8**. Any space between settled eggs indicates the presence of jelly coats. Dejellying usually takes 5–8 min, but should not exceed 10 min. Once all the eggs are completely dejellied, decant the cysteine solution.
10. Quickly wash the eggs 3 times with 0.5× MMR buffer. Add the buffer, stir gently to draw the eggs into the vortex, then stop stirring, and allow them to settle. During this step, remove poor-quality eggs (white and swollen) using a 9-inch glass Pasteur pipette attached to a silicone bulb. After stopping the stirring, poor-quality eggs tend to accumulate at the center of the vortex, making them easy to collect.
11. Wash the eggs 3 times with 1× ELB, removing as many poor-quality eggs as possible, as described in **step 10**.
12. Remove as much buffer as possible; then transfer the eggs to 14 mL round-bottom tubes or 50 mL polycarbonate centrifuge tubes. Pack the eggs by gentle centrifugation for 1 min at 100 *g* in a swinging-bucket rotor. Aim to fill the tubes with eggs. If necessary, aspirate off excess buffer, add more eggs to fill the remaining space, and repack the eggs by centrifugation. Ensure the tubes are at least half-filled (Fig. 2).
13. Aspirate off the excess buffer; then add the aprotinin/leupeptin solution and cytochalasin B solution to the packed eggs (0.5  $\mu$ L of each solution per 1 mL of eggs). Mixing is not necessary.
14. Centrifuge the eggs at 16,000 *g* for 20 min in a swinging-bucket rotor (NS-1). Both the centrifuge and the rotor should be pre-warmed at 22 °C (**step 5**), but set the temperature to 4 °C before starting the spin. This step is crucial to activate the extract and drive it into the interphase while maintaining the temperature at 4 °C after activation. Keep the extract on ice following this step, unless otherwise specified. During this process, thaw the cycloheximide, aprotinin/leupeptin, cytochalasin B, DTT, and nocodazole solutions.
15. Remove the lipid layer using a spatula; then transfer the crude S-phase extract into a 50 mL screw-cap conical centrifuge tube using a disposable plastic Pasteur pipette (*see* Fig. 2, *see also* **Note 13**).
16. Add 5  $\mu$ L of cycloheximide solution (50  $\mu$ g/mL), 1  $\mu$ L of aprotinin/leupeptin solution (10  $\mu$ g/mL each), 1  $\mu$ L of cytochalasin B solution (2.5  $\mu$ g/mL), 1  $\mu$ L of DTT solution (1 mM), 0.67  $\mu$ L of Nocodazole solution (3.3  $\mu$ g/mL), and 100  $\mu$ L 1× ELB per 1 mL extract. Gently invert the 50 mL tube to mix thoroughly.

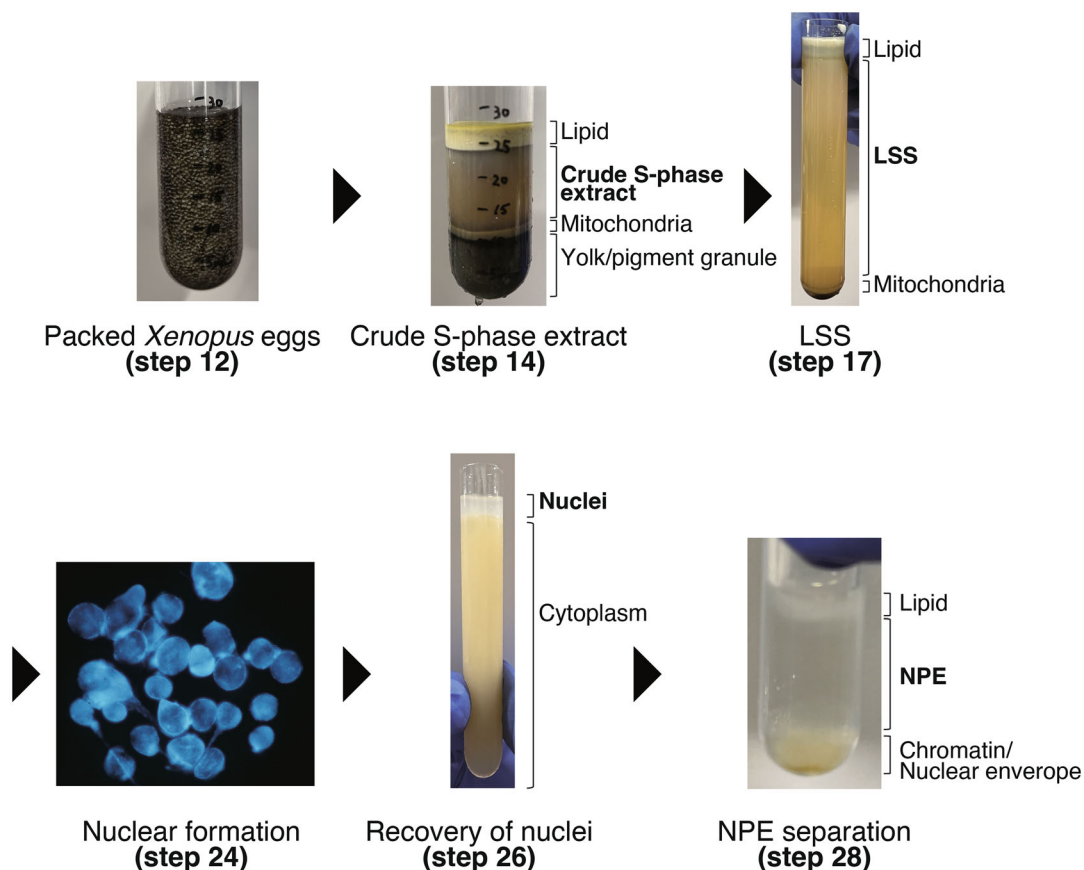


**Fig. 2** Overview of the NPE preparation procedures. Eggs are collected, packed, and spin-crushed, and the cytoplasmic fraction is further purified by ultracentrifugation. Nuclei are assembled in the extract and collected, and the nucleoplasm is extracted. Nuclei were stained with Hoechst 33258 and photographed using a fluorescence microscope

17. Recentrifuge the extract at 110,000  $g$  for 30 min at 4 °C using a swinging-bucket rotor (SW41). During centrifugation, thaw the ATP and PC solutions.
18. Roughly remove the lipid layer from the top of LSS by gently touching it with a Parafilm membrane stretched over the wider opening of a P1000 tip. Twist and lift the tip to help detach the lipid layer. Then, completely aspirate the lipid layer using a gel-loading tip (*see Fig. 2*).
19. Carefully transfer LSS into a new 50 mL tube using a cut-off P1000 tip. Sacrifice the final ~0.5 mL to avoid the mitochondrial layer at the bottom of the tubes (*see Note 14*).
20. Add 10  $\mu$ L of ATP solution (final concentration: 2 mM), 20  $\mu$ L of PC solution (20 mM), and 1  $\mu$ L of CPK solution per 1 mL of LSS. Gently invert the tube to mix thoroughly. If necessary,

add recombinant Geminin to a final concentration of 300 nM (*see Note 15*). Preincubate the extract at 22 °C for 10 min.

21. Add demembranated sperm chromatin to LSS to a final concentration of 4000/μL. Disperse the sperm chromatin completely (*see Note 16*).
22. Transfer LSS into glass test tubes by decantation, aiming to fill the tubes nearly completely. Use an appropriate combination of tube sizes: 13 × 100 mm for 9 mL, 12 × 105 mm for 7 mL, and 10 × 90 mm for 4 mL.
23. Incubate the LSS-sperm mixture at 22 °C, using a sand bath or other appropriate equipment. Gently invert the mixture every 5 min to prevent nuclei from floating.
24. At 60 min, take 1 μL of the LSS-sperm mixture, place it on a glass slide, and mix it with 1 μL of Hoechst solution. Check for nuclear assembly under a fluorescence microscope using the UV/DAPI channel (*see Fig. 2*).
25. Continue checking for nuclear assembly every 10–15 min until the nuclei reach a sufficient size (25–30 μm in diameter). This usually takes 70–90 min.
26. Centrifuge the glass test tubes at 13,000 *g* for 2 min at 4 °C using a swinging-bucket rotor (NS-1). To prevent crushing the glass test tubes, use 14 mL round-bottom tubes filled with 2 mL of water as adaptors. The nuclei will float to the top to form a thick layer (*see Fig. 2, see also Note 17*).
27. Collect the nuclei with a cut-off P200 tip. This step requires careful attention. Always inspect the extract pulled into the tip to avoid contamination with cytoplasm. The nucleus layer appears clearer and more viscous, while the cytoplasmic extract is more brownish and less viscous. Rotate the glass tube while collecting the nuclei to ensure even extraction of the nucleus layer. If cytoplasmic contamination is unavoidable, transfer the mixture of the nuclei and cytoplasmic extract to a new thin tube, and centrifuge at 13,000 *g* for 2 min at 4 °C. The nuclei will float to the top again.
28. Centrifuge the collected nuclei at 260,000 *g* for 30 min at 4 °C using a swinging-bucket rotor (SW55Ti).
29. Aspirate the lipid layer from the top of the tube using an ultrathin pipet tip. Then, recover NPE with a cut-off P200 tip, avoiding contamination of the chromatin layer (*see Fig. 2*).
30. Freeze 10–20 μL aliquots in liquid nitrogen.

### 3.3 DSB End Resection Assay in NPE

1. Digest 4 μg of plasmid DNA (we use a 6 kb plasmid) with 80 units of a restriction enzyme that generates 3'-protruding ends in 150 μL of the appropriate buffer (*Fig. 3*).

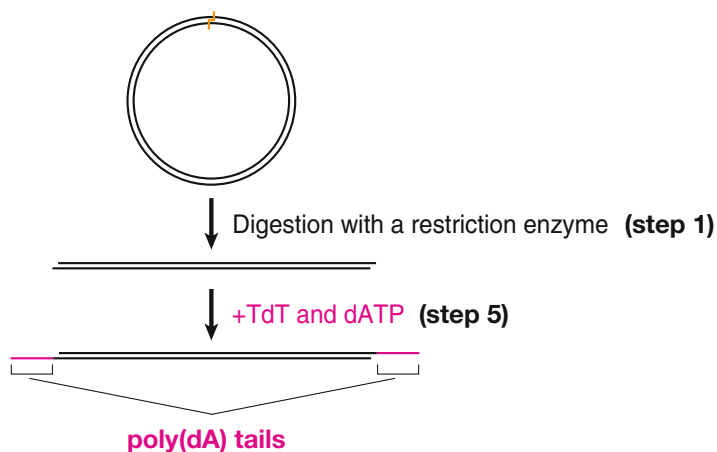


**Fig. 3** Schematic diagram of the preparation of a DNA substrate carrying 3'-ssDNA overhangs. Plasmid DNA is digested with a restriction enzyme that generates 3'-protruding ends. The resulting double-stranded linear DNA is incubated with terminal deoxynucleotidyl transferase (TdT) and dATP to add poly(dA) tails to the 3' termini

2. Purify the DNA by phenol/chloroform extraction: Add 1 volume of phenol/chloroform to 1 volume of the DNA solution, mix vigorously, and centrifuge at 13,000 *g* for 2 min at room temperature. Carefully recover the aqueous (upper) layer.
3. Recover the DNA by ethanol precipitation: Add 2.5 volumes of EtOH-NaAc to 1 volume of the DNA solution, incubate at  $-20^{\circ}\text{C}$  for 1 h, and centrifuge at 18,000 *g* for 15 min at  $4^{\circ}\text{C}$  to pellet the DNA. Add 1 mL of 80% ethanol to the tube, gently invert, centrifuge at 18,000 *g* for 2 min at  $4^{\circ}\text{C}$ , and remove as much of the supernatant as possible. Repeat once and air dry the DNA pellet completely.
4. Resuspend DNA in 10:1 TE to obtain a 250 nM linear double-stranded DNA solution.
5. Append 3'-ssDNA overhangs using a terminal deoxynucleotidyl transferase (TdT) (Fig. 3). Incubate 4  $\mu\text{g}$  of linearized DNA with 20 units of TdT in 20  $\mu\text{L}$  of  $1\times$  TdT buffer containing 250  $\mu\text{M}$   $\text{CoCl}_2$  and 0.5 mM dATP at  $37^{\circ}\text{C}$  for 30 min.
6. Stop the reaction by adding 9 volumes of 10:20 TE to 1 volume of the TdT reaction mixture.
7. Purify the DNA through phenol/chloroform extraction followed by ethanol precipitation.
8. Resuspend the DNA in 10:1 TE to obtain a 200 ng/ $\mu\text{L}$  solution of linearized DNA with 3'-ssDNA overhangs (tailed DNA).

9. Prepare the ATP regeneration system (ATP-RS) and keep it on ice.
10. Thaw the required aliquots of NPE tubes and add 0.3  $\mu\text{L}$  of ATP-RS per 10  $\mu\text{L}$  of NPE.
11. Preincubate the NPE at 22 °C for 5 min (*see Note 18*).
12. Add 1.1  $\mu\text{L}$  of tailed DNA (final concentration: 20 ng/ $\mu\text{L}$ ) into 10  $\mu\text{L}$  of NPE and incubate at 22 °C.
13. At appropriate time points, take aliquots and stop the reaction. For DNA analysis, terminate 0.5  $\mu\text{L}$  of the reaction mixture with 100  $\mu\text{L}$  of stop buffer (*see steps 14–19* for further processing). For immunoblotting, terminate 0.5  $\mu\text{L}$  of the reaction mixture with 9.5  $\mu\text{L}$  of 2 $\times$  SDS sample buffer (*see steps 20–25* for further processing).
14. Add 1  $\mu\text{L}$  of proteinase K solution to 100  $\mu\text{L}$  of stop buffer containing DNA samples and incubate at 37 °C for 2 h. Add 1  $\mu\text{L}$  of glycogen to the sample as a precipitation carrier. Purify the DNA through phenol/chloroform extraction followed by ethanol precipitation.
15. Resuspend the DNA in 10:1 TE containing 10  $\mu\text{g}/\text{mL}$  RNase A (*see Note 19*).
16. Digest 5 ng of DNA with 1 unit of a restriction enzyme that cleaves the linear DNA into two fragments of appropriate sizes, along with 1 unit of S1 nuclease in 1 $\times$  rCutSmart buffer at 37 °C for 2 h.
17. Separate the digested DNA (5 ng) by 0.8% agarose gel electrophoresis in 0.5 $\times$  TBE buffer.
18. Stain the gel with SYBR Gold nucleic acid gel stain at room temperature in 0.5 $\times$  TBE buffer for 1 h with gentle shaking.
19. Scan the gel using a fluorescence scanner, such as the Amersham Typhoon Scanner 5 system (Cytiva).
20. Detect Chk1 phosphorylation as a readout of the ATR checkpoint activation. Separate 4  $\mu\text{L}$  of the immunoblotting sample from **step 13** (containing 0.2  $\mu\text{L}$  of NPE) by SDS-PAGE; then transfer the proteins onto PVDF membranes.
21. Perform immunoblotting: Block the membrane with 5% skim milk in PBST at room temperature for more than 30 min; then incubate the membrane overnight at 4 °C with Chk1 and phospho-Chk1 antibodies, diluted in PBST containing 1% (w/v) BSA.
22. Wash the membrane: Shake the membrane in PBST for 10 min at room temperature, and then discard PBST. Repeat the wash twice.
23. Probe the membrane with fluorescent-dye conjugated secondary antibodies at room temperature for 1 h.

24. Wash the membrane three times.
25. Scan the membrane using a fluorescence scanner.

### 3.4 DNA Pull-Down Assay in NPE

1. Dilute 200  $\mu$ L of 50 mM EZ-Link Amine-PEG3-Biotin solution with 800  $\mu$ L of coupling buffer to a final concentration of 10 mM.
2. Prepare a HiTrap NHS-activated sepharose HP 1 mL column for biotin conjugation. Open a new column and wash it with 5 mL of 1 mM HCl (*see* **Note 20**).
3. Conjugate biotin to the resin via amine coupling. Inject 1 mL of 10 mM EZ-Link Amine-PEG3-Biotin solution into the column. Seal the inlet and outlet of the column with plugs and incubate at room temperature for 30 min. Wash the column with 3 mL of coupling buffer.
4. Inactivate any unused ligands by sequentially injecting 6 mL of blocking buffer, 6 mL of washing buffer, and 6 mL of blocking buffer. Incubate at room temperature for 30 min; then inject 6 mL of washing buffer, 6 mL of blocking buffer, and 6 mL of washing buffer. Finally, replace the buffer by injecting 6 mL of PBS.
5. Open the column from the top connector with a clean razor; then recover the resin with PBS using a cut-off P200 tip.
6. Adjust the resin bed volume to 50% with PBS and add  $\text{NaN}_3$  to a final concentration of 0.2% as a preservative. Store the biotin-Sepharose beads at 4 °C.
7. Linearize 100  $\mu$ g of plasmid DNA (we use a 3 kb plasmid) with 200 units of restriction enzymes that recognize non-palindromic sequences in 1 mL of the appropriate buffer (*see* Fig. 4a and **Note 21**).
8. Purify the DNA through phenol/chloroform extraction followed by ethanol precipitation.
9. Dissolve the DNA in 100  $\mu$ L of 10:1 TE. Remove the restriction enzyme fragment using the S-400 HR spin column.
10. Ligate 160 nM of a hairpin oligonucleotide adaptor carrying a biotin moiety to 25 nM of one terminus of the DNA using 5000 units of T4 DNA ligase in 500  $\mu$ L of 1 $\times$  ligation buffer at 16 °C overnight (Fig. 4a).
11. Purify the DNA through phenol/chloroform extraction followed by ethanol precipitation.
12. Digest 50  $\mu$ g of the DNA with 200 units of a restriction enzyme that generates a 3'-protruding end in 500  $\mu$ L of the appropriate buffer (Fig. 4a).
13. Purify the DNA through phenol/chloroform extraction followed by ethanol precipitation.

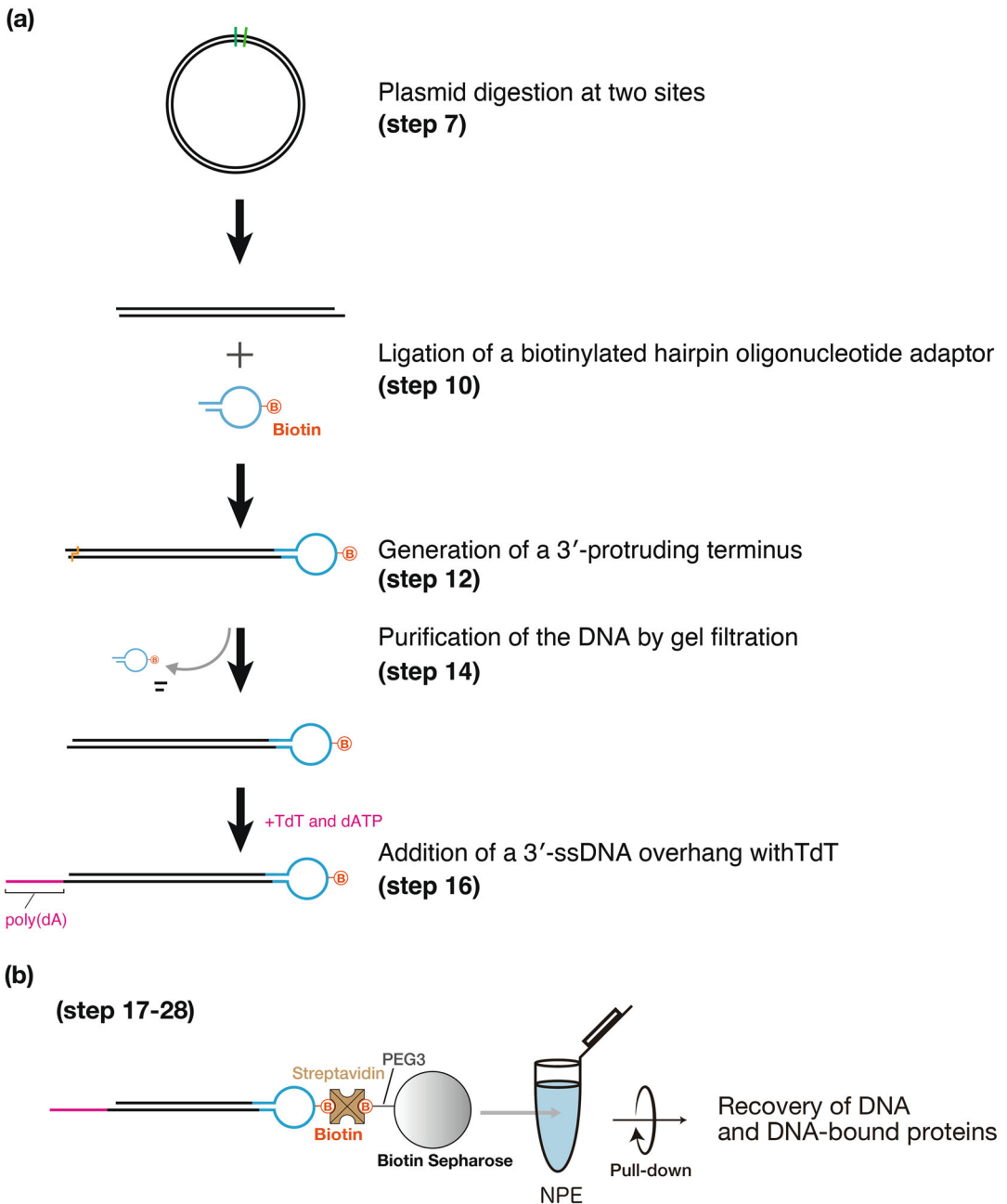


**Fig. 4** DNA Pull-Down Assay with Linearized DNA. **(a)** Schematic diagram of the preparation of a DNA substrate for the DNA pull-down assay. Plasmid DNA is digested with restriction enzymes that recognize non-palindromic sequences at two sites. A biotinylated hairpin oligonucleotide adaptor is ligated to one terminus of the linearized DNA, while the other terminus is digested with a restriction enzyme that generates a 3'-protruding end. Excess hairpin adaptors and small restriction fragments are removed using an open-top gel filtration column. The purified DNA substrate is then incubated with TdT and dATP to add a 3'-ssDNA overhang. **(b)** Schematic illustration of the DNA pull-down assay. The substrate DNA is immobilized onto biotin-Sepharose via streptavidin. The DNA-bead complexes are incubated in NPE and recovered by centrifugation

14. Dissolve the DNA pellet in 100  $\mu\text{L}$  of 10:1 TE. Separate the linearized plasmid DNA from oligonucleotide adaptors using an open-top gel filtration column filled with Sepharose CL-4B. Allow the column to operate by gravity flow. Collect 100  $\mu\text{L}$  fractions (*see* Fig. 4a).
15. Analyze the CL-4B fractions by 1.2% agarose gel electrophoresis and pool the fractions that contain the linearized plasmid DNA but not oligonucleotide adaptors. Concentrate the DNA by ethanol precipitation. Resuspend the DNA pellet in 10:1 TE to obtain a 200 nM solution of hairpin linear DNA.
16. Append 3'-ssDNA overhangs using TdT. *See* steps 5–8 in Subheading 3.3.
17. Immobilize the biotinylated DNA onto biotin-Sepharose beads. Incubate 125 fmol of biotinylated DNA with 1  $\mu\text{g}$  of streptavidin in 25  $\mu\text{L}$  of binding buffer at 4  $^{\circ}\text{C}$  overnight with gentle rotation. Then, mix the DNA–streptavidin complex (125 fmol) with 1  $\mu\text{L}$  (bed volume) of biotin-Sepharose beads in 20  $\mu\text{L}$  of binding buffer, and incubate at room temperature for 3 h with gentle rotation.
18. Wash the beads: Add 200  $\mu\text{L}$  of binding buffer to the beads and centrifuge by a swinging-bucket rotor (TMS-21) at 12,700  $g$  for 1 min at 4  $^{\circ}\text{C}$ . Aspirate the supernatant. Repeat twice.
19. Wash the beads with 1 $\times$  ELB salts 3 times.
20. Prepare NPE. *See* steps 9–11 in Subheading 3.3.
21. Aspirate off any excess buffer from the beads, and mix the DNA beads with NPE at a concentration of 20 ng/ $\mu\text{L}$  with respect to immobilized DNA. Incubate at 22  $^{\circ}\text{C}$  with gentle rotation (*see* Note 22).
22. At appropriate time points, take aliquots and recover the beads. Prepare a 200  $\mu\text{L}$  cushion of 1 $\times$  ELB salts containing 0.5 M sucrose in a 0.65 mL microfuge tube. Take 3.5  $\mu\text{L}$  of the NPE mixture containing DNA beads, quickly dilute it into 200  $\mu\text{L}$  of ELB salts containing 0.2% Triton X-100, and overlay onto the sucrose cushion. Centrifuge the tube in a swinging-bucket rotor (TMS-21) at 12,700  $g$  for 1 min at 4  $^{\circ}\text{C}$ .
23. Aspirate off the supernatant and add 200  $\mu\text{L}$  of 1 $\times$  ELB salts. Centrifuge the tube again in a swinging-bucket rotor at 12,700  $g$  for 1 min at 4  $^{\circ}\text{C}$ , and aspirate the supernatant.
24. Resuspend the beads in stop buffer at a concentration of 1  $\mu\text{L}$  beads per 15  $\mu\text{L}$  buffer.
25. For DNA analysis, take 5  $\mu\text{L}$  of the bead suspension and add 100  $\mu\text{L}$  of stop buffer containing 3 mM biotin and 50  $\mu\text{g}/\text{mL}$  protease K. Incubate at 37  $^{\circ}\text{C}$  for 1 h to disrupt the DNA–streptavidin interaction. *See* steps 26–28 for further

processing. For immunoblotting, take the remaining 10  $\mu\text{L}$  of the bead suspension and add 10  $\mu\text{L}$  of  $2\times$  SDS sample buffer. See **steps 20–25** in Subheading **3.3** for further processing.

26. Purify the DNA through phenol/chloroform extraction followed by ethanol precipitation. Use glycogen as a precipitation carrier (*see step 14* in Subheading **3.3**).
27. Resuspend the DNA in 10:1 TE containing 10  $\mu\text{g}/\mu\text{L}$  RNaseA. Cleave the hairpin adaptor with an appropriate restriction enzyme.
28. Separate the digested sample (5 ng DNA) by neutral or alkaline agarose gel electrophoresis. Stain the gel with SYBR Gold nucleic acid gel stain, and scan the gel using a fluorescence scanner.

---

## 4 Notes

1. Since sucrose takes a long time to dissolve in the buffer, especially at high concentrations, prepare the sucrose-containing buffers before starting the recovery of the testis. Rotating the tubes at 37 °C helps dissolve the sucrose.
2. Since this solution degrades over time, prepare it fresh at least once a month. The 10% SDS stock solution also degrades and should not be stored for more than 6 months.
3. To test the sucking reflex, insert the tip of an index finger deep into the frog's mouth. If the frog does not attempt to remove the finger, it is effectively anesthetized.
4. This step significantly affects the recovery of sperm chromatin. Stack two new razor blades together and finely mince the testes until completely homogenized.
5. This step also affects the recovery of sperm chromatin. We typically use 2 mL of buffer X + 0.2 M sucrose at each step and repeat the procedure 6–7 times to obtain a total of 14 mL in Tube B.
6. Ensure that the interface between the sucrose cushion and the sperm solution is completely disrupted. Incomplete disruption may result in incomplete precipitation of sperm chromatin.
7. Be careful not to touch the upper half of the tube wall, as red blood cells may be present there.
8. Completely remove Triton X-100 by carefully aspirating the supernatant. Avoid pipetting up and down with more than 0.2 mL of buffer X to prevent contamination from detergent that may be present on the upper half of the tube walls.

9. When holding a frog, place your index finger between its legs and grasp it from the back. Covering its eyes with your palm will help calm the frog.
10. Cover the bucket to prevent the frogs from escaping. Placing a weight on the cover will help secure it.
11. Spinning the rotor at a low speed (e.g., 100 rpm) helps quickly bring the temperature to 22 °C.
12. After the dejelling step, proceed as quickly as possible.
13. Remove the lipid layer by pushing it to the side of the tube with a spatula; then gently but quickly transfer the extract from the opening in the lipid plug. During this step, avoid contaminating the extract with mitochondria from beneath the cytoplasmic layer, although some contamination is tolerable.
14. Contamination of the LSS with mitochondria can induce apoptosis during nuclear formation.
15. Using Geminin can improve the recovery of proteins loaded onto post-replicative chromatin, such as cohesin. Since Geminin is naturally concentrated in NPE, adding exogenous Geminin during NPE preparation is not expected to affect its downstream applications.
16. To prevent sperm chromatin aggregation, transfer 1 mL of LSS in a 2 mL round-bottom microfuge tube, add a 90 µL aliquot of sperm chromatin, and mix them thoroughly by pipetting up and down 15 times using a P1000 tip. Return the mixture to the main LSS tube and repeat the procedure as needed until reaching the final sperm chromatin concentration. Finally, gently invert the tube to ensure thorough mixing.
17. The nuclear layer should be between 3 and 5 mm thick.
18. Preincubation is critical for proper activation of NPE. Adding DNA substrates without preincubation leads to poor assay outcomes.
19. RNase A is essential to digest RNA from NPE.
20. The protocol is provided by the supplier.
21. Digesting two different sites with restriction enzymes that recognize non-palindromic sequences avoids self-ligation.
22. Intentionally introduce a small air bubble into the mixture to stir the NPE and DNA beads.

## References

1. Blow JJ, Laskey RA (1986) Initiation of DNA replication in nuclei and purified DNA by a cell-free extract of *Xenopus* eggs. *Cell* 47: 577–587
2. Lohka MJ, Masui Y (1983) Formation in vitro of sperm pronuclei and mitotic chromosomes induced by amphibian ooplasmic components. *Science* 220:719–721

3. Newport J (1987) Nuclear reconstitution in vitro: stages of assembly around protein-free DNA. *Cell* 48:205–217
4. Bell SP, Labib K (2016) Chromosome duplication in *Saccharomyces cerevisiae*. *Genetics* 203:1027–1067
5. Wohlschlegel JA, Dwyer BT, Dhar SK et al (2000) Inhibition of eukaryotic DNA replication by geminin binding to Cdt1. *Science* 290:2309–2312
6. McGarry TJ, Kirschner MW (1998) Geminin, an inhibitor of DNA replication, is degraded during mitosis. *Cell* 93:1043–1053
7. Hodgson B, Li A, Tada S et al (2002) Geminin becomes activated as an inhibitor of Cdt1/RLF-B following nuclear import. *Curr Biol* 12:678–683
8. Raspelli E, Falbo L, Costanzo V (2017) Xenopus egg extract to study regulation of genome-wide and locus-specific DNA replication. *Genesis* 55:e22996
9. Walter J, Sun L, Newport J (1998) Regulated chromosomal DNA replication in the absence of a nucleus. *Mol Cell* 1:519–529
10. Walter J, Newport J (2000) Initiation of eukaryotic DNA replication: origin unwinding and sequential chromatin association of Cdc45, RPA, and DNA polymerase  $\alpha$ . *Mol Cell* 5:617–627
11. Byun TS, Pacek M, Yee M et al (2005) Functional uncoupling of MCM helicase and DNA polymerase activities activates the ATR-dependent checkpoint. *Genes Dev* 19:1040–1052
12. Kwasoe Y, Tsurimoto T, Nakagawa T et al (2016) MutS $\alpha$  maintains the mismatch repair capability by inhibiting PCNA unloading. *elife* 5:e15155
13. Räsche M, Knipscheer P, Enoiu M et al (2008) Mechanism of replication-coupled DNA inter-strand crosslink repair. *Cell* 134:969–980
14. Tatsukawa K, Sakamoto R, Kwasoe Y et al (2024) Resection of DNA double-strand breaks activates Mre11–Rad50–Nbs1- and Rad9–Hus1–Rad1-dependent mechanisms that redundantly promote ATR checkpoint activation and end processing in *Xenopus* egg extracts. *Nucleic Acids Res* 52:3146–3163
15. Hoogenboom WS, Klein Douwel D, Knipscheer P (2017) Xenopus egg extract: a powerful tool to study genome maintenance mechanisms. *Dev Biol* 428:300–309
16. Newport J, Kirschner M (1982) A major developmental transition in early xenopus embryos: I. Characterization and timing of cellular changes at the midblastula stage. *Cell* 30:675–686
17. Newport J, Kirschner M (1982) A major developmental transition in early xenopus embryos: II. Control of the onset of transcription. *Cell* 30:687–696
18. Barrows JK, Long DT (2019) Cell-free transcription in *Xenopus* egg extract. *J Biol Chem* 294:19645–19654
19. Mevissen TET, Kümmecke M, Schmid EW et al (2024) STK19 positions TFIIH for cell-free transcription-coupled DNA repair. *Cell* 187:7091–7106.e24
20. Higashi TL, Ikeda M, Tanaka H et al (2012) The prereplication complex recruits XEco2 to chromatin to promote cohesin acetylation in *Xenopus* egg extracts. *Curr Biol* 22:977–988
21. Takahashi TS, Yiu P, Chou MF et al (2004) Recruitment of Xenopus Scc2 and cohesin to chromatin requires the pre-replication complex. *Nat Cell Biol* 6:991–996
22. Lebofsky R, Takahashi T, Walter JC (2009) DNA replication in nucleus-free Xenopus egg extracts. In: Vengrova S, Dalgaard JZ (eds) DNA replication. Humana Press, Totowa, pp 229–252
23. Sparks J, Walter JC (2019) Extracts for analysis of DNA replication in a nucleus-free system. *Cold Spring Harb Protoc* 2019:pdb.prot097154
24. Tutter AV, Walter JC (2006) Chromosomal DNA replication in a soluble cell-free system derived from xenopus eggs. In: Liu XJ (ed) *Xenopus protocols: cell biology and signal transduction*. Humana Press, Totowa, pp 121–137
25. Duxin JP, Dewar JM, Yardimci H, Walter JC (2014) Repair of a DNA-Protein Crosslink by Replication-Coupled Proteolysis *Cell* 159(2):346–357 <https://doi.org/10.1016/j.cell.2014.09.024>



## Liposome Floatation Assays to Study Membrane Interactions of Nucleoporins

Marianna Tatarek-Nossol and Wolfram Antonin

### Abstract

Many nucleoporins interact with the pore membrane, often via amphipathic helices. Liposome floatation assays are convenient and flexible assays to analyze these protein-membrane interactions and their dependence on specific lipid composition and membrane curvature. We outline here our protocols for the generation of different-sized small unilamellar liposomes of defined lipid compositions and describe how these are employed in floatation assays.

**Key words** Liposome, Small unilamellar vesicle, Protein-membrane interaction, Lipid-protein interaction, Phosphoinositide, Phospholipids, Amphipathic helix, Nuclear pore complex, Nucleoporin, Nuclear envelope

### Abbreviations

PC	L- $\alpha$ -Phosphatidylcholine
PE	L- $\alpha$ -Phosphatidylethanolamine
PI	L- $\alpha$ -Phosphatidylinositol
Chol	Cholesterol
SM	Sphingomyelin
PS	L- $\alpha$ -Phosphatidylserine
Rhod-PE	1,2-dioleoyl-sn-glycero-3-phosphoethanolamine-N-(lissamine rhodamine B sulfonyl)
DOPC	1,2-dioleoyl-sn-glycero-3-phosphocholine
DOPE	1,2-dioleoyl-sn-glycero-3-phosphoethanolamin
DOPS	1,2-dioleoyl-sn-glycero-3-phospho-L-serine (sodium salt)
DOPA	1,2-dioleoyl-sn-glycero-3-phosphate (sodium salt)
PI(4)P	1,2-dioleoyl-sn-glycero-3-phospho-(1'-myo-inositol-4'-phosphate) (ammonium salt)
PI(4,5)P <sub>2</sub>	1,2-dioleoyl-sn-glycero-3-phospho-(1'-myo-inositol-4',5'-bisphosphate) (ammonium salt)
CDP-DG	1,2-dioleoyl-sn-glycero-3-(cytidine diphosphate) (ammonium salt)

# 1 Introduction

Nuclear pore complexes are embedded in the two-membrane structure of the nuclear envelope at sites where the membranes of the outer and inner nuclear membranes are fused and connected by the pore membrane [1–3]. Yet, most of the about thirty nucleoporins do not span with transmembrane regions in the nuclear envelope membranes. Instead, many nucleoporins interact as peripheral membrane proteins with the pore membrane, often with amphipathic helices which immerge into one leaflet of membranes with a preference for already curved membranes [4].

Liposomes, synthetic vesicles composed of lipid bilayers, are versatile tools for drug delivery [5] and setting up artificial or synthetic cells [6, 7] but also for studying membrane-associated processes and interactions [8, 9]. Among the techniques to investigate membrane interactions, liposome flotation assays offer a powerful means to characterize the lipid-binding properties of proteins, peptides, and other membrane-active molecules [10, 11]. In liposome flotation assays, liposomes containing a marker molecule, typically a buoyant lipid or a fluorescent probe, are mixed with a sample of interest containing the protein under investigation. Through centrifugation, liposomes carrying bound proteins migrate to the top of a density gradient, while unbound proteins remain in the lower fractions. This buoyancy-based separation allows quantification and characterization of lipid-protein interactions, membrane insertion, and membrane binding affinities (Fig. 1).

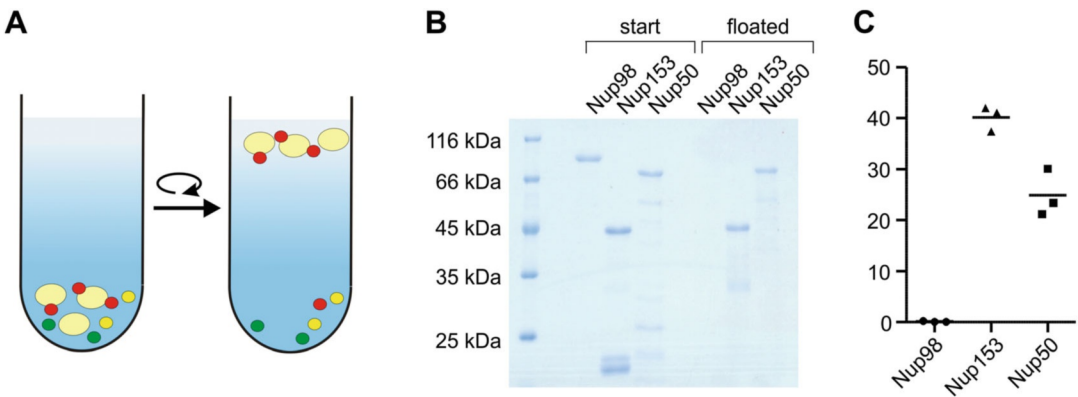


**Fig. 1** Liposome flotation assay. (a). Scheme of the flotation assay. SUV liposomes (light yellow) are floated through a density gradient by centrifugation. At the end of the centrifugation, liposome bound proteins (red) are found in the top fraction while unbound proteins (green, yellow) remain in the lower fraction. (b) Recombinant Nup98 as negative control, a membrane binding domain of Nup153 (aa 1-149) and Nup50 is employed in a liposome flotation assay using 100 nm *E. coli* polar lipids. (c) Quantitation of three independent flotation assays as in (b) with the individual data points and the average (bar) indicated

Liposome floatation assays can be conveniently employed to test for membrane interaction of recombinant expressed and purified nucleoporins [12–14]. Here, full-length proteins or fragments can be employed, e.g., to determine the membrane interaction region. Isolated membrane binding motifs, e.g., an amphipathic helix framed by two inert domains, can be similarly studied [15]. By employing different-sized liposomes, a curvature dependence of the membrane interaction can be determined as smaller-sized liposomes possess a higher membrane curvature. This is especially important for a subclass of amphipathic helices, so-called ALPS motifs, which are sensitive to membrane curvature [16, 17]. In addition, if starting from purified or synthetic lipids, the composition of liposomes can be easily varied. It is thus possible to mimic organism-specific lipid composition of the nuclear envelope of, e.g., budding yeast or vertebrates or analyze the dependence of nucleoporin membrane interaction on specific lipids and lipid classes, e.g., phosphoinositides [18, 19]. On the other hand, minimalistic membrane compositions like pure 1,2-dioleoyl-sn-glycero-3-phosphocholine (DOPC) liposomes or mixtures of 1-palmitoyl-2-oleoyl-sn-glycero-3-phosphocholine (POPC) and 1,2-dioleoyl-sn-glycero-3-phospho-L-serine (DOPS) might be employed [12, 14, 20].

We prefer liposome floatation assays using the lower density of liposomes as compared to proteins over liposome pelleting assays as in the second co-pelleting of proteins because liposome membrane interaction needs to be carefully distinguished from protein pelleting due to protein aggregation. We describe here our protocols to first generate multilamellar vesicle (MLV) liposomes typically from chloroform-dissolved lipids. These are then converted into small unilamellar vesicle (SUV) liposomes of defined sizes using an extruder and filters of defined pore sizes. We then describe how to set up liposome floatation assays, collect the floated liposomes, and analyze these for bound proteins. At the end, we describe an easier method of liposome generation employing *E. coli* polar lipids avoiding chloroform and the need for a rotary evaporator which we often employ as a starting point for exploring membrane interactions of nucleoporins [13, 21].

---

## 2 Materials

### 2.1 Preparation of Multilamellar Vesicle Liposomes

1. Phosphate-buffered saline (PBS): 137 mM NaCl, 2.7 mM KCl, 10 mM Na<sub>2</sub>HPO<sub>4</sub>, pH adjusted to 7.4 (*see Note 1*).
2. Chloroform.
3. Lipid stocks dissolved in chloroform, stored in a glass vial (*see Note 2*), and overlaid with inert gas (argon or nitrogen) at –20 °C.

**Table 1**  
**Composition and pipetting scheme for vertebrate nuclear envelope lipid mix**

	mol %	Mw (g/mol)	Stock in $\text{CHCl}_3$	
			(mg/mL)	Vol. ( $\mu\text{L}$ )
PC	60	770.1	25	244
PE	20	744.1	25	78
PI	10	909.1	25	48
Chol	5	386.7	25	10
SM	2.5	703.0	10	23
PS	2.5	812.0	25	11
Chloroform				586

**Table 2**  
**Composition and pipetting scheme for vertebrate nuclear envelope lipid mix with rhodamine-PE**

	mol %	Mw (g/mol)	Stock in $\text{CHCl}_3$	
			(mg/mL)	Vol. ( $\mu\text{L}$ )
PE	20	744.1	25	78
PI	10	909.1	25	48
Chol	5	386.7	25	10
SM	2.5	703.00	10	23
PS	2.5	812.00	25	11
Rhod-PE	0.2	1301.715	1	34
Chloroform				553

4. 10 mg/mL lipid mixture stock in chloroform (*see* Tables 1, 2, 3, 4 and 5), stored in a glass vial (*see* Notes 2 and 3) and overlaid with inert gas (argon or nitrogen) at  $-20^\circ\text{C}$ .
5. Glass micropipettes (intraMark, Blaubrand).
6. Glass containers (NeoLab cat # 7-0815).
7. 50 mL pear-shaped flask with a glass plug (VWR, cat # 201-1223).
8. Desiccator (Vacuum-Desiccatorator, Duran).
9. Rotary evaporator (IKA RV8) with heating water bath (IKA HB10).

**Table 3****Composition and pipetting scheme for budding yeast ER/nuclear envelope lipid mix with rhodamine-PE**

	mol %	Mw (g/Mol)	Stock in CHCl <sub>3</sub>	
			(mg/mL)	Vol. (μL)
DOPC	49	786.113	25	201
DOPE	21	744.034	25	81
DOPS	8	810.025	25	34
DOPA	5	722.948	10	47
PI	8	902.33	25	38
PI(4)P	2.2	977.147	1	280
PI(4,5)P2	0.8	1074.158	1	112
CDP-DG	2	1040.208	5	54
Rhod-PE	0.2	1301.715	1	34
Chloroform				120

**Table 4****Composition and pipetting scheme for *E. coli* polar lipid mix**

	mol %	Mw (g/Mol)	Stock in CHCl <sub>3</sub>	
			(mg/mL)	Vol. (μL)
<i>E. coli</i> polar lipids	100	827.23	25	400
Chloroform				600

**Table 5****Composition and pipetting scheme for *E. coli* polar lipid mix with rhodamine-PE**

	mol %	Mw (g/Mol)	Stock in CHCl <sub>3</sub>	
			(mg/mL)	Vol. (μL)
<i>E. coli</i> polar lipids	99.8	827.23	25	399
Rhod-PE	0.2	1301.715	1	31
Chloroform				570

10. 1,1'-dioctadecyl-3,3,3',3'-tetramethylindocarbocyanine perchlorate (DiC18), 1 mg/mL in DMSO.
11. 3,3'-dioctadecyloxacarbocyanine perchlorate (DiOC18), 1 mg/mL in DMSO.
12. 1,2-dioleoyl-sn-glycero-3-phosphoethanolamine-N-lissamine rhodamine B sulfonyl ammonium salt (Rhod-PE), 1 mg/mL in ethanol.
13. 1,2-dioleoyl-sn-glycero-3-phosphoethanolamine-N-7-nitro-2-1,3-benzoxadiazol-4-yl ammonium salt (NBD-PE), 1 mg/mL in ethanol.

## **2.2 Preparation of Small Unilamellar Vesicle Liposomes**

1. Mini-Extruder (Avanti Polar Lipids, cat # 610000).
2. Nuklepore Track-Etch Membrane 30 nm, 100 nm, and 400 nm, 19 mm diameter (Whatman).
3. Filter, Drain Disc 10 mm, PE (Whatman).
4. Two 1 mL Hamilton syringes.
5. Dialysis membrane (Spectra/Por 4, 0.3 mL/cm).
6. Phosphate-buffered saline (PBS): 137 mM NaCl, 2.7 mM KCl, 10 mM Na<sub>2</sub>HPO<sub>4</sub>, pH 7.4 (*see Note 1*).
7. Heating block.

## **2.3 Floatation of Liposomes**

1. 1 mg/mL protein solution (*see Note 4*).
2. High sucrose buffer (2.1 M sucrose in PBS). Add 71.9 g sucrose to 40 mL ddH<sub>2</sub>O, add 10 mL of tenfold concentrated PBS-stock, fill ab to 100 mL with ddH<sub>2</sub>O, and stir until dissolved (*see Note 1*).
3. 12% (w/v) sucrose in PBS (*see Note 1*).
4. Ultracentrifuge (Optima MAX-XP, Beckman Coulter).
5. Rotor (TLS-55, Beckman Coulter).
6. Fluorescence Microplate Reader.
7. Thermomixer (Eppendorf).

## **2.4 Protein Isolation from the Floated Liposome Fraction Using Wessel-Flügge Precipitation**

1. Methanol.
2. Chloroform.
3. SDS sample buffer (6×): 187.5 mM Tris pH 6.8, 30% (w/v) sucrose, 9% SDS, 100 mM DTT, 0.1% (w/v) bromophenol blue.
4. Typical SDS-PAGE gel.
5. Typical protein detection instruments (e.g., Coomassie staining, silver staining, Western blotting) after SDS-PAGE.

### **2.5 Liposome Preparation from *E. coli* Polar Lipids in Ethanol and Floatation**

1. *E. coli* polar lipids in ethanol (Avanti Polar Lipids, Cat# 100600).
2. Argon gas or Nitrogen gas.
3. Ethanol.
4. Glass vial.
5. Water bath.
6. Polystyrene tubes 3.5 mL (Carl Roth) or glass tube.
7. High sucrose buffer: 2.1 M sucrose in PBS. Add 71.9 g sucrose to 40 mL ddH<sub>2</sub>O, add 10 mL of tenfold concentrated PBS-stock, fill ab to 100 mL with ddH<sub>2</sub>O, and stir until dissolved (*see* **Note 1**).
8. Sonifier (Branson).

---

## **3 Methods**

### **3.1 Preparation of Multilamellar Vesicle Liposomes**

1. Use glass micropipettes and glass containers for lipid mixtures (*see* **Note 2**). Preferably dissolve lipids in chloroform. Use glass screw cap vials for storage for dissolved lipid stocks and mixtures (*see* **Note 5**).
2. Pipet the required amounts of chloroform-dissolved lipids into a 50 mL pear-shaped flask (*see* Tables 1, 2 and 3), in total not more than 10 mg of lipids (*see* **Note 3**). Adjust the lipid concentration in the flask to 10 mg/mL with chloroform (*see* **Notes 6 and 7**).
3. Evaporate chloroform in a pear-shaped flask using a rotary evaporator. Heat water bath to 42 °C and slowly increase the vacuum to form an even lipid film; chloroform must not boil (Fig. 2a).
4. Regulate the vacuum to stay below boiling point and wait till all chloroform is evaporated (Fig. 2b).
5. Put the flask in an desiccator overnight or longer to remove residual chloroform.
6. Rehydrate lipid film by adding a buffer of choice (e.g., PBS) to reach a final lipid concentration of 10 mg/mL.
7. Seal the flask with a glass plug and parafilm, place it in a water bath at 42 °C, and incubate for 2 h without movement.
8. Put the flask in an incubator at 42 °C and rotate at 150–200 rpm until the lipid film is resolved. This typically takes 2–3 h.
9. Freeze/thaw lipid film/suspension ten times, i.e., put the flask in liquid nitrogen followed by thawing in a 42 °C water bath (*see* **Note 8**).

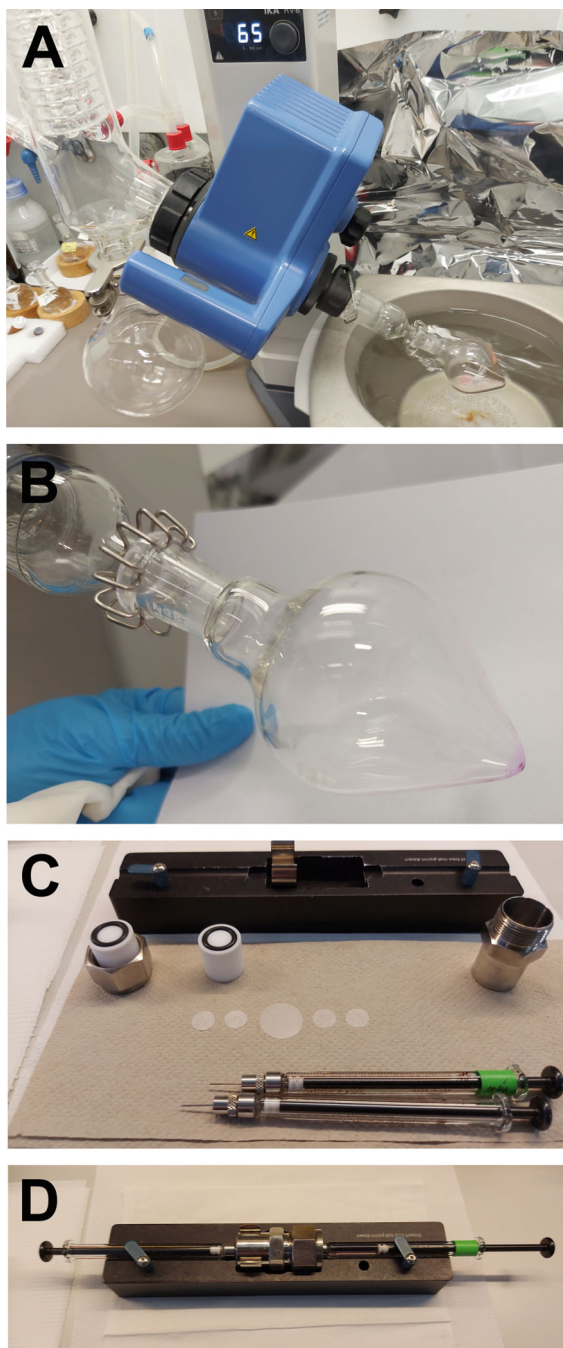


**Fig. 2** Selected steps of the liposomes preparation protocol. **(a)** Chloroform is evaporated from the lipid-chloroform mixture in a pear-shaped flask in a rotary evaporator. **(b)** After evaporation of chloroform, a thin lipid film remains on the glass surface. In this case, the lipid mixture contained Rhod-PE. **(c)** Components required for the SUV preparation using the Mini-Extruder are shown. **(d)** Assembled Mini-Extruder before passing the MLV mixture through the membrane to generate SUVs is shown

10. Transfer MLVs using a glass pipette into a glass tube and proceed with Subheading 3.2 (*see* **Notes 9** and **10**).

### **3.2 Preparation of Small Unilamellar Vesicle (SUV) Liposomes**

1. If starting from stored MLVs, thaw MLVs in a water bath at 42 °C.
2. Dilute MLVs to a final concentration of 6.6 mg/mL with PBS (*see* **Notes 11** and **12**).
3. Preheat Mini-Extruder to >45 °C. Assemble the Mini-Extruder with 400 or 100 nm membrane and filters (two filters, membrane, two filters to be placed, Fig. 2c) to generate 400 nm or 100 nm SUVs, respectively (*see* **Notes 13–15**).
4. Rinse the Mini-Extruder with buffer (e.g., PBS) (purge 2–3 times, exchange buffer, and purge again).
5. Fill 350 µL liposomes in the first Hamilton syringe and assemble the Mini-Extruder including a second Hamilton syringe (*see* **Note 16**, Fig. 2d).
6. Equilibrate the Mini-Extruder on the heating block (>45 °C) for at least 5 min.
7. Pass liposomes 21× through the membrane. To avoid contamination of SUVs with MLVs, we pass the liposomes an uneven number through the membrane. In this way, the SUV liposomes are found at the end of the procedure in the second Hamilton syringe.
8. Fill liposomes in a pre-wetted dialysis membrane (0.3 mL/cm). We typically dialyze against at least 1000 times larger buffer reservoir with a buffer (e.g., PBS) change after 1 h followed by an o/n dialysis.

### **3.3 Floatation of Liposomes**

1. For each sample, mix carefully 50 µL the SUV liposomes with 50 µL of a 1 mg/mL protein solution in an Eppendorf tube (*see* **Notes 17** and **18**).
2. Keep 10 µL of the mixture as “started materials” for the following SDS-PAGE procedure (**step 9** in Subheading 3.4).
3. Incubate the mixture for 30 min at 30 °C shaking at 600 rpm, e.g., in a thermomixer.
4. Per sample, mix 75 µL of the protein-liposome sample with 75 µL of high sucrose buffer in a TLS-55 centrifugation tube. Overlay carefully with 1700 µL of 12% sucrose in PBS and 300 µL PBS (0% sucrose) (*see* **Note 19**). Safe residual protein-liposome sample as starting material (*see* **step 8** in Subheading 3.4).
5. Centrifuge samples in an ultracentrifuge in an TLS-55 rotor at 55000 rpm (259,000 *g*) for 2 h at 25 °C.

6. After centrifugation, collect the liposome containing the top fraction (approx. 150  $\mu\text{L}$ ) in a 2 mL micro tube (*see* **Notes 20** and **21**). For concentration of the liposome, we typically employ a Wessel-Flügge precipitation (*see* Subheading 3.4) [22].

### **3.4 Protein Isolation from the Floated Liposome Fraction Using Wessel-Flügge Precipitation**

1. Determine the volume of the collected floated liposome sample, add four volumes of methanol, and mix using a vortexer.
2. Add one volume of chloroform and mix using a vortexer.
3. Add three volumes of ddH<sub>2</sub>O and mix using a vortexer.
4. Centrifuge for 2 min at 13,300 rpm (16,400  $g$ ) at 4 °C.
5. Remove carefully and discard the upper phase. Take care not to disturb the interphase.
6. Add three volumes of methanol, concerning the starting liposomes volume, and mix with the inter- and bottom-phases using a vortexer.
7. Centrifuge for 10 min at 13,300 rpm (16,400  $g$ ) at 4 °C.
8. Discard carefully supernatant and dry the pellet for 30 s at room temperature. Resuspend the pellet in 20  $\mu\text{L}$  of SDS sample buffer. Add each 20  $\mu\text{L}$  of SDS sample buffer to 10  $\mu\text{L}$  of the “starting material.” Heat samples to 95 °C for 5 min on a heating block.
9. Analyze the starting material of flotations as well as the Wessel-Flügge precipitated liposome fractions by SDS-PAGE followed by Coomassie staining, silver staining, or Western blotting. We typically load 2–4  $\mu\text{L}$  of the starting material and 10  $\mu\text{L}$  of the liposome fractions on a mini-SDS PAGE for staining, for western blotting 1–2  $\mu\text{L}$  of the starting material and 10  $\mu\text{L}$  of the liposome fraction (Fig. 1).

### **3.5 Liposome Preparation from *E. coli* Polar Lipids and Flootation**

1. Heat 100% ethanol to 45 °C on a heating block (*see* **Note 22**).
2. Add in a glass vial 1 mL of warm ethanol to 100 mg *E. coli* polar lipids powder and dissolve the lipid by carefully shaking in a water bath at 60 °C until lipids are dissolved (*see* **Notes 23** and **24**).
3. Transfer the dissolved lipids with a glass micropipette in a screw cap vial. Rinse the glass vial with 500  $\mu\text{L}$  of ethanol and add this to the screw cap vial as well. Overlay the solution with an inert gas such as Argon or nitrogen to avoid lipid oxidation, and store it as a 66.6 mg/mL *E. coli* polar lipid solution in ethanol at –20 °C (*see* **Note 25**).
4. Heat ethanol-dissolved *E. coli* polar lipids (66.6 mg/mL) to 45–50 °C.

5. Inject 50  $\mu\text{L}$  of the ethanol-dissolved *E. coli* polar lipids with one fast pipet stroke into 450  $\mu\text{L}$  working buffer (450  $\mu\text{L}$  PBS) in a 3.5 mL polystyrene or glass tube.
6. Mix with a pipette and swirl gently till the mixture has an opaque appearance. Fill 350  $\mu\text{L}$  in a Hamilton pipette and proceed as described in Subheading 3.2 (*see Note 26*).

---

## 4 Notes

1. Depending on the planned experiments, alternative buffers can be used, e.g., 20 mM HEPES, 50 mM KCl, and 2.5 mM  $\text{MgCl}_2$ , as they might affect protein stability and protein-membrane interaction differently. In this case, the different sucrose buffers need to be prepared within the respective buffer system.
2. Before using, properly rinse glassware with chloroform.
3. Pipette the lipids dissolved in chloroform using glass pipettes.
4. We typically used recombinant protein expressed in *E. coli* and affinity-purified using Ni-agarose (*see, e.g., [12–15]*). After further purification (e.g., by gel filtration), they are dialyzed to PBS and employed in a concentration of 1 mg/mL.
5. Always keep dissolved lipids under inert gas such as argon or nitrogen to prevent lipid oxidation.
6. If Rhod-PE or NBD-PE is used as lipid dye, add this to the chloroform-dissolved lipid mixture, e.g., 34  $\mu\text{L}$  of 1 mg/mL in ethanol (*see Tables 2 and 3*). DiIC18 or DiOC18 can be added at **step 2** in Subheading 3.2.
7. MLVs from *E. coli* polar lipids can be generated by a more effortless and faster protocol (*see Subheading 3.4*). However, generating them following this protocol is also possible, e.g., if they need to be labeled with Rhod-PE or NBD-PE.
8. Fix the flask with a wooden clip.
9. Use a Hamilton pipette.
10. For longer storage, MLVs can be stored with 100  $\mu\text{L}$  aliquots at  $-80^\circ\text{C}$  for up to 2 months. For this, transfer to PCR tubes, overlay with an inert gas (argon or nitrogen), and snap freeze in liquid nitrogen.
11. For dilution of the MLVs, we typically use 3.5 mL polystyrene tubes.
12. If a lipid mixture without Rhod-PE/NBD-PE in chloroform was used for MLVs generation (*see Subheading 3.1*) a fluorescent membrane dye (DiIC18, DiOC18) can be added at this point, e.g., 3.5  $\mu\text{L}$  of 1 mg/mL DiIC18 in DMSO to the 350  $\mu\text{L}$  diluted MLVs.

13. Slight wetting of the filter with ddH<sub>2</sub>O eases the proper assembly.
14. It is difficult to generate 30 nm SUVs by directly passing MLVs through a 30 nm. In this case, start with the double amount of MLVs and pretreat them for 20 min in an ultrasound bath (40% amplitude, 30 s pulse on/5 s pulse off). Then, pass them first through a 100 nm membrane and only then through the 30 nm membrane.
15. The size distribution of the different liposomes can be tested by dynamic light scattering [12, 13].
16. From a 350  $\mu$ L MLV liposome solution, we typically recover 250–280  $\mu$ L. A typical floatation run with four samples in a TLS-55 rotor requires 200  $\mu$ L of SUVs.
17. Cut the pipette tips with scissors to generate a wider opening or use genome DNA tips.
18. As the TLS-55 rotor has four buckets, we typically generate four samples.
19. Mark the phase borders with a marker pen.
20. The liposomes are found at the phase boundary between the 12% and 0% sucrose solution and can be identified by Rhod-PE or the DiIC18 dye. Place the tube in front of a white paper sheet.
21. To check the floatation efficiency of the liposomes, the fluorescence intensities of the start protein/liposome mixture and the top fraction can be determined and related on a fluorometer [13].
22. Always keep the solution warm.
23. One can add the ethanol also directly to the vial provided by the supplier.
24. Do not shake too much as the lipid solution will not come off easily from the glass wall.
25. Transfer must be done quickly before the solution gets cold and sticky.
26. If DiIC18 or DiOC18 is used as membrane dye, add at this point 3.5  $\mu$ L of 1 mg/mL DiIC18 or DiOC18 in DMSO to the solution before filling the Hamilton pipette.

## References

1. Lin DH, Hoelz A (2019) The structure of the nuclear pore complex (an update). *Annu Rev Biochem* 88:725–783. <https://doi.org/10.1146/annurev-biochem-062917-011901>
2. Hampoelz B, Andres-Pons A, Kastiris P et al (2019) Structure and assembly of the nuclear pore complex. *Annu Rev Biophys* 48:515–536. <https://doi.org/10.1146/annurev-biophys-052118-115308>
3. Yang Y, Guo L, Chen L et al (2023) Nuclear transport proteins: structure, function, and disease relevance. *Signal Transduct Target Ther*

- 8(1):425. <https://doi.org/10.1038/s41392-023-01649-4>
4. Hamed M, Antonin W (2021) Dunking into the lipid bilayer: how direct membrane binding of nucleoporins can contribute to nuclear pore complex structure and assembly. *Cells* 10(12). <https://doi.org/10.3390/cells10123601>
5. Torchilin VP (2006) Multifunctional nanocarriers. *Adv Drug Deliv Rev* 58(14):1532–1555. <https://doi.org/10.1016/j.addr.2006.09.009>
6. Göpflich K, Platzman I, Spatz JP (2018) Mastering complexity: towards bottom-up construction of multifunctional eukaryotic synthetic cells. *Trends Biotechnol* 36(9): 938–951. <https://doi.org/10.1016/j.tibtech.2018.03.008>
7. Rideau E, Dimova R, Schwille P et al (2018) Liposomes and polymersomes: a comparative review towards cell mimicking. *Chem Soc Rev* 47(23):8572–8610. <https://doi.org/10.1039/c8cs00162f>
8. Sessa G, Weissmann G (1968) Phospholipid spherules (liposomes) as a model for biological membranes. *J Lipid Res* 9(3):310–318
9. Akbarzadeh A, Rezaei-Sadabady R, Davaran S et al (2013) Liposome: classification, preparation, and applications. *Nanoscale Res Lett* 8(1):102. <https://doi.org/10.1186/1556-276x-8-102>
10. Senju Y, Lappalainen P, Zhao H (2021) Liposome co-sedimentation and co-floitation assays to study lipid-protein interactions. *Methods Mol Biol* 2251:195–204. [https://doi.org/10.1007/978-1-0716-1142-5\\_14](https://doi.org/10.1007/978-1-0716-1142-5_14)
11. Starr ML, Fratti R (2019) Determination of Sec18-lipid interactions by liposome-binding assay. *Methods Mol Biol* 1860:211–220. [https://doi.org/10.1007/978-1-4939-8760-3\\_13](https://doi.org/10.1007/978-1-4939-8760-3_13)
12. Vollmer B, Lorenz M, Moreno-Andres D et al (2015) Nup153 recruits the Nup107-160 complex to the inner nuclear membrane for interphasic nuclear pore complex assembly. *Dev Cell* 33(6):717–728. <https://doi.org/10.1016/j.devcel.2015.04.027>
13. Vollmer B, Schooley A, Sachdev R et al (2012) Dimerization and direct membrane interaction of Nup53 contribute to nuclear pore complex assembly. *EMBO J* 31(20):4072–4084. <https://doi.org/10.1038/emboj.2012.256>
14. von Appen A, Kosinski J, Sparks L et al (2015) In situ structural analysis of the human nuclear pore complex. *Nature* 526(7571):140–143. <https://doi.org/10.1038/nature15381>
15. Amm I, Weberuss M, Hellwig A et al (2023) Distinct domains in Ndc1 mediate its interaction with the Nup84 complex and the nuclear membrane. *J Cell Biol* 222(6). <https://doi.org/10.1083/jcb.202210059>
16. Drin G, Casella JF, Gautier R et al (2007) A general amphipathic alpha-helical motif for sensing membrane curvature. *Nat Struct Mol Biol* 14(2):138–146. <https://doi.org/10.1038/nsmb1194>
17. Giménez-Andrés M, Čopič A, Antonny B (2018) The many faces of amphipathic helices. *Biomol Ther* 8(3). <https://doi.org/10.3390/biom8030045>
18. Mansat M, Picot M, Chicanne G et al (2021) Liposome-based methods to study protein-phosphoinositide interaction. *Methods Mol Biol* 2251:177–184. [https://doi.org/10.1007/978-1-0716-1142-5\\_12](https://doi.org/10.1007/978-1-0716-1142-5_12)
19. Bigay J, Antonny B (2005) Real-time assays for the assembly-disassembly cycle of COP coats on liposomes of defined size. *Methods Enzymol* 404:95–107. [https://doi.org/10.1016/s0076-6879\(05\)04010-3](https://doi.org/10.1016/s0076-6879(05)04010-3)
20. Floch AG, Tareste D, Fuchs PF et al (2015) Nuclear pore targeting of the yeast Pom33 nucleoporin depends on karyopherin and lipid binding. *J Cell Sci* 128(2):305–316. <https://doi.org/10.1242/jcs.158915>
21. Kralt A, Wojtynek M, Fischer JS et al (2022) An amphipathic helix in Brl1 is required for nuclear pore complex biogenesis in *S. cerevisiae*. *elife* 11. <https://doi.org/10.7554/eLife.78385>
22. Wessel D, Flugge UI (1984) A method for the quantitative recovery of protein in dilute solution in the presence of detergents and lipids. *Anal Biochem* 138(1):141–143



# Chapter 16

## Giant Unilamellar Vesicles (GUVs) to Study Membrane Interaction of Nucleoporins

Marianna Tatarek-Nossol and Wolfram Antonin

### Abstract

Giant unilamellar vesicles (GUVs) are large, spherical lipid bilayer vesicles typically ranging from 1 to 100 micrometers in diameter, far exceeding the size of typical small unilamellar vesicles (SUVs) employed, for example, in liposome floatation assays. Their unique size and structural simplicity make them particularly suitable for a wide range of biophysical studies. GUVs serve as versatile model systems for studying membrane-protein interactions, membrane curvature sensing, and membrane remodeling processes. In addition, by micromanipulation, fluorescence recovery after photobleaching, and single-molecule imaging, membrane bending, deformation, and fusion events can be investigated with high spatial and temporal resolution. Here, we summarize our protocols generating GUVs for studying nucleoporin-membrane interaction including protocols reconstituting transmembrane nucleoporins into GUVs.

**Key words** Lipid bilayer, Liposome, Protein-membrane interaction, Lipid-protein interaction, Membrane deformation, Phosphoinositide, Phospholipids, Nuclear pore complex, Nucleoporin, Nuclear envelope

### Abbreviations

PC	L- $\alpha$ -Phosphatidylcholine
PE	L- $\alpha$ -Phosphatidylethanolamine
PI	L- $\alpha$ -Phosphatidylinositol
Chol	Cholesterol
SM	Sphingomyelin
PS	L- $\alpha$ -Phosphatidylserine
Rhod-PE	1,2-dioleoyl-sn-glycero-3-phosphoethanolamine-N-(lissamine rhodamine B sulfonyl)
DOPC	1,2-dioleoyl-sn-glycero-3-phosphocholine
DOPE	1,2-dioleoyl-sn-glycero-3-phosphoethanolamin
DOPS	1,2-dioleoyl-sn-glycero-3-phospho-L-serine (sodium salt)
DOPA	1,2-dioleoyl-sn-glycero-3-phosphate (sodium salt)
PI(4)P	1,2-dioleoyl-sn-glycero-3-phospho-(1'-myo-inositol-4'-phosphate) (ammonium salt)

PI(4,5)P2	1,2-dioleoyl-sn-glycero-3-phospho-(1'-myo-inositol-4',5'-bisphosphate) (ammonium salt)
CDP-DG	1,2-dioleoyl-sn-glycero-3-(cytidine diphosphate) (ammonium salt)
Ni-DOGS	1,2-dioleoyl-sn-glycero-3-[(N-(5-amino-1-carboxypentyl)iminodiacetic acid)succinyl] (nickel salt)

---

## 1 Introduction

Nuclear pore complexes form huge transport gates in the double-membrane structure of the nuclear envelope [1–3]. They sit at point fusions of the two membranes of the nuclear envelope with some nucleoporins spanning as transmembrane proteins the pore membrane and a larger number interacting with the pore membrane as peripheral membrane proteins [4, 5]. Giant unilamellar vesicles (GUVs) can be conveniently employed as minimal membrane systems to study nucleoporin membrane interactions [6] as well as the binding of soluble to transmembrane nucleoporins in a membranous environment [7].

One of the primary advantages of GUVs lies in their large size and homogeneity [8, 9]. Unlike smaller liposomes typically used for liposome floatation assays or electron microscopy analysis, GUVs can be easily visualized using light microscopy techniques. They allow thus direct observation of membrane dynamics [10–15], separation of membrane subdomains [16–19], and binding of membrane interacting proteins at the single-vesicle level [20–22]. Furthermore, GUVs exhibit small size variations within a population, enabling reproducible experimental measurements and quantitative analysis [23].

As with small liposomes, membrane lipid composition of GUVs can be precisely controlled to investigate the effects of specific lipid compositions on membrane properties and membrane binding of proteins. By varying lipid composition, one can mimic the diverse lipid environments of biological membranes and can approximate the lipid composition of the yeast or vertebrate nuclear envelope [6, 7]. By this, one can probe how these different lipid compositions influence membrane organization, phase behavior, and protein-membrane interactions.

GUVs can also serve as versatile platforms for reconstituting functional membrane proteins and studying their activity in a controlled environment [24]. By incorporating proteins of interest into GUV membranes, one can probe protein-lipid interactions, membrane insertion, conformational changes, and enzymatic activities. In the context of nuclear pore complexes, they also allow for studying the soluble nucleoporins with membrane integral proteins in a lipid environment [6, 7].

Of the variety of methods for generating GUVs, lipid film hydration [25], electroforming [26, 27], lipid emulsification, and microfluidic methods [28, 29] are probably the most commonly used. Each of these techniques has its own drawbacks and trade-offs depending on the application. We describe here our protocols for generating GUVs by gel-assisted swelling using polyvinyl alcohol (PVA) and electroformation which involves modulating the spontaneous swelling of lipids within an aqueous solution using an externally applied electric field. We describe how these GUVs can be employed for studying nucleoporin-lipid membrane interaction using light microscopy. For this, we typically employ recombinant expressed nucleoporins or fragments thereof which are either expressed as fluorescent protein fusions (e.g., eGFP, mCherry) [7, 13] or after expression labeled with fluorescent dyes (e.g., Alexa 488, Alexa 546 via succinimidyl ester- or maleimide-mediated coupling) [6, 13].

We explain how transmembrane proteins can be integrated into the GUVs [6, 13]. Although different methods exist here [24], we typically follow a simple pipeline where transmembrane proteins are first inserted into small liposomes by gel filtration-assisted reconstitution [30, 31]. From these proteoliposomes, then GUVs are generated and can be employed for studying behavior of transmembrane proteins in a lipid environment but also to study protein-transmembrane protein interactions [6, 7]. Finally, by spiking the GUVs with small quantities of Ni-NTA-modified lipids (e.g., Ni-NTA-DOGS), His<sub>6</sub>-tagged proteins can be conveniently recruited to the GUV surface for studying their effect on membrane structure and function.

---

## 2 Materials

### 2.1 Preparation of Proteolipid Solution

1. Ultracentrifuge (Optima MAX-XP, Beckman Coulter).
2. Rotor (TLA 120.2, Beckman Coulter).
3. Thermomixer.
4. Gel filtration column (e.g., 20 × 0.5 cm, Econo-Column, Bio-Rad), self-packed with Sephadex G-50.
5. Phosphate-buffered saline (PBS): 137 mM NaCl, 2.7 mM KCl, 10 mM Na<sub>2</sub>HPO<sub>4</sub>, pH 7.4.
6. Membrane protein, approx. 1 mg/mL, dialyzed into PBS (*see* **Notes 1** and **2**).
7. 10% octyl- $\beta$ -D-glucopyranoside solution in ddH<sub>2</sub>O.
8. 1,1'-dioctadecyl-3,3',3',3'-tetramethylindocarbocyanine perchlorate (DilC18) 1 mg/mL in DMSO.

**Table 1**

**Composition and scheme for a 30 mg/mL vertebrate nuclear envelope lipid mix to be dissolved in 10% octyl- $\beta$ -D-glucopyranoside for proteoliposome formation**

	<b>mol %</b>	<b>Mw (g/Mol)</b>	<b>Amount (mg)</b>
PC	60	770.1	18.26
PE	20	744.1	5.88
PI	10	909.1	3.59
Chol	5	386.7	0.76
SM	2.5	703	0.69
PS	2.5	812	0.80

9. 3,3'-dioctadecyloxacarbocyanine perchlorate (DiOC18) 1 mg/mL in DMSO.
10. Marina Blue™ 1,2-dihexadecanoyl-sn-glycero-3-phosphoethanolamine (Marina Blue-DHPE 1 mg/mL in DMSO (*see* **Note 3**).
11. 30 mg/mL lipid mixture in 10% octyl- $\beta$ -D-glucopyranoside (*see* **Note 4**, Table 1).
12. 50 mM Hepes pH 7.5.
13. HB100 buffer: 100 mM NaCl, 20 mM Hepes pH 7.5, 1.5 mM KCl.

## **2.2 Preparation of GUVs on Platinum Grids**

1. Phosphate-buffered saline (PBS).
2. 255 mM sucrose solution (*see* **Notes 5** and **6**).
3. 5% BSA (lipid-free Bovine Serum Albumin) in PBS.
4. Lipid stocks dissolved in  $\text{CHCl}_3$ , stored in a glass vial, and overlaid with inert gas (argon or nitrogen) at  $-20^\circ\text{C}$  (*see* **Note 7**).
5. 10 mg/mL lipid mixture stock in chloroform, stored in glass vial, and overlaid with inert gas (argon or nitrogen) at  $-20^\circ\text{C}$  (*see* **Notes 7** and **8**, Tables 2, 3, 4 and 5).
6. Solid lipid stocks, stored in a glass vial, and overlaid with inert gas (argon or nitrogen) at  $-20^\circ\text{C}$ .
7. Chloroform.
8. Ethanol.
9. Heating block.
10. Desiccator (Vacuum-Desiccatorator, Duran).
11. Platinum grids ( $5 \times 5$  mm, ALS, distributed by BAS Inc.)
12. Cuvette (e.g., Eppendorf, 1 mL UVette).

**Table 2**  
**Composition and pipetting scheme for vertebrate nuclear envelope lipid mix**

	mol %	Mw (g/mol)	Stock in CHCl <sub>3</sub>	
			(mg/mL)	Vol. (μL)
PC	60	770.1	25	244
PE	20	744.1	25	78
PI	10	909.1	25	48
Chol	5	386.7	25	10
SM	2.5	703.0	10	23
PS	2.5	812.0	25	11
Chloroform				586

**Table 3**  
**Composition and pipetting scheme for vertebrate nuclear envelope lipid mix with Rhodamin-PE**

	mol %	Mw (g/mol)	Stock in CHCl <sub>3</sub>	
			(mg/mL)	Vol. (μL)
PE	20	744.1	25	78
PI	10	909.1	25	48
Chol	5	386.7	25	10
SM	2.5	703.00	10	23
PS	2.5	812.00	25	11
Rhod-PE	0.2	1301.715	1	34
Chloroform				553

13. Function generator (e.g. TG315, Aim-TTi).
14. 8-well, chambered cover glass borosilicate (Nunc Lab-Tek, Thermo Scientific), coated with 5% BSA.

### **2.3 Preparation of GUVs Using PVA Method**

1. 2% Mucosal solution.
2. 5% polyvinyl alcohol (PVA) (Mw = 146,000-186,000) in ddH<sub>2</sub>O (*see Note 9*).
3. Phosphate-buffered saline (PBS): 137 mM NaCl, 2.7 mM KCl, 10 mM Na<sub>2</sub>HPO<sub>4</sub>, pH 7.4.

**Table 4****Composition and pipetting scheme for budding yeast ER/nuclear envelope lipid mix with Rhodamin-PE**

	mol %	Mw (g/Mol)	Stock in CHCl <sub>3</sub>	
			(mg/mL)	Vol. (μL)
DOPC	49	786.113	25	201
DOPE	21	744.034	25	81
DOPS	8	810.025	25	34
DOPA	5	722.948	10	47
PI	8	902.33	25	38
PI(4)P	2.2	977.147	1	280
PI(4,5)P <sub>2</sub>	0.8	1074.158	1	112
CDP-DG	2	1040.208	5	54
Rhod-PE	0.2	1301.715	1	34
Chloroform				120

**Table 5****Composition and pipetting scheme for vertebrate nuclear envelope lipid mix containing *N*-NTA-lipids**

	mol %	Mw (g/Mol)	Stock in CHCl <sub>3</sub>	
			(mg/mL)	Vol. (μL)
PC	60	770.1	25	251
PE	20	744.1	25	81
PI	10	909.1	25	49
Chol	5	386.7	25	10
SM	2.5	703	10	24
PS	2.5	812	25	11
Ni-DOGS	0.1	1057.02	10	1
Chloroform				428

4. 10 mg/mL lipid mixture stock in chloroform, stored in glass vial, and overlaid with inert gas (argon or nitrogen) at  $-20^{\circ}\text{C}$  (see **Notes 7** and **8**, Tables **2**, **3**, **4** and **5**).
5. 8-well, chambered cover glass borosilicate (Nunc Lab-Tek, Thermo Scientific), coated with 5% BSA.
6. Glass microscope slide (SuperFrost Plus, Eppredia).

7. Glass micropipettes (intraMark, Blaubrand).
8. Silicone isolators (1–13 Dia × 0.5 mm Depth ID9, GRACE Bio-Labs).
9. Pen (multimark permanent, waterproof, Faber-Castell).

## 2.4 GUV Imaging

1. Inverted microscope Nikon Ti2-E with fully motorized XYZ-stage.
2. Dual operation module (confocal or fluorescence widefield) Crest X-Light V2 Spinning Disc with Single Pattern—22 mm/40 µm Pinhole optimized for 60× objective (*see* **Note 10**).
3. Objective: 60× Lambda Oil 1.4NA WD 0–13 mm.
4. Metal halide 100 W lamp for epifluorescence.
5. LED Light engine Lumencor Spectra X for Crest Spinning Disc.
6. Illumination/filter set compatibility: DAPI, Hoechst, CFP, GFP, FITC, YFP, TRITC, Cy3, Texas Red, mCherry, Cy5.
7. Zyla 4.2 USB3 SCMOS Camera, >80%QE, 40ffps@16bit, 53 ffps@12bit.
8. High-performance computing workstation with a specific hardware and software (Nikon Elements AR<sup>®</sup>) to control the microscope, optic path, illumination, and the cameras.
9. Fiji/ImageJ software for image analysis.

---

## 3 Methods

Here, we describe two methods for generating lipid GUVs, one based on electroformation using Pt-grids (Subheading 3.2). An alternative method describes the gel-assisted GUV preparation (Subheading 3.3). This requires the preparation of small proteoliposomes, which we first describe in Subheading 3.1. While the gel-assisted GUV preparation method is fast and can be quickly done in parallel for many GUV preparations, it cannot be excluded the PVA used in the process in later assays impacts protein-membrane interactions.

### 3.1 Preparation of Proteoliposomes

1. Pre-cool ultracentrifuge.
2. Start washing the gel filtration columns with PBS (*see* **Note 11**).
3. Mix a sample of 5–20 µL membrane protein dialyzed into PBS (can be labeled with fluorescence dye) with 100 µL of PBS and 20 µL of NE lipid-detergent mixture (30 mg/mL NE lipids solubilized in 10% (w/v) octyl-β-D-glucopyranoside (*see*

**Note 2**, Table 1). Membrane dyes such as DiOC18 or DilC18 can be added at this step (1  $\mu$ L of a 1 mg/mL solution).

4. Remove the column lid and remove the excess of PBS above the column bead material. When no buffer is left, carefully apply the sample mixture. If the sample is drained into the bead material, apply 500  $\mu$ L of PBS. Add slowly on top of the gel matrix or the column wall and avoid swirling up the matrix. Add more PBS on top and carefully reconnect the lid with a connection to the buffer reservoir to the column to allow constant buffer flow (*see Note 12*).
5. When the protein is labeled, a faster migrating band separating from the bulk lipid dye can be observed. These are the formed proteoliposomes (*see Notes 13–15*).
6. To concentrate proteoliposomes, pellet them by centrifugation, e.g., in a Beckman tabletop ultracentrifuge using a TLA 120 rotor, 100,000 rpm (435,000 *g*) for 30 min at 4 °C.
7. Resuspend proteoliposome pellet in 10–50  $\mu$ L of 50 mM Hepes pH 7.4 or HB100 (*see Note 16*).
8. Between two gel filtration runs for runs, wash columns with at least two column volumes buffer (*see Note 17*).

### 3.2 Preparation of Giant Unilamellar Vesicles (GUVs) on Pt-Grids

1. Prewarm heating block to 42 °C and 255 mM sucrose to 42 °C.
2. Clean platinum grids with chloroform, ethanol, and then ddH<sub>2</sub>O (*see Note 18*). Dry on heating block for 20–30 min.
3. When grids are completely dry, dilute the chloroform-dissolved lipids (e.g., NE-lipid mixture, *see Tables 1, 2, 3 and 4*) 1:10 with chloroform to a final concentration of 1 mg/mL, and spread 10  $\mu$ L equally on each of the two grids (equally on both sides of the grids) (*see Notes 18 and 19*). For generating proteo-GUVs, apply 5  $\mu$ L of the proteoliposome solution (*see Subheading 3.1*) on each grid. Make sure to spread the 5  $\mu$ L not just on one side of the grid but also on the other side.
4. To generate proteo-GUVs, dry lipids on platinum grids in a desiccator for at least 60 min at room temperature. This step is omitted for the preparation of pure lipid GUVs as the chloroform quickly evaporates.
5. Fill 1 mL of prewarmed 255 mM sucrose into cuvette. Mix the solution before use.
6. Submerge grids in a parallel way with a distance of 5 mm in the cuvette. Use adhesive tape to fix the top of the cuvette if the top does not fit perfectly. Attach (and fix) the grids and connect them to the power supply (Fig. 1).

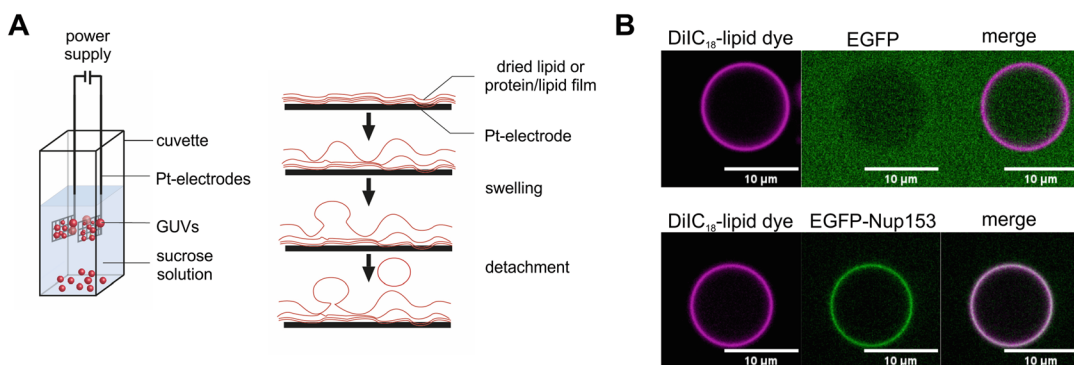


**Fig. 1** GUV assay. (a) Scheme for GUV preparation. Platin grids as electrodes with dried lipid or protein/lipid mixtures are immersed in a cuvette with a sucrose solution and an alternating voltage applied. By that the swelling of the lipid film, formation of large vesicles and their detachment is facilitated. (b) GUVs with a nuclear envelope lipid mixture, identified by the red DiIc18 membrane dye, were incubated with 0.5  $\mu\text{M}$  free EGFP or EGFP fused to the membrane binding domain of Nup153 (aa 1-149). The GUVs were imaged on a Nikon Ti2E spinning disc confocal microscope with 60 $\times$  Lambda Oil 1.4NA objective with light emission at 515 nm after excitation at 470 nm for EGFP and 578 nm excitation/641 nm emission for membrane dye DiIc18

7. For electroformation, apply 2 V, 10 Hz of alternating electric field for 1 h 20 min. Then decrease the frequency to 2 Hz for 20 min.
8. In the meantime, block the chambered cover glass with 5% (w/v) lipid-free BSA in PBS for 1 h, and wash 5 $\times$  with PBS.
9. Stop electroformation and cool down the chamber to room temperature for approximately 5 min (*see Note 20*).
10. Fill 150  $\mu\text{L}$  of PBS into chambered cover glass; transfer 20–30  $\mu\text{L}$  of GUVs onto PBS layer (*see Note 21*).
11. Wait for 5 min for GUVs to sink (*see Note 22*).
12. Analyze GUVs and their behavior by microscopy. Soluble proteins can be studied for deformation or GUV interaction by adding them to the chambered cover glass.

### 3.3 Preparation of GUVs Using PVA Method

1. Clean the glass microscope slides before coating (preferably overnight in glass cleaner (e.g., 2% Mucosol), followed by ddH<sub>2</sub>O and ethanol, and then dry.
2. Mark two circular areas of approx. 1 cm<sup>2</sup> on the reverse side of a microscope slide with a pen (*see Note 23*).
3. On the other microscope glass side, evenly coat the marked areas with 2  $\mu\text{L}$  of 5% PVA solution each (Fig. 2a, b); then dry for 30 min at 60  $^{\circ}\text{C}$  preferably on a heating block (*see Note 24*).
4. Dilute the chloroform-dissolved lipids (e.g., NE-lipid mixture, *see Tables 1, 2, 3 and 4*) 1:10 with chloroform to a final concentration of 1 mg/mL, and spread 3  $\mu\text{L}$  of lipid mixture

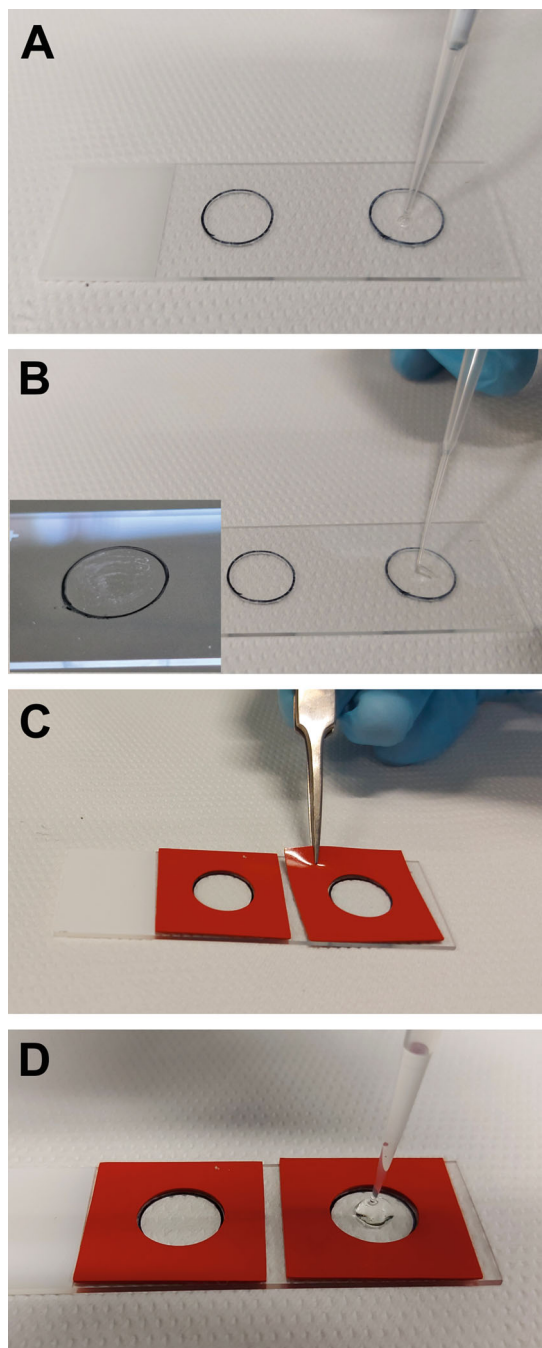


**Fig. 2** Steps of the gel-assisted GUV preparation using PVA. **(a, b)** On a glass microscope slide on two spots encircled with a pen, the PVA solution is brought up and evenly distributed (see inset for thin the PVA film). After drying, the lipids are brought up on the PVA film (not shown). **(c)** The silicone isolators are placed on the PVA coated area with the lipid film. **(d)** Buffer is brought up to the PVA coated area with the lipid film and incubated to form GUVs by rehydration

(e.g., NE-lipid) from 1 mg/mL solution in chloroform or 2  $\mu$ L of proteoliposome solution (*see* Subheading 3.1) evenly on each dried PVA matrix (*see* **Note 25**).

5. Dry the lipids on the gel matrix for at least 1 h in a desiccator.
6. Seal the two matrices with the silicone isolators (Fig. 2c), and incubate the PVA coatings with the lipids each with 90  $\mu$ L of buffer (e.g., PBS) for 1 h at room temperature (Fig. 2d). During this time, the resulting GUVs (proteo-GUVs) are transferred to the buffer (*see* **Note 26**).
7. After 1 h incubation, the GUV-containing buffer is removed from both matrices and transferred to an 8-well chambered cover glass coated with 5% BSA solution.
8. Analyze the GUVs by microscopy.

### 3.4 GUV Imaging

1. Select the light path in confocal mode and the 60 $\times$  1.4NA oil objective.
2. Place the well with the GUVs to be imaged on the objective, and find the focal plane using the ocular and epifluorescence illumination (*see* **Note 27**).
3. When studying the interaction between GUVs and proteins, the proteins should be added to the well with GUVs at this point. After a short incubation of approx. 10 min for equilibration, you can start imaging.
4. Set up the illumination conditions according to labeling (membrane dye, fluorescence-labeled, or fluorescence fusion protein).
5. Start image capture and save the data.

### 3.5 Image Analysis

1. Use Fiji (ImageJ) to extract and assemble multichannel image (galleries) from original files (*see* **Notes 28 and 29**).
2. Quantitative measurement of signal intensities can be extracted using ROIs of the fluorescence of the GUV using the Fiji “segmented line” tool and the ROI manager. The values can be exported as .csv or excel tables for further processing (*see* **Note 30**).

---

## 4 Notes

1. Protein expressed in *E. coli* and affinity-purified using Ni-agarose. Described in detail in [31].
2. The volume of the membrane protein to be added depends on its nature and concentration and needs to be optimized. We typically employ as a start 10  $\mu$ L of protein with a concentration

of 1 mg/mL. If aggregation is observed on the gel filtration column, reduce the amount of membrane protein.

3. The fluorescence of Marina Blue fades relatively quickly.
4. Make 1 mL mixture: weigh lipids into Eppendorf tube (*see* Table 5). Dissolve the solid lipid mixture in 10% octyl- $\beta$ -D-glucopyranoside, shaking for approx. 2 h, at room temperature, 1000 rpm in a shaker (e.g., Thermomixer). 100  $\mu$ L aliquots can be snap-frozen and stored at  $-80^{\circ}\text{C}$  for at least 1 year.
5. 1 mL aliquots can be stored at  $-20^{\circ}\text{C}$ .
6. This solution is isosmotic to PBS. If required, check this on an osmometer.
7. Rinse glassware with  $\text{CHCl}_3$  before use.
8. Pipette the lipids dissolved in chloroform into a screw glass vial using glass pipettes.
9. Prepare a solution at high temperature, e.g., in ThermoMixer at  $80^{\circ}\text{C}$ . PVA stocks can be stored at  $-20^{\circ}\text{C}$ .
10. The GUVs can move slightly in the well. As GUV image recording with a spinning disc confocal microscope is faster than with a laser scanning confocal microscope, we prefer this option. Alternatively, GUVs containing a low amount of biotinylated lipids can be immobilized on a streptavidin-coated surface [32].
11. Do not let the column run dry; otherwise it needs to be replaced.
12. Placing a white paper behind the column helps identify the faster migrating liposome fraction.
13. Collect the fraction of proteoliposome directly into the centrifuge tubes. For the Econo-columns, we typically collect about 12 drops (drop numbers 17–28 if counted after the loaded fraction has completely entered the gel matrix).
14. Do not collect too many drops of proteoliposomes. If mixed with the later eluting detergent containing bulk lipid dye fraction, proteoliposomes are re-solubilized.
15. The proteoliposome can be used directly or 5  $\mu$ L aliquots can be snap frozen in liquid nitrogen and stored at  $-80^{\circ}\text{C}$ .
16. In case precipitated material is deposited in the upper part of the gel matrix, remove, and substitute this and block column again by passing 100  $\mu$ L of 1 (w/v) % lipid-free BSA in PBS over the column.
17. Block the column material by passing 100  $\mu$ L of 1 (w/v) % lipid-free BSA solution in PBS, before first use. It is also recommended to reconstitute first empty liposomes to test

the column, i.e., use 100  $\mu\text{L}$  PBS and 20  $\mu\text{L}$  NE lipid-detergent mixture (*see Step 3* in Subheading 3.3).

18. Avoid contact of plastic materials with chloroform.
19. If needed, one can include a membrane staining at this point: e.g., add 0.4  $\mu\text{L}$  of 1 mg/mL DiIC18 to 40  $\mu\text{L}$  lipid mixture.
20. Use a glass vial; work quickly as chloroform evaporates fast.
21. Before removing the Pt-grids, tap the cuvette lightly so that the GUVs come off the Pt-grids more easily.
22. Use wide-bore tips.
23. As the GUVs are filled with 255 mM sucrose, they will slowly sink in the PBS solution because of their higher buoyant density.
24. Use of a silicone seal later used as a model (Fig. 2c).
25. The prepared glasses can be stored before use for 3–4 weeks.
26. Only use glass capillaries or glass syringes for lipids dissolved in chloroform.
27. To avoid excessive buffer loss, do not allow air bubbles to form between the silicone and glass.
28. Albeit the GUVs slowly settle down, they can be found at different levels.
29. Fiji/ImageJ is a standalone multipurpose image analysis program.
30. Channels and brightness/contrast tools can be used.

## References

1. Lin DH, Hoelz A (2019) The structure of the nuclear pore complex (an update). *Annu Rev Biochem* 88:725–783. <https://doi.org/10.1146/annurev-biochem-062917-011901>
2. Yang Y, Guo L, Chen L et al (2023) Nuclear transport proteins: structure, function, and disease relevance. *Signal Transduct Target Ther* 8(1):425. <https://doi.org/10.1038/s41392-023-01649-4>
3. Dultz E, Wojtynek M, Medalia O et al (2022) The nuclear pore complex: birth, life, and death of a cellular behemoth. *Cells* 11(9). <https://doi.org/10.3390/cells11091456>
4. Mosalaganti S, Obarska-Kosinska A, Siggel M et al (2022) AI-based structure prediction empowers integrative structural analysis of human nuclear pores. *Science* 376(6598): eabm9506. <https://doi.org/10.1126/science.abm9506>
5. Hamed M, Antonin W (2021) Dunking into the lipid bilayer: how direct membrane binding of nucleoporins can contribute to nuclear pore complex structure and assembly. *Cells* 10(12). <https://doi.org/10.3390/cells10123601>
6. Vollmer B, Lorenz M, Moreno-Andres D et al (2015) Nup153 recruits the Nup107-160 complex to the inner nuclear membrane for interphasic nuclear pore complex assembly. *Dev Cell* 33(6):717–728. <https://doi.org/10.1016/j.devcel.2015.04.027>
7. Amm I, Weberruss M, Hellwig A et al (2023) Distinct domains in Ndc1 mediate its interaction with the Nup84 complex and the nuclear membrane. *J Cell Biol* 222(6). <https://doi.org/10.1083/jcb.202210059>
8. Dimova R, Aranda S, Bezlyepkina N et al (2006) A practical guide to giant vesicles. Probing the membrane nanoregime via optical microscopy. *J Phys Condens Matter* 18(28): S1151–S1176. <https://doi.org/10.1088/0953-8984/18/28/s04>

9. Walde P, Cosentino K, Engel H et al (2010) Giant vesicles: preparations and applications. *Chembiochem* 11(7):848–865. <https://doi.org/10.1002/cbic.201000010>
10. Wollert T, Hurley JH (2010) Molecular mechanism of multivesicular body biogenesis by ESCRT complexes. *Nature* 464(7290):864–869. <https://doi.org/10.1038/nature08849>
11. Wollert T, Wunder C, Lippincott-Schwartz J et al (2009) Membrane scission by the ESCRT-III complex. *Nature* 458(7235):172–177. <https://doi.org/10.1038/nature07836>
12. Bacia K, Futai E, Prinz S et al (2011) Multi-budded tubules formed by COPII on artificial liposomes. *Sci Rep* 1:17. <https://doi.org/10.1038/srep00017>
13. Lorenz M, Vollmer B, Unsay JD et al (2015) A single herpesvirus protein can mediate vesicle formation in the nuclear envelope. *J Biol Chem* 290(11):6962–6974. <https://doi.org/10.1074/jbc.M114.627521>
14. Zeev-Ben-Mordehai T, Weberuss M, Lorenz M et al (2015) Crystal structure of the herpesvirus nuclear egress complex provides insights into inner nuclear membrane remodeling. *Cell Rep* 13(12):2645–2652. <https://doi.org/10.1016/j.celrep.2015.11.008>
15. Litschel T, Ramm B, Maas R et al (2018) Beating vesicles: encapsulated protein oscillations cause dynamic membrane deformations. *Angew Chem Int Ed Eng* 57(50):16286–16290. <https://doi.org/10.1002/anie.201808750>
16. Baumgart T, Hess ST, Webb WW (2003) Imaging coexisting fluid domains in biomembrane models coupling curvature and line tension. *Nature* 425(6960):821–824. <https://doi.org/10.1038/nature02013>
17. Sezgin E, Levental I, Grzybek M et al (2012) Partitioning, diffusion, and ligand binding of raft lipid analogs in model and cellular plasma membranes. *Biochim Biophys Acta* 1818 7:1777–1784. <https://doi.org/10.1016/j.bbmem.2012.03.007>
18. Bacia K, Schuette CG, Kahya N et al (2004) SNAREs prefer liquid-disordered over “raft” (liquid-ordered) domains when reconstituted into giant unilamellar vesicles. *J Biol Chem* 279(36):37951–37955. <https://doi.org/10.1074/jbc.M407020200>
19. Bacia K, Schwille P, Kurzchalia T (2005) Sterol structure determines the separation of phases and the curvature of the liquid-ordered phase in model membranes. *Proc Natl Acad Sci USA* 102(9):3272–3277. <https://doi.org/10.1073/pnas.0408215102>
20. Sezgin E, Schwille P (2012) Model membrane platforms to study protein-membrane interactions. *Mol Membr Biol* 29(5):144–154. <https://doi.org/10.3109/09687688.2012.700490>
21. Jalmar O, García-Sáez AJ, Berland L et al (2010) Giant unilamellar vesicles (GUVs) as a new tool for analysis of caspase-8/Bid-FL complex binding to cardiolipin and its functional activity. *Cell Death Dis* 1(12):e103. <https://doi.org/10.1038/cddis.2010.81>
22. Prevost C, Zhao H, Manzi J et al (2015) IRSp53 senses negative membrane curvature and phase separates along membrane tubules. *Nat Commun* 6:8529. <https://doi.org/10.1038/ncomms9529>
23. van Buren L, Koenderink GH, Martínez-Torres C (2023) DisGUVery: a versatile open-source software for high-throughput image analysis of giant unilamellar vesicles. *ACS Synth Biol* 12(1):120–135. <https://doi.org/10.1021/acssynbio.2c00407>
24. Jorgensen IL, Kemmer GC, Pomorski TG (2017) Membrane protein reconstitution into giant unilamellar vesicles: a review on current techniques. *Eur Biophys J* 46(2):103–119. <https://doi.org/10.1007/s00249-016-1155-9>
25. Manley S, Gordon VD (2008) Making giant unilamellar vesicles via hydration of a lipid film. *Current protocols in cell biology* Chapter 24: Unit 24.23. <https://doi.org/10.1002/0471143030.cb2403s40>
26. Angelova MI, Dimitrov DS (1986) Liposome electroformation. *Faraday Discuss* 81:303. <https://doi.org/10.1039/Dc9868100303>
27. Herold C, Chwastek G, Schwille P et al (2012) Efficient electroformation of supergiant unilamellar vesicles containing cationic lipids on ITO-coated electrodes. *Langmuir* 28(13):5518–5521. <https://doi.org/10.1021/la3005807>
28. Matosevic S (2012) Synthesizing artificial cells from giant unilamellar vesicles: state-of-the art in the development of microfluidic technology. *BioEssays* 34(11):992–1001. <https://doi.org/10.1002/bies.201200105>
29. Karamdad K, Law RV, Seddon JM et al (2015) Preparation and mechanical characterisation of giant unilamellar vesicles by a microfluidic

- method. *Lab Chip* 15(2):557–562. <https://doi.org/10.1039/c4lc01277a>
30. Eisenhardt N, Redolfi J, Antonin W (2014) Interaction of Nup53 with Ndc1 and Nup155 is required for nuclear pore complex assembly. *J Cell Sci* 127(Pt 4):908–921. <https://doi.org/10.1242/jcs.141739>
31. Eisenhardt N, Schooley A, Antonin W (2014) Xenopus in vitro assays to analyze the function of transmembrane nucleoporins and targeting of inner nuclear membrane proteins. *Methods Cell Biol* 122:193–218. <https://doi.org/10.1016/b978-0-12-417160-2.00009-6>
32. Di Iorio D, Lu Y, Meulman J et al (2020) Recruitment of receptors at supported lipid bilayers promoted by the multivalent binding of ligand-modified unilamellar vesicles. *Chem Sci* 11(12):3307–3315. <https://doi.org/10.1039/d0sc00518e>



## One-Pot Reconstitution of GPCRs into Unilamellar Vesicles for Fluorescence-Based Phospholipid Scramblase Activity Assay

Indu Menon and Anant K. Menon

### Abstract

Scramblases are membrane proteins that translocate phospholipids bidirectionally between the leaflets of a membrane bilayer. Examples of scramblases include Class A G protein-coupled receptors (GPCRs), members of the TMEM16 and DedA protein families, and protein insertases. To measure scramblase activity, the protein of interest is purified and reconstituted into large unilamellar vesicles that contain trace amounts of a fluorescent phospholipid reporter. The activity assay reports on the translocation of fluorescent lipids from the inner to the outer leaflet of the vesicles by using a membrane-impermeant reducing agent to eliminate the fluorescence of only those molecules that can reach the outer leaflet. Here we describe a one-pot reconstitution protocol whereby phospholipids, solubilized in the non-ionic detergent CHAPS, are combined with a purified GPCR to generate mixed micelles and then treated with detergent-adsorbing polystyrene beads (SM2 BioBeads) to yield proteoliposomes. The proteoliposomes are extruded to generate a more homogeneously sized, unilamellar population suitable for activity assays. We describe protocols for measuring the protein and phospholipid content of the vesicles and for assaying scramblase activity.

**Key words** CHAPS, Dithionite, Fluorescence, GPCR, Opsin, Liposome, Phospholipid, Reconstitution, Scramblase

---

### 1 Introduction

Scramblases are membrane proteins that translocate phospholipids bidirectionally between the leaflets of a membrane bilayer [1–4]. No metabolic energy is required for their activity, i.e., they are ATP-independent. Examples of phospholipid scramblases include Class A G protein-coupled receptors (GPCRs) [5, 6]; members of the TMEM16 [7–9], Xkr [10], and DedA [11–13] protein families; the autophagosomal protein Atg9 [14]; protein insertases [15, 16]; and the voltage-dependent anion channel [17]. Scramblases are important for membrane biogenesis where they facilitate the trans-bilayer equilibration of phospholipids that are synthesized in—or

delivered to—the cytoplasmic leaflet of an organellar membrane. They are also implicated in the regulated loss of the transbilayer lipid asymmetry of the plasma membrane, resulting in cell surface exposure of the signaling lipid phosphatidylserine.

Scramblase activity can be assessed in cells—this is convenient for those scramblases that act at the plasma membrane—but is more typically quantified after detergent-mediated reconstitution of purified proteins into large unilamellar vesicles containing trace quantities of radioactive or fluorescent phospholipids that serve as transport reporters. These tracer lipids are interrogated in the outer leaflet of the vesicles by topological probes, i.e., reagents that cannot enter the vesicles. Thus, only 50% of the tracers (corresponding to the pool located in the outer leaflet) will be detected in a vesicle that lacks scramblase activity. For scramblase-active vesicles, 100% of the tracers will be detected as those lipids in the inner leaflet will be translocated to the outer leaflet by the scramblase.

The activity assay outlined above is often used simply to determine whether a particular protein has scramblase activity, in comparison with a control protein which lacks activity. Thus, reconstitutions are carried out using sufficient protein such that the average number of proteins per vesicle is 10; given the stochastic nature of the reconstitution process, this implies that all vesicles have at least one scramblase. This yields a binary outcome: for protein-free liposomes and liposomes reconstituted with the control protein, only 50% of the tracer lipid is detected, whereas for a scramblase candidate, 100% of the tracer is detected. In this format, the assay can be used to screen for scramblase activity as was done recently for different protein insertases [15]. Once scramblase activity is established, more detailed experiments can be performed. For example, the amount of protein can be varied to characterize the reconstitution [17–19], and the lipid composition of the vesicles can be varied to determine how this affects scrambling [20]. It may also be possible to extract the kinetics of scrambling if the rate of scrambling is lower than that of the reaction used to interrogate the tracer lipid [9].

Here we describe a one-pot reconstitution protocol whereby phospholipids, solubilized in the non-ionic detergent CHAPS, are combined with a purified scramblase protein to generate mixed micelles and then treated with detergent-adsorbing polystyrene beads (SM2 BioBeads) to yield proteoliposomes. The proteoliposomes are extruded to generate a more homogeneously sized, unilamellar population suitable for activity assays. We go on to describe protocols for measuring the protein and phospholipid content of the vesicles and for assaying and analyzing scramblase activity. This one-pot protocol is simpler than a commonly used complementary protocol in which liposomes are first prepared and

then destabilized with detergent to permit reconstitution of protein [21, 22].

## 2 Materials

Prepare all buffers and reagents with double distilled, deionized water.

### 2.1 BioBeads Preparation

1. Reconstitution Buffer: 50 mM HEPES, pH 7.4, 150 mM NaCl.
2. BioBeads SM-2 Adsorbent Media (Bio-Rad 152-3920).
3. Methanol.
4. Glass beaker.
5. Smooth magnetic stir bar.

### 2.2 Vesicle Preparation

1. 1-palmitoyl-2-oleoyl-glycero-3-phosphocholine (POPC, Avanti Polar Lipids 850457C, 25 mg/mL).
2. 1-palmitoyl-2-oleoyl-sn-glycero-3-phospho-(1'-rac-glycerol) (POPG, Avanti Polar Lipids 840457C, 25 mg/mL).
3. 1-palmitoyl-2-{6-[(7-nitro-2-1,3-benzoxadiazol-4-yl)amino]hexanoyl}-sn-glycero-3-phosphocholine (NBD-PC, Avanti Polar Lipids 810130C, 1 mg/mL).
4. Glass tubes 13 × 100 mm (VWR 47729-572).
5. Hamilton syringes for transferring lipids in chloroform.
6. Nitrogen gas for drying.
7. Pentane.
8. CHAPS detergent (Anatrace C316).
9. Vibrax VXR agitator with test-tube attachment (IKA, VWR 444-0022).
10. Bath Sonicator (Elmasonic P30H).
11. 2 mL and 1.5 mL micro tubes.
12. Purified scramblase. We use opsin here, purified as described in ref. [20]. The protein is prepared in 0.1% (w/v) n-dodecyl-β-D-maltoside, 20 mM Hepes pH 7.5, and 150 mM NaCl at a concentration of 0.15 mg/mL (3.75 μM).
13. Handheld mini extruder (Avanti, 6100000).
14. 200 nm pore size polycarbonate filter (GE Healthcare Whatman Nucleopore Track-Etch Membrane 10417004).
15. Sodium dithionite (Sigma-Aldrich 15795305G, molecular weight 174.11); weigh out aliquots (≥10 mg) to make at least 55 μL of a 1 M solution (9.6 mg/55 μL). Dissolve the aliquots in 0.5 M Tris base (pH 10) just before use.

**2.3 Scramblase Assay**

1. Spectrofluorimeter (e.g., Horiba, FluoroMax), equipped with a temperature controller, stirring mechanism, and lid with an injection port.
2. Disposable plastic standard cuvettes for fluorescence measurement, fluorimeter polystyrene cuvettes (Sigma-Aldrich C918-100EA).
3. Mini magnetic stir bars (“fleas” VWR 80062-122).

**2.4 Analysis of Scramblase Activity Data**

1. Microsoft Excel software.
2. GraphPad Prism software.

**2.5 Estimating the Average Number of Proteins Reconstituted per Vesicle**

1. UV-Vis Spectrophotometer.
2. Sodium phosphate, dibasic, anhydrous ( $\text{Na}_2\text{HPO}_4$ ).
3. Perchloric acid (70–72%) (Sigma 30755).
4. Ammonium molybdate tetrahydrate (EMD AX1310-3).
5. L-Ascorbic acid (Sigma A5960).
6. Heating block.
7. Glass tubes.
8. Glass marbles (Fisher Scientific S04581).
9. Solvent-compatible polypropylene tubes.
10. 1% SDS in water
11. Micro BCA™ Protein Assay Kit (ThermoFisher 23235).
12. Bovine serum albumin (BSA).
13. Image J/Fiji software.

---

**3 Methods**

The procedure described here is for the preparation of two 1 mL samples of liposomes, one without protein (“control”) and the other with the scramblase. The size of each sample can be reduced to 0.5 mL, but the preparation time is the same. The basic procedure, adapted from Levy et al. [23, 24], involves combining phospholipids and detergent, with or without protein, to generate mixed micelles. These are then treated with SM2 BioBeads to remove detergent. Finally, the resulting vesicles are extruded to generate a more homogeneous, unilamellar sample suitable for activity assays. The protocol—illustrated as a flow chart in Fig. 1a—is typically initiated in the afternoon of Day 1 to yield extruded vesicles in the late morning of Day 2. The extruded vesicles may be concentrated by ultracentrifugation if needed [20].

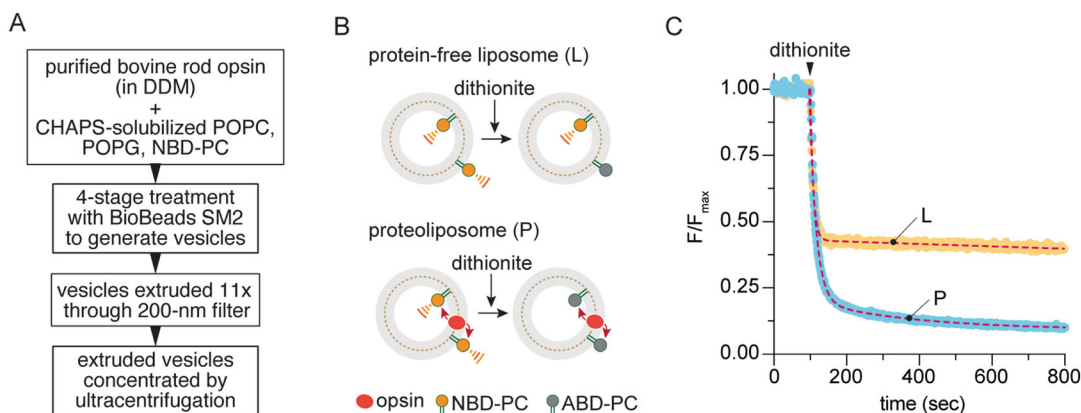


**Fig. 1** Reconstitution protocol and scramblase assay. **(a)** Reconstitution protocol. *See text for details.* Vesicles are used after extrusion but may be concentrated by ultracentrifugation if needed. **(b)** Scramblase assay. Protein-free liposomes (L) or opsin proteoliposomes (P) containing a trace amount (0.5 mol %) of fluorescent NBD-PC are treated with dithionite. Dithionite converts the nitro group in the NBD fluorophore of NBD-PC molecules in the outer leaflet of the vesicles to an amino group; the resulting non-ABD-PC is non-fluorescent. The extent of fluorescence loss is expected to be 50% for protein-free liposomes as dithionite cannot access NBD-PC molecules in the inner leaflet during the time frame of the assay and 100% for opsin-containing vesicles in which NBD-PC molecules are scrambled between leaflets. **(c)** Scramblase assay traces for L and P vesicles. Fluorescence ( $\lambda_{\text{ex}} = 470 \text{ nm}$ ,  $\lambda_{\text{em}} = 530 \text{ nm}$ ) was recorded at a frequency of 1 Hz for 100 s to obtain a stable initial value ( $F_{\max}$ ) before adding dithionite and monitoring fluorescence decay. The dashed lines superimposed on the data points correspond to exponential decay fits (constrained to an initial value of  $F/F_{\max} = 1.0$ ), a single exponential decay plus a linear component for L and a double exponential for P. The plateau values from the fits are 0.43 and 0.09, for L and P, respectively. (The figure is adapted from Ref. [20])

### 3.1 BioBeads Preparation

1. Weigh 2 g of BioBeads in a 100 mL glass beaker (*see Note 1*).
2. Add 50 mL of methanol and stir the beads gently for 15 min at room temperature (*see Note 2*).
3. Let the beads settle and pour off most off the methanol, disposing appropriately.
4. Repeat the methanol wash.
5. Wash the beads with double distilled water (50 mL water, 15 min stirring per wash). Remove the water using a plastic or a glass pipette as the beads do not settle easily.
6. Repeat the water wash two more times.
7. Wash once with 50 mL Reconstitution Buffer.
8. Remove the buffer using a plastic or a glass pipette and store the washed beads in Reconstitution Buffer at 4 °C (*see Note 3*).

### 3.2 Vesicle Preparation

Carry out the following procedures under low light as far as possible to avoid bleaching the fluorescent lipid. It is enough to reduce room lighting and draw window blinds.

1. For each 1 mL reconstitution, use 12 mg (16  $\mu$ mol) of lipids as follows: transfer 432  $\mu$ L POPC, 48  $\mu$ L POPG, and 60  $\mu$ L NBD-PC to a 13  $\times$  100 glass tube using Hamilton syringes of the appropriate capacity. Rinse the syringes several times in chloroform before and after use. The final molar proportion of lipids is 9:1:0.05 (POPC:POPG:NBD-PC).
2. Dry the lipids under a gentle stream of nitrogen for 30 min (*see Note 4*).
3. Add approximately 1 mL pentane to the dried lipids using a glass pasteur pipette. Vortex gently to dissolve.
4. Dry under a gentle stream of nitrogen for 30 min.
5. Add 0.6 mL of 70 mM CHAPS (prepared in Reconstitution Buffer), and parafilm the top of the tube.
6. Using a Vibrax agitator, shake the tube at 1500 rpm for 15 min at room temperature (*in lieu* of Vibrax agitation, samples can be vortexed intermittently until the dried film is dissolved).
7. Sonicate the samples in a bath sonicator (37 Hz, 100% power, pulse mode) for 10 min or longer until clarity is achieved.
8. Add 0.6 mL of Reconstitution Buffer to give 10 mg/mL lipids in 35 mM CHAPS.
9. Transfer 0.9 mL of the lipid solution (9 mg (12  $\mu$ mol) lipids) to a 2 mL Eppendorf tube.
10. For the proteoliposome sample, add 15  $\mu$ g (100  $\mu$ L, 0.375 nmol) of opsin or equivalent mole amount of another scramblase (*see Note 5*).
11. For the protein-free liposome sample, add 100  $\mu$ L 0.1% (w/v) n-dodecyl- $\beta$ -D-maltoside, 20 mM Hepes pH 7.4, and 150 mM NaCl (or, if using a different scramblase preparation, then the same buffer as used to supply the protein) (*see Note 6*).
12. Place the samples on an end-over-end rotator and mix for 30 min at room temperature.
13. Add 140 mg of the prepared BioBeads and mix end-over-end at 4  $^{\circ}$ C for 2 h (BioBeads-1).
14. Transfer the suspension to a fresh 2 mL Eppendorf tube and add 140 mg of BioBeads. Mix end-over-end at 4  $^{\circ}$ C for 2 h (BioBeads-2).
15. Transfer the suspension to a fresh 2 mL Eppendorf tube and add 140 mg of BioBeads. Mix end-over-end at 4  $^{\circ}$ C overnight (BioBeads-3).
16. Transfer the suspension to a fresh 2 mL Eppendorf tube and add 140 mg of BioBeads. Mix end-over-end at 4  $^{\circ}$ C for 2 h (BioBeads-4).

17. Transfer the now turbid suspension, containing liposomes or proteoliposomes, to a  $13 \times 100$  mm glass tube. Make sure that no BioBeads are transferred.
18. Assemble an Avanti handheld mini extruder with a 200 nm pore size polycarbonate filter, and use the provided gas-tight syringes to pass Reconstitution Buffer through the apparatus (*see* **Note 7**).
19. Collect the suspension in a mini extruder syringe (*see* **Note 8**) and extrude 11 times at room temperature.
20. Store the vesicles at 4 °C until use (*see* **Notes 9–11**).

### 3.3 Scramblase Assay

The scramblase assay is illustrated schematically in Fig. 1b, and sample data are shown in Fig. 1c. The reconstituted vesicles prepared in Methods Subheading 3.2 contain fluorescent NBD-PC lipids that are distributed symmetrically between the two leaflets of the bilayer. The NBD fluorophore is susceptible to chemical reduction by dithionite, a negatively charged reagent that does not easily cross membranes. On reduction, the nitro group of the NBD fluorophore is converted to an amino group, eliminating fluorescence irreversibly. Thus, on adding dithionite to protein-free liposomes, NBD-PC molecules in the outer leaflet of the vesicles will be bleached, whereas those in the inner leaflet will be protected. This results in a loss of fluorescence of slightly more than 50% as the outer leaflet of the vesicles has a slightly larger surface area and hence more NBD-PC molecules. For proteoliposomes equipped with a scramblase, NBD-PC molecules from the inner leaflet will be translocated to the outer leaflet where they will be bleached by dithionite—in this case, the extent of fluorescence reduction is expected to be 100%. The rate of fluorescence decay after dithionite addition is usually similar in liposomes and proteoliposomes, indicating that scrambling occurs at the same rate (or faster) than the rate of the chemical reaction that results in bleaching of the NBD fluorophore.

1. Set up the fluorimeter with the following parameters: Excitation and emission wave lengths, 470 nm and 530 nm, respectively; excitation and emission slit widths 2 nm (or adjust to obtain an appropriate signal, in the range  $10^5$ – $10^6$  counts per second); temperature 25 °C (or as needed); stirring speed 900 rpm; data acquisition frequency 1 Hz; total acquisition time 10 min (or as needed).
2. Add a 50  $\mu$ L aliquot of liposomes or proteoliposomes to 2.45 mL of Reconstitution Buffer in a fluorimeter cuvette equipped with a magnetic stir bar(flea) and start recording. Monitor the fluorescence signal for 2–5 min, or until it is stable. Terminate the recording and start a fresh recording for the next step (*see* **Note 12**).

- Record fluorescence for 100 s, then add 50  $\mu\text{L}$  of freshly prepared 1 M dithionite (final concentration 20 mM) through the injection port in the lid of the fluorimeter, and continue recording fluorescence for a further 500–800 s (*see Note 13*).

### 3.4 Analysis of Scramblase Activity Data

- Export the fluorimeter data to Microsoft Excel in the form of columns corresponding to time and associated fluorescence values. Determine the average of the first 100 s of the fluorescence recording (up to the point at which dithionite is added). Divide this value by 1.02 to obtain  $F_{\text{max}}$  (the scale factor corrects for the subsequent drop in signal resulting from dilution when adding 50  $\mu\text{L}$  dithionite to 2.5 mL sample).
- Normalize the fluorescence values ( $F$ ) from the recording by dividing by  $F_{\text{max}}$  and plot  $F/F_{\text{max}}$  versus time (s), with  $t = 0$  corresponding to the time of dithionite addition. It is convenient to use GraphPad Prism software for this purpose, but any suitable graphing program will do. Figure 1c shows fluorescence traces for a typical scrambling assay. Complete traces are shown, including the initial fluorescence recording which establishes  $F_{\text{max}}$ . Dithionite addition prompts loss of fluorescence, reaching different extents for the protein-free liposome (L) and proteoliposome (P) samples.
- The greater extent of fluorescence loss in the proteoliposome sample indicates the presence of a scramblase in the majority of the vesicles. The traces are modeled using single- and double-exponential decay functions for the L and P samples, respectively, constrained to an initial value of  $F/F_{\text{max}} = 1.0$ . Modeling is easily accomplished using GraphPad Prism software. As described in Ref. [18], the L trace is sometimes better fit with a single exponential, modified by a linear component as follows:  $F/F_{\text{max}}(t) = (1 - \text{Plateau}) \cdot \exp(-K \cdot t) + \text{Plateau} - S \cdot t$ , where  $F/F_{\text{max}}(t)$  = fluorescence at time  $t$ ,  $t = 0$  s is the time of dithionite addition, and  $S$  = absolute value of the slope of the linear component (typically of the order of  $10^{-4} \text{ s}^{-1}$ ). The linear component corrects for slow processes that result in fluorescence loss, for example, dithionite leakage or NBD photobleaching. The P trace shown in Fig. 1c has two components, which can be interpreted as follows: a fast component (half-time 10 s) corresponding to the dithionite-mediated reduction of the NBD fluorophore and a slow component (half-time 200 s) associated with scrambling of NBD-PC from the inner to the outer leaflet. In many instances, the P trace shows monophasic behavior (e.g., TMEM16 scramblase in the presence of  $\text{Ca}^{2+}$  [9], or recombinant opsin produced in HEK293 cells [18, 25]), in which case it is concluded that scrambling occurs as fast or faster than the rate of the dithionite-mediated reduction of NBD (*see Note 14*).

4. Despite reconstitution parameters targeted at obtaining approximately 10 copies of opsin per vesicle on average, with the likelihood that all vesicles have at least one scramblase, fluorescence decay for the proteoliposome sample is incomplete, indicating that a fraction of the vesicles is refractory to reconstitution [18]. The fraction of vesicles ( $f$ ) containing a functional scramblase can be calculated as  $f = 1 - \text{Plateau(P)}/\text{Plateau(L)}$  from the exponential fit-derived plateau values, Plateau(P) and Plateau(L) of fluorescence obtained after dithionite treatment of proteoliposomes and matched protein-free liposomes, respectively. For the example shown in Fig. 1c, Plateau(P) and Plateau(L) are 0.09 and 0.43, respectively, and therefore the fraction of scramblase-active vesicles in the  $P$  sample is  $f = 0.79$ , i.e., approximately 80% of the vesicles have scramblase activity.

### 3.5 Estimating the Average Number of Proteins Reconstituted per Vesicle

The reconstitution protocol is set up to generate vesicles with approximately 10 proteins per vesicle on average. Thus, vesicles are generated by combining 15  $\mu\text{g}$  (0.375 nmol) of opsin with 9 mg (12  $\mu\text{mol}$ ) of phospholipids, corresponding to a protein/phospholipid ratio of 1.25  $\mu\text{g}/\mu\text{mol}$  or 1: 32000 mol/mol. As approximately 320,000 phospholipids comprise a 200 nm diameter vesicle, this corresponds to 10 proteins per vesicle on average. This number is based on the input amounts of protein and phospholipid and can be verified post-reconstitution by assaying phospholipid and protein content of the reconstituted vesicles as described below and, if dynamic light scattering instrumentation is available, by additionally obtaining an estimate of the size of the vesicles (*see Note 15*).

#### 3.5.1 Phospholipid Quantification

The phospholipid concentration of the vesicle samples is measured by hydrolyzing the phospholipids and then using a colorimetric assay to measure the released inorganic phosphate [20, 26]. A set of phosphate standards is processed in parallel. The samples—including the standards—are aliquoted in glass tubes and incubated with perchloric acid at 145 °C for 1 h. Following acid treatment, 1 mL of water is added, and samples are allowed to cool. To the cooled samples, ammonium molybdate and ascorbic acid are added, and color development is allowed to proceed for 10 min at 100 °C. The absorbance of the samples is then measured at 797 nm.

1. Prepare a 40 mM stock solution of  $\text{Na}_2\text{HPO}_4$  in water. This can be stored at 4 °C essentially indefinitely, in a glass tube or vial. Make working solutions of 4 mM and 0.4 mM  $\text{Na}_2\text{HPO}_4$  by sequential ten-fold dilution from the stock.
2. Use the working solutions to prepare a series of standards (0–80 nmol  $\text{Na}_2\text{HPO}_4$ ), in 13  $\times$  100 mm glass tubes. A series of 6 or 7 standards is sufficient, including a tube with no

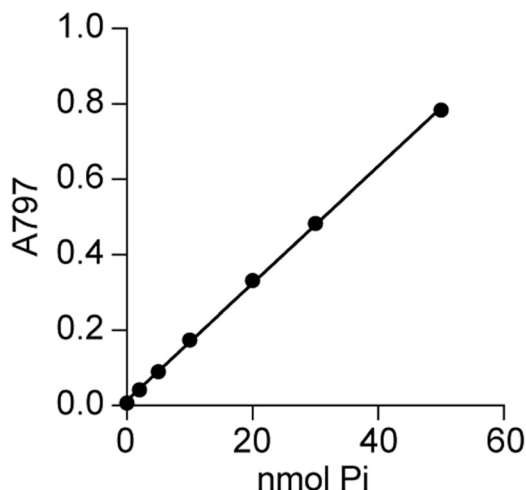


**Fig. 2** Calibration plot for phosphate assay. Inorganic phosphate standards (prepared from 4 mM and 0.4 mM solutions of  $\text{Na}_2\text{HPO}_4$ ) were subjected to perchloric acid treatment and subsequent work-up exactly as described for liposome samples. The color response, measured as absorbance at 797 nm ( $A_{797}$ ), is linear over a 0–80 nmol range (shown here up to 50 nmol phosphate)

$\text{Na}_2\text{HPO}_4$ . The total volume of each standard should be 50  $\mu\text{L}$ . For example, to make a 5 nmol  $\text{Na}_2\text{HPO}_4$  standard, combine 12.5  $\mu\text{L}$  of the 0.4 mM working solution with 37.5  $\mu\text{L}$  water. For a 20 nmol standard, combine 5  $\mu\text{L}$  of the 4 mM working solution with 45  $\mu\text{L}$  water. A table for preparing standards can be found in Ref. [27] (*see Note 16*).

3. Transfer 3  $\mu\text{L}$  of vesicle samples (expected to have 36 nmol phospholipid if recovery is 100%) to 13  $\times$  100 mm glass tubes and add 47  $\mu\text{L}$  water.
4. Add 300  $\mu\text{L}$  perchloric acid to each tube (*see Note 17*).
5. Incubate the tubes at 145  $^\circ\text{C}$  for 1 h in a heating block, with a glass marble on top of each tube to prevent evaporation.
6. Remove the tubes from the heating block, add 1 mL of water to each tube, vortex to mix, and let the samples come to room temperature.
7. Set the heating block to 100  $^\circ\text{C}$ .
8. Make fresh solutions of 12 mg/mL ammonium molybdate and 50 mg/mL ascorbic acid in water.
9. Add 400  $\mu\text{L}$  each of ammonium molybdate and ascorbic acid to the tubes. Vortex to mix.
10. Incubate the tubes at 100  $^\circ\text{C}$  for 10 min. Remove and let the tubes come to room temperature before measuring absorbance at 797 nm using a UV Spectrophotometer (*see Note 18*).

11. Determine the phosphate concentration of the vesicles by comparing with the phosphate standards (Fig. 2).

### 3.5.2 Protein Quantification

Several methods can be used to determine the amount of protein reconstituted into vesicles. As lipids interfere with these measurements, each of the procedures listed below provides a means to eliminate the “lipid background” (*see* **Note 19**). For example:

1. Precipitate a fraction of the reconstituted vesicles using the chloroform/methanol method [28]. It is important to use solvent-compatible polypropylene tubes. Dissolve the resulting protein precipitate in 1% SDS overnight, and measure protein using the Micro BCA™ Protein Assay Kit, which has a linear range of 0–8 µg protein.
2. Use the Kaplan and Pederson assay [29] which measures protein (up to 20 µg) in the presence of high amounts of phospholipid (up to 40 mg) and is therefore well suited to the scale of the reconstitution protocol described here. Proteoliposomes can be used directly for this assay without prior precipitation of protein.
3. Resolve an aliquot (20–30 µL (300–450 ng, based on input protein) will suffice) of the proteoliposomes by SDS-polyacrylamide gel electrophoresis, along with purified protein and bovine serum albumin (BSA) for comparison, and visualize by Coomassie staining. Different amounts of purified protein and BSA, e.g., in the range 0.1–1 µg, should be used and the intensity of Coomassie staining quantified by densitometry using Image J/Fiji software [30] to generate a standard curve. Run an aliquot of protein-free liposomes as a control for any lipid-related artefact affecting the result.
4. Similar to **Step 3** in Subheading 3.5.2 above, use SDS-PAGE-immunoblotting (instead of Coomassie staining) to determine the protein content of proteoliposomes. This requires much less sample.

---

## 4 Notes

1. 840 mg beads are needed per 1 mL reconstitution, but a larger amount is taken as losses occur during washing.
2. Use a small, smooth stir bar and a low stirring speed to avoid generating fines.
3. The beads can be stored in Reconstitution Buffer at 4 °C for at least a week.
4. It is convenient to use a drying manifold for this purpose, but a homemade arrangement works just as well.

5. This results in a protein/phospholipid ratio of 1.25 mg/mmol or 1:32000 mol/mol, or 10 proteins per 200 nm diameter vesicle on average.
6. For **steps 11** and **12**, the amount of buffer brought in by the protein sample should not exceed 100  $\mu$ L. Thus, the protein sample used in **step 11** should have a concentration  $\geq 3.75 \mu$ M.
7. Instructions for using the extruder can be found on the Avanti Polar Lipids website at: <https://avantiresearch.com/products/equipment/category/mini-extruder>.
8. BioBeads will block the syringe, hence the need to take care in the previous step to make sure that the sample does not contain any beads.
9. Reconstituted vesicles appear stable for long periods at 4 °C, but best practice dictates that they should be used within a week.
10. The vesicles that are produced after **Step 20** in Subheading **3.2** can be sized by dynamic light scattering and analyzed by cryoelectron microscopy as described in Ref. [20]. They have an average diameter of roughly 180 nm and are >80% unilamellar, with the remainder corresponding to bilamellar vesicles in which a small vesicle appears trapped within a large unilamellar vesicle [20].
11. Unilamellar vesicles—unlike multilamellar vesicles—will not settle overnight, or even after a few days, so the vesicle suspension should remain visibly uniform in the storage tube. This provides an easy visual corroboration of the quality of the preparation.
12. Separate control liposomes and proteoliposomes can be reconstituted in parallel to test the extent to which dithionite leaks into the vesicles. For these controls, NBD-PC is left out and instead NBD-glucose is included in **Step 2** in Subheading **3.2**. After reconstruction, extravesicular NBD-glucose is removed by dialyzing the vesicles against Reconstitution Buffer or by pelleting the vesicles by ultracentrifugation and resuspending them to the original volume of the sample in Reconstitution Buffer. NBD-glucose that is trapped inside the vesicles should not be susceptible to bleaching by dithionite. See Refs. [9, 12, 19, 25].
13. BSA can be used instead of dithionite as a topological probe. Although the 16:0–06:0 NBD-PC used in the dithionite assay will suffice, it is better to reconstitute vesicles with a shorter chain NBD-PC species (14:0–06:0, Avanti Polar Lipids 810122C) for the BSA-based assay. The short-chain NBD-PC molecules partition to a small extent into the aqueous phase, and from there they can be captured by fatty acid-

free BSA. In complex with BSA, the fluorescence of the NBD-PC is 50% quenched. Thus, when protein-free liposomes are treated with BSA, fluorescence will drop by 25% corresponding to capture of the outer leaflet pool of NBD-PC. For scramblase-equipped proteoliposomes, a 50% drop in fluorescence is expected as all NBD-PC molecules will be captured as those originally in the inner leaflet of the vesicles will be scrambled to the outer leaflet. Examples of this assay can be found in Refs. [5, 9, 17, 19, 25, 31].

14. The fluorescence decay traces obtained on dithionite addition can be analyzed in more detail by considering three pools of NBD-PC: fluorescent lipid in the inner and outer leaflet of vesicles and the non-fluorescent form resulting from dithionite treatment. Such an analysis yields rate constants for the inward and outward scrambling processes, as well as for the dithionite reaction. Examples of this and related analyses can be found in Refs. [32–34].
15. The recovery of both protein and phospholipid after reconstitution is about 60–70%. Thus, the input protein/phospholipid ratio also applies to the final reconstituted vesicle samples.
16. Phosphate standards should be prepared each time a measurement is made.
17. Perchloric acid should be handled in a fume hood, and after completing the assay, all samples should be discarded appropriately.
18. All glass tubes should be placed in the same heating block in **Step 10** in Subheading 3.5.1 as the temperature may vary between individual heating blocks in the same ensemble, affecting the rate of color development.
19. Methods 1–4 described above measure the total amount of protein in the sample, with the assumption that all of the protein is reconstituted into vesicles. This assumption can be verified by floating the vesicles in a density gradient to separate reconstituted protein (which floats with the vesicles) from unincorporated protein (which remains at the bottom of the tube) and then measuring the protein and phospholipid content (as above, and Subheading 3.5) of the “purified” floated vesicles. A protocol for vesicle flotation and subsequent protein and phospholipid analysis is described in Ref. [35].

---

## Acknowledgments

This work was supported by a Research Grant from the Human Frontier Science Program (Ref.-No: RGP009/2023).

## References

1. Pomorski T, Menon AK (2006) Lipid flippases and their biological functions. *Cell Mol Life Sci* 63(24):2908–2921. <https://doi.org/10.1007/s00018-006-6167-7>
2. Wang Y, Kinoshita T (2023) The role of lipid scramblases in regulating lipid distributions at cellular membranes. *Biochem Soc Trans* 51(5):1857–1869. <https://doi.org/10.1042/BST20221455>
3. Sakuragi T, Nagata S (2023) Regulation of phospholipid distribution in the lipid bilayer by flippases and scramblases. *Nat Rev Mol Cell Biol*:1–21. <https://doi.org/10.1038/s41580-023-00604-z>
4. Sebinelli HG, Syska C, Copic A et al (2024) Established and emerging players in phospholipid scrambling: a structural perspective. *Biochimie*. <https://doi.org/10.1016/j.biochi.2024.09.008>
5. Menon I, Huber T, Sanyal S et al (2011) Opsin is a phospholipid flippase. *Curr Biol* 21(2):149–153. <https://doi.org/10.1016/j.cub.2010.12.031>
6. Khelashvili G, Menon AK (2022) Phospholipid scrambling by G protein-coupled receptors. *Annu Rev Biophys* 51:39–61. <https://doi.org/10.1146/annurev-biophys-090821-083030>
7. Kalienkova V, Clerico Mosina V, Paulino C (2021) The groovy TMEM16 family: molecular mechanisms of lipid scrambling and ion conduction. *J Mol Biol* 433(16):166941. <https://doi.org/10.1016/j.jmb.2021.166941>
8. Suzuki J, Umeda M, Sims PJ et al (2010) Calcium-dependent phospholipid scrambling by TMEM16F. *Nature* 468(7325):834–838. <https://doi.org/10.1038/nature09583>
9. Malvezzi M, Chalal M, Janjusevic R et al (2013) Ca<sup>2+</sup>-dependent phospholipid scrambling by a reconstituted TMEM16 ion channel. *Nat Commun* 4:2367. <https://doi.org/10.1038/ncomms3367>
10. Suzuki J, Denning DP, Imanishi E et al (2013) Xk-related protein 8 and CED-8 promote phosphatidylserine exposure in apoptotic cells. *Science* 341(6144):403–406. <https://doi.org/10.1126/science.1236758>
11. Wu L, Liu L, Xu B et al (2022) In vitro and in vivo assay of the ER lipid scramblase TMEM41B. *STAR Protoc* 3(2):101333. <https://doi.org/10.1016/j.xpro.2022.101333>
12. Ghanbarpour A, Valverde DP, Melia TJ et al (2021) A model for a partnership of lipid transfer proteins and scramblases in membrane expansion and organelle biogenesis. *Proc Natl Acad Sci USA* 118(16). <https://doi.org/10.1073/pnas.2101562118>
13. Li YE, Wang Y, Du X et al (2021) TMEM41B and VMP1 are scramblases and regulate the distribution of cholesterol and phosphatidylserine. *J Cell Biol* 220(6). <https://doi.org/10.1083/jcb.202103105>
14. Matoba K, Kotani T, Tsutsumi A et al (2020) Atg9 is a lipid scramblase that mediates autophagosomal membrane expansion. *Nat Struct Mol Biol* 27(12):1185–1193. <https://doi.org/10.1038/s41594-020-00518-w>
15. Li D, Rocha-Roa C, Schilling MA et al (2024) Lipid scrambling is a general feature of protein insertases. *Proc Natl Acad Sci USA* 121(17):e2319476121. <https://doi.org/10.1073/pnas.2319476121>
16. Bartos L, Menon AK, Vacha R (2024) Insertases scramble lipids: molecular simulations of MTCH2. *Structure* 32(4):505–510.e504. <https://doi.org/10.1016/j.str.2024.01.012>
17. Jahn H, Bartos L, Dearden GI et al (2023) Phospholipids are imported into mitochondria by VDAC, a dimeric beta barrel scramblase. *Nat Commun* 14(1):8115. <https://doi.org/10.1038/s41467-023-43570-y>
18. Ploier B, Caro LN, Morizumi T et al (2016) Dimerization deficiency of enigmatic retinitis pigmentosa-linked rhodopsin mutants. *Nat Commun* 7:12832. <https://doi.org/10.1038/ncomms12832>
19. Verchere A, Ou WL, Ploier B et al (2017) Light-independent phospholipid scramblase activity of bacteriorhodopsin from *Halobacterium salinarum*. *Sci Rep* 7(1):9522. <https://doi.org/10.1038/s41598-017-09835-5>
20. Menon I, Sych T, Son Y et al (2024) A cholesterol switch controls phospholipid scrambling by G protein-coupled receptors. *J Biol Chem* 300(2):105649. <https://doi.org/10.1016/j.jbc.2024.105649>
21. Brunner JD, Schenck S (2019) Preparation of proteoliposomes with purified TMEM16 protein for accurate measures of lipid scramblase activity. *Methods Mol Biol* 1949:181–199. [https://doi.org/10.1007/978-1-4939-9136-5\\_14](https://doi.org/10.1007/978-1-4939-9136-5_14)
22. Ploier B, Menon AK (2016) A fluorescence-based assay of phospholipid scramblase activity. *J Vis Exp* 115. <https://doi.org/10.3791/54635>
23. Levy D, Bluzat A, Seigneuret M et al (1990) A systematic study of liposome and

- proteoliposome reconstitution involving bio-bead-mediated triton X-100 removal. *Biochim Biophys Acta* 1025(2):179–190. [https://doi.org/10.1016/0005-2736\(90\)90096-7](https://doi.org/10.1016/0005-2736(90)90096-7)
24. Gummadi SN, Hrafnisdottir S, Walent J et al (2003) Reconstitution and assay of biogenic membrane-derived phospholipid flippase activity in proteoliposomes. *Methods Mol Biol* 228: 271–279. <https://doi.org/10.1385/1-59259-400-X:271>
25. Goren MA, Morizumi T, Menon I et al (2014) Constitutive phospholipid scramblase activity of a G protein-coupled receptor. *Nat Commun* 5:5115. <https://doi.org/10.1038/ncomms6115>
26. Rouser G, Fleischer S, Yamamoto A (1970) Two dimensional thin layer chromatographic separation of polar lipids and determination of phospholipids by phosphorus analysis of spots. *Lipids* 5(5):494–496. <https://doi.org/10.1007/BF02531316>
27. Chauhan N, Jentsch JA, Menon AK (2019) Measurement of intracellular sterol transport in yeast. *Methods Mol Biol* 1949:115–136. [https://doi.org/10.1007/978-1-4939-9136-5\\_10](https://doi.org/10.1007/978-1-4939-9136-5_10)
28. Wessel D, Flugge UI (1984) A method for the quantitative recovery of protein in dilute solution in the presence of detergents and lipids. *Anal Biochem* 138(1):141–143. [https://doi.org/10.1016/0003-2697\(84\)90782-6](https://doi.org/10.1016/0003-2697(84)90782-6)
29. Kaplan RS, Pedersen PL (1989) Sensitive protein assay in presence of high levels of lipid. *Methods Enzymol* 172:393–399. [https://doi.org/10.1016/s0076-6879\(89\)72025-5](https://doi.org/10.1016/s0076-6879(89)72025-5)
30. Schindelin J, Arganda-Carreras I, Frise E et al (2012) Fiji: an open-source platform for biological-image analysis. *Nat Methods* 9(7): 676–682. <https://doi.org/10.1038/nmeth.2019>
31. Chang QL, Gummadi SN, Menon AK (2004) Chemical modification identifies two populations of glycerophospholipid flippase in rat liver ER. *Biochemistry* 43(33):10710–10718. <https://doi.org/10.1021/bi049063a>
32. Hrafnisdottir S, Nichols JW, Menon AK (1997) Transbilayer movement of fluorescent phospholipids in *Bacillus megaterium* membrane vesicles. *Biochemistry* 36(16):4969–4978. <https://doi.org/10.1021/bi962513h>
33. Marx U, Lassmann G, Holzhtutter HG et al (2000) Rapid flip-flop of phospholipids in endoplasmic reticulum membranes studied by a stopped-flow approach. *Biophys J* 78(5): 2628–2640. [https://doi.org/10.1016/S0006-3495\(00\)76807-X](https://doi.org/10.1016/S0006-3495(00)76807-X)
34. Malvezzi M, Andra KK, Pandey K et al (2018) Out-of-the-groove transport of lipids by TMEM16 and GPCR scramblases. *Proc Natl Acad Sci USA* 115(30):E7033–E7042. <https://doi.org/10.1073/pnas.1806721115>
35. Sanyal S, Frank CG, Menon AK (2008) Distinct flippases translocate glycerophospholipids and oligosaccharide diphosphate dolichols across the endoplasmic reticulum. *Biochemistry* 47(30):7937–7946. <https://doi.org/10.1021/bi800723n>



## Identifying Genomic DNA Sequences Near the Nuclear Lamina Using Proximity Biotinylation with Ascorbate Peroxidase

Yixian Zheng, Katherine A. Bossone, Sara Debic, Ross T. A. Pedersen, and Joseph R. Tran

### Abstract

Ascorbate peroxidase (APEX2) is an engineered plant-based enzyme that is used for the proximal ligation of biotin onto nearby proteins and nucleic acids. The APEX2 enzyme can be targeted to a specific subcellular compartment (e.g., the nuclear lamina) by creating a fusion between the APEX2 enzyme and a targeting protein (e.g., Lamin B1). We have found that the APEX2 proximity ligation reaction is very robust and can be performed in both living and formaldehyde-fixed cells. The biotinylated proteins and nucleic acids can then be precipitated with streptavidin beads for the identification of proximal proteins, RNA, and DNA. Here, we detail a protocol for the use of an APEX-Lamin B1 fusion protein to identify DNA in the proximity of the nuclear lamina, including lamina-associated domains (LADs).

**Key words** Ascorbate peroxidase, APEX, Proximity ligation, Nuclear lamina, Lamina-associated domains, LADs

---

## 1 Introduction

Peroxidases are a large group of oxidoreductases used in industrial and scientific applications. In the biological sciences, peroxidases are frequently used in a signal amplification step for antibody-based assays such as enzyme-linked immunosorbent assays (ELISA), western blotting, and immunostaining. The most common peroxidase used for signal amplification is the heme-containing horseradish peroxidase and is familiar as an antibody conjugate used in ELISA and western blotting procedures. Peroxidase-based signal amplification can catalyze the deposition of a traceable biomolecule or the emission of photons at densities that far exceed the original amount of antibody. Traceable biomolecules are diverse and can be chromogenic, chemiluminescent, or deposition of a secondary

molecule that can be directly (e.g., fluorescent tyramide/phenol) or indirectly (e.g., biotin) detected.

Additional peroxidases have been explored for their usefulness. One such example is the ascorbate peroxidase (APEX) endogenous to pea and soybean plants. APEX was engineered into a monomeric form and further engineered to generate a highly active and robust version called APEX2 [1, 2]. APEX2 is used as a fusion to a carrier protein that targets the enzyme to a cellular region of interest. Upon expression of the fusion protein, the APEX2 enzyme, in the presence of biotin-phenol and hydrogen peroxide, catalyzes the formation of a short-lived biotin-phenoxy radicals that covalently attach to the side chains of electron-rich amino acids. Subsequently, the biotinylated material can be precipitated with streptavidin-immobilized beads. The APEX2 system has been extensively used for the identification of proteins at specific subcellular regions and can also be used for the detection of RNA species [3–8]. The APEX2 enzyme is robust and retains its activity under a number of laboratory conditions, including live-cell settings and in cells fixed with paraformaldehyde as demonstrated for electron and fluorescence microscopy.

We recently employed the APEX2 enzyme, fused to the amino-terminus of Lamin B1 protein for the mapping of chromatin that is proximal to the proteinaceous nuclear lamina—the lamina-associated domains (LADs) [3]. LADs are largely gene-poor heterochromatic genomic regions spanning from a few hundred kilobases to the many megabases in size [9]. While most LADs are conserved between cell types, select LADs can vary between cell types [10]. This variability is thought to be part of the developmental program for some cell types and allows the expression or repression of relevant cell-type-specific genes during development and in disease settings.

In this protocol, we describe how to use the APEX2-Lamin B1 construct for the mapping of DNA proximal to the nuclear lamina. As a broad outline, we start with cultured cells that are transfected with the APEX2-Lamin B1 plasmid. Transfected cells are then fixed with formaldehyde prior to performing the APEX reaction. DNA fragmentation, streptavidin pulldown, and DNA isolation are then performed. We detail a number of barriers that we encountered and the approaches we took to overcome them.

---

## 2 Materials

It is imperative to be consistent as to how one does the experiment. We have learned that there can be inconsistencies in mapping if one performs the APEX2 reaction with fixed cells on a plate, or if one trypsinizes the cells into suspension prior to fixation and reaction.

**2.1 Transfection**

1. Cell lines: we used HEK293T/FT and HCT116. Cell culture conditions can vary depending on cell line and lab conditions and should be established in the lab prior to embarking on this experiment. We typically transfect cells at ~40–60% confluency.
2. APEX2-Lamin B1 plasmid (Addgene; 139442). The APEX2-Lamin B1 construct is also tagged with an amino terminal FLAG tag for immunofluorescence.
3. Cell culture hood/incubators.
4. Transfection reagent, e.g., Lipofectamine 2000 (Thermo Fisher; 11668030).
5. Optimem (Thermo Fisher; 11058021).
6. Culture media: McCoy's 5A media (ATCC; 30-2007) containing 10% FBS.

**2.2 Cell Fixation and Chromatin Fragmentation by Sonication**

1. Diagenode Bioruptor Pico with chiller unit, Misonix 3000 probe sonicator, or equivalent (*see Note 1*).
2. 16% paraformaldehyde ("PFA", EMS; 15710). PFA is a polymerized solid of formaldehyde. 16% PFA is a formaldehyde solution composed of 16% weight-by-volume PFA. We routinely use a more dilute formaldehyde solution made in 1× PBS. Prepare a 4% solution in a final of 1× PBS. For example, for a formaldehyde solution containing the equivalent of 4% w/v PFA, 10 mL of 16% paraformaldehyde is added to 4 mL of 10× PBS, and the volume is brought up to 40 mL with nanopure water. Dilutions of this stock PFA solution can then be made with 1× PBS.
3. Ethanol, absolute anhydrous (Pharmco; 111000200).
4. Glycine (Millipore-Sigma; G8898). Prepare a 2 M stock solution. The pH is roughly 5.5.
5. RIPA buffer: 50 mM Tris pH 7.5, 150 mM NaCl, 0.1% (wt/vol) sodium dodecyl sulfate (*see Note 2*), 0.5% (wt/vol) sodium deoxycholate, and 1% (vol/vol) Triton X-100. Adjust the pH to 7.5 with HCl. Add protease inhibitors before use. Store at 4 °C.
6. Circular glass coverslips.
7. 0.1 M phenylmethylsulfonyl fluoride in ethanol.

**2.3 APEX2 Reaction**

1. Biotin-phenol (Iris Biotech; LS-3500.0250). Prepare a 2.75 mM (1 mg/mL) stock of biotin-phenol with DMSO (*see Note 3*).
2. Hydrogen peroxide, 30% wt in H<sub>2</sub>O (Millipore-Sigma; H3410). The solution is approximately 9.8 M as sold.
3. Dulbecco's PBS, pH 7.4 (Gibco; 21600-069). Prepare in 1 liter of nanopure water to give a 10× stock of DPBS.

4. PBSTX: 1× PBS, 0.25% Triton X-100.
5. Neutralization solution; 10 mL PBS containing 0.02 g sodium ascorbate (final = 10 mM), 0.0134 g Trolox (final = 5 mM), 10 mM NaN<sub>3</sub> (*see* **Note 4**).
6. 1.5 mL microtubes.
7. 15 mL conical tubes (Millipore-Sigma; 339650).
8. Reaction media: McCoy's 5A media containing 10% FBS and 100 μM biotin-phenol.

## **2.4 Immuno-fluorescence**

1. Blocking buffer (for immunofluorescence): 1× PBS, 10% BSA, 10% goat serum (Millipore-Sigma; G9023), 10 mM NaN<sub>3</sub>. Store at 4 °C.
2. PBST: 1× PBS, 0.1% Tween-20.
3. Bovine serum albumin (BSA), heat shock fraction 7 (Millipore-Sigma; A7906).
4. Mouse anti-FLAG M2 antibody (Millipore-Sigma; F3165).
5. Streptavidin-conjugated Alexa 488 (Biolegend; 405235).
6. Goat anti-mouse Alexa Fluor 594 conjugated antibody (Millipore-Sigma; A-11032).
7. DAPI (1 μg/mL) solution in PBST.
8. Prolong anti-fade mounting medium.

## **2.5 Lysis and Sonication**

1. Diagenode Bioruptor Pico with chiller unit, Misonix 3000 probe sonicator.
2. RIPA buffer.
3. RIPA buffer with protease inhibitor cocktail (Millipore-Sigma; cComplete, EDTA-free; 11873580001) (*see* **Note 5**).
4. RNase A solution (100 mg/mL; 7000 units/mL).
5. Proteinase K solution (20 mg/mL).
6. 1.5 mL Diagenode Bioruptor microtubes with caps (Diagenode; C30010016).

## **2.6 Streptavidin Pulldown**

1. Streptavidin beads (Fisher Scientific, Pierce; 88817) (*see* **Note 6**).
2. Magnetic rack.
3. High salt wash buffer: 50 mM Tris-HCl pH 8.0, 1 M KCl, 5 mM EDTA (*see* **Note 7**), add one protease inhibitor cocktail tablet to 50 mL. Store at 4 °C.
4. Urea wash buffer: 10 mM Tris-HCl, pH 8.0, and 2 M urea (*see* **Note 8**), add one protease inhibitor cocktail tablet to 50 mL. Store at 4 °C.

### 2.7 DNA Purification and Sequencing

1. 80% ethanol with molecular biology grade water.
2. Ampure XP beads (Agencourt; A63881).
3. SPRI bead buffer: 20% w/v polyethylene glycol 8000 (Millipore-Sigma; P2139), 2.5 M NaCl, 10 mM NaN<sub>3</sub>. Store at 4 °C.
4. Elution buffer: 10 mM Tris-HCl pH 8.0 (*see Note 9*).
5. Qubit 3 fluorometer.
6. Qubit dsDNA HS Assay kit (Thermo-Fisher; Q32854).
7. DNA sequencer (*see Note 10*).

### 2.8 Data Analysis

1. bowtie v2.3.2
2. samtools v1.6
3. bedtools v2.26.0

---

## 3 Methods

### 3.1 Transfection

Cell culture and transfection protocols can vary and should be optimized for the cell line and transfection approach being used. We routinely use the Lipofectamine 2000 transfection reagent and follow the manufacturer's instructions. We place two sterilized circular coverslips in the 10 cm dish before seeding. These two coverslips will be used to check for the APEX2 reaction in Subheading 3.4.

1. Cells are grown to ~70% confluency in a 10 cm dish in a 37 °C incubator at 5% CO<sub>2</sub>.
2. Refresh the cells with 15 mL of cell culture media.
3. Prepare the following separate mixes in 1.5 mL microfuge tubes.
  - (a) Mix 1: 250 µL Optimem and 60 µL Lipofectamine 2000.
  - (b) Mix 2: 250 µL Optimem and 20–25 µg plasmid DNA (*see Note 11*).
4. Incubate for 5 min at room temperature.
5. Take Mix 2 and add it to Mix 1. Gently mix by flicking the tube.
6. Add, dropwise, to the 10 cm dish and gently rock the plate and forth to disperse the transfection mixture.
7. Place back into the cell culture incubator for 6 h.
8. Aspirate the cell culture media and refresh the cells with 10 mL of culture medium.
9. Place back into the cell culture incubator and express the plasmid for a total of 24–48 h (*see Note 12*).

### 3.2 Cell Fixation

Cell fixation is often not discussed in chromatin precipitation studies. While insufficient fixation can lead to sample damage and loss during processing steps, overly fixed cells have chromatin that can be very difficult to fragment to an acceptable size and can frustrate the experimenter (*see Note 13*).

1. Aspirate the cell culture media and wash the cells once with  $1\times$  PBS.
2. Add 5 mL of 1% PFA solution prepared in  $1\times$  PBS. Incubate for 2 min.
3. Add 312.5  $\mu$ L of 2 M glycine and swirl gently to mix.
4. Incubate on ice for 5 min.

### 3.3 APEX2 Reaction

The APEX reaction can be done in both live and fixed cell settings. In our LADs mapping, we perform the APEX reaction using paraformaldehyde-fixed cells.

1. Wash the fixed cells twice with 5 mL of PBS and aspirate in between.
2. Carefully aspirate off the PBS and permeabilize the cells by covering with PBSTX for 10 min at room temperature.
3. Aspirate and wash the cells with PBS.
4. Aspirate and wash the cells with culture media.
5. Aspirate and add 5 mL of Reaction media (*see Note 14*). Gently rock back and forth 5 times. Incubate at room temperature for 5 min.
6. Add an equal volume of 2 mM  $\text{H}_2\text{O}_2$  (the final concentration will be 1 mM; *see Note 14*) to the solution, mix, and incubate for 20 s.
7. Add in 10 mL of neutralization solution and rock the solution back and forth (*see Note 15*).
8. Aspirate and wash twice with PBS. At this point, collect the circular coverslips for immunostaining below in Subheading 3.4.
9. Add 5 mL of PBS and collect the cells with a cell scraper into a 15 mL conical tube.
10. Centrifuge the cells at  $500\text{ g} \times 5\text{ min}$  and aspirate the supernatant.
11. Resuspend the cells with 1 mL of PBS and transfer to a 1.5 mL microfuge tube.
12. Centrifuge the cells at  $500\text{ g} \times 5\text{ min}$  and aspirate.
13. Snap-freeze and store at  $-80^\circ\text{C}$ .

### 3.4 Immuno-fluorescence

The coverslips above from the APEX2 reaction are verified by antibody and streptavidin staining (Fig. 1). The number of cells transfected and the quality of the APEX reaction can be assessed here before moving on to the Lysis and Sonication in Subheading 3.5.

1. Wash the coverslips with PBS.
2. Incubate in the Blocking buffer for 1 h at room temperature.
3. Aspirate the Blocking buffer from the coverslips and cover with PBS.
4. Prepare a solution containing mouse anti-FLAG M2 antibody at 1:500 in Blocking buffer.
5. Aspirate the PBS from the coverslips and replace with the primary antibody solution. Incubate at room temperature for 1 h.
6. Aspirate the primary antibody solution and wash the coverslips three times for 10 min each with PBST.
7. Prepare the secondary and streptavidin solution. We use a goat anti-mouse 594 antibody (1:1000) and a streptavidin conjugated to Alexa Fluor 488 (1:250) resuspended in PBST. Incubate for 1 h at room temperature.
8. Wash with the coverslips two times for 10 min each with PBST.
9. Incubate in PBST with DAPI (1  $\mu\text{g}/\text{mL}$ ) for 10 min.
10. Aspirate the DAPI solution and wash with PBS.
11. Mount the coverslip with prolong anti-fade mounting medium for imaging.

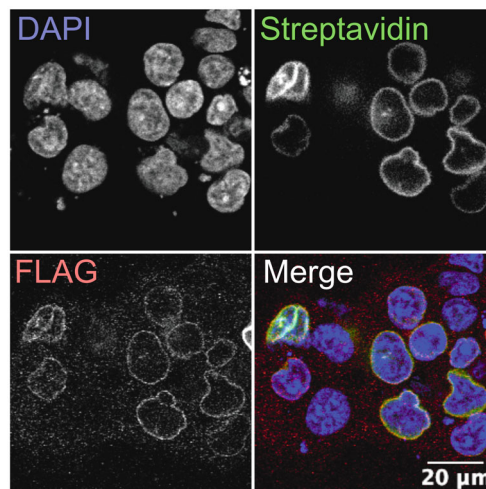


**Fig. 1** Verification of the APEX2 reaction by immunostaining. The APEX2 reaction was performed on PFA-fixed cells transfected with the APEX2-Lamin B1 construct. The cells were permeabilized and stained for an antibody against the FLAG tag (red) on the APEX2-Lamin B1 protein and for streptavidin (green). DAPI staining is presented in blue

### 3.5 Lysis and Sonication

Lysis of cells is relatively straightforward. However, chromatin fragmentation must be optimized. In this protocol, we perform the sonication step using the Bioruptor Pico system.

1. Frozen cells (**Step 13** in Subheading 3.3) are removed from the  $-80^{\circ}\text{C}$  freezer and thawed on ice.
2. Add 300  $\mu\text{L}$  of RIPA buffer containing protease inhibitors and 1  $\mu\text{L}$  of RNase A solution. Completely resuspend the cells.
3. Transfer the lysate to a 1.5 mL Diagenode Bioruptor Pico microtube.
4. Rotate the microfuge tube at  $4^{\circ}\text{C}$  for 30 min.
5. Sonicate this lysate using the empirically determined conditions (*see Note 16*).
6. Centrifuge the lysate at 12,000  $g$  for 60 s.
7. Collect the supernatant to a fresh 1.5 mL microfuge tube.
8. Collect 1/10th of this clarified supernatant (30  $\mu\text{L}$ ) and bring the volume up to 100  $\mu\text{L}$  with RIPA buffer without protease inhibitors.
9. Add in 3  $\mu\text{L}$  of proteinase K and digest at  $50^{\circ}\text{C}$  overnight. This sample will serve as your input DNA and will be processed the next day at Subheading 3.7.

### 3.6 Streptavidin Pulldown

Streptavidin pulldown is an efficient procedure and does not require a lengthy incubation.

1. Aliquot 75  $\mu\text{L}$  of streptavidin beads into 1.5 mL microfuge tubes for each sample.
2. Magnetize the beads using the magnetic rack and aspirate the storage buffer.
3. Wash the beads twice with RIPA buffer containing protease inhibitors.
4. Resuspend in 75  $\mu\text{L}$  of RIPA buffer and add this to the clarified lysate from **Step 7** in Subheading 3.5.
5. Incubate at room temperature for 45 min with end-over-end rotation (*see Note 17*).
6. Magnetize the beads and aspirate the lysate.
7. Wash with 1 mL of the following buffers. Washing involves resuspending the beads in the buffer and letting the suspension sit in a microfuge tube rack for 1 min. Briefly centrifuge the tube to collect liquid that might get trapped in the cap. The beads are then placed back on the magnetic rack and aspirated after the magnetic beads have formed a tight clump near the magnet.

- RIPA buffer with protease inhibitors
  - High salt wash buffer with protease inhibitors
  - Urea wash buffer with protease inhibitors
  - RIPA buffer without protease inhibitors
8. Resuspend the beads with 100  $\mu\text{L}$  of RIPA buffer without protease inhibitors.
  9. Add in 3  $\mu\text{L}$  of proteinase K and digest at 50  $^{\circ}\text{C}$  overnight.

### 3.7 DNA Purification and Sequencing

At this point, one will have two DNA samples. The input sample is obtained in **Step 9** in Subheading 3.5 and the streptavidin pull-down (StrePD) sample from the **Step 9** in Subheading 3.6.

There are many procedures that can be used to isolate DNA from these two samples; however, we found it most convenient to use Solid-Phase Reversible Immobilization (SPRI) beads. A benefit of SPRI bead purification is the ability to perform DNA size selection by adjusting the ratio of SPRI beads to sample solution. Further, the DNA binding capacity of SPRI beads is quite high. One issue we encounter is that it can be difficult to efficiently elute DNA with a small amount of elution buffer when starting from a large amount of SPRI beads. The goal is to obtain a concentrated solution of DNA. We therefore prepare a SPRI buffer that we use in conjunction with Ampure XP beads. Finally, a “double-sided” SPRI clean purification is recommended for this procedure and which is detailed below.

1. Input and StrePD samples (both are  $\sim 103 \mu\text{L}$ ) are “spiked” with another 3  $\mu\text{L}$  of proteinase K and digested for an additional 1–2 h at 50  $^{\circ}\text{C}$ .
2. Freshly prepare 80% ethanol with molecular biology grade water.
3. For the StrePD sample, place the tube on a magnetic rack for 5 min and collect  $\sim 106 \mu\text{L}$  of the supernatant to a fresh 1.5 mL microfuge tube.
4. Add 20  $\mu\text{L}$  of Ampure XP beads and 43.6  $\mu\text{L}$  of SPRI bead buffer to the supernatant ( $\sim 106 \mu\text{L}$ ). Mix it by pipetting up and down 10 $\times$  (*see Note 18*).
5. Incubate at room temperature for 10 min.
6. Place on a magnetic rack for 5 min.
7. Collect the supernatant ( $\sim 165 \mu\text{L}$ ) and transfer to a fresh 1.5 mL microfuge tube. Do not collect the beads (*see Note 19*).
8. Add 20  $\mu\text{L}$  of Ampure XP beads and 20  $\mu\text{L}$  of SPRI bead buffer to the supernatant. Mix it by pipetting up and down 10 $\times$  (*see Note 20*).

9. Incubate for 10 min at room temperature.
10. Place the tube on a magnetic rack for 5 min.
11. Aspirate the supernatant with a P200 pipet and discard. The DNA fragments bound to the beads should be less than 500 bp.
12. Wash the beads by pipetting in 500  $\mu$ L of 80% ethanol while the tube is still on the magnetic rack. Let it sit for 30 s.
13. Aspirate off the ethanol and repeat the wash with 80% ethanol.
14. Aspirate this second ethanol wash.
15. Briefly spin down ( $\sim$ 2–3 s) the sample.
16. Place the tube back on the magnetic rack and remove residual ethanol.
17. Air-dry for  $\sim$ 1 min (*see* **Note 21**).
18. Elute the beads with 15–20  $\mu$ L of elution buffer.
19. Quantitate by Qubit according to the manufacturer's instructions (*see* **Note 22**).
20. Proceed to library production and sequencing using your preferred kit (*see* **Note 23**).

### 3.8 Data Analysis

1. We align input and streptavidin pulldown (StrePD) reads to the corresponding genome with bowtie/2.3.2 using the default parameters.
2. The sam output file is converted to a bam file and sorted with samtools/1.6.
3. We then perform a read count in sequential, nonoverlapping windows using bedtools/2.26.0 and export this data as a bed-graph file. The analysis is usually done using genomic windows that are 20–100 kb in size.
4. The bedgraph counts for the input and StrePD sample are then imported into RStudio for normalization to counts per million, calculating the log<sub>2</sub> of the ratio of StrePD/input and conversion to z-score.
5. A successful experiment is shown in Fig. 2 (*see* **Note 24**).

---

## 4 Notes

1. The chiller unit for the Diagenode Bioruptor Pico is a necessary add-on for this bath sonicator. When using the Misonix 3000 sonicator, we use a microtip probe and place the sample, which is in a 15 mL conical tube, in a beaker containing an ice water slurry.
2. Prepare a 5% stock solution of SDS.

## HCT116, hg38, Chr2

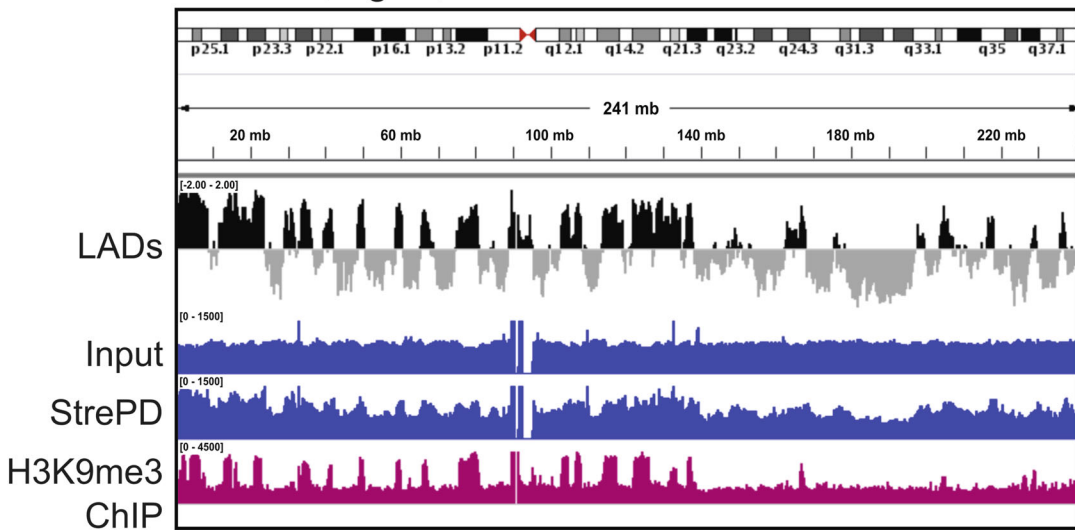


**Fig. 2** IGV v2.3.94 browser view of APEX2 LADs data. APEX2-Lamin B1 LADs data from HCT116 cells is presented for chromosome 2 (hg38). The top track, “LADs” is the log2 of the streptavidin pulldown (StrePD) over input converted to a z-score. The “input” track is the DNA isolated after sonication. The StrePD track is the DNA isolated from the pulldown. “H3K9me3 ChIP” track is a ChIP-seq track for the indicated histone mark in HCT116 cells

3. We aliquot biotin-phenol stocks and store at  $-20^{\circ}\text{C}$ . Avoid more than two freeze-thaw cycles per aliquot. In our experience, this stock is stable for well over a year at  $-20^{\circ}\text{C}$ .
4. Prepare a 0.5 M stock of sodium azide.
5. Use one tablet for 50 mL of solution.
6. Before use, we wash the streptavidin beads with RIPA buffer by collecting them on a magnetic rack. Do not centrifuge these beads since it might result in aggregation. In the event of loss of binding, which can occur during prolonged storage of the bead slurry and is presumably caused by aggregation of the beads, we sonicate the beads with  $2 \times 30$  second pulses 30 s of rest in between using a Diagenode Bioruptor Standard model UCD-200 (high setting) or the Bioruptor Pico.
7. Prepare a 0.5 M stock of EDTA and pH to 8.0.
8. Prepare a 5 M stock solution.
9. Prepare 1 M stock solutions, one at pH 7.5 and one at pH 8.0.
10. We use an Illumina NextSeq1000.
11. Cell culture and transfection protocols can vary and should be optimized for the cell line and transfection approach being used. We aim for at least 50% transfection efficiency. Low transfection efficiencies lead to higher background signal.

12. Overexpression effects can be seen in the HEK293T/FT and HCT116 cell lines that have prolonged expression of the APEX2-Lamin B1 construct. These effects normally manifest as an accumulation of cells in prophase. We do not proceed with experiments that show >5% of APEX2-Lamin B1 expressing cells in prophase. Expression of the APEX2-Lamin B1 construct should be examined in a pilot experiment to determine the ideal length of expression time. The expression of the APEX2-Lamin B1 construct can be detected by immunostaining with an antibody against FLAG tag and by peroxidase activity. The expression of the construct, as assessed by anti-FLAG immunostaining, does not necessarily need to be strong in order to label the nuclear lamina.
13. We suggest performing the following experiment in order to assess the stability of cells to be used in the reaction. We perform a fixation time-course for cells on glass coverslips (for adherent cells) with formaldehyde solutions made with 1%, 2%, or 4% weight-by-volume PFA. We fix for 0.5, 1, 2, 5, and 10 min followed by prompt neutralization with glycine. We then perform a standard immunostaining procedure (described in Subheading 3.4) for nuclear proteins such as Lamin B1 (Fig. 3). The immunostaining results of this test are compared to those obtained from a 10-min fixation with 4% PFA, and the minimum fixation time and PFA concentration are chosen for a sonication test. Inadequate fixations can result in a major loss of cells from the coverslip and distortion of DAPI and antibody staining.
14. Prepare the Reaction media and the 2 mM H<sub>2</sub>O<sub>2</sub> solution in culture media right before use.
15. Prepare these solutions right before starting Subheading 3.3.
16. The length of time required for sonication needs to be empirically determined for each cell line. From our experience, sonicated chromatin covering a size range from ~200 to 800 bp is ideal. However, we often find that the standard fixation procedure (i.e., 10 min with 4% PFA) results in chromatin that is difficult to completely fragment without using very long process times; hence we chose the shortest fixation time possible (Fig. 4). For the Bioruptor Pico, the cell lysate (300 µL) is sonicated in a 1.5 mL Diagenode Bioruptor microtubes. For the Misonix 3000 or similar probe sonicators, we typically use a 1/16th inch tip with a power setting of 6 watts. For probe sonicators, the lysate is brought up to around 1.3 mL with RIPA buffer and transferred to 15 mL conical tube. The location of the probe tip is centered, and its height from the bottom of the conical tube is around 1 cm. The choice of volume was based on a desire to minimize foaming during

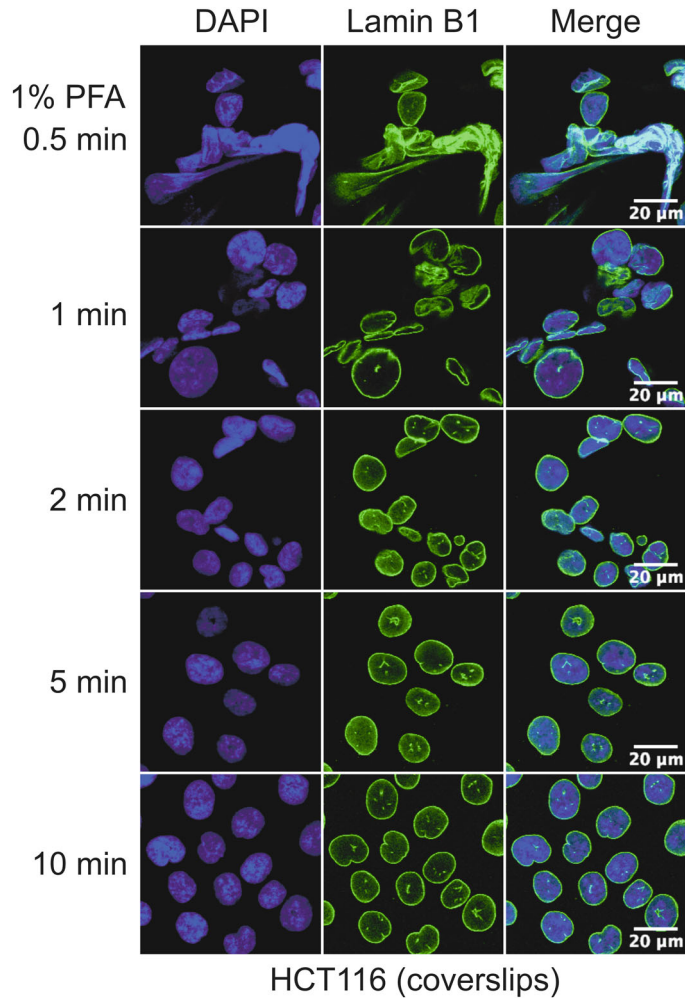


**Fig. 3** Cell fixation time course. HCT116 cells were grown on coverslips and fixed with 1% PFA for the indicated times. The cells were then permeabilized with PBS supplemented with 0.25% Triton X-100 and stained for Lamin B1 (Abcam, ab16048). The Lamin B1 antibody was visualized with a secondary conjugated with Alexa-fluor 488

sonication. We use a small amount of phenylmethylsulfonyl fluoride prepared in ethanol to remove bubbles and foam should they appear during probe sonication.

17. While streptavidin pulldown can be done overnight at 4 °C, we observed higher nonspecific binding when using fragmented chromatin from cells not expressing the APEX2-Lamin B1 construct.
18. The total volume of Ampure XP beads and SPRI bead buffer is 63.6  $\mu$ L, which is around 0.6 $\times$ . This ratio favors the binding of

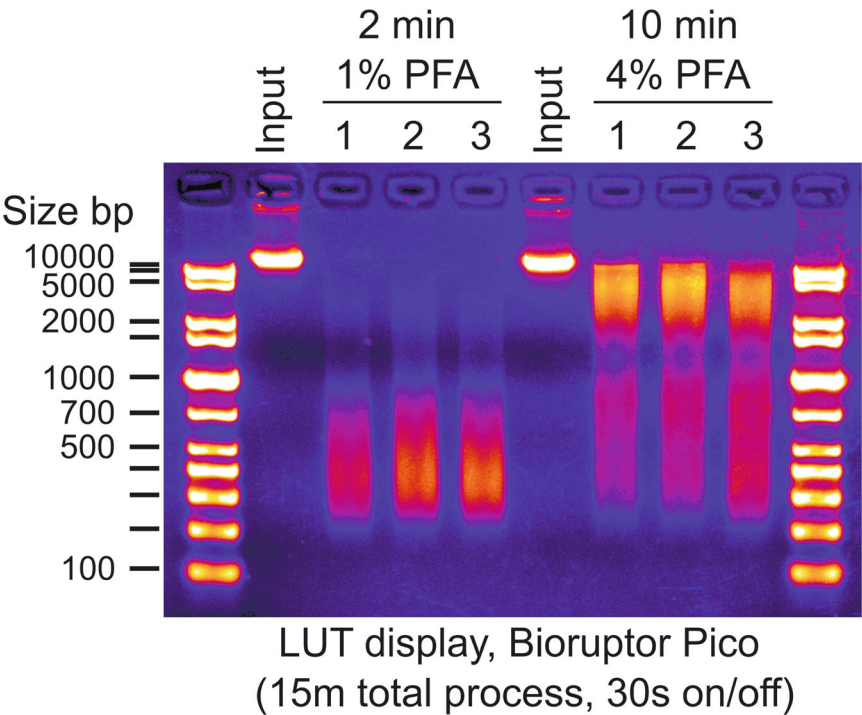


**Fig. 4** Sonication testing. PFA-fixed HCT116 cells were lysed and sonicated. DNA was extracted with phenol-chloroform isoamyl alcohol and resolved by agarose gel electrophoresis. The PFA percentage and fixation times are indicated. The input is from unfixed cells, and the replicates for each condition are sequentially denoted 1–3

DNA that is 500 bp and greater to the beads. It is imperative that the pipetting be as accurate as possible.

19. This supernatant is enriched for fragments that are smaller than 500 bp.
20. The SPRI bead buffer ratio is now around 1×.
21. Do not overdry the beads. The beads will initially appear “reflective” but will become matte once drying is complete.
22. The Qubit can measure sub-nanogram quantities of DNA and is preferred.
23. We use the Takara ThruPlex DNA-seq kit (Takara, R400674) for library production. The Takara ThruPlex DNA-seq library pipeline is entirely additive, and purification of libraries with SPRI beads does not occur until after the final PCR amplification. We perform single-ended sequencing at a read-length of 50–75 bp. 30–40 million reads per sample is sufficient.
24. The input is relatively even, indicating fairly uniform coverage of the genome in the sonicated material. The StrePD sample shows enrichment of reads in regions that are often higher in H3K9me3 ChIPseq signal.

## References

1. Martell JD, Deerinck TJ, Sancak Y et al (2012) Engineered ascorbate peroxidase as a genetically encoded reporter for electron microscopy. *Nat Biotechnol* 30(11):1143–1148. <https://doi.org/10.1038/nbt.2375>
2. Lam SS, Martell JD, Kamer KJ et al (2015) Directed evolution of APEX2 for electron microscopy and proximity labeling. *Nat Methods* 12(1):51–54. <https://doi.org/10.1038/nmeth.3179>
3. Tran JR, Paulson DI, Moresco JJ et al (2021) An APEX2 proximity ligation method for mapping interactions with the nuclear lamina. *J Cell Biol* 220(1). <https://doi.org/10.1083/jcb.202002129>
4. Fazal FM, Han S, Parker KR et al (2019) Atlas of subcellular RNA localization revealed by APEX-Seq. *Cell* 178(2):473–490.e426. <https://doi.org/10.1016/j.cell.2019.05.027>
5. Chen CL, Hu Y, Udeshi ND et al (2015) Proteomic mapping in live *Drosophila* tissues using an engineered ascorbate peroxidase. *Proc Natl Acad Sci USA* 112(39):12093–12098. <https://doi.org/10.1073/pnas.1515623112>
6. Chung CY, Khurana V, Yi S et al (2017) In situ peroxidase labeling and mass-spectrometry connects alpha-synuclein directly to endocytic trafficking and mRNA metabolism in neurons. *Cell Syst* 4(2):242–250.e244. <https://doi.org/10.1016/j.cels.2017.01.002>
7. Hung V, Udeshi ND, Lam SS et al (2016) Spatially resolved proteomic mapping in living cells with the engineered peroxidase APEX2. *Nat Protoc* 11(3):456–475. <https://doi.org/10.1038/nprot.2016.018>
8. Kaewsapsak P, Shechner DM, Mallard W et al (2017) Live-cell mapping of organelle-associated RNAs via proximity biotinylation combined with protein-RNA crosslinking. *elife* 6. <https://doi.org/10.7554/eLife.29224>
9. Guelen L, Pagie L, Brasset E et al (2008) Domain organization of human chromosomes revealed by mapping of nuclear lamina interactions. *Nature* 453(7197):948–951. <https://doi.org/10.1038/nature06947>
10. Meuleman W, Peric-Hupkes D, Kind J et al (2013) Constitutive nuclear lamina-genome interactions are highly conserved and associated with A/T-rich sequence. *Genome Res* 23(2):270–280. <https://doi.org/10.1101/gr.141028.112>



## Pairing Lamin B1-DamID and Immuno-3D-FISH to Resolve and Verify Peripheral Genome Organization of Adipogenesis

Rafal Czapiewski, Jose I. de las Heras, and Eric C. Schirmer

### Abstract

Each tissue has unique patterns of spatial genome organization that contribute to tissue-specific gene regulation, and these patterns are often disrupted in aging, cancer, and developmental diseases such as muscular dystrophy and lipodystrophy. Interactions between nuclear membrane proteins and specific sets of genes drive much of this tissue-specific genome organization; however, identifying specific gene targets of these proteins can be challenging because of their insolubility and interactions with the lamin polymer. The DamID method is a powerful approach to overcome these limitations because, unlike chromatin immunoprecipitation (ChIP) approaches, it does not require isolation of the nuclear membrane protein; however, dam methylase fusions to the nuclear membrane proteins that tether specific chromatin may interfere with the specificity of their genome interactions. Thus, dam methylase is fused to lamin B1 to determine all genes at the nuclear envelope when the nuclear membrane protein is present or absent, and the comparison should identify genes under nuclear membrane protein positional control. However, DamID needs to be optimized for each tissue; so, it is helpful to have each procedure catalogued and to be able to compare different modifications of the procedure when establishing DamID in a new tissue. We present here an optimized protocol for lamin B1-DamID on pre-adipocytes and differentiated adipocytes along with two approaches for analysis. We also present a method for 3D Immuno-FISH in adipocytes to confirm DamID results. This method requires specialized approaches to permeabilize fat cells which otherwise have significant autofluorescence.

**Key words** Nuclear envelope, DamID, LAD, Lamina, FISH, Adipogenesis, Adipocytes

---

### 1 Introduction

Genome regulation can occur at many levels. While transcription factor action on genes remains the actual method for driving transcription, epigenetic marks on chromatin, the local folding of the genome, and the higher-order genome organization all contribute to making genes primed and accessible for transcription factor action. The 3D spatial organization of the genome not only can segregate genes between generally active and inactive regions but can also position super-enhancers to optimally interact with

multiple genes, even when they are on different chromosomes [1–3]. Each tissue has a unique genome organization pattern that tends to position active genes in the nuclear interior and inactive genes at the nuclear envelope (NE) [4–9], though there are exceptions so that the NE should be viewed as a regulatory region rather than a purely repressive one.

Some of this 3D genome organization appears to be driven by epigenetics with a greater tendency for histone silencing marks to accumulate at the NE [10–12]. Mechanistically, this is achieved because some NE transmembrane proteins (NETs) have specific interactions with either markers of silenced chromatin (e.g., NET LBR with HP1; [13]), the enzymes that silence them (e.g., NET LAP2 $\beta$  with HDAC3; [14]), or transcriptional repressors (e.g., NET LAP2 $\beta$  with germ cell-less, GCL; [15]). Moreover, several tissue-specific NETs have been identified that direct much of the more tissue-specific genome organization patterns [5–7, 16–18]. Interestingly, several tissue-specific NETs appear to work together in a particular tissue to establish these genome organization patterns. For example, in the muscle the NETs Tmem38A, NET39, and Wfs1 each affects the positioning and through this the expression of over 100 genes with little overlap between gene sets [5]. However, also in the muscle the NET Tmem214, which has a second cytoskeletal function [19], affects positioning/expression of many of the genes regulated by the other 3 NETs [5]. This suggests that some NETs may exert their functions directly as gene tethers with specificity for particular genes while others may exert their function more indirectly through affecting mechano-signal transduction. The tethering function was confirmed for NET39 [5]; however, potential functions of NETs in mechano-signal transduction still need to be tested. These principles likely apply to all tissues as, though not as extensively screened for such NETs, in fat both Tmem120A and Tmem120B each has many unique as well as partially overlapping sets of genes under their positional regulation [7]. As both epigenetic mechanisms and NET expression can be dynamic during development and both can be misregulated and/or mutated in aging and disease [20–25], it is important to have methods for determining all genes under such regulation in different cell types and states.

Determining genes that change their radial positioning (NE or nuclear interior) during development and in different tissues was initially done on an individual gene basis by fluorescence in situ hybridization (FISH). Among the most prominent early discoveries, a single allele of the *IgH* locus was observed to be released from the NE when it became activated for *v-d-j* recombination in lymphocytes [26], and the *Mash1* gene important for neurons was released from the NE concomitant with its activation and a change in epigenetic marks during neuronal differentiation [27]. Many other examples were found, but the rate of their discovery was

limited by the fact that there were not many developmental labs doing FISH. The initial technical advance of high-throughput/genome-wide technologies did not immediately enhance discovery with regards to radial genome organization because chromosome conformation capture approaches [28] do not distinguish the NE and chromatin. Furthermore, chromatin immunoprecipitation-sequencing (ChIP-Seq) approaches did not work well for most NETs tested, presumably due to their association with the insoluble lamin polymer and membrane integration (anecdotal evidence plus a paucity of papers despite many labs trying). ChIP-Seq has been used with considerable success to determine many aspects of lamin A-chromatin associations [18, 29]; however, these data cannot distinguish the nucleoplasmic pool of lamin A from the NE fraction, and it is hard to determine what may have been missed because of the insolubility of the lamin polymer [30, 31] which takes great skill to break down into ChIP-friendly pieces. To overcome these issues, the DamID method was developed which is based on the unique ability of bacterial Dam methylase that can add adenine methylation to GATC motifs that is not normally present in mammalian genomes [32, 33]. Thus, fusing a NE protein such as lamin B1 to the bacterial Dam methylase enables this unique m6A methylation to be added to proximal genome regions, which can be subsequently enriched for and sequenced to enable the identification of NE-associated regions of the genome.

A typical DamID experiment starts with viral transduction of the bacterial Dam methylase fused to one's protein of interest (to identify peripheral chromatin, most commonly lamin B1) into one's cells of interest. Viral transduction is used because rather than being isolated by affinity, the uniquely methylated DNA is enriched for by preferential amplification; thus, background amplification is reduced when a higher fraction of cells express the fusion protein. Next, DNA is labeled in situ by the Dam methylase which is maintained at a low level by using a leaky *D. melanogaster* heat-shock promoter of *hsp70* in the absence of heat shock to avoid saturating methylation of genomic DNA [34]. After labeling in situ for 72 h, cells are harvested, and total genomic DNA (gDNA) is extracted. The gDNA is digested with *DpnI*, an enzyme that cuts only at adenine methylated GATC sequences and amplified for sequencing. In addition to the fused Dam-lamin B1 construct, free Dam methylase is expressed in control cells to subtract bioinformatically peaks that are potentially unspecific, leaving the lamin B1/NE-conferred methylated sequences. Plotting these yields positive peaks indicating NE localization and negative peaks indicating absence from the NE; however, the intensity of these peaks can vary. Most analysis algorithms to call lamina associated domains (LADs) are binary, but these can cut off LADs that can be confirmed by FISH; therefore, it can potentially be useful to use other cutoffs.

While many protocols already exist for DamID, we have found the need to modify these protocols when adapting it for more differentiated cell types/tissues. Here we present optimized protocols for DamID and FISH on adipocytes. As lamins have already been linked to multiple lipodystrophies and metabolic syndromes [35, 36] and knockout of the fat genome organizing NET Tmem120A in mice yields a lipodystrophy phenotype [7], it seems likely that radial genome organization is important for these disorders and possibly also the epidemic of obesity [37, 38]. The approach presented below can thus be directly used to study these disorders or it can be further adapted by comparing optimization for different tissues [39, 40] to tackle genome organization in the many other models where genome organization defects are being linked to human disease.

## 2 Materials

### 2.1 Lamin B1-DamID Equipment and Materials

#### 2.1.1 Equipment

1. Standard tissue culture labware, i.e., biosafety hood, centrifuge, and tissue culture CO<sub>2</sub> incubator.
2. Swinging bucket centrifuge  $\geq 4000 \times g$ .
3. Swinging bucket ultracentrifuge  $\geq 55,000 \times g$  and rotor, e.g., JA25.50 (Beckman Coulter) with round bottomed 30 mL tubes.
4. PCR thermocycler to amplify Dam-methylated DNA.
5. Centrifuge  $\geq 14,000 \times g$  for purification of DamID products.
6. Standard agarose electrophoresis equipment.
7. Epifluorescence microscope equipped with filters for GFP (488 nm) and if not set up for live cell imaging also DAPI (461 nm). If such a microscope is not available, the level of GFP expression can be assessed by Western blotting in which case equipment and materials for SDS-PAGE will instead be necessary.
8. Access to BIoAnalyzer or Qubit for DNA quality assessment unless this will be done by sequencing provider in which case still a spectrophotometer capable of small volume measurements such as a NanoDrop is necessary.

#### 2.1.2 Lentivirus Production and Transduction

1. PES syringe filter 0.45  $\mu\text{m}^2$  (*see Note 1*).
2. HEK293FT cells (ATCC, cat. PTA-5077) (*see Note 2*) cultured in DMEM supplemented with 10% FBS, 100 U/mL penicillin, 100  $\mu\text{g}/\text{mL}$  streptomycin.
3. Transfection reagents, e.g., Lipofectamine 2000 (Invitrogen, cat. 11668019) and OptiMEM (Gibco, cat. 31985062) (this protocol was optimized with these though any other could be used).

4. Genomic DNA extraction kit for mycoplasma test, e.g., DNeasy Blood and Tissue Lysis kit (Qiagen, cat. 69504).
5. Primers for mycoplasma detection: Fwd. 5' GGGAGCAAA CAGGATTAGATACCCT and Rev 5' TGCACCATCTGTC ACTCTGTAAACCTC.
6. Standard PCR polymerase Mix (e.g., Phusion cat. M05300S).
7. dNTPs.
8. Agarose and standard reagents for electrophoresis to resolve DNA and test for mycoplasma positive lysates.
9. Plasmids for viral packaging:
  - psPAX2, (Addgene, cat. 12260).
  - pMD2.G, (Addgene, cat. 12259).
10. Transfer plasmid:
  - pLGW-empty, (van Steensel lab) (*see* **Note 3**).
  - pLGW-Dam, (Addgene, cat. 59210).
  - pLGW-Dam-Lamin B1, (Addgene, cat. 182671).
  - pRRLSIN.cPPT.PGK-GFP.WPRE (Addgene, cat. 12252).
11. Protamine sulfate.
12. Phosphate-buffered saline (PBS), 137 mM NaCl, 2.7 mM KCl, 10 mM Na<sub>2</sub>HPO<sub>4</sub>, and 1.8 mM KH<sub>2</sub>PO<sub>4</sub>, pH 7.4.
13. DAPI stain and paraformaldehyde (PFA) if a live-cell fluorescence imaging setup is not available in the tissue culture room.
14. Other standard microscopy consumables, i.e., glass slides, coverslips, and anti-fade mounting medium (e.g., Vectashield, Vector Laboratories, cat. H-1000-10 or Fluoromount-G, Invitrogen, cat. 00-4958-02).

**2.1.3 Maintenance and Differentiation of Adipocytes from 3T3-L1 Cells**

1. 3T3-L1 mouse fibroblasts (ATCC, cat. CL-172).
2. Oil Red O (Thermo Scientific, cat. A12989) or LipidTox (Thermo Scientific, cat. H34477).
3. Growth medium: DMEM, 10% FBS, 1X MEM non-essential amino acids, 1 mM Sodium Pyruvate, 100 U/mL penicillin, 100 µg/mL streptomycin.
4. Differentiation induction medium: DMEM, 10% FBS, 0.5 µM insulin, 1 µM dexamethasone, 0.5 µM 3-isobutyl-1-methylxanthine (IBMX), 1 µM rosiglitazone, 100 U/mL penicillin and 100 µg/mL streptomycin.
5. Adipocytes maintenance medium: DMEM, 10% FBS, 0.5 µM insulin, 1 µM rosiglitazone, 100 U/mL penicillin and 100 µg/mL streptomycin.
6. Trypsin for splitting cells.

7. PBS.
8. Standard tissue culture plasticware.

#### 2.1.4 Generation and Enrichment of Dam-Methylated DNA

1. 3T3-L1 preadipocytes and mature adipocytes (generated from above).
2. Lentivirus particles with DamID packaged constructs (generated from above).
3. DNeasy blood and tissue lysis kit.
4. 3 M potassium acetate, pH 5.5.
5. Glycogen.
6. Ethanol.
7. DpnI.
8. T4 DNA Ligase.
9. DpnII.
10. Antarctic phosphatase.
11. Primers:
  - (a) AdRt 5' CTAATACGACTCACTATAGGG-CAGCGTGGTTCGCGGCCGAGGA 3'.
  - (b) AdRb 5' TCCTCGGCCG 3'.
  - (c) Adrp-PCR 5' GGTCGCGGCCGAGGATC 3'.
12. cDNA HF-Advantage PCR kit.
13. PCR purification kit.
14. Access to a sequencing provider capable of at least 90PE reads at the recommended depths of 20–40 M per sample. If the provider does not also do library construction, this will also need to be outsourced or performed by the user. Illumina currently recommends preparing DamID libraries with TruSeq DNA Nano kit (Illumina, cat. 20015964). Alternatively, we can also recommend NEBNext Ultra (NEB, cat. E7645S).

#### 2.1.5 Data Analysis

1. Computer with at least a 4-core processor, Unix operating system (e.g., Linux), 16Gb of RAM memory and at least 50Gb of free space on the hard drive. However, deeper sequencing protocols might require more storage space.
2. Trimmomatic, (<http://usadellab.org/>), v0.35 [41].
3. FastQC, v.0.11.9, (<https://www.bioinformatics.babraham.ac.uk/projects/fastqc/>).
4. Bwa-Mem, v.0.7.16 [42].
5. R package, v.1.46.0, (<https://cran.r-project.org>, R Core Team (2015). R: A language and environment for statistical computing. R Foundation for Statistical Computing, Vienna, Austria. URL <https://www.R-project.org/>).

6. BEDTools [43].
7. EdgeR [44].
8. DESeq2 [45].
9. BioConductor, DNA copy, (<https://bioconductor.org/packages/DNAcopy>).
10. BioConductor, Limma, (<https://bioinf.wehi.edu.au/limma/>) [46].
11. SICER2, for peak calling in the  $\log_2$ (Lamin B1/Dam) ratio, (<https://zanglab.github.io/SICER2/>) [47].
12. IGV, Integrative Genome Browser for DamID peaks visualization, (<https://igv.org/doc/desktop/>) [48].

## **2.2 Immuno-3D-FISH on Cultured Adipocytes and Fat Tissue: Equipment and Materials**

### **2.2.1 Equipment**

1. Microfuge  $\geq 10,000\times g$ .
2. PCR thermocycler.
3. SpeedVac DNA concentrator.
4. UV crosslinker and UV transilluminator.
5. Swinging bucket centrifuge  $\geq 1000\times g$ .
6. Heating blocks at 37 °C and 85 °C.
7. Drying oven at 70 °C.
8. Water baths at 37 °C, 45 °C and 60 °C.
9. Coplin jars for staining glass slides.
10. Isolation of ex vivo adipose tissue will require a CO<sub>2</sub> chamber for humane termination of mice.
11. Dissection of adipose tissue will require surgical instruments available from many manufactures and in a variety of shapes and sizes. We recommend a starting set of tools as follows:
  - (a) Straight Deaver scissors, 5.5" (Roboz Surgical Store, cat. RS-6762).
  - (b) Straight Iris scissors (VWR, cat. 470018-890).
  - (c) Spring micro-dissecting scissors, straight, 5 mm (VWR, cat. 76457-358).
  - (d) Spring micro-dissecting scissors, curved, 5 mm (VWR, cat. 76457-360).
  - (e) Straight dissecting Forceps, fine tip, 114 mm (VWR, cat. 82027-386).
  - (f) Precision straight tweezers, No. 5, 110 mm (VWR, cat. 89259-986).
  - (g) Dissecting Forceps with curved tip, 114 mm (VWR, cat. 89259-946).
12. 7 mL Bijou tubes for sample collection in 4% PFA.

13. Round-bottom 14 mL tubes.
14. Suitable container for warming up paraffin to 58 °C or paraffin embedding station, e.g., EpreDia HistoStar (ThermoFisher, cat. HIS3350).
15. Tissue Path™ IV Tissue Cassettes.
16. Forceps and brushes to handle paraffin blocks.
17. Tissue sectioning will require a Microtome capable of generating 4–10 µm thickness sections.
18. Hydrophobic barrier pen.
19. Epifluorescence microscope: e.g., widefield microscope with 60× or 100× objectives (it is difficult to see loci at lower magnification), appropriate filter set for fluorophores that will be used to visualize hybridized probes, and camera. The FISH signals are often weak with a high background to noise ratio; so at least a mid-range EM-CCD camera is recommended, e.g., Prime 95B camera (Photometrics). It is not necessary if just doing 2D FISH, but to do 3D FISH will also require a motorized stage capable of 0.2 µm Z-steps. If this is not available a comparatively inexpensive option is to purchase a PIFOC Z-axis focus drive (e.g., Physik Instruments) that can be mounted under the objective.

### 2.2.2 *Animals and Cell Lines for Immuno-3D-FISH*

1. BL6/57 mouse or other relevant animal model at age/condition of interest. Preselect adipose tissue depot and plan dissection in advance. For guidance on adipose tissue depot identification and methods of dissection refer to published protocols by Bagchi et al. (2019) [49] and Mann et al. (2014) [50]. As adipose tissue is reported to begin degrading rapidly after death, it is important to plan access to tissues immediately after termination even if this step is being done by animal facility personnel.
2. Cultured 3T3-L1 preadipocytes and differentiated adipocytes are maintained with the same materials as for DamID (*see* Subheading 2.1.3). For FISH, however, cells are cultured on 13 mm glass coverslips in 24-well plates and before the FISH experiment cells are fixed in PFA.

### 2.2.3 *Animal Models Dissection and Cell Culture*

1. PBS.
2. Ethanol.
3. 4% PFA in PBS.
4. Cell culture materials as described above (*see* Subheading 2.1.3).
5. Paraffin, EpreDia, melting point 55–57 °C.

6. Positively charged microscope slides, e.g., EpreDia SuperFrost Plus Adhesion slides (ThermoFisher, cat. J1800AMNZ).

#### 2.2.4 Probe Ordering, Storage, and DNA Isolation Materials

1. Choose genome regions of interest based on DamID data as described in Subheading 3.2.5, purchase BAC or Fosmid clones from a suitable vendor (*see Note 4*). We recommend BacpacResources (<https://bacpacresources.org>). Note that it typically takes 2 weeks to receive clones as a bacterial swab.
2. Appropriate resistance antibiotics for BACs and Fosmids, e.g., typically ampicillin or chloramphenicol.
3. Luria Broth (LB).
4. Glycerol.
5. If not using a kit for plasmid purification, make lysis buffers: 100 mL of GTE buffer: 50 mM glucose, 25 mM Tris pH 8.0, 10 mM EDTA, RNase A with no DNase activity at purchase or from boiling, Lysozyme, 10 mL of fresh lysis buffer: 0.2 M NaOH, 1% SDS. 100 mL of acetate buffer: 5 M KCH<sub>3</sub>COO, 11.5% glacial acetic acid.

#### 2.2.5 Nucleotides for Nick Translation and Probe Detection

1. Choose the probe detection method. One can incorporate into probes nucleotides directly coupled to fluorophores or nucleotides coupled to biotin or digoxigenin followed by staining with antibodies against biotin or digoxigenin coupled to fluorophores. Currently, we recommend the use of nucleotides directly labeled by fluorophores as they give a robust signal and typically give less background from the fluorescent secondary antibody.
2. Purchase labeled dUTPs for the chosen probe detection method. We tested the following with good results: fluorophore labeled: ChromaTide™ Alexa Fluor 488-5-dUTP (ThermoFisher C11397), SEEBRIGHT® Green 496 dUTP (Enzo, ENZ-42831L), ChromaTide™ Alexa Fluor 568-5-dUTP (ThermoFisher C11399), or ChromaTide™ Alexa Fluor 594-5-dUTP (ThermoFisher C11400). Also, we have successfully used digoxigenin-labeled dUTPs (digoxigenin-11-dUTP, Roche, cat. 11093088910) and biotin-labeled dUTPs (biotin-16-dUTP, Roche, cat. 11093070910).
3. If using biotin- or digoxigenin-labeled dUTPs, also purchase secondary antibodies to detect labeled nucleotides. We have gotten good results using the following:
  - (a) Alexa Fluor 488 IgG fraction monoclonal mouse anti-digoxigenin (Jackson ImmunoResearch, cat. 200-542-156).

- (b) Alexa Fluor 594 IgG fraction monoclonal mouse anti-digoxigenin (Jackson ImmunoResearch, cat. 200-582-156).
- (c) Alexa Fluor 488 streptavidin (Jackson ImmunoResearch, cat. 016-540-084).
- (d) Alexa Fluor 594 streptavidin (Jackson ImmunoResearch, cat. 016-580-084).
- 4. Nucleotides, dATP, dCTP, dGTP, and dTTP.
- 5. Polymerase I, 10 U/ $\mu$ L, (Invitrogen, cat. 18010017).
- 6. DNase I, (Roche, cat. 04716728001).
- 7. 10 $\times$  Nick Translation Salts (NTS): 0.5 M Tris pH 7.5, 0.1 M  $\text{MgSO}_4$ , 1 mM DTT, 0.5 mg/mL BSA fraction V, (SIGMA, cat. 810533).
- 8. Efficiency Buffer 1: 0.1 M Tris pH 7.5, 0.15 M NaCl.
- 9. Efficiency Buffer 2: 0.1 M Tris pH 9.5.
- 10. Whatman Protran nitrocellulose membrane cat. BA 85/20; 0.45 $\mu$ m, cat. 10405316.
- 11. G-50 MicroSpin columns, (Amersham, cat. 27533001 or Illustra, GE Healthcare, cat. 27-5330-01; both works equally well).
- 12. Streptavidin alkaline phosphatase to detect biotin, (Roche, cat. 11093274910) and anti-Dig-AP antibodies to detect digoxigenin labeled probes, (Roche, cat. 11093266910).
- 13. Vector BCIP/NBT kit (Vector Lab cat. SK-5400).
- 14. For nuclear envelope counter-staining we use a lamin A antibody generated in an appropriate species to complement other antibodies if biotin or digitoxigenin-labeled nucleotides are used, and appropriate secondary antibody based on other fluorophores used for the FISH probes.

#### 2.2.6 Permeabilization and Hybridization Solutions

- 1. HistoChoice Clearing Agent (SIGMA, cat. H2779) to remove paraffin. Alternatively, standard historical protocols using xylenes can be applied to deparaffinate tissue sections.
- 2. Triton X-100.
- 3. Proteinase K.
- 4. 2 M acetic acid.
- 5. Tris buffer pH 8.0.
- 6. BSA fraction V.
- 7. 20 $\times$  Saline-sodium citrate buffer (SSC): 3 M NaCl, 300 mM  $\text{Na}_3\text{C}_6\text{H}_5\text{O}_7$ , adjusted to pH 7.0 with HCl.
- 8. Make 2 mL per probe of fresh denaturation buffer: 70% formamide in 2 $\times$  SSC in  $\text{H}_2\text{O}$  (*see* **Note 5**).

9. Make 1 mL per probe of fresh hybridization buffer: 2× SSC, 50% formamide, 10% dextran sulfate, 1% tween-20, H<sub>2</sub>O, 0.1% Tween, 0.1× SSC.
10. Mouse Cot1 DNA, (Invitrogen, cat. 18440016).
11. Sheared salmon sperm DNA (Invitrogen, cat. AM9680).
12. Rubber cement (e.g., Marabu, Fixogum) for sealing samples during hybridization.
13. Antifade mounting medium (e.g., Vectashield, Vector Laboratories, cat. H-1000-10).
14. Poly-L-Lysine coated 13 mm coverslips, thickness 0.13–0.16.

#### 2.2.7 Imaging and Data Analysis

1. Software for image acquisition: e.g., ZEN (ZEISS), MetaMorph (Molecular Devices) or Micromanager (open source).
2. If doing 3D FISH, software for image deconvolution, e.g., AutoQuant X3 (Media Cybernetics).
3. Software for Image analysis, e.g., Imaris (Oxford Instruments), ImageJ (open source), or Volocity 3D Visualization (PerkinElmer).

---

## 3 Methods

### 3.1 DamID in 3T3-L1 Adipogenesis Model

#### 3.1.1 Cell Lines Quality Check: Mycoplasma and Differentiation Potential

The first stage of a successful DamID experiment is to confirm the quality of cells used. HEK293FT fibroblasts or any equivalent cell line used for the production of dam domain-carrying lentivirus particles must be free of mycoplasma as these microorganisms encode a dam methylase that might be a source of false positive DamID signals (Fig. 1). Also, cells infected with mycoplasma yield lower levels of viral particles. Similarly, healthy mycoplasma-free 3T3-L1 cells (or other target cell) are a prerequisite for successful DamID experiments. Healthy and mycoplasma-free 3T3-L1 pre-adipocytes will also yield more robust mature adipocytes.

1. Grow cells for 48 h and isolate genomic DNA using DNeasy blood and tissue kit, according to manufacturer instructions.
2. Mix the following reaction for each sample:
  - 1 µL of gDNA at concentration of 50 ng/µL.
  - 4 µL of 5× High Fidelity buffer.
  - 2 µL of primer mix (from 5 µM mix stock).
  - 0.2 µL of 10 mM dNTPs.
  - 12.8 µL of H<sub>2</sub>O.
3. Run the PCR reaction in a thermocycler using the following program:

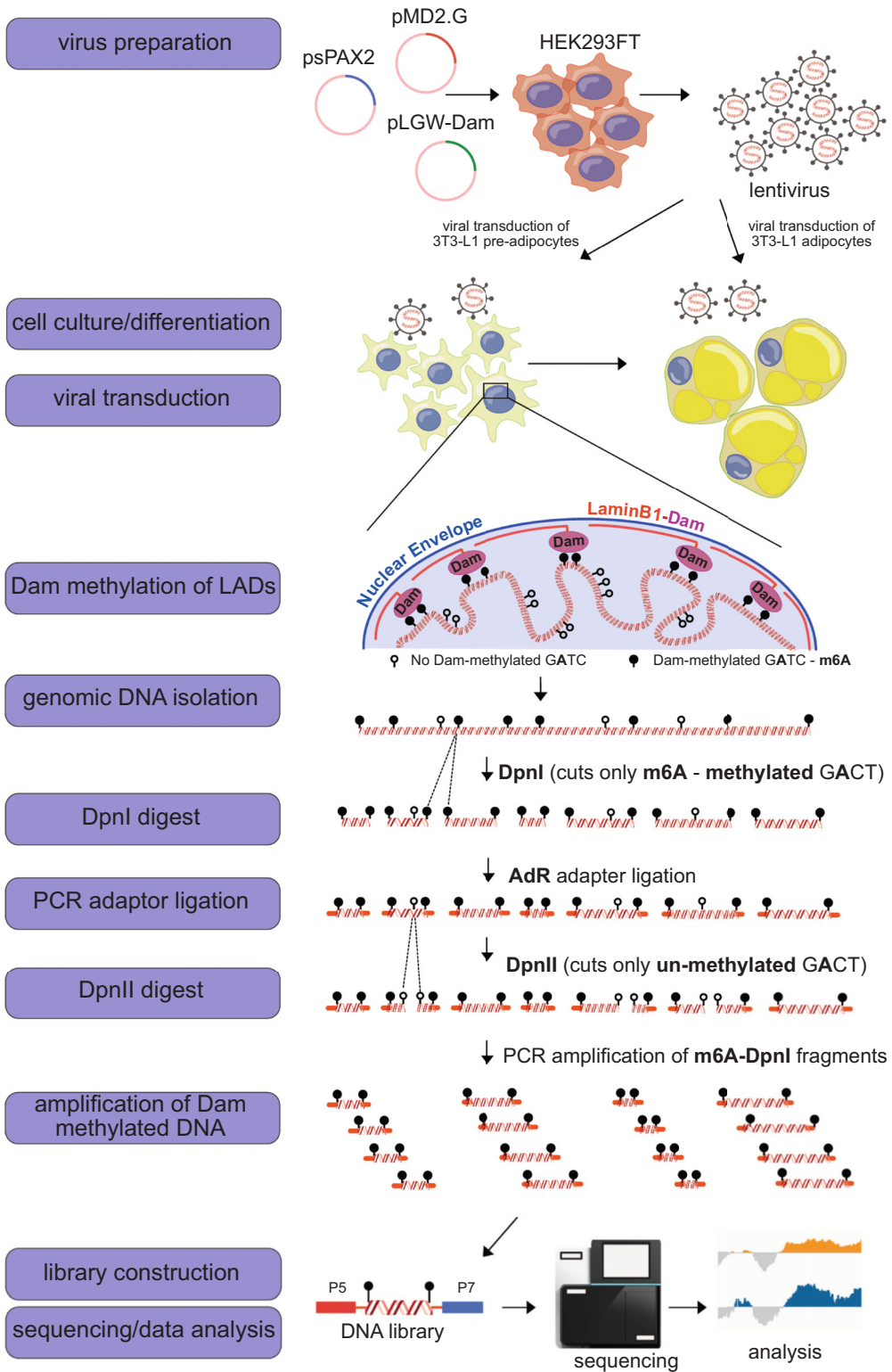


**Fig. 1** Flowchart diagram representing steps and principles of the DamID method. The procedure starts with virus preparation by transfecting HEK293FT cells with virus component plasmids (psPAX2, pMD2.G, and pLGW-Dam) and lentivirus collection. At the same time, quality checks are performed (e.g., mycoplasma, cell

- Sample volume 20  $\mu$ L.
  - Lid temperature 100 °C.
  - Denaturation at 98 °C for 30 s.
  - 32 cycles of: 98 °C for 7 s, 68 °C for 7 s and 72 °C for 5 s.
  - Final elongation at 72 °C for 10 s.
4. Resolve PCR reaction on a 2% agarose gel. Positive control and contaminated sample will yield a 220 bp PCR product.
  5. Mycoplasma contaminated cells are not usable for DamID experiment. If mycoplasma positive cell samples are identified, then the best action is to identify a mycoplasma free batch. Alternatively, cells can be treated with standard mycoplasma treatments using, e.g., BM Cyclin (Roche) or Plasmocin (InvivoGen) kits. However, it is important to note that 3T3-L1 cells can lose differentiation potential the longer they are passaged; thus, it may be better to replace than clean them if contaminated.
  6. If comparing differentiated and undifferentiated adipocytes, it is helpful due to the preceding point to start with low passage number cells and to pre-test them to ensure they are robust, can differentiate well, and can tolerate lentiviral transduction.

### 3.1.2 Lentivirus Production in HEK293FT Cells

It is important to achieve the highest percentages of transfected cells possible because of backgrounds with mitochondrial DNA in DamID experiments (i.e., the mitochondrial background will come from all cells whether or not they express the Dam methylase construct and so the ratio of background noise diminishes the more cells express the Dam methylase construct). The most widely used technique is lentiviral transduction due to its efficiently delivering dam methylase constructs to virtually every proliferating and non-proliferating cell type.

1. If not using the lamin B1-Dam methylase fusion construct, generate whatever Dam fusion you will be using in the same vector for expression in the lentivirus system.

---

**Fig. 1** (continued) viability) as well as the optimization of cell transduction and 3T3-L1 adipocytes differentiation. In the following steps, cells are transduced and the lamin B1-Dam fusion protein is expressed at the nuclear envelope. Subsequently, lamina associated domains (LADs) are Dam methylated at adenines (m6A) of GATC sequences. Next, genomic DNA is extracted and fragmented with DpnI enzyme that digest only m6A methylated GATC sequence. In the following step, AdR adapters are ligated to DpnI fragments. These adapters will act as a template for selective PCR amplification in the subsequent steps. Next, the DpnI fragments are digested by DpnII enzyme that targets only un-methylated GATC sequences. The resulting m6A methylation-flanked DpnI fragments (m6A-DpnI) are PCR amplified with primers complementary to AdR adapters. Subsequently Illumina sequencing libraries are generated and sequenced, and data are analyzed

2. Culture HEK293FT cells in fully supplemented media as described (*see* Subheading 2.1.2).
3. Mix the lentiviral plasmid in Opti-MEM at the following proportions per virus prep:
  - 4.6  $\mu$ g psPAX2.
  - $\mu$ g PMD2.G.
  - 7.5  $\mu$ g transfer vector, i.e., pLGW-empty, pLGW-Dam or pLGW-Dam-lamin B1
  - top up to 1.5 mL with Opti-MEM.
4. Mix 36  $\mu$ L of Lipofectamine 2000 with 1.5 mL of Opti-MEM in a 15 mL tube (*see* Note 6).
5. Incubate solutions from **Steps 2** and **3** in Subheading 3.1.2 at room temperature for 5 min; then combine them and mix gently (final volume is 3 mL). Incubate DNA-Lipofectamine mixture for 20 min at room temperature.
6. During DNA-Lipofectamine incubation, trypsinize and count HEK293FT cells. Use 6 million cells per viral preparation. Plate cells in 6 mL culture media in a 10 cm tissue culture plate and immediately add the 3 mL of preincubated DNA-Lipofectamine solution from **Step 4** in Subheading 3.1.2. Mix culture carefully and place into the tissue culture 5% CO<sub>2</sub> incubator.
7. Next day remove the media from the culture and add fresh 15 mL of media and continue to culture for another 48 h to maximize lentivirus concentration in the media.
8. Harvest the virus-containing media from the cell culture into 50 mL tubes and store at 4 °C. Add fresh media to the cells and collect after 24 h for additional viral particles production.
9. Combine both supernatants and centrifuge at 1000 $\times$  *g* for 15 min to remove cell debris. Transfer the clean, viral-rich supernatant to a new 50 mL tube and discard pelleted debris.
10. To remove small impurities, pass the clarified supernatant through a 0.45  $\mu$ m<sup>2</sup> PES syringe filter.
11. Immediately, transfer filtered viral-rich supernatants into 30 mL Oak Ridge round bottomed tubes and top up with PBS to 25 mL if required and spin at 55,000 $\times$  *g* for 75 min at 4 °C using a JA25.5 rotor in a Beckman Avanti JA-25 centrifuge or equivalent. Lentivirus particles will appear as a semi-translucent pellet of ~3 mm in diameter to the side on the bottom of the tube.
12. Remove the supernatant and resuspend the lentivirus pellet in 1 mL of media used for culture of target cells by gentle agitation on a shaker for 10 min at room temperature. If not used immediately, freeze aliquots at –80 °C.

### 3.1.3 Culture and Differentiation of Adipocytes from 3T3-L1 Fibroblasts

Maintaining the differentiation potential of 3T3-L1 cells is a crucial challenge in culturing these preadipocytes. These fibroblasts once growing beyond 80% confluency will considerably reduce their ability to form mature adipocytes. Thus, we recommend using a fresh batch of cells from an aliquot frozen at an early passage number rather than splitting and differentiating overcultured cells.

1. Maintain 3T3-L1 fibroblasts as described previously [51]. Briefly, plate 300,000 cells in one well of 6-well tissue culture dish in Growth media (*see* Subheading 2.1.3) until ~60% confluency. Overgrowing 3T3-L1 will significantly reduce differentiation potential of these cells so definitely split them well before they reach 80% confluency.
2. To maintain cells, once they reach ~60% confluency, wash them gently with PBS, trypsinize, and passage them 1:6 (typically we seed  $0.2 \times 10^6$  cells into one six-well plate).
3. If differentiating cells, let them continue to full confluency and then let them go for another 2 days before inducing differentiation. At second day post-confluency, wash them gently with PBS and add differentiation induction media (*see* Subheading 2.1.3) and continue culturing cells for 48 h.
4. At this time, replace the media with adipocyte maintenance medium and continue culturing cells for another 96 h, changing the maintenance medium again at the midpoint. By the 96th h point, cells should be fully differentiated into adipocytes and ready for transduction with lentivirus (a total of 6 days from induction of differentiation). Adipogenesis efficiency can be assessed by Oil Red O staining or LipidTOX stain (Fig. 2a).
5. If using 3T3-L1 preadipocytes as controls for DamID experiments, it is wise to time culturing so as to plate them 1 day before transduction. This gives time for genome organization patterns to settle after splitting while having the cells at a low enough density so as to not get confluent during the course of the DamID experiment.

### 3.1.4 Lentiviral Transduction Optimization

Prior to engaging the DamID experiment, it is wise to first optimize the lentiviral transduction, e.g., optimal viral titer levels and concentration of transduction enhancers. If using 3T3-L1 cells, provided they are reasonably early passage number from an ATCC-purchased stock, the optimized conditions listed below should work; however, even if further optimization is not needed, it is necessary to determine virus titers and useful to check that similar transduction efficiencies are obtained. To estimate transduction efficiency, perform a pilot experiment using virus with GFP-only expression (Fig. 2b) (Subheading 2.1.2). This enables the visual assessment of the infected cells (*see* Note 7). To further optimize lentiviral transduction, the process can be enhanced with

several chemicals. These enhancers tend to be cationic molecules that increase virus attachment to the cell membranes by neutralizing the charge repulsion between the virus and the cell surface as both are negatively charged, thus improving the transduction efficiency. These compounds, however, are often toxic to the cells in high concentrations. Previously, we established that for DamID in the myogenesis C2C12 model, the most efficient enhancer with the least interference in differentiation was protamine sulfate [39], while for mouse primary hepatocytes we found that polybrene was better [40]. For adipocytes, we found that protamine sulfate was the best.

1. To test for the optimal protamine sulfate concentration, seed 3T3-L1 cells in several wells of a 24-well plate. Include samples to be cultured in both the undifferentiated and differentiated states if DamID will be performed on both as optimal conditions may differ for each. Maintain the cultures as described (*see* Subheading 3.1.3).
2. Add 1 mL of fresh culture medium containing protamine sulfate at final concentrations of 0  $\mu\text{g/mL}$ , 2  $\mu\text{g/mL}$ , 4  $\mu\text{g/mL}$ , 8  $\mu\text{g/mL}$ , 10  $\mu\text{g/mL}$ , and 12  $\mu\text{g/mL}$  to the different wells and continue culturing for 24 h.
3. Replace the media with fresh culture media and incubate for a further 48 h to assess cell morphology, proliferation, and differentiation potential. For the DamID experiment, choose the maximum concentration of the transduction enhancer with no negative effects on cell viability or differentiation. In our experiments, we used 10  $\mu\text{g/mL}$  protamine sulfate. However, we still recommend this optimization step as we expect some batch variation from both compound and cell line.
4. Optimize viral titer by preparing dilutions of harvested viruses. For each well of a 24-well plate, prepare 1 mL of media supplemented appropriately for preadipocytes and adipocytes. Add the desired concentration of protamine sulfate in five separate wells 25  $\mu\text{L}$ , 50  $\mu\text{L}$ , 100  $\mu\text{L}$ , 250  $\mu\text{L}$ , and 500  $\mu\text{L}$  of viral preparation. Also, leave one well free of virus as a control. Culture cells with the virus for 24 h transduction.
5. At the 24 h point, replace the medium with fresh and culture for another 48 h to give time to express before assessing the GFP signal level.
6. Assess transduction efficiency by fluorescence microscopy. Cells can be checked live if an epifluorescence microscope is available in tissue culture, but if this is only equipped with low magnification objectives, it may be difficult to see the GFP signals. In this case, fix samples with 4% PFA for 10 min, counterstain the nuclei by DAPI and seal the sample with anti-fade mounting

medium, e.g., Vectashield and image cells on an epifluorescence microscope equipped with filters for GFP and DAPI.

7. Alternatively, cells can be trypsinized, sonicated, and GFP detected by Western blotting; however, we recommend microscopy as exact transduced cell numbers can be counted.

### 3.1.5 Lamin B1-DamID Experiment

Once the culture of preadipocytes/adipocytes is established, viral particles have been produced, and transduction conditions have been optimized, the DamID experiment can be performed. Consider the time required for differentiation of mature adipocytes and synchronize accordingly the cultures of pre-adipocytes if needed.

1. Culture pre-adipocytes and adipocytes in 6-well plates as described above. Seed cells for pre-adipocytes 1 day before transduction to avoid over-confluency during the experiment. Differentiate adipocytes for 6 days from the induction day (*see* Subheading 3.1.3 and *see* **Note 8**). As mentioned above, differentiation efficiency can be assessed by Oil Red O or Lipid-TOX staining according to manufacturer protocols (Fig. 2a).

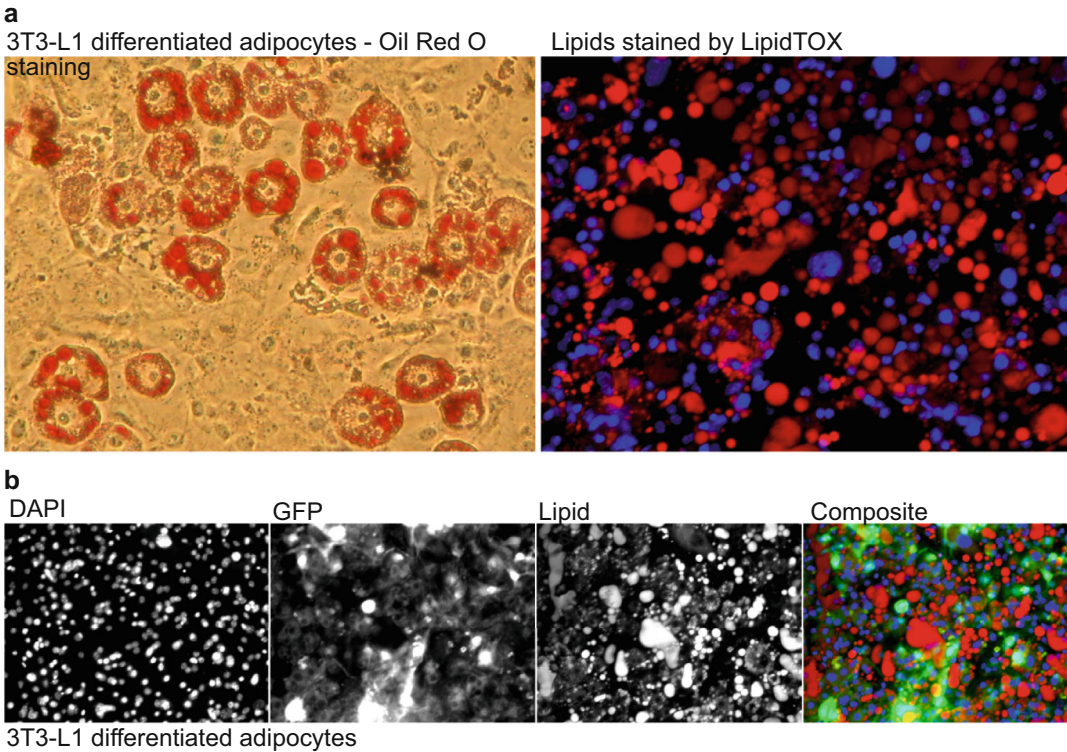


**Fig. 2** (a) 3T3-L1 adipogenesis assessment by Oil Red O staining (left panel), lipid droplets visible in red and LipidTox staining (right panel), nuclei stained by DAPI (blue), and lipids visible in red channel. (b) Assessment of transduction efficiency of GFP virus can be conducted by analysis of the signal with epifluorescence microscope. In our hands, we obtained regularly close to 90% cells GFP positive

2. On the day of transduction, replace media with fresh medium with 10 µg/mL protamine sulfate (or optimized quantity if different) and predetermined quantities (based on titers) of the following lentiviruses:
  - Empty vector.
  - Dam-only.
  - Dam-lamin B1.
  - GFP (for visual control of infection).
3. Culture transduced cells for 3 days to ensure Dam-lamin B1 expression and sufficient methylation of DNA.
4. Assess the transduction efficiency by analyzing GFP signal in control cells (Fig. 2b).
5. Aspirate the media, wash cells gently with PBS considering that mature adipocytes are very easy to detach at this stage. Trypsinize the cells, pellet by centrifugation and isolate total genomic DNA using the DNeasy blood and tissue lysis kit, and include the RNase digestion step.
6. Perform final precipitation of DNA by adding 0.1 volumes of 3 M sodium acetate (pH 5.5), 10 µg of glycogen, and 3 volumes of 100% ethanol. Incubate samples in –80 °C for at least 1 h or overnight and pellet DNA at 13,000× *g* for 15 min at 4 °C.
7. Aspirate the supernatant and wash the pellet with 70% ethanol with a final centrifugation step at 13,000× *g* for 5 min at 4 °C.
8. Remove the supernatant and air-dry the pellet.
9. Resuspend the pellet in nuclease-free water by heating up the solution to 55 °C for 1 h. Additional time might be needed if the DNA pellet is not fully resuspended. Quantify the DNA amount by nano-drop.

### 3.1.6 Enrichment of Dam-Methylated Genomic DNA

The Dam-methylated genomic DNA that has been isolated can now be enriched by specific PCR amplification of generated fragments. The DNA in the region of LADs will contain methylated GATC sequences which are first specifically restriction digested by the DpnI enzyme. Resulting fragments are ligated to adaptors that are complementary to PCR primers enabling specific amplification of the methylated fragments only. After ligation of adaptors, the remaining unmethylated GATC fragments are restriction digested by the DpnII enzyme, which recognizes the same sequence but only cuts if unmethylated, leaving only the fragments of interest flanked with primer-complementary sequences. In the final enrichment step, during the PCR reaction only DpnI-digested fragments are amplified (i.e., fragments flanked with Dam-methylated sequences) (Fig. 1). The product of this amplification is then ready for generating Illumina sequencing libraries. Note that

empty vector transduced cells should not produce any PCR product as there was no Dam methylase expressed. In addition, controls without DpnI enzyme (to control for apoptotic DNA cleavage) and without T4 DNA ligase (to control for dsAdR-independent amplification) should be included.

1. Digest 2.5 µg of isolated genomic DNA with DpnI at 37 °C for a minimum of 8 h. Include a sample transduced with Dam methylase lentivirus in the reaction lacking DpnI as a control. Set up the reaction as follows:
  - 2.5 µg of gDNA
  - 1 µL of 10× NEB buffer 4 (or equivalent buffer for another provider)
  - 0.5 µL of DpnI (20 U/µL)
  - H<sub>2</sub>O top up to 10 µL.
2. Heat inactivate the DpnI enzyme by incubating at 80 °C for 25 min and hold at 18 °C until ready to continue.
3. To anneal the adaptors, first mix equal volumes of 100 µM stocks of AdRt and AdRb primers. Next, denature the solution at 95 °C for 10 min and cool down slowly no faster than 1 °C/min (or denature on heating block and turn of the power after 10 min for slow annealing at room temperature).
4. Set up ligation of adapters reaction (include no T4 ligase control) as follows:
  - 10 µL of the reaction from **Step 2** in Subheading [3.1.6](#) containing digested gDNA
  - 2 µL of NEB ligation buffer
  - 1 µL of T4 DNA ligase (5 U/µL)
  - 0.8 µL of 50 µM dsAdR adaptors (annealed in **Step 3**)
  - 6.2 µM of H<sub>2</sub>O
5. Incubate the ligation reaction at 16 °C for 16 h.
6. Inactivate the T4 ligase by incubating the reaction at 65 °C for 20 min and digest the unmethylated GATC sequences by DpnII, an enzyme specific for unmethylated GATC. Set up the DpnII reaction as follows:
  - 20 µL of the reaction from **Step 4** in Subheading [3.1.6](#) (adaptor-ligated gDNA)
  - 5 µL of 10× NEB DpnII buffer
  - 1 µL of DpnII enzyme (10 U/µL)
  - 24 µL of H<sub>2</sub>O
7. Incubate the DpnII digestion reaction at 37 °C for 1 h.

8. PCR amplify adaptor-ligated DpnI fragments of Dam-methylated DNA. To increase the yields, several PCR reactions for each sample should be prepared. From the DpnII reaction (**Step 6** in Subheading 3.1.6), up to 10 amplification reactions can be set. We advise to set up at least 5 PCR reactions for each sample. Mix the following reaction per sample on ice in 200  $\mu$ L PCR tubes:
  - 5  $\mu$ L of DpnII digested gDNA—reaction from **Step 6** in Subheading 3.1.6
  - 5  $\mu$ L of 10 $\times$  cDNA PCR buffer
  - 1.25  $\mu$ L of Adr-PCR primer (from 50  $\mu$ M stock)
  - 1  $\mu$ L of dNTPs (from 10  $\mu$ M stock)
  - 1  $\mu$ L of 50 $\times$  Advantage PCR enzyme mix
  - 36.75  $\mu$ L of H<sub>2</sub>O
9. Run PCR reaction following the program for the thermocycler as follows:
  - Preheat lid to 100  $^{\circ}$ C.
  - Incubate at 68  $^{\circ}$ C for 10 min.
  - 1 cycle at 94  $^{\circ}$ C for 3 min, 65  $^{\circ}$ C for 5 min, 68  $^{\circ}$ C for 15 min.
  - 4 cycles at 94  $^{\circ}$ C for 1 min, 65  $^{\circ}$ C for 1 min, 68  $^{\circ}$ C for 10 min.
  - 18 cycles at 94  $^{\circ}$ C for 1 min, 65  $^{\circ}$ C for 1 min, 68  $^{\circ}$ C for 2 min.
  - Hold at 4  $^{\circ}$ C until ready to continue.
10. Load 3  $\mu$ L of the PCR reaction from the previous step on a 1% agarose gel for electrophoresis to assess the amplification yield and quality of PCR products. Expected product smear will appear between 200 and 2000 bp for samples transduced with lamin B1-Dam and Dam alone lentivirus (Fig. 3a). No PCR product is expected from negative control samples as described above.
11. Once the quality of PCR amplifications is confirmed and controls are negative, continue with pooling PCR reactions from the same samples and perform PCR cleanup with the Qiagen QIAquick PCR purification kit. Quantify and determine the quality of the purified product using a Bioanalyzer or Qubit (*see Note 9*) and continue with any additional steps required by the sequencing platform/provider. Most sequencing services will also perform library construction, and we recommend this if possible as it is often cost-effective and their frequency in performing this task makes mistakes infrequent; however, if considering other options, it may benefit to compare methods by referring to [52].

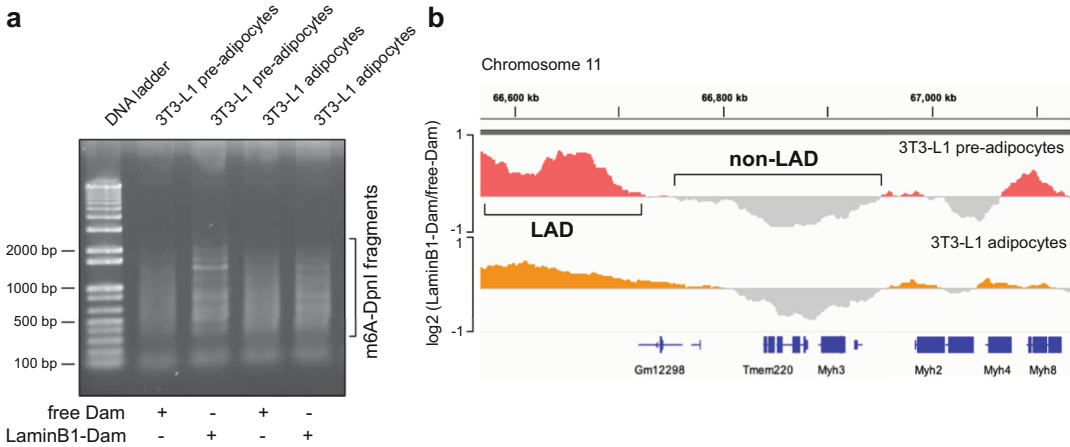


**Fig. 3** (a) Typical pattern of the DamID amplification product smear on the agarose gel. Expected smear size is between 2000 and 300 bp. (b) Examples of DamID tracks. Clear differential regions can be seen corresponding with the *Myh* genes cluster that show differences in association with the lamina when comparing pre-adipocytes and differentiated adipocytes. The tracks represent m6A-DpnI fragments signal as a ratio calculated for lamin B1-Dam samples to free-Dam samples and are shown as  $\log_2$  (lamin B1-Dam/free-Dam) value. Positive values are considered LAD sequences and negative values are considered non-LAD sequences

12. If performing a standard library construction, oneself instead of having the sequencing provider do this, DamID sample libraries can be prepared for Illumina sequencing by any standard protocol that randomly fragments the DNA and ligates standard sequencing adaptors (e.g., protocol refer to [53]). If libraries will be made in the lab, we recommend using a kit such as NEBNext Ultra (NEB, cat. E7645S) or TruSeq DNA Nano kit (Illumina, cat. 20015964) and following the manufacturer's instructions.

### 3.1.7 Sequencing and Data Analysis

1. We recommend paired-end (PE) sequencing with read lengths of at least 90 nucleotides, and a depth of at least 40 million PE reads, with 60 million being optimal in our experience. Lower than 20 million reads tend to lose sensitivity and the smaller LADs are not effectively detected, which can lose important data if searching for changing LADs since it is the smaller LADs that tend to be more dynamic. The use of 2–3 replicates is recommended. Note that mitochondrial sequence contamination is common for some cell types. In our experience, this can account from anything between <1% (HT1080 cell line) and >60% (C2C12 cell line). It is recommended to do a test to assess this and increase the sequencing depth accordingly. We have attempted to remove mitochondria DNA from the sample preparation, but we failed to do so without also losing genomic DNA.

2. Returned sequences should be processed to remove the adaptor sequences using Trimmomatic v0.35 [41] and quality assessed with FastQC v0.11.9. Trimmed sequences should then be aligned to the appropriate genome sequence (e.g., for mouse mm9) using Bwa Mem v0.7.16 [42] in PE mode using default parameters. Subsequent processing is performed using R and BEDTools [43].
3. DamID data should next be quantified at the DpnI fragment level by counting the number of reads that overlapped each DpnI fragment, for each of the Dam-lamin B1 and Dam-control pairs. The log<sub>2</sub> ratios between Dam-lamin B1 and Dam-control are calculated for each DpnI fragment, and the resulting values quantile normalized between samples in R using the BioConductor Limma package [46].
4. There are many peak finding algorithms that can be employed to define LADs. We recommend a circular binary segmentation algorithm available in the BioConductor package called DNACopy, using the default parameters [54]. This method segments the genome into regions of similar signal intensities and is geared towards the detection of signal switches, such as those demarking the transition between LAD/non-LAD regions. The positive signal tracts (signal threshold = 0) should be extracted and merged if less than 8 Kb apart (*see* **Note 10**).
5. To identify genomic regions with differential frequencies of association with the periphery (termed DR for “differential regions”) in the absence of replicates, one can follow a binary approach (LAD vs. non-LAD), i.e., subtract the LADs between conditions using BEDTools and select those regions that are only identified as a LAD in one of the conditions. These selected regions should then be filtered so that the average signal between conditions is at least twofold.

Alternatively, we have noticed that the signal over LADs can vary, sometimes wildly. It is not exactly clear what the biological meaning of a high signal LAD is compared to a low signal LAD. It could represent the likelihood that a given region is at the nuclear periphery in the cell population sampled; however, this is uncertain since similar patterns are observed in single-cell DamID [55]. In order to take into account signal differences to determine DRs, a statistical test was devised and described in Robson et al. (2016) to filter the results [39]. A moving window of 45 DpnI fragments (~25 Kb) is run along each chromosome, with a shift of 10 DpnI fragments (~5 Kb). The average DamID signal difference between two samples is calculated within each window. Windows with a signal difference greater than twofold are flagged as potential DRs. If this approach is undertaken, these regions should be tested for statistical significance compared to a control signal-

shuffled sample ( $\times 1000$  iterations) using Fisher's exact test. Regions that pass with  $p < 0.01$  can be called PI or IP regions, to denote regions that exhibited a significant repositioning moving either to the interior (PI) or to the periphery (IP) between the conditions examined.

If replicates are available, we recommend pooling all the LADs together, dividing them into 20 Kb fragments, and using those for quantification of the signals in all samples using the *featureCounts* algorithm [56]. This produces a matrix of counts that can be assessed for differential signal using standard tools such as *edgeR* [44] or *DESeq2* [45]. One could simply query the whole LADs as they are, but given the large size of many of them, the result would be too conservative as the average signal from many of the LADs is not uniform. For this reason, we recommend dividing LADs into fragments of 10–50 Kb. The higher the sequencing depth, the smaller the fragments can be. From the results, either one could select a binary DR definition where only those regions that belong to a LAD in only one of the conditions are accepted or one could use a nonbinary approach simply adding a  $\log_2(\text{FoldChange})$  as a filter. In this case, it is recommended to choose a range of peak intensities and increase the number of samples to test by FISH so that one can go back and set a threshold based on where LAD confirmation by FISH begins to fail (*see* Subheading 3.2). Representative visualization of DamID peaks by IGV browser is shown in Fig. 3b.

6. Confirmation of individual LADs and estimating the validity of LAD calling in general can best be done by FISH. The next section describes how to select LAD and DR candidates for FISH and how to perform FISH experiments on either tissue culture cells or in ex vivo adipose tissue.

### **3.2 Immuno-3D-FISH on Cultured Adipocytes and Ex Vivo Adipose Tissue: Protocol**

#### **3.2.1 Probe DNA Purification**

The workflow of FISH experiment begins usually with the preparation of the probe (Fig. 4). Extraction of high-quality DNA for generating probes is crucial for subsequent application in a successful FISH experiment. 2  $\mu\text{g}$  of DNA from one preparation is usually optimal for further applications (minimum 500 ng). The below is mostly standard molecular biology practices, but ratios have been modified to improve yields and purity of larger plasmids.

1. Upon delivery, streak bacteria from BAC or Fosmid clone glycerol stock on an agar plate with appropriate antibiotic and grow overnight at 37 °C.
2. Transfer a single colony to 6 mL of LB culture supplemented with ampicillin at final concentration of 100  $\mu\text{g}/\text{mL}$  or chloramphenicol at final conc. 25  $\mu\text{g}/\text{mL}$  (depending on which resistance gene is on the BACs or Fosmids). Divide 3 mL

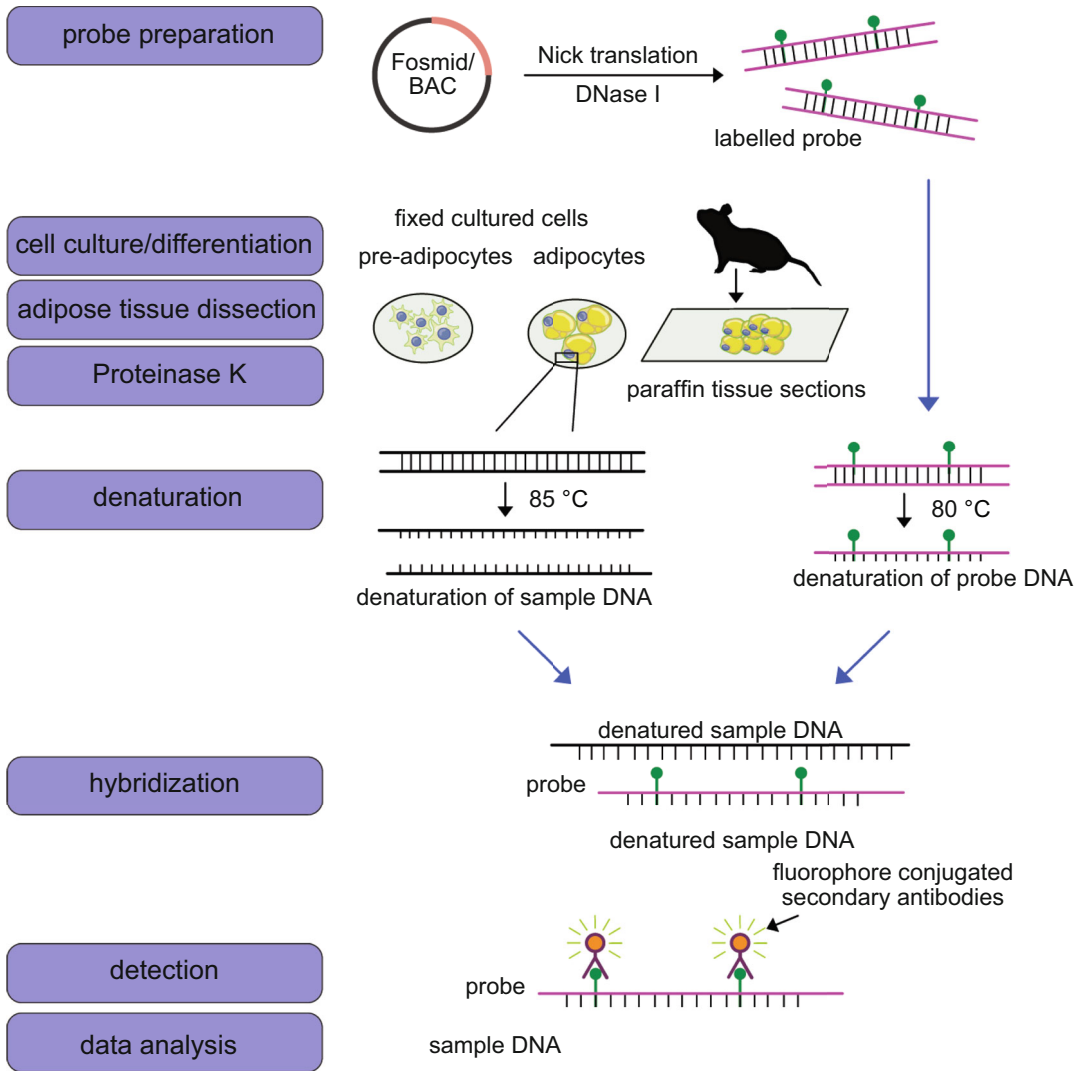


**Fig. 4** Flowchart diagram depicting a workflow of Immuno-3D-FISH protocol. The initial step of every FISH experiment is to prepare a labeled probe from a Fosmid or BAC by Nick translation. The next step is to fix the biological material and to permeabilize cells. In our FISH protocol for cultured adipocytes and adipose tissue, we use proteinase K for permeabilization. In the next step, the DNA of the sample and DNA of the probe is denatured to enable hybridization of the probe. In the final step, the hybridized probe is detected with fluorophore-conjugated antibodies to the digoxigenin or biotin probes that were used for labeling. If directly fluorophore-labeled nucleotides were used for probe production, no secondary antibodies are needed

each 3 mL between two 14 mL round-bottom tubes to optimize aeration and grow overnight at 37 °C.

3. Mix 0.75 mL of the culture with 0.75 mL of a 50% sterile glycerol solution and freeze at -80 °C for long-term storage of the clone.

4. Spin down the rest of the overnight culture and remove the supernatant. The remaining pellet is ready for alkaline lysis plasmid extraction (*see Note 9*).
5. Carry out alkaline lysis extraction to purify probe DNA (the same protocol for Fosmids and BACs). Resuspend the pellet in 200  $\mu\text{L}$  fresh GTE buffer with lysozyme (1 mg/mL) and RNase A (2  $\mu\text{g}/\text{mL}$ ), vortex, and incubate at room temperature T for 5 min.
6. Add 400  $\mu\text{L}$  of lysis buffer, mix by inversion (*see Note 11*), and leave for 5 min on ice.
7. Add 300  $\mu\text{L}$  of acetate buffer, mix gently, and leave for 5 min on ice.
8. Centrifuge for 5 min at 4 °C at a minimum speed of 10,000 $\times g$ .
9. Remove supernatant to fresh tube and add equal volume of phenol-chloroform (1:1) and mix well by inversion. Centrifuge for 4 min at 4 °C at 14,000 $\times g$ . Repeat phenol-chloroform extraction.
10. Transfer the top layer to fresh Eppendorf and add equal volume of chloroform, mix by inversion, and centrifuge for 4 min at 4 °C at 13,000 $\times g$  (*see Note 12*).
11. Transfer the top layer to a fresh tube and add equal volume of isopropanol.
12. Let precipitate at -20 °C for a minimum of 1 h.
13. Centrifuge for 15 min at 4 °C at 14,000 $\times g$ , remove supernatant, wash pellet once in 70% ethanol, and centrifuge for 5 min at 4 °C at 14,000 $\times g$ .
14. Remove supernatant and dry pellet for 2 min at room temperature without over drying (*see Note 13*).
15. Resuspend the DNA pellet in 25–50  $\mu\text{L}$  of TE buffer or nuclease-free water. Confirm concentration by Qubit or nano-drop and continue with Nick translation protocol. Store purified DNA at -80 °C.

### 3.2.2 Nick Translation and Probe Purification

1. Thaw and keep on ice 10 $\times$  NTS and both labeled and unlabeled nucleotides. Place on ice also DNase and DNA polymerase I. Select the labeled dUTPs (*see Note 14*).
2. Mix the ingredients for Nick translation reaction as follows:
  - 4  $\mu\text{L}$  of 10 $\times$  NTS
  - 5  $\mu\text{L}$  of 0.5 mM dATP
  - 5  $\mu\text{L}$  of 0.5 mM dCTP
  - 5  $\mu\text{L}$  of 0.5 mM dGTP
  - 2.5  $\mu\text{L}$  of 1 mM labeled dUTP (*see Note 15*)

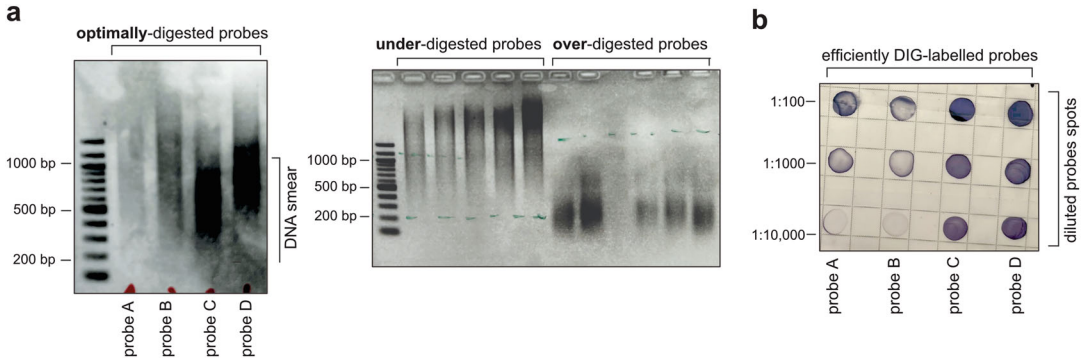


**Fig. 5 (a)** Identification of optimal probe fragment size after DNase I digestion during Nick translation. Optimal DNA smear size guaranteeing high signal-to-background ratio is between 200 and 1000 bp. The left panel shows optimally digested examples of probes, and the right panel depicts examples of under- and over-digested probes. **(b)** The efficiency of labeling probes is assessed by dot blot. Examples of four efficiently DIG-labeled probes. 2  $\mu$ L of diluted probes were spotted onto the membranes as described in point Subheading 3.2.2 of the protocol

- 1  $\mu$ L of DNA polymerase I
  - 200 ng–1  $\mu$ g of probe DNA
  - 1  $\mu$ L of 0.01–0.02 U/ $\mu$ L of DNase I (*see Note 16*)
  - H<sub>2</sub>O to make the reaction up to 40  $\mu$ L volume
3. Place the reaction immediately in the precooled PCR thermocycler and incubate at 16 °C for 90 min.
  4. VAfter incubation place the tube with reactions on ice and confirm the level of DNA digestion by agarose electrophoresis. Optimal DNA fragment size should be from 200 to 1000 bp (Fig. 5a). If samples are under digested, incubate samples at 16 °C for an additional 30 min.
  5. Stop the Nick translation reaction by adding 2  $\mu$ L of 20% SDS and 2  $\mu$ L of 0.5 M EDTA.
  6. Top up the reaction to 100  $\mu$ L with TE buffer and purify the probe to remove free nucleotides using G-50 MicroSpin columns or equivalent according to manufacturer protocol.
  7. Store labeled probes in –20 °C until ready to test labeling efficiency.

### 3.2.3 Detection of Labeling Efficiency

This is an optional step to detect the labeling efficiency of probes only applicable when digoxigenin or biotin conjugate nucleotides are used. We do not test the efficiency of fluorophore-labeled probes before using them in FISH experiments but just infer successful Nick translation from the observed size of digested probe DNA on an agarose gel. To quantify labeling efficiency:

1. Wash a nitrocellulose gridded membrane circle in ddH<sub>2</sub>O for 5 min and then soak in 20× SSC.
2. Make 1:100, 1:1000, and 1:10,000 dilution of reactions in TE and spot 2 µL onto the membrane with 1, 2, 10, and 20 pg standards of either digoxigenin- or biotin-labeled DNA standards. Store the remaining probe at −20 °C.
3. Crosslink DNA onto the membrane using UV crosslinker for 4 min at 150,000 µJ/cm<sup>2</sup>. Importantly, DNA crosslinking also works with a standard UV transilluminator: use “high” setting and crosslink DNA to the membrane for 5 min.
4. Immediately wash filter membrane for 1 min in an Efficiency Buffer 1 (0.1 M Tris pH 7.5, 0.15 M NaCl).
5. Incubate the membrane for 10 min at 60 °C in a 50 mL buffer 1 plus 3% BSA fraction V.
6. Transfer the membrane into a container with 10 mL Efficiency Buffer 1 containing 10 µL of either streptavidin alkaline phosphatase to detect biotin or anti-Dig-AP antibodies to detect digoxigenin. Incubate the membranes for 15 min at room temperature.
7. Wash the membranes with Efficiency Buffer 1, twice for 15 min each.
8. Wash the membranes in Efficiency Buffer 2 (0.1 M Tris pH 9.5) for 1 min at RT.
9. Seal the membrane in a plastic bag with 5 mL of Buffer 2 containing 2 drops each from bottles 1, 2, and 3 of the Vector BCIP/NBT kit. Reaction should be complete within 10–30 min and spots visible (Fig. 5b).
10. Relate spot intensities to determine probe incorporation.

### 3.2.4 Cell Culture and Fixation

1. Prepare *Maintenance* and *Differentiation Induction* media the same as for DamID protocol (*see* Subheading 3.1.3).
2. Plate 3T3-L1 cells on Poly-L-Lysine coated 13 mm coverslips.
3. For preadipocytes, fix at 60% confluence with 4% PFA for 10 min and wash twice in PBS and store at 4 °C for up to a month before further processing (*see* Note 17).
4. For mature adipocytes, 2 days after the cultures achieve confluency, induce differentiation as described earlier and fix adipocytes on day 6 after induction of differentiation. Next fix the adipocytes in 4% PFA for 10 min at room temperature. Wash twice with PBS and store at 4 °C up to a month before further processing.

### 3.2.5 Adipose Tissue Dissection and Sections

1. Humanely euthanize mouse by CO<sub>2</sub> asphyxiation or neck dislocation (*refer to local ethical guidance*).
2. Dissect adipose tissue depots of interest following detailed protocols of Mann et al. (2014) [50] or Bagchi et al. (2019) [49].
3. Wash adipose tissue depots in PBS briefly to remove hair and blood.
4. Place tissues in 4% PFA for 24 h and transfer to 70% ethanol for storage at 4 °C until embedding in paraffin at desired orientation. Keep tissue pieces no bigger than 1 cm<sup>3</sup> for sufficient fixation and further embedding in paraffin. For detailed tissue embedding in paraffin protocol, refer to a chapter by Korach-Andre et al. (2020) [57].
5. Cut paraffin block on microtome into 4 µm (max 10 µm) sections on charged glass slides, and store in dry container protected environment at room temperature.

### 3.2.6 Deparaffinization of the Adipose Tissue Sections

(If working with cultured pre- and adipocytes, skip this section and continue directly with Subheading 3.2.7 Permeabilization section).

1. Incubate slides at 60 °C for 15 min and immediately immerse still warm slides in HistoChoice Clearing Agent twice for 3 min at room temperature (xylenes can be used as alternative with the same results; however, it requires longer incubation times).
2. Rehydrate the samples in decreasing concentrations of ethanol: 100% (twice), 90%, and 70%, 3 min each at room temperature.
3. Wash twice in ddH<sub>2</sub>O and proceed with permeabilization of tissue sections (next section).

### 3.2.7 Permeabilization

(NOTE: sperate protocols for pre-adipocytes, cultured mature adipocytes, and adipose tissue sections!)

- (a) Cultured 3T3-L1 adipocytes and pre-adipocytes
  1. Wash cells twice in PBS.
  2. Permeabilize in 0.5% Triton-X in PBS for 10 min (*see Note 18*).
  3. Wash cells twice in PBS.
  4. For *differentiated adipocytes*, next add proteinase K at 5 µg/mL in 50 mM pH 8.0 to cultured adipocytes and incubate for 2 min at 37 °C. Optimize the proteinase K concentration as overdigestion results in loss of nuclear morphology (*see Note 19*).
  5. Immediately but gently wash cells 5× with cold PBS.
- (b) Adipose tissue sections

1. Wash section slides twice in PBS.
2. Remove slides from Coplin jars and place them horizontally. Use hydrophobic marker pen to mark area around the tissue so the proteinase K is held as a drop on the slide.
3. Load proteinase K to cover tissue sample at concentration 20 µg/mL in 50 mM Tris pH 8.0 and incubate for 15 min at 37 °C. (*optimize every new batch of the enzyme; see Note 19*).
4. Immediately place slides into a Coplin jar with cold distilled H<sub>2</sub>O and wash 5 times.
5. Permeabilize adipose tissue sections in ice-cold 2 M acetic acid for 20 s in precooled Coplin jar and immediately transfer slides to ice-cold ddH<sub>2</sub>O and wash 5×.
6. Transfer samples to PBS and continue with immunostaining if you want to use lamins as positional marker for the edge of the nucleus (*see Subheading 3.2.8*) or alternatively proceed directly with hybridization procedure (*see Subheading 3.2.9*).

### 3.2.8 Optional Labeling of the NE with Lamin A Antibodies

(*The same protocol for cultured pre- and adipocytes as well as for tissue sections*)

1. Wash samples once with PBS.
2. Block in 1% BSA and 0.1% Tween-20 in PBS for 20 min.
3. Dilute primary antibodies in 0.5% BSA and 0.1% Tween-20 in PBS at concentration 1:500 (*concentration might require optimization depending on antibodies and tissues*).
4. Load primary antibodies solution on cells or tissues and incubate for 1 h at room temperature or overnight at 4 °C.
5. Remove antibodies and wash samples three times with PBS with 0.1% Tween.
6. Load secondary antibodies at concentration 1:1000 in the same buffer and incubate for 1 h at room temperature.
7. Wash samples three times with PBS with 0.1% Tween.
8. Wash samples once with PBS for 1 min.
9. Briefly fix the samples again in 2% PFA in PBS for 1 min to ensure antibodies will withstand the harsh FISH procedure.
10. Wash samples twice with PBS and proceed with hybridization procedure (*Subheading 3.2.9*).

### 3.2.9 Working Probe Preparation

Note this should be done during RNase A incubation and approximately 1 h before you are ready to add them. (*The same working probe solutions are used for preadipocytes, cultured mature adipocytes, and tissue sections.*)

1. For one sample, mix approximately 5–10  $\mu\text{L}$  or 100–200 ng efficiently labeled probe (*see Note 20*) with 10  $\mu\text{g}$  of Cot1 DNA and 5  $\mu\text{g}$  of sheared salmon sperm DNA. Next add two volumes of 100% ethanol and vortex mix.
2. Dry probe mixture in a SpeedVac vacuum concentrator—usually it takes 15–30 min for liquid to evaporate and a visible white pellet to form at the bottom of the tube.
3. Make hybridization buffer (2 $\times$  SSC, 50% formamide, 10% dextran sulfate and 1% Tween-20).
4. Once the probe is dried, add 20  $\mu\text{L}$  of hybridization buffer per slide/sample and mix by pipetting and avoiding introduction of bubbles. Continue incubation at room temperature until the DNA pellet is fully resuspended, usually 10–15 min.
5. Denature probe mixture in PCR thermocycler for 5 min at 80 °C and then slowly reanneal by reducing the temperature to 42 °C at a rate of 1 °C/min and hold at 42 °C until ready to load onto the samples.

### 3.2.10 RNase A Treatment, Sample Denaturation, and Hybridization

(*The same step for cultured adipocytes and tissue sections*)

1. Preheat the 70 °C oven, two heating blocks at 42 °C and 85 °C, and water bath at 85 °C. Prewarm glue (rubber cement) at 42 °C heating block and set up a humid chamber (*see Note 21*) in 37 °C incubator or water bath. Prewarm glass slides on 42 °C heating block.
2. Prepare denaturation buffer—70% formamide in 2 $\times$  SSC in  $\text{H}_2\text{O}$ .
3. Prepare RNaseA solution in 2 $\times$  SSC buffer at concentration 100  $\mu\text{g}/\text{mL}$ .
4. Remove PBS from samples and wash with 2 $\times$  SSC buffer for 2 min.
5. Remove 2 $\times$ SSC buffer and add RNase A solution and incubate samples for 1 h at 37 °C.
6. During RNase A incubation, prepare working probe (*see Subheading 3.2.9*).
7. After incubation, wash samples twice with 2 $\times$  SSC and dehydrate samples in increasing ethanol concentrations, i.e., 70% ethanol for 2 min, then 90% ethanol for 2 min, and finally 100% ethanol for 2 min (*transfer some ethanol to –20 °C freezer to be used later*).
8. After incubation in 100% ethanol, transfer samples to 70 °C oven for 10 min.
9. Immediately after that, transfer samples from the oven onto 85 °C heating block and cover specimen with large drop of denaturation buffer. Incubate for 20 min.

10. At the end of the incubation, rapidly transfer samples into  $-20^{\circ}\text{C}$  70% ethanol from the freezer and incubate for 2 min (*see Note 22*).
11. Continue dehydration of the samples with 90% ethanol for 2 min and then 100% ethanol for 2 min. These latter two incubations can be done at room temperature.
12. Briefly dry the samples by quick touch (3–5 s to allow ethanol evaporation) to the  $85^{\circ}\text{C}$  heating block and place samples on the  $42^{\circ}\text{C}$  heating block.
13. Load 15  $\mu\text{L}$  (for cells on 13 mm coverslips) or 50  $\mu\text{L}$  (for tissues and 2 cm cover glass) of working probe solution, close samples with coverslip, and seal with rubber cement.
14. Place samples for 2 min on the  $85^{\circ}\text{C}$  heating block for final denaturation of specimen.
15. Transfer samples to prewarmed humid chamber and incubate overnight at  $37^{\circ}\text{C}$  overnight.

### 3.2.11 Stringency Washing

(*The same protocol for cells and tissues*)

1. Gently remove samples from humid chamber and carefully remove rubber cement and cover slips.
2. Wash samples in  $2\times$  SSC with 0.1% Tween-20, 4 times for 3 min each at  $45^{\circ}\text{C}$ .
3. Wash samples in  $0.1\times$  SSC with 0.1% Tween-20, 4 times for 3 min each at  $60^{\circ}\text{C}$ .
4. Wash samples in  $2\times$  SSC with 0.1% Tween-20, 2 times for 3 min each at room temperature.
5. If probes were made with fluorophore-conjugated dUTPs, i.e., do not require secondary antibodies, stain with DAPI at concentration 50 ng/mL in  $2\times$  SSC for 10 min. To do this, add 300  $\mu\text{L}$  of DAPI solution to a well with cells on coverslips or 500  $\mu\text{L}$  onto tissues on glass slides (make fresh lines around tissue with a hydrophobic marker pen if necessary). Next, wash samples in  $2\times$  SSC, for 10 min at RT. Finally, wash samples with  $1\times$  PBS, add 20  $\mu\text{L}$  Vectashield, close the tissue sample with cover glass, and seal with nail varnish. In the case of using cells on coverslips, add 20  $\mu\text{L}$  of Vectashield on glass slides and place coverslips cells down and also seal with nail varnish. Avoid leaving air bubbles!
6. If probes were made with digoxigenin or biotin-labeled dUTPs, block samples with 4% BSA in  $4\times$  SSC with 0.1% Tween-20 for 20 min at room temperature.
7. Prepare secondary antibody mix, 50  $\mu\text{L}$  per sample in 4% BSA in  $4\times$  SSC buffer. Add Alexa Fluor 594 anti-rabbit antibody at concentration 1:500 (*to enhance lamin A antibody signal from*

*Subheading 3.2.7*. To the same tube, add fluorophore-conjugated secondary antibodies at 1:500 to detect probe (anti-DIG or streptavidin). Mix by flicking tube with finger briefly and centrifuge for 1 min at  $10,000\times g$  to pellet any antibody aggregates, which if not removed can significantly increase background signal and noise.

8. Load antibody mixture on samples, place cover glass, and incubate for 60 min at 37 °C.
9. Wash samples in  $4\times$  SSC with 0.1% Tween-20, 4 times for 3 min each at 37 °C.
10. Add DAPI at concentration 50 ng/mL in  $2\times$  SSC for 10 min and wash samples in  $2\times$  SSC with 0.1% Tween-20, 4 times for 3 min each at room temperature.
11. Wash samples with  $1\times$  PBS and close samples with antifade mounting medium (e.g., Vectashield, Vector Laboratories, cat. H-1000-10) and seal with nail varnish.

### 3.2.12 Imaging and Data Analysis

It is difficult to observe the FISH signals at low magnification; so, it is recommended to use at least a wide-field epifluorescence microscope with a  $60\times$  or  $100\times$  objective. Depending on the type of experiment, more information can be gleaned when using super resolution microscopes; however, this is overkill for most purposes. Also, depending on need, one can either just take images in the plane of the FISH spot or capture images as Z-stacks to generate 3D projections of nuclei and identify the spots in 3D. The former is less accurate and usually requires 50–100 cells to see statistically significant differences while the latter takes more time, but usually 20 cells are more than enough (Fig. 6).

1. Capture 2D images for an appropriate number of nuclei (typically 50) using available microscope and software or for 3D capture an appropriate number of z-stacks (typically 20).
2. If capturing 3D images with the microscope's z-stack function, use software (e.g., AutoQuant X3) to deconvolve them, thereby reducing out-of-focus light and creating accurate 3D reconstructions.
3. Use the measurement tool in Image J or Imaris software to quantify the distance between probes or between probe and the NE. Alternatively, we recommend Volocity 3D Visualization (PerkinElmer) which has special algorithms that measure the localization of the FISH signal within the nucleus (based on DAPI signal, *see Note 23*) as well as the distance between two probes signal or between a probe and the NE.

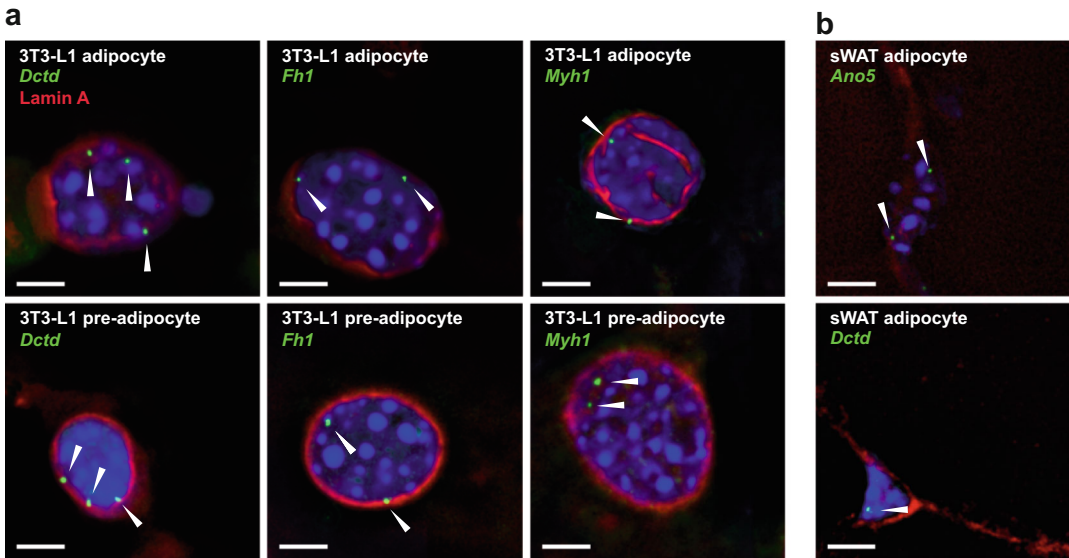


**Fig. 6** Examples of FISH signal for different genes loci (green dots, white arrows), nuclear envelope staining by lamin A antibodies (red), and DAPI stain for nucleus on (a) cultured adipocytes and (b) subcutaneous white adipose tissue (sWAT). Of note, the 3T3-L1 cell line is tetraploid, so it is expected to yield up to 4 dots/signals representing the loci, as opposed to mouse tissues that being diploid would yield only 2 dots. Different numbers of loci may be observed in 2D sections depending on the Z-plane positioning, but the full complement of loci should be observed in 3D reconstructions from Z-series images

## 4 Notes

1. PES (polyether sulfone) membranes allow high flow rate and clog more slowly than the historically used PVDF membranes. Importantly, the pore size enables size exclusion of cells which will not pass through the membranes while the viral particles will, being much smaller than  $0.45 \mu\text{m}^2$ . Smaller pore membranes, like  $0.22 \mu\text{m}^2$ , are not recommended as in our hands they resulted in reduced virus titers and clogged easily.
2. The HEK293FT cell line is superior at lentiviral production when compared to other HEK293 lines. This is due to transformation of these cells with SV40 large T antigen.
3. As this is the only plasmid not available from Addgene, note that it can be generated by just taking the pLGW-Dam plasmid and deleting the Dam insert.
4. Choose a gene loci or genetic region of interest based on DamID data. In our experience, even DRs that have only minor peaks above the line even if they are not called as LADs by the binary algorithm tend to be at the NE by FISH; thus, one can reasonably pick weaker DRs using the second peak calling method described if they are biologically interesting.

However, many of these are short, and if a LAD is very short, then one must be careful to either purchase a clone that more specifically matches the LAD dimensions or further subclone. To be safe in the expectation of LAD confirmation, one can also select regions with stronger loss/gain in the DR LAD peaks. Next, identify the genetic regions of choice on the UCSC genome browser, [www.genome.ucsc.edu](http://www.genome.ucsc.edu). Many BAC and Fosmid clones have been mapped on this server to the latest genome builds (currently for mouse mm10 and for human—hg 38). The general rule of thumb is that the shorter the probe, the more accurate the positional information because it will cover a smaller region; however, this is countered by the fact that shorter probe length also correlates to lower signal intensity. Although many constitutive LADs are hundreds of kb and even several Mb in length so that BACs (~200 kb) should be fine, DRs tend to be shorter such that we recommend for them using Fosmids (~40 kb). The following public sessions in UCSC browser are set up by Schirmer lab to visualize most currently available probes for mouse and human:

- mouse mm9: <http://tinyurl.com/3xecs4cw>
- mouse mm10: <http://tinyurl.com/bdhxt36f>
- human hg19: <http://tinyurl.com/4da7cnt5>
- human hg38: <http://tinyurl.com/3bymta9j>

5. Make enough denaturation buffer to cover the specimen, i.e., if working with cells on cover slips, 200  $\mu$ L of the buffer per sample is usually enough. When working with tissues or cells fixed on glass slides, prepare between 500  $\mu$ L and 1 mL of denaturation buffer per slide. If working with material fixed on glass slides, it is practical to use a hydrophobic marker pen to draw around the specimen to avoid buffer flowing outside the sample boundaries.
6. We give the protocol we optimized for lipofectamine 2000 to make lentiviruses here; however, any transfection reagent can be used.
7. Adding GFP to the Dam fusion construct can reduce its efficacy; so, a control virus just expressing GFP is used here. Thus, titers are estimated based on its efficacy though it may differ somewhat from that with the Dam fusion constructs to be used in the experiments. Nonetheless, if the viruses are generated in parallel, it typically is a good indicator of titers for the relevant constructs.
8. This protocol is for the standard DamID method that uses very low expression of the Dam methylase fusion and so also requires 3 days of labeling. Therefore, it is important to just check stable differentiation states and make certain that the

population has reached a particular state before transducing the Dam expression construct. If one wants to investigate changes occurring at different shorter temporal stages of differentiation, it is possible that increasing the expression level and shortening the timeframe might work; however, we have not directly tested this. It is also possible to make variations based on other developments from the van Steensel lab such as a short burst followed by use of an antibody for the methylated DNA and ChIP; however, again these have not been tested for this purpose.

9. Most providers want to know in advance of shipping that the DNA is of sufficient quality, plus it is in the interest of the researcher to check before shipping to save time and money. If one does not have access to such a machine, then one needs to find a provider that does not require this. However, one still needs to know how much material to send for library preparation or sequencing, but any reasonable spectrophotometer that can assay small volumes such as a nanodrop will work for this.
10. LAD detection from noisy data can often be improved by selecting a small threshold, typically between 0.05 and 0.2. The threshold should be chosen empirically after careful examination of the LAD profiles. When replicates are not available, removal of LADs smaller than about 15–20 Kb is often beneficial as detection of smaller LADs is less reliable than larger LADs. However, if replicates are available, this may not be necessary.
11. It is fine to use a kit, but note that one gets much more DNA doing alkaline lysis than from kits; so, one should use  $\sim 5\times$  the amount starting material recommended here to get the needed amount of DNA if using kits. A key challenge with alkaline lysis is ensuring complete RNA degradation and removal of phenol to obtain high-quality DNA. When the steps outlined here are performed thoroughly, the resulting DNA yield is higher and cleaner than that obtained using commercial kits.
12. Vortexing is bad because it can break the genomic DNA, and the whole point is to pellet that first so the plasmid can be recovered clean of genomic contamination. Thus, the best way to mix is with five strong but slow shakes of the tube, each time like throwing a javelin.
13. It is important to do post-phenol extractions to remove all traces of phenol as slight phenol contamination can inhibit transfection efficiency. This protocol increases yield and purity over kits if done correctly, but it is critical to get rid of all phenol. One can repeat the chloroform extraction or do an additional ether extraction for extra surety. Note also that leaving a small amount of the supernatant behind to ensure

that the interface does not get disrupted is another way to better ensure no phenol contamination. Overdrying DNA pellets makes it hard to resuspend the pellet which in turn reduces the percentage of material labeled. Once the pellet is cracking, it is a sign that it is too dry.

14. We recommend starting with directly labeled dUTPs as secondary antibody detection of digoxigenin or detection of biotin-labeled probes by streptavidin will generate additional background signal since most antibody-antigen interactions have dissociation constants in the  $10^{-7}$ – $10^{-9}$  affinity range whereas the biotin-streptavidin interaction is around  $10^{-14}$ .
15. Digoxigenin-labeled dUTPs require addition of dTTP because it is too big and requires spacing between nucleotides. Thus, we recommend adding 2  $\mu$ L of 0.5 mM dTTP (non-labeled) to the reaction. Other labeled dUTPs do not require additional dTTP for spacing.
16. This step requires optimization due to DNase I batch variation. We noticed that the activity of DNase I differs considerably between manufacturers. For example, in our hands Invitrogen DNase I required 1  $\mu$ L of 0.02 U/ $\mu$ L whereas DNase I from Roche (cat: 04716728001) required 1  $\mu$ L of 2 U/ $\mu$ L per reaction to achieve the same level of DNA digestion. Running the reaction on agarose every time will inform on the efficiency of DNase digestion. Best FISH signal results will be obtained with a probe that shows a smear between 200 and 1000 bp.
17. The cells are fine at 4 °C for a month provided they have not yet been permeabilized. If cells have been permeabilized, the full FISH procedure should be performed within a few days. Note also that there is an aging factor that occurs in the refrigerator which some argue makes FISH cleaner; so, it is actually beneficial to let the (unpermeabilized) cells sit in the refrigerator for at least a week.
18. Triton-X is sufficient to permeabilize *preadipocytes*, but mature *adipocytes* require an additional digestion step by proteinase K. At this step, preadipocytes are ready for immunostaining with lamin A antibodies or denaturation steps for FISH.
19. Proteinase K often shows differences in activity between batches. We recommend to aliquot proteinase K upon arrival and test its strength with the same concentration at three different time points.
20. Quantification of labeled probe is not always accurately assessed; hence, if not certain it is often adequate to use the amount of the final solution suggested in the protocol rather than an exact DNA amount. Cot1 DNA and seared salmon sperm DNA are added to reduce unspecific hybridization and reduce background signal.

21. By humidified chamber, we mean a sealed container (e.g., tupperware), containing wet paper towels that will keep the chamber humid, but not get water soaking up onto slides or coverslips set on the towels.
22. One of the most critical tricks with FISH is the importance of maintaining temperature/ having sharp temperature shifts through rapid transfers. Slides and even more so coverslips at high temperatures will rapidly start dropping temperature if one is carrying it from one bench to another. Thus, it is best to have all equipment collected together in the same space and move fast when engaging temperature shifts. The cold EtOH here will fix what was achieved at the high temperature, i.e., denaturation of chromatin, but if the temperature drops by 10 °C before the transfer to the below 0 °C EtOH, then the FISH signal will be reduced dramatically.
23. Many preexisting algorithms use a DAPI mask to determine the nuclear boundaries for measuring distance from the NE. However, we strongly encourage the use of lamin or another NE marker antibody staining because the distance measured using the DAPI mask can vary greatly depending on the thresholding.

---

## Acknowledgments

The authors would like to thank the current and former members of Schirmer lab, particularly Dzmitry G. Batrakou and Michael Robson who together with Jose de las Heras initially brought the DamID technique into the lab, Bas van Steensel, Carolyn de Graaf, and Job Kind who provided considerable guidance on the method initially. Funding for this work was provided by MRC Project grants 18GRO-PG24-0248 and MR/W001241/1.

## References

1. Wang X, Cairns MJ, Yan J (2019) Super-enhancers in transcriptional regulation and genome organization. *Nucleic Acids Res* 47: 11481–11496
2. Kai Y, Li BE, Zhu M et al (2021) Mapping the evolving landscape of super-enhancers during cell differentiation. *Genome Biol* 22:269
3. Uyehara CM, Apostolou E (2023) 3D enhancer-promoter interactions and multi-connected hubs: organizational principles and functional roles. *Cell Rep* 42:112068
4. Peric-Hupkes D, Meuleman W, Pagie L et al (2010) Molecular maps of the reorganization of genome-nuclear lamina interactions during differentiation. *Mol Cell* 38:603–613
5. Robson MI, de Las Heras JI, Czapiewski R et al (2016) Tissue-specific gene repositioning by muscle nuclear membrane proteins enhances repression of critical developmental genes during myogenesis. *Mol Cell* 62:834–847
6. Gatticchi L, de Las Heras JI, Sivakumar A et al (2020) Tm7sf2 disruption alters radial gene positioning in mouse liver leading to metabolic defects and diabetes characteristics. *Front Cell Dev Biol* 8:592573
7. Czapiewski R, Batrakou DG, de las Heras JI et al (2022) Genomic loci mispositioning in

- Tmem120a knockout mice yields latent lipodystrophy. *Nat Commun* 13(1):321
8. Shah PP, Keough KC, Gjoni K et al (2023) An atlas of lamina-associated chromatin across twelve human cell types reveals an intermediate chromatin subtype. *Genome Biol* 24(1):16
9. Shah PP, Lv W, Rhoades JH, Poleshko A et al (2021) Pathogenic LMNA variants disrupt cardiac lamina-chromatin interactions and de-repress alternative fate genes. *Cell Stem Cell* 28(938–954):e939
10. de Wit E, Braunschweig U, Greil F et al (2008) Global chromatin domain organization of the *Drosophila* genome. *PLoS Genet* 4:e1000045
11. Pindyurin AV, Ilyin AA, Ivankin AV et al (2018) The large fraction of heterochromatin in *Drosophila* neurons is bound by both B-type lamin and HP1a. *Epigenetics Chromatin* 11:65
12. Eberhart A, Feodorova Y, Song C et al (2013) Epigenetics of eu- and heterochromatin in inverted and conventional nuclei from mouse retina. *Chromosome Res* 21:535–554
13. Ye Q, Callebaut I, Pezhman A, Courvalin JC et al (1997) Domain-specific interactions of human HP1-type chromodomain proteins and inner nuclear membrane protein LBR. *J Biol Chem* 272:14983–14989
14. Somech R, Shalkai S, Geller O et al (2005) The nuclear-envelope protein and transcriptional repressor LAP2beta interacts with HDAC3 at the nuclear periphery, and induces histone H4 deacetylation. *J Cell Sci* 118:4017–4025
15. Nili E, Cojocaru GS, Kalma Y et al (2001) Nuclear membrane protein LAP2beta mediates transcriptional repression alone and together with its binding partner GCL (germ-cell-less). *J Cell Sci* 114:3297–3307
16. Korfali N, Wilkie GS, Swanson SK et al (2010) The leukocyte nuclear envelope proteome varies with cell activation and contains novel transmembrane proteins that affect genome architecture. *Mol Cell Proteomics* 9:2571–2585
17. Zuleger N, Boyle S, Kelly DA et al (2013) Specific nuclear envelope transmembrane proteins can promote the location of chromosomes to and from the nuclear periphery. *Genome Biol* 14:R14
18. Ramirez-Martinez A, Zhang Y, Chen K et al (2021) The nuclear envelope protein Net39 is essential for muscle nuclear integrity and chromatin organization. *Nat Commun* 12:690
19. Wilkie GS, Korfali N, Swanson SK et al (2011) Several novel nuclear envelope transmembrane proteins identified in skeletal muscle have cytoskeletal associations. *Mol Cell Proteomics* 10(M110):003129
20. Meinke P, Kerr ARW, Czapiewski R et al (2020) A multistage sequencing strategy pinpoints novel candidate alleles for Emery-Dreifuss muscular dystrophy and supports gene misregulation as its pathomechanism. *EBioMedicine* 51:102587
21. Martins F, Sousa J, Pereira CD et al (2020) Nuclear envelope dysfunction and its contribution to the aging process. *Aging Cell* 19:e13143
22. Carollo PS, Barra V (2023) Chromatin epigenetics and nuclear lamina keep the nucleus in shape: examples from natural and accelerated aging. *Biol Cell* 115:e2200023
23. Bione S, Maestrini E, Rivella S et al (1994) Identification of a novel X-linked gene responsible for Emery-Dreifuss muscular dystrophy. *Nat Genet* 8:323–327
24. Bonne G, Di Barletta MR, Varnous S et al (1999) Mutations in the gene encoding lamin A/C cause autosomal dominant Emery-Dreifuss muscular dystrophy. *Nat Genet* 21:285–288
25. Hellemans J, Preobrazhenska O, Willaert A et al (2004) Loss-of-function mutations in LEMD3 result in osteopoikilosis, Buschke-Ollendorff syndrome and melorheostosis. *Nat Genet* 36:1213–1218
26. Kosak ST, Skok JA, Medina KL et al (2002) Subnuclear compartmentalization of immunoglobulin loci during lymphocyte development. *Science* 296:158–162
27. Williams RR, Azuara V, Perry P et al (2006) Neural induction promotes large-scale chromatin reorganisation of the *Mash1* locus. *J Cell Sci* 119:132–140
28. Lieberman-Aiden E, van Berkum NL, Williams L et al (2009) Comprehensive mapping of long-range interactions reveals folding principles of the human genome. *Science* 326:289–293
29. Madsen-Osterbye J, Abdelhalim M, Baudent MO et al (2022) Local euchromatin enrichment in lamina-associated domains anticipates their repositioning in the adipogenic lineage. *Genome Biol* 23(1):91
30. Lund E, Oldenburg AR, Delbarre E et al (2013) Lamin A/C-promoter interactions specify chromatin state-dependent transcription outcomes. *Genome Res* 23:1580–1589
31. Dorner D, Gotzmann J, Foisner R (2007) Nucleoplasmic lamins and their interaction partners, LAP2alpha, Rb, and BAF, in transcriptional regulation. *FEBS J* 274:1362–1373
32. Vogel MJ, Peric-Hupkes D, van Steensel B (2007) Detection of in vivo protein-DNA

- interactions using DamID in mammalian cells. *Nat Protoc* 2:1467–1478
33. Guelen L, Pagie L, Brasset E et al (2008) Domain organization of human chromosomes revealed by mapping of nuclear lamina interactions. *Nature* 453:948–951
  34. Greil F, Moorman C, van Steensel B (2006) DamID: mapping of in vivo protein-genome interactions using tethered DNA adenine methyltransferase. *Methods Enzymol* 410: 342–359
  35. Cao H, Hegele RA (2000) Nuclear lamin A/C R482Q mutation in Canadian kindreds with Dunnigan-type familial partial lipodystrophy. *Hum Mol Genet* 9:109–112
  36. Shackleton S, Lloyd DJ, Jackson SN et al (2000) LMNA, encoding lamin A/C, is mutated in partial lipodystrophy. *Nat Genet* 24:153–156
  37. Pan DZ, Garske KM, Alvarez M et al (2018) Integration of human adipocyte chromosomal interactions with adipose gene expression prioritizes obesity-related genes from GWAS. *Nat Commun* 9:1512
  38. Siersbaek R, Madsen JGS, Javierre BM et al (2017) Dynamic rewiring of promoter-anchored chromatin loops during adipocyte differentiation. *Mol Cell* 66(420–435):e425
  39. Robson MI, Schirmer EC (2016) The application of DamID to identify peripheral gene sequences in differentiated and primary cells. *Methods Mol Biol* 1411:359–386
  40. Gatticchi L, de Las Heras JI, Roberti R et al (2019) Optimization of DamID for use in primary cultures of mouse hepatocytes. *Methods* 157:88–99
  41. Bolger AM, Lohse M, Usadel B (2014) Trimmomatic: a flexible trimmer for Illumina sequence data. *Bioinformatics* 30:2114–2120
  42. Li H, Durbin R (2009) Fast and accurate short read alignment with Burrows-Wheeler transform. *Bioinformatics* 25:1754–1760
  43. Quinlan AR, Hall IM (2010) BEDTools: a flexible suite of utilities for comparing genomic features. *Bioinformatics* 26:841–842
  44. Robinson MD, McCarthy DJ, Smyth GK (2010) edgeR: a Bioconductor package for differential expression analysis of digital gene expression data. *Bioinformatics* 26:139–140
  45. Love MI, Huber W, Anders S (2014) Moderated estimation of fold change and dispersion for RNA-seq data with DESeq2. *Genome Biol* 15:550
  46. Ritchie ME, Phipson B, Wu D et al (2015) Limma powers differential expression analyses for RNA-sequencing and microarray studies. *Nucleic Acids Res* 43:e47
  47. Zang C, Schones DE, Zeng C et al (2009) A clustering approach for identification of enriched domains from histone modification ChIP-Seq data. *Bioinformatics* 25:1952–1958
  48. Robinson JT, Thorvaldsdottir H, Winckler W et al (2011) Integrative genomics viewer. *Nat Biotechnol* 29:24–26
  49. Bagchi DP, MacDougald OA (2019) Identification and dissection of diverse mouse adipose depots. *J Vis Exp* 149:10.3791/59499
  50. Mann A, Thompson A, Robbins N et al (2014) Localization, identification, and excision of murine adipose depots. *J Vis Exp* 94:52174
  51. Batrakou DG, de Las Heras JI, Czapiewski R et al (2015) TMEM120A and B: nuclear envelope transmembrane proteins important for adipocyte differentiation. *PLoS One* 10: e0127712
  52. Head SR, Komori HK, LaMere SA, et al (2014) Library construction for next-generation sequencing: overviews and challenges. *Biotechniques* 56:61–64, 66, 68, passim
  53. Wu F, Olson BG, Yao J (2016) DamID-seq: genome-wide mapping of protein-DNA interactions by high throughput sequencing of adenine-methylated DNA fragments. *J Vis Exp* 107:e53620
  54. Seshan VE, Olshen A (2016) DNACopy: DNA copy number data analysis. R Package Version. 1.46.0
  55. Kind J, Pagie L, Ortabozkoyun H et al (2013) Single-cell dynamics of genome-nuclear lamina interactions. *Cell* 153:178–192
  56. Liao Y, Smyth GK, Shi W (2014) featureCounts: an efficient general purpose program for assigning sequence reads to genomic features. *Bioinformatics* 30:923–930
  57. Korach-Andre M (2020) In vivo investigation of high-fat diet-induced hepatic lipid dysfunctions. *Methods Mol Biol* 2164:109–119



## Measurement of Spatial Contact Map Using Sequential FISH

Hiroaki Ohishi

### Abstract

The spatial organization of genomes within the cell nucleus is fundamental to gene expression and chromosome folding processes. DNA sequential fluorescence in situ hybridization (DNA-seqFISH) facilitates the examination of higher-order genome structures across the genome by spatially mapping specific genomic coordinates. Leveraging this spatial data allows for the precise calculation of distances between genomic regions within cells, allowing analyses of region-associated gene transcription and protein localization at single-cell and single-allele resolutions. This chapter presents a methodology for generating DNA spatial distance maps using bright spot coordinate data derived from DNA-seqFISH. The corresponding code is available on GitHub (<https://github.com/hirohishi/MicEASH.git>).

**Key words** seqFISH, Distance matrix, Single cell, Single allele, Mouse embryonic stem cells

---

### 1 Introduction

The human genome, extending nearly 2 m, is intricately folded and compactly stored within a cell nucleus merely 6  $\mu\text{m}$  in diameter. This efficient packaging enables cells to precisely access genetic information, critical for their functions. Gene function modulation primarily occurs through gene expression regulation, encompassing DNA transcription into RNA and subsequent mRNA translation into proteins. Understanding gene transcription, closely associated with protein synthesis, is essential for elucidating the control mechanisms underlying gene expression. In specific cell types, gene transcription is influenced by the physical interactions between distal enhancers and proximal promoters, with transcription-related factors binding to these regions to initiate transcription. Additionally, gene spatial positioning within the nucleus and localized accumulation of transcription-related factors markedly influence transcriptional regulation [1–4]. Therefore, comprehending genomic element spatial arrangement and transcription-related factor localization within the nucleus is crucial

for elucidating the complex mechanisms governing gene expression regulation.

Sequential fluorescence in situ hybridization (seqFISH) is a powerful method for achieving multimodal profiling, including RNA, DNA, and protein spatial localization [5, 6]. Traditional DNA-FISH employs fluorescently labeled DNA probes, typically derived from bacterial artificial chromosomes or yeast artificial chromosomes, which contain the specific sequences of the target genomic regions to be visualized. These probes hybridize with the corresponding sequences in fixed cells, identifying specific genomic regions as distinct fluorescent spots. However, this approach is limited to visualizing a maximum of four DNA regions concurrently owing to restricted fluorescent dye availability and wavelengths. Such limitations present challenges for analysis of complex higher-order genomic structures. DNA-seqFISH overcomes these limitations through the use of an extensive primary DNA oligonucleotide pool for hybridization, tagged with unique sequence identifiers (readout binding sequences) for each specific genomic region. This setup includes a fluorescently labeled DNA probe (readout probe) that binds directly to the sequence identifier, enabling precise genomic region detection as discrete spots within the nucleus. These readout probes are designed with a lower binding affinity than that of the DNA probes attached to the genome, facilitating their selective removal using high formaldehyde concentrations, thereby eliminating unwanted fluorescent signals [6, 7]. Comprising cycles of hybridization, imaging, and stripping of readout probes, DNA-seqFISH enables visualization of specific genomic regions at the single-cell and single-allele levels. Each round of fluorescence is decoded using a pseudocolor-based barcoding system, enabling the visualization of multiple DNA molecules across the entire genome [6, 8]. Technological advancements based on these principles, including seqFISH, multiplexed error-robust FISH, and optical reconstruction of chromatin architecture, have enabled direct observation and analysis of multiple genomic regions' spatial configurations within the nucleus [8, 9]. Furthermore, integrating DNA-seqFISH with live imaging and computational simulations provides additional options for exploring gene transcription regulation dynamics [10]. Moreover, DNA-seqFISH enables chromosome arrangement determination and genome-wide size measurement.

In experimental setups, cells or tissues undergo initial treatment with paraformaldehyde and bis(sulfosuccinimidyl)suberate to fix and preserve their structure. Subsequently, RNase treatment is employed to degrade RNA, and heat denaturation converts double-stranded genomic DNA into single strands, preparing the genomic template for probing. Hybridization involves applying tens to hundreds of primary DNA probes for each specific genomic region under investigation. For instance, approximately 200 probes,

each comprising about 35 nucleotides, enable clear visualization of a 25 kb genomic region. To visualize larger genomic regions, such as a 10 Mb region, with a discrete 25 kb resolution, over 80,000 probes are necessary. These probes are synthesized with high precision by vendors. Following synthesis, the oligonucleotide pool undergoes PCR amplification, with the resultant DNA subsequently transcribed into RNA *in vitro*. The RNA is then reverse-transcribed back into single-stranded DNA. The resulting primary oligo pool is hybridized to the single-stranded genomic DNA, after which the cells are washed. Following padlock construction to enhance probe genomic DNA binding, target genomic regions are visualized using readout probes binding to specific sites within the hybridized DNA, enabling precise spatial mapping of genetic elements.

Spatial data, including bright spot coordinates and nuclear configurations, can be derived from image datasets obtained through rounds of imaging. Precise data extraction from these images is pivotal for comprehensive analysis. For example, seqFISH images are captured using a confocal microscope in a  $1024 \times 1024 \times 51$  voxel format at 130 nm XY resolution and 200  $\mu\text{m}$  Z-step, employing lasers at 647, 568, 488, and 405 nm wavelengths, with a 16-bit depth [10]. Across 30 imaging sessions spanning 100 fields of view, cumulative data can reach approximately 1.28 Tb. To efficiently process this voluminous data, a computing system with robust computational capabilities and substantial memory capacity is required, as graphical user interface-based methods are insufficient. Consequently, semiautomatic analyses are implemented using programming languages, including macros in Fiji/ImageJ, Python, or MATLAB. The image analysis protocol includes preprocessing steps to normalize fluorescence unevenness induced by excitation lasers, correction of positional shifts observed across imaging rounds, detection of bright spots, and their alignment based on these data. Additionally, a decoding step is used to correlate the bright spots with their respective spatial coordinates and barcode data, precisely identifying specific genomic regions within any chromosome [8, 11].

To perform spatial analysis using spatial coordinate information linked to specific chromosomal regions, association of bright spot information must be carefully conducted. This includes classifying homologous chromosomes, handling doublets from DNA replication, and addressing dropout issues due to low bright spot detection efficiency. During DNA replication, if two genomic regions are sufficiently separated in space, they may appear as two distinct bright spots when observed using DNA-FISH. Methods such as main chromosome selection based on bright spot intensity or polymer model usage have been proposed for this distinction [6, 12]. Additionally, in diploid cells, two bright spots are expected for one target region on autosomes (excluding sex chromosomes in

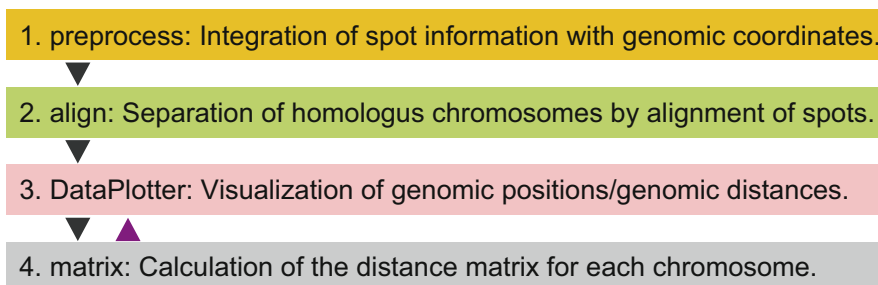


**Fig. 1** Workflow for analyzing DNA-seqFISH data via miceash module. The miceash module provides a computational analysis for DNA-seqFISH data within the MicEASH package. The preprocess command in the module integrates spot information from seqFISH data with reference genomic coordinates. The align command clusters data to specific chromosomal alleles. The DataPlotter command generates chromosomal diagrams and distance heatmaps. The matrix command calculates distances between genomic regions within chromosomes. Analytical data from the matrix can also be visualized using DataPlotter (indicated by purple arrows)

males). To distinguish two homologous autosomal chromosomes, it is necessary to separate the bright spots into two alleles. A set of bright spots can be defined as a single cluster to distinguish homologous chromosomes. Using allele-categorized coordinate information, distances between genomic coordinates associated with spatial genomic coordinates are measured. For a deeper understanding of higher-order genomic structures, a matrix representation used in Hi-C methods is employed. Specifically, pairwise distance information for each genomic region is organized and stored within a region-by-region-structured matrix. Using the matrix data for individual cells, a median distance matrix is calculated. This matrix allows for heatmap visualization of each genomic distance and comparison with genome interaction matrix information obtained through Hi-C methods.

In this chapter, I introduce computational analysis methods using the bright spot information obtained from DNA-seqFISH (Fig. 1). I use a package named “Micro Environment Analysis of Sequential fluorescence *in situ* Hybridization” (MicEASH) for preprocessing bright spot spatial coordinates, connecting bright spots based on genomic coordinates by distinguishing alleles and subsequently calculating distances. MicEASH has been consolidated into commands, enabling analysis to be performed in relatively few steps. It can be downloaded from GitHub and installed on a personal laptop (<https://github.com/hirohishi/MicEASH.git>). Regarding decoding bright spot information and experimental methods, refer to the original protocol [6, 7, 11].

---

## 2 Materials

### 2.1 Execution via a Personal Computer

For this analysis, a personal computer (PC) terminal is used. I have verified that PCs with 16–32 GB of memory and 500 GB to 2 TB of solid state drive (or hard disk drive) storage can effectively accommodate the analysis. Additionally, various PC operating systems are compatible, including Mac OS, Windows OS (using wsl2, allowing Linux OS to be run within Windows OS), and Linux OS (Ubuntu).

### 2.2 Setting Up the Execution Environment

The MicEASH package is employed to analyze spatial information using test data from DNA-seqFISH. This package requires Jupyter Notebook, an integrated development environment capable of executing Python code within a web browser. The packages necessary for the analysis are available on GitHub.

The tools required to set up the analysis environment can be downloaded from the provided URLs:

- Anaconda (<https://www.anaconda.com/products/distribution>).
- Git (<https://github.com/git-guides/install-git>).

The MicEASH package can be downloaded from GitHub. An individual analysis execution folder can be created, for example, named “analysis\_folder” or “codes\_folder.” This folder can be created in the home directory navigated to, and the MicEASH package can then be downloaded. To create a directory and install the MicEASH package from GitHub, the following commands can be used in the terminal, replacing [desired folder name] with the chosen folder name:

```
cd ~
mkdir [desired folder name] # This command creates a new
                             directory with your specified name.
cd [desired folder name] # This changes the directory to the
                           one you just created.
git clone https://github.com/hirohishi/MicEASH.git # This
                                                    clones the
                                                    MicEASH repository
                                                    into your current
                                                    directory.
```

Using Anaconda, all required packages can be managed within a conda environment, facilitating the easy setup of the desired analysis environment. To install MicEASH, the following command can be executed in the terminal:

```
cd MicEASH
conda create --name mice_env python=3.11
conda activate mice_env
pip install -e .
pip install notebook
```

```
python -m ipykernel install --user --name mice_env --display-
name "mice_env"
```

### 2.3 Downloading Test Data

For seqFISH analysis, the test file in zip format can be downloaded by entering the following URL into your Internet browser:

<https://zenodo.org/records/3735329/files/DNAseqFISH+.zip?download=1>

This compressed zip file will require decompression. It is assumed that the file is downloaded to the Downloads folder. A folder named “test\_data” can be used in the directory containing the MicEASH folder from Subheading 2.2, and the downloaded data can be dragged and dropped into the new folder.

The following command can be executed in the terminal to move and unzip the file:

```
# Before proceeding with the commands, manually drag and drop
the downloaded file from your Downloads folder to the "test_-
data" folder. Subsequently, execute the following commands in
the command line:
cd test_data/ # This changes the directory to the "test_data"
folder.
unzip DNAseqFISH+.zip # This command unzips the downloaded
file within the "test_data" folder.
mv DNAseqFISH+/DNAseqFISH* ./
```

To download the supplementary files necessary for conducting analysis, the following URL can be entered into an Internet browser to download the zip file:

[https://www.science.org/doi/suppl/10.1126/science.abj1966/suppl\\_file/science.abj1966\\_tables\\_s1\\_to\\_s4.zip](https://www.science.org/doi/suppl/10.1126/science.abj1966/suppl_file/science.abj1966_tables_s1_to_s4.zip)

Subsequently, the file can be manually dragged and dropped from the Downloads folder to the “test\_data” folder in the MicEASH folder from Subheading 2.2.

The following commands can then be executed in the terminal:

```
# Before executing the command, ensure that the downloaded file
has been moved from your Downloads folder to the "test_data"
folder. Subsequently, execute the following command in the
command line to unzip the file within the "test_data" folder:
unzip science.abj1966_tables_s1_to_s4.zip
```

---

## 3 Methods

### 3.1 Preprocessing Bright Spot Information Data

For this analysis, I use genome-wide DNA-seqFISH bright spot coordinates at a 1 Mb resolution obtained from male mouse embryonic stem cells (refer to Subheadings 2.2 and 2.3 in Materials for data download details). The file “Spatial\_distance\_analysis.ipynb” in the MicEASH package includes data analysis for replicates 1 and 2 (*see* **Note 1**). For simplicity, this protocol introduces commands for analyzing data from replicate 1.

To perform spatial analysis using bright spot information for genomic coordinates, I begin with file preprocessing using the “preprocess” command from the “micesh” module. First, I load the specified bright spot coordinate and target region information files. Subsequently, I merge the target region information with the coordinate data and then expand it. I adjust X, Y, and Z coordinates based on voxel size. Additionally, I add a column named “hyb,” sequentially numbering from zero based on chromosome coordinate order. Finally, I save the preprocessed file in CSV format. A detailed step-by-step guide to processing your data using the Jupyter Notebook in the MicEASH environment is provided below:

1. Open your terminal: Access the terminal application on your PC.
2. Navigate to the MicEASH folder: Type the command “cd [desired folder name]/MicEASH/jupyter” in your terminal to move to the MicEASH folder located within the folder created in your home directory. Replace [desired folder name] with your folder’s name. Refer to “2.2 Setting up the execution environment” for details on the MicEASH setup.
3. Activate the conda environment: Enter “conda activate mice\_env” in your terminal. This command activates the conda environment required to run the analysis tools provided in MicEASH.
4. Launch Jupyter Notebook: Type “jupyter notebook” in your terminal. This command should automatically open your web browser; if this does not occur, manually open your default web browser (e.g., Chrome, Safari, or Edge) and enter the Jupyter Notebook address shown in the terminal.
5. Access the Jupyter Notebook file: In the open Jupyter Notebook interface in your browser, navigate to and double-click the file named “Spatial\_distance\_analysis.ipynb.” This opens the notebook for performing data analysis.
6. Change the kernel: After opening the Notebook, select Kernel → Change kernel → mice\_env from the menu. If the kernel is already set to mice\_env, please ignore this step.

7. Execute the Notebook code: Locate the section titled “1. Preprocess bright spot information data.” Select the code under this heading and run it by pressing Shift+Enter or clicking the start button near the column. This processes the data and generates a DataFrame named “df\_preprocessed\_rep1,” which is automatically saved in a folder named “analysis.”

```
from miceash.preprocess import preprocess
path_1 = "../test_data"
df_preprocessed_rep1 = preprocess(data_path=path_1, posi_file="DNaseqFISH+1Mbloci-E14-replicate1.csv", anno_file="science.abj1966_table_s1.xlsx")
df_preprocessed_rep1
```

### 3.2 Spot Alignment to an Allele

Using the preprocessed DNA-seqFISH data file from Subheading 3.1, I perform allele separation for the two homologous chromosomes using the “align” command. This enables allele distinction across all chromosomes by assuming two clusters from the groups of spots on each homologous chromosome and classifying them. Clustering methods can be selected from KMeans (default), spectral clustering, hierarchical clustering, or Gaussian models. Clustering results are saved in a new file. Although this study focuses on diploid male cells, there is an option to switch to diploid female cells.

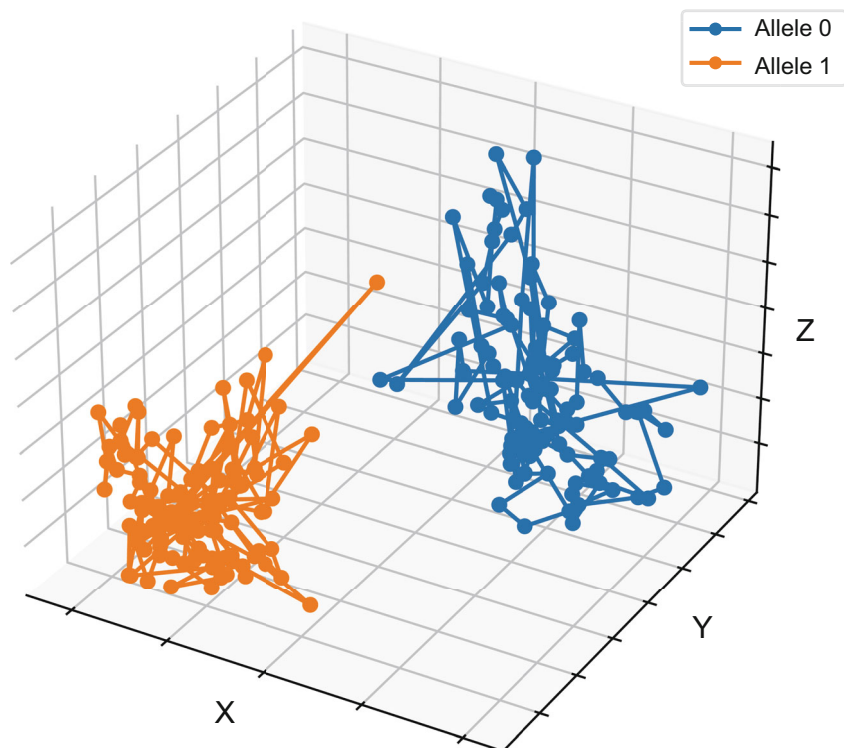
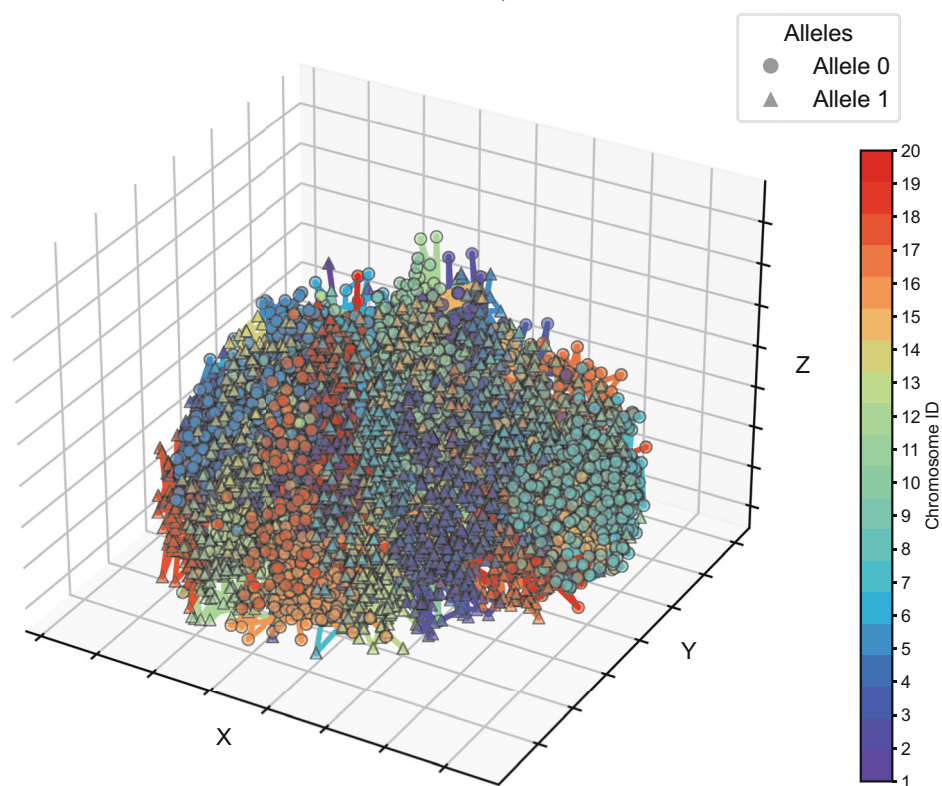
1. Select and execute the code under the column labeled “2. Align spots to each allele” (use Shift+Enter or the start button near the column). This will generate the “df\_preprocessed\_align\_rep1” file, and the data will automatically be saved in a folder named “analysis.”

```
from miceash.align import align
df_preprocessed_align_rep1 = align(path_1, "DNaseqFISH+1Mbloci-E14-replicate1_preprocessed.csv", "kmeans")
df_preprocessed_align_rep1
```

### 3.3 Visualization of Nuclear Spot Information

Using the file created in Subheading 3.2. containing annotated allele information for each homologous chromosome, I visualize chromosome 12 and all chromosomes in a cell using the “Data-Plotter” command (Fig. 2). This step enables the visual confirmation of allele distinction.

1. Select and execute the code under the column titled “3. Visualize allelic information” (use Shift+Enter or the start button near the column). After running the code, the output will display the two alleles in chromosome 12 (Fig. 2a).

**A****B**

**Fig. 2** Visualizing nuclear spot arrangements within a cell. **(a)** Coordinates of spots on chromosome 12 in a single cell are divided into two alleles, with each spot's spatial coordinates mapped based on its genomic coordinates. **(b)** Information for all chromosomes in a single cell. Alleles 0 and 1 are represented by circles and triangles, respectively. Chromosome ID 20 corresponds to chromosome X

```

from miceash.plot import DataPlotter
plotter = DataPlotter()
df_filtered = df_preprocessed_align_rep1[(df_preprocessed_align_rep1['cellID'] == 10) & (df_preprocessed_align_rep1['fov'] == 3) & (df_preprocessed_align_rep1['Chrom'] == "chr12")]
plotter.plot3D_onechr(df_filtered, path_1, "cellID_10_fov_3_-Chrom_chr12", show = True, save = True)

```

2. Select and execute the following code (use Shift+Enter or the start button near the column), which will produce an output showing spots for all distinguished chromosomes (Fig. 2b).

```

df_filtered = df_preprocessed_align_rep1[(df_preprocessed_align_rep1['cellID'] == 10) & (df_preprocessed_align_rep1['fov'] == 3)]
plotter.plot3D_allchr(df_filtered, path_1, "cellID_10_fov_3_-Chrom_all", show = True, save = True)

```

### 3.4 Calculating Distances Between Spots

After confirming the allelic information in Subheading 3.3, I calculate the pairwise distances between all genomic regions within each chromosome, generating the distance matrix for individual cells as well as the median distance matrix across all cells using the “matrix” command. Specifically, I calculate the Euclidean distances between the spatial coordinates of genomic regions within any chromosome at the single-allele level, storing these distances in a distance matrix. Next, I compute the median and average values of the distance matrices for each allele and save the data as a Numpy array. I perform this analysis for all chromosomes.

1. Select and execute the code under the column titled “4. Calculate distance matrix for each chromosome” (use Shift+Enter or the start button near the column). This will generate an output file containing spot distances for each chromosome. The output data include the distance matrix at the single-cell level as well as the median and mean distances.

```

from miceash.matrix import matrix
path_1 = "../test_data"
chromosomes = df_preprocessed_rep1["Chrom"].unique()
results = {chrom: matrix(path_1, "DNaseqFISH+1Mbloci-E14-replicatel_preprocessed_marked.csv," chrom, (103, 103, 250)) for chrom in chromosomes}

```

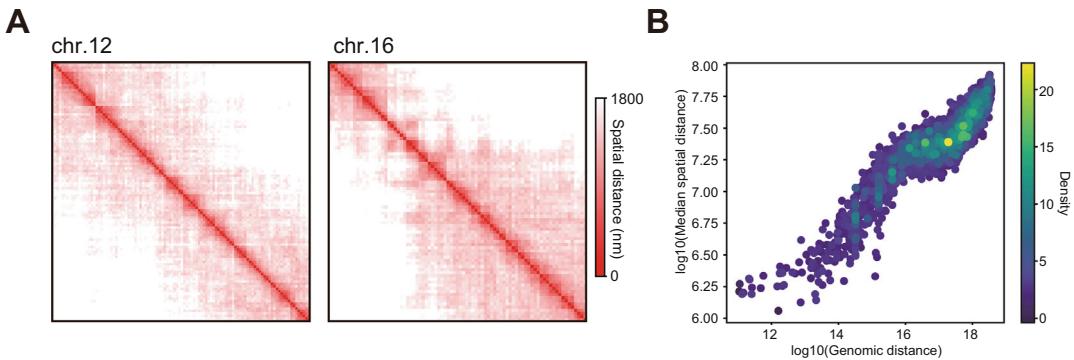


**Fig. 3** Visualization of distance matrices and comparison with genomic coordinates. **(a)** Visualization of chromosomes 12 and 16 using median spatial distance matrices, highlighting varying close regions between chromosomes and offering insights into chromosomal architecture and interactions. **(b)** Density scatter plot comparing actual spatial distances with genomic coordinate distances. As genomic coordinates become more distant, spatial distances increase, albeit nonlinearly due to nuclear size constraints. This plot illustrates the complex folding and DNA organization within the nucleus, where genomic distances do not necessarily correlate with physical proximities

### 3.5 Visualization of Distance Matrix Information

By visualizing the distance matrix information in a heatmap, I can reveal the features of higher-order genomic structures [9]. I produce heatmaps of the spatial distance matrix data using the “Data-Plotter” command. This provides an intuitive understanding of the structural differences between chromosomes and between regions with high contact frequencies within chromosomes (Fig. 3a).

1. Select and execute the code under the column titled “5. Plot the distance matrix for one chromosome” (use Shift+Enter or the start button near the column). This will generate an image file depicting the genomic distances of one chromosome. The output data are automatically saved in the “output\_images” folder (optional).

```
from miceash.plot import DataPlotter
from matplotlib.colors import LinearSegmentedColormap
plotter = DataPlotter()
path_1 = "../test_data"
file_name = "DNAseqFISH+1Mbloci-E14-replicate1_preprocessed_-marked_chr12_medi.npy"
cmap = LinearSegmentedColormap.from_list("bright_red",
[(1, 0, 0), (1, 1, 1)])
plotter.plot2D(path_1, file_name, C_MIN=None, C_MAX=1800,
c=cmap, show=True, save=False)
```

2. Select and execute the code under the column titled “Plot the distance matrix for all chromosomes” (use Shift+Enter or the start button near the column). This will generate an image file depicting the genomic distances of each chromosome. The

output data are automatically saved in the “output\_images” folder (optional).

```
chromosomes = df_preprocessed_align_rep1["Chrom"].unique()
path_1 = "../test_data"
for chrom in chromosomes:
    file_name = f"DNaseqFISH+1Mbloci-E14-replicate1_preprocessed_marked_{chrom}_medi.npy"
    plotter.plot2D(path_1, file_name, C_MIN=None, C_MAX=1800,
c=cmap, show=False, save=True)
```

### 3.6 Comparison of Genomic Coordinate-Pair Distances and Actual Genomic-Pair Distances

The genome, although extensive, is folded and stored within the nucleus, ensuring that any chromosome’s size does not exceed the nucleus’ size. Thus, the actual distances between far-separated genomic coordinates will not exceed a certain limit compared with neighboring regions. To explore the relationships among distances within chromosomes, I compare the actual genome structure to the genomic coordinates (Fig. 3b).

1. Select “6. Comparison of genome coordinates and genomic distances.”
2. Proceed with this section using Shift+Enter until completed.

### 3.7 Comparison of Hi-C Contact Count Information and seqFISH Data

The spatial distance matrix data from seqFISH are compared with the contact count matrix data from Hi-C using mouse embryonic stem cells as a reference [13]. I use an additional library called “straw” for handling Hi-C data (*see Note 2*). First, I create a heatmap showing the contact and distance matrices from Hi-C and seqFISH, respectively, to compare these data directly (Fig. 4a). Next, using each dataset, I compute the correlation coefficient and create a scatter plot. A negative correlation is shown by higher contact in Hi-C data corresponding to shorter distance in seqFISH data (Fig. 4b). However, determining a threshold for genomic regions in close contact based solely on spatial distance data is challenging; therefore, I use the Hi-C data as a reference to determine the contact frequency (Fig. 4c). This procedure enables a detailed comparative analysis of interactions between genomic regions.

1. Select “7. Heatmap of spatial distance (seqFISH) and contact count (Hi-C)” and proceed with Shift+Enter until completed, thereby visualizing the Hi-C contact data and seqFISH distance matrices in a comparative heatmap (Fig. 4a).
2. Select “8. Scatter plot of spatial distance (seqFISH) and contact count (Hi-C)” and continue with Shift+Enter until completed. This calculates the correlation between Hi-C contact data and

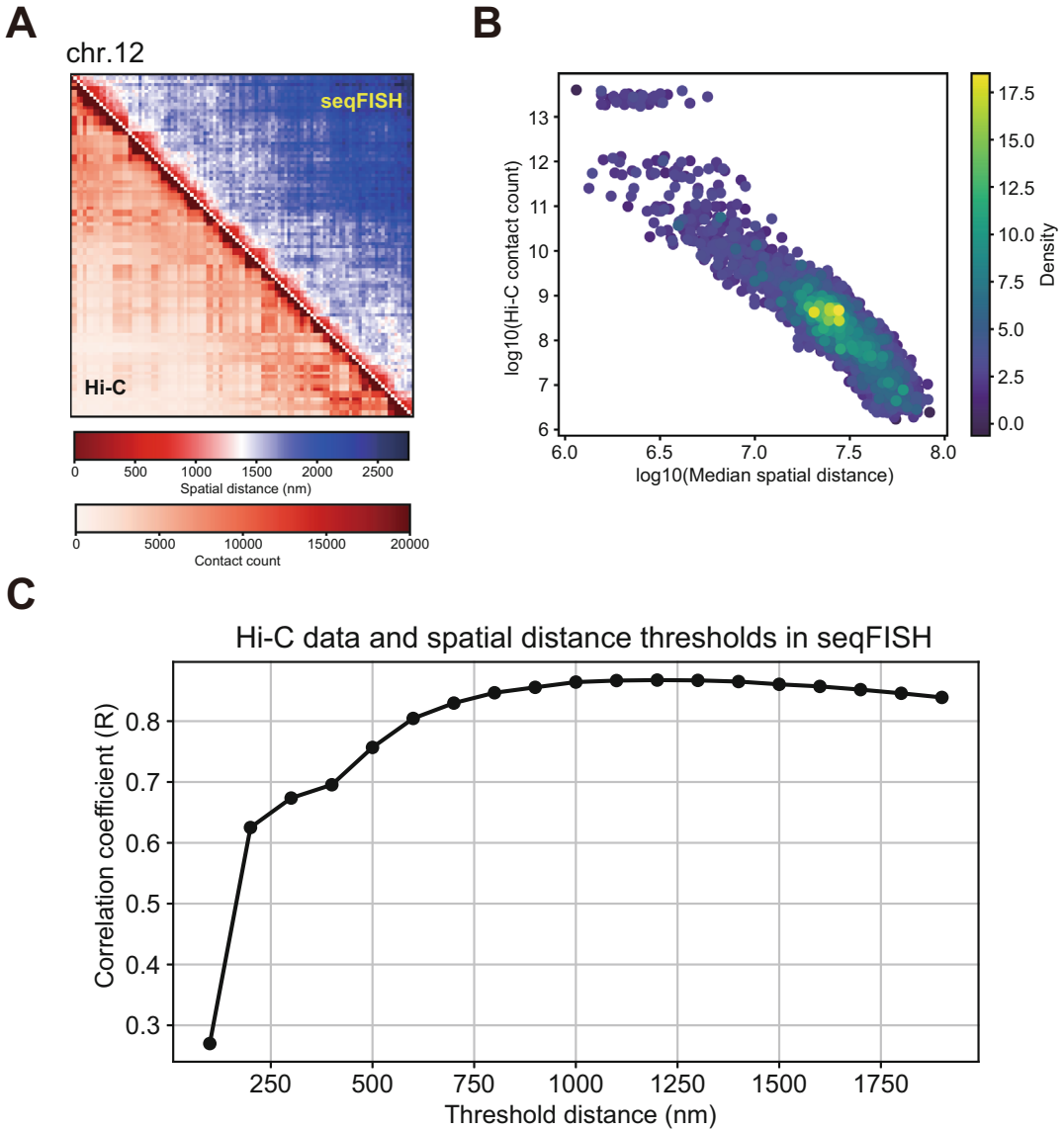


**Fig. 4** Comparison of seqFISH data with Hi-C data. (a) Heatmap of median spatial distance matrix from seqFISH data compared with Hi-C contact count matrix between genomic coordinates. The physical DNA segment proximity within the nucleus, determined through seqFISH, is comparable to the interaction (contact count), detected using Hi-C techniques. (b) Scatter plot comparing median spatial distances from seqFISH with Hi-C contact counts between genomic coordinates. As the distance between spots in seqFISH (x-axis) increases, the Hi-C contact count (y-axis) decreases, showing a negative correlation. (c) Correlation analysis between Hi-C contact counts and the contact frequency determined by the spatial distance threshold of seqFISH. At the 1100 nm threshold, seqFISH contact frequency at a 1 Mb resolution shows the strongest correlation with Hi-C contact counts, indicating an optimal threshold for comparing these genomic data types

seqFISH distance data, displaying the correlation on a scatter plot (Fig. 4b).

3. Select “9. Contact frequency with various thresholds” and proceed with Shift+Enter until completed. This calculates the optimal threshold for converting seqFISH distance data to contact frequency data based on Hi-C contact data (Fig. 4c).

---

## 4 Notes

1. **Steps 1** to **7** in Subheading **3.1.** are contained within a single Jupyter Notebook. Although you can proceed with each section individually, selecting “Run All” executes all the code at once. For sequential execution from **steps 1** to **5** in Subheading **3.1**, you may create a new Jupyter Notebook and either copy and paste the specified code from the Methods Subheadings **3.1**, **3.2**, **3.3**, **3.4** and **3.5** into this notebook or write the code directly. For Methods **3.2** and **3.3**, i.e., distinguishing alleles and selecting observation options, you can manipulate the data to determine the best options. This flexibility allows you to customize analysis to fit your research needs.
2. To perform Subheading **3.7**, the “hic-straw” library needs to be installed in the conda environment “mice\_env.” Please follow the installation instructions available at the following URL: <https://github.com/aidenlab/straw> or <https://pypi.org/project/hic-straw/>.

---

## Acknowledgments

I thank Hiroshi Ochiai (Kyushu University) and Soya Shinkai (RIKEN BDR) for their invaluable comments on the methods. This work was supported by JSPS KAKENHI to Hiroaki Ohishi (JP22K15084 and JP25K02255); JST, PRESTO grant to Hiroaki Ohishi (JPMJPR24O3); The Nakajima Foundation to Hiroaki Ohishi.; Nakatani Foundation to Hiroaki Ohishi.; Astellas Foundation for Research on Metabolic Disorders to Hiroaki Ohishi.

## References

1. Ohishi H, Au Yeung WK, Unoki M et al (2020) Characterization of genetic-origin-dependent monoallelic expression in mouse embryonic stem cells. *Genes Cells* 25:54–64
2. Ohishi H, Shimada S, Uchino S et al (2022) STREAMING-tag system reveals spatiotemporal relationships between transcriptional regulatory factors and transcriptional activity. *Nat Commun* 13:7672
3. Bonev B, Cavalli G (2016) Organization and function of the 3D genome. *Nat Rev Genet* 17: 661–678
4. Ochiai H, Ohishi H, Sato Y et al (2023) Organization of transcription and 3D genome as

- revealed by live-cell imaging. *Curr Opin Struct Biol* 81:102615
5. Kempfer R, Pombo A (2020) Methods for mapping 3D chromosome architecture. *Nat Rev Genet* 21:207–226
  6. Takei Y, Yun J, Zheng S et al (2021) Integrated spatial genomics reveals global architecture of single nuclei. *Nature* 590:344–350
  7. Takei Y, Zheng S, Yun J et al (2021) Single-cell nuclear architecture across cell types in the mouse brain. *Science* 374:586–594
  8. Su JH, Zheng P, Kinrot SS et al (2020) Genome-scale imaging of the 3D organization and transcriptional activity of chromatin. *Cell* 182:1641–1659
  9. Mateo LJ, Murphy SE, Hafner A et al (2019) Visualizing DNA folding and RNA in embryos at single-cell resolution. *Nature* 568:49–54
  10. Ohishi H, Shinkai S, Owada H et al (2024) Transcription-coupled changes in genomic region proximities during transcriptional bursting. *Sci Adv* 10:eadn0020
  11. Takei Y, Yang Y, White J et al (2025) Spatial multi-omics reveals cell-type specific nuclear compartments. *Nature* 641:1037–1047
  12. Jia BB, Jussila A, Kern C et al (2023) A spatial genome aligner for resolving chromatin architectures from multiplexed DNA FISH. *Nat Biotechnol* 41:1004–1017
  13. Bonev B, Mendelson Cohen N, Szabo Q et al (2017) Multiscale 3D genome rewiring during mouse neural development. *Cell* 171:557–572

# INDEX

## A

- Adipocytes
  - differentiation .....291, 294, 299, 301, 302, 307
  - maintenance..... 291, 294, 301
  - permeabilization ..... 314
  - 3D Immuno-FISH.....293–297, 308–318
- Adipogenesis..... 287–323
- Adipose tissue
  - deparaffinization of the tissue sections ..... 314
  - dissection ..... 293, 294, 314
  - permeabilization of the tissue sections ..... 314
- Agrobacterium tumefaciens*..... 29
- Amphipathic helix ..... 101, 227
- Analytical digestion ..... 103, 108
- Anti-GFP antibody-conjugated bead.....169
- APEX2 reaction
  - APEX2-Lamin B1 plasmid ..... 272, 273, 277, 281–283
  - ascorbate peroxidase (APEX2) ..... 271–284
- Arabidopsis thaliana* ..... 21, 30
- Artificial nucleus
  - in mouse oocytes ..... 183–198
- Atomic force microscopy (AFM) ..... 45–68

## B

- Beads incorporation
  - into living cells ..... 170, 173
  - into mouse oocytes ..... 184
- Biolistic bombardment ..... 76
- Biolistic transformation ..... 74–78
- Budding yeast *Saccharomyces cerevisiae*
  - fixation ..... 95
  - immunostaining ..... 83–97
  - nuclear membrane..... 83–97
  - preparation for super-resolution fluorescent microscopy ..... 83–97
  - spheroplasting ..... 86–88, 93
  - staining ..... 93

## C

- Calculating genomic distance
  - calculating distances between spots ..... 336–337

- comparison of calculated distance and actual distance ..... 338
- comparison of Hi-C contact count information ..... 338
- preprocessing bright spot information data ..... 333
- spot alignment to an allele ..... 334
- visualization of distance matrix information ..... 337
- visualization of nuclear spot information ..... 334
- Cell culture
  - cell lysis ..... 3, 7, 8
  - cell synchronization ..... 153, 155, 157
- Cell line
  - HCT116 ..... 282
  - HEK293FT fibroblasts ..... 297
  - HeLa cells ..... 35–42
  - Hepa1c1 (hepatocytes) cells ..... 8
  - human hTERT-immortalized retinal pigment epithelium (hTERT RPE-1) ..... 144
  - mouse 3T3-L1 fibroblasts ..... 291–292
  - U2OS cells..... 47
- CHAPS ..... 256, 257, 260
- Chemical transformation in yeast ..... 109, 110
- Chromatin condensation ..... 152, 153, 155, 156
- Chromatin fragmentation..... 273, 278
- Circadian clock ..... 1, 11
- Class A G protein-coupled receptors (GPCRs)..... 255–267
- Closed mitosis ..... 71
- Confining cell migration..... 160
- Confocal microscopy ..... 56, 114, 152
- Coomassie staining ..... 22, 23, 26, 228, 234, 264
- Correlated light-electron microscopy (CLEM) ..... 67, 170–175
- Correlation between fluorescence microscopy (FM) and EM images ..... 178
- Correlative fluorescence imaging ..... 126
- Cytoplasm..... 14, 17, 18, 33, 41, 46, 71, 100, 119–121, 125, 127, 133–135, 143, 191, 198, 215
- Cytoskeleton..... 18, 120, 127, 145, 147, 152, 154

## D

- DamID
  - Dam methylase ..... 289, 297, 299, 320
  - Dam-methylated DNA

detection of labeling efficiency .....	312–313
enrichment .....	292
generation .....	292
Data analysis	
of Dam-methylated DNAs .....	290, 292, 306
of FISH results .....	322
of GUV images .....	250
of pulled down DNAs .....	207–209, 218–221
of Scramblase activity data .....	262
Deflection measurement .....	161, 164
Diacylglycerol (DG) .....	2, 99–116
Direct Stochastic optical reconstruction microscopy (dSTORM) .....	47, 49, 56, 57, 59–61, 63, 65, 67
Distance matrix .....	330, 336–340
Dithionite .....	257, 259, 260, 262, 263, 266, 267
DNA double-strand break (DSB) .....	203
DNA sequencing .....	29
DNA sequential fluorescence in situ hybridization (DNA-seqFISH) .....	328, 330, 331, 333, 334
DSB end resection assay in NPE .....	205–207, 213–218
<b>E</b>	
Egg extract	
high-speed supernatant (HSS) .....	202
low-speed supernatant (LSS) .....	202, 203
nucleoplasmic extract (NPE) .....	202, 203
Endoplasmic reticulum (ER) .....	17, 18, 25, 33, 35, 46, 71–73, 79, 83, 145–147, 169, 229, 244
Estimating the number of proteins per vesicle .....	263–264
Extracellular matrix (ECM) fibers .....	159–167
<b>F</b>	
FISH	
data analysis .....	318
imaging .....	297, 318
preparing DNA probe .....	328
Fission yeast <i>Schizosaccharomyces pombe</i>	
chemical transformation .....	109, 110
genotyping .....	110
molecular genetics .....	104
selection .....	110
Fixation	
for live CLEM .....	175
for TEM imaging .....	36, 38
Flexural rigidity .....	166
Fluorescence microscopy (FM) .....	26, 45–68, 83–97, 122, 124, 126, 170, 173, 175, 178, 180, 272, 302
Fluorescent labeling .....	47, 49, 54, 55, 57
Fluorescent NBD-PC lipids .....	260
Frequency distribution map .....	145–148

**G**

Gaussian fit .....	164
--------------------	-----

**I**

Imaging	
of FISH probes .....	296
of GUVs .....	244, 249
high speed imaging .....	72, 73, 116, 153
label free imaging .....	120, 125
Immunoblotting for Chk1 phosphorylation .....	217
Immunofluorescence/immunostaining	
in HeLa cells for CLEM .....	174
using antibodies for nuclear lamina/ membrane .....	83–97, 282
using anti-FLAG antibody .....	274, 277, 282
Indirect immunofluorescence staining .....	171
In gel digestion .....	23, 27, 31, 32
Inner nuclear membrane (INM) .....	17, 18, 46, 47, 55, 59, 83, 84, 99, 100, 114
In vitro biochemical perturbations .....	127
In vitro transcription of RNA .....	188
In vivo biochemical perturbations .....	127
Isolation	
of microsomal membrane .....	22
of nuclear membrane .....	22, 26
of nucleus from cell culture .....	2, 3, 7
of nucleus from mouse liver .....	2, 6
of reconstructed nuclei in egg extract .....	202

**L**

Label-free quantification .....	20
Lamina associated domains (LADs) .....	272, 276, 281, 289, 299, 304, 305, 307–309, 319–321
Lamin B1 .....	55, 145, 195, 272, 282, 283, 289, 293
Lentiviral transduction optimization .....	301
Lentivirus production in cell culture .....	290, 299
Lipid	
bilayer .....	46, 226
composition .....	1, 11, 83, 227, 240, 256
dynamics .....	100
extraction .....	2, 9
metabolism .....	1
Lipid-protein interaction .....	226
Lipid sensor	
fluorescent lipid biosensor .....	100
Liposome	
giant unilamellar vesicles (GUVs) .....	240
large unilamellar vesicles .....	256
liposome floatation assays .....	226–236, 240
multilamellar vesicle (MLV) liposomes .....	227, 231, 236
preparation from <i>E. coli</i> polar lipids .....	227, 231, 234

proteo-liposome ..... 241, 242, 244, 246, 249,  
250, 256, 259–264, 266, 267

small unilamellar vesicle (SUV)  
liposomes ..... 226–228, 233

Live-cell imaging  
in HeLa cells ..... 155, 176  
in mouse oocytes ..... 184, 186, 193  
of nuclear membrane ..... 71–79  
of nuclear shape fluctuations ..... 152, 153, 155  
using correlated light-electron microscopy  
(CLEM) ..... 170  
using fluorescence microscopy ..... 170, 175  
in yeasts ..... 111–113

## M

Mass density ..... 119–137

Mass spectrometry ..... 2, 10, 14, 23, 28, 30, 31, 33

Microfabrication of negative mold ..... 162, 163, 165

Microinjection in mouse oocytes  
of DNA ..... 184–186, 191–193, 196–198  
of RNA ..... 186, 190–192, 196–198

Micropost  
coating with Fibronectin ..... 163  
design ..... 160–163  
etching ..... 161  
fabrication ..... 160–163  
fixed-cell imaging ..... 164  
live-cell imaging ..... 164  
seeding cell ..... 164  
washing ..... 163

Miniprep ..... 103, 108, 109

Mitotic progression ..... 151

Molecular cloning ..... 29, 103, 105, 106

Mouse  
embryonic stem cells ..... 333, 338  
liver ..... 1, 2, 6, 11  
oocytes ..... 183–198

Mouse oocyte activation ..... 185, 186, 192

Mouth pipette preparation ..... 185, 188, 189, 195, 196

## N

NE transmembrane proteins (NETs) ..... 288–290

Nick translation ..... 295, 296, 310–312

Nuclear assembly in LSS ..... 202

Nuclear envelope (NE)  
break down ..... 152, 202  
detection ..... 157  
reformation ..... 169

Nuclear flickering spectroscopy ..... 156

Nuclear invagination analysis ..... 156

Nuclear lamina ..... 17, 18, 46, 159, 272, 282

Nuclear lipid composition ..... 1, 11

Nuclear lipidome ..... 1, 2, 11

Nuclear localizing signal (NLS) ..... 9–12, 15, 100–102,  
112, 115

Nuclear mechanics ..... 152

Nuclear membrane ..... 17, 18, 20, 22, 26, 41, 46,  
71–73, 83–97, 119, 143–149, 155, 169–181,  
201, 202, 226

Nuclear pore complex (NPC) ..... 18, 35, 41, 46, 47,  
61, 63, 64, 83, 85, 169–181, 195

Nuclear shape fluctuation ..... 151–158

Nuclei extraction ..... 21, 48, 50–53, 64

Nuclei immobilization ..... 48, 52, 54

Nucleoplasm ..... 71, 119, 127, 134, 143, 214

Nucleoporin (Nup)  
Nup-beads ..... 169–181

## O

Opsin ..... 257, 259, 260, 262, 263

Optical diffraction tomography (ODT)  
field retrieval ..... 129  
initialization ..... 128  
ODT setup ..... 121–125, 130, 132, 137  
post-processing ..... 129–133  
segmentation ..... 133  
setup ..... 121–122, 124, 125, 130, 132, 137  
tomogram acquisition ..... 128–130  
tomogram reconstruction ..... 129, 132

Optional spectral autofluorescence image correction by  
regression (SAIBR) ..... 112

Oxygen plasma treatment ..... 162

## P

Particle coating ..... 76

Particle preparation ..... 75

PCR ..... 23, 29, 102, 103, 105–107, 109,  
110, 235, 284, 290–293, 297, 299, 304–306,  
312, 316, 329

Peptide preparation ..... 20, 23

Permeabilization  
of adipocytes ..... 314  
of adipose tissue sections ..... 314

Pharmacological agent ..... 152, 153, 155

Phosphatidic acid (PA) ..... 2, 5, 99–116, 160

Phosphoinositide ..... 227

Phospholipid ..... 135, 255–267

Photoresist ..... 160–162

Plant nuclear envelope transmembrane proteins  
(PNETs) ..... 20, 30

Polydimethylsiloxane (PDMS) ..... 160, 162, 163,  
165–167

Preparation of GUVs  
on platinum grids ..... 242, 246  
using PVA method/gel-assisted method ..... 241,  
243, 244, 247, 248

- Preparation of oocytes
  - in mouse ..... 183–198
  - in *Xenopus laevis*..... 203, 205
- Pronucleus in mouse oocytes ..... 183
- Prophase ..... 152, 155, 282
- Protein isolation from the floated liposome
  - fraction ..... 228, 234
- Protein-membrane interaction ..... 235, 240, 244
- Proteoliposome
  - concentration ..... 246
  - preparation ..... 244, 246
- Pull-down
  - of DNA in NPE ..... 207, 216–221
  - of streptavidin..... 274, 278–281, 283
- Q**
- Quantification
  - distribution of nuclear proteins ..... 143–149
  - phospholipid ..... 263
  - protein on liposomes ..... 264
- R**
- Rehydration of lipid film ..... 248
- S**
- Saccharomyces cerevisiae*..... 100, 101
- Schizosaccharomyces pombe*..... 100–102, 104, 105, 109–114, 116
- Scramblase assay
  - scramblase ..... 260
- seqFISH..... 328–330, 332, 338–340
- Shotgun lipidomics ..... 2, 4–6, 9–12
- Single molecule localization microscopy
  - (SMLM)..... 46, 47, 51, 54, 57, 59, 64
- Sonication for chromatin fragmentation ..... 273
- Spinning disk confocal super-resolution fluorescence
  - microscopy ..... 187, 193, 197
- Stochastic optical reconstruction microscopy
  - (STORM)..... 85, 89
- Structured illumination microscopy (SIM) ..... 78, 84–86, 91, 93, 94
- Subtractive proteomics ..... 17–33
- Super-resolution fluorescence microscopy
  - stochastic optical reconstruction microscopy (STORM) ..... 85, 89
  - structured illumination microscopy (SIM) ..... 85, 91, 93
- T**
- T4 DNA
  - T4 DNA-induced reconstruction of artificial nuclei ..... 183–198
- Tetrahymena* culture..... 74, 79
- 3D Immuno-FISH
  - of cultured adipocyte ..... 293–297, 308–318
  - DNA probe preparation ..... 308, 315
  - of fat tissue ..... 293–297
  - hybridization of DNA probes ..... 316
  - RNase A treatment..... 316
  - stringency washing ..... 317
- Transfection of plasmids ..... 273
- Transmission electron microscopy (TEM)
  - fixation ..... 36, 38
  - resin embedding..... 36, 38, 39
  - staining ..... 37, 40
  - trimming..... 37, 39, 40
  - visualization ..... 37
- V**
- Visualization
  - for in vitro sample ..... 126–127
  - for in vivo sample ..... 124–126
- X**
- Xenopus laevis*
  - egg extract ..... 201
  - oocytes ..... 46
  - sperm chromatin preparation ..... 203
- Y**
- Young's modulus ..... 62, 160, 166, 167